The Redistribution of Argon Through a Metamorphic Cycle: Causes, Effects, and Consequences on Understanding Cooling Rates

Thesis

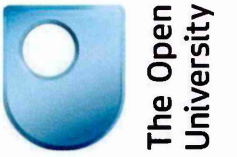

The Redistribution of Argon through a Metamorphic Cycle:

Causes, Effects and Consequences on Understanding Cooling Rates

Christopher S. McDonald

MGEOL. University of Leicester (2011)

A thesis submitted for the degree of Doctor of Philosophy

Department of Environment, Earth and Ecosystems,

The Open University,

Walton Hall,

Milton Keynes,

MK7 6AA

November 2014

This Dissertation is the result of my own work and included nothing which is the outcome of work done in collaboration except where specifically indicated in the text.

Christopher S. McDonald

November 2014

Abstract

$^{40}Ar/^{39}Ar$ thermochronology is commonly used to constrain the timing, and rates, of cooling in exhumed metamorphic terranes. Metamorphic micas that crystallise at high temperatures are usually considered to lose ^{40}Ar via thermally-activated volume diffusion, and the resulting age is commonly linked to temperature via Dodson's closure temperature (T_c) formulation. $^{40}Ar/^{39}Ar$ ages from many metamorphic terranes commonly do not fit within a chronological framework defined by other, higher T chronometers, such as U-Pb zircon, suggesting that linking age to temperature via pure open system diffusion may not always be a correct interpretation.

The Western Gneiss Region of Norway documents isothermal decompression from high pressures (from ~3.0 GPa to ~1.0 GPa) at 700°C. White mica, biotite, amphibole, and feldspar single grain fusion and laser ablation $^{40}Ar/^{39}Ar$ ages yield a broad range that spans the known timing of the metamorphic cycle and that cannot be readily reconciled with models of simple thermal diffusion.

Instead, the $^{40}Ar/^{39}Ar$ data record the cumulative effects of a complex interplay of processes that affected the rocks during decompression and exhumation. Recrystallization, deformation, partial melting, and fluid infiltration all acted to add or remove Ar from the system at different times in different lithologies. Samples that show significant recrystallization and deformation yield younger white mica but older biotite ages than more pristine samples. Furthermore, migmatisation acted to make biotite ages younger in the amphibolite-facies gneisses whereas fluid infiltration acted to increase biotite ages. Data from white mica breaking down to form a symplectite of biotite and plagioclase show that during recrystallization, Ar was not lost to the grain boundary, but instead becomes incorporated into biotite and plagioclase.

These physical processes appear to have dominated over thermally-activated volume diffusion as the means by which Ar was (re)distributed within, and between, different lithologies. Overall, these data support the observation that $^{40}Ar/^{39}Ar$ ages from K-bearing minerals in high-temperature and high-pressure metamorphic terranes may not always be interpretable as cooling ages and that metamorphic $^{40}Ar/^{39}Ar$ ages require careful assessment with respect to metamorphic stage and petrographic evolution.

Acknowledgements

I owe the success and the completion of this thesis to so many people and I hope to thank them all here.

Firstly I'd like to thank my supervisory team: thanks to Clare for giving me the opportunity to work on this interesting project and for your unfailing enthusiasm, optimism, for asking the tough questions, for striving for perfection and for always having patience with me. Thanks to Darren, Simon, and Sarah for all your help and support throughout the PhD and all your interesting discussions regarding the finer points of Ar dating.

Thanks you also to the technical staff at the OU for all their help with during the PhD. Thank you Alison and Jam for all their help in the Ar lab and advise on mass specs and sample preparation. Thank you to Michelle and Kay for putting up with me in the thin section lab for my first three months. Thanks you to Sam, Andy and Susanne for the all their help with the microprobe work.

Thank you also goes to my fellow metamorphic people at the OU, Catherine, Lucy, Big Tom, Little Tom, and Nigel for their many chats, even if they were Himalayan-based. Thank you to Julian and Daniele for all their assistance in Norway and particularly to Dani for teaching me all of the finer points of the Italian language!

A big thank you to all my friends I have made during my time at the OU: Encarni, Peter, Sam, Tom, Alice, Kat, Kate (scoobs), Adele, Hayley, Frazer, Catherine, Sion, Bertie, runty Pete etc. for the numerous laughs, interesting lunchtime discussions, beers, and for the oodles of cake that were always very tasty! A massive thank you to my office mates Leanne, Alice, and Kat for many laughs and sound advice, especially Leanne, my unofficial wife, for putting with me at home too!!

To my fellow geology friends from Leicester: Camille, Jon, Mikey, Phil, Pat, Steve, Bella, Bedders, Mike, Fev, Mark, Sophie, and Rob a massive thank you for being there and making my undergraduate days fun and interesting. No doubt, without you guys I would not have enjoyed the subject half as much as I do. Thank you to Pete for all the laughs and good times, despite not being able to warn off the PhD path! To my friends Mark and Mike from outside the OU; thanks for all the laughs, and for distracting me from geology every once in a while. To my friends from home: John, Holly, Paul, and Steve, and everyone else, thank you for all your support through the PhD, for being understanding about my silence during writing up, for putting up with my random talk of rocks. Soon I shall return to 'normality' and there will be wine!

To my family, thank you for being there mum and dad, despite not having a clue about what it is I do. Your support throughout this PhD has been immense and without you I would not have made it through. Thank you to my sister and brother for all your support too.

And finally, thank you Nan. I know you would have never understood what I was doing or why I was doing it, but you'll always be there for me and you are always in my heart.

Contents

Chapter 4: Symplectites: Tracking Ar though Metamorphic Reactions

Chapter 5: $^{40}Ar/^{39}Ar$ Dating of the Minor Lithologies of the WGR: Eclogites, Amphibolites, and Granulties

List of Figures

Chapter 1: Introduction

Chapter 2: Modelling Ar Diffusion: Creating the Framework for Interpreting Metamorphic $^{40}Ar/^{39}Ar$ Ages

Chapter 3: Tracking Ar through a Metamorphic Cycle: Consequences for Understanding Cooling Rates

Chapter 4: Symplectite: Tracking Ar through Metamorphic Reactions

Chapter 5: $^{40}Ar/^{39}Ar$ Dating of Minor Lithologies of the WGR: Eclogites, Amphibolites, and Granulites

Appendix A: Sample Petrography and Mineral Geochemistry

List of Tables

Chapter 2: Modelling Ar Diffusion: Creating the Framework for Interpreting Metamorphic $^{40}Ar/^{39}Ar$ Ages

Chapter 3: Tracking Ar through a Metamorphic Cycle: Consequences for Understanding Cooling Rates

Chapter 4: Symplectites: Tracking Ar through a Metamorphic Reaction

Chapter 5: $^{40}Ar/^{39}Ar$ Dating of the Minor Lithologies of the WGR: Eclogites, Amphibolites, and Granulites

Appendix A: Sample Petrography and Mineral Geochemistry

Appendix B: Electron Microprobe Analysis Datasets

Appendix C: Single Grain Fusion $^{40}Ar/^{39}Ar$ Datasets

Appendix D: *In-situ* Laser Ablation $^{40}Ar/^{39}Ar$ Datasets

Appendix E: Whole Rock XRF Datasets

Appendix F: DiffArg_inverse Model Results

List of Publications and Conference Papers resulting from this Thesis

Manuscripts under Preparation:

McDonald, C. S., Warren, C. J., Mark, D. F., Regis, D., Halton, A. M., Kelley, S. P. & Sherlock, S. C. *$^{40}Ar/^{39}Ar$ Age Systematics of Eclogites and Granulites from the Western Gneiss Region, Norway.*

McDonald, C. S., Warren, C. J., Mark, D. F., Halton, A. M., Kelley, S. P. & Sherlock, S. C. *Tracking Ar though a Metamorphic Cycle: Consequences for Understanding Cooling Rates.*

McDonald, C. S., Warren, C. J., Regis, D., Kelley, S. P. & Sherlock, S. C. *Symplectites: Tracking Ar though a Metamorphic Reaction.*

McDonald, C. S., Warren, C. J., Hanke, F., Regis, D., Chard, J. & Ingvorsen, L. *Modelling P-T Paths and Cooling Rates: Creating the Framework for Interpreting Metamorphic $^{40}Ar/^{39}Ar$ Ages.*

Conference Abstracts:

McDonald *et al.*, (2014). *Recycling Ar through Metamorphic Reactions: The Record in Symplectites.* Goldschmidt, Sacramento, CA; U.S.A. (oral presentation)

McDonald *et al.*, (2014). *Recycling Ar through Metamorphic Reactions: The record in Symplectites.* Metamorphic Studies Group, Milton Keynes, U.K.

McDonald *et al.*, (2013). *Argon Dates and Cooling Rates: Argon Age Heterogeneities and Implications for the Exhumation History of the WGR, Norway.* Building Strong Continents, Portsmouth, U.K. (oral and poster presentation)

McDonald *et al.*, (2013). *Do Ar Dates Yield Cooling Rates in Metamorphic Terranes? A Case Study from the WGR of Norway.* William Smith Meeting, Geological Society of London, London, U.K. (Poster presentation)

McDonald *et al.*, (2013). *When is a Date not an Age? An $^{40}Ar/^{39}Ar$ Investigation of a UHP Metamorphic Cycle.* Metamorphic Studies Group, Cambridge, U.K. (oral presentation)

McDonald *et al.*, (2012). *Eclogites, Amphibolites, and Argon: Tracking Argon through a Metamorphic Cycle.* European Mineralogical Society, Frankfurt, Germany. (poster presentation)

McDonald *et al.*, (2012). *Eclogites, Amphibolites, and Argon: Tracking Argon through a Metamorphic Cycle.* Metamorphic Studies Group, 2012, Cambridge, U.K. (poster presentation)

Chapter 1

Introduction

Folded mafic eclogite at Geitebruvika

Radioisotopic dating, known as geochronology, is a technique that uses the natural radioactive decay of one element to another to measure time. The commonest used methods in the study of metamorphic rocks and metamorphic timescales are lutetium-hafnium (Lu-Hf), samarium-neodymium (Sm-Nd), uranium-lead (U-Pb) and potassium-argon (K-Ar). Each of these methods can be used to date particular parts of the metamorphic cycle. Lu-Hf and Sm-Nd analysis of garnet provides timings of the prograde metamorphic path (Duchene *et al.,* 1997). U-Pb dating of zircon can be used to constrain timing of peak metamorphism and K-Ar dating of micas provides details of the cooling history (Root *et al.,* 2004, McDougall & Harrison 1999). This thesis will focus on the use of K-Ar dating, via the $^{40}Ar/^{39}Ar$ method, to understanding the cooling history of a metamorphic terrane, the effects the metamorphic cycle has on the K-Ar chronometer, and the consequences for understanding cooling or recrystallization histories.

1.1 The $^{40}Ar/^{39}Ar$ Dating Method

The K-Ar method, *sensu stricto*, requires the individual measurements of the concentrations of K and Ar isotopes (Dalrymple & Lanphere 1969). For K-Ar dating, measurement was performed using separate aliquots of a sample, which were then measured using two different instruments (commonly a flame photometer and a gas source mass spectrometer). The drawbacks of this method is that large volumes of material were required and the use of two different instruments and additional weighing errors leading to large errors on the resulting age (McDougall & Harrison 1999). An advance of the K-Ar method is $^{40}Ar/^{39}Ar$ dating (Merrihue & Turner 1966). ^{39}K is converted to ^{39}Ar via fast neutron bombardment in a nuclear reactor. ^{40}Ar and ^{39}Ar (which is a proxy for the ^{39}K) can thus be measured using a single mass spectrometer, reducing the uncertainty (McDougall & Harrison 1999).

$^{40}Ar/^{39}Ar$ chronology is a relative dating method and ages are calculated relative to a standard of a known age. The standard, which is irradiated in conjunction with the unknowns, acts as a monitor for the neutron flux that converts the ^{39}K to ^{39}Ar that the unknown receives during the irradiation process. This neutron flux is calculated into a *J*-value which allows ages to be calculated by comparison with the $^{40}Ar/^{39}Ar$ age of the known standard (McDougall & Harrison 1999).

The age equation is defined as:

$$t = \frac{1}{\lambda} ln\left(1 + J\frac{^{40}Ar^*}{^{39}Ar_K}\right) \qquad (1.1)$$

Where t is time, λ is the decay constant of ^{40}K to ^{40}Ar, $^{40}Ar^*/^{39}Ar_K$ is the ratio of radiogenic ^{40}Ar to ^{39}Ar produced from ^{39}K, and J is the irradiation parameter (a measure of the neutron flux and thus a measure of how much ^{39}K is converted to ^{39}Ar. J is defined by the equation:

$$J = \frac{(exp^{\lambda t})-1}{^{40}Ar^*/^{39}Ar_K} \qquad (1.2)$$

Where t, in this case, is the age of the standard (which is known) and that was irradiated in in conjunction with the unknowns. The $^{40}Ar/^{39}K$ ratio is proportional to the $^{40}Ar/^{39}Ar$ ratio and is therefore proportional to the age. This is because the production of ^{39}Ar from ^{39}K depends on the concentration of ^{39}K present in the sample and measurements of the $^{40}K/^{39}K$ ratio in natural systems indicates variations less than 1 per mil, a variation which is well within the experimental errors so it is valid to assume a single, constant natural ratio (McDougall & Harrison 1999).

The $^{40}Ar/^{39}Ar$ method is used to date K-bearing igneous and metamorphic rocks (e.g. whole-rock basalts where the grain size is fine or on mineral separates from coarser-grained lithologies such as granites and gneisses; McDougall & Harrison (1999)). The most commonly dated minerals in metamorphic rocks are white micas (muscovite and/or its high-pressure equivalent phengite), biotite, amphibole, and alkali feldspars (McDougall & Harrison 1999).

1.1.1 Diffusion and the Closure Temperature Formulation

The $^{40}Ar/^{39}Ar$ dating technique, unlike other geochronometers such as U-Pb, is regarded as a thermochronometer as generally there is less ^{40}Ar within a mineral than expected for age of crystal formation given the radioactive decay of the parent isotope ^{40}K. This is because Ar, being a noble gas and geochemically inert, does not bond to the mineral structure and/or lattice. This inert nature makes Ar more mobile than many other elements, and at elevated temperatures Ar is able to escape from a mineral via diffusion.

Diffusion of a radiogenic element within geological materials below recrystallization or melting temperatures is assumed to be predominately controlled by temperature (i.e. is thermally activated), and the concentration of the diffusing species (i.e. radiogenic Ar) is governed by a modified version of Fick's 2nd Law of diffusion:

$$\frac{\partial \emptyset}{\partial t} = D\frac{\partial^2 \emptyset}{\partial x^2} + S \qquad (1.3)$$

Where $\emptyset$ is the concentration of ^{40}Ar and t is time. X is the diffusion length and D is the temperature (T)-dependent diffusion coefficient determined by the pre-exponential coefficient D_0, the activation energy E_a and the gas constant R defined by the equation:

$$D = D_0 e^{(-E_a/RT)} \qquad (1.4)$$

S is the source term and relates the production of ^{40}Ar via the radioactive decay of ^{40}K within the grain and is defined by the equation:

$$S = \lambda[^{40}K]_i e^{-\lambda t} \qquad (1.5)$$

Where λ is the total decay constant of ^{40}K to ^{40}Ar, $[^{40}K]_i$ is the concentration of ^{40}K at time zero (Dodson 1973).

Dodson (1973) provided an analytical solution to the diffusion equation which provided a simple way of relating age to cooling rate. This solution, known as the closure temperature formulation or T_c, is defined by the equation:

$$T_c = \frac{R}{[E_a ln(A\tau D_0/a^2)]} \qquad (1.6)$$

In which R is the universal gas constant, E_a is the activation energy, A is a numerical constant that depends on mineral geometry, a is a characteristic diffusion radius, D_0 is the pre-exponential component, and τ is the time constant at which the diffusion coefficient (D) diminishes. It is this function τ that relates the T_c to cooling rate by:

$$\tau = \frac{R}{(E_a dT^{-1}/dt)} = -\frac{RT^2}{(E_a dT/dt)} \qquad (1.7)$$

It is important to note that the calculation of the T_c requires that the cooling rate (dT/dt) be estimated, however the cooling rate is one of the unknown variables, causing the formulation to be circular (Warren *et al.*, 2012c). However, the other variables of D_0, E and a within the formulation have a much greater influence than cooling rate (Lee 2009).

The T_c formulation is best applied to systems that experienced a simple, slow, 1/T-shaped, cooling history. This 1/T cooling rate is the main mathematical assumption inherent within the T_c formulation. It is assumed that ^{40}Ar is able to diffuse out of the mineral grain and is lost to the grain boundary medium (which is assumed to act as an infinite reservoir with a zero concentration of Ar). As the system begins to cool, Ar will become progressively retained within the mineral (Fig. 1.1).

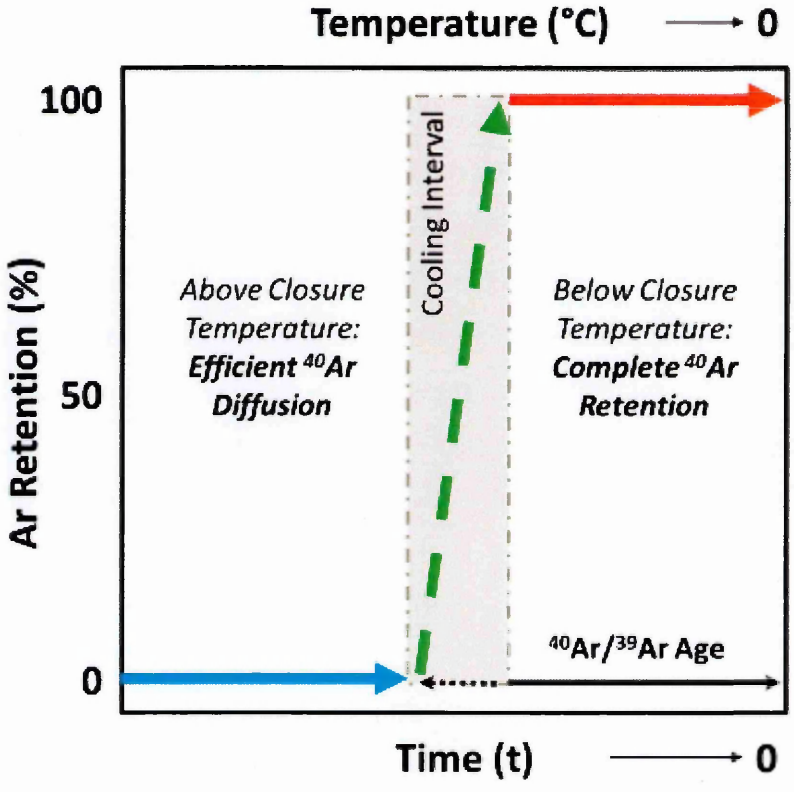

Fig. 1.1. A schematic representation of the Dodson (1973) closure temperature (Tc) showing that with decreasing time and temperature, Ar retention increases within a grain until all Ar is retained, thereby age = temperature. Modified after (McDougall & Harrison 1999).

This retention is not instantaneous and occurs across a temperature interval; therefore the value of T_c is an estimated average temperature at the time of the grain's apparent age.

The formulation only holds true when the following assumptions regarding the behaviour of Ar can be deemed to be in operation during the exhumation and cooling path:

(1) That the concentration of Ar within a grain is governed only by thermally-activated volume diffusion that adheres to Fick's 2nd law of diffusion (modified for a source term),

(2) That the mineral grain crystallised or recrystallized with no inherited ^{40}Ar within its crystal lattice, and

(3) That the grain boundary network operates as an 'open system', i.e. that the concentration of Ar in the grain boundary is negligible such that the grain boundary network acts as an 'infinite' sink for Ar.

However, some of these assumptions may not hold true for rocks that experience metamorphic cycles. In all metamorphic systems, rocks experience changes in pressure and temperature with time during their evolution, which may follow rapid metamorphic cycles. Mineralogical changes, changes in mineral grain size, and the extent to which the system is open or closed to the loss of Ar during the metamorphic cycle may affect how Ar partitions between the mineral and the grain boundary. Furthermore, temperatures may be too low during the metamorphic cycle for Ar to efficiently diffuse out of a mineral. In addition, if temperatures are high, and there are measureable amounts of Ar in the grain boundary, Ar can diffuse into the mineral from the grain boundary if the mineral/fluid partition coefficients are not very low. These effects can cause one or more of the assumption within the T_c formulation to become invalid. Therefore, $^{40}Ar/^{39}Ar$ ages from rocks that experience metamorphic cycles require careful interpretation before they can be linked to either cooling or crystallisation, this is particularly important in dry rocks or during short metamorphic cycles.

The evaluation and understanding of how Ar is incorporated, released and transported within and between different minerals during a metamorphic cycle is therefore key to the interpretation of metamorphic $^{40}Ar/^{39}Ar$ data, especially with regards to linking 'age' to 'stage' along the pressure-temperature (P-T) path, and it is important to constrain how/where Ar is produced, stored and transported during exhumation-related, retrograde metamorphic reactions.

1.1.2 $^{40}Ar/^{39}Ar$ Dating Techniques

Three techniques have chiefly been employed in $^{40}Ar/^{39}Ar$ thermochronology. These are step heating (of single or multiple grains), single grain fusion and *in-situ* laser ablation analyses. In step heating samples are heated incrementally, starting at low temperatures and increased until the sample fuses, with Ar released and measured at each temperature increment. A series of steps is produced which are commonly plotted as the apparent $^{40}Ar/^{39}Ar$ age vs. the cumulative proportion of ^{39}Ar released (McDougall & Harrison 1999). This plot is known as an age spectrum and will yield a flat profile, or plateau, if the rock and/or mineral have been closed to the loss or gain of Ar (McDougall & Harrison 1999).

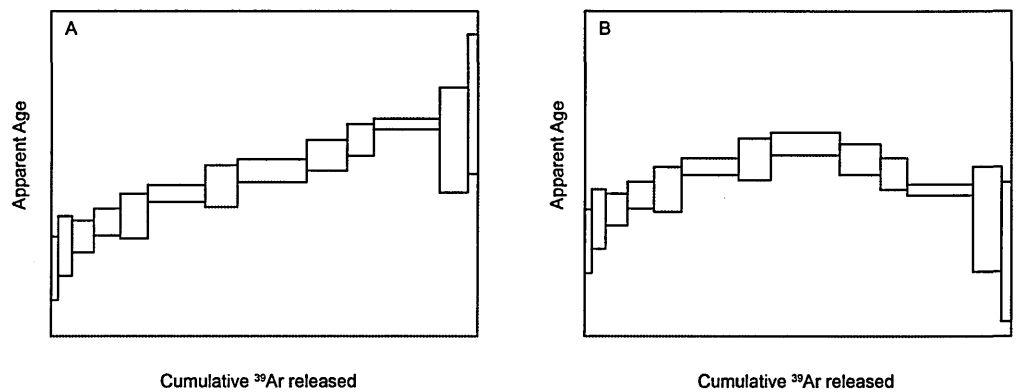

Fig. 1.2. A schematic representation of 'disturbed' step heating spectra. A) A staircase profile, and B) a 'hump' shaped step heating profile.

Analysis of micas via the step heating method also commonly yields 'staircase' or 'hump-shaped' non-plateau spectra (Fig. 1.2). These complex spectra have been attributed to the heterogeneous breakdown of micas during heating, the presence of a mixture of mineral compositions, or disturbed system including addition of excess argon (Sletten & Onstott 1998, Di Vincenzo 2006). This is problematic because complex age spectra may not yield a resolvable age and also the step heating method may mask the underlying Ar heterogeneity.

Single grain fusion is the analysis of individual mineral grains that, unlike the step heating method, are fused in one step, producing a bulk mineral age. This method allows for a more rapid collection of $^{40}Ar/^{39}Ar$ age data and allows for the analysis of many different mineral separates from the same sample so that the age variability within a rock can be assessed.

Finally *in-situ* laser ablation $^{40}Ar/^{39}Ar$ analysis can be performed on mineral separates or on polished slabs, providing key spatial context to the resulting $^{40}Ar/^{39}Ar$ ages. The *in-situ* technique is a useful tool for mapping intra- and inter-grain age heterogeneities. Step heating and single grain fusion techniques are commonly only used to analyse a single mineral species, such as muscovite or biotite, whereas the *in-situ* technique can be used to analyse these minerals as well as other K- and non K-bearing minerals (e.g. quartz, feldspar, garnet) that may be acting as sources or sinks for Ar.

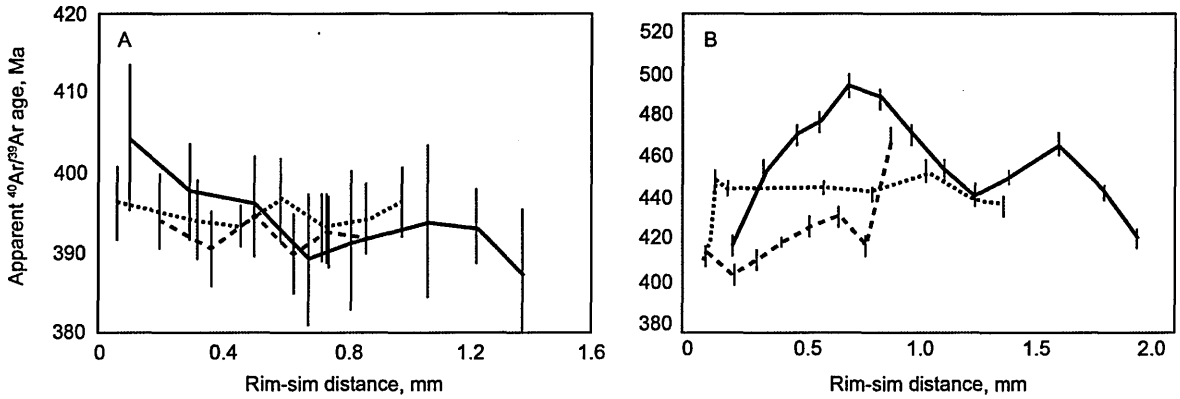

Fig. 1.3. Examples of core-rim *in-situ* analyses from white micas modified after (Warren *et al.*, 2012a), showing A) relatively flat profiles, and B) heterogeneous core-rim $^{40}Ar/^{39}Ar$ age profiles. Note the solid, dashed, and dotted lines represent different profiles in different grains.

The *in-situ* method also provides the opportunity for collecting core-rim age profiles that allow for the testing of whether or not diffusion has occurred within the grain (Fig. 1.3).

1.2 HP Pressure Metamorphism

High-pressure (HP) metamorphism occurs when oceanic and/or continental crustal material is subducted during oceanic-continent and continent-continent collisions. Subduction results in the transport of the oceanic and/or continental crust to mantle depths. The presence of HP metamorphic rocks at the Earth's surface testifies to exhumation of these rocks from mantle to crustal depths. HP terranes typically contain lenses of mafic lithologies enclosed within crustal rocks that are of either metasedimentary (marbles and schists) and/or igneous (quartzofeldspathic gneisses) origin. Although these crustal rocks record lower pressures than the mafic lithologies, they experienced the same P-T history (Chopin 1984). The lithologies include blueschists that are characterised by the presence of the blue amphibole glaucophane, and eclogites with their characteristic garnet-omphacite (a HP Na-pyroxene) mineral assemblage. Eclogites were first identified as a HP lithology by Eskola (1921) in the Western Gneiss Region (WGR) of Norway.

Studies by Smith (1984) and Chopin (1984) identified coesite (a variant of quartz that is stable at $P > 2.6$ GPa) in the mafic eclogites of the Western Gneiss Region and the Alps, respectively. This discovery showed that crustal rocks could be subducted to depths of at least 100 km and exhumed back to the Earth's surface. The study of HP and ultrahigh-

pressure (UHP) metamorphic terranes offers a fascinating insight into the geodynamics of orogenic cycles, in particular, how and when continental crust is subducted to mantle depths and subsequently returned to the surface. However, while the subduction-related processes are fairly well understood, how these rocks are exhumed to the surface still remains a matter of controversy.

Numerous mechanisms have been proposed for the exhumation of (U)HP terranes through the mantle and crust (Hacker & Gerya 2013). These include processes such as eduction, whereby the subducted (U)HP rocks are exhumed due to a reversal in the direction of subduction, rollback of the subducted crustal slab, channel flow, and buoyancy-driven processes due to continental crust being less dense than the mantle into which it has been subducted (Hacker & Gerya 2013). The latter two processes have been proposed for the exhumation of small (U)HP terranes, while eduction and buoyancy have been proposed as the mechanism by which the WGR was exhumed (Andersen *et al.,* 1991, Hacker & Gerya 2013).

The mechanisms of exhumation are based on numerical modelling and/or tectonic studies of exhumed HP metamorphic terranes. The key to determining the mechanism of exhumation is providing temporal constraints on the rates and timings at which exhumation occurs. The $^{40}Ar/^{39}Ar$ thermochronological technique is a powerful tool in understanding the mechanism of exhumation since age should be able to be linked to temperature, via the Dodson T_c formulation, and therefore to a specific point along a metamorphic P-T path.

1.2.1 Previous $^{40}Ar/^{39}Ar$ Studies of HP Metamorphic Terranes

For many decades, $^{40}Ar/^{39}Ar$ thermochronology has been applied to the decompression and cooling histories of many HP metamorphic terranes (Armstrong *et al.,* 1966, Clark & Jager 1969, Copeland *et al.,* 1987, Foster *et al.,* 1990, Baldwin *et al.,* 1993, Sherlock *et al.,* 1999, Warren *et al.,* 2011, Warren *et al.,* 2012a). However, it has become increasingly apparent that many HP metamorphic terranes yield $^{40}Ar/^{39}Ar$ ages that cannot be interpreted as the result of cooling through a T_c. Analysis of white mica, biotite (± amphibole) from many HP terranes commonly yield ages that are older than expected given the P-T history of the HP terrane. $^{40}Ar/^{39}Ar$ ages are commonly older than the timing of peak metamorphic conditions, older than the timing of mica crystallisation, or yield $^{40}Ar/^{39}Ar$ ages that span the entirely of the HP metamorphic cycle. (Sherlock & Kelley 2002, Putlitz *et al.,* 2005, De Sigoyer *et al.,* 2000, Warren *et al.,* 2011, Warren *et al.,* 2012a, Li *et al.,* 1999, Villa 1997,

Hacker *et al.,* 2003, Di Vincenzo 2006). Common interpretations for these elevated ages include:

1) The presence (or lack) of fluids during the metamorphic cycle. Ar-bearing fluids can bring Ar into the system, providing the potential for Ar to diffuse into a grain (if the temperature is high enough; Warren *et al.,* (2011)). However, if there is no fluid phase present during the metamorphic cycle, Ar will be retained within the mineral's grain boundary since there would be no medium to facilitate the removal of Ar,
2) Microtextural and/or microstructural defects and fluid inclusions within grains can act as sinks for Ar within the mineral structure (Di Vincenzo 2006, Camacho *et al,.* 2012),
3) inefficient diffusion of Ar from a grain due to either the temperature being too low to allow for diffusion to occur or the PT path too rapid to allow time for diffusion to occur efficiently, and
4) Excess Ar ($^{40}Ar_E$). This is the component of ^{40}Ar that is incorporated into a mineral by processes other than the in-situ decay of ^{40}K (McDougall & Harrison 1999).

However, this is not the whole problem since HP metamorphic terranes are typically subdivided into two groups that experienced differences in their P-T evolution (Kylander-Clark *et al.,* 2012 and references therein). These are:

1) Small (<1000 km^2), cold (450-650°C) HP terranes that are exhumed as boudins or slices of crustal material. These terranes tend to be exhumed from peak metamorphic conditions to upper crustal conditions in less than 10 Ma (Gebauer *et al.,* 1997, De Sigoyer *et al.,* 2000). Examples of small, cold HP terranes include the Tso Morari of the Himalaya, and the Dora Maira of the western Alps (De Sigoyer *et al.,* 2000, Di Vincenzo 2006).
2) Large (up to 40,000 km^2), hot (650-1000°C) HP terranes that are exhumed as intact terranes. The larger size of these terranes means that exhumation from peak metamorphic conditions can take tens of millions of years (Hacker *et al.,* 2000, Schärer & Labrousse 2003, Zheng *et al.,* 2003, Root *et al.,* 2005). Examples of these large HP terranes include the Dabie-Sulu of China and the Western Gneiss Region of Norway (Li *et al.,* 1999, Hacker 2007)

The cold temperatures and rapid P-T paths experienced by small HP terranes means that there may not have been sufficient time or reached sufficiently high temperatures for

efficient diffusion of Ar to occur. The low temperatures and rapid P-T paths result in $^{40}Ar/^{39}Ar$ ages that yield crystallisation ages and not cooling ages when other factors such as excess or inherited argon don't mask the in-situ ^{40}Ar produced by K decay. The higher temperatures and the slower rates of exhumation experienced by larger HP terranes means that, unlike the small HP terranes, $^{40}Ar/^{39}Ar$ ages could, potentially, yield reliable cooling ages.

$^{40}Ar/^{39}Ar$ analyses from HP terranes, regardless of size, have focussed primarily on the study of phengite (the HP, Si-rich variant of muscovite). Lithologies that are commonly analysed are mafic eclogites and blueschist that record the peak metamorphic conditions and gneisses and pelites that host the mafics. These host lithologies generally do not record the peak metamorphic conditions, but rather, document the exhumation of the HP terranes and therefore should provide constraints on the exhumation history.

Step heating of phengites from eclogites and gneisses from the Dabie-Sulu of China and the Western Gneiss Region of Norway display disturbed $^{40}Ar/^{39}Ar$ step heating spectra (Li *et al.,* 1994, Li *et al.,* 1999, Root *et al.,* 2005, Walsh *et al.,* 2007, Young *et al.,* 2011, Walsh *et al.,* 2013). $^{40}Ar/^{39}Ar$ phengite ages are often older than, or equivalent to the timing of peak metamorphism defined by U-Pb zircon dating (Li *et al.,* 1994, Li *et al.,* 1999, Andersen *et al.,* 1998, Hacker & Gans 2005, Root *et al.,* 2005, Walsh *et al.,* 2007, Young *et al.,* 2011, Walsh *et al.,* 2013). In the case of the Western Gneiss Region, the HP terrane documented in this study, single grain fusion and *in-situ* laser ablation studies have shown that $^{40}Ar/^{39}Ar$ phengite ages from mafic eclogites and felsic gneisses yielded ages that range from 759-379 Ma, a far greater range than what would be expected from simple models of cooling through a mineral-specific closure temperature (Warren *et al.,* 2012a).

It is clear that the interpretation of $^{40}Ar/^{39}Ar$ ages from HP metamorphic terranes is complex. Regardless of the dimensions and the P-T history of the HP terrane, ^{40}Ar-^{39}Ar mica ages from many HP terranes are $^{40}Ar/^{39}Ar$ ages are elevated relative to other chronometers (e.g. U-Pb zircon), and yield $^{40}Ar/^{39}Ar$ ages that do not conform to our current understanding of how Ar should behave during a metamorphic cycle.

1.3 Aims and Objectives

The main objective of this study is to provide an in-depth understanding of the behaviour of Ar during a HP metamorphic cycle and to create a means by which future metamorphic Ar age data in these types of terranes can be interpreted.

This PhD aims to investigate the $^{40}Ar/^{39}Ar$ ages from various lithologies of the Outer Nordfjord area of the Western Gneiss Region, Norway, in order to determine whether these ages are spatially consistent with modification via thermally-activated volume diffusion. If the ages are not consistent with diffusion, what impact does this have for understanding and interpreting $^{40}Ar/^{39}Ar$ from the WGR and from HP metamorphic terranes in general?

Computational modelling of the pressure-temperature history and Ar diffusional modelling will provide the framework by which the $^{40}Ar/^{39}Ar$ age data from this study can be assessed in terms of a cooling history.

$^{40}Ar/^{39}Ar$ ages of white mica, biotite, and amphibole mineral separates and grains in polished slabs are compared with the results of diffusion and petrographic modelling to:

(1) Create a conceptual modelling framework, with which $^{40}Ar/^{39}Ar$ ages can be interpreted in terms of the metamorphic evolution of the WGR,

(2) Understand how the physical processes that affect rocks during exhumation, such as recrystallization, deformation, and fluids, have affected the Ar isotopic signature of the crustal gneisses of the Western Gneiss Region and to use $^{40}Ar/^{39}Ar$ thermochronology to track these processes from decompression from eclogite-facies conditions to amphibolite-facies conditions,

(3) To investigate how Ar is redistributed during the breakdown of HP white mica to biotite and plagioclase symplectites in order to determine how Ar behaves during an exhumation-related metamorphic reaction, and

(4) To compare and contrast the behaviour of Ar in the anhydrous mafic eclogite and felsic granulite lithologies in order to understand how these lithologies behaved, with respect to the Ar isotope systematics, during the Caledonian Orogeny.

These aims will be investigated by studying three key locations in the Outer Norfjord area of the WGR.

1.4 The Geological Evolution of the Western Gneiss Region, Norway

The Western Gneiss Region (WGR) in western Norway is a 50,000 km^2, basement window within the Scandinavian Caledonides that outcrops between Bergen and Trondheim. It is bounded in the east by the Jotunheim Décollement, to the south by the Bergen Arc Shear Zone and by the Nordfjord-Sogn Detachment Zone to the west (Wain *et al.,* 2000, Austrheim *et al.,* 2003, Labrousse *et al.,* 2004, Root *et al.,* 2005).

85% of the WGR is composed of quartzofeldspathic gneiss that has an amphibolite-facies paragenesis with approximately 25% of this gneiss being garnet-bearing (Peterman *et al.,* 2009). The remaining 15% of the WGC is comprised of minor lithologies which include:

- 5-10% eclogite-facies metabasites that occur as ovoid to tabular, decimetre-kilometre scale bodies hosted within the quartzofeldspathic gneisses and commonly occur as trails of boudins along specific horizons (Wain 1998). The eclogites possibly represent boudinaged sheets of basic dykes or gabbroic bodies (Wain 1998).
- 2-5% relict, Precambrian granulite-facies gneiss which include the Flatraket mangerite (an pyroxene-bearing quartz monzonite) and the Kråkenes metagabbro (Wain 1998). These lithologies have been dated at 1641 ± 5 Ma and 1255 ± 8 Ma, respectively (U-Pb zircon; Corfu *et al.,* 2013).

The WGR formed from material accreted to Baltica during the Gothian orogeny 1750-1500 Ma; and is comprised of a wide composition of plutonic rocks ranging from ultramafic to felsic (Gaal & Gorbatschev 1987). By the end of the Gothian orogeny, approximately 80% of the crust observed at the present day surface was formed (Skar 2000). Following this period of orogenesis, the WGR experienced a period of relative quiescence until the Sveconorwegian-Grenvillian orogeny at 1250-900 Ma which saw the addition of the remaining 20% of the WGC (Skar 2000).

The Caledonian orogeny is the result of the oblique collision between Baltica and Laurentia in the Late Silurian to Early Devonian which involved the subduction of Baltica beneath Laurentia (Roberts 2003). The Caledonian orogeny (450-380 Ma) saw the reworking of the Proterozoic gneisses and the formation of the allochthonous nappes that now overlie the Baltican basement (Skar 2000). Evidence of UHP metamorphism is provided by coesite (the high-pressure form of quartz stable above 2.6 GPa) and has been recorded mostly within the eclogite-facies metabasites, but rare occurrences have been documented within the felsic host gneisses, showing that the gneisses experienced the same UHP metamorphism as the eclogites (Wain 1997). Rare microdiamonds from granitic gneisses indicate that the subduction of Baltica beneath Laurentia may have reached peak metamorphic conditions of 800°C and 3.6 GPa, equivalent to a depth of 120 km (Dobrzhinetskaya *et al.,* 1995).

The UHP lithologies occur in three separate domains which, from south to north, are the Nordfjord-Stadlandet, the Sorøyane, and the Nordøyane domains, together covering an

area of 5,000 km^2 (Root *et al.,* 2005). This study focuses on the Nordfjord-Stadlandet domain because it is the largest (2500 km^2) and most studied of the WGR's UHP domains. Recorded/preserved P-T gradients in this area range from the quartz eclogite-facies in the southeast (~2.5 GPa and 600°C) to coesite-stable eclogite-facies in the northwest (~3.0 GPa and 700°C) (Young *et al.,* 2007, Root *et al.,* 2005).

Following decompression from HP/UHP conditions, the entire WGR began to undergo hinterland-directed extension under amphibolite-facies conditions at ~700°C and 1 GPa (Walsh & Hacker 2004). Initially extension was accommodated by the basal décollement, with foreland-directed thrusting overprinted by later extensional structures (Fossen 2010). The extension is accommodated by later regional-scale extensional shear zones that cross-cut the basement and the nappes (Fossen 2010). The Nordfjord-Sogn Detachment Zone forms one of the largest extensional shear zones in the Scandinavian Caledonides (Fossen 2010).

These major, crustal-scale extensional shear zones may have been the mechanism by which the UHP terrane was exhumed from depth, however, the timing of UHP metamorphism and crustal-scale extension roughly overlap, indicating that UHP metamorphism may or may not have acted as the catalyst for the extension. Nevertheless, by 390-385 Ma, the UHP terranes in the WGR were exhumed to lower crustal depths (Fig. 1.4; Root *et al.,* 2004). This exhumation caused amphibolite-facies supra-Barrovian and subsequent Buchan overprinting of the basement gneisses that characterise the WGR as a whole (Walsh *et al.,* 2007, Hacker *et al.,* 2010).

1.4.1 Previous Geochronology of the Western Gneiss Region

Multiple radioisotopic techniques including Sm-Nd, Lu-Hf, U-Pb, and $^{40}Ar/^{39}Ar$ from both eclogites and their host gneisses have been employed to constrain the timing of both peak metamorphism and exhumation (Fig. 1.5). Lu-Hf and Sm-Nd garnet + whole rock (± clinopyroxene) ages from eclogite and gneisses suggest that prograde metamorphism occurred from 419.5 ± 4.3 Ma to 403.9 ± 0.8 Ma (Kylander-Clark *et al.,* 2007, Peterman *et al.,* 2009).

U-Pb dating within the WGR has largely been restricted to zircon and titanite with two studies focussing on monazite and one on rutile (Terry *et al.,* 2000, Schärer & Labrousse 2003, Root *et al.,* 2004, Walsh *et al.,* 2007, Spencer *et al.,* 2013). U-Pb zircon dating constrains the timing of the peak metamorphic event, while U-Pb titanite and monazite ages documents the recrystallization of the gneisses under amphibolite-facies conditions.

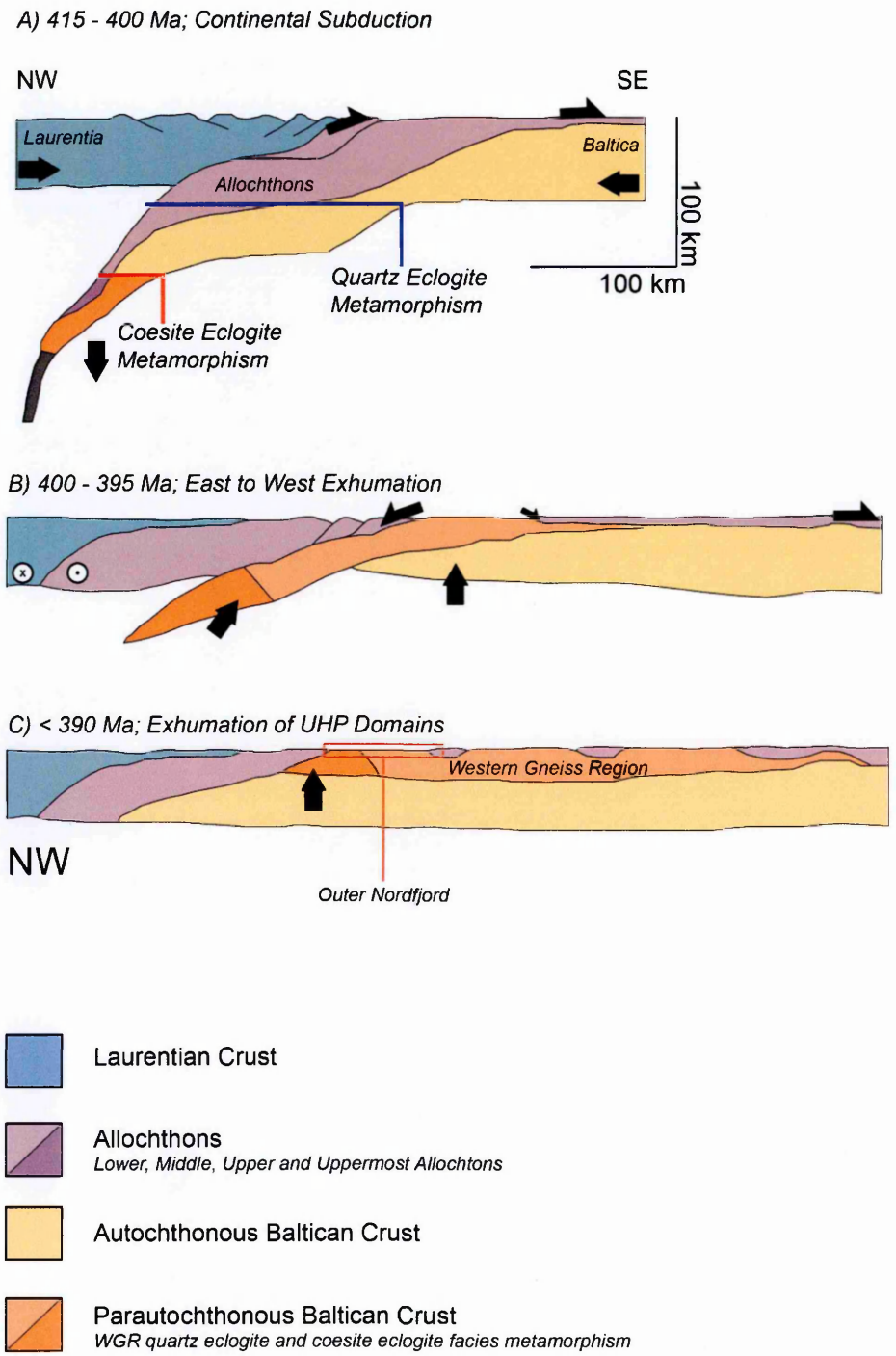

Fig. 1.4. A cross-section reconstruction of the evolution of the Western Gneiss Region modified after (Hacker *et al.*, 2010). A) Continental collision and the subduction of the Baltican margin to HP and UHP depth. B) Exhumation along of the HP/UHP terrane through the mantle to the Lower Crust and C) Continued exhumation, bringing the HP/UHP terranes to the surface. The approximate location of the Outer Nordfjord is marked by the red box.

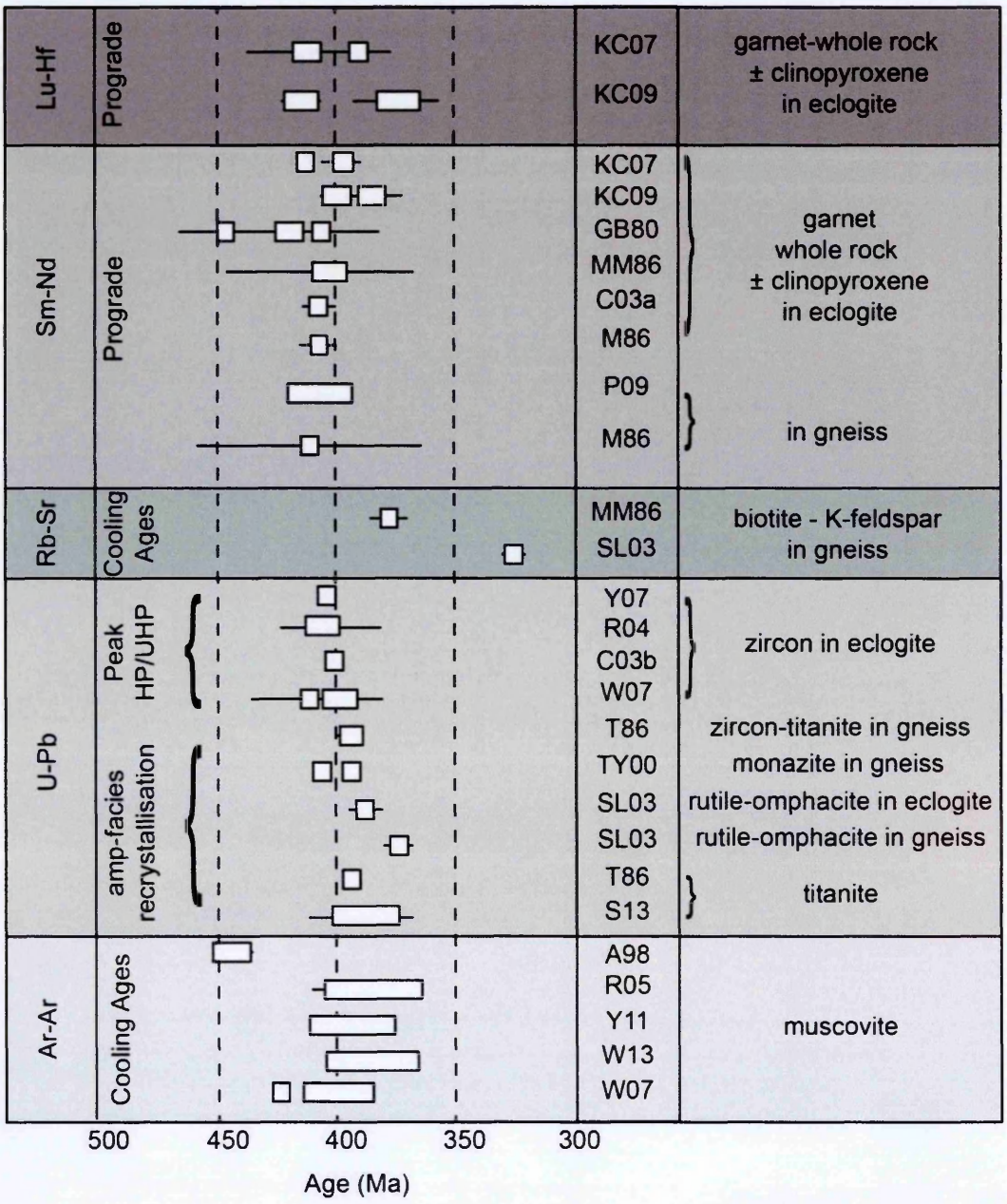

Fig. 1.5. Compilation of geochronological studies from the Western Gneiss Region, modified after (Kylander-Clark *et al.,* 2009). Lu-Hf and Sm-Nd studies document the prograde evolution, U-Pb indicates the timing of peak metamorphism and amphibolite-facies recrystallization and $^{40}Ar/^{39}Ar$ and Rb-Sr studies record the timings of cooling. Most notably there is a strong overlap between many of these different chronometers. References: KC07: (Kylander-Clark *et al.,* 2007); KC09: (Kylander-Clark *et al.,* 2009); GB80: (Griffin & Brueckner 1980); MM86: (Mork & Mearns 1986); C03a: (Carswell *et al.,* 2003b); M86: (Mearns 1986); P09: (Peterman *et al.,* 2009); SL03: (Schärer & Labrousse 2003); Y07: (Young *et al.,* 2007); R04: (Root *et al.,* 2004), C03b: (Carswell *et al.,* 2003a); W07: (Walsh *et al.,* 2007); T86: (Tucker *et al.,* 1986), TY00: (Terry *et al.,* 2000); S13: (Spencer *et al.,* 2013); A98: (Andersen *et al.,* 1998); R05: (Root *et al.,* 2005); Y11: (Young *et al.,* 2011); and W13: (Walsh *et al.,* 2013).

U-Pb zircon ages from mafic eclogite bodies suggest that peak eclogite-facies metamorphic conditions were achieved from 405-400 Ma (Root *et al.,* 2004, Walsh *et al.,* 2007). U-Pb rutile ages from mafic eclogites suggest cooling through 600-700°C at 395-392 Ma (Schärer & Labrousse 2003). The U-Pb titanite ages of 399-379 Ma in the Nordfjord area, have been interpreted to represent the timing at which the host gneisses recrystallized under amphibolite-facies conditions (Spencer *et al.,* 2013). U-Pb-(Th) dating of monazites yields highly scattered ages from 1692-375 Ma. Published weighted mean ages lie between 407-375 Ma, a broad spread that spans the peak- to amphibolite-facies metamorphic conditions defined by U-Pb zircon and U-Pb titanite (Terry *et al.,* 2000, Walsh *et al.,* 2007).

Extensive $^{40}Ar/^{39}Ar$ age studies have been undertaken in the WGR in order to constrain the timing of cooling and exhumation. The majority of these have consisted of step heating analyses of muscovite, biotite, and minor hornblende multi- and single-grain mineral separates (Andersen *et al.,* 1998, Hacker & Gans 2005, Root *et al.,* 2005, Walsh *et al.,* 2007, Young *et al.,* 2011, Walsh *et al.,* 2013). Published plateau ages for the Outer Nordfjord area range from 389-374 Ma, although many of these age spectra show disturbance. The plateau ages are generally interpreted as the time at which the white mica cooled through a T_c of 400°C during cooling and exhumation and showed that there is a trend in the $^{40}Ar/^{39}Ar$ that youngs from east to west across the WGR (Hacker 2007). These studies however, do not consider the age data in terms of the metamorphic history and whether the application of the T_c is applicable to these ages.

A study of phengites from mafic eclogites and felsic host gneisses using single-grain fusion and *in-situ* techniques demonstrated that many samples yielded $^{40}Ar/^{39}Ar$ ages that were significantly older than the timing of peak metamorphism reported by U-Pb zircon ages (405-400 Ma; Root *et al.,* (2004). Eclogites yielded $^{40}Ar/^{39}Ar$ ages that ranged from c. 755-398 Ma and felsic gneisses yielded $^{40}Ar/^{39}Ar$ ages that span 507-379 Ma, ages that span the entirety of the WGR metamorphic cycle (Warren *et al.,* 2012a). $^{40}Ar/^{39}Ar$ ages were shown to be heterogeneously distributed both within individual grains and between different grains within the same sample and across different samples. These results imply that lithologies of the WGR are variously affected by $^{40}Ar_E$ and that the assumptions inherent in the Dodson (1973) T_c formulation may not hold true for HP terranes.

These results prove problematic when it comes to interpreting mica $^{40}Ar/^{39}Ar$ ages as cooling ages if the T_c formulation is not applicable to HP metamorphic terranes. The study

undertaken in this thesis was motivated by the need to understand the behaviour of Ar during the metamorphic cycle.

The WGR is a suitable natural laboratory for testing the behaviour of Ar during a metamorphic cycle because; the WGR is composed of gneisses that are broadly similar in composition but preserve different stages of the metamorphic evolution. The petrography of the gneisses can therefore be used to document the exhumation history of the WGR and the behaviour of Ar during each stage. The WGR experienced high temperatures (~700°C) for a long-enough period of time (10-15 Ma; Spencer *et al.,* 2013) for diffusion (i.e. Ar loss), in theory, to have been efficient at resetting the $^{40}Ar/^{39}Ar$ chronometer, so $^{40}Ar/^{39}Ar$ ages in a perfect system should be interpretable in terms of thermally-activated volume diffusion. This thesis aims to determine whether the $^{40}Ar/^{39}Ar$ ages of WGR are consistent with Ar redistribution via volume diffusion and if not, what the consequences are for the understanding of Ar behaviour in these types of terrane.

1.4.2 Study Sites

Three localities were chosen from the Nordfjord-Stadlandet area of the WGR; Krokkenakken (south), Flatraket Harbour (centre), and Drage (north; Fig. 1.6). The study sites expose eclogite-facies mafic lithologies that have undergone varying degrees of amphibolitisation, hosted within felsic gneisses. The three localities were chosen for their similar petrographical and lithological associations but differences in their recorded peak metamorphic conditions. These peak metamorphic conditions range from ~600°C at 2.1 GPa at Krokkenakken to ~750°C at 3.2 GPa at Drage (Cuthbert *et al.,* 2000). All three locations record similar P-T conditions for the amphibolite-facies retrogression of ~700°C at 1 GPa (Spencer *et al.,* 2013).

The felsic gneisses are subdivided into two categories; Group 1 garnet-bearing gneisses and Group 2 biotite-epidote gneisses. Group 1 gneisses are subdivided in those that contain relicts of the high-pressure evolution (Group 1a); those that do not contain relicts of the high-pressure evolution (Group 1b) and garnet-biotite gneisses that do not contain high-pressure relicts or white mica (Group 1c). The Group 2 gneisses are also subdivided into those that contain relicts of garnet and white mica (Group 2a) and gneisses that contain an amphibolite-facies assemblage of biotite + epidote (Group 2b).

The location and sample numbers of the samples analysed in this study are documented on outcrop maps of Krokkenakken, Flatraket Harbour and Drage (Plates 1-3). Full petrological and geochemical descriptions of each sample are given in Appendix A.

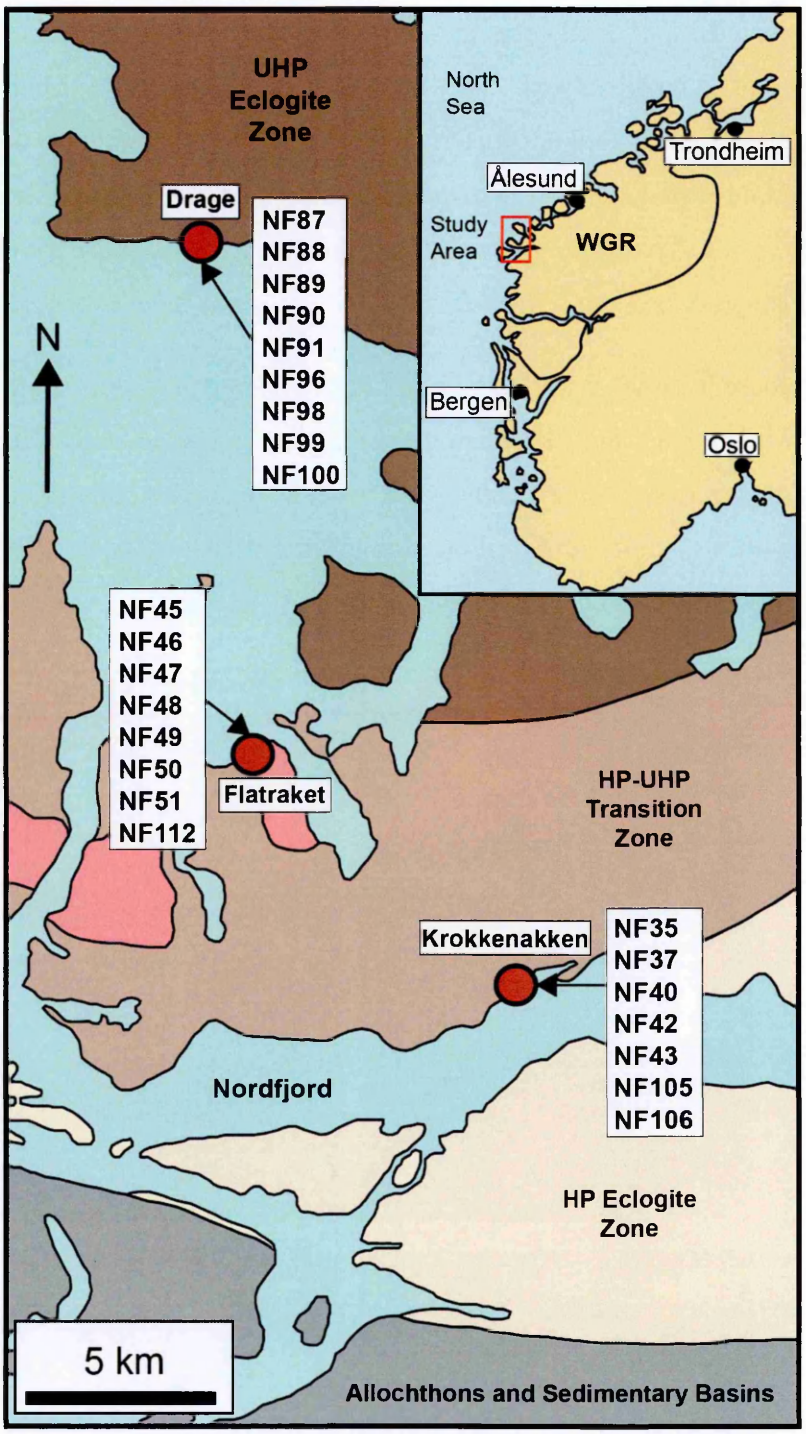

Fig. 1.6. Simplified map of the Outer Nordfjord area of the Western Gneiss Region, modified after (Wain *et al.*, 2000). The three locations studied in this thesis are marked by the red circles.

1.4.2.1 Krokkenakken

Krokkenakken is located on the north shore of the Nordfjord at 61°54'53.73" N 005°20'16.49"E. The 300+ metre exposure consists of both Group 1 and Group 2 gneisses, and their associated mafic eclogites and amphibolites (Fig. 1.7; Plate 1). From SW to NE the outcrop at Krokkenakken is comprised of amphibolite-facies, banded, grey granodioritic gneisses belonging to Group 2b gneisses. They contain the assemblage of biotite + epidote + plagioclase; these gneisses also contain decimetre length amphibolite stringers and pods. These Group2b gneisses grade into Group 2a, with millimetre-sized garnets and isolated flakes of white mica.

Adjacent to these gneisses is a ~10 m wide transition zone of Group 1b gneisses composed of garnet + white mica + biotite + quartz + plagioclase. Close to the contact with the Group 2a gneisses, this transition zone contains many decimetre-sized lenses of biotite-amphibole amphibolites after eclogite. Progressing through the transition zone, these lenses show a progressive preservation of the original eclogitic paragenesis.

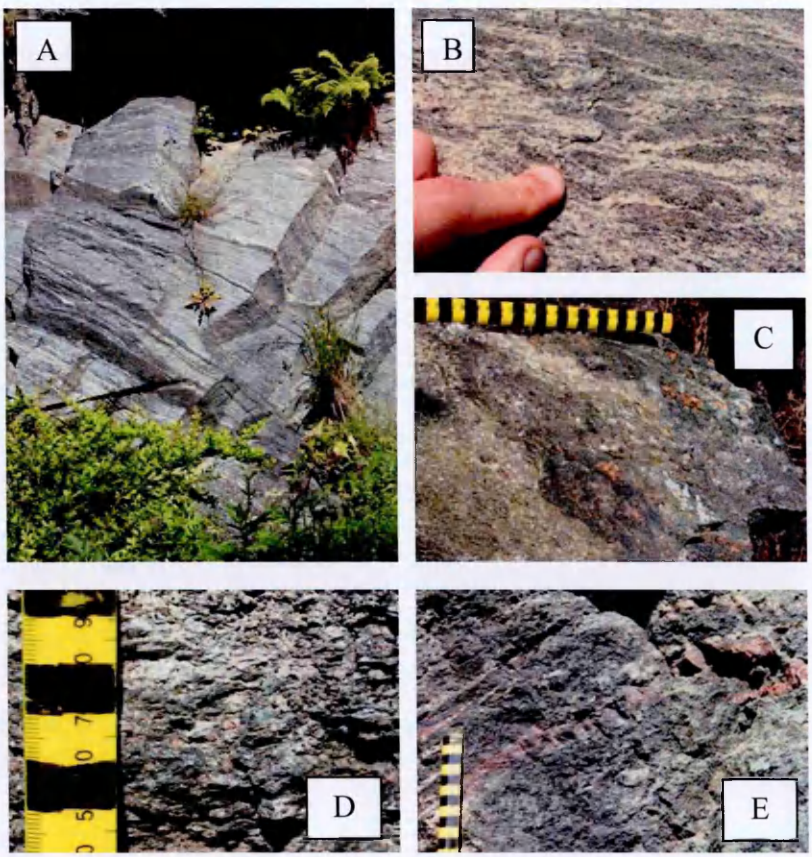

Fig. 1.7. Field photographs of the Krokkenakken locality. A) Banded (**Group2b**) granodioritic gneisses, B) **Group 1b** gneisses close to the contact with **Group 2b** gneisses, containing cm-scale mafic lenses. C) **Group 1a** gneisses that contain HP relicts, interleaved with mafic eclogite. D) **Group 1a** gneiss showing relict omphacite lenses, and E) massive eclogite with a folded layer of garnetite.

This transition zone gives way to Group 1a gneisses with an assemblage of quartz + white mica + garnet with minor kyanite, clinozoisite and symplectites of clinopyroxene-plagioclase and biotite-plagioclase after omphacite and white mica, respectively. Intercalated within these gneisses are numerous mafic eclogite pods that range from decimetre to meter in scale. Continuing along the exposure for 15 meters, there is a sharp contact between the Group 1a gneisses and the main mafic eclogite body at Krokkenakken.

This eclogite is medium-grained and granular with garnetite layers that define a weak eclogite-facies foliation. The peak assemblage consists of garnet + omphacite + phengite + quartz with accessory phases of rutile and clinozoisite.

1.4.2.2 Flatraket Harbour

Flatraket Harbour is located on the southern shore of Sildagapet at 61°58'42.60"N 005°14'03.80"E. This locality comprises a small islet that is located within the harbour wall (Fig. 1.8, Plate 2). The exposure at the outcrop is small (< 10 m) and, like at Krokkenakken, consists of a mafic eclogite and its associated host gneisses. The eclogite is course-grained and unfoliated with a peak assemblage of garnet + omphacite + phengite + quartz + rutile + kyanite. Inclusions of polycrystalline quartz inclusions in garnet and omphacite attest to the former presence of coesite. The eclogite is surrounded by a ~40 cm think amphibolitised rind composed of biotite + amphibolite + epidote + calcite.

Close to the contact with the mafic eclogite are Group 1c gneisses with a primary mineral assemblage of biotite + garnet + plagioclase with minor epidote group minerals. These gneisses grade over a distance of tens of centimetres into a band of Group 1b gneisses that contain abundant white mica. Associated with these Group 1b gneisses are several, metre-long garnet amphibolite lenses. The gneiss then grades back into Group 1c gneisses for approximately 2 m before meeting a sharp contact with Group 2b gneisses. This sharp contact is defined by discontinuous veins of plagiogranite + titanite. The rest of the outcrop comprises Group 2b biotite-epidote gneisses, with abundant epidote porphyroblasts and minor cm-sized alkali feldspar augen.

Located approximately 550 m east of the Flatraket Harbour locality is the Flatraket granulite. This is a 2 km^2 low strain enclave of pre-Caledonian granulite that was subducted and exhumed during the Caledonian Orogeny and yet, still preserves much of its original textures and mineralogy. The core of the granulite is dominated with decimetre-sized spherical to ovoid augen of alkali feldspar in a fine-grained matrix. These augen give the granulite a rapakivi-like texture (Krabbendam *et al.,* 2000). Cross-cutting the

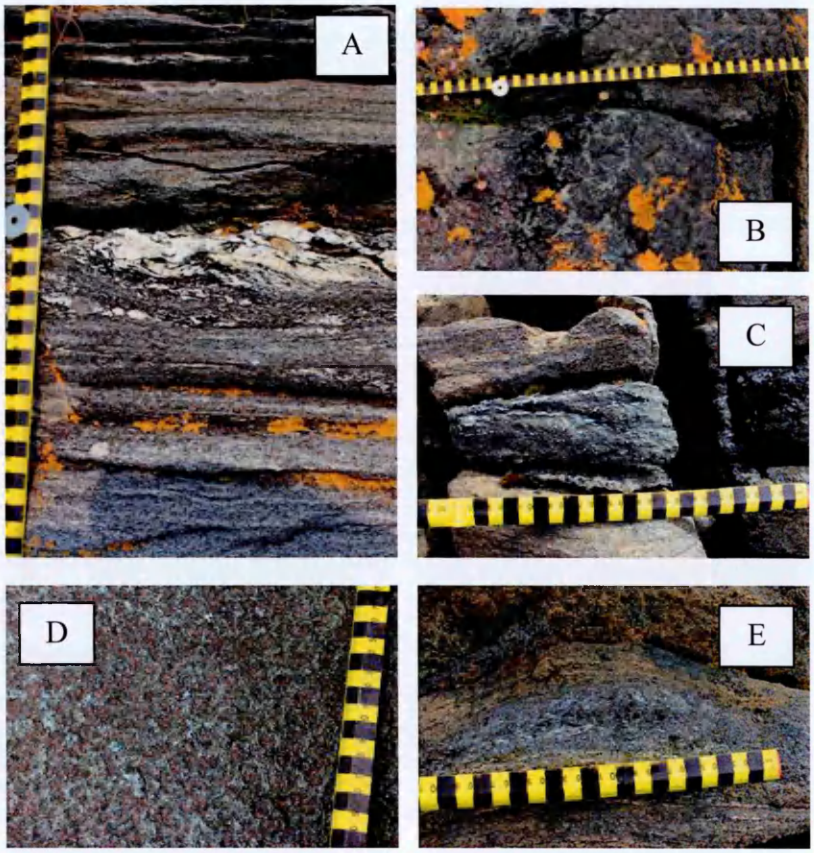

Fig. 1.8. Field photographs of the Flatraket Harbour locality. A) the contact between **Group 1c** and **Group 2b** gneisses demarcated by the presence of plagiogranitic melt containing an oval titanite crystal. B) the contact between the mafic eclogite body and the host gneisses showing intense amphibolitisation over a decimetre-scale. Garnet and omphacite in the eclogite are gradually replaced by amphibolite + biotite. C) garnet-amphibolite lens in the **Group 2b** gneiss. D) Pristine, granular eclogite showing pink garnet, green omphacite and blue kyanite, and E) garnet- and mica-rich layer within the **Group 2b** gneiss.

granulite body are numerous anastomosing shear zones, which preserve an amphibolite-facies parageneses. These shear zones have been interpreted as forming during the exhumation of the WGR (Corfu *et al.,* 2013).

1.4.2.3 Drage

Drage is located on the southern shore of the Stadlandet Peninsula at 62°06'08.3"N 005°12'48.0"E. Drage shows the most intense deformation of the three localities, with highly migmatised and folded gneisses and deformed metabasic lenses (Fig. 1.9, Plate 3). The folding in the gneisses verges to the west and this has been interpreted to represent a top-to-the-west shear sense (Labrousse *et al.,* 2004). Predominately, the gneisses belong to Group 2b with subordinate layers of garnet-bearing Group 1b and 1c gneisses.

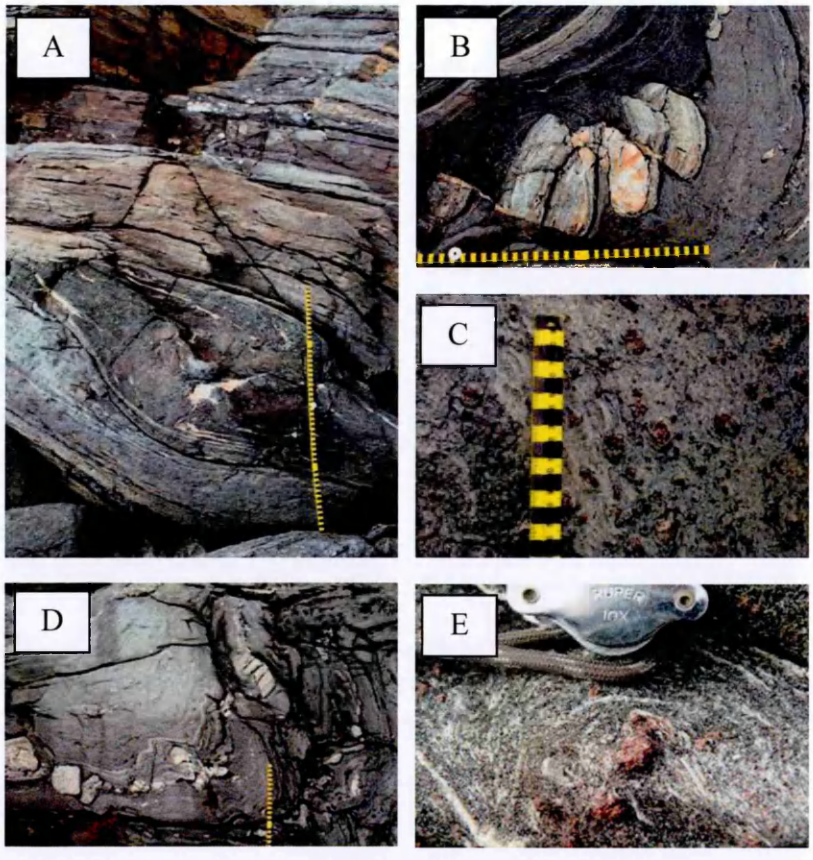

Fig. 1.9. Field photographs of the outcrops on the Drage foreshore. A) Sampled section that contains an amphibolitised mafic boudin surrounded by host, crustal gniesses. These gneisses grade from **Group 1c** close to the boudin, though to **Group 2b** gneisses. These gneisses are adjacent to **Group 2b** gneisses. B) Brittle deformed felsic layer in highly deformed and folded gneisses. C) garnet-rich **Group 2b** gneiss with cm-sized garnets. D) Folded and migmatised gneisses typical of the Drage locality, and E) degraded garnets hosted in **Group 2a** gneiss.

Eclogite-facies metabasic lenses vary from metre to decimetre-scale with a peak assemblage of garnet + omphacite + quartz + rutile with accessory phases of kyanite and phengite, which vary in abundance from mafic body to mafic body. Polycrystalline quartz inclusions in garnet from the eclogites indicate the former presence of coesite and that this locality experienced UHP metamorphic conditions.

The gneisses show evidence of intense ductile deformation. Within these gneisses are felsic blocks, which represent more competent granitic layers within the granodioritic gneisses, and have been brittley deformed, rotated and boudinaged. Garnet-bearing gneisses are particularly garnet-rich at this locality with garnets ranging from mm to cm in size.

Samples were collected from two key sections at Drage. Firstly, a transect from an amphibolitised eclogite, over a distance of approximately 1.5 meters (Fig. 1.9A). The gneisses closest to the eclogite body belong to Group 1c and grade into Group 1b with increasing distance. The transition from Group 1b to Group 2b gneisses is demarcated by a thin (~10 cm) band of alkali feldspar augen gneiss. The second section lies 10 meters further to the west where samples were collected across the Group 2b and Group 1b contacts.

1.5 Structure of Thesis

Chapter 2: Modelling Ar Diffusion: Creating the Framework for Interpreting Metamorphic $^{40}Ar/^{39}Ar$ Ages

This chapter will introduce the Ar diffusion modelling produced via a modified form of DiffArg (DiffArg_inverse) to demonstrate the importance modelling $^{40}Ar/^{39}Ar$ age data from metamorphic terranes before interpretations age data can be applied.

Chapter 3: Tracking Ar through a Metamorphic Cycle: Consequences for Understanding Cooling Rate

This chapter will document the single grain fusion and *in-situ* $^{40}Ar/^{39}Ar$ age data from white mica and biotite derived from the crustal gneisses and will link the patterns observed in these age data to processes that have affected the gneisses during the retrograde metamorphic path, from the eclogite-facies to the amphibolite-facies conditions. This chapter is written as a paper that will be submitted to Chemical Geology.

Chapter 4: Mica $^{40}Ar/^{39}Ar$ Crystallisation Ages Preserved in High Temperature Rocks

This chapter presents *in-situ* analysis from a single sample from Krokkenakken that demonstrates how Ar is recycled during retrograde metamorphic reactions from phengite to biotite via the process of symplectization. This chapter is written as a paper that will be submitted to Geology.

Chapter 5: $^{40}Ar/^{39}Ar$ Dating of Minor Lithologies of the WGR: Eclogites, Amphibolites, and Granulites

This chapter presents $^{40}Ar/^{39}Ar$ single grain fusion and *in-situ* analyses of eclogites, amphibolites, and granulite from the Outer Nordfjord area. In conjunction with P-T modelling of the eclogites, this chapter aims to investigate the behaviour of Ar in these

minor lithologies. This chapter will be submitted to Contributions to Mineralogy and Petrology or Lithos.

Chapter 6 provides some of the overarching conclusions derived from the thesis and will include recommendations and ideas for potential future work.

The appendices of this thesis include a petrographic description of the samples documented in the above chapters, electron microprobe mineral chemistry data and the single grain fusion and *in-situ* $^{40}Ar/^{39}Ar$ age datasets, XRF datasets and DiffArg_inverse modelling results.

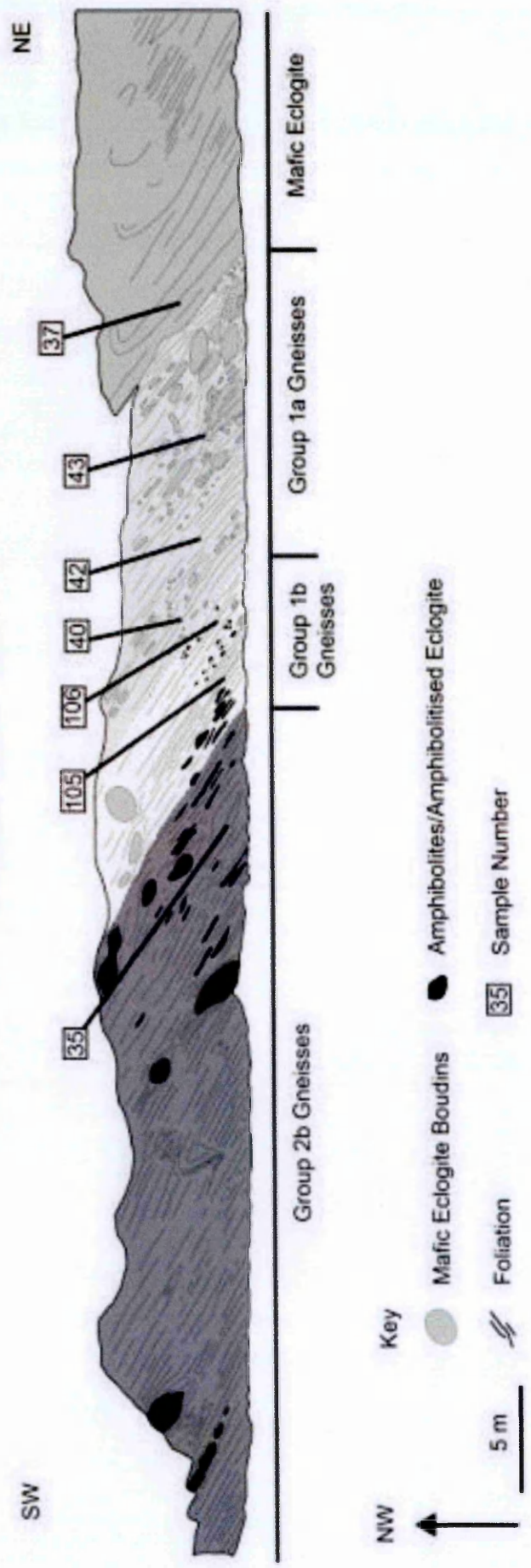

Plate 1: Outcrop sketch of Krokkenakken, modified after (Dransfield 1994)

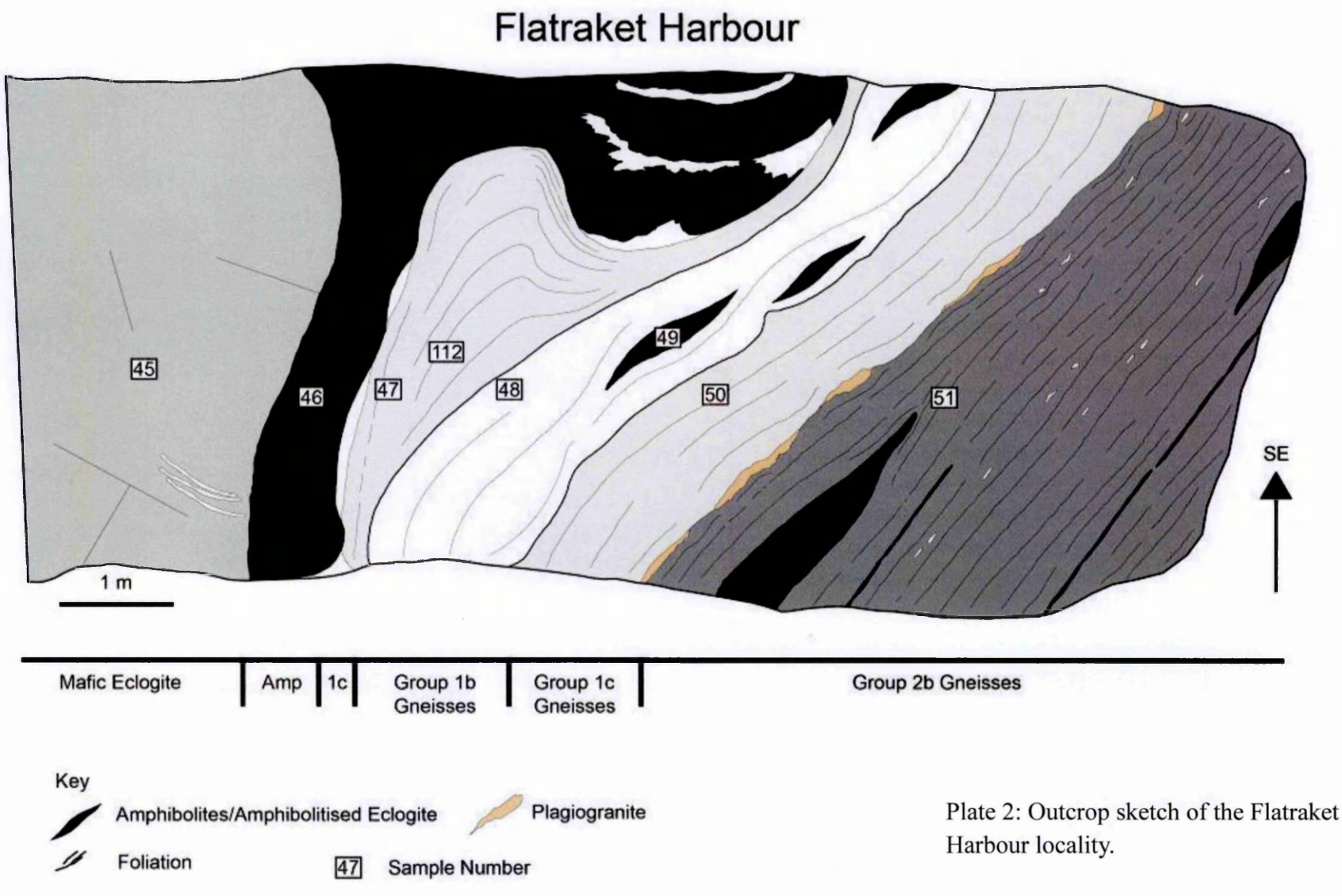

Plate 2: Outcrop sketch of the Flatraket Harbour locality.

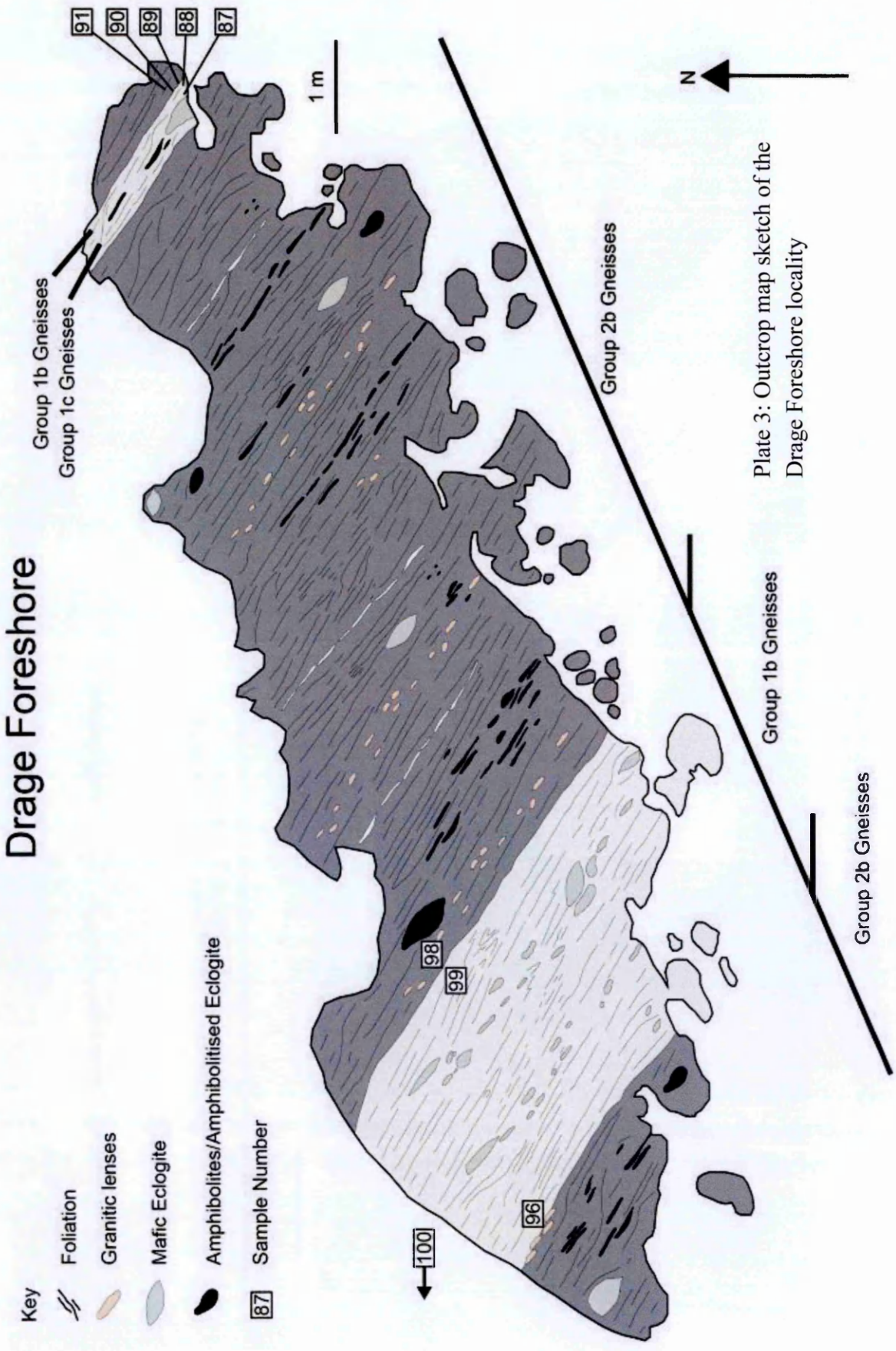

Plate 3: Outcrop map sketch of the Drage Foreshore locality

Chapter 2

Modelling Ar Diffusion: Creating the Framework for Interpreting Metamorphic $^{40}Ar/^{39}Ar$ Ages

The view east across the Sildegapet from Vågsøy

This chapter forms part of the paper:

McDonald, C. S., Warren, C. J., Hanke, F., Regis, D., Chard, J. & Ingvorsen, L. Modelling P-T paths and Cooling Rates: Creating the Framework for Interpreting Metamorphic $^{40}Ar/^{39}Ar$ Ages. In Prep for *Chemical Geology*.

2.1 Introduction

The expected $^{40}Ar/^{39}Ar$ ages of K-bearing minerals that experienced different P-T histories during a metamorphic cycle, can be modelled using the finite-difference algorithm DiffArg (Wheeler 1996). DiffArg has previously been used to model Ar diffusion in different minerals that experienced complex metamorphic histories in a variety of tectonic environments (e.g. Mark *et al.,* (2008), Warren *et al.,* (2011), Warren *et al.,* (2012a), Warren *et al.,* (2012b). DiffArg allows the user to input any thermal and (de)compression history experienced by a K-bearing metamorphic mineral, and outputs both expected single grain (bulk) ages and diffusional age profiles.

DiffArg solves the diffusion equation (Equation 1.3) numerically. This approach has advantages over the solution provided by the Dodson T_c formulation (Equation 1.6), since it does not require prior knowledge of, or the assumption of, a singular cooling rate; this is the unknown that is commonly to be determined.

The original DiffArg code was subsequently modified to take into account the pressure dependence of Ar diffusion in muscovite suggested by experimental data (Harrison *et al.,* 2009). This modified code is called DiffArgP (Warren *et al.,* 2012c). DiffArgP was further modified to allow for the computation of 1/T (and also 1/P) cooling paths which closely approximate the 1/T assumption in the T_c formulation (Dodson 1973). This new code is called DiffArg_inverse (Hanke pers. comm, 2013). In this study, DiffArg_inverse was used to explore the possible bulk Ar ages for white mica and biotite that experience various temperatures and cooling rates during exhumation of metamorphic terranes for a number of different grain sizes.

This chapter will focus on how diffusion modelling can be used to construct a framework for interpreting metamorphic $^{40}Ar/^{39}Ar$ ages. The modelling will focus on two minerals, white mica and biotite, which are the commonest minerals in metamorphic rocks dated using $^{40}Ar/^{39}Ar$ thermochronology.

2.2 Methodology

2.2.1 Operating DiffArg_inverse

The code in DiffArg_inverse is divided into five simple components that allow the user to define the temperature and pressure history, the conditions at the grain boundary-mineral interface, the mineral characteristics, the model solver, and the duration of the model. The inputs for each of these components are outlined below.

1) Temperature and Pressure History

The temperature and pressure histories can be modelled as either linear, flat-top pulse, piecewise, or user defined. The units for temperature are always in °C. Linear histories are the simplest models that can be run in DiffArg_inverse and are defined in terms of an initial temperature and the cooling rate (Wheeler 1996). Flat-top pulse allows the user to model a thermal pulse relative to an ambient background temperature. Flat-top pulse temperature histories would model the effects of an igneous intrusion into country rock (Wheeler 1996). Piecewise temperature history allows the user of DiffArg_inverse to define the temperature history of a mineral as a series of temperature-time points (Wheeler 1996). Within this option is the new ability to model the temperature changes as either being linear or an inverse time segment (a 1/T cooling path). A user defined temperature history enables the user of DiffArg_inverse to create an arbitrary temperature history.

The pressure history works in a very similar manner to the temperature history and has the same options as the temperature history function, whereby pressure can be modelled linearly, pulsed, piecewise or user defined. The units for pressure are expressed in GPa.

2) Grain Boundary-Mineral Interface Conditions

This function allows the user to define the concentration of Ar (expressed as time in Ma) at the grain boundary mineral interface. The edge history, again, can either be linear, flat-top pulse piecewise or user defined. The edge history can be zero, to reflect an open system boundary condition, or can vary during the model run to represent an influx of Ar into the modelled grain boundary system.

3) Mineral Characteristics

This component of the DiffArg_inverse code is where the user selects the mineral that is to be modelled, the geometry of the mineral, grain size, and mesh length. The K-bearing minerals that can be modelled in DiffArg_inverse are muscovite, K-feldspar, biotite, and hornblende. The diffusion parameters for these minerals are outlined in Table 2.1.

The geometries of the mineral that can be selected are plate, cylinder, and sphere. Typically micas are modelled using a cylindrical geometry and K-feldspar and hornblende are modelled using a spherical geometry. Despite the use of a spherical geometry in the calculation of Harrison *et al.,* (2009) for the diffusion of Ar in muscovite, natural samples have shown that diffusion occurs within a cylindrical geometry (Hames & Bowring 1994). The grain size can be as large or as small as the user defines, and is entered as the radius of

the grain. For example, a muscovite that is 1 mm in length would be modelled as a 0.5 mm grain. It should be noted that the smaller the grain size the more computationally time consuming the model becomes.

Parameter	Units	White Mica	K-Feldspar	Biotite	Hornblende
E_a	$kJmol^{-1}$	263 ± 29	43.8 ± 1	197 ± 8	64.1 ± 1.7
D_0	cm^2s^{-1}	2.3 +70/-2.2	0.00982 +0.0066/-0.00371	0.077 +0.21/-0.06	0.024 +0.053/-0.011
V_0	cm^3mol^{-1}	14	0	0	0
P_0	GPa	1	0	0	0

Table 2.1. The diffusion parameters for the K-bearing minerals that can be modelled in DiffArg_inverse. White mica diffusion parameters from Harrison *et al.,* (2009), K-Feldspar from Foland (1974), biotite from Harrison *et al.,* (1985), and hornblende from Harrison (1981).

The mesh length, unlike the previous parameters entered into DiffArg_inverse, is not related to the physical properties of the mineral or metamorphic cycle being modelled (Wheeler 1996). This function defines a value that represents the number of intervals (or separations) that the grain radius is divided into for the finite difference calculation (Wheeler 1996). The larger the value entered (as an integer), the more precise the finite difference calculation. For example, a mesh length of 10 will divide the grain radius into 10 separations and a value of 100 will divide the grain in 100 separations. The larger mesh length value, the more segments the grain is divided into and the more precise the calculation. However, the larger the value, the more computationally time consuming the model becomes.

DiffArg_inverse uses Simpson's rule over the radial mesh to calculate the bulk age, with the effect that the bulk age is a direct function of the specified mesh length interval. This means that the calculated bulk age may have a large associated numerical error, especially when small values are specified for the mesh lengths. Wheeler (1996) recommends a mesh length of 20 to be a reasonable value to begin with. The main numerical error on the bulk age arises from the point closest to the grain edge and is proportional to the mesh length (Warren *et al.,* 2012c). The numerical error on the bulk age may be minimised by running the same model calculation for different mesh lengths, plotting the resulting mesh separations against age for each of the three model runs and regressing the results back to a zero mesh length (Fig. 2.1; Warren *et al.,* (2012a).

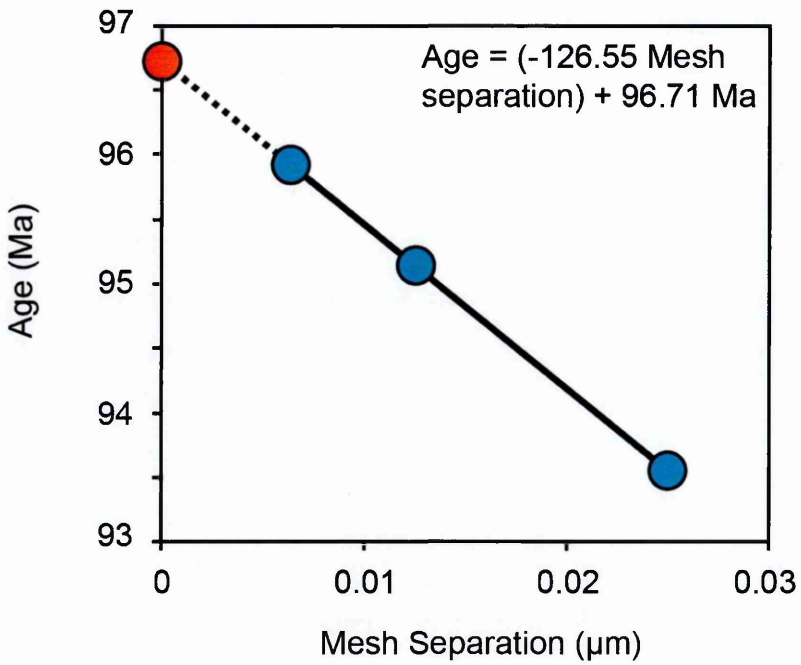

Fig. 2.1. A plot of apparent age vs. the mesh separation showing that the numerically correct bulk age can be determined by regressing the age/mesh separation relationship to a zero mesh separation. Modified after Warren *et al.*, (2012a).

4) Model Solver

The user of DiffArg_inverse can choose from two numerical algorithms for performing the time integration. These algorithms are "fully explicit" and "Crank-Nicholson". Crank-Nicholson was chosen for this study as it allows for faster computation (Wheeler 1996).

5) Model Duration

Upon selecting the display options, DiffArg_inverse prompts for time until the next display. This value, in Ma, tells DiffArg_inverse how long to run the resulting model for. This value can be related to the specific metamorphic terrane that is being modelled; however, the 'older' the age entered the longer the model will run. This can be circumvented by selected a smaller value and adding the remaining time onto the model output. For example, for modelling the Caledonian Orogeny at 400 Ma would take time but by running DiffArg_inverse for only 100 Ma, the model will run faster and the user merely has to add the remaining 300 Ma on the model output. It is assumed that the rocks are at 0°C for this 300 Ma period.

2.2.2 Model Inputs for this Study

For the purposes of this study, white mica and biotite were modelled using a piecewise temperature and pressure history, using both a simple linear time segments and inverse (1/T) time segments with cooling rates of 5°CMa^{-1}, 10°CMa^{-1}, 25°CMa^{-1}, 50°CMa^{-1}, and 70°CMa^{-1}, representing slow to rapid cooling. Both minerals were modelled cooling from temperatures of 700°C, 600°C, 500°C, and 450°C at a constant pressure of 1 GPa. These temperature and pressure conditions were chosen to represent 'hot' to 'cold' metamorphic terranes exhuming from mid-crustal conditions. Grain radii of 1 mm, 0.5 mm, and 0.25 mm were selected since these are typical grain sizes used in $^{40}Ar/^{39}Ar$ thermochronological studies. The grain boundary conditions in all models were modelled with a zero Ar concentration at the grain boundary-mineral interface, so as to model the expected bulk muscovite and biotite Ar ages in a purely open system. All model data are calculated for cylindrical diffusion geometry and the time integration in the models was performed using the Crank– Nicholson solver, with a recommended time step that is 10 times larger than the value suggested for a stable fully-explicit method (Wheeler 1996).

The results for white mica and biotite linear and 1/T models are plotted in Fig. 2.2 and 2.3, respectively and the model data are presented in Appendix F. The modelled curves derived from the 1/T and linear models are not designed to match the geological history of any particular region, but instead are designed to illustrate the potential of DiffArg_inverse as a tool for assisting in the interpretation of $^{40}Ar/^{39}Ar$ bulk age data in yielding a potential cooling rate for a given metamorphic terrane.

2.3 Results

Figs. 2.2A-D and 2.3A-D graphically show the age difference between the model start time and the resulting bulk age with variations in the grain size, the temperature, and the cooling rate for white mica and biotite, respectively. These simple graphs are a useful tool for determining whether $^{40}Ar/^{39}Ar$ analyses of white mica and biotite would yield estimates of the cooling rate for different metamorphic conditions. The 1/T models are also a useful tool to understand whether or not the $^{40}Ar/^{39}Ar$ mica ages can be interpreted as cooling ages that adhere to thermally-activated volume diffusion in an open system.

All graphs have the same general asymptotic trends, with:

(1) Decreasing age difference with increasing cooling rate [i.e. the faster a grain cools, the less the age difference from the starting temperature] and,

(2) Decreasing age difference with decreasing temperature [i.e. the colder the initial starting temperature, the less of a difference there will be between the starting age and the modelled age].

Figs. 2.2A-D and 2.3A-D also show that a reduction in grain radius from 1 mm to 0.5 mm to 0.25 mm shifts the age differences in the white mica and biotite to greater values due to the increased efficiency of Ar diffusion out of small grains. This effect is more pronounced in the linear models than in the 1/T models.

The main results of the diffusion modelling may be summarised as follows:

(1) The plotted model curves show clearly that very little diffusive loss is expected in white mica and biotite that experience low peak temperatures, e.g. from 450°C (Figs 2.2A and 2.3A). White mica would only yield an age differences between the model start time and the bulk age of 0.1 Ma to 0.6 Ma and 0.5 Ma to 2.2 Ma for a 1/T and linear cooling history, respectively. Overall the bulk ages are very close to the nominal starting age of the models and within error of typical analytical uncertainty (2%).

Biotite would show a much greater age difference between the model start time and the bulk age, ranging from 6 Ma to 11 Ma and 18 Ma to 25 Ma for a 1/T and linear cooling history. Unlike with the white mica, the differences in model start age and the model bulk age may be resolvable in $^{40}Ar/^{39}Ar$ age data, implying that at low temperatures of ~450°C biotite would make the better mineral to analyse instead of white mica in order to understand cooling rates in exhumed metamorphic terranes.

(2) The difference between the model start time and the resulting model bulk age increases with increasing temperature for both muscovite and biotite. However, the two different model types (1/T and linear) behave differently. The age differences generated by the 1/T models are consistently less than those generated by the linear models. The age differences between grain sizes are also smaller in the 1/T models compared to the linear models. This implies that the choice of model is crucial for making an appropriate estimation of cooling rate. The use of 1/T or linear models may result in an under- or over-estimation of the cooling rate.

(3) At the highest modelled temperature of 700°C white mica and biotite show the most diffusive loss, and the greatest age differences between the model start time and resulting bulk age (Fig. 2.2D and 2.3D).

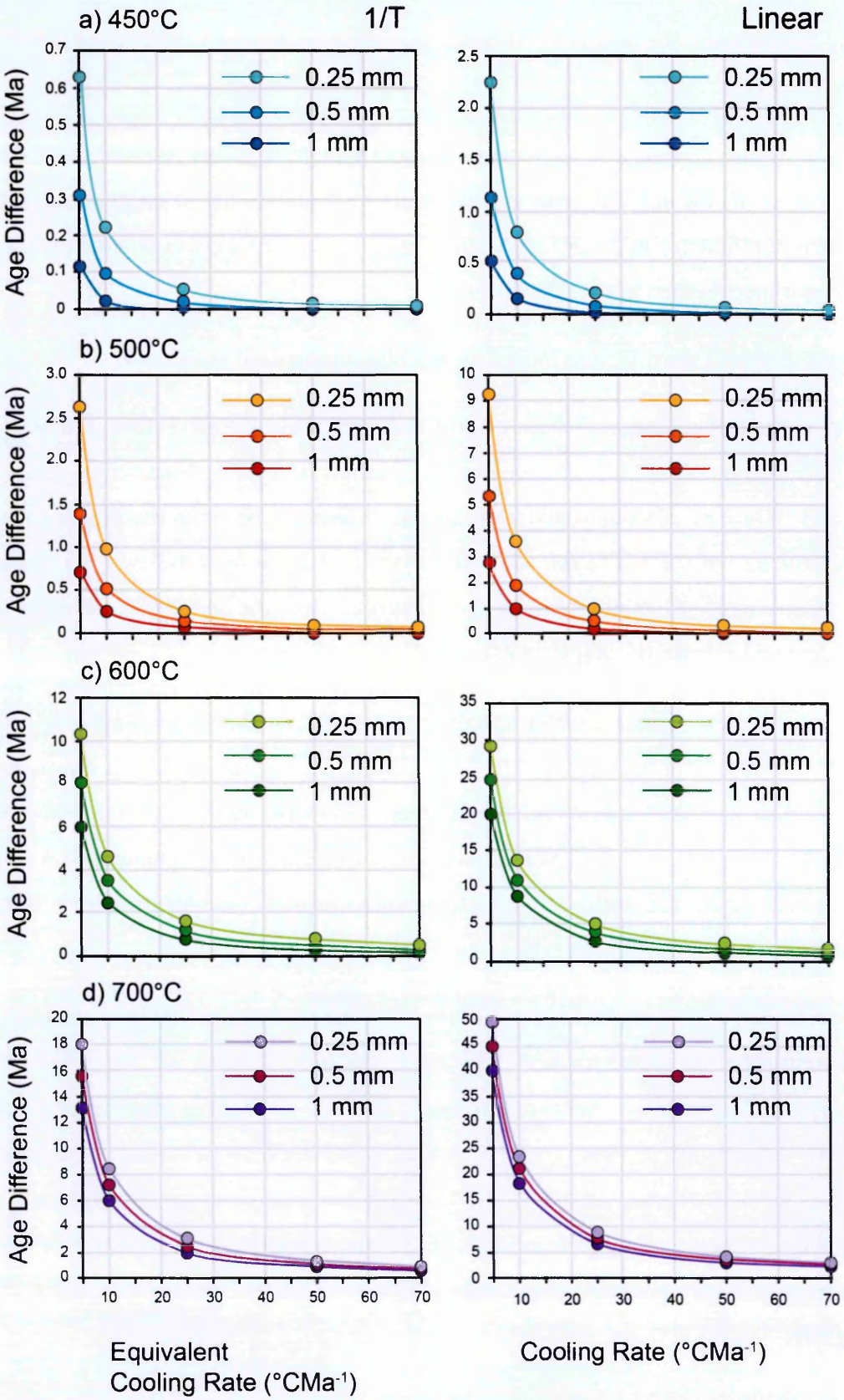

Fig. 2.2. White mica 1/T and linear model results plotted as age difference between model start time and model bulk age vs. cooling rate. Note the differences in the vertical scales between the two model types.

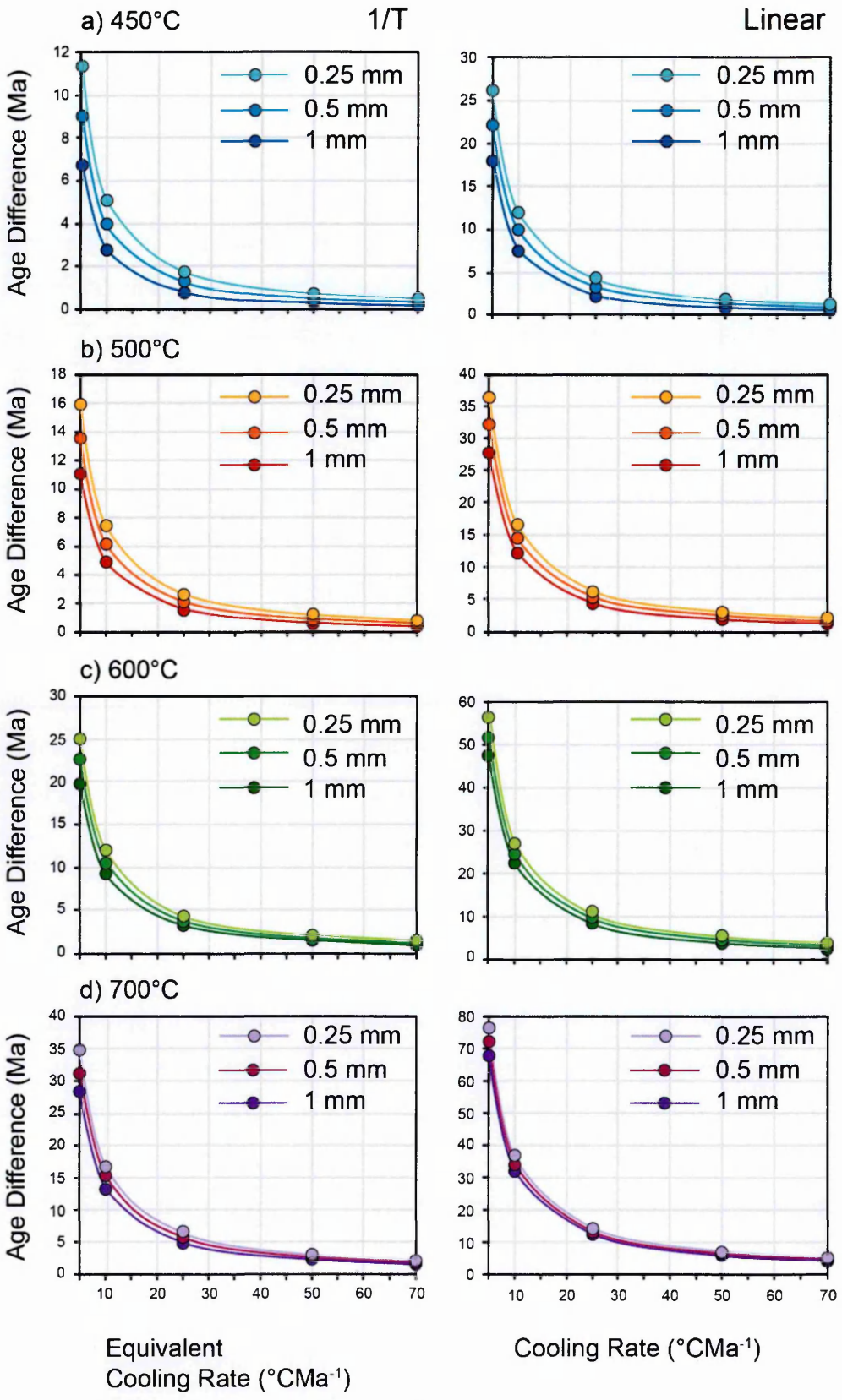

Fig. 2.3. Biotite 1/T and linear model results plotted as age difference between model start time and model bulk age vs. cooling rate. Note the differences in the vertical scales between the two model types.

2.4 Discussions

2.4.1 Model Uncertainties

The model results are sensitive to a number of uncertainties, which are induced from systematic unknowns in the activation energy and diffusion coefficients; experimental unknowns derived from uncertainties in the grain size used in experiments; and from geological uncertainties in the P-T history. In summary, systematic errors derived from uncertainties in the activation energy (E_a) and the diffusion coefficient (D) lead to an uncertainty of ± 4 Ma on the resulting model age (Warren *et al.*, 2012a). Variations in grain size (diffusion radius) from 1 mm to 0.25 mm yield a ± 2 Ma uncertainty on the age.

Variations in the cooling rate from 5-70°CMa^{-1} will result in a +41 to -5 Ma and +15 to -2 Ma uncertainty on the white mica age for the linear and 1/T cooling paths respectively. Variations in the cooling rate from 5-70°CMa^{-1} for biotite yields a range from +62 to -9 Ma and +28 to -4 Ma for the linear and 1/T cooling paths. The large uncertainties are due to the variations in T and grain size as the cooling rate varies from 5-70°Ma^{-1}.

There are of course other geological errors that arise from uncertainties on the timings of the metamorphic path (e.g. U-Pb zircon constraints on the timing of peak metamorphic conditions). However, these errors are terrane-specific and will not be explored further in this chapter, but should be considered when applying DiffArg_inverse to determine terrane-specific cooling rates.

2.4.2 Caveats

It is important to note that the numerical model adheres to a number of approximations: the models solve the modified formulation of Fick's Law of diffusion, the modelled white mica and biotite grains contain no initial Ar and no additional Ar is introduced to the grains during cooling, and the modelled grains have a zero-age boundary condition i.e. an open system operates within the grain boundary network. The 1/T and linear models only apply to cases of volume diffusion.

In those cases where secondary recrystallization or similar effects apply, care will be needed before comparing the measured data to model results. Recrystallization and deformation on a retrograde metamorphic path will, of course, have an effect on the Ar systematics of any grain as these processes act on faster timescales than volume diffusion alone (Villa 1997). Therefore the conditions that the white mica and biotite experience, not

only during growth but also during the exhumation and cooling must be known or at least estimated in order for model interpretations to be applied correctly.

These models also assume that the system is open to the loss of Ar throughout the cooling path and that the grain boundary network remains an 'infinite' reservoir for Ar. Lastly, the models also assume that the cooling path experienced by the white mica or biotite (whether linear or 1/T) is representative of the natural system being modelled.

2.4.3 Applying Model Results to Natural Systems

With these uncertainties and caveats in mind, the models generated from DiffArg_inverse can be applied to any metamorphic terrane to assess whether $^{40}Ar/^{39}Ar$ ages can reflect cooling rates. The prior knowledge that is required to use these model results is:

1) A basic petrographic understanding of when the mica grew along the metamorphic cycle, whether prograde, peak, or during decompression,

2) The temperature at which mica growth occurred,

3) The absolute timing of mica growth. This could be from U-Pb zircon ages if, petrographically, the mica grew at peak metamorphic conditions, or from Rb-Sr mica crystallisation ages,

4) The empirical $^{40}Ar/^{39}Ar$ age data that has been collected via single grain fusion, and,

5) An estimation of the grain size of the white mica or biotite that was analysed.

The age difference is calculated from subtracting the analysed white mica or biotite $^{40}Ar/^{39}Ar$ age from the timing of mica growth to create an age difference, which can subsequently be read off the Y axis of figures 2.2 or 2.3 to yield an estimated cooling rate. For example, a 0.5 mm radius white mica, crystallising at 700°C with an age difference between crystallisation and $^{40}Ar/^{39}Ar$ age of 10 Ma, would suggest an estimated cooling rate of ~7°CMa^{-1} for a 1/T model curve and ~20°CMa^{-1} for a linear cooling curve.

The clear difference between the results of the 1/T and the linear model results indicates that the choice of model curve used for interpreting metamorphic $^{40}Ar/^{39}Ar$ ages is important. 1/T model curves replicate the 1/T cooling rate assumption inherent to the Dodson T_c formulation (Equation 1.6); however, the diffusion models are more robust than the T_c formulation as they do not rely on an over simplification of the cooling curve that

the formulation requires and the diffusional models do not make an assumption of the cooling rate to calculate the bulk age of a grain.

Linear model curves are a very simplistic representation of the cooling history that a metamorphic terrane can experience. These model curves, however, may not be representative of a natural system but may be a close approximation.

2.5 Conclusions

A modified version of the original Wheeler (1996) DiffArg code, DiffArg_inverse solves the diffusion equation numerically, allowing for the computation of $^{40}Ar/^{39}Ar$ ages expected for rocks following simple linear and 1/T cooling paths. The latter replicates the 1/T cooling rate assumption in the Dodson T_c formulation, making the comparison between the 1/T models and the Dodson T_c formulation feasible. DiffArg_inverse can be used to model multiple scenarios for K-bearing minerals rapidly, with variations in temperature, pressure, grain size, and cooling rate. The advantage of using numerical models is that there is no assumption of the shape of the cooling curve that the analytical approach of the Dodson T_c formulation requires.

The technique of modelling Ar diffusion outlined in this chapter is a more robust method for interpreting metamorphic $^{40}Ar/^{39}Ar$ ages as cooling ages than the T_c formulation of Dodson (1973). The models include the effects of pressure on Ar diffusion in white mica, and the diffusion modelling is capable of modelling linear cooling histories, which the T_c formulation cannot. By modelling multiple scenarios that reflect the potential metamorphic conditions, robust cooling rate estimations can be made using the $^{40}Ar/^{39}Ar$ ages of white mica and biotite.

Moreover, by graphically representing the model outputs as the age difference between the model start time (a proxy for the timing of mica crystallisation) and the resulting modelled bulk age, the results are not specific to any one given metamorphic terrane and are widely applicable to all exhumed metamorphic terranes, assuming the assumption of an open system can be demonstrated. In practice, an open system can be demonstrated if white mica or biotite $^{40}Ar/^{39}Ar$ ages can be matched to those generated through diffusional modelling.

Chapter 3

Tracking Ar through a Metamorphic Cycle: Consequences for Understanding Cooling Rates

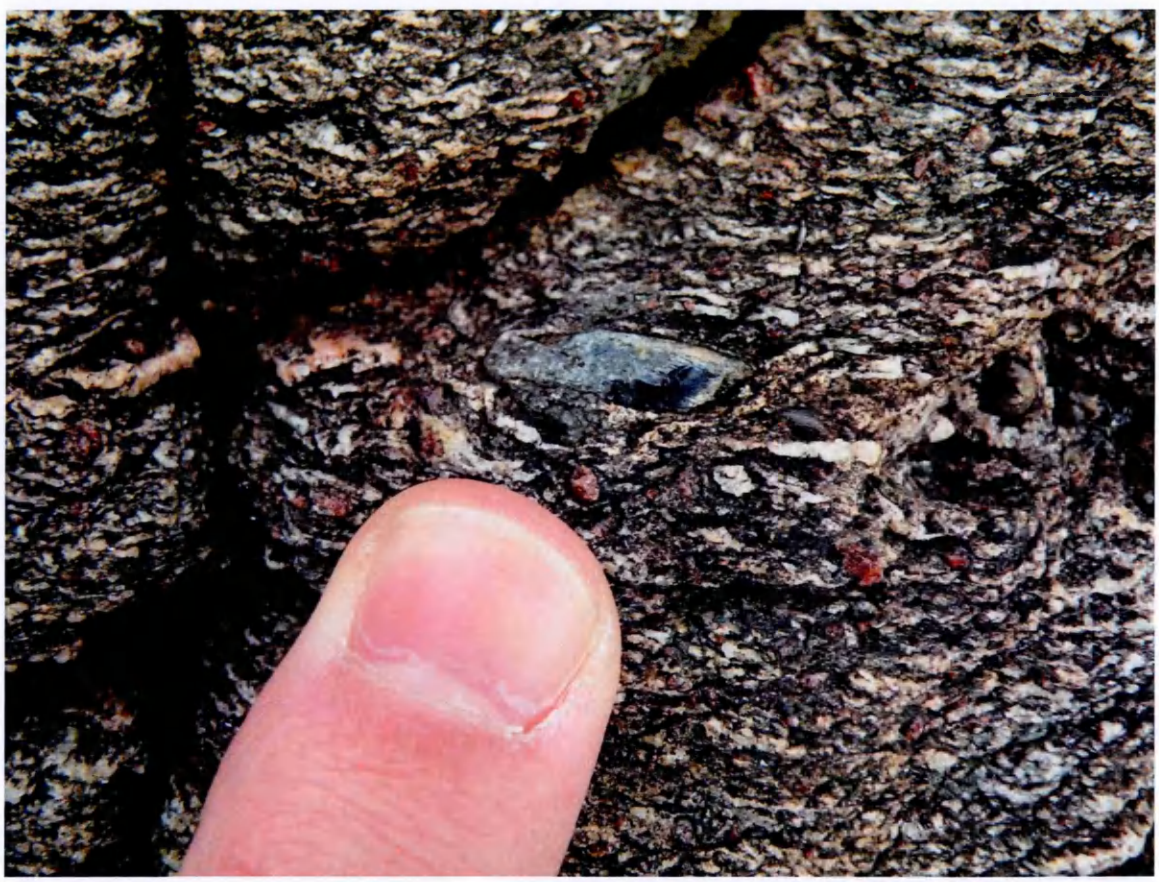

Kyanite-garnet schist at Vetrhus

This Chapter forms the paper:

McDonald, C. S., Warren, C. J., Mark, D. F., Halton, A. M., Kelley, S. P. & Sherlock, S. C. Tracking Ar through a Metamorphic Cycle: Consequences for Understanding Cooling Rates. In prep for *Chemical Geology*.

Abstract

$^{40}Ar/^{39}Ar$ thermochronology is commonly used to constrain the timing, and rates, of cooling in exhumed metamorphic terranes and is usually linked to temperature via Dodson's closure temperature (T_c) formulation. $^{40}Ar/^{39}Ar$ ages in many metamorphic rocks commonly do not fit within a chronological framework defined by other, higher T chronometers, such as U-Pb zircon, suggesting that this link may not always be a correct interpretation. We report white mica and biotite single-grain fusion and laser ablation $^{40}Ar/^{39}Ar$ ages from felsic gneisses from the Western Gneiss Region, Norway. The rocks record isothermal decompression from peak eclogite-facies conditions to amphibolite-facies conditions at 700°C. White mica and biotite yield a range of single grain fusion ages ranging from 411-383 Ma and 430-360 Ma respectively. UV laser ablation yields similar results, with white mica ages ranging from 502-349 Ma and biotite ages ranging from 449-357 Ma. These ages span the entirety of the known timing of the metamorphic cycle previously reported from other chronometers. Simple diffusion models cannot readily provide an explanation for the range of $^{40}Ar/^{39}Ar$ ages recorded by each sample. Physical processes such as recrystallization, deformation, partial melting and fluid fluxes appear to have had a greater effect on Ar distribution. Samples that show significant recrystallization and deformation yield younger white mica ages than more pristine samples, but older biotite ages. Furthermore, migmatisation acts to make biotite ages younger in the amphibolite-facies gneisses whereas fluid infiltration acts to increase biotite ages. The $^{40}Ar/^{39}Ar$ ages yielded by these samples therefore cannot be reconciled with the T_c formulation. Our data support the observation that the $^{40}Ar/^{39}Ar$ ages of micas from high-temperature metamorphic terranes may not always be interpretable as cooling ages and that metamorphic $^{40}Ar/^{39}Ar$ ages require careful assessment with respect to metamorphic stage and petrographic evolution.

3.1 Introduction

Understanding the timing and rate at which metamorphic terranes are exhumed through the Earth's mantle and crust is important in constraining many geodynamic models. $^{40}Ar/^{39}Ar$ thermochronology of micas is typically employed to constrain exhumation and cooling rates, with age most commonly being linked to temperature via the Dodson closure temperature (T_c) formulation (Dodson 1973). T_c in theory yields the "temperature at the time of the grain's apparent age", only if three inherent assumptions regarding the behaviour of Ar in a mineral crystal can be shown to be upheld: (1) that the mineral (re)crystallised with no inherited ^{40}Ar within its crystallographic lattice, (2) that the Ar

distribution within the mineral is controlled only by thermally-activated volume diffusion that adheres to Fick's 2nd law of diffusion (modified for a source term) and (3) that the grain boundary network operates as an 'open system' i.e. the grain boundary effectively has an Ar concentration of zero.

Experimental data have demonstrated that Ar diffusion in white mica is pressure- as well as temperature-dependent (Harrison *et al.,* 2009). These new data affect the way that T_c is calculated, especially in rocks that have experienced metamorphic pressures >10 kbar. This has profound implications when it comes to interpreting metamorphic $^{40}Ar/^{39}Ar$ ages, particularly white micas from high-pressure (HP) terranes, as Ar becomes more retentive in white mica with increasing pressure.

Micas in metamorphic rocks commonly yield $^{40}Ar/^{39}Ar$ step heating ages that show either disturbed "non-plateau" spectra or are too "old" relative to other geochronologically well-constrained 'events' along the (P-T) path e.g. U-Pb zircon of peak metamorphism (Baxter *et al.,* 2002, Sherlock & Arnaud 1999). These apparently "older" ages have been attributed to processes including:

(1) The incorporation of ^{40}Ar into the mineral by ^{40}Ar that has diffused into the grain from the grain boundary. This additional ^{40}Ar is termed excess Ar ($^{40}Ar_E$) and represents ^{40}Ar that has become decoupled from its parent ^{40}K and not ingrown via *in situ* decay; (2) inefficient degassing of grains due in part to the sometimes rapid and cool P-T paths that metamorphic rocks experience during their evolution; (3) non-zero grain boundary conditions which would hinder efficient diffusion of Ar out of a grain and/or (4) recrystallization that may cause $^{40}Ar_E$ to become incorporated within a mineral's crystallographic lattice (Warren *et al.,* 2012a, Sherlock & Kelley 2002, Villa 1997, Di Vincenzo 2004).

The evaluation and understanding of how Ar is incorporated, released and transported within and between different minerals during a metamorphic cycle is therefore important for the interpretation of metamorphic $^{40}Ar/^{39}Ar$ age data, especially with regards to linking 'age' to 'stage' along the pressure-temperature (P-T) path. Of particular interest and importance is how/where Ar is produced, stored and transported during exhumation-related, retrograde metamorphic reactions. The study of such reactions informs the assessment of whether diffusion is the main mechanism for redistributing Ar within minerals, and hence whether the $^{40}Ar/^{39}Ar$ ages may be linked to temperature via the

Dodson T_c formulation (Di Vincenzo *et al.,* 2001, Sherlock *et al.,* 1999, Warren *et al.,* 2011, Warren *et al.,* 2012a, Warren *et al.,* 2012b, Smye *et al.,* 2013).

Here we systematically document differences in $^{40}Ar/^{39}Ar$ ages and age ranges in micas separated from samples of crustal gneisses exposed in the Western Gneiss Region (WGR) of western Norway. This region is a suitable natural laboratory for testing the behaviour of Ar during a metamorphic cycle because geochemically, the Western Gneiss Region is composed of gneisses that are broadly similar in composition but preserve different stages of the metamorphic evolution. Also, the WGR experienced a high temperature evolution (~700°C) for a long-enough period of time (10-15 Ma; Spencer *et al.,* (2013)) for diffusion (i.e., Ar loss), in theory, to have been efficient at resetting the $^{40}Ar/^{39}Ar$ chronometer. This study tests the hypothesis that the application of T_c to metamorphic rocks from the WGR, may be invalid and that instead, Ar can be used as a tracer for physical processes that affect rocks during exhumation.

Hence, we provide an in-depth study into $^{40}Ar/^{39}Ar$ age heterogeneity in an attempt to constrain the behaviour of Ar during a retrograde metamorphic cycle. Ultimately we will test whether apparent $^{40}Ar/^{39}Ar$ ages can be linked to the cooling history of the Western Gneiss Region and thus to tectonic models of exhumation.

3.2 Regional Geology

The Western Gneiss Region (WGR) of western Norway is a 50,000 km^2 basement window within the Scandinavian Caledonides, formed during the subduction of the leading edge of Baltica beneath Laurentia during the Scandian Phase of the Caledonian Orogeny (Roberts 2003, Hacker 2007). The dominant lithology in the WGR is amphibolite-facies felsic gneiss, that locally contain eclogite-facies metabasic eclogites (Hacker *et al.,* 2010).

Remnants of ultrahigh-pressure metamorphism (UHP; >2.6 GPa) are preserved across c. 5,000 km^2 of the WGR (Root *et al.,* 2005). Coesite (the high-pressure polymorph of quartz) has been documented mostly within the eclogite-facies metabasites, but rare occurrences have been documented within the felsic host gneisses (Wain 1997). These UHP lithologies occur in three separate domains, from south to north, the Nordfjord-Stadlandet; the Sorøyane and the Nordøyane. This study focuses on the Nordfjord-Stadlandet domain, where the recorded/preserved P-T gradient ranges from the quartz eclogite-facies in the southeast (~2.5 GPa and 600°C) to coesite-stable eclogite-facies in the northwest (~3.0 GPa and 700°C) across 2500 km^2 (Young *et al.,* 2007, Root *et al.,* 2005). Following (near)isothermal decompression from (U)HP conditions, the entire WGR

experienced retrograde amphibolite-facies metamorphism at ~700°C and 1 GPa (Walsh & Hacker 2004).

3.2.1 Study Sites

From the Nordfjord-Stadlandet area of the WGR three localities, Krokkenakken, Flatraket Harbour and Drage (Fig. 3.1), were chosen for their similar petrographical and lithological associations yet varying preserved P-T conditions. Although each locality preserves evidence for different peak metamorphic conditions, ranging from ~600°C at 2.1 GPa at Krokkenakken to ~750°C at 3.2 GPa at Drage (Cuthbert *et al.,* 2000), all three locations record similar amphibolite-facies retrogression P-T conditions.

The study sites comprise eclogite-facies mafic lithologies that underwent varying degrees of amphibolitisation, hosted within felsic gneisses. The mafic lithologies are known to be plagued with $^{40}Ar_E$ and do not yield geologically meaningful $^{40}Ar/^{39}Ar$ ages (Warren *et al.,* 2012a). The eclogites and their associated amphibolites will be discussed in further detail in Chapter 5. The felsic gneisses record varying P-T conditions along the retrograde metamorphic path, from garnet-bearing gneisses that contain relicts from the HP evolution (e.g. symplectites after omphacite) to amphibolite-facies biotite-epidote gneisses that only record mid-crustal amphibolite-facies conditions. The garnet-bearing gneisses with HP relicts are located within strain shadows adjacent to the mafic lithologies with amphibolite-facies assemblages increasingly overprinting the HP assemblages with increased distance from the mafic units.

3.2.2 Previous Chronology of the Nordfjord-Stadlandet Area

Multiple radioisotopic dating techniques have previously been employed to constrain the timing of both peak metamorphism and exhumation throughout the WGR, including Sm-Nd, Lu-Hf, U-Pb, and $^{40}Ar/^{39}Ar$. Both eclogites and their host gneisses have been targeted.

Sm-Nd and Lu-Hf garnet ages suggest that prograde metamorphism occurred from 419.5 ± 4.3 Ma (Kylander-Clark *et al.,* 2007) to 403.9 ± 0.8 Ma (Peterman *et al.,* 2009) while U-Pb zircon ages in mafic eclogite bodies suggest that peak eclogite-facies metamorphic conditions were achieved by c. 405-400 Ma (Root *et al.,* 2004).

U-Pb rutile from mafic eclogites suggest cooling through 600-700°C at c. 395-392 Ma (Schärer & Labrousse 2003). The U-Pb titanite ages of c. 399-379 Ma in the Nordfjord area have been interpreted to represent the timing at which the host gneisses recrystallized under amphibolite-facies conditions (Spencer *et al.,* 2013).

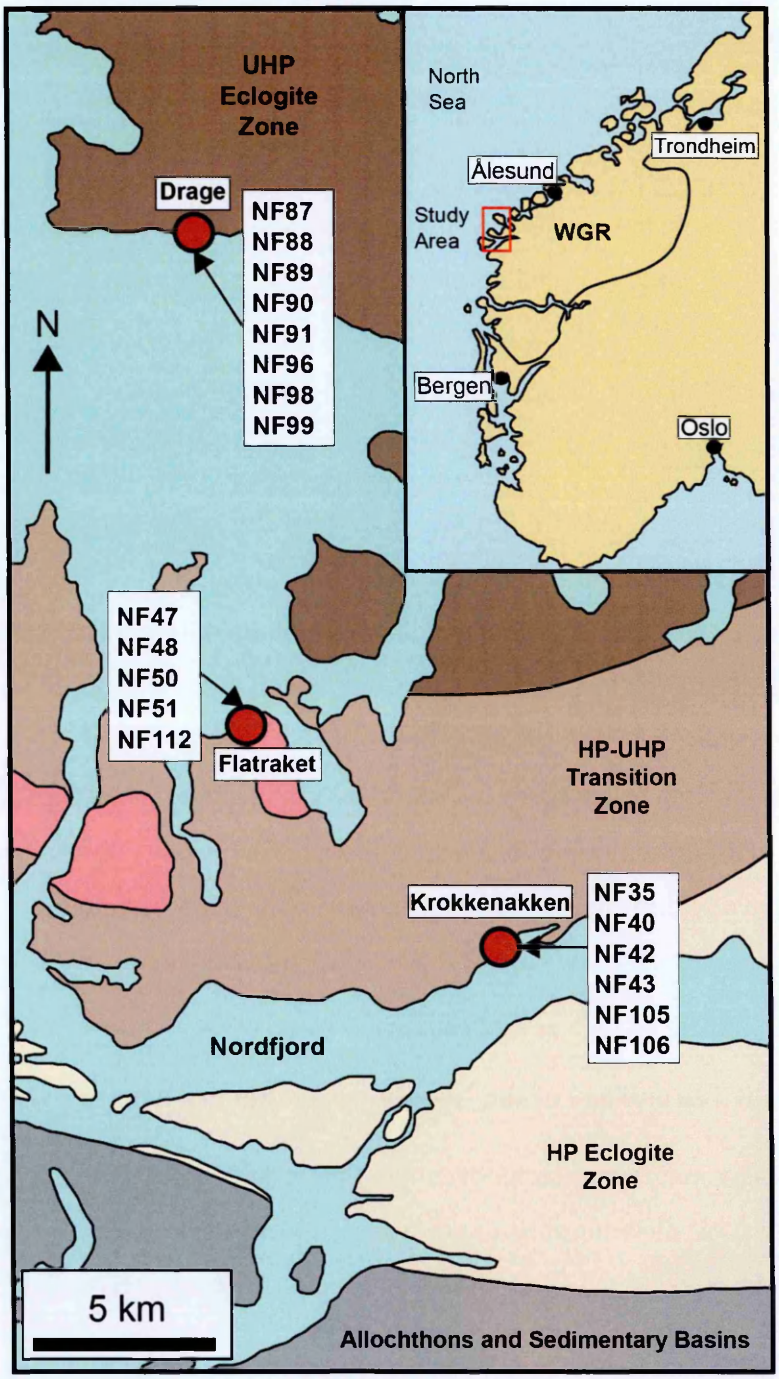

Fig.3.1. A simplified geological map of the Outer Nordfjord region of the WGR showing the locations of the study sites in the Outer Nordfjord region and the samples numbers collected from each locality. Modified after Wain, (1997).

$^{40}Ar/^{39}Ar$ age data is restricted to multi- and single-grain step heating of white micas and biotite. Published plateau ages for the Outer Nordfjord area range from c. 389-374 Ma for white mica and c. 467-379 Ma for biotite, respectively. These age data have been interpreted as cooling through white mica and biotite T_c's (Andersen *et al.,* 1998, Hacker & Gans 2005, Root *et al.,* 2005, Hacker 2007, Walsh *et al.,* 2007, Young *et al.,* 2011, Walsh *et al.,* 2013). A single grain fusion and *in-situ* study of Warren *et al.,* (2012a) showed that white mica $^{40}Ar/^{39}Ar$ ages are highly variable both within grains and between different samples, with ages ranging from 507-379 Ma. The study by Warren *et al.,* (2012a) demonstrated that the assumption that white mica $^{40}Ar/^{39}Ar$ ages represent cooling age may not always be the correct interpretation of $^{40}Ar/^{39}Ar$ white mica age data and thus was the impetus for this study.

3.3 Petrology and Mineral Chemistry

Major-element compositions of muscovite (henceforth, "white mica" so as to remove any pressure or geochemical context that stems from using the terms phengite or muscovite) and biotites were analysed using the Open University Cameca SX-100 5 wavelength-dispersive spectrometer electron microprobe using a defocused beam with spot size of 10 μm, and conditions of 15 kV, 20 nA and 30 s collection time. Calibrations were performed on natural standards, and analyses were corrected using a ZAF matrix correction routine. Analyses were bracketed by analyses of secondary standards to check for major element reproducibility of 1%. The composition of the white mica and biotite from each sample is presented in Table 3.1 and 3.2, respectively.

The felsic gneisses form two petrographic groups: garnet-bearing gneisses that record exhumation from eclogite-facies conditions (**Group 1**) and biotite-epidote gneisses that record the amphibolite-facies overprinting (**Group 2**). A full petrographic description of each sample is provided in Appendix A, but the gneisses are briefly described below.

The garnet-bearing (**Group 1**) gneisses can be further subdivided into three subgroups: those that still preserve high pressure (HP) relicts (**Group 1a**), those that lack HP minerals and contain white mica (**Group 1b**) and those that lack HP relicts but do not contain white mica (**Group 1c**).

Group 1a gneisses are found in a low-strain region adjacent to a large (>300 m long) eclogite boudin at Krokkenakken (samples NF40, NF42 and NF43; Fig. 3.2A). These are medium-grained, unfoliated gneisses with a peak assemblage of quartz, white mica and garnet with accessory apatite, rutile, zircon, clinozoisite and kyanite. Symplectites of

Table 3.1
Core-rim chemical composition of the white mica analysed in each sample

Gneiss Group	1A						1B					
Sample	NF40		NF42		NF43		NF106		NF48		NF88	
Position	Core	Rim	Core	Rim	Core	Rim	Core	Rim	Core	Rim	Core	Rim
F	0.22	0.14	0.05	0.02	0.10	0.08	0.00	0.00	0.07	0.15	0.10	0.00
Cl	0.00	0.01	0.00	0.01	0.00	0.00	0.01	0.00	0.00	0.00	0.01	0.00
Na_2O	0.67	0.75	0.39	0.41	0.20	0.17	0.32	0.46	0.53	0.63	0.46	0.54
K_2O	9.44	9.70	9.59	9.92	10.41	10.59	10.29	10.32	9.90	9.89	10.33	10.45
MgO	2.58	2.16	3.68	3.04	3.29	2.74	2.62	1.06	1.98	1.38	1.64	1.03
CaO	0.00	0.00	0.01	0.00	0.00	0.02	0.00	0.01	0.00	0.05	0.01	0.01
MnO	0.01	0.00	0.02	0.00	0.02	0.00	0.01	0.00	0.00	0.00	0.02	0.01
FeO	2.66	2.72	1.99	1.81	2.68	2.69	2.95	2.85	2.51	2.67	2.22	1.99
Al_2O_3	28.41	29.72	27.32	29.00	26.73	28.14	28.19	32.96	29.28	31.17	30.65	32.55
Cr_2O_3	0.02	0.01	0.02	0.03	0.07	0.07	0.03	0.00	0.01	0.02	0.00	0.00
SiO_2	50.24	49.08	49.68	48.86	50.25	48.80	47.75	43.72	48.86	46.60	47.12	45.88
TiO_2	0.33	0.56	0.19	0.41	0.30	0.38	0.40	0.59	0.73	0.91	1.20	1.12
Total	94.58	94.88	93.00	93.49	94.07	93.68	92.58	91.97	93.89	93.48	93.76	93.58
F	0.09	0.06	0.02	0.01	0.04	0.03	0.00	0.00	0.03	0.07	0.04	0.00
Cl	0.00	0.00	0.00	0.00	0.00	0.00	0.00	0.00	0.00	0.00	0.00	0.00
Na	0.18	0.19	0.10	0.11	0.05	0.04	0.09	0.13	0.14	0.17	0.12	0.14
K	1.62	1.66	1.67	1.72	1.80	1.84	1.82	1.84	1.71	1.73	1.79	1.82
Mg	0.52	0.43	0.75	0.62	0.67	0.56	0.54	0.22	0.40	0.28	0.34	0.21
Ca	0.00	0.00	0.00	0.00	0.00	0.01	0.00	0.00	0.00	0.01	0.00	0.00
Mn	0.00	0.00	0.01	0.00	0.00	0.00	0.00	0.00	0.00	0.00	0.00	0.00
Fe	0.30	0.31	0.23	0.20	0.30	0.31	0.34	0.33	0.29	0.30	0.25	0.23
Al	4.50	4.71	4.38	4.63	4.27	4.53	4.59	5.42	4.68	5.03	4.92	5.23
Cr	0.00	0.00	0.00	0.01	0.01	0.01	0.01	0.00	0.00	0.00	0.00	0.00
Si	6.75	6.59	6.77	6.62	6.82	6.66	6.60	6.11	6.62	6.38	6.42	6.25
Ti	0.03	0.06	0.02	0.04	0.03	0.04	0.04	0.06	0.07	0.09	0.12	0.12
Total	14.00	14.01	13.94	13.95	14.00	14.03	14.02	14.11	13.94	14.05	14.02	14.00

Table 3.1 cont.
Core-rim chemical composition of the white mica analysed in each sample

Gneiss Group	1B						2A			
Sample	NF89		NF96		NF99		NF98		NF105	
Position	Core	Rim	Core	Rim	Core	Rim	Core	Rim	Core	Rim
F	0.05	0.10	0.12	0.00	0.11	0.00	0.04	0.10	0.07	0.09
Cl	0.00	0.00	0.01	0.01	0.00	0.01	0.01	0.00	0.01	0.00
Na_2O	0.35	0.37	0.52	0.53	0.36	0.52	0.22	0.25	0.22	0.22
K_2O	10.54	10.81	10.53	10.51	10.22	10.41	10.81	10.78	10.79	10.82
MgO	1.38	1.05	1.78	0.85	2.32	0.97	1.90	1.33	2.17	2.16
CaO	0.01	0.00	0.01	0.01	0.02	0.03	0.00	0.01	0.00	0.00
MnO	0.02	0.03	0.04	0.00	0.01	0.02	0.02	0.00	0.02	0.03
FeO	2.71	2.70	2.84	2.50	2.68	2.71	4.34	4.23	4.56	4.55
Al_2O_3	30.61	32.00	30.00	32.69	28.40	32.56	28.12	30.13	26.70	27.16
Cr_2O_3	0.01	0.02	0.04	0.03	0.01	0.00	0.02	0.00	0.00	0.03
SiO_2	47.09	46.16	47.98	45.57	49.65	45.31	47.63	46.04	48.05	47.80
TiO_2	1.13	0.74	1.19	0.90	0.86	0.42	1.23	0.94	0.87	0.86
Total	93.93	93.98	95.06	93.61	94.64	92.96	94.34	93.80	93.46	93.72
F	0.02	0.04	0.05	0.00	0.04	0.00	0.02	0.04	0.03	0.04
Cl	0.00	0.00	0.00	0.00	0.00	0.00	0.00	0.00	0.00	0.00
Na	0.09	0.10	0.14	0.14	0.09	0.14	0.06	0.07	0.06	0.06
K	1.83	1.89	1.82	1.83	1.75	1.83	1.89	1.90	1.91	1.91
Mg	0.28	0.21	0.36	0.18	0.47	0.20	0.39	0.28	0.45	0.45
Ca	0.00	0.00	0.00	0.00	0.00	0.01	0.00	0.00	0.00	0.00
Mn	0.01	0.01	0.01	0.00	0.00	0.00	0.00	0.00	0.00	0.01
Fe	0.31	0.31	0.32	0.29	0.30	0.31	0.50	0.49	0.53	0.53
Al	4.92	5.15	4.77	5.27	4.51	5.29	4.55	4.91	4.36	4.43
Cr	0.00	0.00	0.01	0.01	0.00	0.00	0.00	0.00	0.00	0.01
Si	6.42	6.31	6.48	6.23	6.69	6.24	6.53	6.36	6.66	6.62
Ti	0.12	0.08	0.12	0.09	0.09	0.04	0.13	0.10	0.09	0.09
Total	14.00	14.09	14.06	14.03	13.96	14.06	14.07	14.14	14.10	14.12

Table 3.1: Representative core-rim white mica compositions

Table 3.2
Core-rim chemical composition of the biotite analysed in each sample

Gneiss Group	1A						1B			
Sample	NF40		NF42		NF43		NF106		NF48	
Position	Core	Rim	Core	Rim	Core	Rim	Core	Rim	Core	Rim
F	0.14	0.22	0.12	0.15	0.10	0.02	0.14	0.21	0.13	0.13
Cl	0.01	0.01	0.00	0.00	0.00	0.00	0.01	0.02	0.04	0.03
Na_2O	0.27	0.25	0.15	0.10	0.13	0.09	0.08	0.09	0.14	0.10
K_2O	8.61	8.92	9.07	8.76	9.53	9.46	8.84	9.34	9.18	9.31
MgO	12.58	12.43	15.37	15.63	10.61	10.64	11.32	11.47	10.62	10.69
CaO	0.13	0.06	0.03	0.08	0.00	0.00	0.06	0.01	0.02	0.02
MnO	0.07	0.05	0.03	0.03	0.17	0.16	0.16	0.17	0.14	0.15
FeO	15.54	15.36	12.96	12.59	17.21	17.38	18.38	17.95	18.22	18.22
Al_2O_3	17.94	17.90	16.95	17.40	18.52	18.64	16.70	16.41	17.73	17.88
Cr_2O_3	0.04	0.03	0.03	0.02	0.04	0.05	0.02	0.01	0.02	0.00
SiO_2	37.13	36.73	37.85	37.65	35.81	35.74	36.26	36.78	35.76	36.07
TiO_2	1.89	1.95	2.27	2.22	2.64	2.70	2.93	3.28	2.43	2.35
Total	94.43	93.98	94.93	94.68	94.81	94.92	94.90	95.74	94.48	94.96
F	0.07	0.10	0.06	0.07	0.05	0.01	0.07	0.10	0.07	0.07
Cl	0.00	0.01	0.00	0.00	0.00	0.00	0.01	0.01	0.01	0.01
Na	0.08	0.08	0.04	0.03	0.04	0.03	0.02	0.03	0.04	0.03
K	1.65	1.72	1.71	1.65	1.85	1.83	1.72	1.80	1.79	1.81
Mg	2.82	2.81	3.39	3.44	2.40	2.40	2.57	2.59	2.43	2.43
Ca	0.02	0.01	0.01	0.01	0.00	0.00	0.01	0.00	0.01	0.00
Mn	0.01	0.01	0.01	0.01	0.02	0.02	0.02	0.02	0.02	0.02
Fe	1.95	1.95	1.61	1.56	2.19	2.21	2.34	2.27	2.34	2.32
Al	3.18	3.20	2.95	3.03	3.32	3.33	3.00	2.93	3.20	3.21
Cr	0.01	0.01	0.01	0.00	0.01	0.01	0.00	0.00	0.00	0.00
Si	5.58	5.57	5.60	5.57	5.44	5.42	5.52	5.56	5.48	5.49
Ti	0.21	0.22	0.25	0.25	0.30	0.31	0.34	0.37	0.28	0.27
Total	15.58	15.68	15.64	15.61	15.61	15.55	15.61	15.68	15.67	15.65

Table 3.2 cont.
Core-rim chemical composition of the biotite analysed in each sample

Gneiss Group	1B								1C	
Sample	NF88		NF89		NF96		NF99		NF47	
Position	Core	Rim	Core	Rim	Core	Rim	Core	Rim	Core	Rim
F	0.09	0.12	0.00	0.18	0.24	0.11	0.12	0.08	0.06	0.17
Cl	0.03	0.03	0.05	0.05	0.06	0.05	0.04	0.08	0.07	0.07
Na_2O	0.11	0.10	0.13	0.10	0.07	0.06	0.11	0.09	0.15	0.19
K_2O	9.44	9.39	9.59	9.60	9.59	8.57	9.54	8.96	9.06	9.13
MgO	9.36	9.37	9.25	9.27	10.41	11.00	9.96	9.76	11.84	11.85
CaO	0.01	0.05	0.00	0.02	0.00	0.02	0.02	0.05	0.07	0.08
MnO	0.16	0.20	0.36	0.39	0.22	0.22	0.18	0.20	0.26	0.21
FeO	20.20	19.81	19.52	19.27	18.95	19.07	19.45	20.42	18.51	18.54
Al_2O_3	17.84	18.35	17.82	17.91	17.85	17.81	17.90	17.96	16.04	16.04
Cr_2O_3	0.02	0.01	0.04	0.04	0.04	0.03	0.00	0.03	0.04	0.03
SiO_2	35.98	35.80	35.83	36.05	36.09	34.73	35.96	35.12	36.71	36.73
TiO_2	2.64	2.50	3.02	2.87	2.74	2.57	2.34	2.51	2.80	2.62
Total	95.87	95.74	95.60	95.75	96.25	94.24	95.60	95.26	95.63	95.77
F	0.04	0.06	0.00	0.09	0.12	0.06	0.06	0.04	0.03	0.08
Cl	0.01	0.01	0.01	0.01	0.02	0.01	0.01	0.02	0.02	0.02
Na	0.03	0.03	0.04	0.03	0.02	0.02	0.03	0.03	0.04	0.06
K	1.83	1.83	1.86	1.87	1.85	1.69	1.85	1.75	1.75	1.77
Mg	2.12	2.13	2.10	2.11	2.35	2.53	2.26	2.23	2.67	2.68
Ca	0.00	0.01	0.00	0.01	0.00	0.00	0.01	0.01	0.01	0.01
Mn	0.02	0.03	0.04	0.05	0.03	0.03	0.02	0.03	0.03	0.03
Fe	2.57	2.52	2.49	2.46	2.40	2.46	2.48	2.62	2.34	2.35
Al	3.20	3.29	3.20	3.22	3.18	3.23	3.22	3.25	2.87	2.87
Cr	0.01	0.00	0.01	0.01	0.01	0.01	0.00	0.01	0.01	0.01
Si	5.48	5.45	5.46	5.49	5.47	5.35	5.48	5.40	5.56	5.57
Ti	0.30	0.29	0.35	0.33	0.31	0.30	0.27	0.29	0.32	0.30
Total	15.63	15.64	15.56	15.66	15.75	15.68	15.69	15.67	15.66	15.76

Table 3.2 cont.
Core-rim chemical composition of the biotite analysed in each sample

Gneiss Group	1C						2A			
Sample	NF112		NF50		NF87		NF98		NF105	
Position	Core	Rim	Core	Rim	Core	Rim	Core	Rim	Core	Rim
F	0.07	0.06	0.09	0.18	0.04	0.07	0.06	0.21	0.25	0.08
Cl	0.06	0.05	0.05	0.05	0.03	0.03	0.02	0.02	0.02	0.01
Na_2O	0.14	0.12	0.16	0.14	0.14	0.10	0.10	0.07	0.06	0.05
K_2O	9.34	9.39	9.04	9.05	9.13	9.46	9.68	9.67	9.63	9.56
MgO	12.54	12.44	12.71	12.46	11.86	11.81	10.31	10.64	8.85	8.72
CaO	0.03	0.04	0.03	0.02	0.09	0.07	0.02	0.02	0.00	0.00
MnO	0.21	0.20	0.18	0.23	0.15	0.15	0.23	0.25	0.54	0.56
FeO	16.27	15.83	17.10	17.01	16.23	16.18	18.89	18.84	20.98	20.83
Al_2O_3	17.31	16.74	16.13	16.51	17.79	18.26	17.72	17.44	15.88	16.59
Cr_2O_3	0.00	0.03	0.02	0.06	0.05	0.04	0.02	0.05	0.00	0.00
SiO_2	36.71	36.57	36.26	36.20	37.07	37.06	35.90	36.16	34.65	34.12
TiO_2	2.47	2.53	2.34	2.24	1.98	1.62	2.29	2.27	2.94	2.86
Total	95.15	94.00	94.18	94.17	94.57	94.85	95.22	95.64	93.80	93.41
F	0.03	0.03	0.04	0.09	0.02	0.03	0.03	0.10	0.13	0.04
Cl	0.02	0.01	0.01	0.01	0.01	0.01	0.01	0.01	0.01	0.01
Na	0.04	0.03	0.05	0.04	0.04	0.03	0.03	0.02	0.02	0.02
K	1.79	1.83	1.77	1.77	1.75	1.82	1.89	1.88	1.95	1.94
Mg	2.82	2.82	2.90	2.84	2.67	2.65	2.34	2.42	2.09	2.06
Ca	0.01	0.01	0.01	0.01	0.02	0.01	0.01	0.01	0.00	0.00
Mn	0.03	0.03	0.02	0.03	0.02	0.02	0.03	0.03	0.07	0.08
Fe	2.05	2.01	2.19	2.18	2.05	2.04	2.41	2.40	2.78	2.76
Al	3.07	3.00	2.91	2.98	3.16	3.24	3.18	3.14	2.96	3.10
Cr	0.00	0.01	0.00	0.01	0.01	0.01	0.00	0.01	0.00	0.00
Si	5.52	5.57	5.54	5.54	5.59	5.58	5.48	5.51	5.49	5.41
Ti	0.28	0.29	0.27	0.26	0.23	0.18	0.26	0.26	0.35	0.34
Total	15.65	15.64	15.71	15.76	15.54	15.60	15.67	15.77	15.85	15.74

Table 3.2 cont.
Core-rim chemical composition of the biotite analysed in each sample

Gneiss Group	2B							
Sample	NF35		NF51		NF90		NF91	
Position	Core	Rim	Core	Rim	Core	Rim	Core	Rim
F	0.21	0.17	0.13	0.15	0.15	0.17	0.32	0.32
Cl	0.01	0.01	0.05	0.04	0.05	0.04	0.07	0.07
Na_2O	0.08	0.09	0.24	0.24	0.06	0.04	0.07	0.06
K_2O	9.65	9.73	9.28	9.27	9.60	8.01	9.60	9.57
MgO	10.08	9.96	11.34	11.33	7.67	6.63	7.96	8.05
CaO	0.00	0.00	0.06	0.08	0.00	2.29	0.04	0.03
MnO	0.39	0.43	0.25	0.24	0.31	0.29	0.44	0.43
FeO	19.21	19.49	19.24	18.94	22.34	20.44	22.22	22.50
Al_2O_3	16.24	16.30	15.30	15.13	16.43	16.22	15.54	15.42
Cr_2O_3	0.03	0.00	0.00	0.00	0.00	0.01	0.01	0.00
SiO_2	36.60	36.22	36.19	36.16	36.02	38.19	36.12	35.89
TiO_2	2.27	2.60	2.59	2.58	2.78	2.37	2.61	2.37
Total	94.84	95.06	94.72	94.25	95.39	94.70	95.00	94.72
F	0.10	0.08	0.06	0.07	0.07	0.08	0.16	0.16
Cl	0.00	0.01	0.01	0.01	0.01	0.01	0.02	0.02
Na	0.02	0.03	0.07	0.07	0.02	0.01	0.02	0.02
K	1.90	1.91	1.83	1.83	1.90	1.57	1.93	1.93
Mg	2.32	2.29	2.61	2.62	1.78	1.52	1.86	1.89
Ca	0.00	0.00	0.01	0.01	0.00	0.37	0.01	0.01
Mn	0.05	0.06	0.03	0.03	0.04	0.04	0.06	0.06
Fe	2.48	2.51	2.48	2.45	2.90	2.63	2.92	2.97
Al	2.95	2.96	2.78	2.77	3.01	2.94	2.88	2.87
Cr	0.01	0.00	0.00	0.00	0.00	0.00	0.00	0.00
Si	5.64	5.58	5.59	5.60	5.60	5.87	5.67	5.67
Ti	0.26	0.30	0.30	0.30	0.32	0.28	0.31	0.28
Total	15.74	15.73	15.79	15.79	15.66	15.32	15.82	15.86

Table 3.2: Representative core-rim biotite compositions

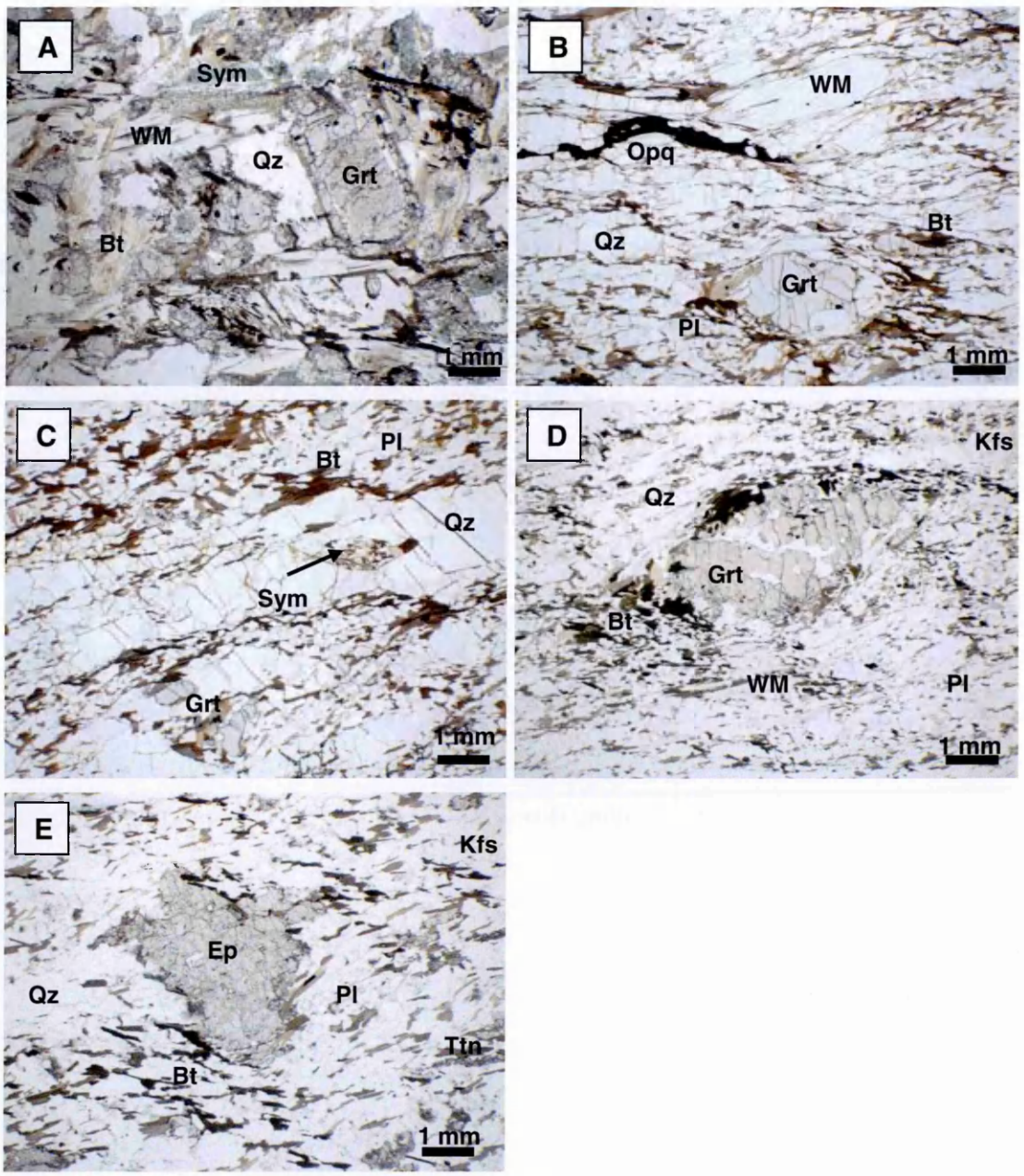

Fig. 3.2: Photomicrographs of samples from the five petrographic types of gneiss documented in this study. (A) **Group 1a** gneiss with preserved high-pressure relicts (NF43), (B) **Group 1b** gneiss (NF48) no longer contains relicts from the high-pressure evolution. Note the formation of white mica fish and foliation defined by biotite. (C) **Group 1c** gneiss (NF112) with relict symplectites of biotite + plagioclase after white mica preserved in quartz ribbons. (D) **Group 2a** gneiss showing highly degraded garnet and minor flakes of white mica (NF98) and (E) **Group 2b** gneiss (NF51). Mineral abbreviations after Whitney & Evans (2010), WM = white mica and Sym = symplectite

clinopyroxene and plagioclase provide evidence for precursor omphacite (Wain *et al.* 2000).

White micas are 0.5-2.5 mm in length, with Si compositions ranging from 6.8-6.3 per formula unit (pfu; core to rim). Crystals are ubiquitously surrounded by replacement biotite-plagioclase symplectites. Biotite grains within the symplectite are generally <0.5 mm in size and are chemically variable with Mg/Mg+Fe ($Mg^{\#}$) of 0.52-0.73 and Ti concentrations of 0.2-0.3 pfu.

Group 1b gneisses (that are white-mica bearing and do not preserve HP phases) occur at all three localities (Krokkenakken: NF106; Flatraket Harbour: NF48; Fig. 3.2B) and Drage: NF88, NF89, NF96 and NF99). These gneisses are foliated and composed of quartz, plagioclase feldspar, garnet, white mica, biotite and rare alkali feldspar with accessory phase of rutile, apatite and zircon.

White micas, 0.5-2.5 mm in length, show strong zonation in Si from core to rim from 6.8-6.1 pfu. There is minor rim alteration to biotite. Biotite is <0.5 mm in length in these samples and forms euhedral laths that define the fabric in the samples. They show a wide range in composition with $Mg^{\#}$ ranging from 0.46-0.51 and Ti concentrations between 0.23-0.34 pfu.

Subordinate in volume to Group 1b gneisses, **Group 1c** gneisses preserve neither HP minerals nor white mica (Flatraket Harbour: NF47, NF50 and NF112; Drage: NF87). These gneisses are located close to the contact with the mafic eclogites and are also found close to the contact with the amphibolite-facies biotite-epidote gneisses described below. They contain quartz, plagioclase feldspar, garnet, epidote (commonly with allanite cores), and biotite with accessory phases of ilmenite, apatite and zircon. Rare biotite-plagioclase symplectites preserved in quartz ribbons attest to the former presence of white mica (Fig 3.2C.). Biotite laths are generally <1 mm in length and yield a narrow range in composition with $Mg^{\#}$ values from 0.53-0.58 and Ti concentrations from 0.20- 0.34 pfu.

Group 2 gneiss is found across the Outer Nordfjord area of the WGR and forms approximately 70% by volume of the felsic gneisses in the study area (Peterman *et al.* 2009). Typically these gneisses are foliated, and grey in colour in the field. These gneisses preserve the lowest metamorphic grade assemblages in the basement. At Drage (Fig. 3.1), within the core of the Nordfjord-Stadlandet UHP domain, these gneisses are intensely migmatised. Biotite-epidote gneisses can be further subdivided into those that still preserve relict white mica (**Group 2a**) and those that do not (**Group 2b**).

Located close to the contact with **Group 1c** gneisses, **Group 2a** gneisses contain an amphibolite-facies assemblage of biotite, epidote, quartz, and plagioclase and preserve skeletal relicts of white mica and garnet. The garnets are small, <1 mm in diameter, and are heavily corroded, as shown by Fig 2D. The white mica shows evidence of melting, converting to alkali feldspar + quartz at the rims. This type of gneiss occurs only at Krokkenakken (NF105) and at Drage (NF98; Fig 3.2D).

The relict white mica is <0.5 mm in length and shows a zonation in Si from core to rim from 6.6-6.3 pfu. The biotite is 0.5-1 mm in length and forms subhedral to euhedral laths that define the fabric. Biotite yields a broad range of compositions with $Mg^{\#}$ ranging from 0.40-0.51 and Ti concentrations from 0.12-0.42 pfu.

Group 2b samples include NF35 from Krokkenakken, NF51 from Flatraket Harbour (Fig. 3.2E) and samples NF90 and NF91 from Drage. They have a broadly similar petrology to **Group 2a** gneisses of quartz, plagioclase, biotite, epidote (with common allanite cores and forming predominant porphyroblasts) and minor amphibole and K-feldspar. Accessory phases include titanite, ilmenite, apatite and zircon.

Biotite defines the fabric in these samples and is often inter-grown with titanite. The fabric both wraps around and is overprinted by the epidote porphyroblasts, suggesting epidote growth during and after deformation during amphibolite-facies metamorphism. Biotite grains are ~1 mm in length and yield a broad range in chemistry, with $Mg^{\#}$ varying from 0.37 to 0.55 and with Ti concentrations from 0.20 to 0.37 pfu.

3.4 $^{40}Ar/^{39}Ar$ Analysis

White mica and biotite were picked from crushed samples for single-grain fusion analysis. Those grains that showed the least deformation and the fewest inclusions were selected. Care was taken when selecting white mica grains from symplectised samples, to avoid the grains rimmed by biotite-plagioclase symplectites.

Samples were analysed at two facilities: the Ar/Ar and Noble Gas Laboratory at the Open University (OU), and the NERC-funded Argon Isotope Facility (AIF) housed at the Scottish Universities Environmental Research Centre (SUERC)

3.4.1 Open University

50 grains of white mica and/or biotite were separated from each sample and were washed in acetone, methanol and distilled water before being packed into aluminium foil packets.

Polished thick sections (~250 μm) were prepared by adhesion to glass slides with cyanoacrylate. Sections were removed from the glass by soaking in acetone for up to 24 hours and then cut into 5 x 5 mm squares before washing and packing as above.

Samples (to be analysed at the Ar/Ar and Noble Gas Research Laboratory at the Open University) were first irradiated at McMaster University Reactor, Ontario. Irradiation flux was monitored using the biotite standard GA1550 with an age of 99.80 ± 0.1 Ma (Renne *et al.,* 2010). The following corrections were applied to the standards: $(^{39}Ar/^{37}Ar)_{Ca}$ = 0.00065 ± 0.0000033, $(^{36}Ar/^{37}Ar)_{Ca}$ = 0.0002654 ± 0.0000013, $(^{40}Ar/^{39}Ar)_{K}$ = 0.0085 ± 0.0000425 based on analyses of Ca and K salts; only the K correction was applied to the analysed samples. Sample *J* values (± 0.5 %) are presented in Appendix C and were calculated by linear interpolation between two bracketing standards with standards included between every 8-10 samples in the irradiation tube. Background measurements bracketed every 1-2 sample measurements. Analyses were corrected for mass spectrometer discrimination, using a value of 283 for the samples analysed on the MAP 215-50 and 295 for samples analysed on the Nu instruments Noblesse. Age data was reduced using the decay constants of Min *et al.,* (2000).

As with many small-volume $^{40}Ar/^{39}Ar$ studies, the measured ^{36}Ar approaches the detection limits. The correction for atmospheric argon magnifies the error on the final $^{40}Ar/^{39}Ar$ age (Sherlock *et al.* 2005). Samples were only corrected for atmospheric argon when the measured ^{36}Ar was <2x that of the background measurement. The uncertainty on the non-atmosphere-corrected analyses was doubled to compensate (Sherlock *et al.,* 2005, Sherlock *et al.,* 2008, Warren *et al.,* 2011, Warren *et al.,* 2012a); these instances are marked on the data table.

Samples were loaded into an ultra-high vacuum laser port and placed under a heat lamp for 8 hours to reduce atmospheric background levels. Total fusion of single grains of the unknowns and flux monitors was achieved using a 1062nm CSI Fibre laser coupled to an automated gas handling vacuum system and admitted to a MAP 215-50 noble gas mass spectrometer with a gettering time of 210 seconds.

Higher resolution single spot and traverse analyses on polished thick sections were achieved using a New Wave Systems Nd-YAG 213 nm ultraviolet (UV) laser coupled to a Nu Instruments Noblesse gas mass spectrometer. UV analyses consisted of ablating 30 μm diameter spots for 90 seconds followed by 90 seconds gettering time.

Both mass spectrometers were run in single-collector mode and unwanted gas species were gettered using two SAES AP10 Zr-Al getters (one at room temperature and the other at 450°C). A liquid nitrogen cold trap on the MAP 215-50 provided additional gas cleaning prior to inlet to the mass spectrometer. Peaks of ^{40}Ar, ^{39}Ar, ^{38}Ar, ^{37}Ar and ^{36}Ar were scanned ten times each and the data extrapolated back to the inlet time (time zero). Data were reduced using the in-house software package ArMaDiLo developed by James Schwanethal. Age uncertainties are reported to 2σ and uncertainties on the analytical precision are reported to 1σ.

3.4.2 SUERC

Single crystals of muscovite and biotite were loaded into Al discs, and stacked in a flame-sealed glass vial for irradiation. Standards of GA1550 with an age of 99.80 ± 0.1 Ma (Renne *et al.,* 2010) were placed within wells adjacent to the samples and throughout the entire stack to permit detailed characterisation of the irradiation flux both horizontally and vertically. Samples were irradiated in the Cd-lined (CLICIT) facility of the Oregon State University (USA) TRIGA reactor.

Samples were fused with a CO_2 laser (full details are explained in Mark *et al.,* (2011)). The *J* parameter was determined to a precision of 0.2%. Isotope data were collected using a GVI ARGUS multi-collector mass spectrometer (Mark *et al.,* 2009). Samples were heated for 20 seconds prior to 300 seconds clean-up. Extracted gases were cleaned using 2 GP50 SAES getters (one operated at 450°C and one at room temperature). The extraction, clean up and data collection processes were entirely automated. Average backgrounds ± standard deviations from all five blank runs were used to correct isotope abundances. Air calibrations were collected after every 8 analyses to monitor mass discrimination. A $^{40}Ar/^{36}Ar$ value of 300.08 ± 0.19 was used to correct the data for mass discrimination. A power law function was used for the mass discrimination correction (Renne *et al.,* 2009b).

Berkeley Geochronology Centre software 'massspec' was used to regress and reduce age data using the decay constants of Min *et al.,* (2000). The isotope data were corrected for blank, radioactive decay, mass discrimination and interfering reactions. All data are reported according to the recommendations of Renne *et al.,* (2009a). Data are reported to 1σ as measurement ± analytical precision.

3.5 $^{40}Ar/^{39}Ar$ Results

3.5.1 Single grain fusion data

19 samples of gneiss from the 5 petrographic types were selected for single grain fusion analysis to understand the age variations between the different petrographic types of gneiss. A summary of the single grain fusion data is provided in Table 3.3 and 3.4 and shown in Fig. 3.3. The full dataset is provided in Appendix C.

3.5.1.1 Garnet-bearing Gneisses

Three **Group 1a** samples from Krokkenakken (NF40, NF42 and NF43), totalling 33 white mica analyses and 34 biotite analyses, yielded single grain fusion (SGF) ages that range from 407 ± 5.3 Ma to 383 ± 4.1 Ma for the white mica and 438 ±2.0 Ma to 360 ± 1.9 Ma for biotite (Fig. 3.3A).

Six **Group 1b** samples, from Krokkenakken (NF106); Flatraket Harbour (NF48) and Drage (NF88, NF89, NF96 and NF99), totalling 107 white mica and 107 biotite SGF analyses, yielded white mica ages ranging from 423 ± 7.1 Ma to 378 ± 4.5 Ma and biotite ages ranging from 414 ± 5.7 Ma to 363 ± 5.2 Ma (Fig. 3.3B).

Four samples of white-mica-free **Group 1c** gneisses from Flatraket Harbour (NF47, NF112 and NF50) and Drage (NF87), totalling 63 biotite SGF analyses, yielded ages from 423 ± 7.5 Ma to 382 ± 4.3 Ma (Fig. 3.3C).

3.5.1.2 Biotite-Epidote Gneisses

Two samples of **Group 2a** gneisses from Krokkenakken (NF105) and Drage (NF98), totalling 30 white mica and 30 biotite SGF analyses, yielded white mica ages that range from 411 ± 8.7 Ma to 377 ± 8.3 Ma and biotite ages ranging from 398 ± 11.8 Ma to 371 ± 8.2 Ma (Fig. 3.3D).

Four **Group 2b** samples from Krokkenakken (NF35); Flatraket Harbour (NF51) and Drage (NF90 and NF91), totalling 94 biotite SGF analyses, yielded ages that range from 430 ± 1.9 Ma to 374 ± 2.0 Ma (Fig. 3.3E).

3.5.2 UV Laser Ablation data

Five samples were selected for detailed *in-situ* laser ablation analysis to provide spatial context to the observed single grain fusion age variations. A summary of the ages is

					IR Single Grain Fusion Ages				UV *In-situ* Ages		
					Oldest Age	Youngest Age	WMA		Oldest Age	Youngest Age	WMA
Lithology	Sample	Location	Mineral	n#	Ma (± 1σ)	Ma (± 1σ)	Ma (± 1σ)	n#	Ma (± 1σ)	Ma (± 1σ)	Ma (± 1σ)
Group 1a	NF40	Krokkenakken	White Mica	8	396 ± 2.6	388 ± 2.8	390 ± 3.3	45	414 ± 5.4	382 ± 6.1	395 ± 2.7
	NF42	Krokkenakken	White Mica	12	405 ± 5.2	387 ± 5.0	399 ± 3.8	41	492 ± 6.0	389 ± 4.5	411 ± 6.6
	NF43	Krokkenakken	White Mica	14	407 ± 5.3	383 ± 4.1	395 ± 3.9	87	502 ± 15.5	348 ± 11.3	403 ± 2.5
Group 1b	NF106	Krokkenakken	White Mica	15	423 ± 7.1	391 ± 4.6	407 ± 5.0		nd	nd	
	NF48	Flatraket Harbour	White Mica	13	391 ± 6.5	381 ± 2.9	385 ± 2.7	19	394 ± 5.4	381 ± 10.2	388 ± 5.4
	NF88	Drage	White Mica	25	399 ± 1.4	387 ± 0.8	392 ± 1.1		nd	nd	
	NF89	Drage	White Mica	24	397 ± 1.5	379 ± 4.4	393 ± 1.1		nd	nd	
	NF96	Drage	White Mica	15	410 ± 3.7	386 ± 5.6	394 ± 4.3		nd	nd	
	NF99	Drage	White Mica	15	409 ± 14.1	378 ± 9.5	384 ± 4.7		nd	nd	
Group 2a	NF98	Drage	White Mica	15	395 ± 3.6	377 ± 4.5	389 ± 3.8		nd	nd	
	NF105	Krokkenakken	White Mica	15	411 ± 4.8	385 ± 4.7	397 ± 4.6		nd	nd	

nd = not determined n# = number of grains or spots WMA = Weighted Mean Age

Krokkenakken ***61°54'53.73" N 005°20'16.49" E*** Flatraket Harbour **61°58'42.60" N** ***005°14'03.80" E***

Drage ***62°06'08.30" N 005°12'48.0" E***

Table 3.3: Summary data table of white mica single grain fusion and *in-situ* analyses

					IR Single Grain Fusion Ages				UV *In-situ* Ages		
					Oldest Age	Youngest Age	WMA		Oldest Age	Youngest Age	WMA
Lithology	Sample	Location	Mineral	n#	Ma (± 1σ)	Ma (± 1σ)	Ma (± 1σ)	n#	Ma (± 1σ)	Ma (± 1σ)	Ma (± 1σ)
Group 1a	NF40	Krokkenakken	Biotite	12	438 ± 2.0	377 ± 1.9	386 ± 11	16	394 ± 7.7	387 ± 5.1	390 ± 5.5
	NF42	Krokkenakken	Biotite	10	360 ± 1.9	423 ± 2.0	381 ± 12	26	400 ± 5.8	377 ± 5.3	390 ± 4.0
	NF43	Krokkenakken	Biotite	12	390 ± 2.4	383 ± 2.1	385 ± 2.5	21	400 ± 9.8	371 ± 14.1	388 ± 6.0
Group 1b	NF106	Krokkenakken	Biotite	15	414 ± 5.7	398 ± 4.8	404 ± 4.6		nd	nd	
	NF48	Flatraket Harbour	Biotite	12	392 ± 2.3	383 ± 2.3	387 ± 3.0	18	448 ± 15.9	377 ± 5.1	386 ± 6.0
	NF88	Drage	Biotite	25	392 ± 0.9	379 ± 2.2	389 ± 0.9		nd	nd	
	NF89	Drage	Biotite	25	394 ± 0.7	378 ± 4.7	390 ± 1.2		nd	nd	
	NF96	Drage	Biotite	15	386 ± 3.6	363 ± 5.2	374 ± 3.7		nd	nd	
	NF99	Drage	Biotite	15	396 ± 6.2	378 ± 3.8	384 ± 4.4		nd	nd	
Group 1c	NF47	Flatraket Harbour	Biotite	12	415 ± 1.9	386 ± 1.8	397 ± 4.9		nd	nd	
	NF112	Flatraket Harbour	Biotite	15	423 ± 7.5	400 ± 5.4	408 ± 4.6		nd	nd	
	NF50	Flatraket Harbour	Biotite	12	401 ± 2.0	383 ± 2.0	392 ± 3.1	33	422 ± 8.2	371 ± 8.6	394 ± 4.4
	NF87	Drage	Biotite	25	394 ± 1.3	382 ± 4.3	388 ± 1.0		nd	nd	
Group 2a	NF98	Drage	Biotite	15	394 ± 3.9	371 ± 8.2	387 ± 4.4		nd	nd	
	NF105	Krokkenakken	Biotite	15	398 ± 11.8	377 ± 4.5	386 ± 4.4		nd	nd	
Group 2b	NF35	Krokkenakken	Biotite	12	430 ± 1.9	379 ± 2.0	387 ± 8.3		nd	nd	
	NF51	Flatraket Harbour	Biotite	25	417 ± 5.3	385 ± 1.8	396 ± 1.7	24	441 ± 8.7	381 ± 7.2	395 ± 5.6
	NF90	Drage	Biotite	25	399 ± 0.4	378 ± 3.2	396 ± 1.0		nd	nd	
	NF91	Drage	Biotite	20	391 ± 1.2	374 ± 2.0	389 ± 1.6	20	441 ± 9.6	360 ± 2.8	369 ± 8.0

nd = not determined n# = number of grains or spots WMA = Weighted Mean Age

Krokkenakken ***61°54'53.73" N 005°20'16.49" E*** Flatraket Harbour **61°58'42.60" N** ***005°14'03.80" E***

Drage ***62°06'08.30" N 005°12'48.0" E***

Table 3.4: Summary of biotite single grain fusion and *in-situ* analyses

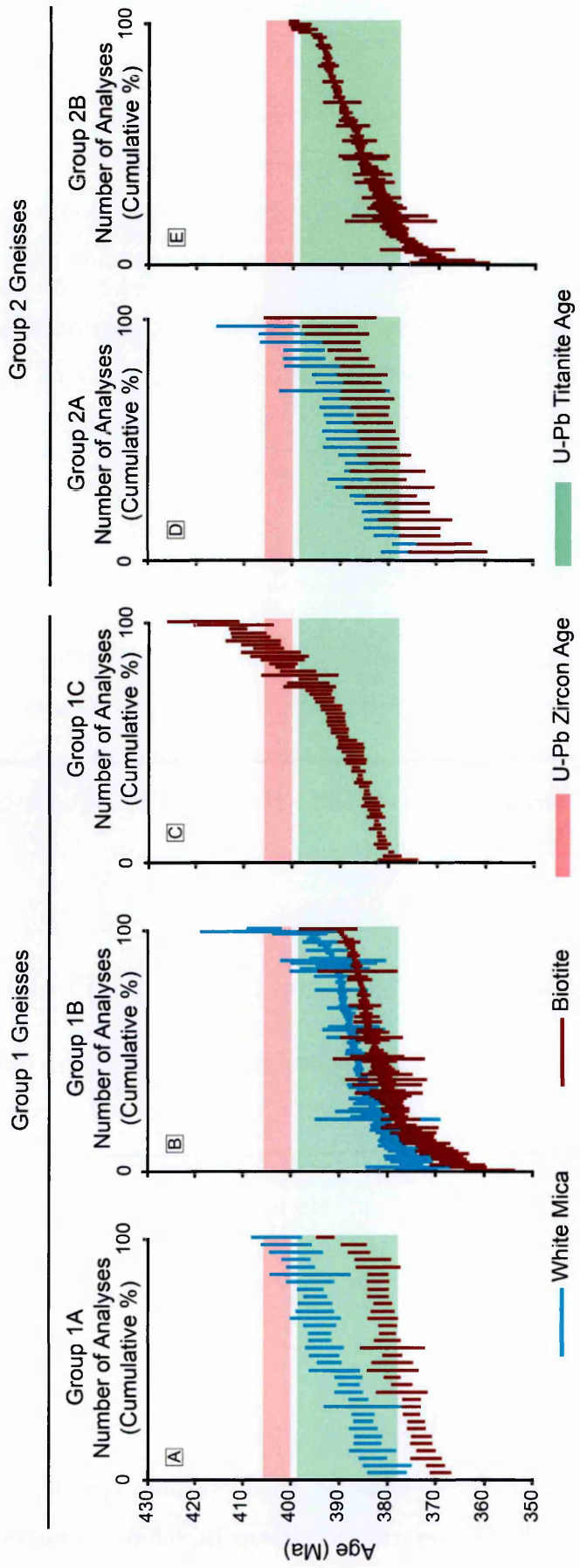

Figure 3.3: Cumulative graphs of white mica and biotite single-grain fusion $^{40}Ar/^{39}Ar$ data from the five petrographic types. (A - C) Group 1 garnet-bearing gneisses of **Group 1a** that contain HP relicts; **Group 1b** that no longer contain HP relicts and **Group 1c** that no longer contains white mica or HP relicts. (D-E) Group 2 epidote-bearing gneisses of **Group 2a** that contains relicts of white mica and garnet from the garnet-bearing gneisses; and **Group 2b** that comprise an amphibolite-facies assemblage of biotite-epidote that is typical of WGR gneisses. The red boxes represent the U-Pb zircon ages for the timing of peak metamorphism of Root *et al.*, (2004) and the green boxes represent the U-Pb titanite ages of the amphibolite-facies recrystallization of Spencer *et al.*, (2013).

provided in Table 3.3 and 3.4 and on the representative photomicrographs in Fig. 3.4. The full dataset is provided in Appendix D.

45 spots on four white mica grains from **Group 1a** sample NF40 and 87 spots on three white mica grains from NF43 (Fig 3.4A) yielded single spot ages ranging from 414 ± 2.7 Ma to 382 ± 3.1 Ma and 502 ± 7.8 Ma to 349 ± 5.7 Ma, respectively. Within uncertainty, each grain yielded internally consistent ages with no consistent core–rim variations.

16 and 21 spots on five biotite grains in each of the same samples yielded ages that range from 394 ± 3.8 Ma to 387 ± 2.5 Ma for sample NF40 and 400 ± 4.9 Ma to 371 ± 7.1 Ma for sample NF43.

19 spots on one large grain (~1 mm) of white mica and 18 spots on nine biotite grains from a **Group 1b** sample (NF48) yielded a range of ages from 394 ± 2.7 Ma to 382 ± 5.1 Ma and 449 ± 8.0 Ma to 378 ± 2.5 Ma (Fig. 3.4B).

23 spots on eight grains of biotite, three included within a garnet and five within the matrix, were analysed from a sample of **Group 1c** gneiss (NF50) from Flatraket Harbour (Fig. 3.4C). A range of ages from 422 ± 4.1 Ma to 371 ± 8.6 Ma was yielded. 24 spots on 8 grains of biotite from the matrix of **Group 2b** sample NF51 (Fig. 3.4D) from Flatraket Harbour yielded a range of ages from 441 ± 4.4 Ma to 381 ± 3.6 Ma.

3.6 Discussion

3.6.1 Comparison between single grain fusion and *in-situ* data

Single-grain fusion data from white mica and biotite separates from felsic gneisses from across the three localities and across the different petrological associations, show a broad spread in $^{40}Ar/^{39}Ar$ ages from 411 ± 8.7 Ma to 383 ± 4.1 Ma in white mica and 430 ± 1.9 Ma to 360 ± 1.9 Ma in biotite. *In-situ* UV laser data from selected samples shows that the distribution of Ar both within and between grains of white mica and biotite is non-systematic and highly variable. Overall the yielded age range is greater with the *in-situ* analyses but the two methods yield broadly similar weighted means.

3.6.2 Comparison of Ages vs. Mineral Chemistry

Both the white mica and the biotite show geochemical zonation (Section 3.3). The Si content of the white mica ranges from 6.8-6.3 (core-rim) in **Group 1a**, 6.8-6.1 in **Group 1b**, and 6.6-6.3 in **Group 2a**. Biotite core-rim vary in $Mg^{\#}$ (Mg/Mg+Fe) range from 0.52-0.71,

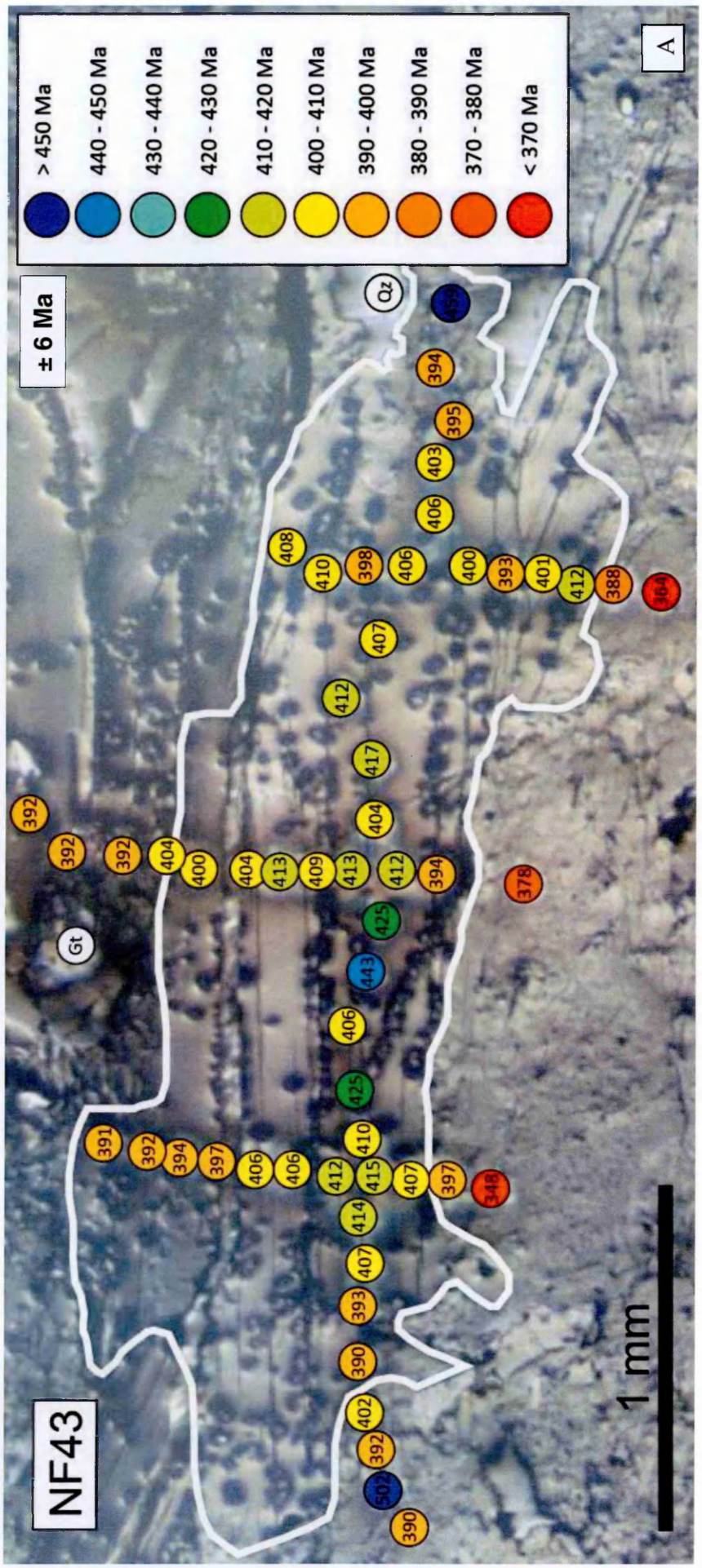
NF43
± 6 Ma
> 450 Ma
440 - 450 Ma
430 - 440 Ma
420 - 430 Ma
410 - 420 Ma
400 - 410 Ma
390 - 400 Ma
380 - 390 Ma
370 - 380 Ma
< 370 Ma
Qz
Gt
1 mm
A

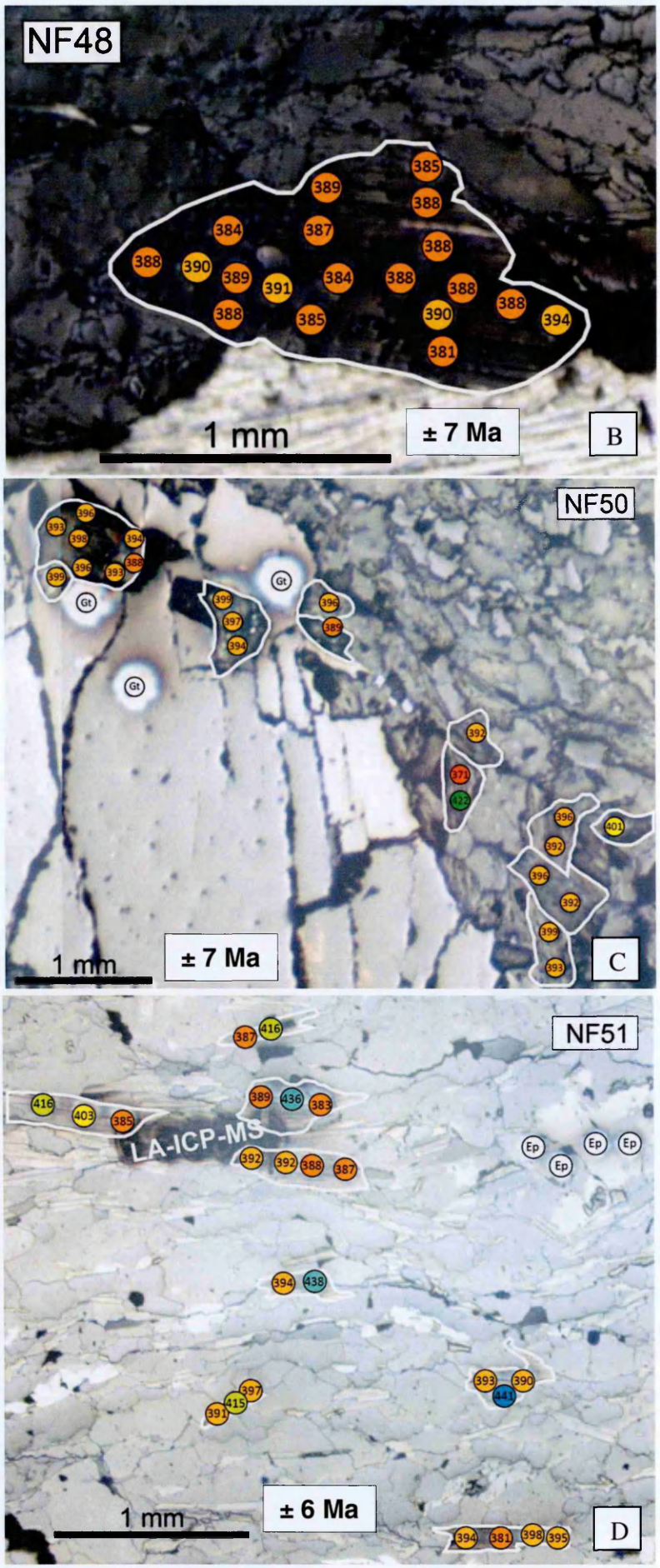

Figure 3.4: Photomicrographs of the *in-situ* UV laser ablation $^{40}Ar/^{39}Ar$ analyses. A and B show analyses of white mica grains while C and D show analyses of biotite grains. (A) Sample NF43 (**Group 1a**), (B) White mica from sample NF48 (**Group 1b**), (C) Biotite from sample NF50 (**Group 1c**), (D) **Group 2b** gneiss (sample NF51).

0.46-0.51, 0.53-0.58, 0.40-0.51, and 0.37-055 for **Groups 1a-c** and **Groups 2a-b**, respectively.

A way to test whether the composition of the analysed mica has an effect on the resulting $^{40}Ar/^{39}Ar$ age is to compare the $^{37}Ar/^{39}Ar$ and $^{38}Ar/^{39}Ar$ ratios with age. ^{37}Ar is produced from Ca and ^{38}Ar is produced from Cl during the irradiation process and these ratios reflect the Ca/K and the Cl/K ratios. In Fig 3.5.A and 3.5.B the $^{37}Ar/^{39}Ar$ and $^{38}Ar/^{39}Ar$ vs. age are shown for the single grain fusion dataset for all analysed samples. 97% of white mica and 99% of biotite $^{37}Ar/^{39}Ar$ ratios lie between 0 and +0.2. 98% of white and 99% of biotite $^{38}Ar/^{39}Ar$ data lie between 0.005 and 0.02. These plots show that there is no statistical correlation between age and the Ar isotopic composition of the micas (regardless of mineral type and despite the varying geochemistry of the micas) and therefore no link between mineral chemistry and $^{40}Ar/^{39}Ar$ age.

The *In-situ* laser ablation dataset also shows a correlation in $^{37}Ar/^{39}Ar$ and $^{38}Ar/^{39}Ar$ vs. age (Fig. 3.5.C and 3.5.D). 96% of white mica and 98% of biotite $^{37}Ar/^{39}Ar$ ratios lie between 0 and 1. However, there is a difference in the $^{38}Ar/^{39}Ar$ ratios when compared with the single grain fusion dataset. 99 % of white mica ratios lie between 0.005 and 0.02 but there is a pattern in the $^{38}Ar/^{39}Ar$ ratios of the biotite. Different samples cluster together and have different ranges in $^{38}Ar/^{39}Ar$ ratios. These clusters do not relate to the petrographic groups as **Group 1a** gneisses (NF42 and NF43) group with **Group 2b** gneiss NF91. Instead this apparent spread in $^{38}Ar/^{39}Ar$ vs. age is due to the higher sensitivity of the Nu instruments Nobelesse over the MAP215-50 used for the *in-situ* analyses.

3.6.3 Comparison between new and previously published ages and age ranges

The yielded $^{40}Ar/^{39}Ar$ ages span the timing of the entire metamorphic cycle from prograde metamorphism at c. 420-404 Ma (Sm-Nd and Lu-Hf garnet; Kylander-Clark *et al.,* (2007), through peak metamorphism at c. 405-400 Ma (U-Pb zircon; Root *et al.,* (2005) to the timing of amphibolite-facies recrystallization at c. 399-379 Ma (U-Pb titanite; Spencer *et al.,* (2013).

15% of all white mica and 38% of all biotite single grain fusion ages fall within the 20 Ma spread in the U-Pb titanite ages (Spencer *et al.,* 2013), with 85% of white mica and 59% of biotite ages being older. Only 56% of the *in-situ* white mica ages fall within the range of titanite ages, with 41 % being older. Biotite *in-situ* data yield a more tightly constrained dataset with 73% of biotite $^{40}Ar/^{39}Ar$ ages falling within the range of the titanite age and only 11% being older.

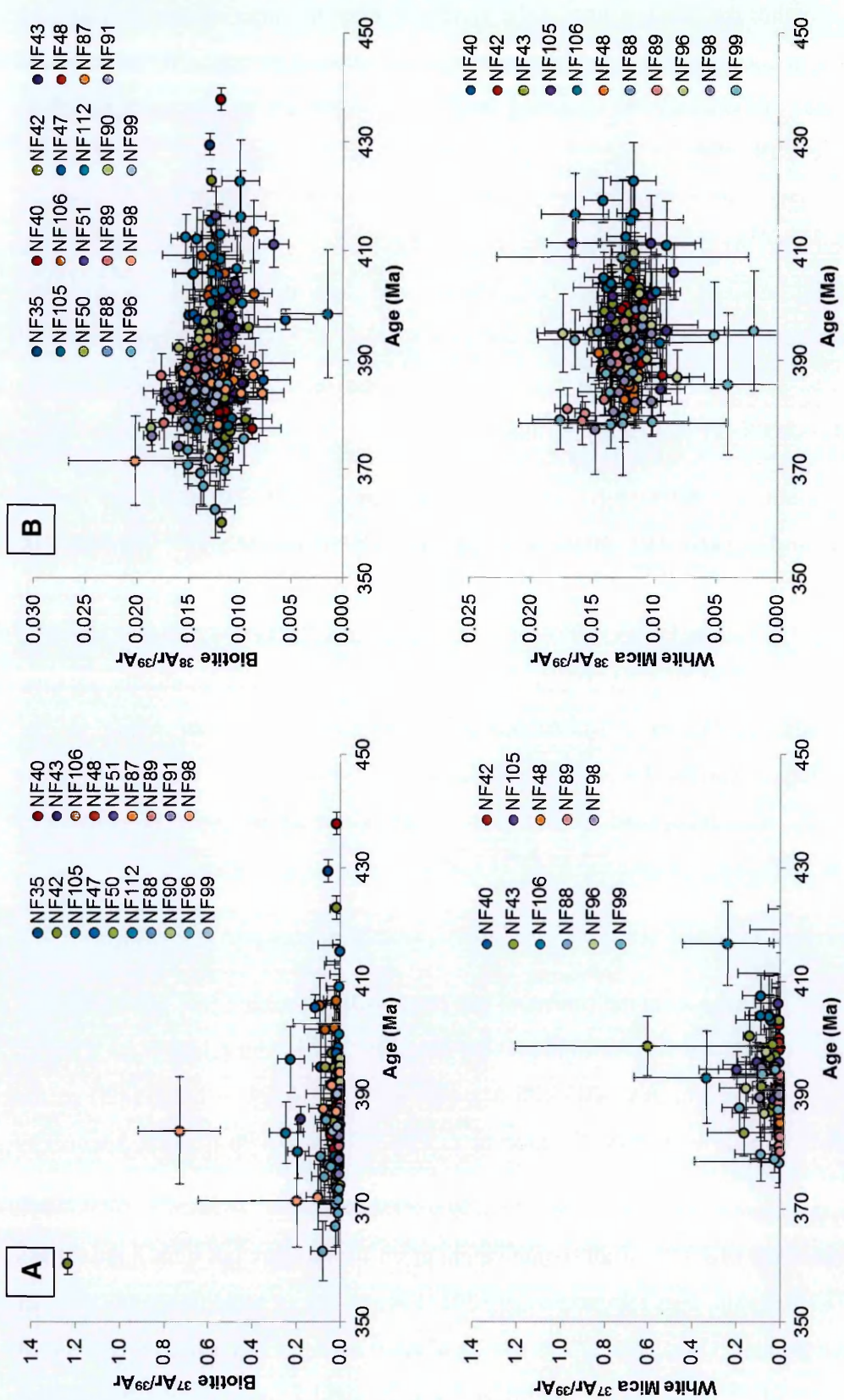

Figure 3.5: Plots of the A) $^{37}Ar/^{39}Ar$ and B) $^{38}Ar/^{39}Ar$ vs. age for all analyses samples of white mica and the biotite from the single grain fusion datasets showing little correlation between age and the isotopic composition of the mica.

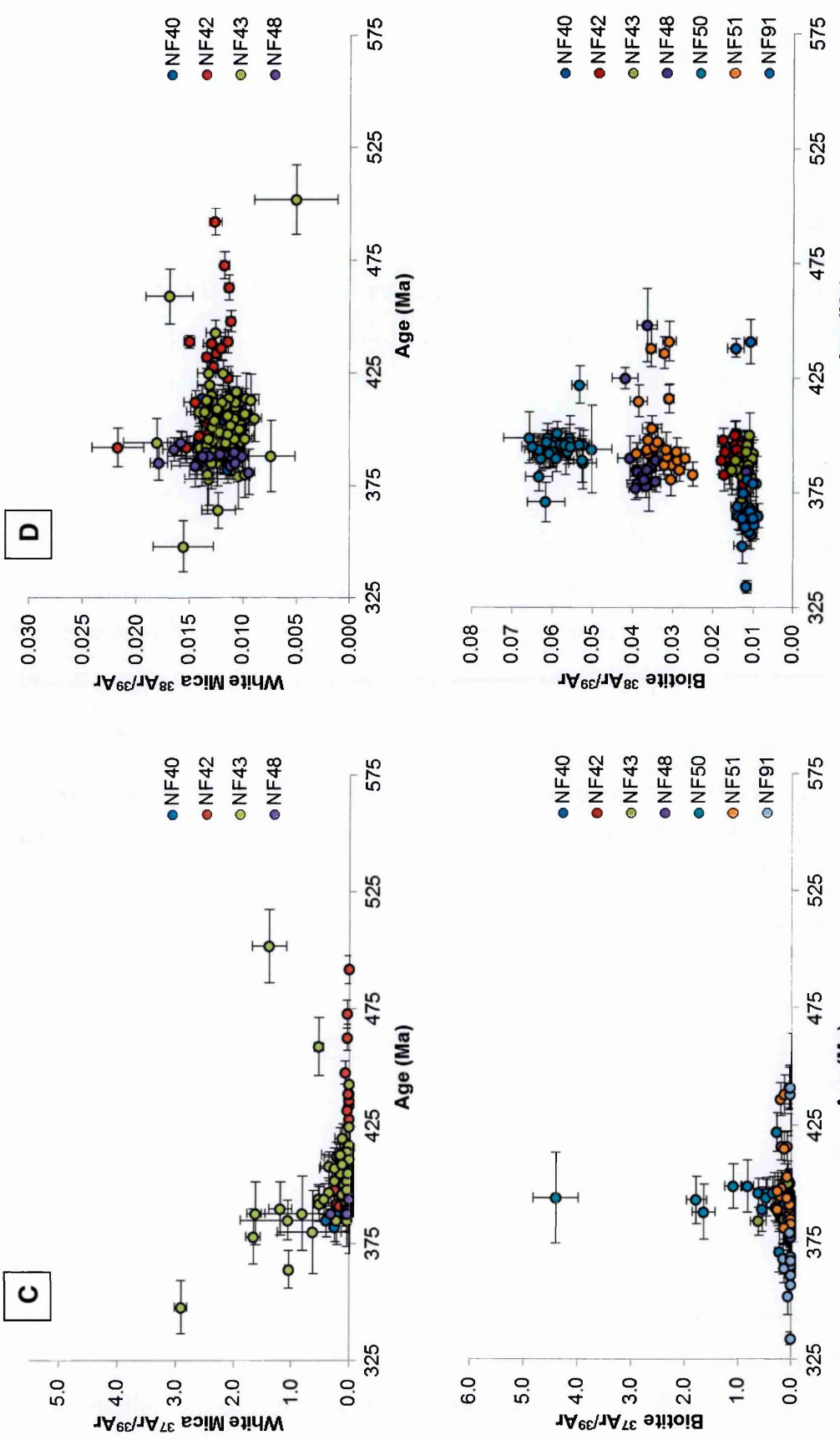

Figure 3.5: Plots of the C) $^{37}Ar/^{39}Ar$ and D) $^{38}Ar/^{39}Ar$ vs. age for all analyses samples of white mica and the biotite from the *in-situ* datasets showing little correlation between age and the isotopic composition of the mica.

Published white mica $^{40}Ar/^{39}Ar$ step heating plateau ages for the Outer Nordfjord area, range from 389-374 Ma (Andersen *et al.,* 1998, Hacker & Gans 2005, Root *et al.,* 2005, Walsh *et al.,* 2007, Young *et al.,* 2011, Walsh *et al.,* 2013). White mica single grain fusion and *in-situ* $^{40}Ar/^{39}Ar$ ages from this study range from 423-377 Ma and 502-348 Ma, respectively. This is a far greater range than what is observed in the step heating plateau ages. This spread is due, in part, to step heating method masking Ar distributions by averaging within grain Ar variability.

Published biotite $^{40}Ar/^{39}Ar$ step heating plateau ages range from 467-379 Ma (Hacker & Gans 2005, Root *et al.,* 2005). Biotite single grain fusion and *in-situ* analysis from this study range from 438-360 Ma and 449-360 Ma, respectively. The range of biotite $^{40}Ar/^{39}Ar$ age from this study is well within the range of those observed in other studies.

The published plateau ages have been interpreted as representing the time at which the white mica and biotite cooled through T_c's of 400°C and 350°C (Andersen *et al.,* 1998, Hacker & Gans 2005, Root *et al.,* 2005, Hacker 2007, Walsh *et al.,* 2007, Young *et al.,* 2011, Walsh *et al.,* 2013). These studies however, did not consider the age data in terms of the metamorphic history and whether the application of the T_c formulation is applicable to these ages.

A single grain fusion and *in-situ* study of white mica from felsic lithologies from the Outer Nordfjord area showed that in detail, white mica ages are highly variable, both within and between samples with white mica $^{40}Ar/^{39}Ar$ ages that range from 413-379 Ma (Warren *et al.,* 2012a). The white mica $^{40}Ar/^{39}Ar$ ages from this study show a very similar spread (420-385 Ma).

The age ranges yielded by this study prove problematic for interpretation in terms of a cooling history because they span almost the entirety of the known timing of the metamorphic cycle. The different lithologies studied here allow the ages to be considered in relation to the recorded reaction history.

3.6.4 Ar (re)distribution during a metamorphic cycle

There are several possible explanations for the wide range of $^{40}Ar/^{39}Ar$ dates yielded within/between petrologically similar samples and within/between grains. These include the loss or gain of Ar due to diffusion, recrystallization, deformation, partial melting and/or the availability/influence of fluids.

3.6.4.1 Diffusion

In order to determine whether the white mica and biotite ages reflect diffusive loss during the exhumation of the WGR, it is useful to assess the $^{40}Ar/^{39}Ar$ ages that would be expected under the assumptions inherent in the Dodson (1973) T_c formulation and given the published constraints on the WGR P-T-t cycle. The amount of diffusion depends on: 1) the mineral type (diffusion parameters are different for different minerals), 2) grain size (maximum diffusion radius in most cases is taken to be the grain radius, and diffusive equilibration is faster in smaller grains); 3) the temperature, and to a lesser extent the pressure, history since crystallisation experienced by the grain being dated (the higher the initial temperature, and the lower the initial pressure the more rapidly diffusion will operate to reset the mineral's age), and 4) the grain boundary Ar concentration (an 'open' boundary, with low Ar concentration, will allow efficient Ar removal).

Ar diffusion was modelled numerically in order to determine the $^{40}Ar/^{39}Ar$ 'cooling' ages that would be expected for a purely diffusive, open system, given the P-T-t history of the WGR using DiffArg_inverse modified from Diffarg Wheeler (1996), (Warren *et al.*, 2012c). For a more in-depth explanation of the diffusion modelling, the reader is referred to Chapter 2. Two main model series were investigated:

(1) White mica models: an average grain radius of 0.5 mm was chosen, growing at peak conditions of 600-750°C at 2.3-3.5 GPa, representing the peak metamorphic conditions of the three chosen localities, since white mica forms part of the peak metamorphic assemblage in the felsic gneisses. This was followed by decompression to amphibolite-facies conditions of 700°C at 1GPa, 2 Ma later. This was subsequently followed by cooling at a rate of 25°CMa^{-1} from amphibolite-facies conditions, with decompression set so that P reaches zero at the same time as T.

(2) Biotite models: an average grain radius of 0.5 mm was chosen, growing at amphibolite-facies conditions of 700°C at 1.0 GPa. This was followed by cooling at a rate of 25°CMa^{-1} from amphibolite-facies conditions, with decompression set so that P reaches zero at the same time as T.

Petrographic studies of biotite show that it grew during the decompressive breakdown of white mica and forms part of the amphibolite-facies assemblage. However, what is unknown is the exact point along the decompression path biotite began to grow. DiffArg_inverse does not have a pressure variable written into the code for biotite (*cf.* Chapter 2). This is because experimental data has shown that pressure has a negligible

effect on Ar diffusion in biotite above 0.4 GPa (Harrison *et al.* 1985). Therefore, as the decompression path from peak metamorphic conditions is isothermal, with only changes in P, biotites were modelled from amphibolite-facies conditions.

The model results show that for an assumed cooling rate of 25°CMa^{-1}, white mica ages should be 8 Ma younger and biotite ages should be 13 Ma younger than the timing of cooling initiation. For a cooling initiation age of 393 Ma (weighted average U-Pb titanite for the Nordfjord area; Spencer *et al.,* (2013)) this means that white mica should yield bulk ages of 385 Ma with core-rim ages that range from 388-386 Ma. Biotite should yield bulk ages of 380 Ma and core-rim ages that range from 385-379 Ma.

It can be expected that mica from samples collected from the same locality would experience the same cooling history. The results of the diffusion models show that regardless of the timing of peak metamorphic conditions, white mica and biotite should only record the cooling from amphibolite-facies conditions because of the high temperatures involved. Since the temperature at amphibolite-facies conditions is ~700°C, much greater than the T_c's of white mica and biotite, volume diffusion should be efficient to reset the mica $^{40}Ar/^{39}Ar$ ages. This implies that the amphibolite-facies P-T conditions should have the greatest effect on the resulting white mica and biotite $^{40}Ar/^{39}Ar$ ages; all $^{40}Ar/^{39}Ar$ ages should in theory reflect the timing of cooling and exhumation.

The diffusion model results are sensitive to a number of input uncertainties, which can be divided into those that cause spread within the modelled ages and those that shift the whole population. Uncertainties that cause spread in the resulting modelled bulk ages are the grain size and the temperature. Variations in grain radius between 0.25-1 mm and variations in the amphibolite-facies temperatures of ± 50°C yield only a ± 2 Ma uncertainty in the modelled age. Input variables that shift the whole population are the diffusion parameters inherent within DiffArg_inverse, and the modelled cooling rate. The uncertainty in the diffusion parameters yields a ± 4 Ma uncertainty. These uncertainties are well within the 1σ error of the single grain fusion and *in-situ* $^{40}Ar/^{39}Ar$ ages observed in this study. Altering the cooling rate between 10-50°CMa^{-1} causes a -6 to a +2 Ma variance in the modelled age. This is also within the 1σ error of the single grain fusion and *in-situ* data. Differences in the cooling rate cannot provide an explanation for the heterogeneity observed in the single grain fusion and *in-situ* datasets, since different grains from a hand-specimen sized sample from the same locality would not experience differing cooling rates.

A key prediction of the pure diffusion model for Ar distribution is the presence of systematic core-rim age variations within grains. Ar loss by diffusion should result in grains with older cores and younger rims. Ar gain from the grain boundary could result in younger cores and older rims (Warren *et al.,* 2011). The *in-situ* white mica data, documented in this chapter and Chapter 4, reveals that $^{40}Ar/^{39}Ar$ ages are patchily distributed, with the oldest ages not concentrated within the geographic cores of the white mica grains and no clear-cut core-rim profiles. Biotite yields a relatively homogeneous spread in *in-situ* ages and yields little variation in age between the different petrographic types, despite the variations in composition and metamorphic grade. This, in conjunction with the spread in single grain fusion ages (for white mica and biotite both within and between the three localities) implies that diffusion was not the principal mechanism by which Ar was redistributed within both the white mica and the biotite, despite cooling from an ambient temperature of ~700°C during amphibolite-facies overprint (Spencer *et al.,* 2013).

3.6.4.2 Role of White Mica Breakdown

Mica recrystallization during metamorphism may exert a far greater influence on the resetting of isotopic ages than diffusion, and should outpace diffusion e.g. Villa (1997) and Allaz *et al.,* (2011). The garnet-bearing gneisses documented in this study clearly reflect the effects of increasing recrystallization along the retrograde metamorphic path on mica $^{40}Ar/^{39}Ar$ ages.

Under peak metamorphic conditions, white mica was the only stable K-bearing phase. As exhumation and decompression initiated and progressed, the white mica recrystallized via symplectization to biotite + plagioclase. Further recrystallization led to the loss of white mica, leaving biotite as the only K-bearing phase (Fig. 3A-C). 3 different samples (NF43, NF48 and NF50) document different stages of this. In general, biotite in samples which preserve white mica yields younger ages than the white mica (Fig. 3.6A and 3.6B).

Sample NF43 (**Group 1a**) documents the initial breakdown of white mica to biotite via symplectization. White mica single grain fusion $^{40}Ar/^{39}Ar$ ages in this sample range from 407-383 Ma with a weighted mean age of 394 Ma. Biotite yields 390-383 Ma with a weighted mean of 385 Ma (Fig. 3.6A and 3.6B).

Further breakdown of white mica to biotite leads to the formation of the **Group 1b** gneiss. In sample NF48, white mica yields younger $^{40}Ar/^{39}Ar$ ages than those of NF43, from 391-381 Ma, with a weighted mean age of 386 Ma. Biotite conversely shows similar $^{40}Ar/^{39}Ar$

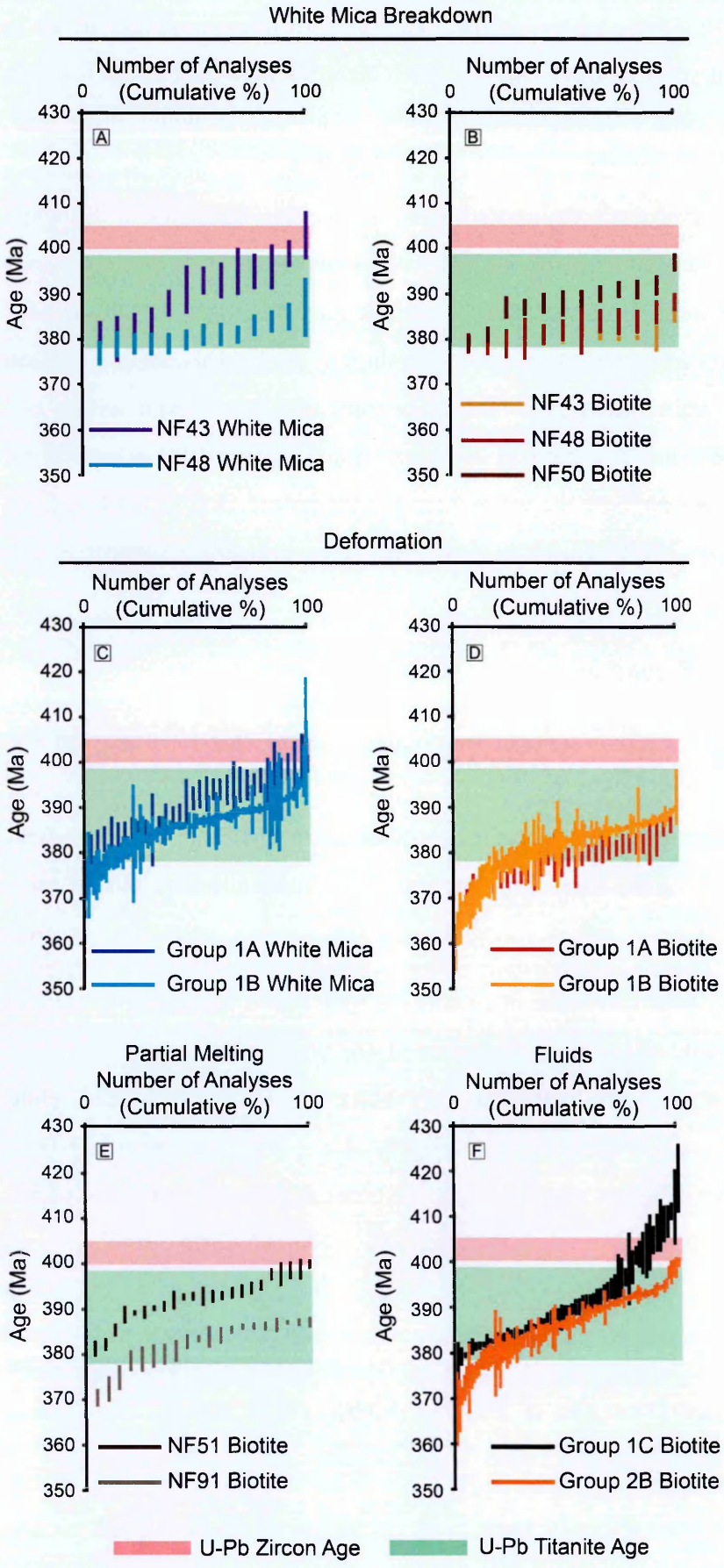

Figure 3.6: Cumulative graphs of single-grain fusion data. A and B show the effects of recrystallization on white mica and biotite ages between sample NF43, NF48, and NF50. C shows the effect of deformation between two samples of biotite-epidote gneiss NF51 and NF91. D shows a comparison between garnet-biotite and biotite-epidote gneisses showing the possible effects of fluid interaction in the rock on the $^{40}Ar/^{39}Ar$ biotite ages. The red boxes represent the U-Pb zircon ages for the timing of peak metamorphism of Root *et al.*, (2004) and the green boxes represent the U-Pb titanite ages of the amphibolite-facies recrystallization of Spencer *et al.*, (2013).

ages as NF43, with a range from 392-383 Ma and a weighted mean age of 387 Ma (Fig. 3.6A and 3.6B).

This younging shift in the white mica $^{40}Ar/^{39}Ar$ ages and a corresponding "aging" of the biotite $^{40}Ar/^{39}Ar$ dates demonstrates that there is a loss of the "old" Ar from the white mica and only a corresponding partial uptake of Ar by biotite during the recrystallization process. Overall, recrystallization has led to an apparent 8 Ma decrease in the weighted mean white mica age and a 2 Ma increase in the weighted mean biotite age.

The loss of the white mica (documented in the **Group 1c** gneisses, Fig. 3.6B) is reflected in the remaining biotite data by a shift towards older ages. Sample NF50 yielded biotite $^{40}Ar/^{39}Ar$ ages that range from 401-391 Ma, with a weighted mean age of 392 Ma (Fig. 3.4A-C). This continued shift towards older biotite ages implies continued uptake of Ar from the white mica, as older ages are otherwise inconsistent with the later crystallisation of biotite.

In-situ analyses of the white micas from samples NF43 and NF48 show patchy distributions of Ar, older patches of 443-425 Ma and younger patches of 397-391 Ma. In contrast, biotite from samples NF43, NF48 and NF50 shows much more homogeneously distributed Ar, both within and between grains. The combination of single grain fusion and *in-situ* analyses therefore show that Ar is released from different grain reservoirs at different times as the white micas recrystallizes, creating varying fluxes in the grain boundary network Ar concentration.

3.6.4.3 Role of Deformation

Deformation can affect Ar isotope concentration within different portions of the same mineral by:

(i) Decreasing the grain size (which affects diffusion rate) (Reddy & Potts 1999, Camacho *et al.,* 2012), and by

(ii) Forming microstructural defects, including dislocations and micropores, that effectively increase the rate at which Ar can migrate through a grain by orders of magnitude compared to volume diffusion (Reddy & Potts 1999, Camacho *et al.,* 2012). In order for these defects to be effective sinks for Ar, they must connect to an external reservoir (i.e. the grain-boundary network) to allow Ar loss. Without this connection, these defects may trap ^{40}Ar within the mineral (Camacho *et al.,* 2012).

Evidence for the effect of exhumation-related deformation on the Ar ages yielded by the felsic lithologies can be demonstrated by comparing the single grain fusion white mica and biotite $^{40}Ar/^{39}Ar$ ages from **Group 1a** gneisses and **Group 1b** gneisses (Fig. 3.3A and B). **Group 1a** gneisses preserve biotite-plagioclase symplectites that form from the breakdown of white mica. These structures are delicate and indicate that little or no deformation affected these gneisses during and/or after decompression (Hacker *et al.,* 2010). These gneisses also preserve relicts from the HP evolution which are not documented in the other gneiss groups. White mica from **Group 1a** gneisses range in $^{40}Ar/^{39}Ar$ age from 407-383 Ma with a weighted mean age of 394 Ma while biotite range in age from 438-360 Ma with a weighted mean age of 382 Ma.

As deformation increases and the **Group 1b** gneisses develop, the delicate symplectite structures are lost and replaced by the development of a gneissose fabric formed from biotite + plagioclase. White micas become kinked, folded and form "fish" and the HP relicts are lost. The white mica also has a greater difference in the Si content from core to rim than white mica from **Group 1a** gneisses. White mica in these gneisses yield a broader range of $^{40}Ar/^{39}Ar$ age, with a mean age that is younger than that observed in the **Group 1a** gneisses, ranging from 423-378 Ma (weighted mean 392 Ma). Biotite from these gneisses also yield a broader spread in age from 414-363 Ma, with an older weighted mean age of 389 Ma compared to **Group 1a**.

The $^{40}Ar/^{39}Ar$ ages from these two petrographic types of gneiss show that deformation and the formation of the gneissose fabric from the original symplectic texture results in an overall decrease in the weighted mean age difference between the white mica and the biotite chronometers (13 Ma in the **Group 1a** gneisses and only 5 Ma in the **Group 1b** gneisses). This implies that during deformation, Ar is redistributed between the white mica and the biotite, leading to their ages converging.

3.6.4.4 Role of Migmatisation

Migmatites have been documented in many exhumed HP metamorphic complexes (Faure *et al.,* 1999, Hermann *et al.,* 2001, Ganzhorn *et al.,* 2014), with their formation in many places (including the WGR) linked to decompression from eclogite to the amphibolite facies conditions (Labrousse *et al.,* 2002). At Drage, the amphibolite-facies gneisses show intense migmatisation. A key **Group 2b** gneiss (sample NF91), shows similar petrography to sample NF51 from Flatraket Harbour, although the latter shows no evidence for migmatisation.

Biotite from NF91 yielded $^{40}Ar/^{39}Ar$ ages that range from 391-374 Ma with a mean age of 389 Ma. Sample NF51 yields much older ages from 417-385 Ma with a weighted mean age 396 Ma; (Fig. 3.6B). Migmatisation therefore appears to have acted to increase the interconnectivity of the grain boundary network, hence aiding the local removal of Ar from biotite. Overall migmatisation led to a younging in the weighted mean biotite $^{40}Ar/^{39}Ar$ ages of 7 Ma.

3.6.4.5 Role of Fluids

Fluids may control the redistribution and resetting of $^{40}Ar/^{39}Ar$ mineral ages in metamorphic rocks (Cumbest *et al.,* 1994, Kelley 2002). Fluids can be derived internally, from dehydration reactions during retrogression (e.g. symplectization of white mica produces biotite + plagioclase + fluid), or be derived from external sources (e.g. from surrounding lithologies).

The behaviour of Ar at the mineral-grain boundary interface depends strongly upon the concentration of Ar in the fluid and the temperature. Ar, being a highly incompatible trace element, strongly partitions into the grain boundary network. This partitioning is dependent on the temperature and salinity of the fluid (Kelley 2002). If the fluid is super-saturated in Ar and the temperature is high, Ar will potentially diffuse into the mineral (Warren *et al.,* 2011). If the fluid has a low concentration of Ar and the temperature is high, then Ar will diffuse out of the grain and into the fluid. If there is no fluid present in the grain boundary network, Ar will remain within the mineral since there is no host for Ar outside the grain, unless of course it partitions into a neighbouring grain.

The felsic lithologies of the Outer Nordfjord region preserve evidence for fluid-based reactions during their decompression history. The white mica breaks down during the decompression and forms biotite + plagioclase. This reaction releases fluid. In contrast, the replacement of garnet (**Group 1c** gneisses) by epidote–group minerals (**Group 2b** gneisses) consumes water. Together these reactions show that water was both produced and consumed in the felsic rocks during the exhumation history, and that fluid was likely mobile at least on the local cm-scale.

The influence of fluid availability on the biotite $^{40}Ar/^{39}Ar$ age data between garnet-bearing and epidote-bearing lithologies can clearly be seen (Fig. 3.6C). The garnet-bearing rocks of **Group 1c** yield biotite ages of 423-382 Ma (weighted mean age 389 Ma). The epidote-bearing rocks of **Group 2b** yield older ages of 430-374 Ma (weighted mean age of 395 Ma). Fluid percolation within these gneisses has thus increased the weighted mean single

grain fusion biotite age by ~5 Ma and increased the age range from 41 Ma to 56 Ma. Conversely, the percolation of fluids within these gneisses has reduced the youngest biotite $^{40}Ar/^{39}Ar$ age by 8 Ma, from 382 Ma to 374 Ma.

In-situ biotite analyses from NF50 of **Group 1c** and NF51 of **Group 2b** indicate an opposite trend. The age spread within each sample is lowered from **Group 1c** to **Group 2b** (441-381 Ma and 422-371 Ma, respectively). The weighted means of these samples are, however, identical at ~395 Ma, and the range in biotite $^{40}Ar/^{39}Ar$ ages is reduced from 60 Ma to 51 Ma.

On the petrographic-scale, the single grain fusion analysis shows that the fluids involved during the exhumation of the WGR acted as an Ar source, elevating the mean ages. On the individual sample-scale, *in-situ* analysis shows that the fluids behaved (at least partially) as a sink for Ar, reducing the overall range of biotite ages by ~9 Ma and the youngest biotite $^{40}Ar/^{39}Ar$ age by ~10 Ma. Therefore although fluids clearly played a role in re-distributing Ar within and between samples during the metamorphic cycle, the overall effect is complex.

3.6.5 Summary

Recrystallization caused white mica weighted mean ages to be reduced by ~8 Ma and biotite weighted mean ages to increase by ~5 Ma. Recrystallization also reduced the spread in the age ranges from 24 Ma to 10 Ma in the white mica and causes the biotite age spread to increase from 7 Ma to 10 Ma. Deformation reduced white mica weighed mean ages by ~2 Ma and increased the biotite weighted mean ages by ~7 Ma. However, unlike recrystallization, deformation caused the spread in white mica ages to increase from 24 Ma to 45 Ma and reducd the spread in biotite age data from 78 Ma to 51 Ma. The process of migmatisation reduced the weighted mean biotite ages in the amphibolite-facies gneisses by ~7 Ma and caused the spread in $^{40}Ar/^{39}Ar$ biotite ages to increase from 17 Ma to 32 Ma. Finally, the influx of fluids into the gneisses resulted in an increase in the weighted mean biotite ages by ~5 Ma and an increase in the spread in ages data from 41 Ma to 56 Ma.

3.7 Consequences for the Interpretation of Metamorphic Ar Ages

Geochemically-similar felsic gneisses in the Outer Nordfjord area of the WGR record different 'snapshots' of the exhumation-portion of the PT path. White mica and biotite $^{40}Ar/^{39}Ar$ ages and age ranges progressively change as the lithology changes, but not in a simple way.

The 30 Ma mean spread between oldest and youngest $^{40}Ar/^{39}Ar$ white mica single grain fusion ages and 31 Ma mean spread in biotite single grain fusion ages across and within different samples cannot be explained in terms of pure diffusion. Instead, these data record a complex interplay between recrystallization, deformation, partial melting and fluid percolation, all of which have had an impact on the local Ar isotopic signature. No one single process appears to have dominated, and no single sample has an easily-interpretable pattern of $^{40}Ar/^{39}Ar$ ages.

White micas, which were stable at peak metamorphic conditions, do not show the core-rim age profiles that would be expected from simple diffusive-loss histories. Despite ~700°C temperatures estimated for both the peak metamorphic conditions and the amphibolite-facies overprint (Spencer *et al.,* 2013); thermally-activated volume diffusion appears to have been inefficient at removing Ar from the white mica.

Biotite in many samples can be clearly texturally linked to white mica breakdown, suggesting that it formed during exhumation. The yielded ages suggest that the biotite did not crystallise in an environment in which ^{40}Ar concentrations were negligible. The single grain fusion and *in-situ* biotite ages are younger than the timing of peak metamorphism at c. 405-400 Ma but, 77% of the single grain fusion and 79% of the *in-situ* ages correlate with the timing of amphibolite-facies recrystallization (estimated at 399-379 Ma from U-Pb titanite; Spencer *et al.,* (2013)). Diffusion modelling suggests that biotite ages should be younger than the timing of the amphibolite-facies overprint by at least 11 Ma. However, the correlation between titanite U-Pb and biotite $^{40}Ar/^{39}Ar$ ages implies instead that biotite age data may reflect crystallisation at amphibolite-facies conditions.

The breakdowns of the assumptions in the T_c formulation (no diffusion and Ar in the grain at the time of crystallisation) suggest that the Outer Nordfjord $^{40}Ar/^{39}Ar$ dates cannot represent the timing of cooling through T_c's of ~400-450°C for white mica and ~300°C for biotite (Grove & Harrison 1996, Harrison *et al.,* 2009). This study instead demonstrates that during the exhumation of the WGR, the diffusive redistribution of Ar within micas in felsic lithologies was overwhelmed by Ar redistribution caused by recrystallization, deformation and fluids.

This study also demonstrates how the $^{40}Ar/^{39}Ar$ thermochronological technique can be applied to understand the physical processes that affect metamorphic terranes during exhumation. Lithologies that preserve different portions of the same PT path and record different amounts of recrystallization, deformation, migmatisation, and fluid interactions

preserve different ages. These samples (in conjunction with diffusion modelling) allow the behaviour of Ar during exhumation-related retrograde metamorphism to be documented, assessed and quantified.

3.8 Conclusions

Geochemically-similar felsic gneisses from the Outer Nordfjord area of the UHP Western Gneiss Region, Norway preserve textural and petrological evidence of different stages of the exhumation from mantle- to mid-crustal-depths. Gneisses can be differentiated into two main groups: garnet-bearing gneisses that record decompression from eclogite-facies to upper amphibolite-facies (Group 1), and biotite-epidote gneisses that record the main amphibolite-facies overprint and associated deformation that is ubiquitous of the WGR (Group 2). These samples, and the snapshots into the different parts of the decompression path that they record, provide a unique opportunity for exploring how Ar is incorporated into, hosted by, and ultimately lost by different K-bearing minerals during metamorphism.

White mica and biotite separates analysed via single-grain fusion yield a spread in ages from 411 Ma to 383 Ma and 430 Ma to 360 Ma, respectively. UV laser ablation *in-situ* analyses of white mica reveal a similar (but older, 502-349 Ma) spread in ages within individual grains, and no clear core-rim patterns. *In-situ* analyses of biotite yield a similar, yet slightly older age spread than the single-grain fusion data (449-357 Ma).

Numerical modelling using DiffArg_inverse predicts that white mica and biotite from the WGR should reflect cooling post-amphibolite-facies conditions given the P-T-t history that is known from other HT chronometers (e.g. U-Pb zircon) and from P-T modelling. However, $^{40}Ar/^{39}Ar$ single grain fusion and *in-situ* age data from white mica and biotite yield highly heterogeneously distributed ages that vary between rocks of differing petrography yet are of similar geochemical composition.

The white mica and biotite $^{40}Ar/^{39}Ar$ dates cannot be explained in terms of simply cooling through a mineral-specific T_c as more than one of the inherent assumptions built in the Dodson (1973) T_c formulation are violated. Whist diffusion may have been in operation during the exhumation of the WGR (the temperatures experienced during the amphibolite-facies overprint were ~700°C), the physical processes that affected these gneisses during exhumation, including recrystallization, deformation, partial melting and the interaction of fluids, had a greater effect on Ar isotopic signature at all scales from grain to outcrop.

Samples that show significant recrystallization and deformation yield younger white mica ages than more pristine sample, but older biotite ages. Recrystallization, acts to reduce the apparent age spread in the white mica and increase the age spread in biotite ages. Deformation results in an inverse effect, by increasing the spread in white mica ages and decreasing the age spread in biotite. Furthermore, migmatisation acts to make biotite ages younger in the amphibolite-facies gneisses whereas fluid infiltration acts to increase biotite ages. Both migmatisation and fluid influx act to increase the resulting spread in biotite ages. Recrystallization, migmatisation, and fluid ingress have the greatest influence on the redistribution of Ar within crustal gneisses, whereas the effect of deformation is within the uncertainty of the $^{40}Ar/^{39}Ar$ age data.

This study shows that the interpretation of $^{40}Ar/^{39}Ar$ data collected from HT metamorphic terranes needs to be carefully considered by analysing multiple Ar chronometers (i.e. white mica and biotite) from multiple samples that record different parts of the metamorphic cycle, as this dataset shows that not all ages may be directly linkable to cooling. Instead, these data show that recrystallization, deformation, partial melting, and fluid flux play an important role in redistributing Ar in the crustal gneisses during decompression, despite the high metamorphic temperatures. This dataset has profound implications for interpreting $^{40}Ar/^{39}Ar$ ages from other HT and HP terranes. Data from different lithologies need to be considered on a case by case basis, in conjunction with detailed petrographic analysis, before $^{40}Ar/^{39}Ar$ mica ages can be interpreted.

Chapter 4

Symplectites: Tracking Ar though Metamorphic Reactions

Interlayered felsic gneiss and mafic eclogite at Drage

This chapter forms the paper:

McDonald, C. S., Warren, C. J., Regis, D., Kelley, S. P. & Sherlock, S. C. Symplectites: Tracking Ar though a Metamorphic Reaction. In prep for *Geology*.

Abstract

Metamorphic micas that crystallised at high temperatures are commonly thought to lose ^{40}Ar via thermally-driven diffusion. We report $^{40}Ar/^{39}Ar$ ages from a high temperature-high pressure metamorphic rock from the Western Gneiss Region, Norway, which preserves different mineralogical stages formed during decompression (2.4 -1.0 GPa) at 700°C. The effect of the breakdown of phengite to biotite-plagioclase symplectites on their $^{40}Ar/^{39}Ar$ ages was analysed using *in-situ* laser ablation techniques with <30μm spatial resolution. Phengite yielded ages ranging from 492-389 Ma, overlapping the previously reported ~405-400 Ma U-Pb zircon age interpreted as the timing of high pressure metamorphism at >2.6 GPa. Biotite and plagioclase in the symplectite yielded ages ranging from 389-380 Ma and 705-269 Ma, respectively, overlapping the previously reported U-Pb titanite ages that constrain the timing of the amphibolite-facies overprint at 1 GPa. Coarser, texturally later, biotite yielded a wider range of ages than the symplectite biotite (400-377 Ma). A pressure-temperature-time framework constructed using pseudosections, provides the relative order of crystallization and aids in the interpretation of whether $^{40}Ar/^{39}Ar$ ages can be related to cooling ages, crystallisation ages or contamination due to the presence ^{40}Ar within a closed grain boundary network. These samples show that even when rocks experience T>700°C for several Ma, Ar may not readily diffuse in mica and Ar ages may not be interpretable as a cooling age. Our data show the importance of understanding the petrographic evolution in order to provide a basis for interpreting the behaviour of Ar, thus allowing the $^{40}Ar/^{39}Ar$ data to be linked more accurately to a metamorphic 'stage'.

4.1 Introduction

$^{40}Ar/^{39}Ar$ dating is commonly used to constrain the timing and rate of cooling in high temperature metamorphic terranes via the closure temperature (T_c) formulation (Dodson 1973). This approach assumes that (1) the mineral in question (re)crystallised with an insignificant initial ^{40}Ar concentration; (2) thermally-activated volume diffusion, observing Fick's 2nd law, redistributed Ar within the mineral after its production and, (3) the grain boundary network surrounding the mineral had a sufficiently low Ar concentration and high connectivity to act as an infinite reservoir (i.e. an 'open' grain boundary system) during the time at which temperatures were high enough for efficient diffusion.

Many studies have shown metamorphic $^{40}Ar/^{39}Ar$ muscovite, phengite (high pressure (HP) muscovite) and biotite ages that are 'too old' to be interpreted as representing the timing of cooling when assessed within a chronological framework defined by higher temperature

(HT) chronometers such as U-Pb zircon e.g. (Baxter *et al.,* 2002, Warren *et al.,* 2012a). These studies have most commonly focussed on HP metamorphic terranes, where temperatures are commonly low (<600°C), the timescales of metamorphic cycles commonly short (<10 Ma), and fluid availability and permeability is low, thus limiting the efficiency of diffusion and efficiency of Ar removal from the grain boundary network. These limitations on diffusion have an impact on the T_c formulation, because if diffusion cannot operate then the application of the T_c to a metamorphic rock may be an invalid interpretation.

HP metamorphic rocks undergo a number of processes during exhumation, including recrystallization (*cf.* Chapter 3). It has recently been suggested that recrystallization may play a far greater role than diffusion in mobilising Ar during metamorphism and deformation (Villa 1997, Allaz *et al.,* 2011, Villa *et al.,* 2014). Recrystallization operates on a much faster timescale than diffusion, thus the determination of when the target mineral grew in the metamorphic cycle provides a key relative chronological framework for Ar age interpretation. Therefore, in HP metamorphic terranes where the T_c formulation may not operate, what effect does recrystallization have on the Ar systematics.

The common occurrence of symplectites in terranes that have decompressed from pressures > 2.0 GPa at temperatures >650°C provides an opportunity to test the effects of recrystallization at high temperatures on element remobilisation. Of specific interest to $^{40}Ar/^{39}Ar$ chronology is the breakdown of phengite to symplectites of biotite plus plagioclase. This reaction, and the symplectites it produces, provides an excellent opportunity to assess the transport distances, pathways, sources and sinks of ^{40}Ar in a K-rich assemblage as HT minerals break down and recrystallize during exhumation.

4.2 Petrography, Mineral Chemistry and P-T Evolution

The Western Gneiss Region (WGR) in Norway is a 50,000km^2 window into the lowest structural levels of the Scandinavian Caledonides (Hacker 2007). Eclogite-facies conditions reached 700-800°C and up to 3.6 GPa between 405-400 Ma (Root *et al.,* 2004, Hacker *et al.,* 2010). Exhumation of the WGR from UHP conditions to amphibolite-facies conditions within the lower crust was near-isothermal and was achieved by 399-379 Ma (U-Pb titanite; Spencer *et al.,* (2013)).

Eclogite-facies metabasites are hosted by biotite-epidote amphibolite-facies gneisses. Garnet-bearing gneisses preserving relicts of HP metamorphic assemblages are locally preserved in strain shadows around mafic boudins and preserve evidence of the

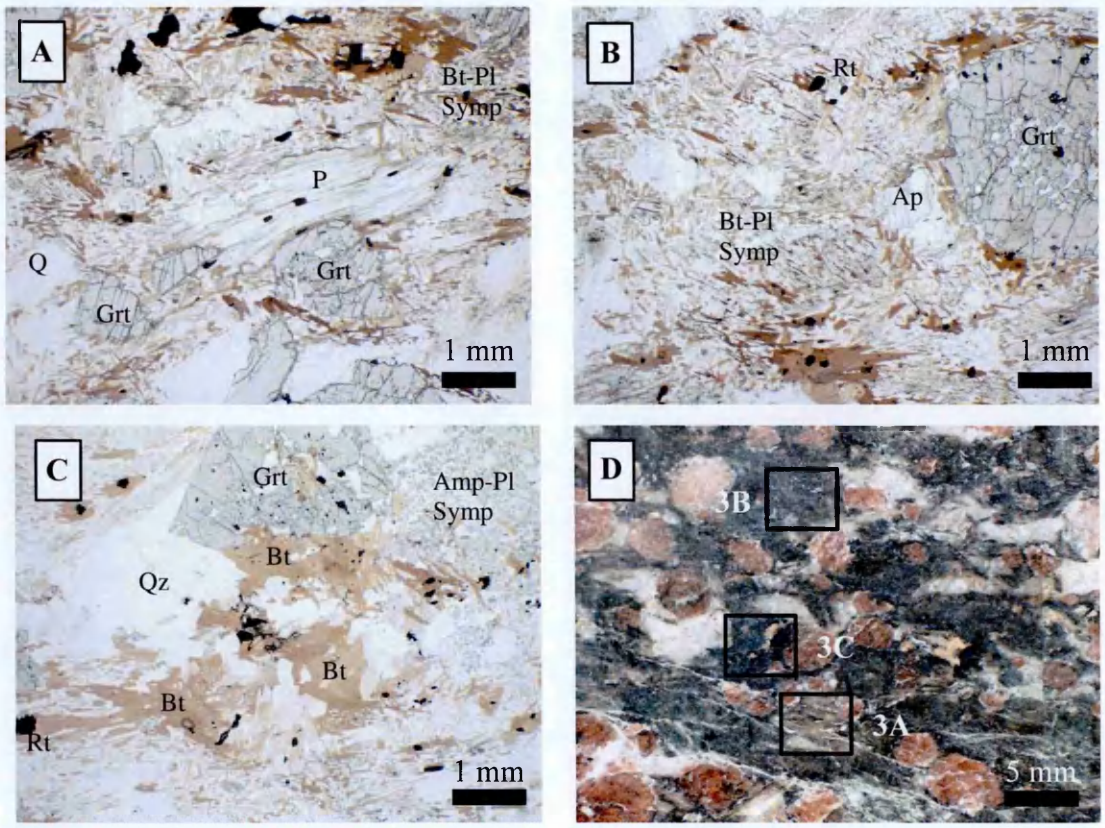

Fig. 4.1. Photomicrographs of symplectic gneiss; A) HP assemblage of Ph-Grt-Qtz; B) biotite-plagioclase symplectites after Ph; C) idioblastic biotite growing from the biotite-plagioclase symplectite and D) photograph of the polished slab showing the locations of the *in-situ* analyses in Fig. 4.3.

mineralogical transition from phengite to biotite via symplectization (Wain *et al.,* 2000). The preservation of the symplectites testifies to a lack of deformation during decompression (Hacker *et al.,* 2010). This lack of deformation means that this sample records only the effects of recrystallization on the Ar systematics.

Our sample (NF42 from Krokkenakken; Fig. 4.1) contains a peak assemblage of Grt + Ph + Qtz + Omp with an overprinting amphibolite-facies assemblage of Bt-Pl and Cpx-Amph-Pl symplectites after phengite and omphacite respectively, followed by a later generation of idioblastic Bt. Texturally, the idioblastic biotite represents continued biotite growth from the symplectites.

Major-element compositions of phengite, biotite and plagioclase were analysed on The Open University Cameca SX-100 electron microprobe using a defocussed 10μm beam, and conditions of 15 kV, 20 nA and 30 s collection time. Calibrations were performed on natural and synthetic standards and analyses were corrected using a ZAF matrix correction

Table 4.1
Average EMP Data of Sample NF42

Mineral	Phengite		Idioblastic Biotite		Symplectic Biotite		Plagioclase	
Position	Core	Rim	Core	Rim	Core	Rim	Core	Rim
SiO2	49.70	49.80	39.30	37.70	38.00	37.60	54.30	65.80
TiO_2	0.20	0.30	2.40	2.10	1.70	2.60	0.00	0.00
Al_2O_3	27.30	28.10	15.70	17.60	17.10	16.70	28.90	21.60
Cr_2O_3	0.00	0.00	0.00	0.10	0.10	0.10	0.00	0.00
FeO	2.00	1.70	10.90	12.80	12.40	13.70	0.00	0.10
MnO	0.00	0.00	0.00	0.00	0.00	0.00	0.00	0.00
MgO	3.70	3.20	16.40	14.50	16.10	14.60	0.00	0.00
CaO	0.00	0.00	0.00	0.00	0.00	0.10	11.60	2.40
Na_2O	0.40	0.30	0.10	0.10	0.10	0.10	5.20	10.40
K_2O	9.60	9.80	8.80	9.40	9.40	9.50	0.10	0.10
Cl	0.10	0.10	0.30	0.10	0.20	0.20	0.00	0.00
F	0.00	0.00	0.00	0.00	0.00	0.00	0.00	0.00
Total	93.00	93.40	93.90	94.50	95.10	95.10	100.00	100.40
Si	6.80	6.70	5.80	5.60	5.60	5.60	2.50	2.90
Ti	0.00	0.00	0.30	0.20	0.20	0.30	0.00	0.00
Al	4.40	4.50	2.70	3.10	3.00	2.90	1.50	1.10
Cr	0.00	0.00	0.00	0.00	0.00	0.00	0.00	0.00
Fe	0.20	0.20	1.30	1.60	1.50	1.70	0.00	0.00
Mn	0.00	0.00	0.00	0.00	0.00	0.00	0.00	0.00
Mg	0.70	0.70	3.60	3.20	3.50	3.20	0.00	0.00
Ca	0.00	0.00	0.00	0.00	0.00	0.00	0.60	0.10
Na	0.10	0.10	0.00	0.00	0.00	0.00	0.50	0.90
K	1.70	1.70	1.70	1.80	1.80	1.80	0.00	0.00
Cl	0.00	0.00	0.10	0.00	0.10	0.10	0.00	0.00
F	0.00	0.00	0.00	0.00	0.00	0.00	0.00	0.00
Total	13.90	13.90	15.60	15.60	15.70	15.70	5.00	5.00

Table 4.1. Representative core to rim electron microprobe analyses of phengite, biotite and plagioclase. Cations normalised at 22 O for phengite and biotite and 8 O for plagioclase feldspar.

routine. Analyses were bracketed by analysis of secondary standards to check for major element reproducibility of 1%. Representative core-rim analyses of phengite, biotite and plagioclase are shown in Table 4.1.

Phengite Si values range from 6.8 apfu in the geographic core to 6.6 at the rim (per 22 O) with grain sizes that vary from 300 μm to 1100 μm (Fig. 4.1A). Geochemical maps (Fig 4.2A) show that the Si composition is homogeneous throughout the grains, with only minor decrease in Si content at the very rim of the grains, that are < 50μm in thickness.

In the symplectite (Fig. 4.1B), plagioclase is intergrown with biotite. Plagioclase has a core-rim composition ranging from An_{45} to An_{11} and a typical grain size of 80 μm to 140 μm. Biotite grains within the symplectite form 40-200 μm laths that either form randomly orientated grains or pseudomorphs after the original phengite grain. These biotites are Mg-rich with Mg/(Mg+Fe) values of 0.65-0.70 and Ti contents ranging from 0.12-0.31 apfu. Geochemical maps of the symplectites are shown in Figs. 4.2B and 4.2C. The geochemistry maps show that the biotite within the symplectite is very homogeneous in composition and also that the biotite grains are coarsest at the edges of the original phengite grain and fine inwards. Plagioclase geochemical maps show that the grains are strongly zoned with high Ca-Al contents in the cores of the grains and low Ca-Al contents at the grain rims.

The idioblastic biotite grains (Fig. 4.1C) are Mg-rich with Mg/(Mg + Fe) values of 0.67-0.73 and Ti contents ranging from 0.21-0.32 apfu. Their diameter ranges from 300 μm to 1200 μm. Geochemical maps show that these grains are relatively homogeneous in composition (Fig. 4.2D).

The petrological evolution of the symplectic gneiss was modelled in the MnNCKFMASTH system using Perple_X version 6_6_8 (Connolly 1990), to determine the relative timing of the symplectite-forming reaction compared to the growth of titanite and the initiation of cooling. The pseudosection was calculated using the internally consistent thermodynamic dataset (hp11ver.dat) and the equation of state for H_2O (Holland & Powell 1998, Holland & Powell 2011). Solid solution models include garnet (Holland & Powell 1998), omphacite (Holland & Powell 1996), plagioclase (Newton *et al.,* 1980), K-feldspar (Thompson & Hovis 1979), phengite (Holland & Powell 1998), biotite (Tajčmanová *et al.,* 2009), chlorite (Holland *et al.,* 1998) and amphibole (Dale *et al.,* 2000). Pseudosections were employed to document (1) where in P-T space does phengite breakdown, (2) where in

P-T space does symplectization occur and biotite growth begins, (3) where titanite grows and (4) where cooling starts.

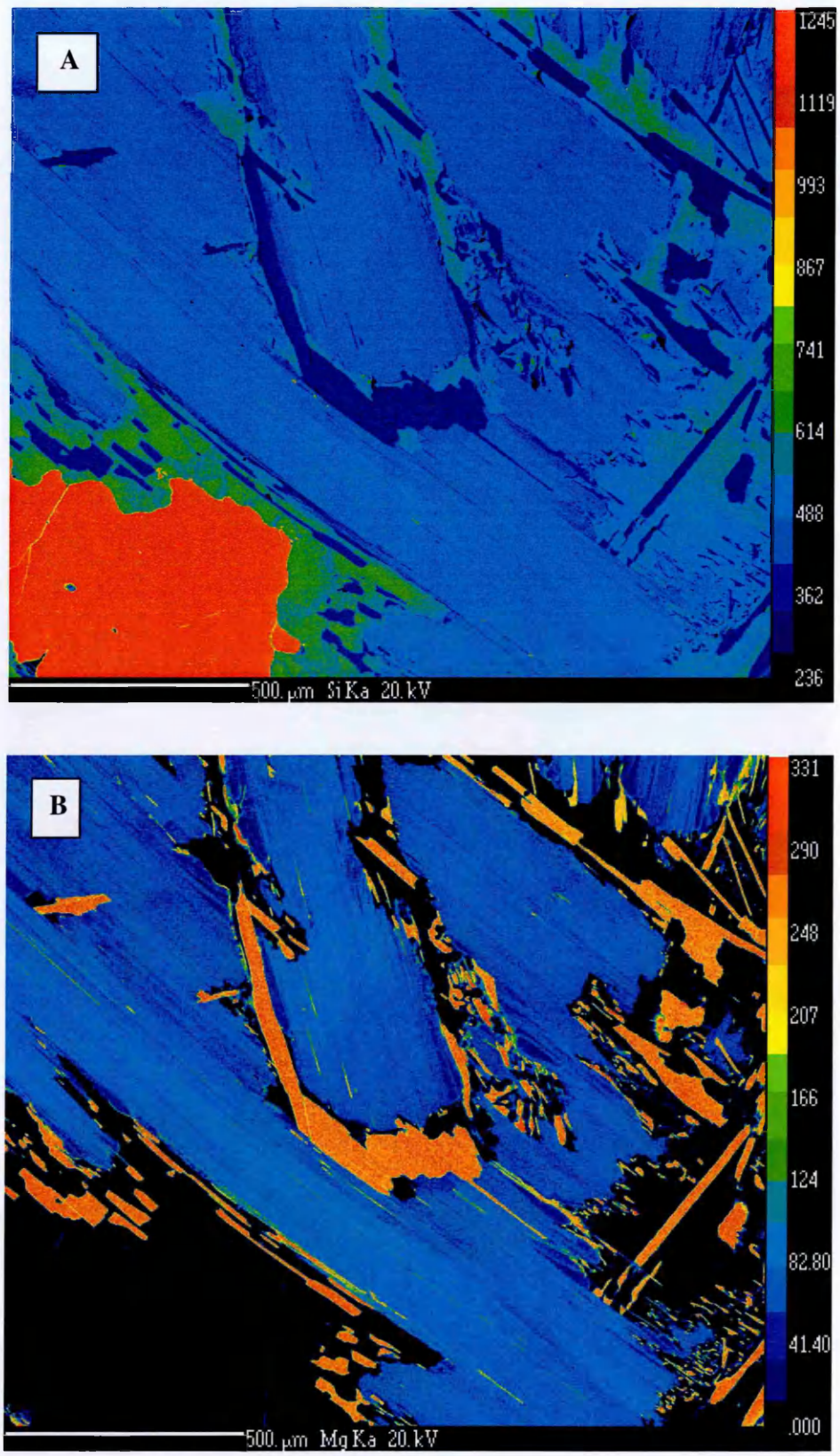

Fig. 4.2A. Geochemical maps of the phengite. A) Si map showing a homogeneous grains and B) Mg map showing that the phengite is surrounded by biotite.

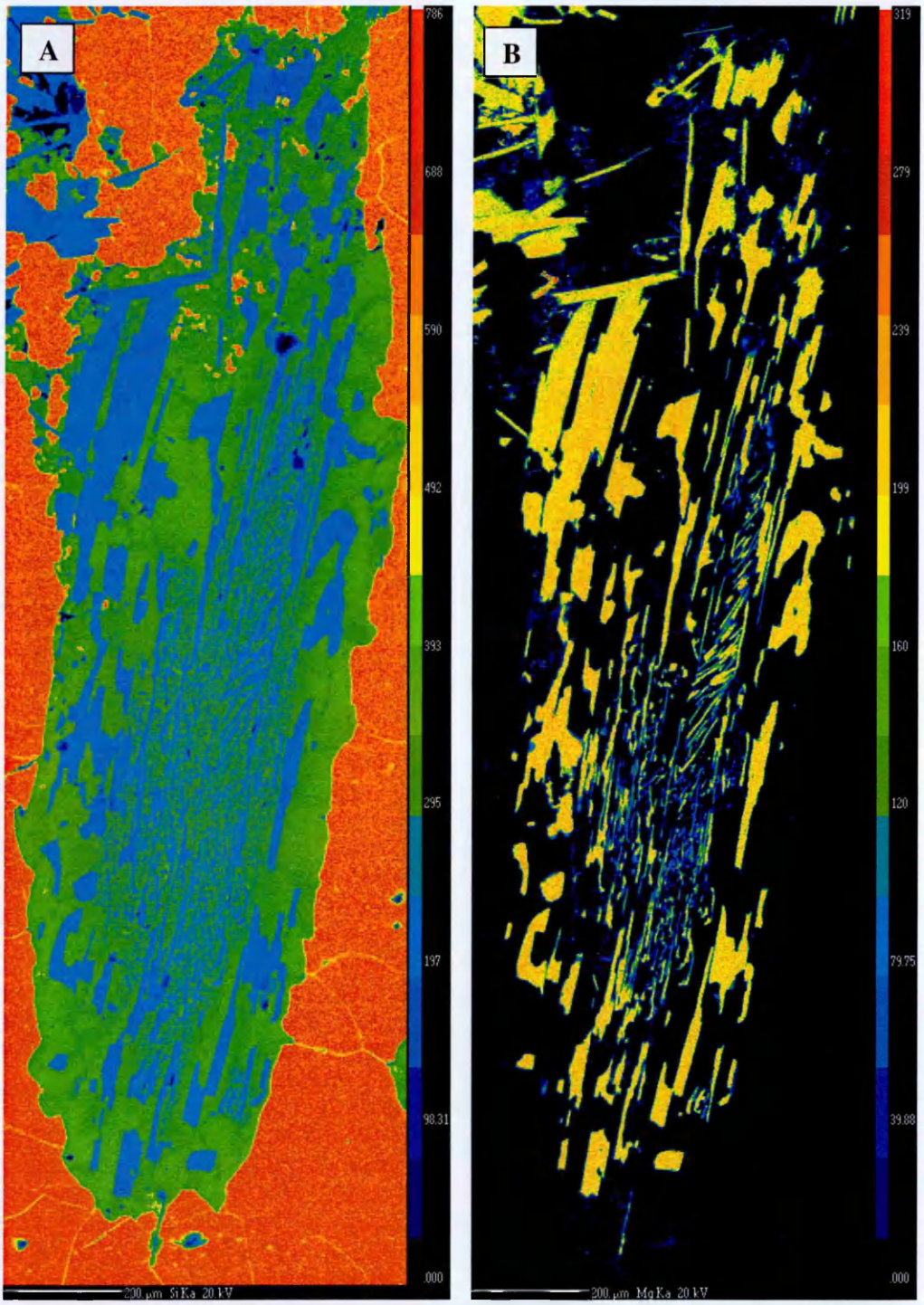

Fig. 4.2B. Geochemical maps of a symplectite that still preserves the original phengite grain morphology. A) Si map – orange: quartz, green: plagioclase and blue: biotite. B) a Mg map of the biotite that composes the symplectite showing homogeneous chemistry and a decrease in grain size from rim to core.

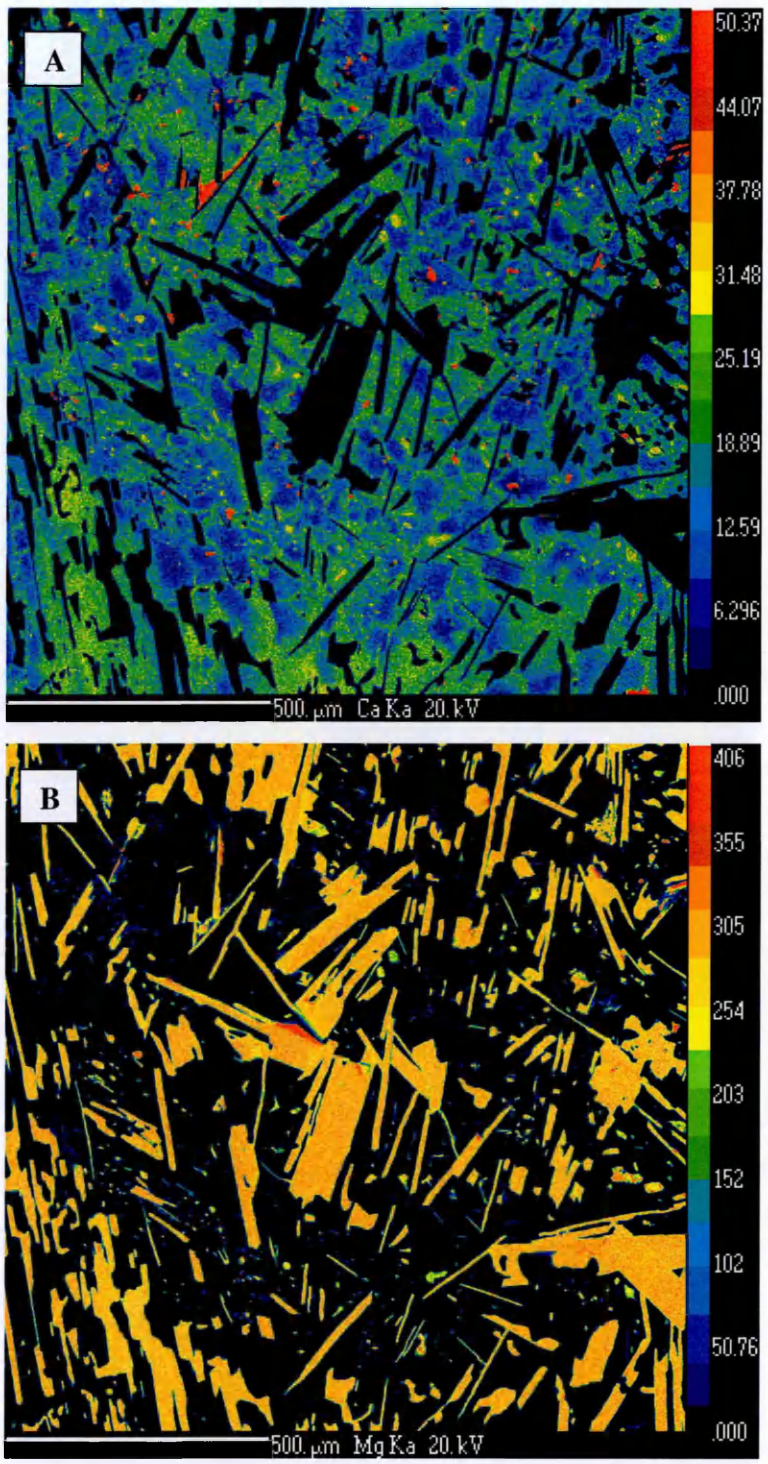

Fig. 4.2C. Geochemical maps of more randomly orientated biotite-plagioclase symplectites. A) Ca map showing zoned plagioclase within the symplectite and B) Mg map of the biotite showing homogeneous grain compositions.

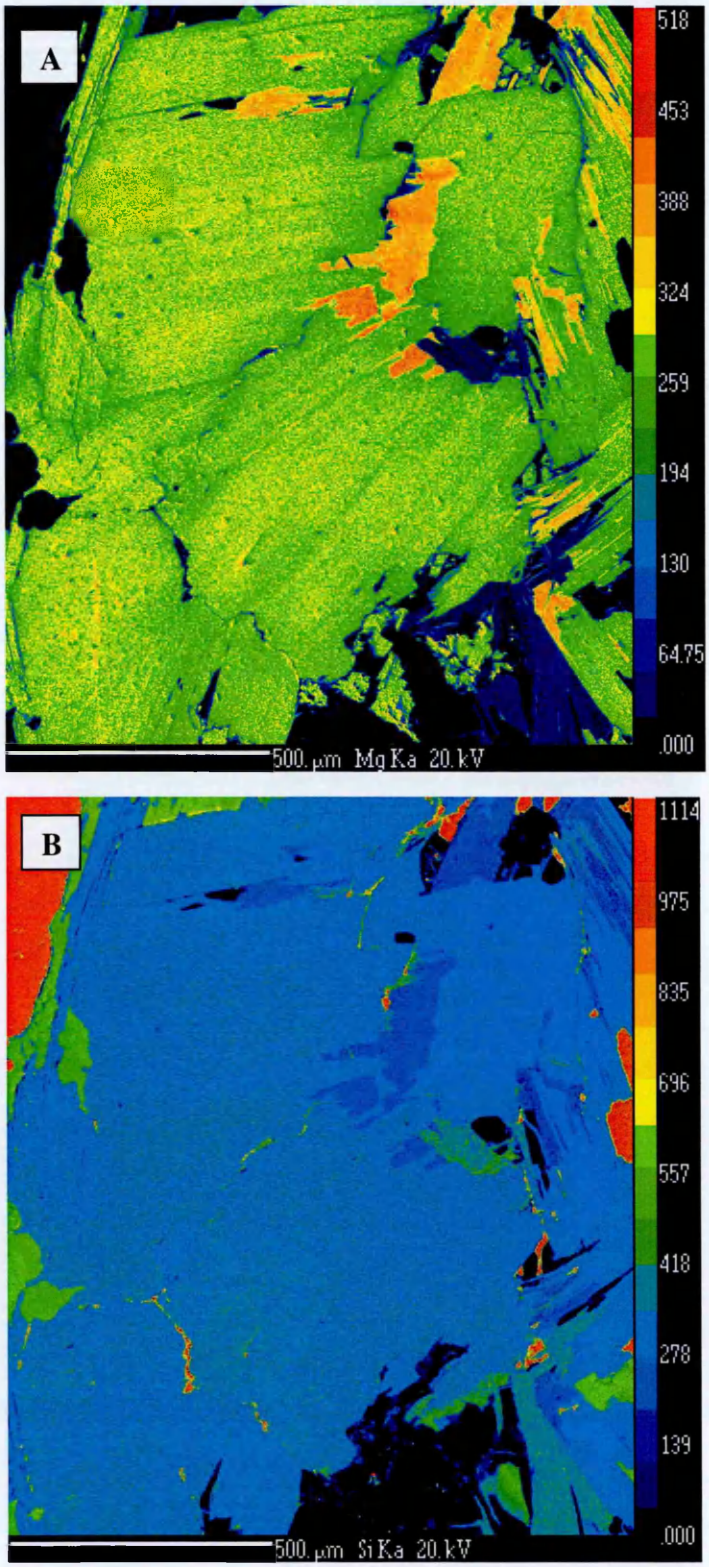

Fig. 4.2D. Geochemical maps of the idioblastic biotite. A) Mg map showing homogeneous biotite (green) and B) Si map of the biotite.

The pseudosection (Fig. 4.4), along with optical petrographic analysis, shows that phengite was the only K-bearing phase in the peak assemblage. Isothermal decompression from 2.4 to 1.0 GPa at 700°C resulted in the breakdown of phengite and the formation of biotite and plagioclase symplectites and the loss of phengite by 1.1 GPa. Post-symplectite growth of biotite resulted in the formation of more idioblastic crystals and an increase in the modal proportion of biotite. Crucially, the pseudosection shows that the growth of the symplectite and the idioblastic biotite occurred prior to the reaction that formed titanite from rutile.

4.3 Diffusion Modelling Methods and Results

In order to determine the $^{40}Ar/^{39}Ar$ 'cooling' ages of phengite, biotite and plagioclase that would be expected for a purely diffusive, open system given the best-fit post-crystallisation P-T-t history, diffusion ages were modelled using DiffArg_inverse (modified from DiffArg after Wheeler (1996); Warren *et al.,* (2012c)). Phengite and idioblastic biotite were modelled with a grain radius of 0.5 mm, and the symplectite biotite and plagioclase with a grain radius of 0.25 mm, closely matching the grain sizes in the sample. The models were based on a cooling history involving cooling from 700°C at linear cooling rates of 5, 10, 25, 50, and 70°CMa^{-1}, with a zero-age grain boundary condition. Model results (Table 4.2) are reported as bulk (area-integrated) age differences between the timing of cooling initiation based on the maximum, weighted mean and minimum U-Pb titanite ages, and the modelled grain age.

The model results suggest that in an open, purely diffusive system, 0.5 mm radius phengite grain should yield ages that are 6 Ma younger than the time at which cooling started (t_{cool}) if cooling took place at 25°CMa^{-1}. This age difference from the timing of cooling varies from 45-3 Ma depending on whether cooling was slow or rapid (5-70°CMa^{-1}). 0.5 mm biotite grain should be 11 Ma younger than t_{cool} at 25°CMa^{-1} and this too varies from 72-4 Ma depending on the rate of cooling. A 0.25 mm biotite grain should be 14 Ma younger and a 0.25 mm plagioclase grain should be 17 Ma younger, with variations in the age difference of 76-5 and 90-6 Ma, respectively, depending on the cooling rate (Table 4.2).

4.4 $^{40}Ar/^{39}Ar$ Dating Methods and Results

Polished thick section slabs (~250 μm thick; Fig. 4.1D) were prepared, cleaned, packed, irradiated and analysed by laser ablation following previously reported methods (Warren *et al.,* 2012a), and those detailed in Chapter 3. A typical laser spot size of 30 μm was used to collect Ar isotope data from the phengite and idioblastic biotite, a smaller spot size of 15 μm was used to analyse biotite and plagioclase in the symplectite. No statistically

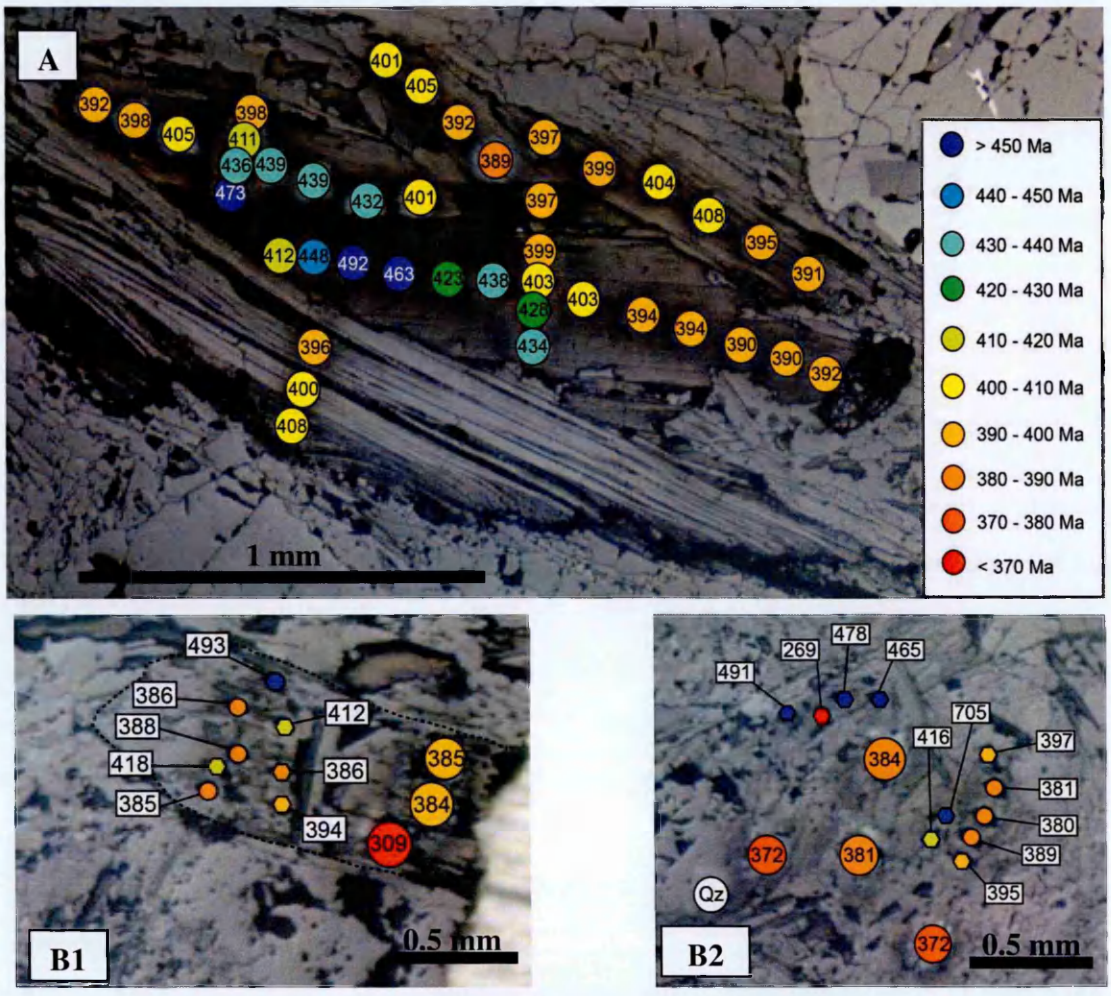

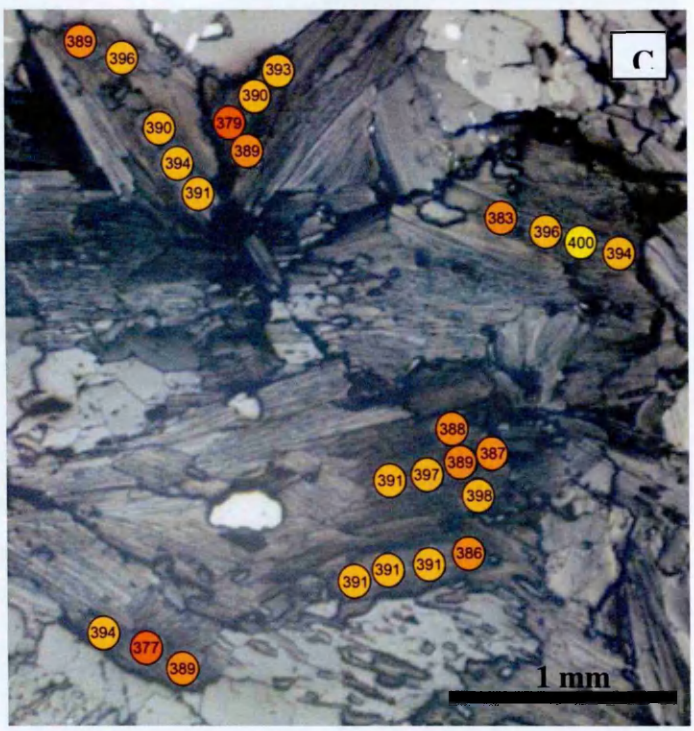

Fig.4.3. Reflected-light photomicrographs of *in-situ* $^{40}Ar/^{39}Ar$ analyses. A) phengite showing a heterogeneous age distribution, with patchy "old" ages; B1) and B2) *in-situ* analysis of the symplectites produced from the breakdown of phengite. B1 shows analysis of symplectite that pseudomorphs the original phengite while B2, shows analysis from randomly orientated symplectite; C) $^{40}Ar/^{39}Ar$ *in-situ* analysis of idioblastic biotite showing a more homogeneous age distribution.

significant link between $^{36}Ar/^{40}Ar$, $^{37}Ar/^{39}Ar$ or $^{38}Ar/^{39}Ar$ and age was found between grains of the same mineral or between different minerals.

41 spots on 5 grains of phengite yielded ages varying from 492 ± 6 Ma to 389 ± 5 Ma (Fig. 4.3A; population weighted mean: 411 ± 7 Ma). Age distributions are patchy, with clusters of 'older' ages in regions that are neither associated with the geographical nor geochemical cores of the phengite (Fig. 4.2A).

7 spots on 7 different symplectite biotite grains yielded a range of ages from 389 ± 6 Ma to 380 ± 3 Ma, with a mean age of 384 ± 6 Ma (ignoring the single 493 ± 6 Ma outlier; Figs 4.3B1, 4.3B2). 12 spots on 12 different symplectite plagioclase grains yielded highly variable $^{40}Ar/^{39}Ar$ ages from 705 ± 115 to 269 ± 82 Ma.

26 spots on 6 grains of idioblastic biotite yielded a range of ages from 400 ± 6 Ma to 377 ± 5 Ma (mean 390 ± 5 Ma). There was no systematic distribution of age within the grains (Fig. 4.3C).

4.5 Discussion

4.5.1 Petrographic Evolution

The pseudosection (Fig. 4.4) shows the evolution of the sample between 0.25-2.5 GPa and 300-900°C and documents the stability of phengite and its subsequent breakdown to biotite + plagioclase via symplectization. The pseudosection correlates with previous petrographic studies of gneisses of the WGR (Wain *et al.,* 2000, Hacker *et al.,* 2010).

Phengite crystallization occurred under eclogite-facies conditions of ~650°C, 2.4 GPa at 405-400 Ma (Cuthbert *et al.,* 2000, Root *et al.,* 2004), followed by isothermal decompression to amphibolite-facies conditions of ~700°C at 1 GPa (Hacker *et al.,* 2010). During this decompression, phengite began to break down at $P < 1.9$ GPa, to form the biotite-plagioclase symplectites. Phengite was 'lost' at ~1.1 GPa, and replaced by biotite, which represents continued growth into the idioblastic biotite from symplectic biotite. Following the growth of the idioblastic biotite, continued cooling resulted in the formation of titanite from rutile.

The pseudosection shows that in this bulk rock composition, the breakdown of phengite and the growth of biotite-plagioclase symplectites occurred prior to the growth of titanite (the date of which constrains the timing of the amphibolite-facies recrystallization). In other

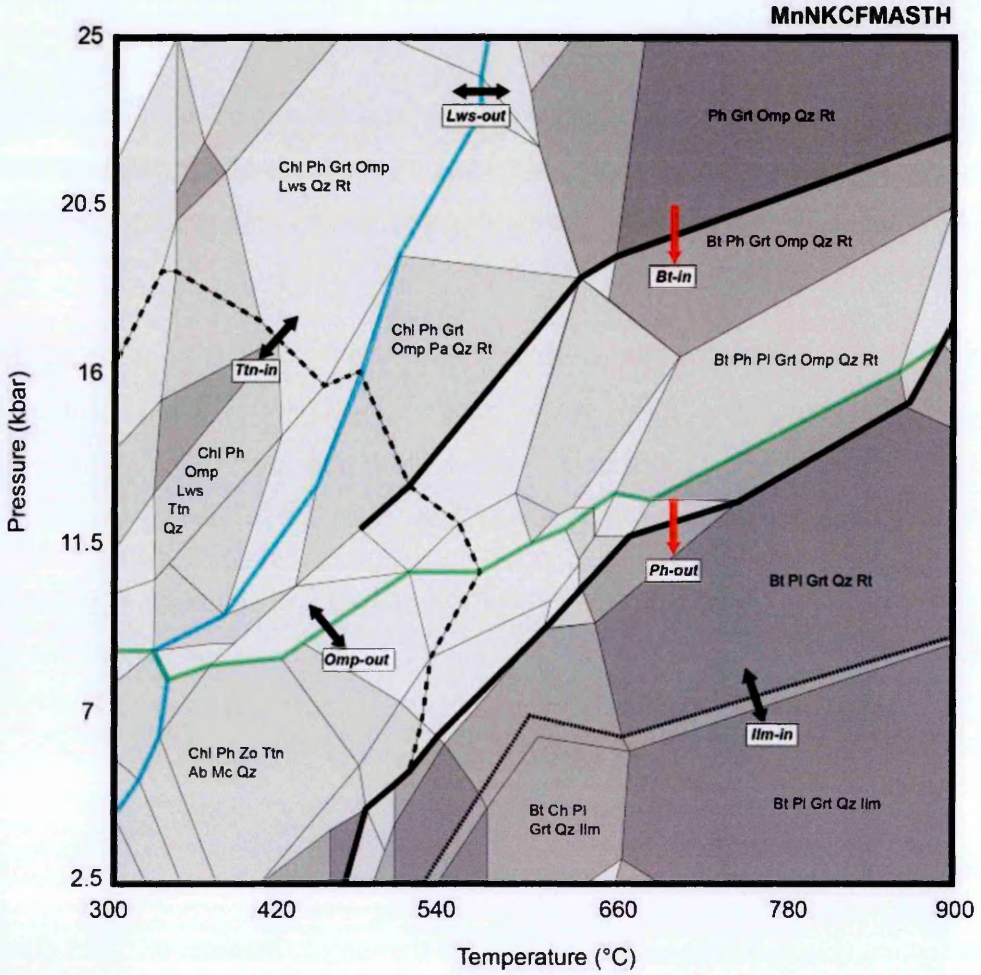

Fig.4.4. P-T pseudosection constructed for the bulk composition of the sample of symplectic gneiss showing the P-T path for Krokkenakken, WGR with approximate positions of the symplectite-forming reaction and the titanite-in field (in wt. % SiO_2: 60.02, TiO_2: 1.12, Al_2O_3: 16.86, FeO: 7.74, MnO: 0.10, MgO: 4.90, CaO, 3.77, Na_2O: 2.19, K_2O: 2.32). The red arrows indicate the biotite-in and phengite-out reactions at ~700°C.

pseudosections that model the evolution of the WGR, the symplectite-forming reaction is synchronous with titanite growth (Spencer *et al.*, 2013).

The disparity between the pseudosections of Spencer *et al.*, (2013) and this study may indicate that the U-Pb titanite ages may not represent the timing of cooling initiation. The differences in pseudosection may be due to a number of causes including: (1) differences in the bulk rock composition of the samples which would create different pseudosections, (2) sample NF42 records different P-T conditions to those of Spencer *et al.*, (2013). NF42 documents decompression from eclogite-facies conditions to amphibolite-facies conditions

while the gneisses of Spencer *et al.,* (2013) record amphibolite-facies only and (3) the pseudosection of Spencer *et al.,* (2013) is a compilation of 9 samples and only documents the Ti-bearing phases. The pseudosection also does not show the Ti phases relative to other phases and reactions in the bulk rock. For the purposes of comparison between the U-Pb titanite ages, $^{40}Ar/^{39}Ar$ phengite and biotite ages, and the P-T evolution, confidence can be placed in the pseudosection of Fig. 4.4 as it is specific to sample NF42 and documents the metamorphic reactions that occurred in the sample during its decompression history.

4.5.2 Modelled vs. Observed Age Ranges

The diffusion modelling predicts that the phengite, idioblastic biotite, symplectite biotite and symplectite plagioclase grains should yield ages that are 8 ± 2, 13 ± 2, 14 ± 2 and 17 ± 2 Ma younger than the timing of initiation of cooling in the WGR respectively, if cooling took place at 25°CMa^{-1} (uncertainties include the uncertainties in the observed grain radii but not uncertainty in the estimated cooling rate).

The model results are variably sensitive to a number of uncertainties, many of which have previously been discussed in detail (Warren *et al.,* 2012a). In summary, systematic errors derived from uncertainties in the activation energy (E_a) and the diffusion coefficient (D) lead to an uncertainty of ± 4 Ma on the resulting model age. A 50°C variation in the starting temperature (650-750°C) yields a ± 2 Ma uncertainty. Variations in the cooling rate, as discussed above, from 5-70°CMa^{-1} can result in a very large uncertainty in the model bulk age. These are 'regional' uncertainties, affecting the sample as a whole. Conversely, variations in diffusion radius would have the effect of varying the yielded age of each grain, thus increasing the range of ages yielded from each sample. Uncertainty in the diffusion radius between 1 mm to 0.25 mm yields a ± 2 Ma uncertainty on the final age.

Dependent upon the bulk rock composition, titanite crystallisation either occurs post-symplectization (as documented in this study), or is contemporaneous with symplectite growth (Spencer *et al.,* 2013). U-Pb titanite ages for the Nordfjord area of the WGR range from 399-379 Ma, with a weighted mean of 393 ± 5 Ma (Spencer *et al.,* 2013). Since the diffusion modelling results are relative to the U-Pb titanite age, the 20 Ma spread in the titanite U-Pb data results in an equal spread in the model ages. Cooling may have begun prior to 393 Ma but the ± 5 uncertainty on the U-Pb and the ± 6 Ma uncertainty on the $^{40}Ar/^{39}Ar$ phengite and biotite data means that any variation on the timing of amphibolite-

Modelled Cooling of the Western Gneiss Region From Titanite U-Pb Age (Ma)

Phengite		Cooling Rate (°CMa^{-1})				
		5	10	25	50	70
U-Pb Titanite Age (Ma)	T_{cool}	45	21	8	4	3
	399 Ma (Max)	354	378	391	395	396
	393 Ma (Wtd Av)	348	372	385	389	390
	379 Ma (Min)	334	358	371	375	376
	Grain Radius	*0.5 mm*				

Symplectite Biotite		Cooling Rate (°CMa^{-1})				
		5	10	25	50	70
U-Pb Titanite Age (Ma)	T_{cool}	76	37	14	7	5
	399 Ma (Max)	323	362	385	392	394
	393 Ma (Wtd Av)	317	356	379	386	388
	379 Ma (Min)	303	342	365	372	374
	Grain Radius	*0.25 mm*				

Idioblastic Biotite		Cooling Rate (°CMa^{-1})				
		5	10	25	50	70
U-Pb Titanite Age (Ma)	T_{cool}	72	35	13	6	4
	399 Ma (Max)	327	364	386	393	395
	393 Ma (Wtd Av)	321	358	380	387	389
	379 Ma (Min)	307	344	366	373	375
	Grain Radius	*0.5 mm*				

Symplectite Plagioclase		Cooling Rate (°CMa^{-1})				
		5	10	25	50	70
U-Pb Titanite Age (Ma)	T_{cool}	90	44	17	8	6
	399 Ma (Max)	309	355	382	391	393
	393 Ma (Wtd Av)	303	349	376	385	387
	379 Ma (Min)	289	335	362	371	373
	Grain Radius	*0.25 mm*				

Table 4.2. Diffusion modelling results for phengite, symplectite biotite, idioblastic biotite, and plagioclase showing the predicted $^{40}Ar/^{39}Ar$ bulk ages from each of the minerals, for varying cooling rates (5-70°CMa^{-1}) and varying times of the initiation of cooling from the U-Pb titanite ages of Spencer et al., (2013) from the max age, weighted mean age and the minimum age.

facies crystallization is lost within the uncertainties of the data. Given these uncertainties in the U-Pb age data, diffusion modelling, and those within the pseudosection calculations, for the purposes of comparison the weighted mean age of the titanite (393 Ma) is taken to represent the timing of cooling initiation.

Measured age ranges for phengite, symplectite biotite, symplectite plagioclase and idioblastic biotite are 492-389 Ma, 389-380 Ma, 705-269 Ma and 400-377 Ma, respectively. These age ranges are much greater than the age range predicted by simple diffusion models, which predicts a single bulk age for each mineral.

Regardless of whether the weighted mean or the youngest $^{40}Ar/^{39}Ar$ age for the phengite is used, the phengite yield generally older ages than those predicted by diffusion models. If the weighted mean age for the titanite is taken as the most reliable constraint on the timing of initiation of cooling, then all $^{40}Ar/^{39}Ar$ phengite ages should be younger than this if the ages are to interpreted in terms of a cooling age. The $^{40}Ar/^{39}Ar$ ages from the phengite are for the most part older than this reference titanite age indicating that the grains display little diffusive resetting despite the high temperatures (700°C). This implies that the phengite $^{40}Ar/^{39}Ar$ ages may not be linked to thermally-activated volume diffusion and are interpreted as being the result of contamination, which will be discussed in Section 4.6.1.

Biotite grains yield a smaller range of ages than phengite, and are consistently younger. There is no consistent difference in age between the smaller, earlier-crystallised biotite in the symplectite and the larger, later idioblastic grains, although the idioblastic grains yield a wider range of ages around a similar weighted mean. A comparison between the modelling results and the weighted mean ages of the symplectite and idioblastic biotite, taking into account the different grain sizes of these biotites, shows that cooling in the WGR took place at a rate of ~35 $°CMa^{-1}$ for the symplectite biotite and a rate of >70$°CMa^{-1}$ for the idioblastic biotite. This disparity between the possible cooling rates recorded by the two forms of biotite implies that diffusion may not have been operation in the one or both types of biotite, since one rock cannot experience multiple cooling rates at the same time. These results suggest that biotite also did not lose Ar via diffusion efficiently, or, that the loss of Ar was partially counteracted by variable influxes of excess Ar even at 700°C. The yielded ages are always older than expected from the diffusion modelling. However, this interpretation is dependent on a correct understanding of the variables that go into the T_c formulation (*cf.* Chapter 2).

The ages yielded by the plagioclase grains also span a considerable range. The plagioclase has low K concentrations, and consequently some of the variability may be due to low measured ^{39}Ar concentrations. It is therefore plausible to consider that these plagioclase $^{40}Ar/^{39}Ar$ ages represent either contamination or indicate the presence of fluid inclusions within the plagioclase crystal lattice.

Despite the uncertainty in the timing of initiation of cooling of the WGR, there is clearly a disparity between both the observed $^{40}Ar/^{39}Ar$ ages (and age ranges) and the modelled ages derived from DiffArg_inverse. Overall these data suggests that a pure diffusion model for Ar distribution is inadequate for the interpretation of the phengite dataset and yields mixed results for the biotite datasets.

4.6 Implications

4.6.1 Phengite

Information from the pseudosection in Fig. 4.4 and petrographic textures (Fig. 4.2A) suggest that phengite grew at peak metamorphic conditions of 2.4 GPa and c. 650°C. The timing of peak metamorphism has been constrained by U-Pb zircon at c. 405-400 Ma (Root *et al.,* 2004). Therefore, if these $^{40}Ar/^{39}Ar$ phengite ages are to be interpreted as crystallisation ages, they should fall within and around this 405-400 Ma timeframe (Fig. 4.5).

The observed phengite $^{40}Ar/^{39}Ar$ ages span a range of 490-389 Ma, far greater than the spread expected for crystallisation ages (Fig. 4.5). The age spread implies that the phengite has undergone some diffusional loss, to make the $^{40}Ar/^{39}Ar$ younger than the age of crystallisation, but not enough to allow the ages to be linked to a cooling age given the existing diffusion parameters. The age spread also indicates that the phengite may have been affected by contamination from Ar, producing ages that are greater than the expected crystallisation ages. This contamination may have occurred during decompression, with Ar becoming incorporated into the phengite from either the grain boundary fluid or maybe adjacent grains, or incorporated into the phengite crystal lattice during crystallisation, but it is difficult to unravel when the contamination occurred from these data.

The 'old' ages within the phengite are concentrated in patches that are not associated with the geographic cores of the grains. Geochemical maps (Fig. 4.2A) show that the phengite is homogeneous and do not indicate the presence of relict phengite cores within the grains.

This information indicates that the contaminating Ar is possibly held within microstructural defects within the phengite.

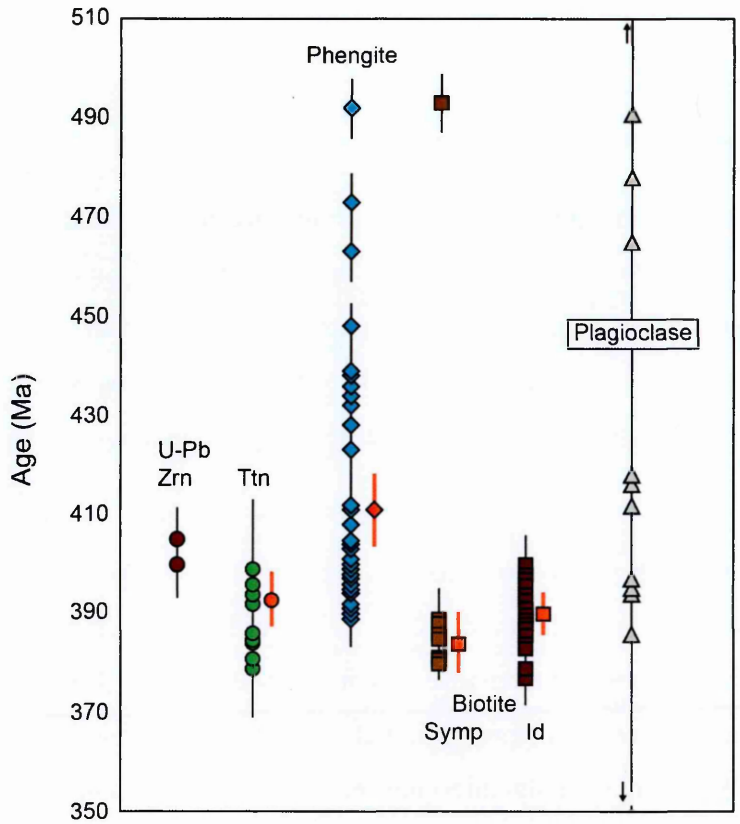

Fig. 4.5. A graphical representation of the *in-situ* $^{40}Ar/^{39}Ar$ ages of phengite, biotite (symp: symplectite, Id: idioblastic) and plagioclase in conjunction with the U-Pb zircon (Zrn) ages for the timing of peak metamorphism in the WGR and the U-Pb titanite ages for the timing of recrystallization under amphibolite-facies conditions according to Root *et al.,* (2004) and Spencer *et al.,* (2013). The data in red indicate the weighted mean age (plus error) for the titanite, phengite and biotite ages, showing that on average the phengite data are older than the U-Pb titanite while the biotite are younger. Also that as biotite grows from symplectite to idioblastic forms, the age heterogeneity increases within the biotite datasets.

4.6.2 Biotite

The pseudosection in Fig. 4.4 suggests the biotite formed initially via the symplectization of phengite during the decompression path from 1.9 GPa. In the bulk composition of this sample, the formation and growth of biotite from the phengite occurred prior to the formation of titanite. Therefore, if the biotite $^{40}Ar/^{39}Ar$ ages are to be interpreted in terms

of crystallisation ages, biotite ages should fall between the youngest U-Pb zircon ages for the timing peak metamorphism (i.e. 400 Ma) and the weighted mean titanite age (393 Ma).

The biotite from the symplectite yields an age from 389-380 Ma, which is younger than the proposed range expected for biotite crystallisation. The idioblastic biotites range in age from 400-377 Ma; these ages are equal to, and younger than, the age range expected for crystallisation ages given the timeframe above.

The symplectite biotite is texturally older than idioblastic biotite, since the symplectite grows first along the decompression path. If interpreted as crystallisation ages, the symplectite biotite should be older than the idioblastic biotite. However, the symplectite biotite is equivalent in age (and with less spread) to the $^{40}Ar/^{39}Ar$ ages of the idioblastic biotite. Also, the $^{40}Ar/^{39}Ar$ ages for the symplectite are younger than the weighted mean titanite age of 393 Ma.

The data raises the possibility that the $^{40}Ar/^{39}Ar$ age from the symplectite biotite reflect a cooling age. If so, according to the model data in Table 4.2, the symplectite biotite age range of 389-380 Ma yield cooling rates that vary from 70-27°CMa^{-1}. If the weighted mean of the symplectite biotite is used as representing closure through the biotite T_c, then a mean cooling rate of 35°CMa^{-1} can be assigned to the biotite. This result, however, could simply be coincidence.

The cooling rate from the symplectite biotite falls within the 30-60°CMa^{-1} estimates from previous studies (Kylander-Clark *et al.*, 2008, Root *et al.*, 2005, Walsh *et al.*, 2013). These studies estimated the cooling rates from phengite and not biotite, yet data from this study suggests that phengite does not yield ages interpretable in terms of a cooling age. This implies that the correlation in cooling rates between this study and published data may be purely coincidence.

The idioblastic biotite, despite being texturally younger than the symplectite biotite, is equal to, and older in age than the symplectite biotite. This means that despite the ages of the symplectite biotite being able to infer a potential cooling rate, this later biotite has, like the phengite, been affected by Ar contamination. This contamination mostly likely occurred during the growth of the idioblastic biotite during post-symplectite growth.

4.6.3 Plagioclase

Evidence for the presence of Ar that has contaminated the biotite comes from the plagioclase that co-crystallised with the biotite during symplectization. The low K content

of the plagioclase allows for the discrimination of this contaminating Ar from that which is produced via the *in-situ* decay of K as the low K content would yield low levels of *in-situ* produced Ar. As the plagioclase forms from the breakdown of phengite, some of the Ar that is released during this reaction is incorporated into the plagioclase.

Whether Ar is incorporated into the plagioclase during the breakdown of the phengite is controlled by the solubility of Ar between the mineral (plagioclase) and the grain boundary network. Ar, being a geochemically inert element is commonly assumed to partition into the grain boundary rather than into a mineral solid. Although it is difficult in nature to measure the solubility of Ar, experimental work has shown that the solubility of Ar in a solid to range from 0.01 – 0.0001 ppm bar^{-1} (Kelley, 2002 and reference therein). These low values indicate this assumption to be correct. Studies have also demonstrated that Ar displays this preferential partitioning even in anhydrous systems (Baxter *et al.,* 2007).

Processes that may drive the partition of Ar from the mineral to grain boundary may include:

1) The temperature, since chemical reactions occur faster at high temperature than at lower temperatures and,
2) The concentration of Ar present in the grain boundary network. Lower concentrations of Ar in grain boundary network would mean that more Ar can be incorporated into the grain boundaries.

In cooling metamorphic systems, it has been shown that solubility decreases and partition coefficients increase as temperatures decrease, likely through exhumation. A common observation of this behaviour in nature is the late influxes of argon into mineral grain boundaries (McDougall & Harrison 1999; Pickles *et al.,* 1997, Kelley, 2002). Conversely, if temperatures are high enough, and the concentration of Ar in the grain boundary sufficient, Ar will partition into the solid mineral phase due to dynamic equilibration (Kelley, 2002).

The incorporation of Ar into the plagioclase implies that the grain boundary network, at least in the local-scale, had a highly variable concentration of Ar, and that the elevated temperatures experienced by the rock (~700°C), led to partial uptake of Ar by the plagioclase and idioblastic biotite where mineral-grain boundary partition coefficients were high enough to allow Ar to become incorporated into the minerals. This uptake of Ar led to the increase in the spread of the $^{40}Ar/^{39}Ar$ biotite ages between the symplectite and idioblastic datasets.

4.7 Conclusions

The texturally-preserved evidence for the reactions between different K-bearing minerals within the same sample can offer insights into how Ar is recycled during HT metamorphism. In the WGR, gneisses that experienced eclogite facies (2.4 GPa) conditions at c. 405-400 Ma followed by isothermal decompression to c. 1.0 GPa, record mineralogical evidence for all these stages. *In-situ* laser ablation $^{40}Ar/^{39}Ar$ data from phengite and the biotite-plagioclase symplectites that replace it yield wide age ranges in all K-bearing minerals that help to constrain how Ar behaves during the recrystallization reactions that occur during retrogression.

Phengite that grew at 700°C and 2.4 GPa and subsequently partially broke down during decompression yields ages ranging from 486-385 Ma. Heterogeneous distributions of $^{40}Ar/^{39}Ar$ ages within and between grains suggest little diffusive resetting despite the high temperatures experienced after crystallisation, and that contamination may have occurred during crystallisation or decompression.

Symplectites that grew from phengite during decompression between 1.9-1.1 GPa document how Ar is (re)distributed during the breakdown of phengite. $^{40}Ar/^{39}Ar$ ages from symplectite biotite grains indicate that they did not incorporate much Ar during their growth and may be useful in determining cooling rates. Ages yielded by the plagioclase that co-crystallized with the symplectite biotite reflect contamination and incorporation of Ar that is not related to its K content. These data also point towards plagioclase acting as a sink for the Ar released by phengite during breakdown. $^{40}Ar/^{39}Ar$ ages of idioblastic biotite that grew at <1.1 GPa and ~700°C show that as biotite continues to grow from symplectite to idioblastic forms, contamination by Ar released during the breakdown of phengite was still prevalent.

None of the measured ages can be reconciled with models of simple thermally-activated diffusion during cooling in an open system. Instead the ages of the phengite reflect contamination (that may have occurred during either crystallisation or along the decompression path) and the partial diffusional loss of Ar. However, this loss was insufficient to produce cooling ages. The ages of plagioclase and idioblastic biotite reflect continued contamination by Ar released during the breakdown of phengite, within a locally closed grain boundary network. The symplectite biotite from this sample is the best candidates for interpreting the $^{40}Ar/^{39}Ar$ ages in terms of cooling.

Overall, these data demonstrate that even at HT metamorphic conditions, Ar may not readily diffuse in micas. These datasets show that the interpretation of $^{40}Ar/^{39}Ar$ data may vary from sample to sample and mineral to mineral, even in the same terrain. The petrographic evolution of each rock should be carefully documented in order to provide a framework in which to interpret the $^{40}Ar/^{39}Ar$ data. Furthermore, the analysis of multiple minerals aids the determination of how Ar has behaved during metamorphic recrystallization. Overall this approach allows $^{40}Ar/^{39}Ar$ ages to be more precisely linked to metamorphic stage.

Chapter 5

$^{40}Ar/^{39}Ar$ Dating of Minor Lithologies of the WGR: Eclogites, Amphibolites, and Granulites

Orthopyroxene-bearing eclogite at Grytting

This chapter forms the paper:

McDonald, C. S., Warren, C. J., Mark, D. F., Regis, D., Halton, A. M., Kelley. S. P. & Sherlock, S. C. Systematic of the $^{40}Ar/^{39}Ar$ system in Eclogites and Granulites from the Western Gneiss Region, Norway. In prep for *Lithos*.

5.1 Introduction

The eclogite-facies metabasites are one of the most striking lithologies of the Western Gneiss Region (WGR) of western Norway. They occur as decimetre- to kilometre-scale boudins hosted within amphibolite-facies granodioritic gneiss. In the Outer Nordfjord area, eclogites range from quartz-stable (high pressure – HP) in the southeast to coesite-stable (ultrahigh-pressure – UHP) in the northwest and their formation has been linked to the subduction of Baltica beneath Laurentia during the Caledonian Orogeny. During the decompression and exhumation of the WGR, many of these eclogite-facies metabasic lithologies underwent varying degrees of retrogression and hydration, to form amphibolites, with only the largest (> 1m in diameter) bodies, preserving the eclogite-facies parageneses in their cores.

Subordinate to the eclogites are granulite-facies felsic lithologies. The protolith of the granulites was formed during the Gothian Orogeny c. 1750-1500 Ma and metamorphosed to granulite-facies during the Sveconorwegian Orogeny c. 1250-900 Ma (Gaal & Gorbatschev 1987). These granulites were subsequently involved in the Caledonian Orogeny, being subducted and exhumed during the collision of Baltica with Laurentia, yet preserve many of their original granulite-facies parageneses and textures. In the Outer Nordfjord area, two granulite bodies are preserved (the Flatraket and Ulvesund granulites) in low strain enclaves.

Approximately 1.8% of the WGR comprises metabasic lithologies of which half still preserve an eclogite-facies assemblage, and 1% of the WGR is composed of the granulite-facies relicts (Peterman *et al.,* 2009). Despite comprising < 3% of the total volume of material within the WGR, these lithologies are still important in understanding the evolution of the WGR and it is important to understand how these lithologies behaved during exhumation in terms of their Ar systematics.

The Flatraket Granulite is located within the HP-UHP transition zone (Wain *et al.,* 2001) (Fig. 5.1) and is a c. 2 km^2 enclave that is hosted within amphibolite-facies gneisses. Structurally above and below the Flatraket granulite are UHP eclogites indicating that the granulite body experienced UHP conditions during the Caledonian orogeny (Wain *et al.,* 2001). The margins are cross-cut by veins with an eclogite-facies paragenesis mineral assemblage (Fig. 5.3B), indicating that fluids infiltrated the granulite during UHP eclogite-facies metamorphism (Wain *et al.,* 2001). The interior of the body comprises unstrained quartz monzonite, with large (up to 10 cm) K-feldspar augen that are variably deformed. It

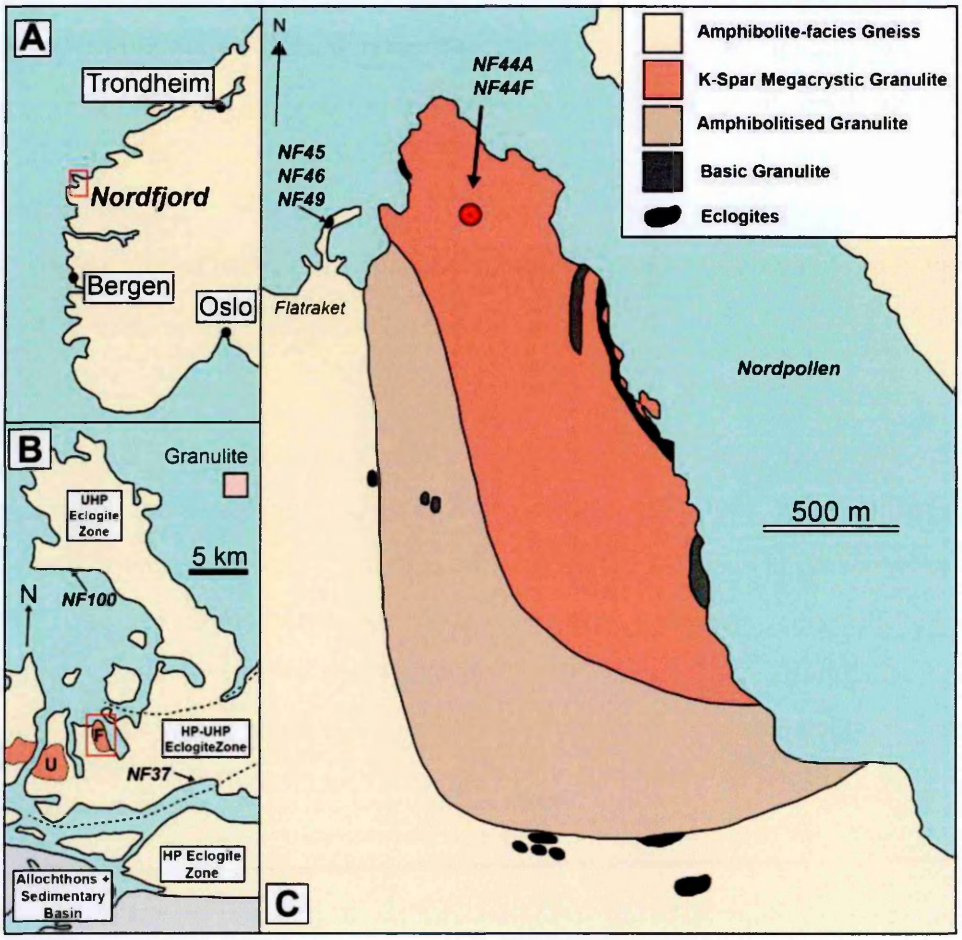

Fig.5.1. Simplified geological map of the Flatraket granulite (modified after Wain *et al.*, (2001). A) Location of the Outer Nordfjord study area in western Norway. B) Simplified map of the Outer Nordfjord area showing the locations of the Flatraket (F) and the Ulvesund (U) granulites. Also shown are the locations of the Krokkenakken eclogite (NF37) and the Drage eclogite (NF100). C) Close up map of the Flatraket granulite showing the location of the quarry (red circle) where the granulite samples were collected and the location of the Flatraket eclogite (NF45) and associated amphibolites (NF46 and NF49).

is also cross-cut by fine-grained dolerite dykes and sets of thin (<10cm wide) coaxial shear zones (Wain *et al.*, 2000, Wain *et al.*, 2001). P-T conditions for the undeformed Flatraket granulite have been calculated to be 0.9-1.1 GPa and 700-800°C (Wain *et al.*, 2001).

Many $^{40}Ar/^{39}Ar$ age studies of white micas from mafic eclogites in exhumed metamorphic HP and UHP terranes have demonstrated that mica $^{40}Ar/^{39}Ar$ ages are usually elevated in comparison with other chronometers (Li *et al.*, 1999, Sherlock *et al.*, 1999, Giorgis *et al.*,

2000, Warren *et al.,* 2011, Warren *et al.,* 2012a). These other chronometers include U-Pb zircon ages that document the timing of eclogite formation at peak metamorphic conditions and Rb-Sr mica ages that have been interpreted to represent the timing of mica crystallisation (Ruffet *et al.,* 1997, Sherlock *et al.,* 1999, Root *et al.,* 2005, Di Vincenzo 2006). This elevation of mica $^{40}Ar/^{39}Ar$ ages relative to independent chronometers has been interpreted to be the result of limited fluid transport within the eclogite, which results in the inefficient removal from the eclogites of Ar that has diffused from K-bearing minerals to the grain boundary network (Ruffet *et al.,* 1995).

To investigate the behaviour of Ar in mafic eclogites and felsic granulite during the exhumation of the WGR, three samples of eclogite and two samples of amphibolite were collected to understand, (1) how Ar behaved in the eclogites during the exhumation of the WGR and (2) how the transformation of eclogite to amphibolite affected the Ar systematics. Furthermore, undeformed and sheared samples from the Flatraket granulite were collected to understand (1) whether the Ar systematics within the granulite, which did not react under eclogite-facies conditions, were perturbed by the Caledonian Orogeny and (2) when the shear zones that cross-cut the granulite were active.

5.2 Previous Chronology of WGR Eclogites and the Flatraket Granulite

Sm-Nd and Lu-Hf garnet ages from eclogites suggest that prograde metamorphism occurred from 419.5 ± 4.3 Ma (Kylander-Clark *et al.,* 2007) to 403.9 ± 0.8 Ma (Peterman *et al.,* 2009) while U-Pb zircon ages in mafic eclogite bodies suggest that peak eclogite-facies metamorphic conditions were achieved from c. 405-400 Ma (Root *et al.,* 2004).

Recent U-Pb zircon and monazite analysis of the Flatraket granulite yielded an upper intercept age of c. 1670-1640 Ma and a lower intercept age of c. 1100-1000 Ma (Corfu *et al.,* 2013). These ages were interpreted as representing the timing of magmatic emplacement of the original protolith to the granulite during the Palaeoproterozoic, and the timing of granulite-facies metamorphism, respectively.

$^{40}Ar/^{39}Ar$ analysis of mafic eclogites in the Outer Nordfjord area of the WGR is thus far restricted to two studies. White mica from the Verpeneset eclogite yielded a step heating plateau age of 401.3 Ma (Root *et al.,* 2005). A single grain fusion and UV laser ablation study of multiple white micas from several eclogites (including the aforementioned Verpeneset eclogite) found that $^{40}Ar/^{39}Ar$ white mica ages in mafic eclogites were highly variable, ranging from 756 ± 2 Ma to 398 ± 2 Ma (Warren *et al.,* 2012). To date, there has been no $^{40}Ar/^{39}Ar$ study on the Flatraket Granulite.

5.3 Petrography, Mineral Chemistry and P-T Evolution

Major-element compositions of white mica, biotites, and amphibole from the eclogites and granulite were analysed using the Open University Cameca SX-100 5 wavelength-dispersive spectrometer electron microprobe using the methods outlined in Chapter 3. The representative core-rim compositions of the white mica, biotite, and amphibole are presented in Table 5.1-5.3. A full petrographic description of each sample is provided in Appendix A; the lithologies are briefly described below.

5.3.1 Eclogite

One sample of metabasic eclogite each was selected from Krokkenakken, Flatraket Harbour, and Drage (NF37, NF45, and NF100, respectively).

NF37 is a granoblastic eclogite from Krokkenakken containing an eclogite-facies assemblage of garnet, omphacite quartz, white mica, clinozoisite and rutile (Figs. 5.2A and 5.4A). This peak assemblage has been partially overprinted by symplectites of clinopyroxene-plagioclase around omphacite; biotite-plagioclase symplectites around phengite, and blue-green amphibole at the contact between garnet and omphacite. Phengite grains are 1-2 mm in length and have Si core-rim concentrations of 6.9-6.6 per 22 O per formula unit (pfu).

Garnets are anhedral to subhedral in shape and commonly contain concentric inclusions of quartz, white mica and omphacite. The garnets are almandine-pyrope in composition with a composition that range from $Alm_{41-51}Sps_{0-1}Py_{28-37}Grs_{17-21}$. Omphacite shows only minor retrogression to symplectite along the grain boundaries and have a composition of Jd_{30-39}.

Minor amphibole occurs at garnet-omphacite grain boundaries. This amphibole is magnesiokatophorite-magnesiotaramite, with minor barroisite. The amphibole has a Si content that ranges from 5.9-7.0 and $Mg^{\#}$ of 0.61-0.80. Epidote forms a minor component of this sample, occurring as isolated grains within the matrix and as inclusions in garnet and omphacite. The composition of the epidote ranges from XEp 0.23-0.47.

NF45, from Flatraket Harbour, is a coarse-grained granoblastic eclogite and contains a peak assemblage of garnet, omphacite, white mica, kyanite and rutile (Figs. 5.2B and 5.4B). Polycrystalline quartz (PCQ) inclusions in omphacite and garnet are interpreted to represent the former presence of coesite, the HP polymorph of quartz. This peak eclogite-facies assemblage is partially replaced by symplectites of clinopyroxene-plagioclase around omphacite, biotite-plagioclase around phengite and blue-green amphibole at

Table 5.1
Core-rim chemical composition of the white mica analysed in each sample

Lithology	Eclogite					
Sample	NF37		NF45		NF100	
Position	Core	Rim	Core	Rim	Core	Rim
F	0.04	0.00	0.04	0.06	0.18	0.15
Cl	0.00	0.00	0.01	0.01	0.01	0.02
Na_2O	0.52	0.40	0.56	0.58	0.28	0.35
K_2O	10.59	10.63	10.64	10.56	10.85	10.66
MgO	4.13	3.80	3.82	4.02	3.87	3.85
CaO	0.00	0.02	0.02	0.03	0.03	0.01
MnO	0.01	0.02	0.00	0.01	0.01	0.00
FeO	1.53	1.76	1.32	1.43	0.94	1.15
Al_2O_3	25.67	26.23	28.12	27.88	27.24	27.84
Cr_2O_3	0.07	0.18	0.09	0.09	0.08	0.05
SiO_2	51.78	49.62	50.48	50.39	51.03	50.71
TiO_2	0.28	0.42	0.42	0.46	0.62	0.58
Total	94.64	93.09	95.51	95.52	95.13	95.37
F	0.02	0.00	0.02	0.03	0.07	0.07
Cl	0.00	0.00	0.00	0.00	0.00	0.01
Na	0.14	0.10	0.14	0.15	0.07	0.09
K	1.81	1.85	1.80	1.79	1.85	1.81
Mg	0.83	0.78	0.76	0.80	0.77	0.76
Ca	0.00	0.00	0.00	0.00	0.01	0.00
Mn	0.00	0.00	0.00	0.00	0.00	0.00
Fe	0.17	0.20	0.15	0.16	0.10	0.13
Al	4.05	4.23	4.40	4.37	4.29	4.37
Cr	0.01	0.02	0.01	0.01	0.01	0.01
Si	6.94	6.79	6.71	6.70	6.81	6.75
Ti	0.03	0.04	0.04	0.05	0.06	0.06
Total	14.00	14.03	14.04	14.06	14.05	14.05

Table 5.1: Representative geochemical core-rim analyses of white mica

Table 5.2
Core-rim chemical composition of the biotite analysed in each sample

Lithology	Granulite				Amphibolite			
Sample	NF44A		NF44F		NF46		NF49	
Position	Core	Rim	Core	Rim	Core	Rim	Core	Rim
F	0.37	0.31	0.35	0.47	0.03	0.02	0.04	0.10
Cl	0.18	0.16	0.12	0.10	0.05	0.05	0.06	0.04
Na_2O	0.07	0.06	0.06	0.06	0.34	0.27	0.12	0.14
K_2O	9.60	9.69	9.75	9.70	9.14	9.26	9.20	9.20
MgO	8.69	8.63	9.60	9.55	14.27	14.29	12.25	12.38
CaO	0.03	0.02	0.01	0.02	0.06	0.07	0.00	0.02
MnO	0.31	0.34	0.30	0.31	0.10	0.10	0.20	0.19
FeO	21.37	21.27	20.09	20.05	16.34	16.40	17.80	17.30
Al_2O_3	16.31	16.32	16.04	16.09	17.25	17.35	16.96	16.97
Cr_2O_3	0.02	0.00	0.01	0.01	0.04	0.05	0.03	0.04
SiO_2	36.10	35.95	36.60	36.48	36.24	36.24	36.67	37.09
TiO_2	3.02	2.89	2.89	2.65	2.12	1.90	2.37	2.24
Total	96.07	95.64	95.83	95.51	95.98	95.98	95.77	95.73
F	0.18	0.15	0.17	0.23	0.01	0.01	0.02	0.05
Cl	0.04	0.04	0.03	0.03	0.01	0.01	0.02	0.01
Na	0.02	0.02	0.02	0.02	0.10	0.08	0.03	0.04
K	1.90	1.92	1.91	1.91	1.72	1.74	1.77	1.76
Mg	2.00	2.00	2.21	2.21	3.14	3.14	2.75	2.77
Ca	0.01	0.01	0.00	0.01	0.01	0.01	0.00	0.01
Mn	0.04	0.04	0.04	0.04	0.01	0.01	0.03	0.02
Fe	2.77	2.76	2.59	2.60	2.02	2.02	2.24	2.17
Al	2.98	2.99	2.91	2.94	3.00	3.02	3.01	3.00
Cr	0.01	0.00	0.00	0.00	0.00	0.00	0.01	0.01
Si	5.59	5.58	5.63	5.65	5.35	5.35	5.52	5.57
Ti	0.35	0.34	0.34	0.31	0.24	0.21	0.27	0.25
Total	15.87	15.85	15.85	15.93	15.60	15.61	15.66	15.66

Table 5.2: Representative geochemical core-rim analyses of biotite

Table 5.3
Core-rim chemical composition of the amphibole analysed in each sample

Lithology	Eclogite				Amphibolite			
Sample	NF37		NF45		NF46		NF49	
Position	Core	Rim	Core	Rim	Core	Rim	Core	Rim
F	0.00	0.00	0.09	0.00	0.03	0.04	0.00	0.00
Cl	0.00	0.00	0.00	0.00	0.05	0.03	0.04	0.06
Na_2O	3.94	3.91	4.40	4.48	1.57	1.94	1.36	1.30
K_2O	0.45	0.49	0.06	0.06	0.69	0.70	1.00	0.66
MgO	13.37	12.92	10.20	10.21	10.47	11.02	9.39	9.30
CaO	9.03	9.05	9.22	9.09	11.69	11.30	10.57	11.00
MnO	0.10	0.09	0.20	0.21	0.18	0.29	0.44	0.44
FeO	10.46	10.55	12.19	12.48	14.52	14.62	16.58	16.80
Al_2O_3	14.11	14.31	21.06	21.13	15.23	14.02	14.74	14.64
Cr_2O_3	0.02	0.11	0.04	0.06	0.04	0.03	0.04	0.02
SiO_2	44.44	44.68	38.76	38.94	41.10	41.90	41.74	41.40
TiO_2	0.33	0.34	0.03	0.01	0.29	0.41	0.41	0.58
Total	96.25	96.45	96.25	96.66	95.92	96.32	96.30	96.25
F	0.00	0.00	0.04	0.00	0.01	0.02	0.00	0.00
Cl	0.00	0.00	0.00	0.00	0.01	0.01	0.01	0.02
Na	1.12	1.11	1.27	1.29	0.46	0.56	0.40	0.39
K	0.09	0.09	0.01	0.01	0.13	0.14	0.20	0.13
Mg	2.92	2.82	2.27	2.25	2.36	2.48	2.12	2.11
Ca	1.42	1.42	1.47	1.44	1.90	1.83	1.72	1.79
Mn	0.01	0.01	0.02	0.02	0.02	0.03	0.06	0.06
Fe	1.28	1.29	1.52	1.55	1.84	1.85	2.10	2.13
Al	2.44	2.47	3.70	3.69	2.72	2.49	2.63	2.62
Cr	0.00	0.01	0.01	0.01	0.01	0.01	0.01	0.00
Si	6.51	6.53	5.77	5.77	6.22	6.32	6.33	6.29
Ti	0.03	0.04	0.01	0.00	0.03	0.05	0.05	0.07
Total	15.83	15.79	16.08	16.03	15.72	15.78	15.62	15.61

Table 5.3: Representative geochemical core-rim analyses of amphibole

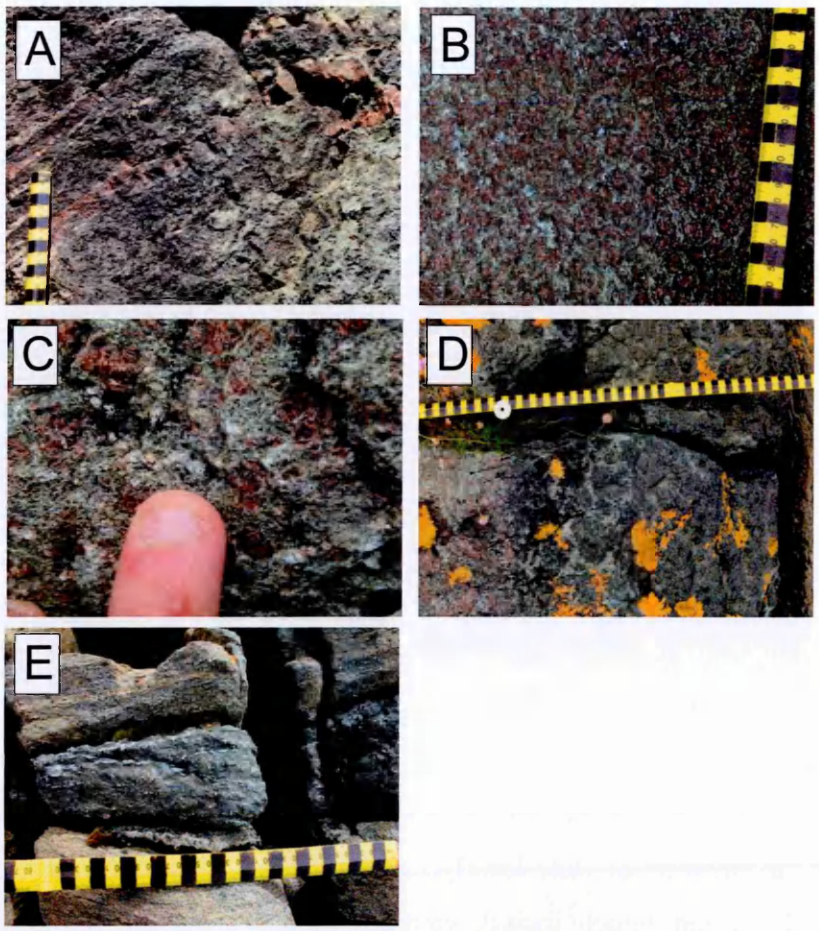

Fig.5.2. Field photographs of the eclogites and amphibolites analysed in this study. A) The Krokkenakken eclogite, showing its massive nature with bands of garnet-rich layers. B) The Flatraket Harbour eclogite with anhedral garnet, symplectised omphacite and blue kyanite. C) The Drage eclogite consisting of red garnet, green omphacite and blue kyanite. D) The amphibolitised margin of the Flatraket eclogite, showing the transition from fresh eclogite on the left of the image to amphibolite on the right. E) The NF49 garnet amphibolite.

contacts between garnet and omphacite. The phengite from this locality display chemical zonation with Si concentrations that range from 6.8 pfu at the core to 6.5 pfu at the rims.

Garnets are large (~20 mm) and are anhedral with a 'spongy' texture. They are typically zoned from more pyrope-rich cores to rim to more almandine-rich rims. The composition ranges from $Alm_{34-45}Sps_{0-2}Py_{30-49}Grs_{14-22}$. Omphacite show varying degrees of symplectization along the grain boundaries and has a composition that ranges from Jd_{34-42}. The blue-green amphibole that occurs at the garnet-omphacite contact is magnesiokatophorite-magnesiotaramite with a composition that ranges from 5.8-7.6 Si per 23 O and $Mg^{\#}$ of 0.59-0.86.

NF100 from Drage is a medium-grained, granoblastic eclogite with a peak metamorphic assemblage of garnet, omphacite, white mica, kyanite and rutile (Figs. 5.2C and 5.4C). PCQ inclusions are present in garnet and are inferred to represent the former presence of coesite. The eclogite shows minor symplectization with clinopyroxene/amphibole-plagioclase symplectites after omphacite and biotite-plagioclase symplectites after phengite.

The white mica grains are commonly rimmed with very fine-grained biotite-plagioclase symplectites and have typical core to rim compositions of 6.9-6.5 Si per 22 O. Garnets are subhedral to anhedral and range in size from 0.5-1.5 mm. They are pyrope-almandine ($Alm_{33-36}Sps_{0-1}Py_{36-41}Grs_{22-28}$) with moderate grossular content. Omphacite forms anhedral grains within the matrix and has a composition of Jd_{22-32}.

The petrological evolution of the eclogites was modelled in the NCKFMASTH system using Perple_X version 6_6_8 (Connolly, 1990), to determine the P-T conditions of the eclogite-facies metamorphism at each of the three localities (Figs. 5.5-5.7). The pseudosection was calculated using the internally consistent thermodynamic dataset (hp11ver.dat) and the equation of state for H_2O of (Holland & Powell 1998, Holland & Powell 2011). Solid solution models include garnet (Holland & Powell 1998), omphacite (Holland & Powell 1996), plagioclase (Newton *et al.,* 1980), phengite (Holland & Powell 1998), biotite (Powell & Holland 1999), chlorite (Holland & Powell 1998) and amphibole (Dale *et al.,* 2000).

Further constraints on the peak metamorphic conditions for the eclogite samples were obtained from Fe-, Mg- and Ca-in-garnet, Na-in-omphacite, and Si-in-phengite isopleth calculations. Pseudosections show that sample NF37 formed at 600-660°C at 2.1-2.5 GPa, NF45 formed at 680-760°C at 2.8-3.3 GPa and NF100 formed at 720-740°C and 3.0-3.2 GPa. These P-T data strongly correlate with previous estimates on the eclogite-facies P-T conditions of eclogites from the Outer Nordfjord area (Cuthbert *et al.,* 2000).

5.3.2 Amphibolite

Two samples of mafic amphibolite were collected from Flatraket Harbour. These samples document the re-equilibration of the eclogite-facies metabasites at the amphibolite-facies conditions.

NF46 is a sample of the amphibolitised rind of sample NF45 (Figs. 5.2D and 5.4D). The principle garnet-omphacite eclogite-facies mineralogy has been replaced by an assemblage of biotite-amphibole-plagioclase with minor epidote, rutile and secondary calcite.

Garnet has been pseudomorphed into biotite-amphibole "clots" while the eclogite matrix omphacite is replaced with pyroxene/amphibole-plagioclase symplectites. Amphiboles, in all structural positions, are tschermakite-magnesiohornblende with a composition that ranges from 5.8-7.3 Si per 23 O and $Mg^{\#}$ of 0.49-0.77. Biotite has compositions of $Mg^{\#}$ 0.55-0.62 and Ti 0.16-0.25 pfu. Plagioclase feldspar occurs within the symplectised matrix, associated with the amphibole. The plagioclase has a composition that ranges from andesine to oligoclase, with anorthite content of An_{13-35}. The epidote that is associated with the biotite and amphibole form isolated clusters of anhedral grains with compositions of XEp 0.53-0.70.

NF49 is a fully retrogressed eclogite that is equilibrated at amphibolite-facies conditions (Figs. 5.2E and 5.4E). This sample contains typical amphibolite-facies mineralogy of quartz, garnet, biotite and amphibole with minor epidote. Accessory phases include rutile, chlorite, and apatite.

Amphibole is ferrotschermakite-tschermakite with a composition that ranges from 6.21-6.56 Si per 23 O and $Mg^{\#}$ of 0.46-0.54. Biotite has a relatively homogeneous composition of Mg# 0.53-0.58 and Ti 0.19-0.29 pfu. The garnet is also fairly homogeneous and is almandine-pyrope with moderate grossular content ($Alm_{52-63}Sps_{1-6}Py_{20-32}Grs_{11-17}$). Plagioclase is oligoclase-andesine in composition with anorthite content ranging from An_{19-31}. Epidote group minerals form small (0.5-1 mm) porphyroblasts that cross-cut the fabric defined by the biotite. Epidote is commonly anhedral, unzoned and contains inclusions of the matrix phases (biotite, quartz, and plagioclase) with a composition that ranges from XEp 0.53-0.63.

5.3.3 Granulite

Two samples were collected from the Flatraket Granulite body. NF44A is an undeformed granulite and contains an assemblage of quartz, biotite, plagioclase with minor garnet, and pyroxene (Figs. 5.3A and 5.4F-H). This sample contain large (3-10 cm) augen of alkali feldspar that range from near-circular to ovoid in shape. The texture of these augen has been likened to that of rapakivi granite (Krabbendam *et al.,* 2000). The biotite forms 'clots' that separate quartz-rich domains from plagioclase-rich domains. The plagioclase forms a granoblastic texture that contains numerous fine-grained clinozoisite and kyanite crystals

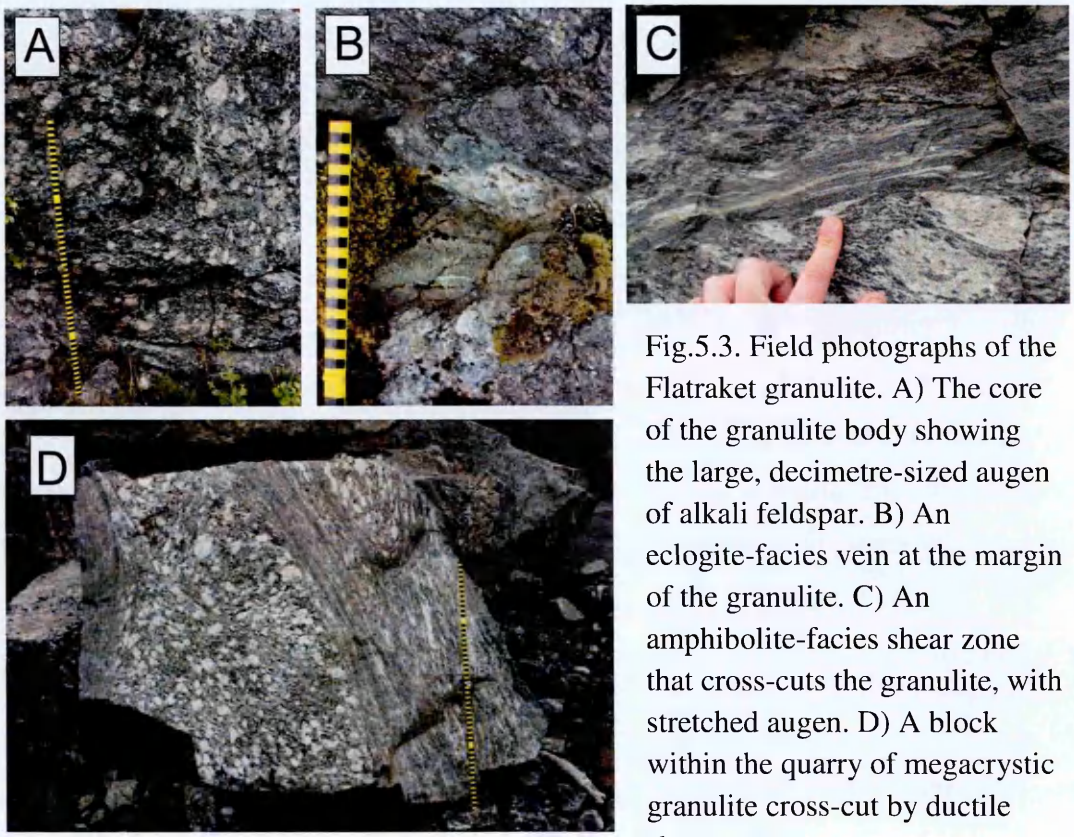

Fig.5.3. Field photographs of the Flatraket granulite. A) The core of the granulite body showing the large, decimetre-sized augen of alkali feldspar. B) An eclogite-facies vein at the margin of the granulite. C) An amphibolite-facies shear zone that cross-cuts the granulite, with stretched augen. D) A block within the quarry of megacrystic granulite cross-cut by ductile shear zones.

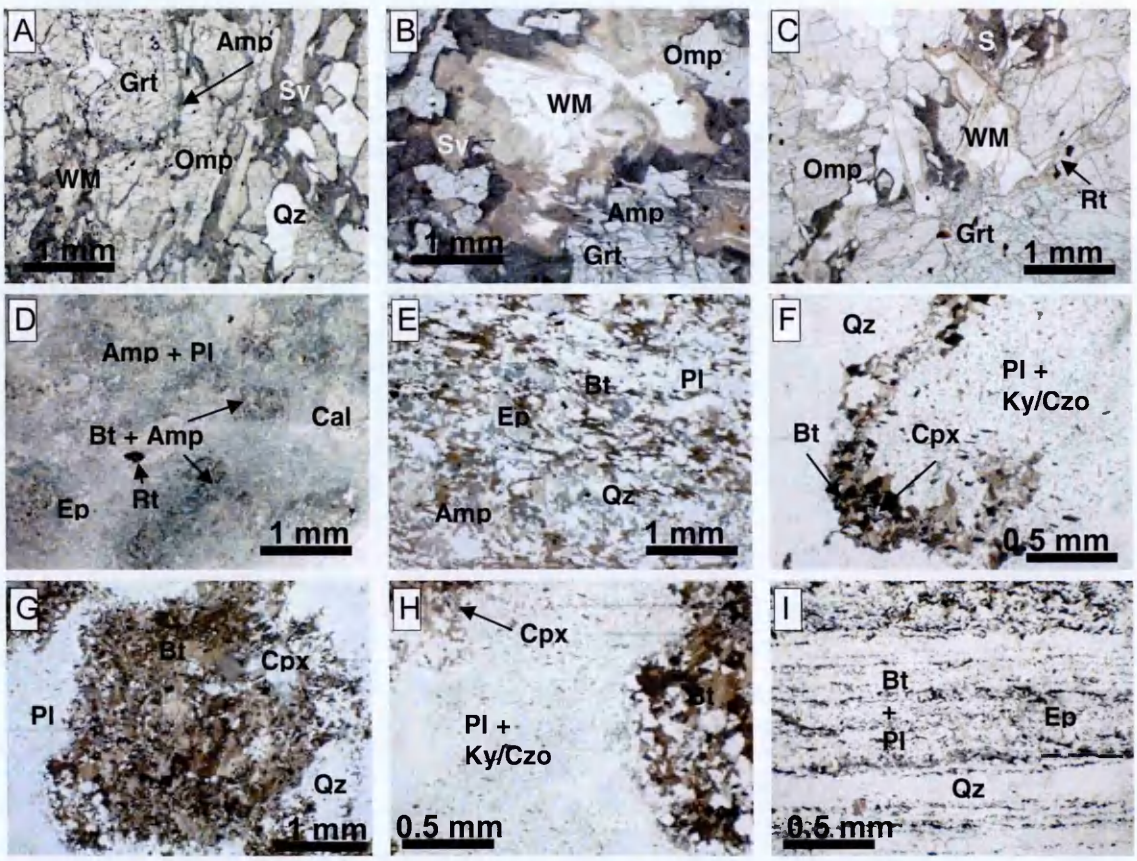

Fig.5.4. Photomicrographs of eclogite, amphibolite, and granulite samples. A) eclogite NF37, B) eclogite NF45, C) eclogite NF100, D) amphibolite NF46, E) amphibolite NF49, F-H) granulite NF44A, and I) sheared granulite NF44F. Mineral abbreviations after Whitney & Evans (2010).

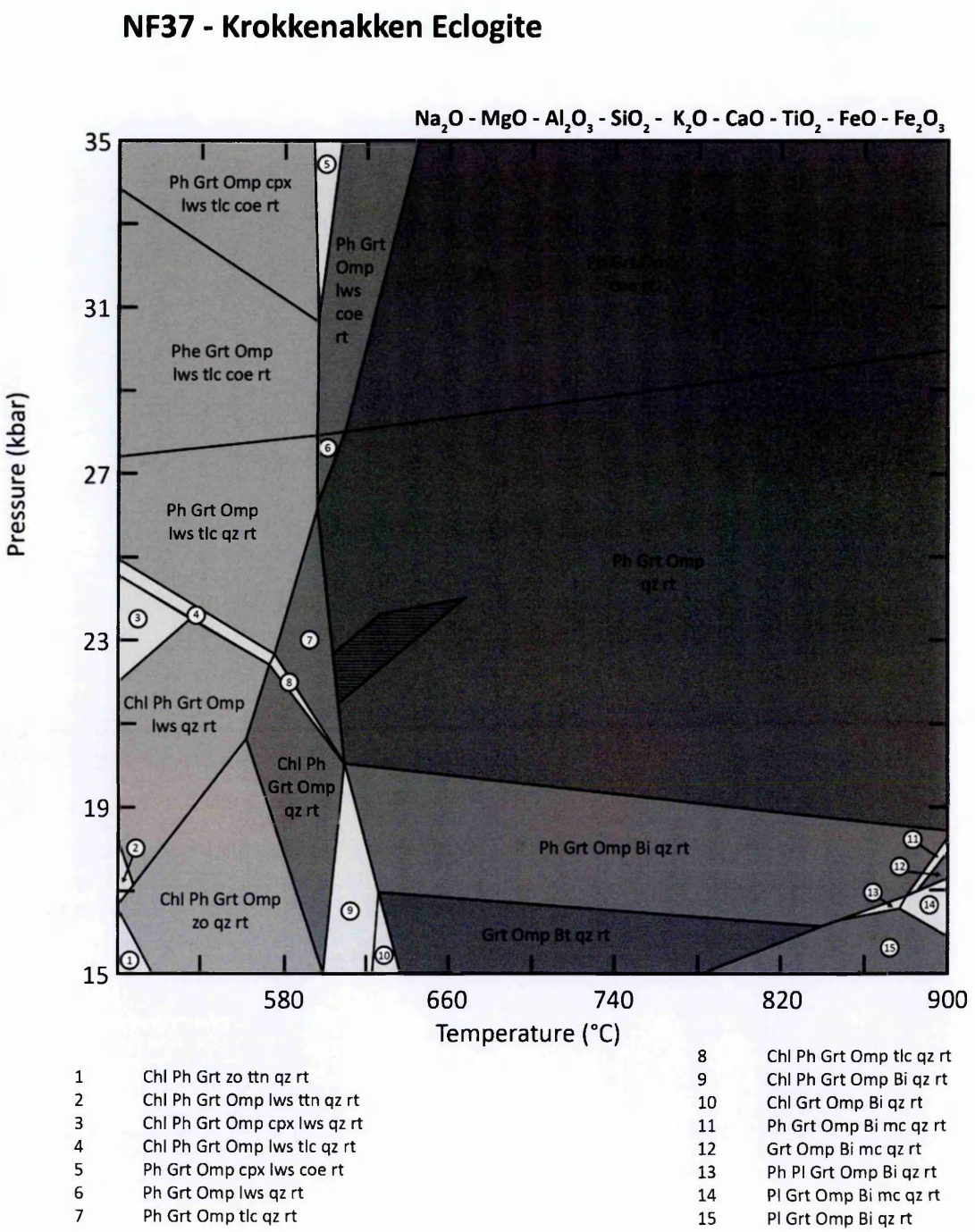

Fig.5.5. P-T pseudosection constructed for the Krokkenakken eclogite NF37, for the bulk composition (in wt. %), SiO_2: 49.48, TiO_2: 2.14, Al_2O_3: 16.30, Fe_2O_3: 0.71, FeO: 12.77, MgO: 7.15, CaO: 9.45, K_2O: 0.32, Na_2O: 1.66. The hatched area denotes the convergence of the Fe, Mg, and Ca isopleths in garnet, the Na isopleth from omphacite, and the Si isopleth of phengite.

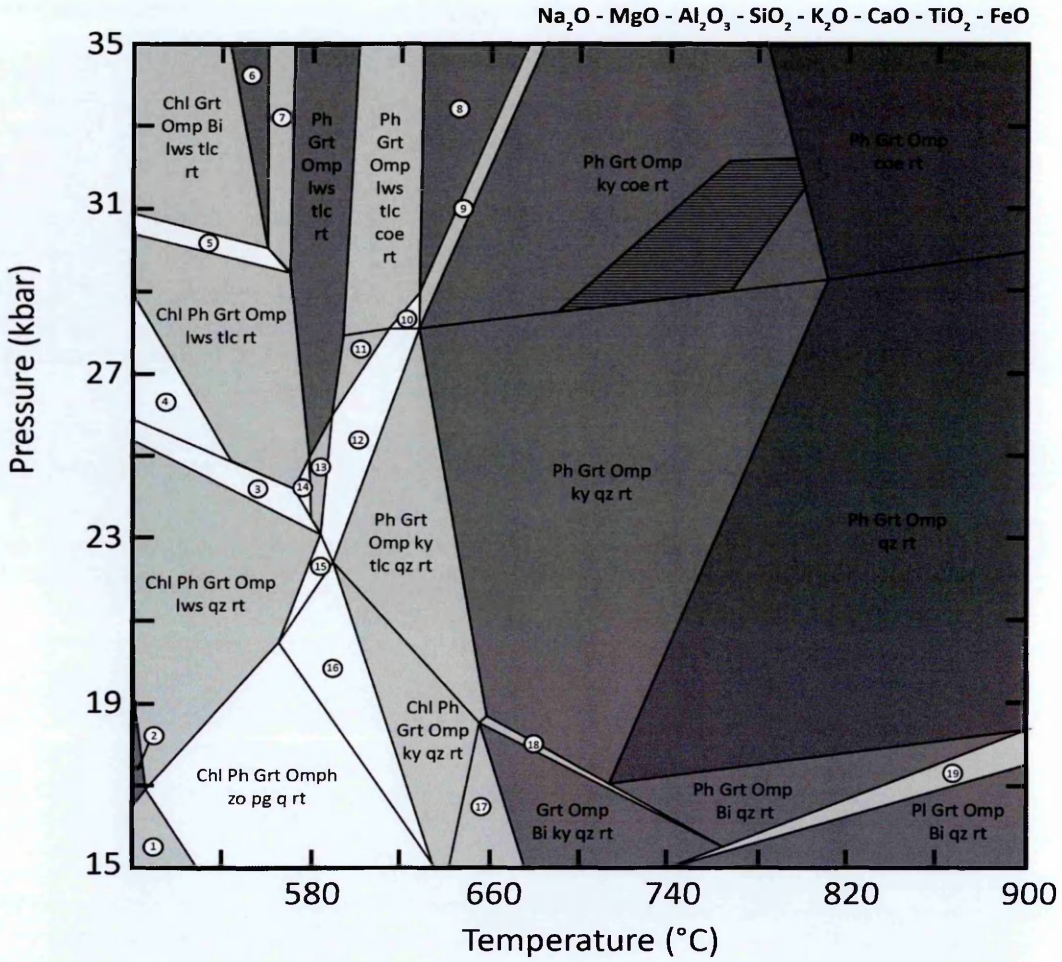

1	Chl Ph Omp zo pa qz rt
2	Chl Ph Omp lws qz rt
3	Chl Ph Grt Omp lws tlc qz rt
4	Amp Chl Ph Grt Omp lws tlc rt
5	Chl Ph Grt Omp Bi lws tlc qz rt
6	Grt Omp Bi lws tlc rt
7	Ph Grt Omp Bi lws tlc rt
8	Ph Grt Omp lws coe rt
9	Ph Grt Omp ky lws coe rt
10	Ph Grt Omp ky lws tlc cow rt
11	Ph Grt Omp lws tlc qz rt
12	Ph Grt Omp ky lws tlc q rt
13	Ph Grt Omp ky lws tlc rt
14	Chl Ph Grt Omp ky lws tlc rt
15	Chl Ph Grt Omp ky lws q rt
16	Chl Ph Grt Omp ky zo qz rt
17	Chl Grt Omp Bi ky qz rt
18	Ph Grt Omp Bi ky q rt
19	Ph Pl Grt Omp Bi qz rt

Fig.5.6. P-T pseudosection constructed for the Flatraket Harbour eclogite NF45, for the bulk composition (in wt. %), SiO_2: 46.94, TiO_2: 2.05, Al_2O_3: 19.45, FeO: 10.10, MgO: 9.94, CaO: 9.15, K_2O: 0.22, Na_2O: 2.15. The hatched area denotes the convergence of the Fe, Mg, and Ca isopleths in garnet, the Na isopleth from omphacite, and the Si isopleth of phengite.

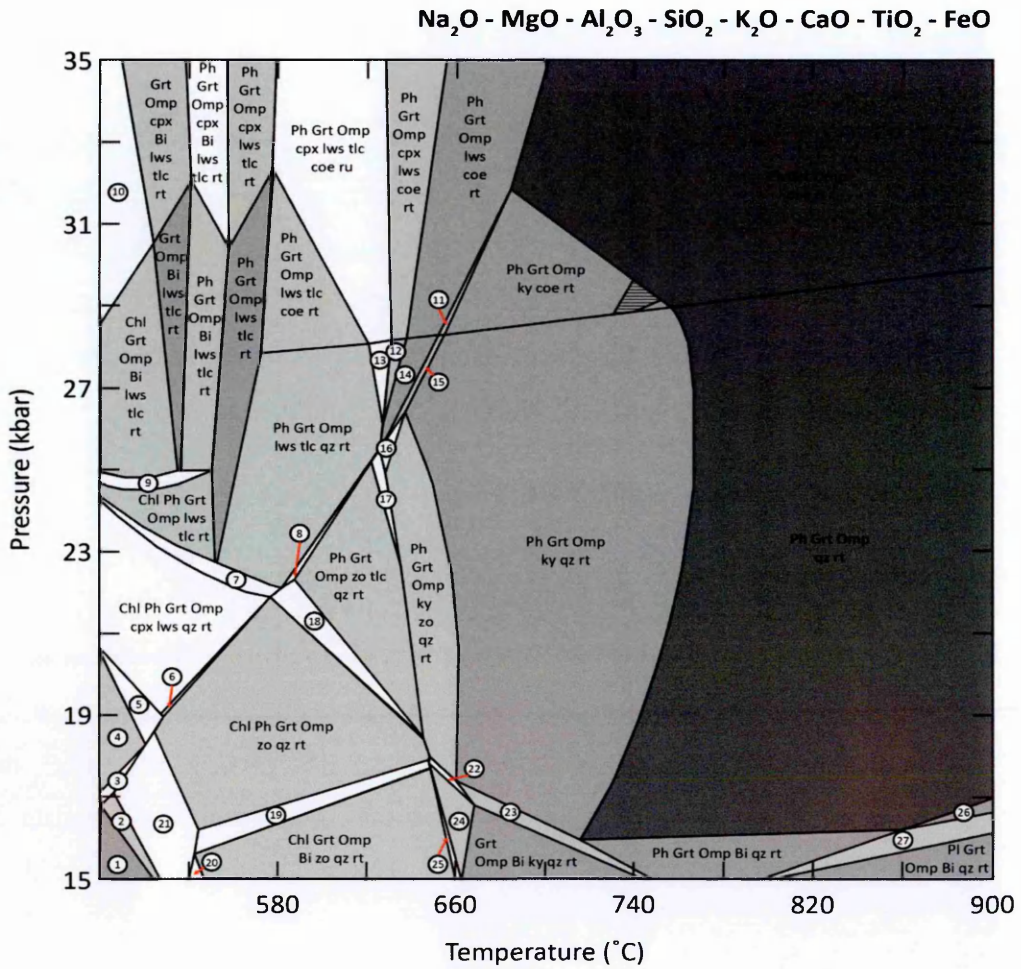

1	Chl Ph Omp zo ttn qz	10	Chl Ph Grt Omp Bi cpx lws tlc rt	19	Chl Ph Grt Omp Bi zo qz rt
2	Chl Ph Grt Omp zo ttn qz	11	Ph Grt Omp ky lws coe rt	20	Chl Grt Omp Bi zo ttn qz rt
3	Chl Ph Grt Omp zo lws ttn qz	12	Ph Grt Omp cpx lws qz rt	21	Chl Ph Grt Omp zo ttn qz rt
4	Chl Ph Grt Omp lws ttn qz	13	Ph Grt Omp cpx lws tlc qz rt	22	Ph Grt Omp Bi ky zo qz rt
5	Chl Ph Grt Omp lws ttn qz rt	14	Ph Grt Omp lws qz rt	23	Ph Grt Omp Bi ky qz rt
6	Chl Ph Grt Omp zo lws qz rt	15	Ph Grt Omp ky lws qz rt	24	Grt Omp Bi ky zo qz rt
7	Chl Ph Grt Omp lws tlc qz rt	16	Ph Grt Omp cpx ky zo qz rt	25	Chl Grt Omp Bi ky zo qz rt
8	Ph Grt Omp zo lws tlc qz rt	17	Ph Grt Omp ky zo tlc qz rt	26	Ph Pl Grt Omp qz rt
9	Chl Ph Grt Omp Bi lws tlc rt	18	Chl Ph Grt Omp zo tlc qz rt	27	Ph Pl Grt Omp Bi qz rt

Fig.5.7. P-T pseudosection constructed for the Drage eclogite NF100, for the bulk composition (in wt. %), SiO_2: 49.18, TiO_2: 2.07, Al_2O_3: 16.88, FeO: 8.01, MgO: 9.26, CaO: 12.16, K_2O: 0.21, Na_2O: 2.21. The hatched area denotes the convergence of the Fe, Mg, and Ca isopleths in garnet, the Na isopleth from omphacite, and the Si isopleth of phengite.

that have been previously been interpreted to represent the onset of static eclogitisation within the Flatraket granulite (Wain *et al.,* 2001). Biotite from this sample ranges in composition from 0.41-0.43 $Mg^{\#}$ and Ti 0.34-0.41.

NF44F (Figs. 5.3C-D and 5.4I), was collected from a shear zone that cross-cuts the undeformed granulite. These shear zones have been interpreted to have formed under amphibolite-facies conditions (Corfu *et al.,* 2013). The sample contains an assemblage of quartz, plagioclase, and biotite with minor alkali feldspar, epidote, and titanite. This sample is finer grained than NF44A, with no alkali feldspar augen preserved. NF44F has a strong mylonitic fabric defined by alternating layers of biotite-rich and quartz-rich domains. Biotite from this sample has a different chemistry from those from the undeformed sample, with a composition of Mg# 0.45-0.46 and Ti 0.30-0.35.

5.4 $^{40}Ar/^{39}Ar$ Dating Methods and Results

5.4.1 Single Grain Fusion Data

Single grain fusion analysis was undertaken at the Ar/Ar and Noble Gas Laboratory at the Open University (OU), and the NERC-funded Argon Isotope Facility (AIF) housed at the Scottish Universities Environmental Research Centre (SUERC) following the methodologies outlined in Chapter 3. A summary of the single grain fusion data is provided in Table 5.4 and shown in Figs. 5.8-5.10. The full dataset is provided in Appendix C.

5.4.1.1 Eclogite

Analysis of 20 white mica grains and 13 amphibole grains from sample NF37 from Krokkenakken yielded ages that range from 464 ± 3.4 Ma to 412 ± 2.2 Ma for the white mica and 1850 ± 15.5 Ma to 438 ±6.9 Ma for amphibole (Fig. 5.8A).

19 white mica and 23 amphibole grains from eclogite NF45 from Flatraket Harbour yielded ages that range from 607 ± 0.9 Ma to 396 ± 6.3 Ma and 2325 ± 7.3 Ma to 391 ± 12.9 Ma for white mica and amphibole, respectively (Fig. 5.8B).

14 white mica grains from the eclogite at Drage (NF100) yielded ages that range from 757 ± 9.1 Ma to 423 ± 9.7 Ma (Fig. 5.8C).

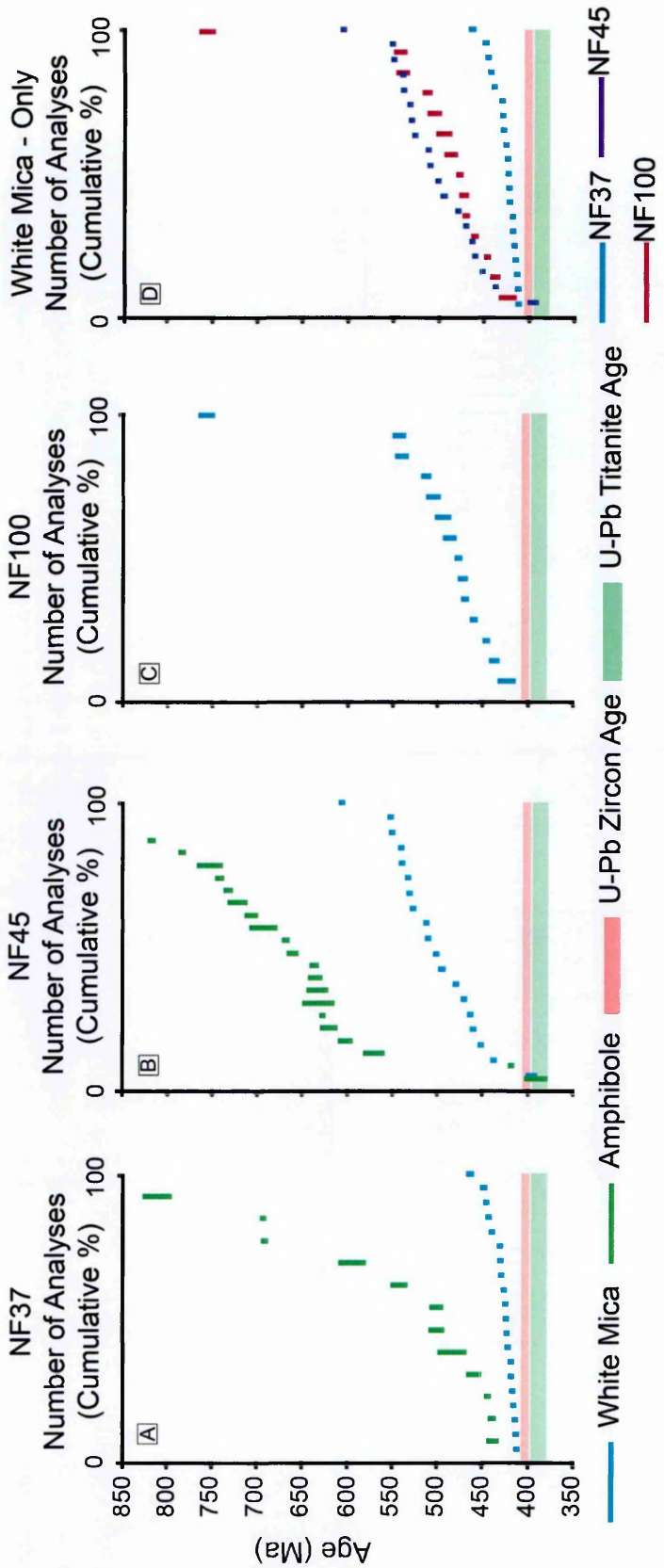

Fig.5.8. Cumulative graphs of white mica and amphibole single grain fusion analyses for the mafic eclogites. A) Sample NF37 from Krokkenakken, B) Sample NF45 from Flatraket Harbour, and C) sample NF100 from Drage. D) White mica only analyses from the three mafic eclogites. The pink boxes represent the U-Pb zircon ages for the timing of peak metamorphism of Root *et al.*, (2004) and the green boxes represent the U-Pb titanite ages of the amphibolite-facies recrystallization of Spencer *et al.*, (2013).

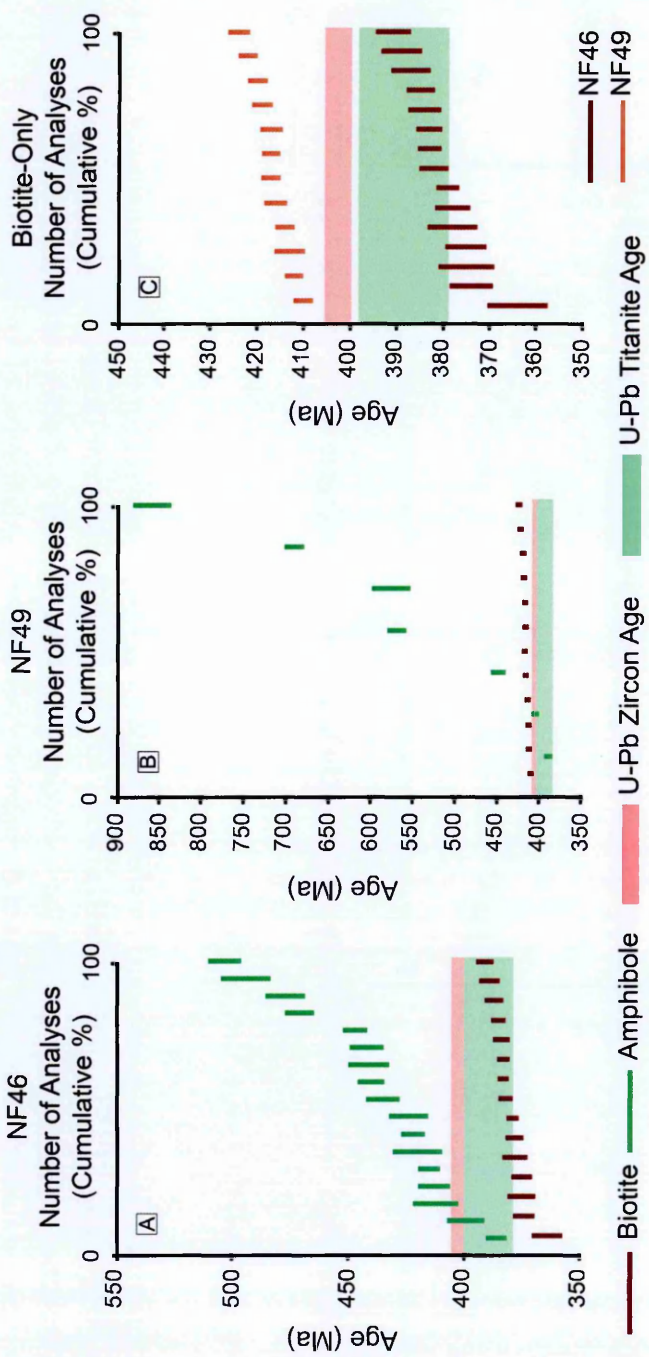

Fig.5.9. Cumulative graphs of biotite and amphibole single grain fusion analyses for the amphibolites. A) Sample NF46 from the margin of the Flatraket eclogite NF45, and B) sample NF49 from the garnet amphibolite. C) Biotite only analyses from the two amphibolites. The pink boxes represent the U-Pb zircon ages for the timing of peak metamorphism of Root *et al.*, (2004) and the green boxes represent the U-Pb titanite ages of the amphibolite-facies recrystallization of Spencer *et al.*, (2013).

5.4.1.2 Amphibolite

Sample NF46 yielded 15 biotite and 17 amphibole ages that range from 391 ± 3.7 Ma to 364 ± 6.5 Ma and 503 ± 7.0 Ma to 386 ± 4.4 Ma, respectively (Fig. 5.9A).

12 biotite grains and 7 amphibole grains from the garnet amphibolite NF49 yielded ages that range from 424 ± 2.4 Ma to 410 ± 2.1 Ma and 858 ± 22.3 Ma to 389 ± 4.1 Ma, respectively (Fig. 5.9B).

5.4.1.3 Granulite

14 analyses of biotite grains from the undeformed Flatraket granulite sample NF44A and 15 biotite grains from the sheared sample NF44F yielded very similar ages that range from 405 ± 4.7 Ma to 383 ± 2.4 Ma and 409 ± 3.8 Ma to 382 ± 2.3 Ma, respectively (Fig. 5.10).

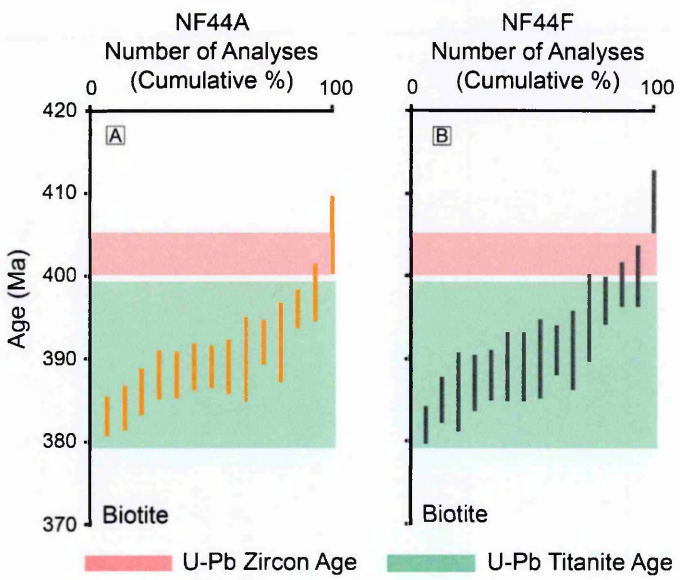

Fig.5.10. Cumulative graphs of biotite single grain fusion analyses for the Flatraket granulite. A) Sample NF44A from the undeformed granulite, and B) sample NF44F from the amphibolite-facies shear zones. The pink boxes represent the U-Pb zircon ages for the timing of peak metamorphism of Root *et al.,* (2004) and the green boxes represent the U-Pb titanite ages of the amphibolite-facies recrystallization of Spencer *et al.,* (2013).

					IR Single Grain Fusion Ages			UV *In-situ* Ages	
					Oldest Age	Youngest Age		Oldest Age	Youngest Age
Lithology	Sample	Location	Mineral	n#	Ma (± 1σ)	Ma (± 1σ)	n#	Ma (± 1σ)	Ma (± 1σ)
Eclogite	NF37	Krokkenakken	White Mica	20	464 ± 3.4	412 ± 2.2	18	438 ± 2.3	402 ± 10.6
			Amphibole	13	1850 ± 15.5	438 ± 6.9		nd	nd
Eclogite	NF45	Flatraket Harbour	White Mica	19	607 ± 0.9	396 ± 6.3		nd	nd
			Amphibole	23	2325 ± 7.3	391 ± 12.9		nd	nd
Eclogite	NF100	Drage	White Mica	14	757 ± 9	423 ± 9		nd	nd
Amphibolite	NF46	Flatraket Harbour	Biotite	15	391 ± 3.7	364 ± 6.5		nd	nd
			Amphibole	17	503 ± 7.0	386 ± 4.4		nd	nd
Amphibolite	NF49	Flatraket Harbour	Biotite	12	424 ± 2.4	410 ± 2.1		nd	nd
			Amphibole	7	858 ± 22.3	389 ± 4.0		nd	nd
Granulite	NF44A	Flatraket Quarry	Biotite	14	405 ± 4.7	383 ± 2.4	9	404 ± 4.0	386 ± 7.3
			Feldspar		nd	nd	3	1502 ± 78.6	360 ± 2.6
Granulite	NF44F	Flatraket Quarry	Biotite	15	409 ± 3.8	382 ± 2.3		nd	nd

nd = not determined n# = number of grains or spots

Krokkenakken	***61°54'53.73'' N***	***005°20'16.49'' E***
Drage	***62°06'08.30'' N***	***005°12'48.0'' E***
Flatraket Harbour	**61°58'42.60'' N**	***005°14'03.80'' E***
Flatraket Quarry	**61°58'41.50'' N**	***005°14'43.20'' E***

Table 5.4: Summary data table of white mica, biotite, and amphibole single grain fusion and *in-situ* analyses

5.4.2 UV Laser Ablation Data

Eclogite sample NF37 and granulite sample NF44A were selected for detailed *in-situ* laser ablation analysis to provide spatial context to the observed single grain fusion age variations and to analyses other phases associated with the micas. UV laser ablation was undertaken at the Ar/Ar and Noble Gas Laboratory at the Open University (OU) following the methodology outlined in Chapter 3. A summary of the ages is provided in Table 5.4 and on the representative photomicrograph in Fig. 5.11. The full dataset is provided in Appendix D.

18 spots on white mica grains from eclogite sample NF37 (Fig. 5.11) yielded single spot ages ranging from 438 ± 2.3 Ma to 402 ± 10.6 Ma. Within uncertainty, the white mica data yielded internally consistent ages with no consistent core–rim variations. Spot analysis of garnet and omphacite within the eclogite revealed negligible concentrations of Ar above background levels, indicating that no Ar was contained within these minerals.

9 spots on two biotite grains and 3 spots on a feldspar grain in sample NF44A yielded ages that range from 404 ± 4.0 Ma to 386 ± 7.3 Ma and 1502 ± 78.6 Ma to 360 ± 2.6 Ma, respectively. The biotite ages are consistent with those documented from the single grain fusion analysis.

5.5 Discussion

5.5.1 Eclogites

White mica and amphibole grains from eclogites from the Outer Nordfjord area show a very large spread in $^{40}Ar/^{39}Ar$ ages, from 727-396 Ma for white mica and 2325-391 Ma for amphibole. 98% of white mica and 97% of amphibole grains yielded ages that are far greater than the timing of peak metamorphism (405-400 Ma. U-Pb zircon; Root *et al.*, (2004)) and amphibolite-facies recrystallization (399-379 Ma. U-Pb titanite; Spencer *et al.*, (2013)). The factors that have caused elevated $^{40}Ar/^{39}Ar$ ages in the eclogites could be a lack of a fluid phase and a system that was closed to the loss of Ar. A lack of a fluid phase within the eclogites would mean that there was no medium by which Ar can be removed from the grain boundary network. Coupled with a system that is closed to the loss of Ar, these factors would cause the Ar that is produced to be retained within the eclogites.

The white mica analyses from the mafic eclogites (Fig. 5.8D), also show that there are differences between the eclogites from the different localities. NF45 and NF100 from Flatraket Harbour and Drage yield identical $^{40}Ar/^{39}Ar$ age patterns, which are consistently

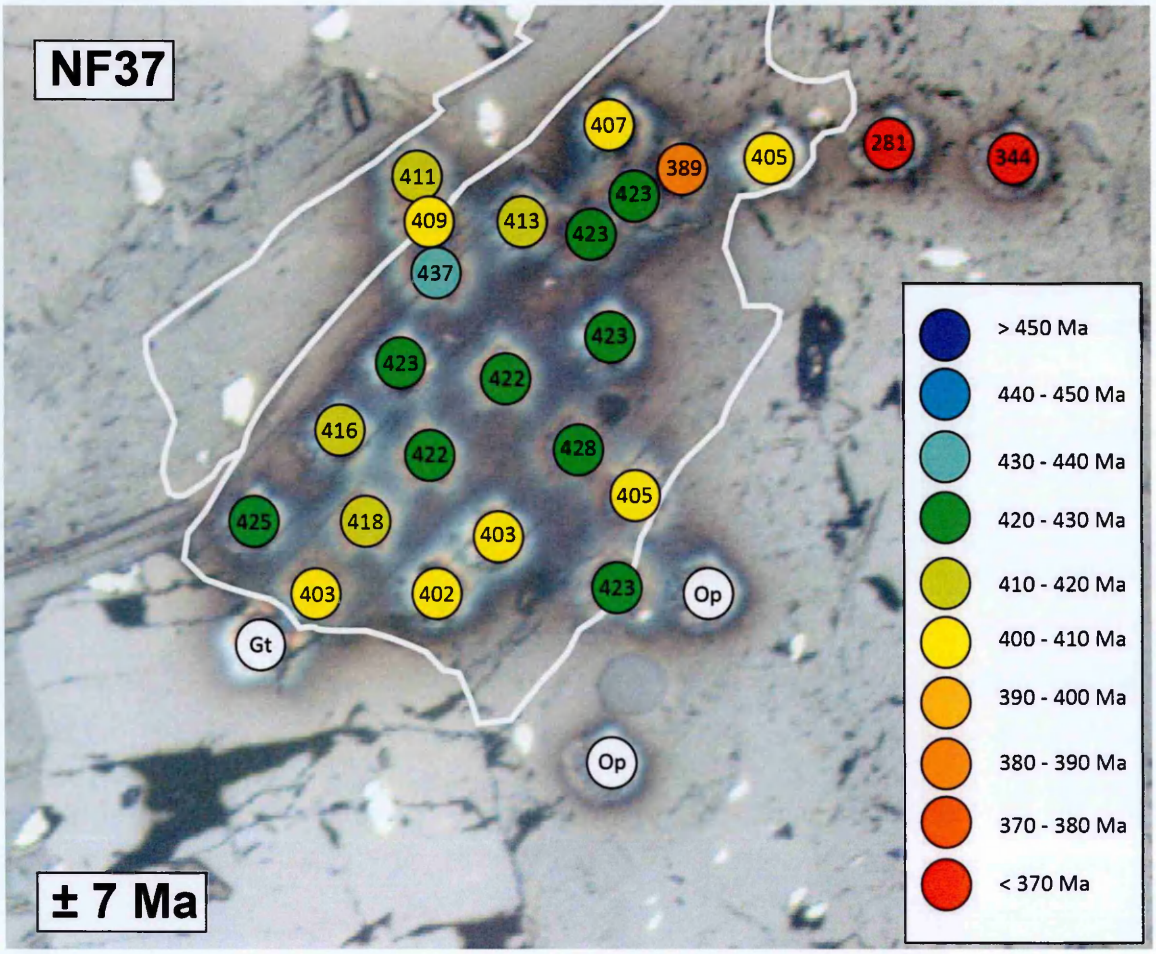

Fig.5.11. A reflected light photomicrograph showing *in-situ* UV laser ablation $^{40}Ar/^{39}Ar$ analysis in white mica from sample mafic eclogite sample NF37. Gt = garnet, Op = omphacite

older, and with a greater spread, than NF37. This may be due to petrological difference between the eclogites, with NF45 and NF100 being kyanite-bearing and NF37 being clinozoisite-bearing. Clinozoisite may be acting as a sink for Ar within eclogite NF37; however, this remains untested. Solubility studies indicates that minerals with open crystal structures, such as clinozoisite, may indeed act as sinks for Ar (Jackson *et al.*, 2013).

The presence of clinozoisite in NF37, an additional hydrous phase that is not present in eclogites NF45 and NF100, implies that NF37 had a greater fluid component. This increased fluid component in NF37 would have aided in the removal of Ar from the grain boundary network, yielding younger $^{40}Ar/^{39}Ar$ white mica ages and reduced the overall spread in age data on NF37, compared to samples NF45 and NF100.

The amphibole analysed from the eclogites is texturally younger than the white mica yet yields a far greater spread in $^{40}Ar/^{39}Ar$ ages, from 2325-391 Ma (a spread of 1934 Ma).

The amphiboles form at the contact between garnet and omphacite and contain very little K (~0.5 wt. %), therefore the $^{40}Ar/^{39}Ar$ ages most likely represent contamination by Ar within a closed grain boundary network, and the contamination mostly probably occurred during amphibole crystallisation. This relationship of texturally younger amphiboles yielding $^{40}Ar/^{39}Ar$ ages that are older than those recorded by white mica has also been documented in other eclogites from HP and UHP terranes, indicating that these age patterns might be a common occurrence within mafic eclogites (Sherlock *et al.*, 1999, Sherlock & Kelley 2002, Di Vincenzo 2006).

Overall, the $^{40}Ar/^{39}Ar$ ages from white mica and amphibole from the mafic eclogites of the Outer Nordfjord area indicate that during the decompression and exhumation of the WGR, mafic eclogites behaved as a closed system to Ar loss. *In-situ* analysis of garnet and omphacite in the eclogite did not reveal any measurable Ar above background, indicating that these phases did not act as sources or sinks for Ar during exhumation. This closed system nature meant that Ar could not be expelled from the rock and was instead redistributed between the white mica, the amphibole and/or other phases present in the rock such as clinozoisite.

5.5.2 Amphibolite

Samples NF46 and NF49 were selected to understand what happens to the Ar systematics at the periphery of the large eclogites and to smaller mafic lenses during the exhumation of the WGR. Petrographically, the amphibolites document mineralogical changes that occur to mafic eclogites during exhumation. These include the conversion of garnet to biotite + amphibole, formation of amphibole + plagioclase from omphacite, and biotite + plagioclase from the breakdown of white mica via symplectization (*cf.* Chapter 4). Both these reactions require the influx of fluid into the mafic eclogite.

Biotite and amphibole $^{40}Ar/^{39}Ar$ single grain fusion analysis from NF46 yield much narrower age ranges than the white mica and amphibole from the associated mafic eclogite (NF45). Biotites range from 391-364 Ma and the amphiboles range from 503-386 Ma, with biotite yielding consistently younger ages. The amphibole dataset is also more scattered than the biotite dataset, with a total age range of 117 Ma, rather than only 27 Ma in the biotite. The biotite ages are the same as the biotite ages yielded by the felsic gneisses documented in Chapter 3.

Biotite and amphibole from NF49 range in $^{40}Ar/^{39}Ar$ age from 424-410 Ma and 849-385 Ma, respectively. The biotite grains in NF49 show older relative ages, with a narrower

range in age, than those in NF46 (14 Ma compared with 27 Ma from NF46, Fig. 5.9C). The spread in the amphibole ages is also increased in sample NF49 with respect to sample NF46, from 117 Ma to 464 Ma.

These data show that during the amphibolitisation of mafic eclogites, the influx of fluids required for the process of amphibolitisation initially resets the amphibole $^{40}Ar/^{39}Ar$ chronometer, leading to both a reduction in age and age range from 1934 Ma in the mafic eclogite to 117 Ma in the amphibolites. The initial amphibolitisation reaction also reduces the mica $^{40}Ar/^{39}Ar$ ages from 727-396 Ma in the eclogite-bearing white mica to 381-364 Ma in the amphibolite-bearing biotite.

As amphibolitisation progresses, continued hydration of the mafic lenses causes the biotite and amphibole ages to become increasingly older, to ages greater than the 405-400 Ma timing of peak metamorphism (Root *et al.,* 2004). During decompression and exhumation, the felsic gneisses that host the mafic lithologies are undergoing dehydration reactions (e.g. symplectization of white mica to produce biotite + plagioclase; *cf.* Chapter 4). Since the amphibolites are hosted wholly within granodioritic gneisses, which are undergoing dehydration reactions during exhumation, the age increase documented in the amphibolites is most likely caused by contamination of Ar derived from these gneisses. Therefore during exhumation, the mafic amphibolites are acting as sinks for Ar that is being sourced from the felsic lithologies.

5.5.3 Granulite

The granulite at Flatraket is a relic lithology from prior to the Caledonian Orogeny. Its crystallisation age and granulite-facies metamorphism age are constrained by U-Pb zircon at c. 1670-1640 Ma and c. 1100-1000 Ma, respectively (Corfu *et al.,* 2013). During the Caledonian Orogeny, when much of the WGR was converted to eclogite-facies assemblages, the Flatraket Granulite only underwent minor eclogite-facies metamorphism within the core of the body as evidenced by the static conversion of plagioclase to zoisite + kyanite (Wain *et al.* 2001). At the margins of the granulite body, eclogite-facies assemblages are found in cross-cutting veins (Fig. 5.3B; Wain *et al.,* (2001)).

The arrested eclogitisation of the precursor granulite has been attributed to sluggish reaction kinetics, caused by the lack of a fluid phase (Wain *et al.,* 2001). In essence, the body remained 'dry' during much of the Caledonian Orogeny thus preserving its original granulite-facies mineral assemblages. The $^{40}Ar/^{39}Ar$ biotite age data, however suggests that

the biotite was still able to degas. The yielded biotite 401-379 Ma age range is within the range of the biotite $^{40}Ar/^{39}Ar$ ages documented from the felsic gneisses (Chapters 3 and 4).

In-situ analysis of the undeformed granulite hints at a possible sink for the Ar released during the degassing of the biotite. 3 spot ages on feldspar within the granulite yielded $^{40}Ar/^{39}Ar$ ages that range from 1485-356 Ma. This broad spread in ages implies that the feldspar, like those documented in the symplectites of Chapter 4, act as sinks for Ar within the granulite as well as the felsic gneisses of the WGR. However, further data from the feldspars within the granulite would be required to fully explore this interpretation.

Single grain fusion analysis of biotites from the amphibolite-facies shear zones that cross-cut the Flatraket Granulite yield $^{40}Ar/^{39}Ar$ ages that range from 404-379 Ma. These are, within error, identical to the ages from the undeformed granulite and the felsic host gneisses. The weighted means of the biotite $^{40}Ar/^{39}Ar$ from the sheared and undeformed granulite are also identical at 387-386 Ma.

The coincidence in biotite $^{40}Ar/^{39}Ar$ age data from the undeformed granulite, the sheared granulite and those of the felsic gneisses that host the Flatraket Granulite indicate that during the exhumation of the WGR biotite appears to have behaved in a very similar manner regardless of the lithology. The similarities between the biotite $^{40}Ar/^{39}Ar$ ages from the undeformed and sheared granulite also make interpreting the timing of when the shear zones were active within the granulite difficult.

5.6 Further Discussions

What is clear from this study is that the mafic eclogites and the felsic granulite behaved differently during the Caledonian Orogeny. Both eclogites and granulites are traditionally considered 'dry' or anhydrous lithologies, despite containing some hydrous phases. Biotite within the granulite was able to equilibrate and yield Caledonian $^{40}Ar/^{39}Ar$ ages whilst the white mica in the eclogite does not seem to have equilibrated. Three possibilities for the difference in behaviour of the mica in the eclogite and the granulite are:

(1) Lithological differences between the two rock types,

(2) Petrological differences between the two rock types, and

(3) Mineralogical differences between white mica and biotite.

Lithologically, the eclogites and the granulite from the Outer Nordfjord are fundamentally different. The eclogites are derived from a basaltic protolith while the granulite has a

granitic (quartz monzonitic) protolith. Whole rock data (Appendix E) shows that the eclogites contain only ~0.4 wt. % K_2O and the granulite contains ~3.4 wt. % K_2O. Since ^{40}Ar is produced from the radioactive decay of ^{40}K (*cf.* Chapter 1), it would stand to reason that the granulite, with its greater K content, should be able to produce more ^{40}Ar as described by Foland (1979) and Sherlock & Kelley (2002).

The anhydrous nature of the eclogites and granulite would hinder the diffusional loss of Ar from the white mica and biotite since there is little to no fluid present in the grain boundary network to remove Ar from the rock (e.g. Foland (1979), Scaillet (1996)). The greater capacity for the granulite to produce ^{40}Ar than the mafic eclogites would imply that the granulite should be more affected by excess Ar contamination. However, the eclogite white mica ages show more contamination than the granulite biotite. Therefore, it seems that a lithological control on the observed $^{40}Ar/^{39}Ar$ signatures from the eclogites and the granulite is unlikely.

Another possibility for understanding the differences in behaviour of Ar between the eclogites and the granulite is the retentivity to Ar of white mica and the biotite. Experimental studies on white mica have shown that the Ar retention of white mica increases with increasing pressure (Harrison *et al.,* 2009). These experimental data imply that the high pressures (2.6-3.2 GPa) experienced by the eclogites and the granulite during the peak of the Caledonian Orogeny had a greater effect on the white mica than on the biotite, causing Ar to be more readily retained within the white mica. This allowed the biotite in the granulite to degas and record $^{40}Ar/^{39}Ar$ ages that are equivalent to those observed in the felsic gneisses, whereas the white mica retained only 'anomalous' ages that are older than the timing of its crystallization.

Experimental work on biotite has shown that composition has a greater effect on Ar retention (Harrison *et al.,* 1985, Grove & Harrison 1996). These studies demonstrated that with igneous biotites, with the increasing replacement of Mg^{2+} by Fe^{2+} within the biotite crystal lattice, Ar can diffuse more readily from biotite. The change in the Fe/Mg content of biotite results in reducing the T_c of biotite, therefore Fe-rich biotites should yield younger ages than Mg-rich biotites (Harrison *et al.,* 1985). However, data from this study suggests that the composition of biotites may not have had much of an influence on the resulting $^{40}Ar/^{39}Ar$ ages.

Biotites from the amphibolites show a marked contrast to the experimental data. NF46 biotites have a very broad range in composition and are more Mg-rich than biotites from

NF49 ($Mg^{\#}$ 0.55-0.62 and 0.53-0.58, respectively). Yet the more Mg-rich biotites of NF46 yield the youngest ages, from 391-364 Ma, when compared with the more Fe-rich biotites of NF49 at 424-410 Ma.

An explanation for the differences between the experimental diffusion data of biotite and the data documented in this study is that the amphibolites show evidence for recrystallization and the interaction with fluids. As documented in Chapter 3, the processes of recrystallization and fluid interaction can affect the Ar isotopic signature of biotite. Recrystallization causes biotite ages to become elevated compared to ages that are expected from a simple diffusional interpretation (*cf.* Chapter 3). Fluid interactions can cause elevated $^{40}Ar/^{39}Ar$ age by bringing Ar into a system from an external source. For the amphibolites, this external source is probably the dehydrating host felsic gneisses. These results show, like with $^{40}Ar/^{39}Ar$ age data from felsic gneisses, that the physical processes that are affecting the amphibolites during the exhumation and decompression of the WGR have a far greater impact on the (re)distribution of Ar than simple thermal diffusion alone.

Since biotite in the granulite was able to degas and the white mica in the eclogites was not, there are hints that there might also be a petrographic control on the movement of Ar within these rock types. *In-situ* analyses of feldspar in the granulite, and omphacite and garnet in the eclogite show that the feldspar contains variable amount of Ar, whist the omphacite and garnet do not contain any measurable Ar. Feldspar acts a sink for Ar within the felsic gneisses (Chapter 4), allowing Ar degassed from white mica to be absorbed. This process also appears to have operated in the granulite as well, with feldspar acting as a sink for Ar during biotite degassing during decompression and exhumation.

The lack of measurable Ar in the omphacite and garnet indicates that these minerals did not act as a sink for Ar within the eclogite. Other phases within the eclogite, such as clinozoisite or kyanite, may have acted as sinks for Ar. A single study by Itaya *et al.,* (2008) of detrital kyanites indicates that kyanite may be a potentially large sink for Ar. However, the Ar content of the kyanite present in the eclogite this study was not analysed due to its rarity and small grain size. As previously mentioned, clinozoisite may also act as a sink for Ar, based upon solubility studies, but to date no $^{40}Ar/^{39}Ar$ studies have been undertaken in natural clinozoisite. Therefore, the elevated age in the eclogites implies that either Ar diffused out of the white mica and was later reincorporated or it never managed to diffuse out of the white mica in the first place. If Ar was able to diffuse out of the white mica but was subsequently reincorporated, then older $^{40}Ar/^{39}Ar$ ages would be expected at the rims of the white mica, relative to the core, where Ar had diffused back into the white

mica forming convex age profiles. If Ar had not been able to diffuse at all, the elevated ages would occur throughout the grains. *In-situ* analysis of white mica shows a slight pattern in the $^{40}Ar/^{39}Ar$ age, with patchy 'older' ages and 'younger' ages within the grain (Fig. 5.11). These age are still equal to, and older than, the timing of peak metamorphism (405-400 Ma; Root *et al.,* (2004)) indicating that while diffusion may have occurred, it was insufficient to reset the $^{40}Ar/^{39}Ar$ ages.

5.7 Conclusion

Mafic eclogites and granulites form only a minor lithological component of the WGR, yet provide important information regarding the differing behaviour of Ar in mafic and felsic lithologies during the exhumation of the WGR. White mica that forms part of the peak metamorphic assemblage in the mafic eclogites yields ages that range from 727 Ma to 396 Ma, while secondary amphibole that grew from the reaction between garnet and omphacite yields highly scattered ages that range from 2325 Ma to 391 Ma. These ages are older than the timing of peak metamorphism defined by U-Pb zircon and older than the relative timing of crystallisation of these phases (Root *et al.,* 2004). Overall, the eclogite $^{40}Ar/^{39}Ar$ age data show that mafic eclogites behaved as a closed system to Ar loss during the exhumation of the WGR.

Amphibolites that form from the hydration of the mafic eclogites during exhumation and decompression of the WGR provide a record of processes at the mafic eclogite – felsic gneiss interface. Initial amphibolitisation and recrystallization of the mafic eclogites results in the younging of the $^{40}Ar/^{39}Ar$ chronometers, yielding biotite ages that range from 391 Ma to 364 Ma and amphibole ages that range from 503 Ma to 386 Ma. These data imply that the influx of fluids derived from the dehydrating felsic gneisses initially reset the $^{40}Ar/^{39}Ar$ chronometers in the edges of the mafic eclogites. With continued amphibolitisation, the biotite and amphibole grains in the amphibolites acquire apparently older $^{40}Ar/^{39}Ar$ ages, yielding ages that range from 424 Ma to 410 Ma and 849 Ma to 385 Ma, respectively. These data indicate that during exhumation of the WGR, amphibolites, hydrated by fluids derived from the host felsic gneisses, acted as a sink for Ar.

The Flatraket Granulite body documents the fact that, despite the lack of metamorphic reaction that failed to convert the granulite to eclogite and/or amphibolite-facies assemblages, the biotite behaved as an open system with regards to Ar loss. The biotites recorded Caledonian ages with feldspar acting as a sink for Ar and recording highly variable ages.

Overall, these data indicate that during the Caledonian Orogeny, the anhydrous lithologies behaved differently with respect to their abilities to redistribute Ar within the rock volume. The difference in behaviour may be a combination of the different retention properties of white mica and biotite to Ar loss, but also the other minerals associated with the micas. The mafic eclogites have no sinks for Ar other than the white mica, whereas the feldspars within the granulite act as a sink for the Ar degassing from the biotite. This allows the biotite to remain relatively contamination-free in comparison to the white mica in the eclogite and allows them to record Caledonian ages.

Chapter 6

Conclusions

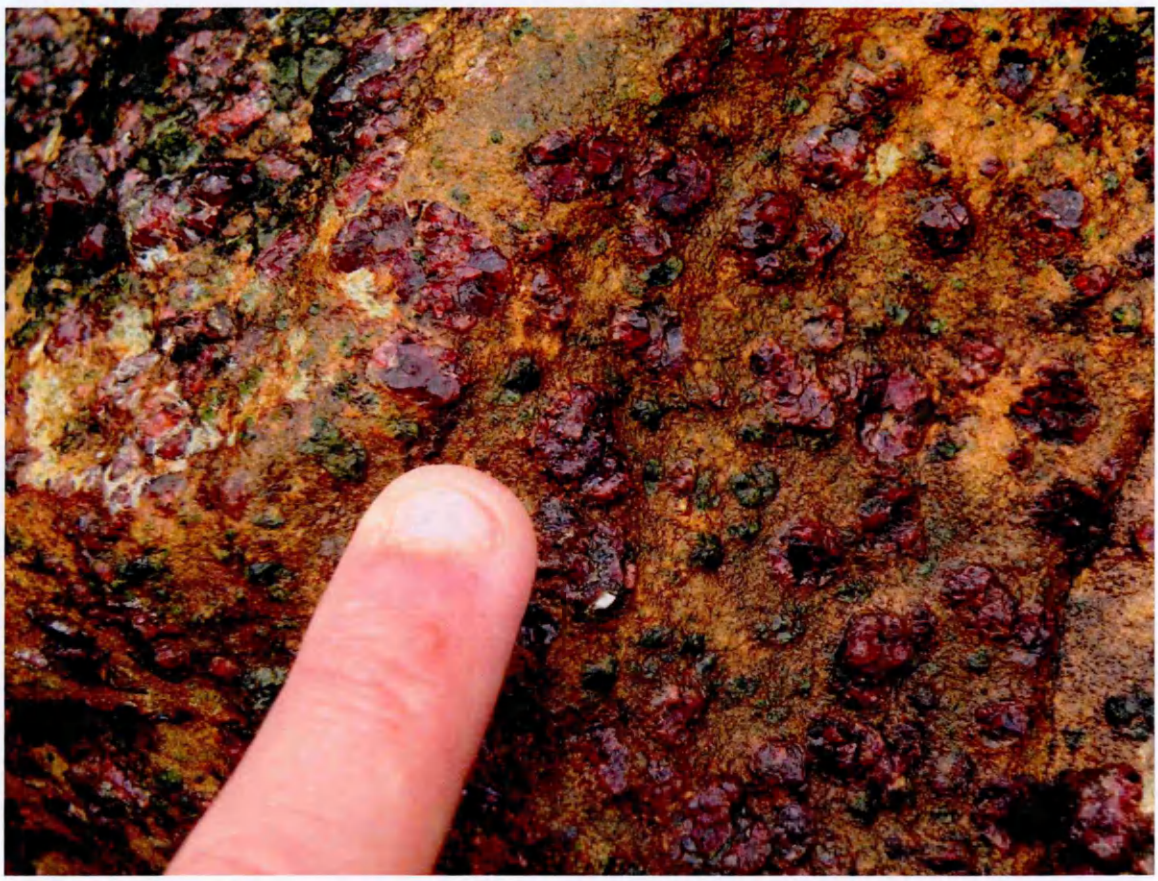

Garnet peridotite, Almklovdalen: D. Regis

The main aims of this study, as outlined in Chapter 1, were:

(1) To create a conceptual diffusion modelling framework, in which $^{40}Ar/^{39}Ar$ ages may be interpreted in terms of the metamorphic evolution of the WGR,

(2) To understand how the physical processes that affect rocks during exhumation, such as recrystallization, deformation, and fluids, have affected the Ar isotopic signature of the crustal gneisses of the WGR and to use $^{40}Ar/^{39}Ar$ chronology to track these processes during decompression from eclogite-facies conditions to amphibolite-facies conditions,

(3) To investigate how Ar is redistributed during the breakdown of high-pressure white mica to biotite and plagioclase symplectites in order to determine how Ar behaves during an exhumation-related metamorphic reaction, and

(4) To compare and contrast the behaviour of Ar in anhydrous mafic eclogite and felsic granulite lithologies in order to how these lithologies behaved, with respect to the Ar isotope systematics, during the Caledonian Orogeny.

These aims were achieved by using infra-red (IR) laser single grain fusion of white mica, biotite, and amphibole mineral separates in conjunction with ultraviolet (UV) laser ablation *in-situ* analysis of white mica, biotite, and plagioclase in polished slabs from selected samples. Non-K-bearing mineral phases including quartz, garnet, and omphacite were analysed to determine whether these phases were acting as sinks for Ar during exhumation.

(1) Diffusion modelling has been shown to be a powerful tool for estimating the expected bulk ages for white mica and biotite, for a known P-T history, and in turn the modelling can be used to gauge whether the measured $^{40}Ar/^{39}Ar$ ages can be interpreted as cooling ages. These models solve the diffusion equation (Equation 1.3) numerically and do not assume the shape of the cooling curve that the Dodson T_c formulation requires. WGR models suggest that white mica and biotite should yield ages that are 6 Ma and 11 Ma younger, respectively, than the timing of mica crystallisation, for a moderate cooling rate of $25°CMa^{-1}$. Assuming cooling from 393 Ma (the weighted mean U-Pb titanite age; Spencer *et al.* (2013)), white mica should yield an age of ~387 Ma and biotite should yield an age of ~382 Ma.

The petrographic evolution and the relative timing of white mica and biotite growth for the felsic gneisses and eclogites were constrained by using the P-T modelling software Perple_X. Petrogenetic modelling indicates that the felsic gneisses and the eclogites shared a common P-T path and that during exhumation and decompression, white mica in the

gneisses broke down to form biotite + plagioclase symplectites over a broad pressure interval of 1.9-1.1 GPa.

(2) The modelling results were used to assess the single grain fusion $^{40}Ar/^{39}Ar$ ages in terms of the petrographic evolution of the rock and the open system assumption of the T_c formulation. IR laser single fusion analysis of white mica and biotite mineral separates of felsic gneisses from the Outer Nordfjord area of the WGR, which are geochemically similar, yet record different stages of the metamorphic cycle, yield broad ranges in $^{40}Ar/^{39}Ar$ ages. White mica $^{40}Ar/^{39}Ar$ ages range from 423 ± 7 Ma to 377 ± 8 Ma, while biotite yields $^{40}Ar/^{39}Ar$ ages of 438 ± 3 Ma to 353 ± 5 Ma. These ages span the entirety of the known metamorphic cycle for the Caledonian Orogeny and cannot be interpreted as mica cooling ages through a mineral specific T_c.

Simple diffusion models cannot readily explain the youngest or the weighted mean observed $^{40}Ar/^{39}Ar$ ages, nor explain the range of ages documented in the felsic gneisses; instead these data show that physical processes such as recrystallization, deformation, partial melting and the influx of fluids appear to have had a greater effect on Ar distribution. Samples that show significant recrystallization and deformation yield younger white mica ages, but older biotite ages, than more pristine samples. Furthermore, migmatisation acts to make biotite ages younger in the amphibolite-facies gneisses whereas fluid infiltration acts to increase biotite ages.

UV laser ablation *in-situ* analysis was used to understand the spatial distribution of the heterogeneous single grain fusion ages, both within grains in the same sample and between samples. *In-situ* analysis yields a similar, broad range in $^{40}Ar/^{39}Ar$ age to the single grain fusion dataset. White mica and biotite spot ages ranged from 502-348 Ma and 441-360 Ma, respectively. The *in-situ* studies also demonstrated a lack of core-rim age profiles in the white mica and biotite that could not be attributed to diffusion. Instead, 'old' ages in the white mica were patchily distributed within the grains and were not associated with the geographic cores of the grains. Biotite, however, yielded more homogeneous within-grain age distributions.

(3) A detailed UV-laser ablation study was undertaken to understand how Ar was (re)distributed within the felsic gneisses during the decompression-related breakdown of white mica, and which minerals acted as Ar sources and/or sinks. White mica yields a patchy distribution of 'old' ages (≥492 Ma) that are not associated with the geographic core of the grain. 'Younger' ages within the white mica range from 412-389 Ma. Biotite

and plagioclase within the replacement symplectite yield ages that range from 389-380 and 705-269 Ma, respectively. Texturally younger idioblastic biotites yield ages that range from 400-377 Ma. These data indicate that as HP white mica breaks down, some released Ar is incorporated into the symplectic biotite and some into plagioclase. The texturally younger idioblastic biotites yield a larger range in $^{40}Ar/^{39}Ar$ age than the texturally older symplectite biotite. These data indicate that during the continued growth of biotite from symplectic to idioblastic form, Ar became increasingly incorporated into the idioblastic biotite. These data show that white mica acts as a source for Ar in the biotite during its crystallisation from white mica and that plagioclase is a major sink for Ar in the felsic gneisses during the exhumation of the WGR.

(4) The eclogites and granulites from the Outer Nordfjord area behaved differently with regards to their Ar systematics. The eclogites yielded white mica and amphibole single grain fusion $^{40}Ar/^{39}Ar$ ages that ranged from 757-396 Ma and 2325-391 Ma, respectively. Meanwhile the biotite and feldspar from the felsic granulite yielded $^{40}Ar/^{39}Ar$ ages that range from 405-383 Ma and 1502-360 Ma, respectively. The younger ages in the granulite biotite indicate that biotite was able to degas during the exhumation of the WGR, thus yielding ages that are similar to the biotite in the felsic gneisses. The white mica in the eclogite was not able to degas, however, thus recording 'old(er)' $^{40}Ar/^{39}Ar$ ages. What these data show is that granulite behaved locally as an open system, allowing Ar to be lost during exhumation. The eclogites, however, behaved as a closed system to the loss of Ar. With the absence of a fluid phase within both rocks types, it can be argued that the feldspar in the granulite acted as a sink for Ar, since the $^{40}Ar/^{39}Ar$ ages of the feldspar are highly variable. Since feldspar is absent from the mafic eclogites, there was no mineralogical sink for Ar released from the white mica within the rock volume.

At the margins of some of the larger eclogites the presence of amphibolites shows that fluid influx initially catalysed the recrystallization of the HP eclogite-facies parageneses to an amphibolite-facies mineral assemblage of biotite + amphibole + plagioclase. Biotite single grain fusion $^{40}Ar/^{39}Ar$ ages range from 391-364 Ma and amphibole single grain fusion $^{40}Ar/^{39}Ar$ ages range from 503-386 Ma. These ages are younger than the white mica and amphibole ages reported for the associated eclogite, suggesting that recrystallization to an amphibolite-facies paragenesis reset the $^{40}Ar/^{39}Ar$ ages at the margin of the eclogite. Prolonged fluid influx, presumably derived from the dehydrating felsic gneisses, led to older biotite and amphibole $^{40}Ar/^{39}Ar$ ages in these samples (424-410 Ma and 849-385, respectively) indicating that the amphibolites acted as sinks for Ar on the outcrop scale.

Overall these data show that white mica and biotite $^{40}Ar/^{39}Ar$ ages from the eclogites, amphibolites, felsic gneisses, and felsic granulites cannot be reconciled with simple model of diffusional loss, and that at HT, Ar may not readily diffuse out of micas. By combining $^{40}Ar/^{39}Ar$ ages with diffusion modelling and detailed petrographic analysis, these data can instead shed light on the sources and sinks for Ar within the rock volume and show how processes such as recrystallization affect the behaviour of Ar during the exhumation of metamorphic terranes.

These study shows that white mica and biotite $^{40}Ar/^{39}Ar$ ages may not always be interpretable as cooling ages and that they require careful assessment in terms of their metamorphic and petrological evolution of HP terranes. Understanding the petrographic evolution is necessary to provide a basis for interpreting the behaviour of Ar, thus allowing $^{40}Ar/^{39}Ar$ age data to be linked more accurately to a metamorphic 'stage'.

6.2 Broader Implications of This Study

6.2.1 Implications for the Dodson Closure Temperature Formulation

For metamorphic $^{40}Ar/^{39}Ar$ to be considered robust cooling ages, they must be shown to adhere to the three inherent assumptions of the Dodson (1973) T_c formulation:

1) The concentration of Ar within a grain is governed only by thermally-activated volume diffusion that adheres to Fick's 2nd law of diffusion.

2) The mineral grain crystallised or recrystallized with no inherited Ar within its crystal lattice, and

3) The grain boundary network operates as an 'open system' i.e. the concentration of Ar in the grain boundary is negligible such that the grain boundary network acts as an 'infinite' sink for Ar.

The evidence documented in this study from the gneisses and minor lithologies of the WGR indicates that all three of the inherent assumptions implied within the Dodson T_c formulation are invalidated on some level and that the $^{40}Ar/^{39}Ar$ ages produced cannot be linked to mineral specific closure temperatures. Firstly, diffusion model results do not match the in-situ age profiles, suggesting that thermally-activated volume diffusion was not one of the primary mechanisms acting in the Nordfjord high-temperature metamorphic rocks for redistributing Ar within micas. Other physical processes such as white mica breakdown, partial melting, and the influence of fluids had a far greater impact on

redistributing Ar within this metamorphic system, thereby invalidating the first assumption if the Tc formulation. Secondly, Ar data from different portions of the symplectite breakdown reaction documented in Chapter 4 showed that Ar can be reincorporated into mineral grains during (re)crystallisation, thereby invaliding the second assumption of the T_c formulation. Thirdly, the broad, heterogeneous spreads in Ar ages documented in the symplectites and gneisses indicates that Ar was not able to readily leave the system but instead acted as a contaminant. This implies that the grain boundary network not operating as a fully open system and the grain boundary network was not acting as an 'infinite' sink for Ar, invalidating the third assumption of the T_c formulation.

Overall these data show that even when, on average, the yielded Ar ages are younger than ages yielded from higher temperature chronometers, it is important to consider and test the full implications of the Dodson (1973) T_c formulation assumptions. The interpretation of these ages as 'cooling ages' is not valid in this terrane even though high enough temperatures were encountered for long enough after mica crystallisation. It is therefore important to assess the role that diffusion plays in future $^{40}Ar/^{39}Ar$ geochronological studies of metamorphic terranes. This can be achieved by detailed *in-situ* spot analysis of mica grains to determine the presence of diffusion profiles which would point towards diffusion being the primary mechanism for redistributing Ar within mineral grains.

6.2.2 Assessing Suitability of Grains for Dating: White Mica or Biotite? Which Mineral for Which Circumstance?

This study has shown that, particularly during high-temperature exhumation paths (~700°C and ~3-1 GPa), white mica and biotite may not yield information about the metamorphic terranes cooling history. Therefore it is important to assess which mineral is suitable for understanding the evolution of high-temperature metamorphic terranes. Diffusion models can be used to extrapolate expected $^{40}Ar/^{39}Ar$ ages from K-bearing minerals given a set of P-T conditions given the same set of assumptions as the Dodson (1973) T_c formulation.

Diffusion models suggest that due to its more diffusive nature, biotite would make a more ideal Ar chronometer than white mica for understanding quantifying cooling histories at low temperature metamorphic conditions (~450°C at 1 GPa). At higher temperature metamorphic conditions (> ~650°C at 1 GPa), either white mica or biotite could theoretically be used to determine the cooling histories of a given metamorphic terrane.

This modelled behaviour is, however, not observed in the natural samples from the WGR because the assumptions mentioned above are not met. White mica and biotite display

variable contamination from Ar that was unable to leave the system during decompression and exhumation. Therefore because the spatial Ar distributions in natural samples may or may not correspond with those predicted by diffusion models, it is important to assess the Ar data from each mineral within each sample on a case by case basis, in conjunction with the P-T and petrological evolution of the sample.

In the WGR, white mica is almost always associated with the peak metamorphic assemblage, and is present as a relic phase in lower pressure lithologies. Biotite, on the other hand, is the result of the breakdown of the white mica during decompression as a result of symplectisation. This petrological evolution is for the most part reflected in the $^{40}Ar/^{39}Ar$ data: where biotite is associated with white mica breakdown then the biotite yields younger ages. The youngest biotite $^{40}Ar/^{39}Ar$ ages of the entire sample set are found within these symplectites and yield the most plausible cooling ages. In the case of the WGR, it is biotite and not white mica that appears to yield cooling age information and therefore any future mica studies of high-temperature metamorphic terranes will require then investigation of phases in multiple petrological positions in order to determine which minerals in which circumstances yield be most reliable information regarding the cooling history of the WGR.

6.2.3 Strategies for Collection of Metamorphic $^{40}Ar/^{39}Ar$ Age Data

In this study, 24 samples of similar geochemical composition in which the petrographic evolution was well-constrained were analysed. In detail, data were collected from 224 grains and 210 spots on white mica, 373 grains and 167 spots on biotite, and 60 grains of amphibole as well as non-K-bearing phases such as garnet, plagioclase, and epidote. This in-depth study allowed the sources and sinks for Ar during a metamorphic cycle to be assessed. Only by performing such an in-depth study can the behaviour of Ar in high-temperature metamorphic rocks be characterised and understood within a petrological and geochronological framework.

This study has shown that no one single sample from a metamorphic terrane will necessarily yield the desired information regarding the cooling history. Instead by applying a multi-sample, multi-technique study, on samples that are petrologically and geochronologically well constrained such as the one described here will allow future studies a detailed overview of the behaviour of the Ar within the system and for the role of diffusion to be assessed.

6.3 Suggestions for Future Work

The work carried out in this study could be enhanced and complimented by numerous other studies that would further our understanding of the behaviour of Ar during a metamorphic cycle. These include:

(1) A Rb-Sr geochronological study of the white mica and biotite analysed in this study. Rb-Sr ages of mica from other HP terranes have suggested that Rb-Sr records the timing of mica crystallisation (Li *et al.,* 1994, Sherlock *et al.,* 1999, Glodny *et al.,* 2008). This technique would not only compliment the $^{40}Ar/^{39}Ar$ age data, but would also place temporal constraints on when mica crystallised in the WGR.

(2) Further $^{40}Ar/^{39}Ar$ data from the plagioclase feldspar and alkali feldspar within the gneisses of the WGR, would allow the role that feldspars play as sinks for Ar during metamorphism to be further assessed.

(3) A transmission electron microprobe (TEM) study, coupled with in-situ laser ablation $^{40}Ar/^{39}Ar$ analysis, could be employed to understand how microstructural defects within the micas (particularly in the white mica) affect the incorporation of excess Ar.

(4) A fluid inclusion study on the gneisses that record differing points along the P-T path from eclogite-facies conditions to amphibolite-facies conditions would provide information on the Ar isotopic composition of the fluid and how the concentration of Ar evolved and changed during the exhumation of the WGR.

(5) Further analysis of non-K-bearing mineral phases associated with the white mica and biotite (e.g. epidote, kyanite, quartz, garnet, and pyroxenes) to determine which phases act as sinks for Ar during the exhumation of the WGR.

(6) Solubility vs. diffusion study of the white mica and biotite would shed light on which of these fundamental processes ultimately control whether Ar is (re)incorporated in the minerals. Although diffusion of Ar out of minerals is believed to be the main process by which Ar is lost from the grain to the grain boundary network, it's the solubility of Ar at the grain boundary-mineral interface that controls whether not Ar is reincorporated back into a mineral from the grain boundary. During recrystallization, deformation, migmatisation, and fluid influx, the boundary conditions are altered and may, or may not, favour the reincorporation of Ar into minerals. This study would shed light on the behaviour of Ar at the grain boundary-mineral interface.

References

Allaz, J., Engi, M., Berger, A. & Villa, I. M. 2011. The Effects of Retrograde Reactions and of Diffusion on $^{40}Ar/^{39}Ar$ Ages of Micas. *Journal of Petrology*, **52**, 691–716.

Andersen, T. B., Jamtveit, B., Dewey, J. F. & Swensson, E. 1991. Subduction and eduction of continental crust: major mechanism during continent-continent collision and orogenic extensional collapse, a model based on the south Caledonides. *Terra Nova*, **3**, 303–310.

Andersen, T. B., Berry IV, H. N., Lux, D. R. & Andersen, A. 1998. The tectonic significance of pre-Scandian $^{40}Ar/^{39}Ar$ phengite cooling ages in the Caledonides of western Norway. *Journal of the Geological Society, London*, **155**, 297–309.

Armstrong, R., Jäger, E. & Eberhardt, P. 1966. A comparison of K-Ar and Rb-Sr ages on Alpine biotites. *Earth and Planetary Science Letters*, **1**, 13–19.

Austrheim, H., Corfu, F., Bryhni, I. & Aandersen, T. B. 2003. The Proterozoic Hustad igneous complex: a low strain enclave with a key to the history of the Western Gneiss Region of Norway. *Precambrian Research*, **120**, 149–175.

Baldwin, S. L., Lister, G. S., Hill, E. J., Foster, D. A. & McDougall, I. 1993. Thermochronologic constraints on the tectonic evolution of active metamorphic core complexes, D'Entrecasteaux Islands, Papua New Guinea. *Tectonics*, **12**, 611–628.

Baxter, E. F., DePaolo, D. J. & Renne, P. R. 2002. Spatially correlated anomalous $^{40}Ar/^{39}Ar$ "age" variations in biotites about a lithologic contact near Simplon Pass, Switzerland: A mechanistic explanation for excess Ar. *Geochimica et Cosmochimica Acta*, **66**, 1067–1073.

Camacho, A., Lee, J. K. W., Ftiz Gerald J. D., Zhao, J., Abdu, Y. A., Jenkins, D. M., Hawthorne, F. C., Kyser, T. K., Creaser, R. A., Armstrong, R. & Heaman, L. W. 2012. Planar defects as Ar traps in trioctahedral micas: A mechanism for increased Ar retentivity in phlogopite. *Earth and Planetary Science Letters*, **341-344**, 255–267.

Carswell, D. A., Tucker, R. D., O'Brien, P. J. & Krogh, T. E. 2003a. Coesite micro-inclusions and the U/Pb age of zircons from the Hareidland Eclogite in the Western Gneiss Region of Norway. *Lithos*, **67**, 181–190.

Carswell, D. A., Brueckner, H. K., Cuthbert, S. J., Metha, K. & O'Brien, P. J. 2003b. The timing of stabilisation and the exhumation rate for the ultra-high pressure rocks in the Western Gneiss Region of Norway. *Journal of Metamorphic Geology*, **21**, 601–612.

Chopin, C. 1984. Coesite and pure pyrope in high-grade blueschists of the western Alps: a first record and some consequences. *Contributions to Mineralogy and Petrology*, **86**, 107–118.

Clark, S. P. & Jäger, E. 1969. Denudation rate in the Alps from geochronologic and heat flow data. *American Journal of Science*, **267**, 1143–1160.

Connelly, J. A. D. 1990. Multivariable Phase Diagrams: An Algorithm Based on Generalized Thermodynamics. *American Mineralogist*, **290**, 666–718.

Copeland, P., Harrison, T. M., Kidd, W. S. F., Ronghua, X. & Yuquan, Z. 1987. Rapid early Miocene acceleration of uplift in the Gangdese Belt, Xizang (southern Tibet), and its bearing on accommodation mechanisms of the India-Asia collision. *Earth and Planetary Science Letters*, **86**, 240–252.

Corfu, F., Austrheim, H. & Ganzhorn, A. C. 2013. Localized granulite and eclogite facies metamorphism at Flatraket and Kråkeneset, Western Gneiss Region: U-Pb data and tectonic implications. *Geological Society, London, Special Publications*, **390**, 425–442.

Cumbest, R. J., Johnson, E. L. & Onstott, T. C. 1994. Argon composition of metamorphic fluids: Implications for $^{40}Ar/^{39}Ar$ geochronology. *Geological Society of America Bulletin*, **106**, 942–951.

Cuthbert, S. J., Carswell, D. A., Krogh-Ravna, E. J. & Wain, A. 2000. Eclogites and eclogites in the Western Gneiss Region, Norwegian Caledonides. *Lithos*, **52**, 165–195.

Dale, J., Holland, T. M. & Powell, R. 2000. Hornblende-garnet-plagioclase thermobarometry: a natural assemblage calibration of the thermodynamics of hornblende. *Contributions to Mineralogy and Petrology*, **140**, 353–362.

Dalrymple, G. B. & Lanphere, M. A. 1969. *Potassium-Argon Dating: Principals, Techniques and Applications to Geochronology*. San Francisco, W. H. Freeman & Co.

De Sigoyer, J., Chavagnac, V., Blichert-Toft, J., Villa, I. M., Luais, B., Cosca, M. A. & Mascle, G. 2000. Dating the Indian continental subduction and collisional thickening in the northwest Himalaya : Multichronology of the Tso Morari eclogites. *Geology*, **28**, 487–490.

Di Vincenzo, G. 2004. The Relationship between Tectono-metamorphic Evolution and Argon Isotope Records in White Mica: Constraints from in situ $^{40}Ar/^{39}Ar$ Laser Analysis of the Variscan Basement of Sardinia. *Journal of Petrology*, **45**, 1013–1043.

Di Vincenzo, G. 2006. Comparison of $^{40}Ar/^{39}Ar$ and Rb-Sr Data on Phengites from the UHP Brossasco-Isasca Unit (Dora Maira Massif, Italy): Implications for Dating White Mica. *Journal of Petrology*, **47**, 1439–1465.

Di Vincenzo, G., Ghiribelli, B., Giorgetti, G. & Palmeri, R. 2001. Evidence of a close link between petrology and isotope records: constraints from SEM, EMP, TEM and in situ $^{40}Ar/^{39}Ar$ laser analysis on multiple generations of white micas (Lanterman Range, Antarctica). *Earth and Planetary Science Letters*, **192**, 389–405.

Dobrzhinetskaya, L. F., Eide, E. A., Larsen, R. B., Sturt, B. A., Trønnes, R. G., Smith, D. C., Taylor, W. R. & Posukhova, T. V.. 1995. Microdiamond in high-grade metamorphic rocks of the Western Gneiss region, Norway. *Geology*, **23**, 597.

Dodson, M. H. 1973. Closure temperature in cooling geochronological and petrological systems. *Contributions to Mineralogy and Petrology*, **40**, 259–274.

Dransfield, M. 1994. *Extensional Exhumation of High-Grade Rocks in Western Norway and the Zanskar Himalaya*. University of Oxford.

Duchêne, S., Bilchert-Toft, J., Luais, B., Télouk, P., Lardeaux, J. -M. & Albarède, F. 1997. The Lu-Hf dating of garnets and the ages of the Alpine high-pressure metamorphism. *Nature*, **387**, 586–589.

Eskola, P. 1921. On the eclogites of Norway. *Norske vidsenskaps-akademi i Oslo. Matematisk-naturvidenskabelig klasse 8*, 1–118.

Faure, M., Lin, W., Shu, L., Sun, Y. & Schärer, U. 1999. Tectonics of the Dabieshan (eastern China) and possible exhumation mechanism of ultra high-pressure rocks. *Terra Nova*, **11**, 251–258.

Foland, K. A. 1979. Limited mobility of argon in a metamorphic terrane. *Geochimica et Cosmochimica Acta*, **43**, 793–801.

Foland, K. A. 1974. ^{40}Ar diffusion in homogeneous orthoclase and an interpretation of Ar diffusion in K-feldspar. *Geochimica et Cosmochimica Acta*, **38**, 151–166.

Fossen, H. 2010. Extensional tectonics in the North Atlantic Caledonides: a regional view. *Geological Society, London, Special Publications*, **335**, 767–793.

Foster, D. A., Harrison, T. M., Millar, C. F. & Howard, K. A. 1990. The $^{40}Ar/^{39}Ar$ thermochronology of the eastern Mojave Desert, California, and adjacent western Arizona with implications for the evolution of metamorphic core complexes. *Journal of Geophysical Research*, **95**, 20005–20024.

Gaál, G. & Gorbatschev, R. 1987. An outline of the Precambrian evolution of the Baltic Shield. *Precambrian Research*, **35**, 15–52.

Ganzhorn, A. C., Labrousse, L., Prouteau, G., Leroy, C., Vrijmoed, J. C., Andersen, T. B. & Arbaret, L. 2014. Structural, petrological and chemical analysis of syn-kinematic migmatites: insights from the Western Gneiss Region, Norway. *Journal of Metamorphic Geology*, **32**, 647–673.

Gebauer, D., Schertl, H. –P., Brix, M. & Schreyer, W. 1997. 35 Ma old ultrahigh-pressure metamorphism and evidence for very rapid exhumation in the Dora Maira Massif, Western Alps. *Lithos*, **41**, 5–24.

Giorgis, D., Cosca, M. A. & Li, S. 2000. Distribution and significance of extraneous argon in UHP eclogite (Sulu terrain, China): insight from in situ $^{40}Ar/^{39}Ar$ UV-laser ablation analysis. *Earth and Planetary Science Letters*, **181**, 605–615.

Glodny, J., Kühn, A. & Austrheim, H. 2008. Diffusion versus recrystallization processes in Rb–Sr geochronology: Isotopic relics in eclogite facies rocks, Western Gneiss Region, Norway. *Geochimica et Cosmochimica Acta*, **72**, 506–525.

Griffin, W. & Brueckner, H. 1980. Caledonian Sm–Nd ages and a crustal origin for Norwegian eclogites. *Nature*, **285**, 319–321.

Grove, M. & Hsrrison, T. M. 1996. $^{40}Ar^*$ diffusion in Fe-rich biotite. *American Mineralogist*, **81**, 940–951.

Hacker, B. R. 2007. Ascent of the ultrahigh-pressure Western Gneiss Region, Norway. *Geological Society of America Special Paper*, **419**, 171–184.

Hacker, B. R. & Gans, P. B. 2005. Continental collisions and the creation of ultrahigh-pressure terranes: Petrology and thermochronology of nappes in the central Scandinavian Caledonides. *Geological Society of America Bulletin*, **117**, 117–134.

Hacker, B. R. & Gerya, T. V. 2013. Paradigms, new and old, for ultrahigh-pressure tectonism. *Tectonophysics*, **603**, 79–88.

Hacker, B. R., Calvert, A., Zhang, R. Y., Ernst, W. G. & Liou, J. G. 2003. Ultrarapid exhumation of ultrahigh-pressure diamond-bearing metasedimentary rocks of the Kokchetav Massif, Kazakhstan? *Lithos*, **70**, 61–75.

Hacker, B. R., Andersen, T. B., Johnston, S., Kylander-Clark, A. R. C., Peterman, E. M., Walsh, E. O. & Young, D. J. 2010. High-temperature deformation during continental-margin subduction & exhumation: The ultrahigh-pressure Western Gneiss Region of Norway. *Tectonophysics*, **480**, 149–171.

Hacker, B. R., Ratschbacher, L., Webb, L., McWilliams, M. O., Ireland, T., Calvert, A., Dong, S., Wenk, H. –R. & Chateigner, D. 2000. Exhumation of ultrahigh-pressure continental crust in east central China : Late Triassic-Early Jurassic tectonic unroofing. *Journal of Geophysical Research*, **105**, 13339–13364.

Hames, W. E. & Bowring, S. A. 1994. An empirical evaluation of the argon diffusion geometry in muscovite. *Earth and Planetary Science Letters*, **124**, 161–167.

Harrison, T. M. 1981. Diffusion of ^{40}Ar in hornblende. *Contributions to Mineralogy and Petrology*, **78**, 324–331.

Harrison, T. M., Duncan, I. & McDougall, I. 1985. Diffusion of ^{40}Ar in biotite : Temperature , pressure and compositional effects. *Geochimica et Cosmochimica Acta*, **49**, 2461–2468.

Harrison, T. M., Célérier, J., Aikman, A. B., Hermann, J. & Heizler, M. T. 2009. Diffusion of ^{40}Ar in muscovite. *Geochimica et Cosmochimica Acta*, **73**, 1039–1051.

Hermann, J., Rubatto, D., Korsakov, A. & Shatsky, V. S. 2001. Multiple zircon growth during fast exhumation of diamondiferous, deeply subducted continental crust (Kokchetav Massif, Kazakhstan). *Contributions to Mineralogy and Petrology*, **141**, 66–82.

Holland, T. J. B., Baker, J. & Powell, R. 1998. Mixing properties and activity-composition relationships of chlorites in the system MgO-FeO-Al_2O_3-SiO_2-H_2O. *European Journal of Mineralogy*, **10**, 395–406.

Holland, T. J. B. & Powell, R. 1996. Thermodymanics of Order-Disorder in Minerals. 2. Symmetric Formulism Applied to Solid Solutions. *American Mineralogist*, **81**, 1425–1437.

Holland, T. J. B. & Powell, R. 1998. An internally consistent thermodynamic data set for phases of petrological interest. *Journal of Metamorphic Geology*, **16**, 309–343.

Holland, T. J. B. & Powell, R. 2011. An improved and extended internally consistent thermodynamic dataset for phases of petrological interest, involving a new equation of state for solids. *Journal of Metamorphic Geology*, **29**, 333–383.

Jackson, C. R. M., Parman, S. W., Kelley, S. P. & Cooper, R. F. 2013. Noble gas transport into the mantle facilitated by high solubility in amphibole. *Nature Geoscience*, **6**, 562–565.

Kelley, S. P. 2002. Excess argon in K–Ar and Ar–Ar geochronology. *Chemical Geology*, **188**, 1–22.

Krabbendam, M., Wain, A. & Andersen, T. B. 2000. Pre-Caledonian granulite and gabbro enclaves in the Western Gneiss Region, Norway: indications of incomplete transition at high pressure. *Geological Magazine*, **137**, 235–255.

Kylander-Clark, A. R. C., Hacker, B. R., Johnson, C. M., Beard, B. L., Mahlen, N. J. & Lapen, T. 2007. Coupled Lu–Hf and Sm–Nd geochronology constrains prograde and exhumation histories of high- and ultrahigh-pressure eclogites from western Norway. *Chemical Geology*, **242**, 137–154.

Kylander-Clark, A. R. C., Hacker, B. R. & Mattinson, J. M. 2008. Slow exhumation of UHP terranes: Titanite and rutile ages of the Western Gneiss Region, Norway. *Earth and Planetary Science Letters*, **272**, 531–540.

Kylander-Clark, A. R. C., Hacker, B. R., Johnson, C. M., Beard, B. L. & Mahlen, N. J. 2009. Slow subduction of a thick ultrahigh-pressure terrane. *Tectonics*, **28**.

Labrousse, L., Jolivet, L., Agard, P., Hébert, R. & Andersen, T. B. 2002. Crustal-scale boudinage and migmatization of gneiss during their exhumation in the UHP Province of Western Norway. *Terra Nova*, **14**, 263–270.

Labrousse, L., Andersen, T. B., Agard, P., Hébert, R., Maluski, H. & Schärer, U. 2004. Pressure-temperature-time deformation history of the exhumation of ultra-high pressure rocks in the Western Gneiss Region, Norway. *Geological Society of America Special Paper*, **380**, 155–183.

Lee, J. K. W. 2009. Using argon as a temporal tracer of large-scale geologic processes. *Chemical Geology*, **266**, 104–112.

Li, S., Wang, S., Chen, Y., Lui, D., Qiu, J., Zhou, H. & Zhang, Z. 1994. Excess argon in phengite from eclogite: Evidence from dating of eclogite minerals by Sm-Nd, Rb-Sr and $^{40}Ar/^{39}Ar$ methods. *Chemical Geology*, **112**, 343–350.

Li, S., Jagoutz, E., Lo, C. -H., Chen, Y., Li, Q. & Xiao, Y. 1999. Sm/Nd, Rb/Sr, and $^{40}Ar/^{39}Ar$ Isotopic Systematics of the Ultrahigh-Pressure Metamorphic Rocks in the Dabie-Sulu Belt, Central China: A Retrospective View. *International Geology Review*, **41**, 1114–1124.

Mark, D. F., Kelley, S. P., Lee, M. R., Parnell, J., Sherlock, S. C. & Brown, D. J. 2008. Ar–Ar dating of authigenic K-feldspar: Quantitative modelling of radiogenic argon-loss through subgrain boundary networks. *Geochimica et Cosmochimica Acta*, **72**, 2695–2710.

Mark, D. F., Barfod, D., Stuart, F. M. & Imlach, J. 2009. The ARGUS multicollector noble gas mass spectrometer: Performance for $^{40}Ar/^{39}Ar$ geochronology. *Geochemistry, Geophysics, Geosystems*, **10**.

Mark, D. F., Rice, C. M., Fallick, A. E., Trewin, N. H., Lee, M. R., Boyce, A. & Lee, J. K. W. 2011. $^{40}Ar/^{39}Ar$ dating of hydrothermal activity, biota and gold mineralization in the Rhynie hot-spring system, Aberdeenshire, Scotland. *Geochimica et Cosmochimica Acta*, **75**, 555–569.

McDougall, I. & Harrison, T. M. 1999. *Geochronology and Thermochronology by the $^{40}Ar/^{39}Ar$ Method*, 2nd ed. New York, Oxford University Press.

Mearns, E. W. 1986. Sm-Nd ages for norwegian garnet peridotite. *Lithos*, **19**, 269–278.

Merrihue, C. & Turner, G. 1966. Potassium-argon dating by activation with fast neutrons. *Journal of Geophysical Research*, **71**, 2852–2857.

Min, K., Mundil, R., Renne, P. R. & Ludwig, K. R. 2000. A test for systematic errors in $^{40}Ar/^{39}Ar$ geochronology through comparison with U/Pb analysis of a 1.1-Ga rhyolite. *Geochimica et Cosmochimica Acta*, **64**, 73–98.

Mørk, M. B. E. & Mearns, E. W. 1986. Sm-Nd isotopic systematics of a gabbro-eclogite transition. *Lithos*, **19**, 255–267.

Newton, R. C., Charlu, T. V. & Kleppa, O. J. 1980. Thermochemistry of the high structural state plagioclases. *Geochimica et Cosmochimica Acta*, **44**, 933–941.

Peterman, E. M., Hacker, B. R. & Baxter, E. F. 2009. Phase transformations of continental crust during subduction and exhumation: Western Gneiss Region, Norway. *European Journal of Mineralogy*, **21**, 1097–1118.

Powell, R. & Holland, T. J. B. 1999. Relating Formulations of the Thermodynamics of mineral Solid Solutions: Activity Modeling of Pyroxenes, Amphiboles, and Micas. *American Mineralogist*, **84**, 1–14.

Putlitz, B., Cosca, M. A. & Schumacher, J. C. 2005. Prograde mica $^{40}Ar/^{39}Ar$ growth ages recorded in high pressure rocks (Syros, Cyclades, Greece). *Chemical Geology*, **214**, 79–98.

Reddy, S. M. & Potts, G. J. 1999. Constraining absolute deformation ages: the relationship between deformation mechanisms and isotope systematics. *Journal of Structural Geology*, **21**, 1255–1265.

Renne, P. R., Deino, A. L., Hames, W. E., Heizler, M. T., Hemming, S. R., Hodges, K. V., Koppers, A. A. P., Mark, D. F., Morgan, L .E., Phillips, D., Singer, B. S., Turrin, B. D., Villa, I. M., Villeneuve, M. & Wijbrans, J. R.. 2009a. Data reporting norms for $^{40}Ar/^{39}Ar$ geochronology. *Quaternary Geochronology*, **4**, 346–352.

Renne, P. R., Cassata, W. S. & Morgan, L. E. 2009b. The isotopic composition of atmospheric argon and $^{40}Ar/^{39}Ar$ geochronology: Time for a change? *Quaternary Geochronology*, **4**, 288–298.

Renne, P. R., Mundil, R., Balco, G., Min, K. & Ludwig, K. R. 2010. Joint determination of ^{40}K decay constants and $^{40}Ar*/^{40}K$ for the Fish Canyon sanidine standard, and improved accuracy for $^{40}Ar/^{39}Ar$ geochronology. *Geochimica et Cosmochimica Acta*, **74**, 5349–5367.

Robers, D. 2003. The Scandinavian Caledonides: event chronology, palaeogeographic settings and likely modern analogues. *Tectonophysics*, **365**, 283–299.

Root, D. B., Hacker, B. R., Mattinson, J. M. & Wooden, J. L. 2004. Zircon geochronology and ca. 400 Ma exhumation of Norwegian ultrahigh-pressure rocks: an ion microprobe and chemical abrasion study. *Earth and Planetary Science Letters*, **228**, 325–341.

Root, D. B., Hacker, B. R., Gans, P. B., Ducea, M. N., Eide, E. A. & Mosenfelder, J. L. 2005. Discrete ultrahigh-pressure domains in the Western Gneiss Region, Norway: implications for formation and exhumation. *Journal of Metamorphic Geology*, **23**, 45–61.

Ruffet, G., Feraud, G., Ballévre, M. & Kienest, J. R. 1995. Plateau ages and excess argon on phengites: a $^{40}Ar/^{39}Ar$ laser probe study of alpine micas (Sesia zone). *Chemical Geology*, **121**, 327–343.

Ruffet, G., Gruau, G., Ballévre, M., Feraud, G. & Philippot, P. 1997. Rb-Sr and $^{40}Ar/^{39}Ar$ laser probe dating of high-pressure phengites from the Sesia Zone (Western Alps): underscoring of excess argon and new constraints on the high-pressure metamorphism. *Chemical Geology*, **141**, 1–18.

Scaillet, S. 1996. Excess ^{40}Ar transport scale and mechanism in high-pressure phengites : A case study from an eclogitized metabasite of the Dora-Maira nappe , western Alps. *Geochimica et Cosmochimica Acta*, **60**, 1075–1096.

Schärer, U. & Labrousse, L. 2003. Dating the exhumation of UHP rocks and associated crustal melting in the Norwegian Caledonides. *Contributions to Mineralogy and Petrology*, **144**, 758–770.

Sherlock, S. C. & Arnaud, N. O. 1999. Flat plateau and impossible isochrons: Apparent $^{40}Ar/^{39}Ar$ geochronology in a high-pressure terrain. *Geochimica et Cosmochimica Acta*, **63**, 2835–2838.

Sherlock, S. C. & Kelley, S. 2002. Excess argon evolution in HP-LT rocks: a UVLAMP study of phengite and K-free minerals, NW Turkey. *Chemical Geology*, **182**, 619–636.

Sherlock, S. C., Kelley, S., Inger, S., Harris, N. & Okay, A. 1999. $^{40}Ar/^{39}Ar$ and Rb/Sr geochronology of high-pressure metamorphism and exhumation history of the Tavsanli Zone, NW Turkey. *Contributions to Mineralogy and Petrology*, **137**, 46–58.

Sherlock, S. C., Lucks, T., Kelley, S. P. & Barnicoat, A. 2005. A high resolution record of multiple diagenetic events: Ultraviolet laser microprobe Ar/Ar analysis of zoned K-feldspar overgrowths. *Earth and Planetary Science Letters*, **238**, 329–341.

Sherlock, S. C., Jones, K. A. & Park, R. G. 2008. Grenville-age pseudotachylite in the Lewisian: laserprobe $^{40}Ar/^{39}Ar$ ages from the Gairloch region of Scotland (UK). *Journal of the Geological Society*, **165**, 73–83.

Skår, Ø. 2000. Field relations and geochemical evolution of the Gothian rocks in the Kvamsoy area, southern Western Gneiss Complex, Norway. *Norges Geologiske Undersokelse Bulletin*, **437**, 5–23.

Sletten, V. W. & Onstott, T. C. 1998. The effect of the instability of muscovite during in vacuo heating on $^{40}Ar/^{39}Ar$ step-heating spectra. *Geochimica et Cosmochimica Acta*, **62**, 123–141.

Smith, D. C. 1984. Coesite in Clinopyroxene in the Caledonides and its Implications for Geodymanics. *Nature*, **310**, 641–644.

Smye, A. J., Warren, C. J. & Bickle, M. J. 2013. The signature of devolatisation: Extraneous ^{40}Ar systematics in high-pressure metamorphic rocks. *Geochimica et Cosmochimica Acta*, **113**, 94–112.

Spencer, K. J., Hacker, B. R., Kylander-Clark, A. R. C., Andersen, T. B., Cottle, J. M., Stearns, M. A., Poletti, J. E. & Seward, G. G. E. 2013. Campaign-style titanite U–Pb dating by laser-ablation ICP: Implications for crustal flow, phase transformations and titanite closure. *Chemical Geology*, **341**, 84–101.

Tajčmanová, L., Connolly, J. A. D. & Cesare, B. 2009. A thermodynamic model for titanium and ferric iron solution in biotite. *Journal of Metamorphic Geology*, **27**, 153–165.

Terry, M. P., Robinson, P., Hamilton, M. A. & Jercinovic, M. J. 2000. Monazite geochronology of UHP and HP metamorphism, deformation, and exhumation, Nordøyane, Western Gneiss Region, Norway. *American Mineralogist*, **85**, 1651–1664.

Thompson, J.B. & Hovis, G.L. 1979. Entropy of Mixing in Sanidine. *American Mineralogist*, **64**, 57–65.

Tucker, R. D., Råheim, A., Krogh, T. E. & Corfu, F. 1986. Uranium-lead zircon and titanite ages from the northern portion of the Western Gneiss Region, south-central Norway. *Earth and Planetary Science Letters*, **81**, 203–211.

Villa, I.M. 1997. Isotopic closure. *Terra Nova*, **10**, 42–47.

Villa, I. M., Bucher, S., Bousquet, R., Kleinhanns, I. C. & Schmid, S. M. 2014. Dating Polygenetic Metamorphic Assemblages along a Transect across the Western Alps. *Journal of Petrology*, **55**, 803–830.

Wain, A. 1997. New evidence for coesite in eclogite and gneisses: Defining an ultrahigh-pressure province in the Western Gneiss region of Norway. *Geology*, **25**, 927.

Wain, A. 1998. *Ultrahigh-Pressure Metamorphism in the Western Gneiss Region of Norway*. University of Oxford.

Wain, A., Waters, D. J., Jephcost, A. & Olijynk, H. 2000. The high-pressure to ultrahigh-pressure eclogite transition in the Western Gneiss Region, Norway. *European Journal of Mineralogy*, **12**, 667–687.

Wain, A., Waters, D. J. & Austrheim, H. 2001. Metastability of granulites and processes of eclogitisation in the UHP region of western Norway. *Journal of Metamorphic Geology*, **19**, 609–625.

Walsh, E. O. & Hacker, B. R. 2004. The fate of subducted continental margins: Two-stage exhumation of the high-pressure to ultrahigh-pressure Western Gneiss Region, Norway. *Journal of Metamorphic Geology*, **22**, 671–687.

Walsh, E. O., Hacker, B. R., Gans, P. B., Grove, M. & Gehrels, G. 2007. Protolith ages and exhumation histories of (ultra)high-pressure rocks across the Western Gneiss Region, Norway. *Geological Society of America Bulletin*, **119**, 289–301.

Walsh, E. O., Hacker, B. R., Gans, P. B., Wong, M. S. & Andersen, T. B. 2013. Crustal exhumation of the Western Gneiss Region UHP terrane, Norway: $^{40}Ar/^{39}Ar$ thermochronology and fault-slip analysis. *Tectonophysics*, **608**, 1159–1179.

Warren, C. J., Sherlock, S. C. & Kelley, S. P. 2011. Interpreting high-pressure phengite $^{40}Ar/^{39}Ar$ laserprobe ages: an example from Saih Hatat, NE Oman. *Contributions to Mineralogy and Petrology*, **161**, 991–1009.

Warren, C. J., Kelley, S. P., Sherlock, S. C. & McDonald, C. S. 2012a. Metamorphic rocks seek meaningful cooling rate: Interpreting $^{40}Ar/^{39}Ar$ ages in an exhumed ultra-high pressure terrane. *Lithos*, **155**, 30–48.

Warren, C. J., Smye, A. J., Kelley, S. P. & Sherlock, S. C. 2012b. Using white mica $^{40}Ar/^{39}Ar$ data as a tracer for fluid flow and permeability under high-P conditions: Tauern Window, Eastern Alps. *Journal of Metamorphic Geology*, **30**, 63–80.

Warren, C. J., Hanke, F. & Kelley, S. P. 2012c. When can muscovite $^{40}Ar/^{39}Ar$ dating constrain the timing of metamorphic exhumation? *Chemical Geology*, **291**, 79–86.

Watson, J.S. 1996. Fast , Simple Method of Powder Pellet Preparation for X-Ray Fluorescence Analysis. *X-Ray Spectometry*, **25**, 173–174.

Wheeler, J. 1996. Diffarg: A program for simulating argon diffusion profiles in minerals. *Computers & Geosciences*, **22**, 919–929.

Whitney, D. L. & Evans, B. W. 2010. Abbreviations for names of rock-forming minerals. *American Mineralogist*, **95**, 185–187.

Young, D. J., Hacker, B. R., Andersen, T. B. & Corfu, F. 2007. Prograde amphibolite facies to ultrahigh-pressure transition along Nordfjord, western Norway: Implications for exhumation tectonics. *Tectonics*, **26**.

Young, D. J., Hacker, B. R., Andersen, T. B. & Gans, P. B. 2011. Structure and $^{40}Ar/^{39}Ar$ thermochronology of an ultrahigh-pressure transition in western Norway. *Journal of the Geological Society*, **168**, 887–898.

Zheng, Y. -F., Fu, B., Gong, B. & Li, L. 2003. Stable isotope geochemistry of ultrahigh pressure metamorphic rocks from the Dabie–Sulu orogen in China: implications for geodynamics and fluid regime. *Earth-Science Reviews*, **62**, 105–161.

Appendix A:

Sample Petrography and Mineral Chemistry

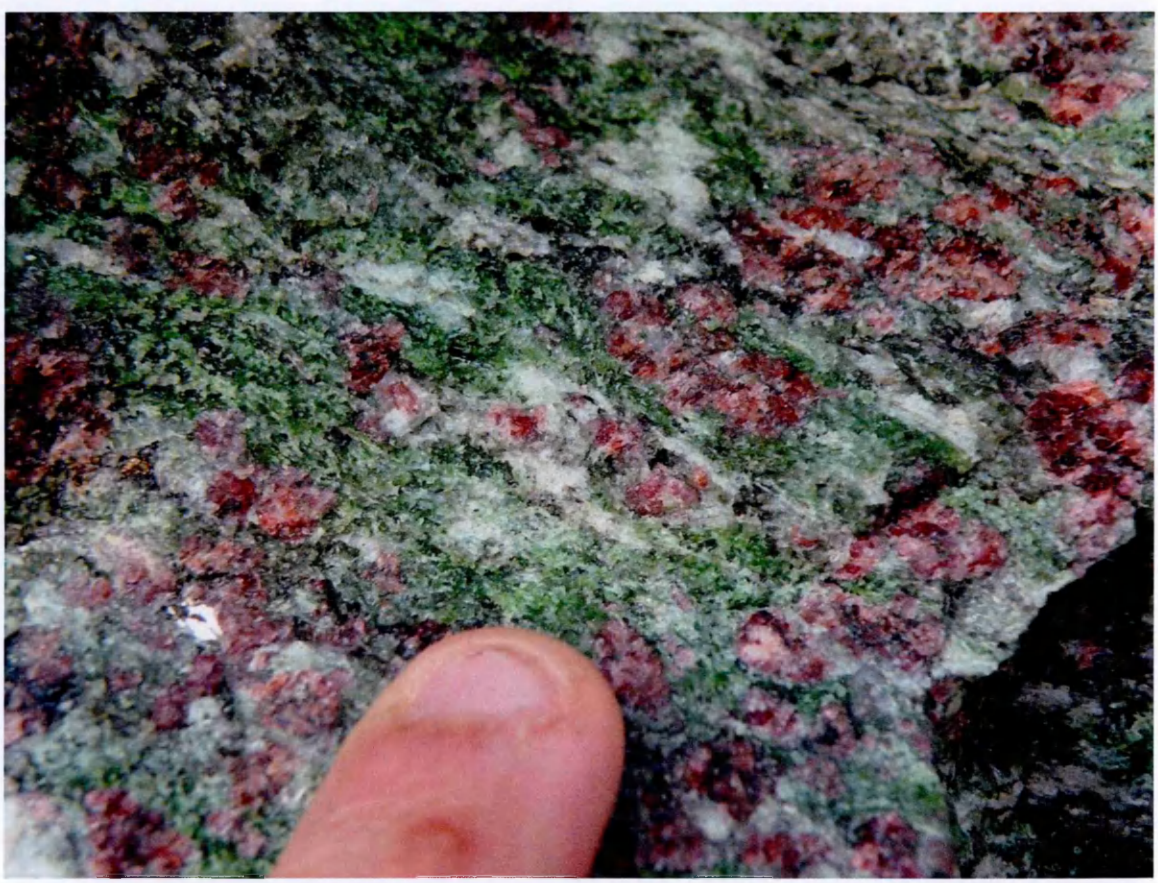

Verpeneset eclogite

Mineral abbreviations from Whitney & Evans (2010)

Aln – allanite	Amp – amphibole
Ap – apatite	Bt – biotite
Cpx – clinopyroxene	Czo – clinozoisite
Ep – epidote	Grt – garnet
Kfs – K-feldspar	Ky – kyanite
Omp – omphacite	Pl – plagioclase
Qz – quartz	Rt – rutile
Ttn – titanite	Zrn – zircon

Also:

Sym – symplectite	WM – white mica

Eclogites

NF37: is a granoblastic eclogite from Krokkenakken containing an eclogite-facies of garnet, omphacite quartz, white mica, clinozoisite, and rutile. This peak assemblage has been partially overprinted by symplectites of clinopyroxene-plagioclase around omphacite; biotite-plagioclase symplectites around phengite and blue-green amphibole at the contact between garnet and omphacite. Phengite grains are 1-2 mm in length and have Si core-rim concentrations of 6.94-6.63 per 22 O per formula unit (pfu).

Garnets are anhedral to subhedral in shape and commonly contain concentric inclusions of quartz, white mica and omphacite. The garnets are almandine-pyrope in composition with a composition that range from $Alm_{41-51}Sps_{0-1}Py_{28-37}Grs_{17-21}$. Omphacite show only show minor retrogression to symplectites along their grain boundaries and have a composition of Jd_{30-39}. Minor amphibole occurs around garnet and within the matrix as isolated grains. This amphibole is magnesiokatophorite-magnesiotaramite with minor barroisite components. The amphibole has a Si content that ranges from 5.92-7.00 and Mg# of 0.61-0.80. Epidote forms a minor component of this sample, occurring as isolated grains within the matrix and as inclusions in garnet and omphacite. The composition of the epidote ranges from XEp 0.23-0.47.

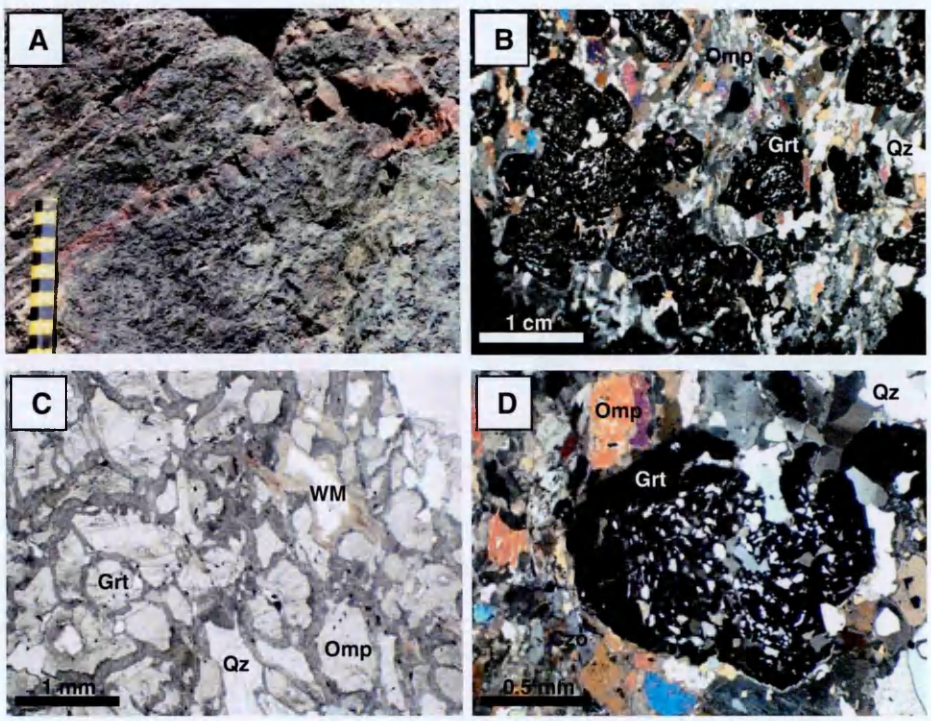

Fig. A1: A) Outcrop photo of sample NF37, B) Whole thin section image, C) close up of the eclogite NF37 showing the assemblage of garnet + omphacite + quartz + white mica + rutile. Omphacite and white mica show varying degrees of symplectization, D) Close up of garnet showing inclusion-rich core and inclusion-poor rim.

NF45: from Flatraket Harbour, is a coarse-grained granoblastic eclogite and contains a peak assemblage of garnet, omphacite, white mica, kyanite, and rutile. Polycrystalline quartz inclusions in omphacite and garnet are interpreted to represent the former presence of coesite. This peak eclogite-facies assemblage is partially replaced by symplectites of clinopyroxene-plagioclase around omphacite, biotite-plagioclase around phengite and blue-green amphibole at contacts between garnet and omphacite. The phengites from this locality display minor chemical zonation with Si concentrations that range from 6.81 pfu at the core to 6.52 pfu at the rims.

Garnets are large (~20 mm) and are anhedral with a 'spongy' texture. They are typically zoned core to rim with a pyrope-almandine in composition ($Alm_{34-45}Sps_{0-2}Py_{30-49}Grs_{14-22}$). Omphacite show varying degrees of symplectization along the grain boundaries and has a composition that ranges from Jd_{34-42}. The blue-green amphibole that occurs at the garnet-omphacite contact is magnesiokatophorite-magnesiotaramite with a composition that range from 5.76-7.60 Si per 23 O and Mg# of 0.59-0.86.

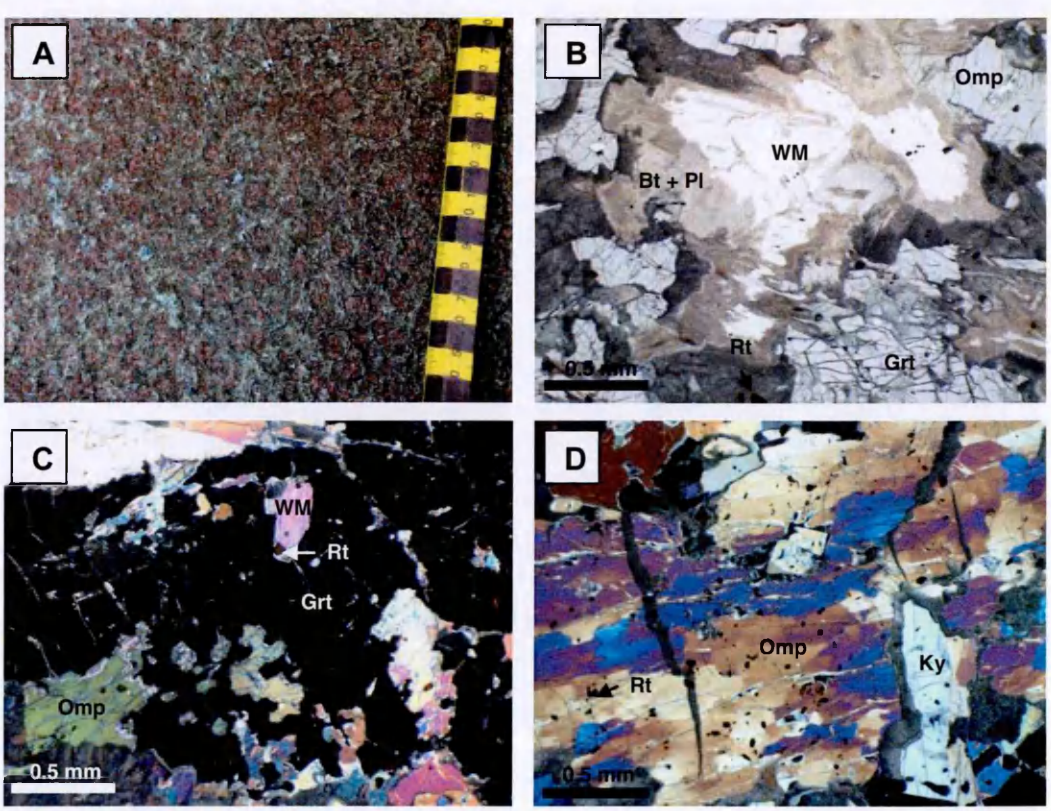

Fig. A2: A) Field photographs of the Flatraket eclogite, B) symplectised white mica surrounded by fine-grained pyroxene + plagioclase after omphacite, fractures in garnet are filled with blue-green amphibole, C) 'spongy' garnets with inclusion of omphacite, white mica and rutile, D) omphacite showing undulose birefringence patterns.

NF84: is from Drage, is a fine-grained granoblastic eclogite that is layered into garnet-rich and omphacite-rich bands. It contains a peak assemblage of garnet, omphacite, amphibole, carbonate, and rutile. There is no phengite present in this sample. Amphibole is a minor constituent and contains inclusions of vermicular quartz and is barroisitic in compositions. The composition of the amphibole ranges from 7.00-7.30 Si per 23 O and Mg# of 0.80-0.82.

Garnets are small (~0.5 mm) and have a fairly homogeneous almandine-pyrope composition of $Alm_{44-47}Sps_{0-1}Py_{38-42}Grs_{11-15}$. Omphacite is fresh with little sign of symplectization. They are commonly anhedral in shape and have a composition of Jd_{24-28}.

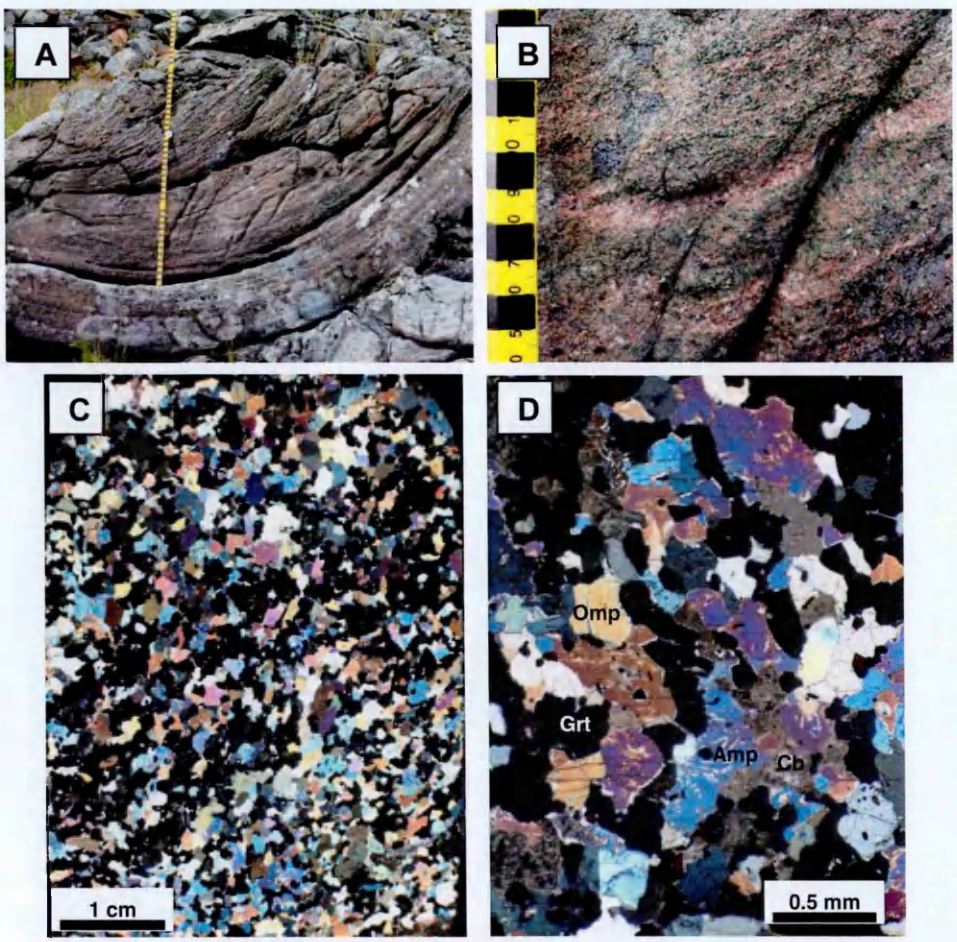

Fig. A3. Drage amphibole-bearing eclogite. A and B) close-up field photograph of the eclogite showing alternating garnet-rich and omphacite-rich layers, C) whole thin section image of eclogite sample NF84 showing a granular texture. The alternating garnet-rich and omphacite-rich layers are evident at the thin section level; D) clos up photomicrograph of eclogite NF84 showing isotropic garnets, omphacite and amphibole with contain vermicular inclusions of quartz.

NF100: collected at Drage on the southern coast of the Stadlandet Peninsula, is a medium-grained granoblastic, eclogite with a peak metamorphic assemblage of garnet, omphacite, white mica, kyanite, and rutile. Two inclusions of polycrystalline quartz are present in garnet and are inferred to represent for coesite. The eclogite show minor symplectisation with clinopyroxene/amphibole-plagioclase symplectites after omphacite and biotite-plagioclase symplectites after phengite.

The white mica are commonly rimmed with very fine-grained biotite-plagioclase symplectites and have a typical core to rim compositions of 6.89-6.51 Si per 22 O. Garnets are subhedral to anhedral and range in size from 0.5-1.5 mmm. They are pyrope-almandine ($Alm_{33-36}Sps_{0-1}Py_{36-41}Grs_{22-28}$) in composition with moderate grossular content. Omphacite form anhedral grains between the garnets and have a composition of Jd_{22-32}.

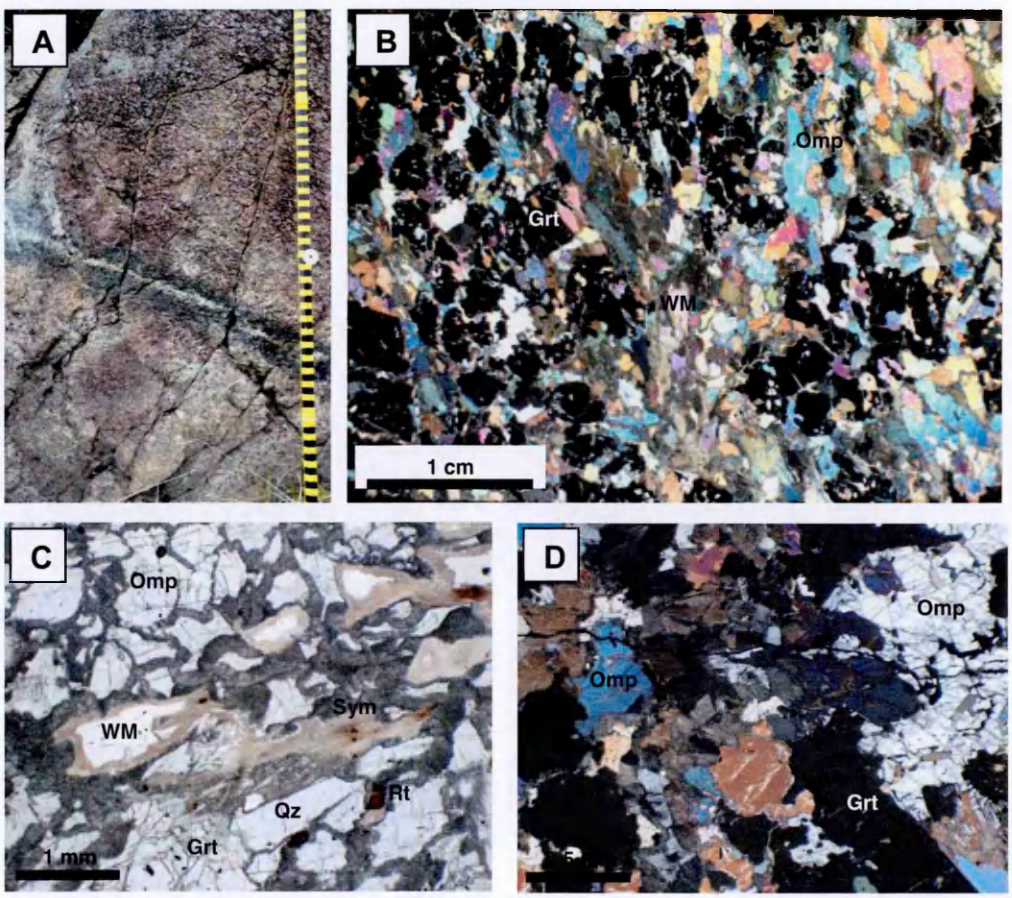

Fig. A4. The Drage kyanite-coesite-bearing eclogite. A) field photograph of the massive eclogite body showing a vein of amphibolite-facies minerals cross-cutting the eclogite, B) whole thin section image of eclogite NF100 showing a similar texture to the Flatraket eclogite NF45, C) photomicrograph showing the principal mineralogy of garnet + omphacite + white mica + rutile. Omphacite and white mica are variably symplectised, D) photomicrograph showing the anhedral morphology of the garnet and omphacite.

Amphibolites

NF46: is the amphibolitised rind to the previously described eclogite, NF45. The principle eclogite-facies mineralogy of garnet-omphacite has been replaced an assemblage of biotite-amphibole-plagioclase with minor epidote, rutile and secondary calcite.

Garnet has been pseudomorphed into biotite-amphibole "clots" while the eclogite matrix is replaced with pyroxene/amphibole-plagioclase symplectites. Amphiboles are tschermakite-magnesiohornblende in composition and the biotite has compositions of Mg# 0.55-0.62 and Ti 0.16-0.25 pfu. Plagioclase feldspar occurs within the symplectised matrix, associated with the amphibole. The plagioclase has a composition that ranges from andesine to oligoclase, with anorthite content of An_{13-35}. The epidote that is associated with the biotite and amphibole form isolated clusters of anhedral grains with compositions of XEp 0.53-0.70.

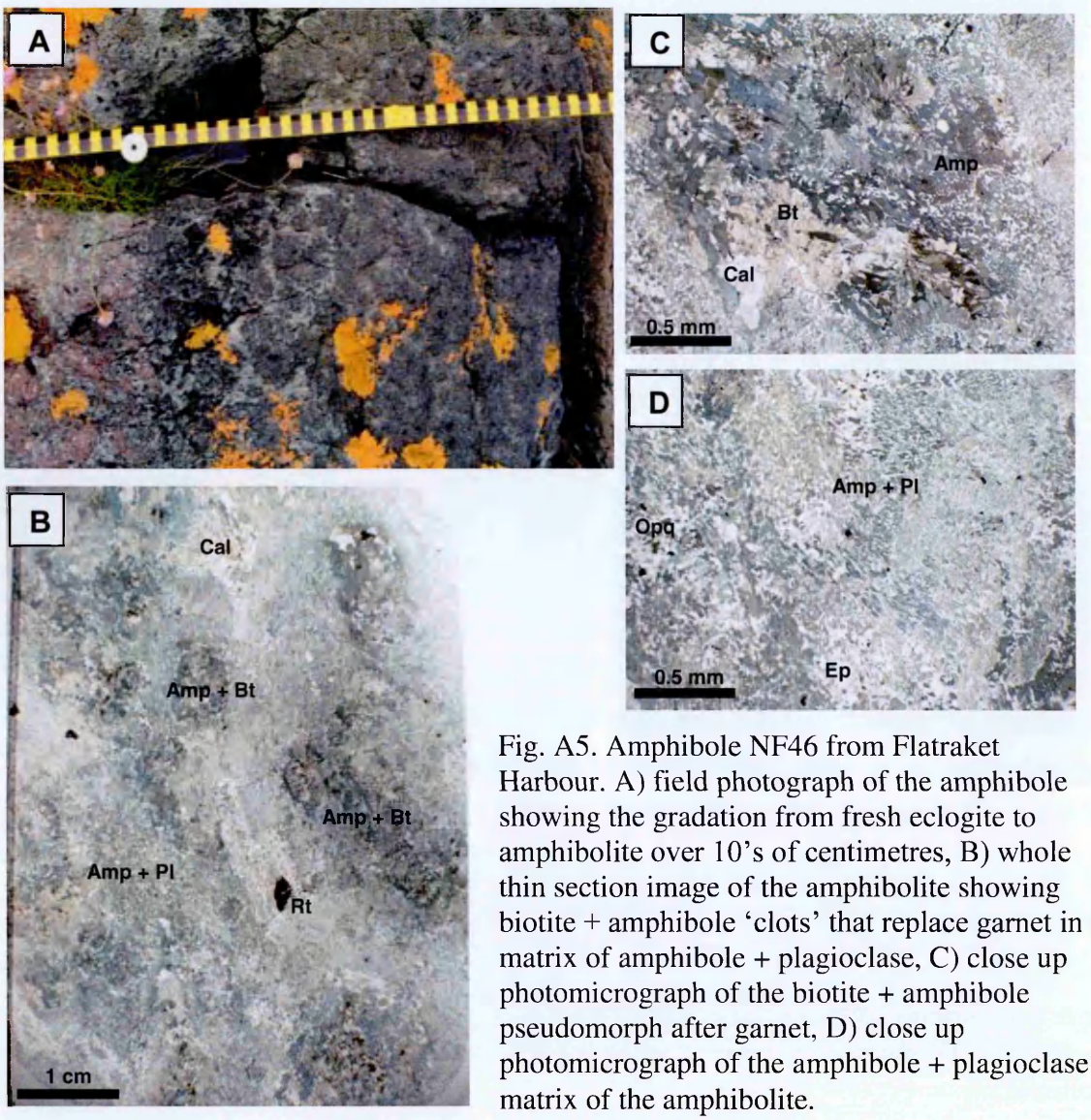

Fig. A5. Amphibole NF46 from Flatraket Harbour. A) field photograph of the amphibole showing the gradation from fresh eclogite to amphibolite over 10's of centimetres, B) whole thin section image of the amphibolite showing biotite + amphibole 'clots' that replace garnet in a matrix of amphibole + plagioclase, C) close up photomicrograph of the biotite + amphibole pseudomorph after garnet, D) close up photomicrograph of the amphibole + plagioclase matrix of the amphibolite.

NF49: is a garnet amphibolite that represents a wholly retrogressed eclogite that is equilibrated with the country rock. This sample contains typical amphibolite-facies mineralogy of quartz, garnet, biotite, and amphibole with minor epidote. Accessory phases include rutile, chlorite and apatite.

Amphibole is ferrotschermakite-tschermakite in composition and biotite has a relatively homogeneous composition of Mg# 0.53-0.58 and Ti 0.19-0.29 pfu. The garnet also fairly homogeneous and are almandine-pyrope with a moderate grossular content ($Alm_{52-63}Sps_{1-6}Py_{20-32}Grs_{11-17}$). Plagioclase is oligoclase-andesine in composition with anorthite content ranging from An_{19-31}. Epidote group minerals form small (0.5-1 mm) porphyroblasts that cross cut the biotite fabric. Epidote is commonly anhedral, unzoned and contains inclusions of the matrix phases (biotite, quartz, and plagioclase) with a composition that ranges from XEp 0.53-0.63.

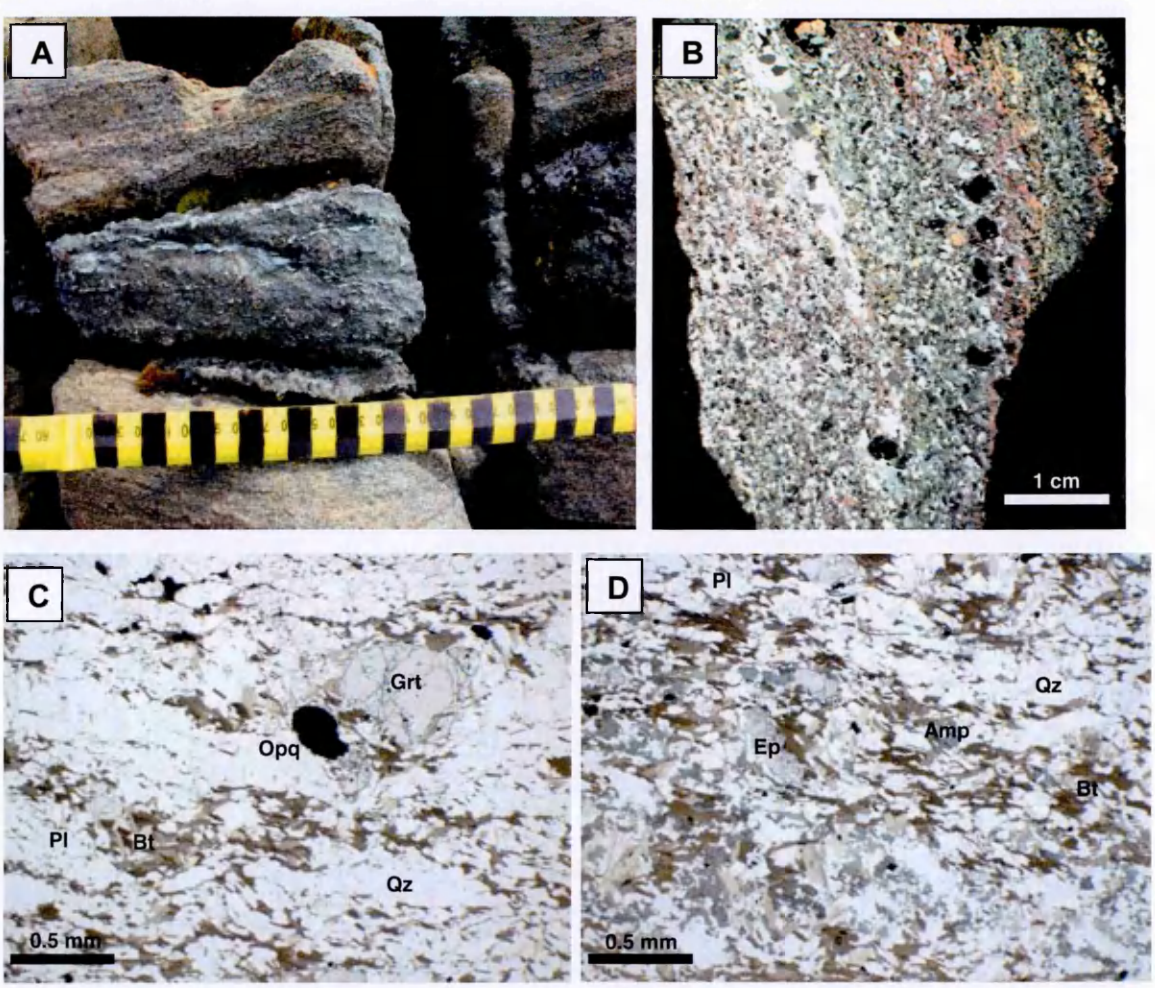

Fig. A6. Flatraket Harbour amphibolite NF49. A) Field photograph of the amphibolite lens, B) whole thin section image of the amphibolite, C and D) photomicrographs of the amphibolite showing a typical amphibolite-facies assemblage of garnet + quartz + plagioclase feldspar + biotite + amphibole.

Host Gneisses

Group 1 Gneisses: Garnet-bearing Gneisses

Group 1a Gneisses: Garnet-bearing Gneisses with high-pressure relicts

Relicts of high-pressure (HP) gneisses are found in low-strain areas adjacent to the eclogite boudin at Krokkenakken. These low-strain regions preserve gneisses that are (near)isofacial to adjacent mafic eclogites.

NF40: is a medium-grained, unfoliated gneiss that is adjacent to the mafic eclogite. It contains a primary assemblage of garnet, quartz, and white mica with accessory phases of kyanite, rutile, apatite and zircon. Phengite is commonly rimmed with biotite-plagioclase symplectites.

The white mica forms the major fabric in this sample and is zoned from core to rim with Si ranging from 6.83-6.31 Si per 22 O. Biotite form elongate sub-mm grains that border the white mica with only minor well-formed laths within the matrix. Chemically, the biotite is homogeneous with Mg# of 0.58-0.61 and Ti 0.17-0.24 pfu. Kyanite is associated with muscovite in the fabric and shows no retrogression to a lower pressure polymorph, indicating muscovite growth at peak metamorphic conditions.

Garnet form anhedral grains, many with embayed edges. Compositionally the garnets are almandine-pyrope with highly variable grossular content ($Alm_{51-58}Sps_{1-3}Py_{26-35}Grs_{9-22}$). Garnets are inclusion-poor with only minor grains of quartz, rutile, and kyanite. The plagioclase associated with the biotite has narrow anorthite content, ranging from An_{22-29}.

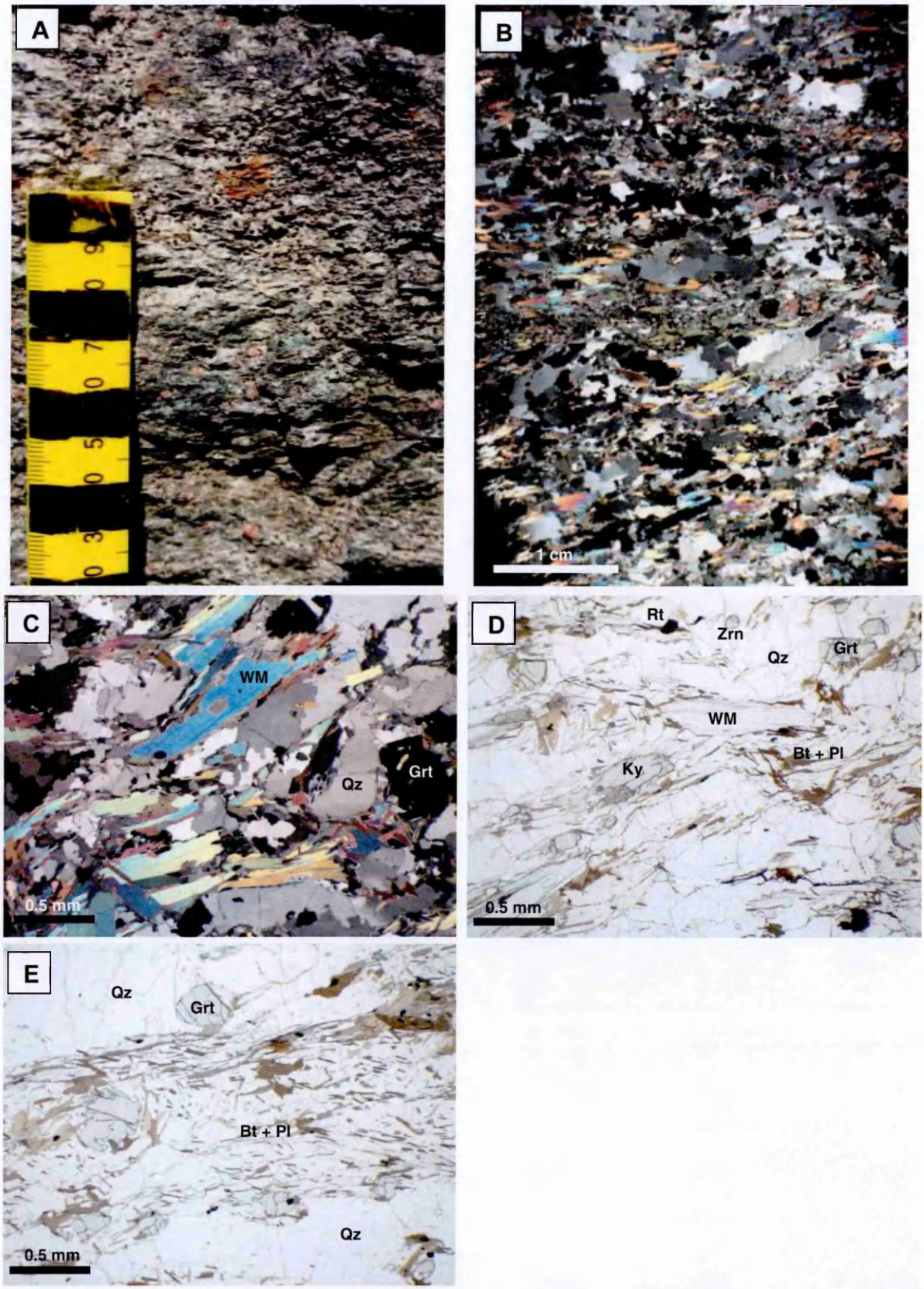

Fig. A7. Group 1a Gneiss, NF40. A) Field photograph of sample NF40, the dark green patches are relic omphacite, attesting to the high pressure experienced by this gneiss, B) whole thin section image, C – D) photomicrographs of sample NF40 showing the principal mineralogy of quartz, garnet, white mica, kyanite, and rutile. Many of the white mica grains are rimmed with biotite-plagioclase symplectites, E) a layer of biotite + plagioclase symplectite that has replaced the original white mica.

NF42: is a medium-grained, unfoliated and highly symplectised gneiss that contains a primary assemblage of garnet, quartz, and white mica-biotite with accessory phases of rutile, clinozoisite, and zircon. Symplectites of biotite-plagioclase and amphibole/clinopyroxene-plagioclase attest to the former presence of phengite and omphacite. Phengite is commonly rimmed with biotite-plagioclase symplectites

Large (~1 mm) relict phengite form the fabric the envelopes garnets and core-rim variations in Si ranging from 6.77-6.50 pfu. Biotites, observed to be the breakdown product of phengite, are Mg-rich with Mg# of 0.67.-0.73 and Ti 0.21-0.32. They form small (sub-micron) laths intergrown with plagioclase and large (~1 mm) clusters.

Garnets form sub- to euhedral grains, ranging from 0.5 – 1.5 mm in diameter. Compositionally the garnets are almandine-pyrope and are zoned from rim to core ($Alm_{51-68}Sps_{0-3}Py_{13-31}Grs_{14-31}$). Garnets are inclusion-rich with grains of quartz, kyanite, rutile, white mica, and apatite. The plagioclase associated with the biotite has a broad composition, with an anorthite content ranging from An_{11-55}.

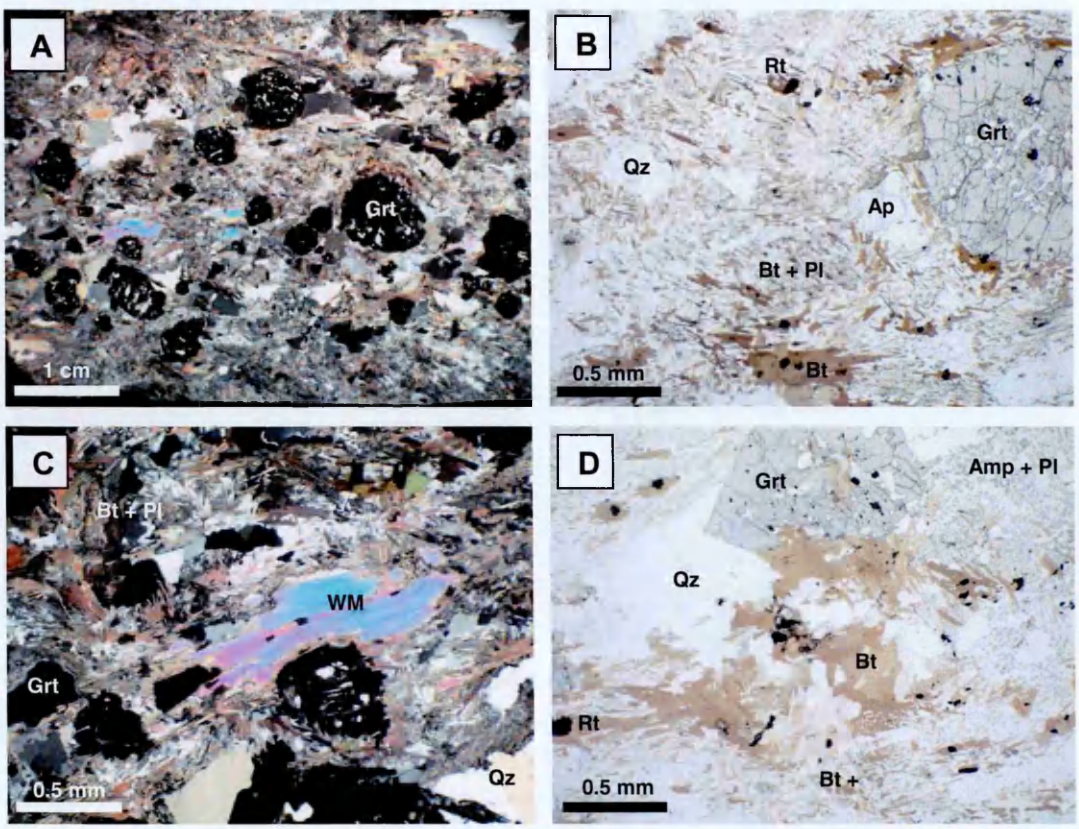

Fig. A8. Group 1a gneiss, NF42. A) whole thin section image of NF42 showing large garnets in a heavily symplectised matrix, B – E) photomicrographs of NF42 showing the samples mineralogy. B) randomly orientated biotite + plagioclase symplectite after white mica, C) relic white mica wrapping around garnet, D) idioblastic biotite that represent continued biotite growth from the symplectites. Top left is amphibole + plagioclase symplectite after omphacite.

NF43: is a medium-grained, unfoliated gneiss that is in contact with a small mafic eclogite. It contains a primary assemblage of garnet, quartz, and white mica with accessory phases of clinozoisite, rutile, apatite, and zircon. Symplectites of biotite-plagioclase and amphibole/clinopyroxene-plagioclase attest to the former presence of phengite and omphacite. Phengite is commonly rimmed with biotite-plagioclase symplectites.

The white mica forms the major phase in this sample and is zoned from core to rim with Si ranging from 6.84-6.55 Si per 22 O. Biotite form elongate sub-mm grains that border the white mica with only minor well-formed laths within the matrix. Chemically, the biotite is homogeneous with Mg# of 0.52-0.56 and Ti 0.27-0.31 pfu.

Garnets form sub- euhedral grains, ranging from 0.5 – 1.5 mm in diameter. Compositionally the garnets are almandine-pyrope and are zoned from rim to core ($Alm_{49-55}Sps_{1-5}Py_{25-30}Grs_{14-22}$). Garnets are inclusion-rich with grains of quartz, white mica, and rutile.

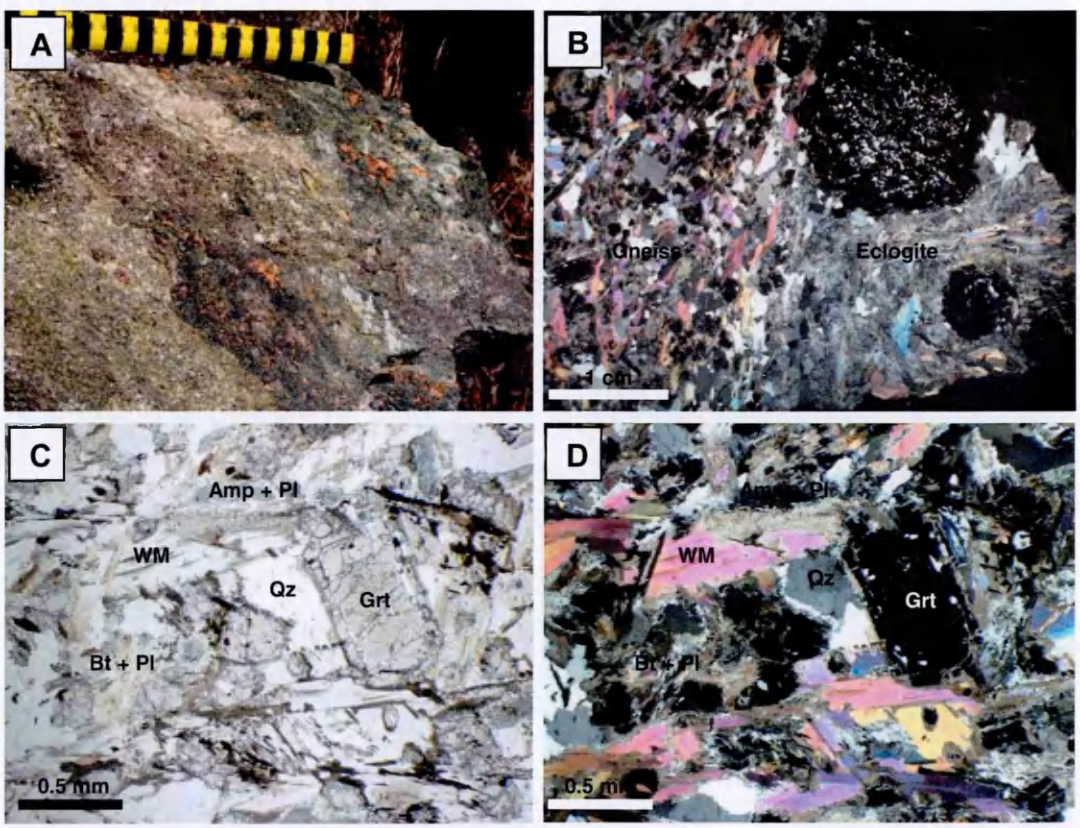

Fig. A9. Group 1a gneiss, NF43. A) field photograph of the sample showing felsic gneisses interlayered with mafic eclogite, B) whole thin section image of sample NF43 showing felsic gneiss to the left of the image and heavily symplectised eclogite on the right, C – D) photomicrographs in ppl and cpl showing the mineralogy of garnet + quartz + white mica with symplectites of biotite + plagioclase and amphibole + plagioclase.

Group 1b Gneisses: Garnet-bearing Gneisses without high-pressure relicts

The most commonly occurring petrographic type of garnet-bearing gneiss. This type of gneiss occurs at all three localities of Krokkenakken, Flatraket Harbour, and Drage.

NF106: is a medium-grained, foliated gneiss that is close to the contact with the Group 2 gneisses at Krokkenakken, described below. It contains a primary assemblage of garnet-quartz, white mica, biotite, and plagioclase with accessory phases of clinozoisite, rutile, apatite, and zircon. Phengite is commonly rimmed with biotite-plagioclase symplectites. The white mica and biotite forms major phases in this sample and the white mica is zoned from core to rim with Si ranging from 6.77-6.44 Si per 22 O. Biotite form elongate sub-mm grains that form distinct domains within the sample, with only minor well-formed laths within the matrix. Chemically, the biotite is homogeneous with Mg# of 0.50-0.54 and Ti 0.24-0.37 pfu. Garnets form sub- euhedral grains, ranging from 0.5 – 1.0 mm in diameter. Compositionally the garnets are almandine-pyrope and are zoned from rim to core ($Alm_{51-62}Sps_{0-1}Py_{12-22}Grs_{22-30}$). Garnets are inclusion-rich with grains of quartz, white mica, apatite, clinozoisite and rutile. The plagioclase associated has a broad composition, with an anorthite content ranging from An_{17-34}.

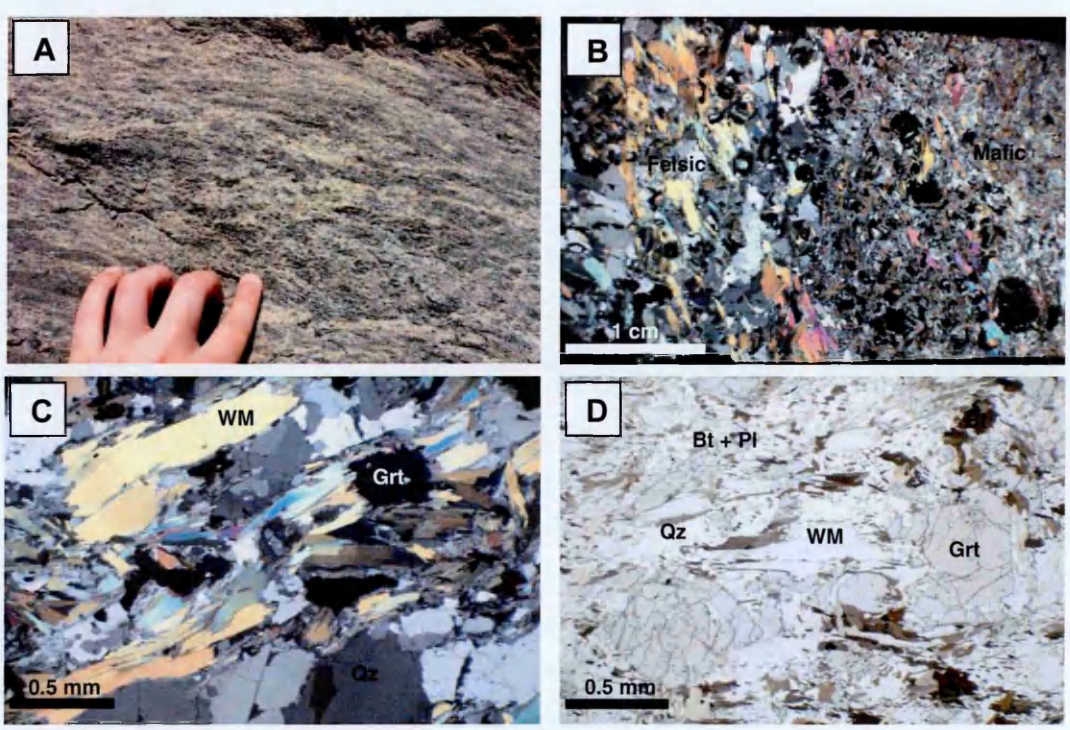

Fig. A10. Sample NF106. A) field photograph showing a mingling of felsic and mafic layers, B) whole thin section image, C – D) photomicrographs of NF106 showing the felsic layers have a mineralogy of quartz + garnet + white mica and the mafic layers have a mineralogy of garnet + quartz + biotite + white mica. Many of the white mica in the mafic layer is symplectised to biotite + plagioclase.

NF48: is a medium-grained, foliated gneiss from Flatraket Harbour. It contains a primary assemblage of garnet, quartz, white mica, biotite, and plagioclase with accessory phases of rutile, apatite, and zircon.

The white mica and biotite forms major phases in this sample and the white mica is zoned from core to rim with Si ranging from 6.70-6.26 Si per 22 O. Biotite form elongate sub-mm grains and define the fabric within the sample. Chemically, the biotite is homogeneous with Mg# of 0.51-0.54 and Ti 0.19-0.30 pfu.

Garnets form sub- euhedral grains, ranging from 0.5 – 1.0 mm in diameter. Compositionally the garnets are almandine-pyrope and are zoned from rim to core ($Alm_{52-63}Sps_{1-5}Py_{20-32}Grs_{11-17}$). Garnets are inclusion-poor with minor grains of quartz and rutile. The plagioclase associated has a broad composition, with an anorthite content ranging from An_{19-31}.

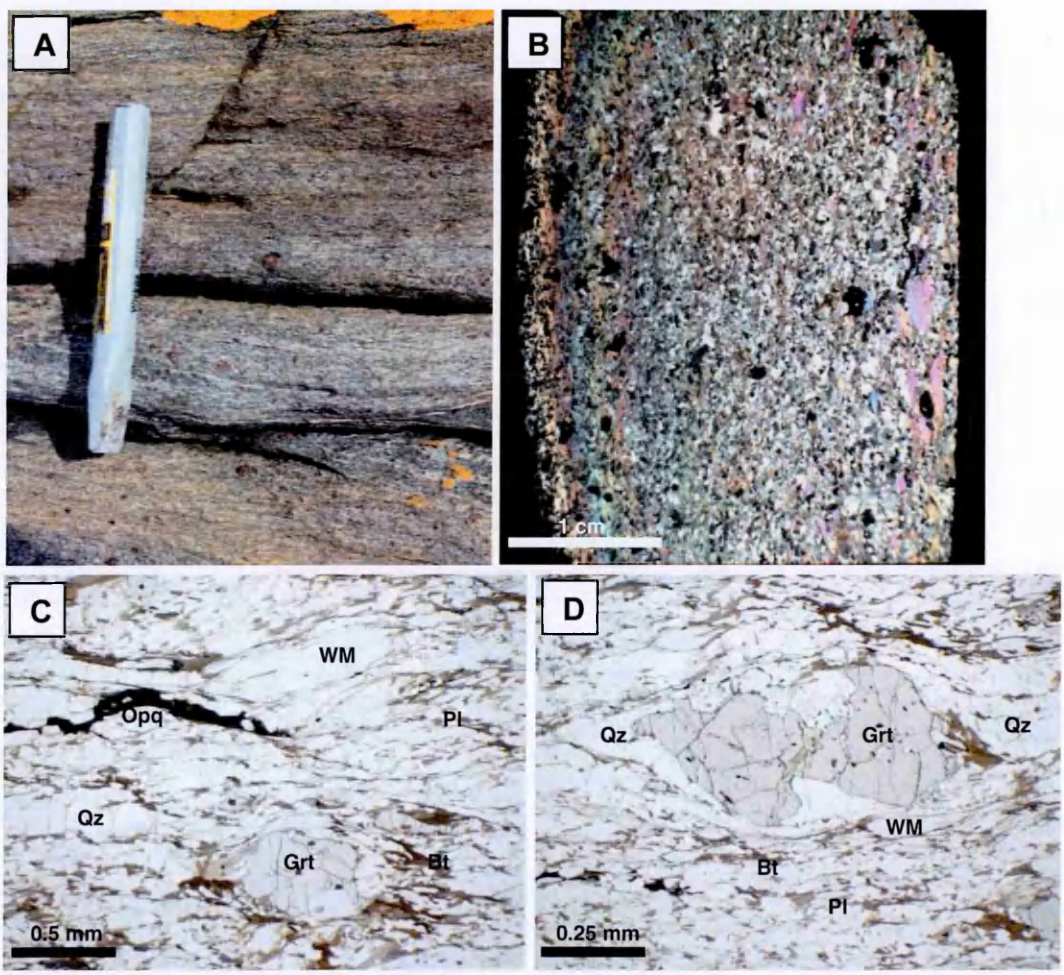

Fig. A11. Sample NF48. A) field photograph showing foliated, garnet-rich gneiss, B) whole thin section image, C – E) photomicrographs of NF48 displaying the mineralogy of white mica + biotite + garnet + quartz + plagioclase. C) white mica fish, D) Sheared garnet indicating that this sample has experienced deformation.

NF88: is a medium-grained, foliated gneiss from Drage. It contains a primary assemblage of garnet, quartz, white mica, biotite, and plagioclase with accessory phases of rutile, apatite, and zircon.

The white mica and biotite forms major phases in this sample and the white mica is zoned from core to rim with Si ranging from 6.72-6.25 Si per 22 O. Biotite form elongate sub-mm grains that define the fabric within the sample. Chemically, the biotite is homogeneous with Mg# of 0.44-0.47 and Ti 0.25-0.37 pfu.

Garnets form sub- anhedral grains, ranging from 0.5 – 1.0 mm in diameter. Compositionally the garnets are almandine-pyrope and are zoned from rim to core ($Alm_{55-60}Sps_{1-9}Py_{9-25}Grs_{16-28}$). Garnets are inclusion-poor with minor grains of quartz and rutile. The plagioclase associated has a broad composition, with an anorthite content ranging from An_{21-32}.

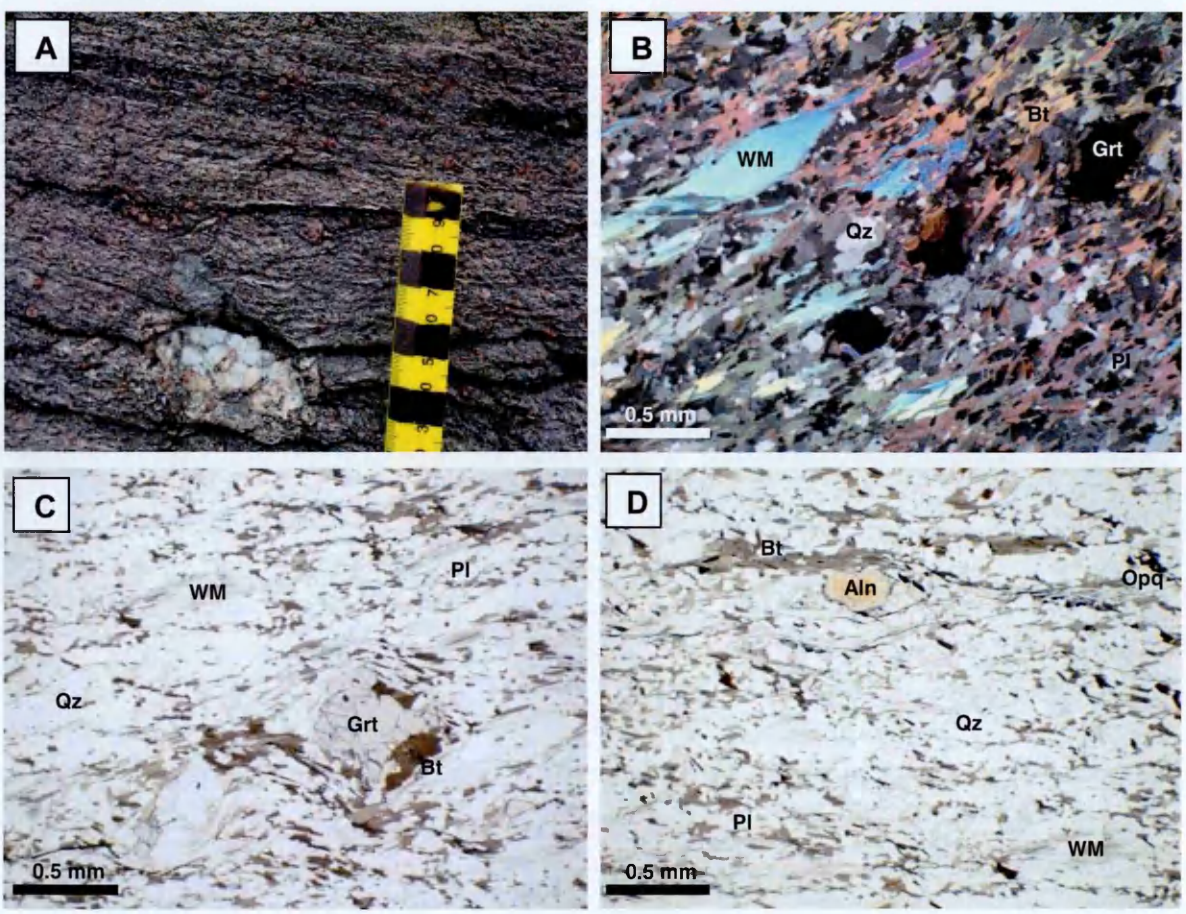

Fig. A12. Sample NF88. A) field photograph of sample NF88. B – D) photomicrograph showing the mineralogy of white mica + biotite + quartz + garnet. White mica form fish within the main biotite + plagioclase fabric. Also present are rare pleochroic allanite.

NF89: is a medium-grained, foliated gneiss from Drage. It contains a primary assemblage of garnet, quartz, white mica, biotite, and plagioclase with accessory phases of rutile, apatite, and zircon.

The white mica and biotite forms major phases in this sample and the white mica is zoned from core to rim with Si ranging from 6.79.6.26 Si per 22 O. Biotite form elongate sub-mm grains that define the fabric within the sample. Chemically, the biotite is variable with Mg# of 0.42-0.51 and Ti 0.26-0.35 pfu.

Garnets form sub- anhedral grains, ranging from 0.5 – 1.0 mm in diameter. Compositionally the garnets are almandine-pyrope and are zoned from rim to core ($Alm_{55-63}Sps_{1-15}Py_{12-30}Grs_{11-17}$). Garnets are inclusion-poor with minor grains of quartz, white mica, and rutile. The plagioclase associated has a broad composition, with an anorthite content ranging from An_{21-32}.

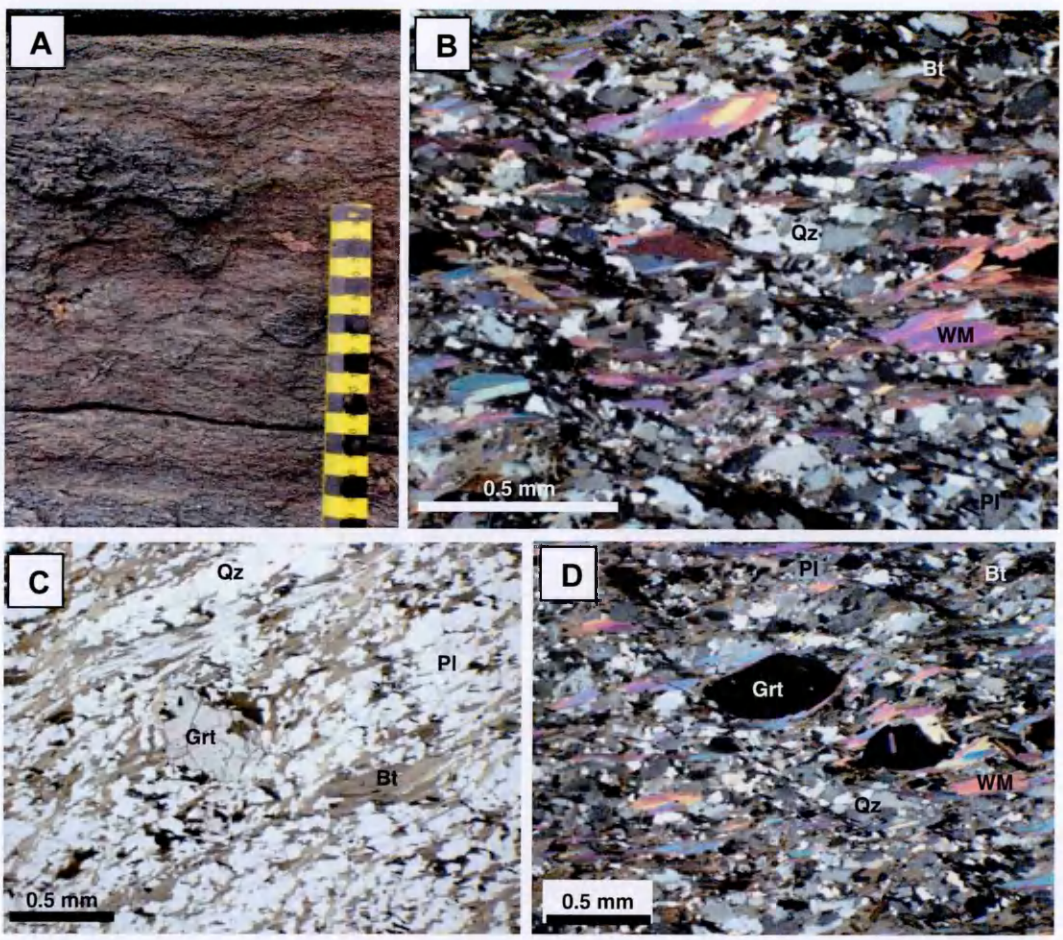

Fig. A13. Sample NF89. A) field photograph of the gneiss in outcrop, B – D) photomicrographs of sample NF89 showing the mineralogy of white mica + biotite + garnet + quartz + plagioclase. White mica, like those of other group 1b gneisses forms fish. Many of the garnet show rounded to anhedral crystal. The fabric of this sample is defined by biotite + plagioclase.

NF96: is a medium-grained, foliated gneiss from Drage. It contains a primary assemblage of garnet, quartz, white mica, biotite, and plagioclase with accessory phases of rutile, apatite, and zircon.

The white mica and biotite forms major phases in this sample and the white mica is zoned from core to rim with Si ranging from 6.77-6.17 Si per 22 O. Many of the white micas are kinked and folded. Biotite form elongate sub-mm grains that define the fabric within the sample. Chemically, the biotite is homogeneous with Mg# of 0.50-0.52 and Ti 0.27-0.32 pfu.

Garnets form sub- anhedral grains, ranging from 0.5 – 1.0 mm in diameter. Compositionally the garnets are almandine-pyrope and are zoned from rim to core ($Alm_{57-59}Sps_{1-4}Py_{18-21}Grs_{16-21}$). Garnets are inclusion-poor with minor grains of quartz, white mica, and rutile. The plagioclase associated has a broad composition, with an anorthite content ranging from An_{17-25}.

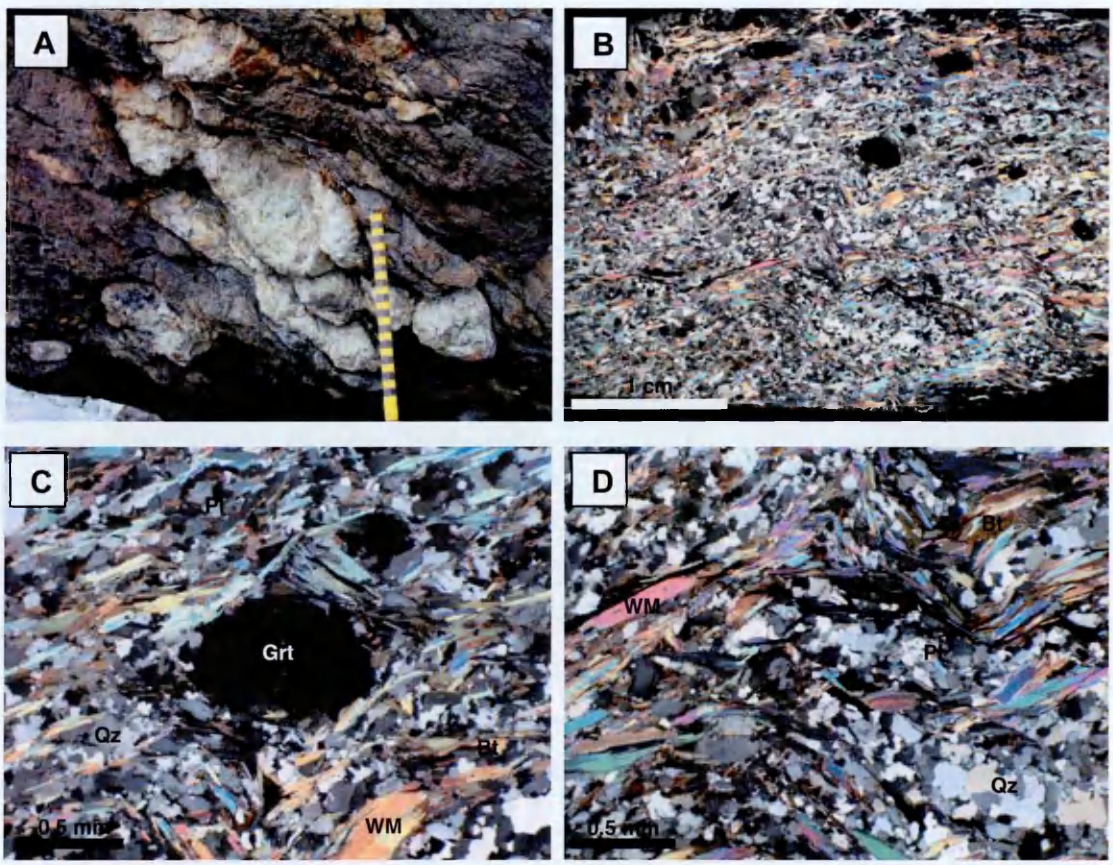

Fig. A14. Sample NF96. A) field photograph show group 1b gneisses in association with leucogranitic melt pods. B) whole thin section photomicrograph of sample NF96, C – D) photomicrographs showing mineralogy of white mica + biotite + garnet + quartz + plagioclase. Garnets are rounded to anhedral and many of the white mica are kinked and deformed.

NF99: is a medium-grained, foliated gneiss from Drage. It contains a primary assemblage of garnet, quartz, white mica, biotite, and plagioclase with accessory phases of rutile, apatite, and zircon.

The white mica and biotite forms major phases in this sample and the white mica is zoned from core to rim with Si ranging from 6.72-6.19 Si per 22 O. Biotite form elongate sub-mm grains that define the fabric within the sample. Chemically, the biotite is variable with Mg# of 0.46-0.53 and Ti 0.25-0.35 pfu.

Garnets form sub- anhedral grains, ranging from 0.5 – 1.0 mm in diameter. Compositionally the garnets are almandine-pyrope and are zoned from rim to core ($Alm_{60-63}Sps_{1-3}Py_{15-18}Grs_{17-22}$). Garnets are inclusion-poor with minor grains of quartz, white mica, and rutile. The plagioclase associated has a broad composition, with anorthite content ranging from An_{11-26}.

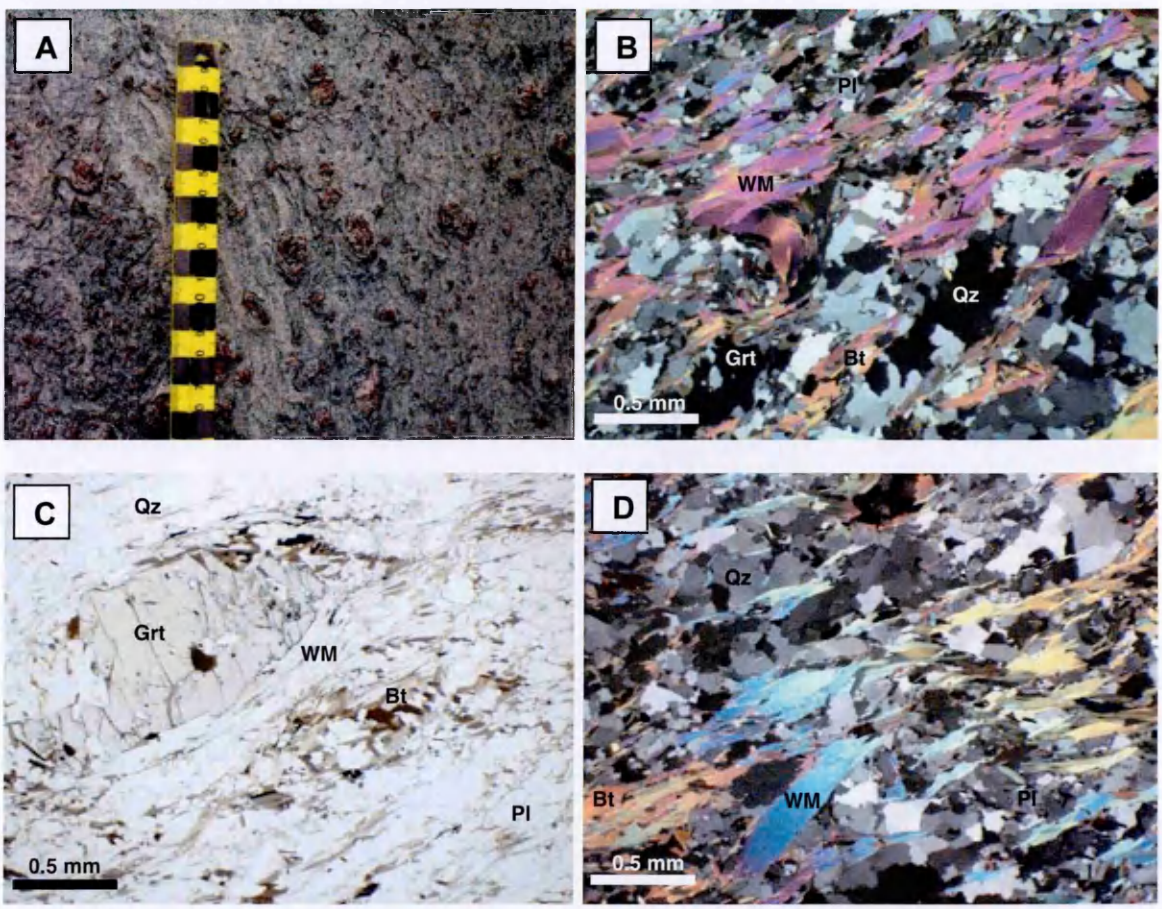

Fig. A15. Sample NF99. A) field outcrop photograph showing cm-sized red garnets, B – D) photomicrographs of sample NF99 showing mineralogy of white mica, biotite + quartz + garnet + plagioclase. White micas are kinked and deformed and many of the garnet are anhedral.

Group 1c Gneisses: Garnet-bearing Gneisses without high-pressure relicts and white mica

Subordinate to the Group 1b gneisses are Group 1c gneisses that contain neither white mica nor high-pressure relict. These gneisses are found at Flatraket Harbour and Drage and are generally associated adjacent to mafic eclogites or the Group 2 gneisses.

NF47: is a medium-grained, foliated gneiss from Flatraket Harbour and is located adjacent to the large, mafic eclogite. It contains a primary assemblage of garnet, quartz, biotite, plagioclase, and epidote with accessory phases of rutile, apatite, and zircon. The biotite forms the major K-bearing phase in this sample and form elongate sub-mm grains that define the fabric within the sample. Chemically, the biotite is variable with Mg# of 0.47-0.55 and Ti 0.23-0.35 pfu.

Garnets form anhedral grains, ranging from 0.5 – 1.0 mm in diameter. Compositionally the garnets are almandine-pyrope and are zoned from rim to core ($Alm_{49-57}Sps_{1-9}Py_{16-29}Grs_{13-21}$). Garnets are inclusion-poor with minor grains of quartz and rutile. The plagioclase associated has a broad composition, with anorthite content ranging from An_{21-37}. Epidote group minerals form large (1-1.5 mm) porphyroblasts that cross cut the biotite fabric. Epidote is commonly anhedral, unzoned and contains inclusions of the matrix phases (biotite, quartz, and plagioclase) with a composition that ranges from XEp 0.53-0.58.

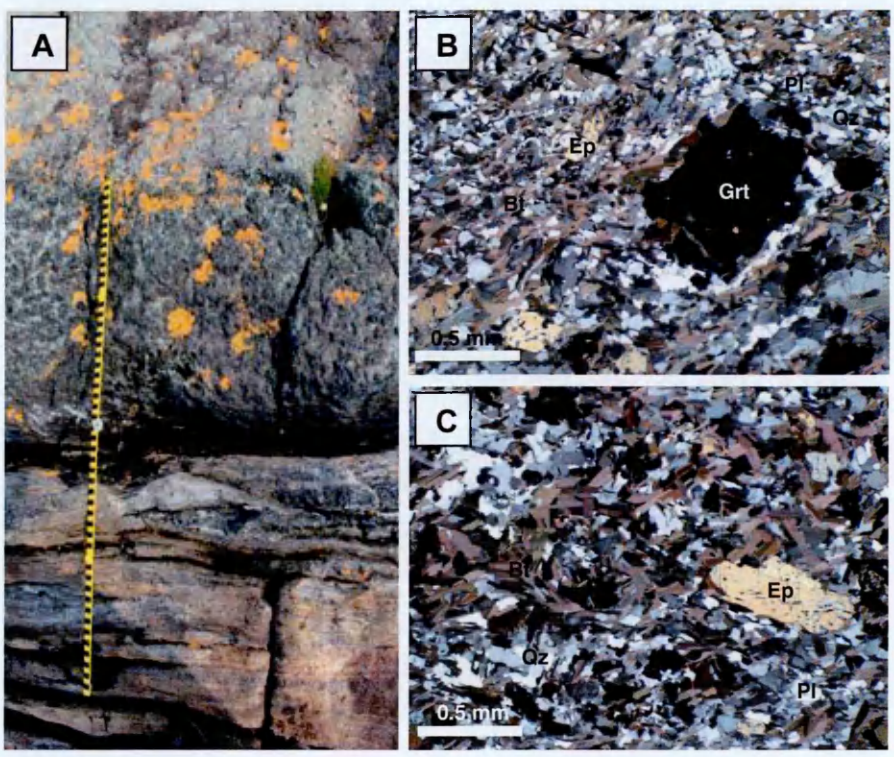

Fig. A16. Sample NF47. A) field photograph of the outcrop showing the close relationship between sample NF47 and the amphibolite NF46. B – C) photomicrographs showing the mineralogy of biotite + quartz + garnet + plagioclase + epidote.

NF50: is a medium-grained, foliated gneiss from Flatraket Harbour. It is located close to the contact with the Group 2b gneiss at this locality. It contains a primary assemblage of garnet, quartz, biotite, plagioclase, and epidote with accessory phases of rutile, apatite, and zircon. The biotite forms the major K-bearing phase in this sample and form elongate sub-mm grains that define the fabric within the sample. Chemically, the biotite is variable with Mg# of 0.55-0.59 and Ti 0.18-0.32 pfu.

Garnets form anhedral grains, ranging from 0.5 – 1.0 mm in diameter. Compositionally the garnets are almandine-pyrope and are zoned from rim to core ($Alm_{48-54}Sps_{1-2}Py_{36-31}Grs_{13-18}$). Garnets are inclusion-poor with minor grains of quartz, white mica, and rutile. The plagioclase associated has a broad composition, with anorthite content ranging from An_{22-38}. Epidote group minerals form large (1-1.5 mm) porphyroblasts that cross cut the biotite fabric. Epidote is commonly unzoned and contains inclusions of the matrix phases (biotite, quartz, and plagioclase) with a composition that ranges from XEp 0.50-0.69. Several grains are cored by allanite.

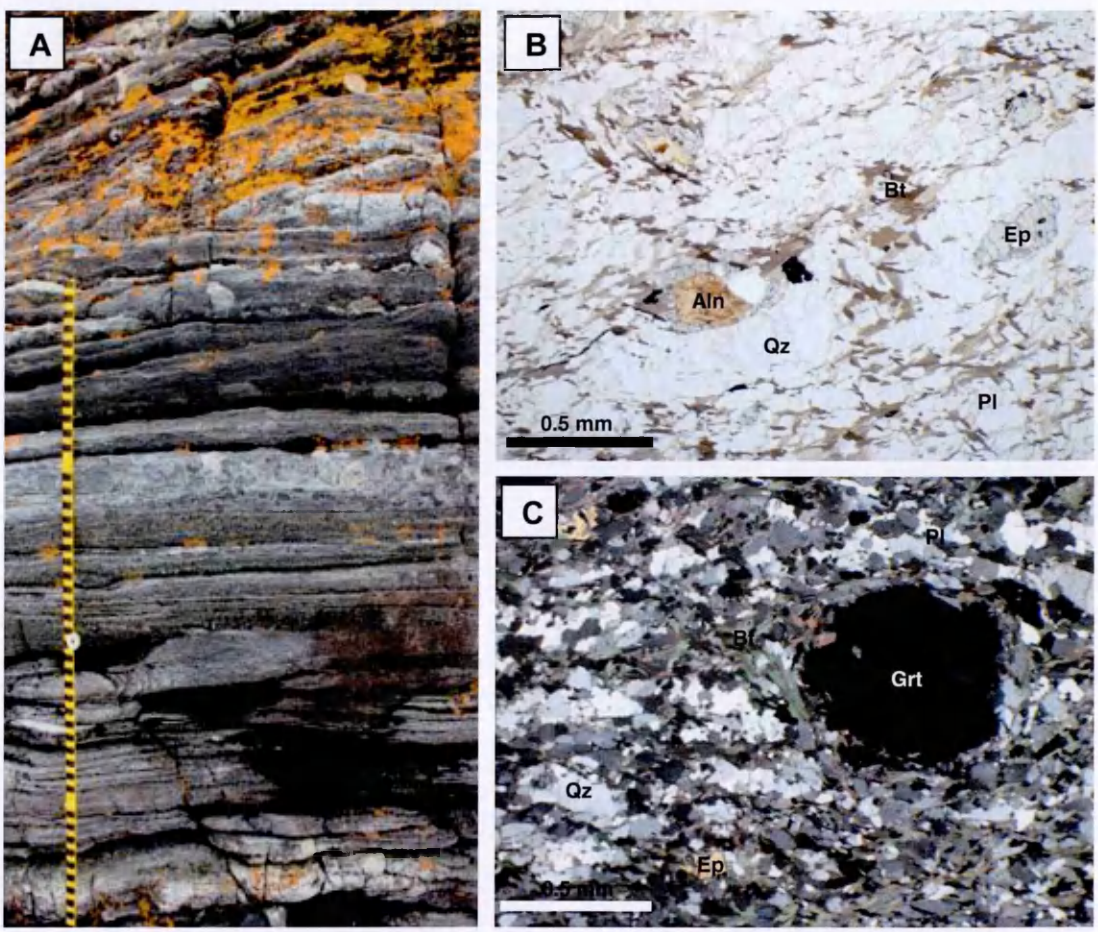

Fig. A17. Sample NF50. A) field photograph of the outcrop at Flatraket Harbour, B – C) photomicrographs showing the assemblage of garnet + biotite + quartz + plagioclase + epidote. Some of the epidote grains show pleochroic allanite cores.

NF87: is a medium-grained, foliated gneiss from Drage and is located adjacent to an amphibolitised mafic eclogite. It contains a primary assemblage of garnet, quartz, biotite, and plagioclase with accessory phases of rutile, apatite, and zircon. The biotite forms the major K-bearing phase in this sample and form elongate sub-mm grains that define the fabric within the sample. Chemically, the biotite is variable with Mg# of 0.52-0.61 and Ti 0.18-0.34 pfu.

Garnets form anhedral grains, ranging from 0.5 – 1.0 mm in diameter and many are heavily corroded. Compositionally the garnets are almandine-pyrope and are zoned from rim to core ($Alm_{54-58}Sps_{1-3}Py_{19-25}Grs_{18-21}$). Garnets are inclusion-poor with minor grains of quartz, white mica, and rutile. The plagioclase associated has a broad composition, with anorthite content ranging from An_{26-54}.

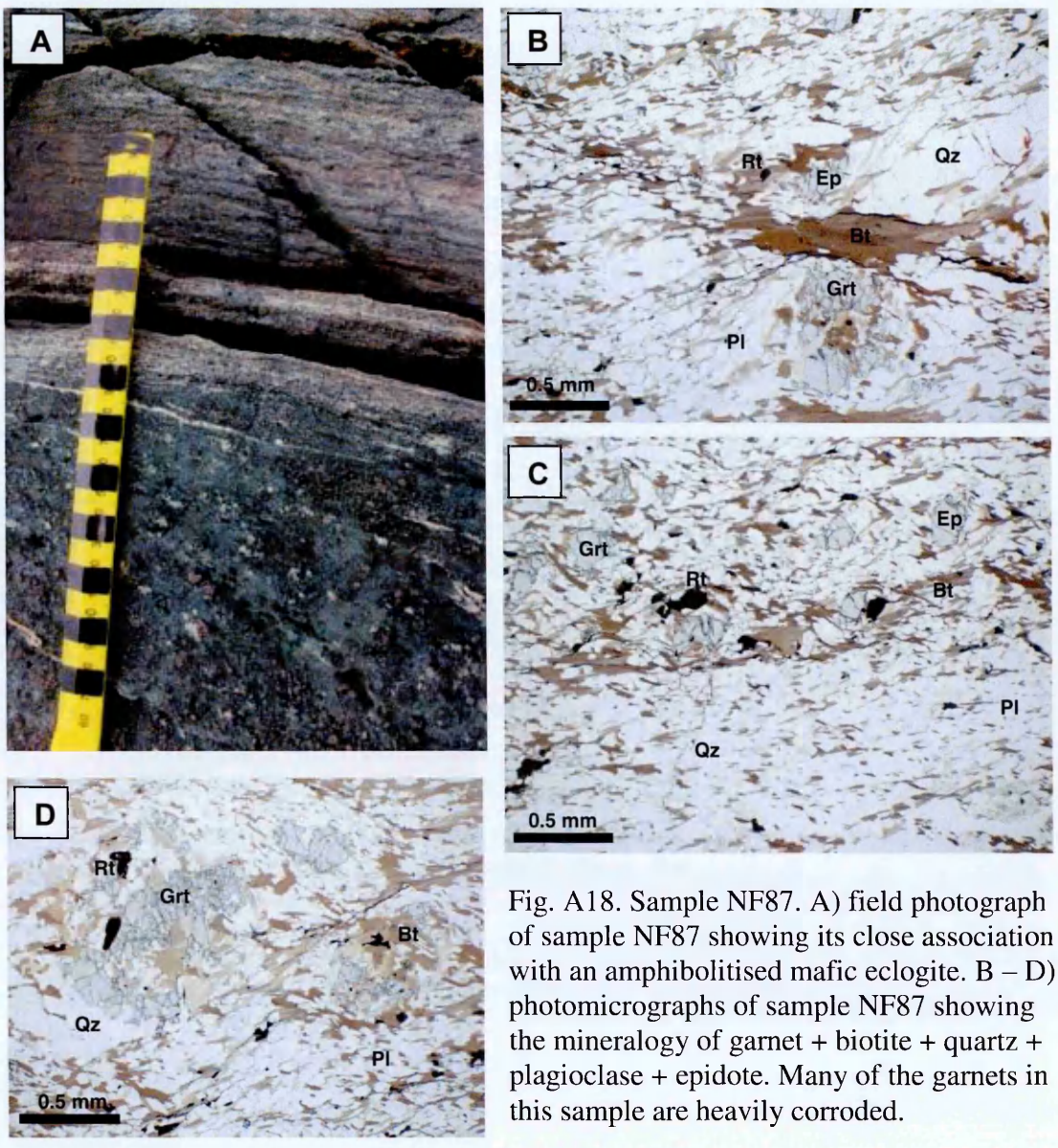

Fig. A18. Sample NF87. A) field photograph of sample NF87 showing its close association with an amphibolitised mafic eclogite. B – D) photomicrographs of sample NF87 showing the mineralogy of garnet + biotite + quartz + plagioclase + epidote. Many of the garnets in this sample are heavily corroded.

NF112: is a medium-grained, foliated gneiss from Flatraket Harbour. It is located close to the contact with the Group 2b gneiss at this locality. It contains a primary assemblage of garnet, quartz, biotite, and plagioclase with accessory phases of rutile, epidote, apatite, and zircon. The biotite forms the major K-bearing phase in this sample and form elongate sub-mm grains that define the fabric within the sample. Chemically, the biotite is homogeneous with Mg# of 0.53-0.58 and Ti 0.22-0.31 pfu.

Garnets form anhedral grains, ranging from 0.5 – 1.0 mm in diameter. Compositionally the garnets are almandine-pyrope and are zoned from rim to core ($Alm_{49-57}Sps_{1-9}Py_{16-29}Grs_{13-21}$). Garnets are inclusion-poor with minor grains of quartz, white mica, and rutile. The plagioclase associated has a broad composition, with anorthite content ranging from An_{21-37}. Epidote group minerals form small (< 0.5 mm) anhedral porphyroblasts that cross cut the biotite fabric. Epidote is commonly unzoned and contains inclusions of the matrix biotite, quartz, and plagioclase.

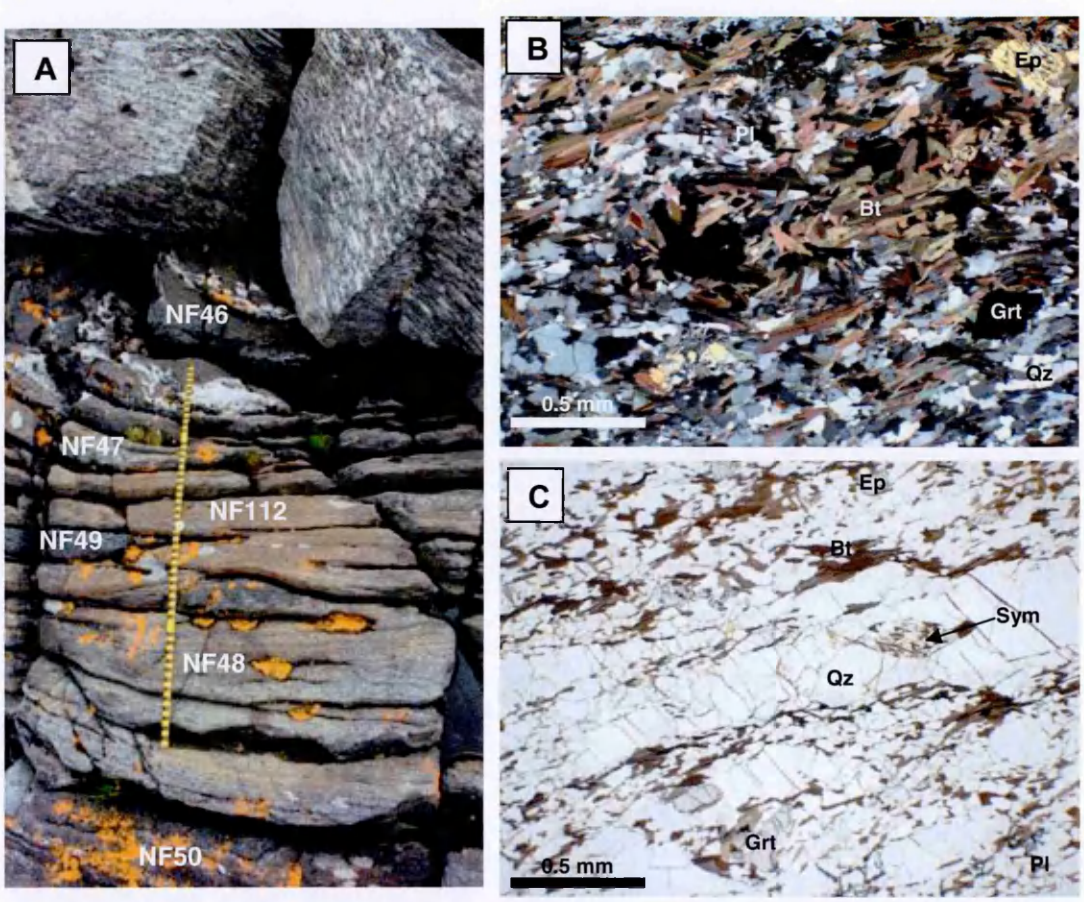

Fig. A19. Sample NF112. A) field photograph of sample NF112 showing its association with sample NF46, NF47 and NF48, B- C) photomicrographs showing the mineralogy of sample NF112 as biotite + garnet + quartz + plagioclase + epidote. In coarse quartz ribbon, relicts of biotite + plagioclase symplectites after white mica are preserved.

Group 2 Gneisses: Biotite-epidote Gneisses

Group 2a Gneisses: Biotite-epidote Gneisses with relict garnet and white mica

Group 2a gneisses are located at the contact between the garnet-bearing gneisses documented above and the amphibolite-facies gneisses are the predominant lithology in the Outer Nordfjord area. These gneisses contain minor relicts of garnet and white mica, preserved from the garnet-bearing gneisses. The two samples analysed in this study were collected at Krokkenakken and Drage

NF98: is a medium-grained, foliated gneiss from Drage. It contains a primary assemblage of quartz, biotite, plagioclase, epidote, and alkali feldspar with accessory phases of garnet, white mica, apatite, rutile, and zircon. The biotite forms the major K-bearing phase in this sample and form elongate sub-mm grains that define the fabric within the sample. Chemically, the biotite is variable with Mg# of 0.46-0.51 and Ti 0.12-0.42 pfu.

White Mica form isolated laths within the matrix that range from 0.5-1mm in length. Chemically, the white mica is moderately zoned, with Si ranging from 6.56-6.24 from core to rim. Commonly, the white mica has corroded margins that contain alkali feldspar + quartz, indicating partial melting.

Garnets form anhedral grains, ranging from 0.5 – 1.0 mm in diameter and are heavily corroded. Compositionally the garnets are almandine-pyrope and are zoned from rim to core ($Alm_{53-56}Sps_{1-5}Py_{9-11}Grs_{30-34}$). Garnets are inclusion-poor with minor grains of quartz and rutile. The plagioclase associated has a broad composition, with anorthite content ranging from An_{28-51}. Alkali feldspar form isolated grains within the matrix and are subordinate to plagioclase. Geochemically, the alkali feldspar has a composition that ranges from Or_{92-94}.

Epidote group minerals form large (1-1.5 mm) porphyroblasts that cross cut the biotite fabric. Epidote is commonly unzoned and contains inclusions of the matrix phases (biotite, quartz, and plagioclase) with a composition that ranges from XEp 0.55-0.62. Several grains are cored by allanite.

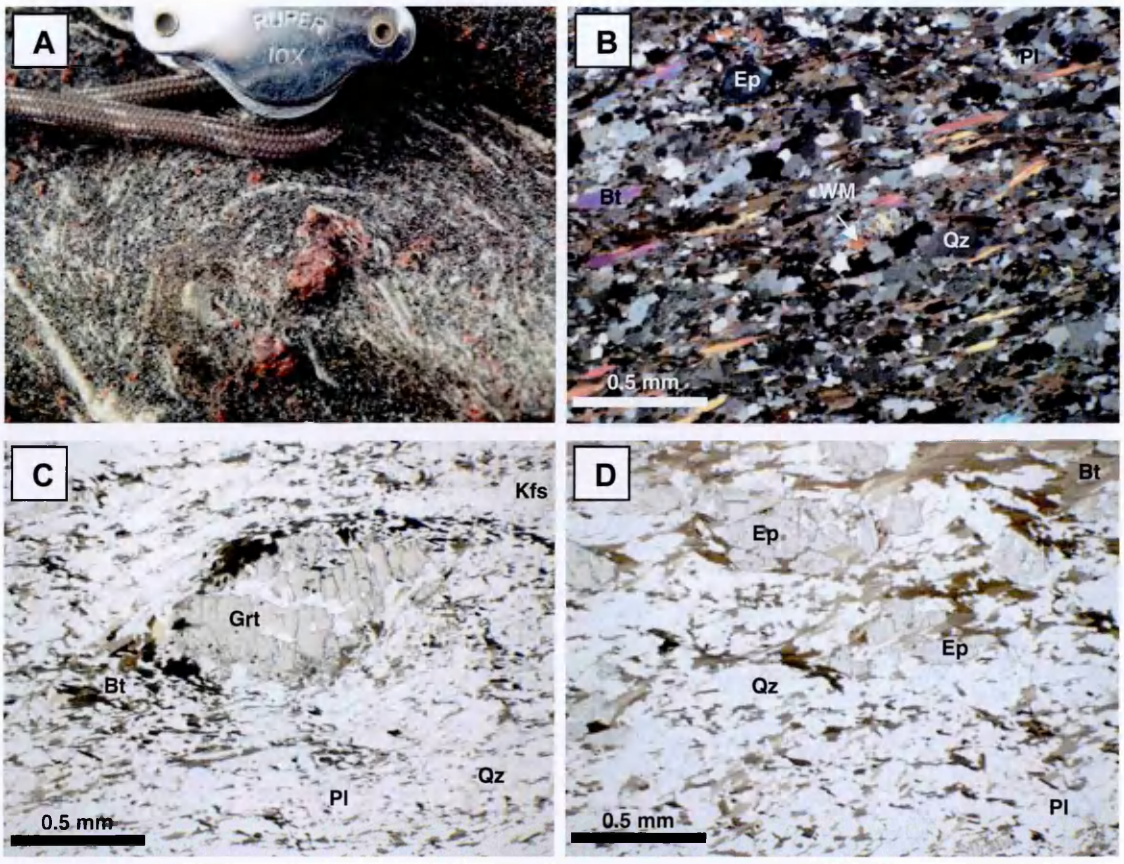

Fig. A20. Sample NF98. A) field outcrop photograph of sample NF98, B – D) photomicrographs showing the mineralogy of biotite + plagioclase + epidote + alkali feldspar. Relic garnets are heavily corroded and white mica show evidence of partial melting to alkali feldspar + quartz.

NF105: is a medium-grained, foliated gneiss from Krokkenakken. It contains a primary assemblage of quartz, biotite, plagioclase, epidote, and alkali feldspar with accessory phases of garnet, white mica, apatite, titanite, and zircon. The biotite forms the major K-bearing phase in this sample and form elongate sub-mm grains that define the fabric within the sample. Chemically, the biotite is homogeneous with Mg# of 0.40-0.43 and Ti 0.32-0.39 pfu.

White Mica form isolated laths within the matrix that range from 0.5-1mm in length. Chemically, the white mica is moderately zoned, with Si ranging from 6.38-6.25 from core to rim. Commonly, the white mica has corroded margins that contain alkali feldspar + quartz, indicating partial melting.

Garnets form rare anhedral grains that are ~0.5 mm in diameter and are heavily corroded. The plagioclase associated has a broad composition, with anorthite content ranging from An_{18-30}. Alkali feldspar form isolated grains within the matrix and are subordinate to plagioclase. Geochemically, the alkali feldspar has a composition that ranges from Or_{91-97}.

Epidote group minerals form large (1-1.5 mm) porphyroblasts that cross cut the biotite fabric. Epidote is commonly zoned and contains inclusions of the matrix phases (biotite, quartz, and plagioclase) with a composition that ranges from XEp 0.58-0.70. Several grains are cored by allanite.

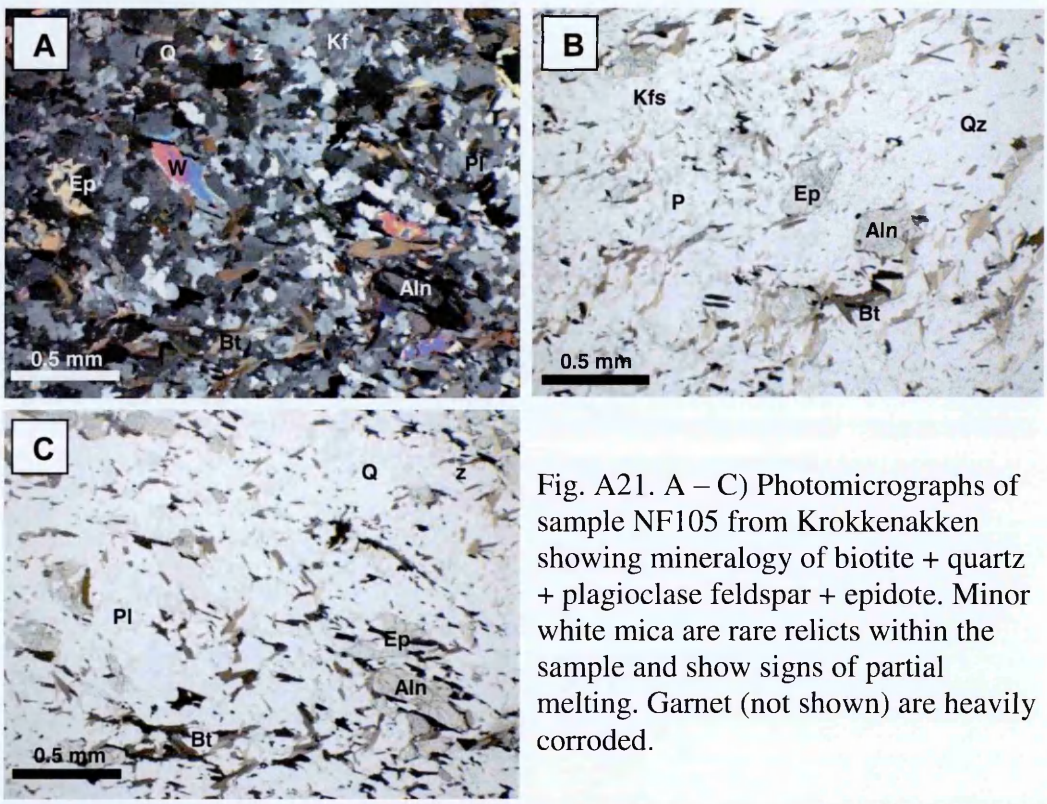

Fig. A21. A – C) Photomicrographs of sample NF105 from Krokkenakken showing mineralogy of biotite + quartz + plagioclase feldspar + epidote. Minor white mica are rare relicts within the sample and show signs of partial melting. Garnet (not shown) are heavily corroded.

Group 2b Gneisses: Biotite-epidote Gneisses

Group 2b gneisses represent the majority of the amphibolite-facies gneisses that are the dominant lithology in the Outer Nordfjord area.

NF35: is a medium-grained, foliated gneiss from Krokkenakken. It contains a primary assemblage of quartz, biotite, plagioclase, and epidote with accessory phases of amphibole, apatite, titanite, alkali feldspar, and zircon. The biotite forms the major K-bearing phase in this sample and form elongate sub-mm grains that define the fabric within the sample. Chemically, the biotite is homogeneous with Mg# of 0.44-0.49 and Ti 0.26-0.37 pfu. Minor amphibole form sub-micron grains within the matrix and belong to the hornblende group.

The plagioclase associated has a broad composition, with anorthite content ranging from An_{15-32}. Alkali feldspar form isolated augen within the matrix. In this sample, titanite forms the major Ti-bearing phase and several grains rim rutile, indicating titanite growth from rutile under amphibolite-facies conditions. Epidote group minerals form large (1-1.5 mm) porphyroblasts that cross cut the biotite fabric. Epidote is commonly zoned and contains inclusions of the matrix phases (biotite, quartz, and plagioclase) with a composition that ranges from XEp 0.46-0.64.

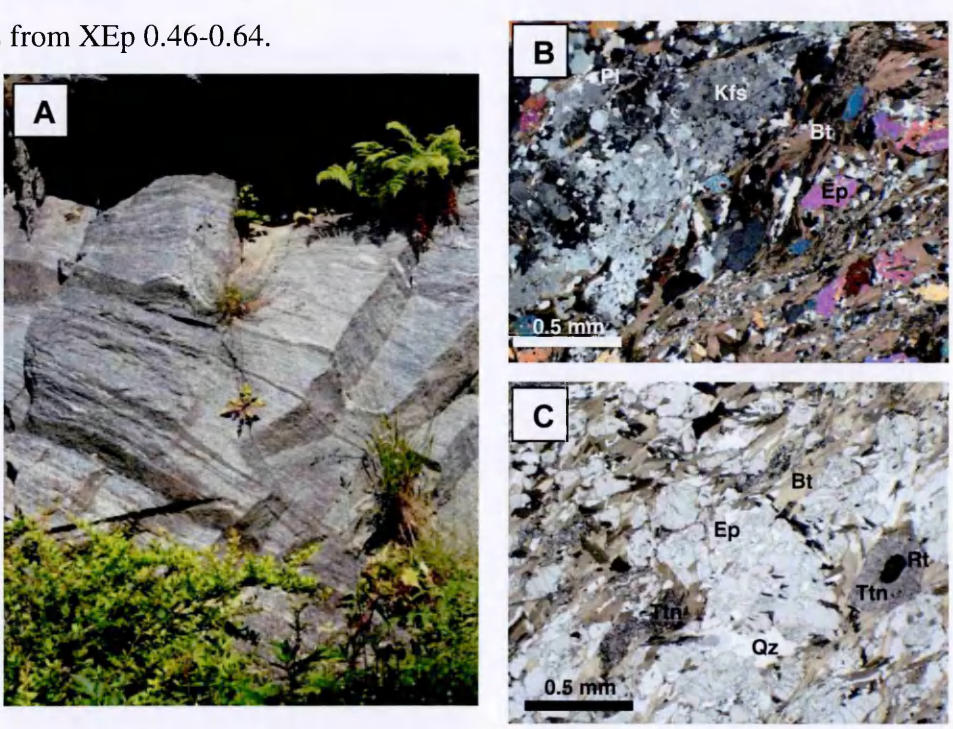

Fig. A22. Sample NF35. A) field photograph of the outcrop at Krokkenakken showing foliated nature of the gneiss, B – C) photomicrographs of NF35 showing mineralogy of biotite + epidote + quartz + plagioclase + alkali feldspar + titanite. Some titanite rim rutile.

NF51: is a medium-grained, foliated gneiss from Flatraket Harbour. It contains a primary assemblage of quartz, biotite, plagioclase, and epidote with accessory phases of amphibole, apatite, titanite, and zircon. The biotite forms the major K-bearing phase in this sample and form elongate sub-mm grains that define the fabric within the sample. Chemically, the biotite is variable with Mg# of 0.49-0.55and Ti 0.14-0.31 pfu. Minor amphibole form sub-micron grains within the matrix and belong to the hornblende group.

The plagioclase associated has a broad composition, with anorthite content ranging from An_{12-26}. Epidote group minerals form large (1-1.5 mm) porphyroblasts that cross cut the biotite fabric. Epidote is commonly zoned and contains inclusions of the matrix phases (biotite, quartz, titanite, and plagioclase) with a composition that ranges from XEp 0.42-0.76.

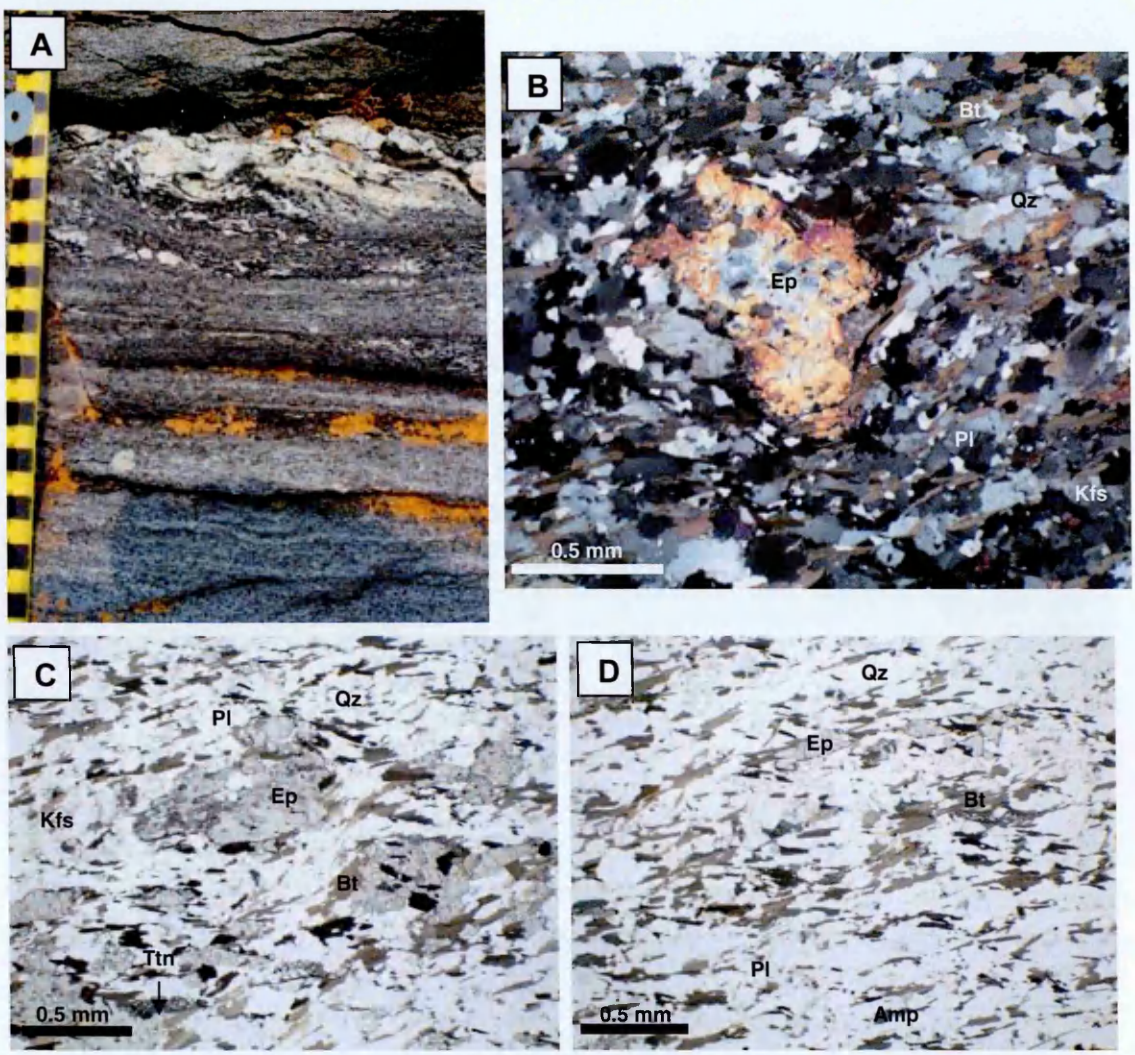

Fig. A23. Sample NF51. A) field photograph of the outcrop at Flatraket. NF51 was collected below the trondhjemite layer. The ovoid grain within this layer is a titanite crystal, B – D) photomicrographs of sample NF51 showing mineralogy of biotite + epidote + plagioclase + quartz + amphibole + titanite. Epidote porphyroblasts cross-cut the biotite fabric.

NF90: is a medium-grained, foliated gneiss from Drage. It contains a primary assemblage of quartz, biotite, plagioclase, and epidote with accessory phases of apatite, titanite, and zircon. Present in this sample are large (>2 mm) augen of alkali feldspar. The biotite form elongate sub-mm grains that define the fabric within the sample. Chemically, the biotite is variable with Mg# of 0.37-0.48 and Ti 0.19-0.41 pfu.

The plagioclase associated has a broad composition, with anorthite content ranging from An_{24-34}. The alkali feldspar augen have a variable composition, with an orthoclase content ranging from Or_{77-95}. Epidote group minerals form large (1-1.5 mm) porphyroblasts that cross cut the biotite fabric. Epidote is commonly zoned and contains inclusions of the matrix phases (biotite, quartz, and plagioclase) with a composition that ranges from XEp 0.63-1.00. Many of the epidote grains are cored by brown, pleochroic allanite.

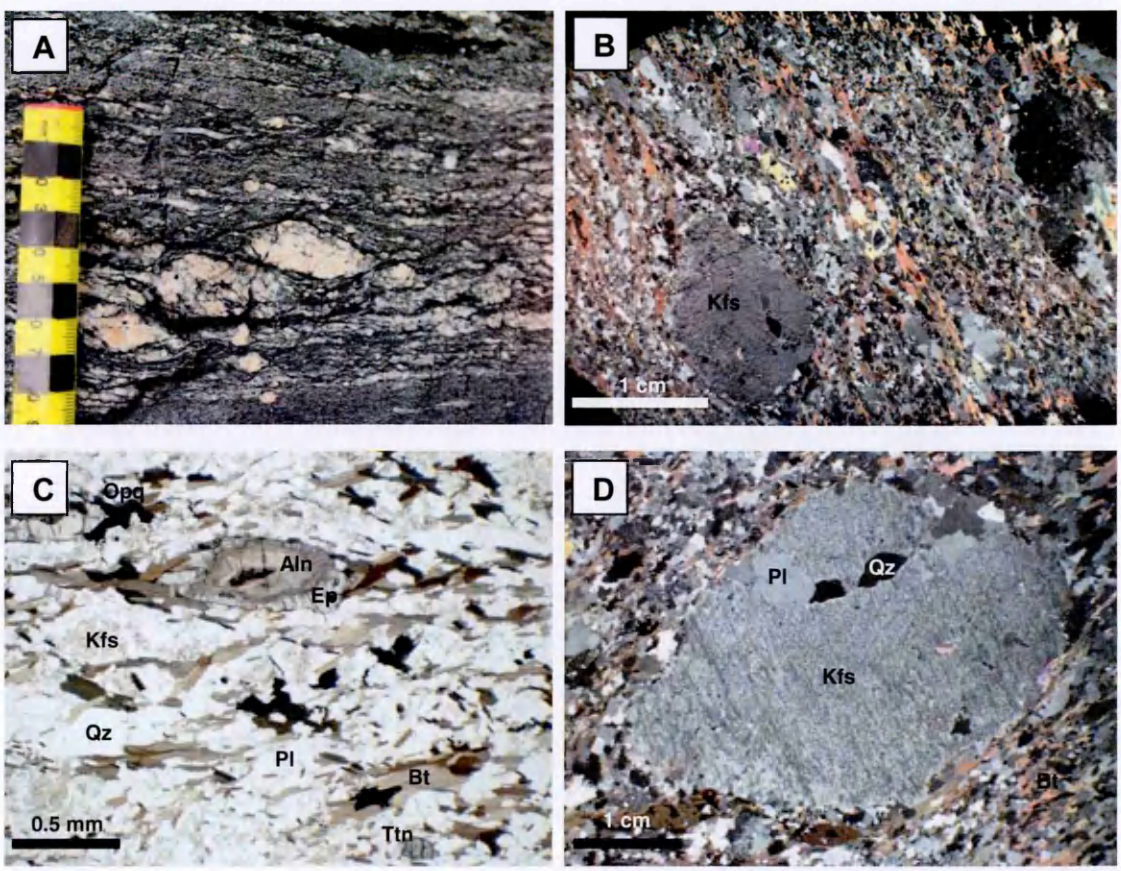

Fig. A24. Sample NF90. A) photograph of the outcrop at Drage showing alkali feldspar augen in a fine-grained matrix, B) whole thin section photograph of the sample, C – D) photomicrographs showing mineralogy of biotite + epidote + quartz + plagioclase + alkali feldspar + titanite. Many of the epidote grains are cored with allanite. Alkali feldspar augen are sub-rounded and contain inclusions of quartz.

NF91: is a fine-grained, migmatised gneiss from Drage. It contains a primary assemblage of quartz, biotite, plagioclase, epidote, and alkali feldspar with accessory phases of apatite, titanite, and zircon. The biotite form elongate sub-mm grains that define the fabric within the sample. Chemically, the biotite is variable with Mg# of 0.39-0.48 and Ti 0.21-0.35 pfu.

The plagioclase associated has a broad composition, with anorthite content ranging from An_{19-25}. The alkali feldspar has a more homogeneous composition than the plagioclase, with an orthoclase content ranging from Or_{93-97}. Epidote group minerals form large (1-1.5 mm) porphyroblasts that cross cut the biotite fabric. Epidote is commonly zoned and contains inclusions of the matrix phases (biotite, quartz, and plagioclase) with a composition that ranges from XEp 0.56-0.82. Many of the epidote grains are cored by brown, pleochroic allanite.

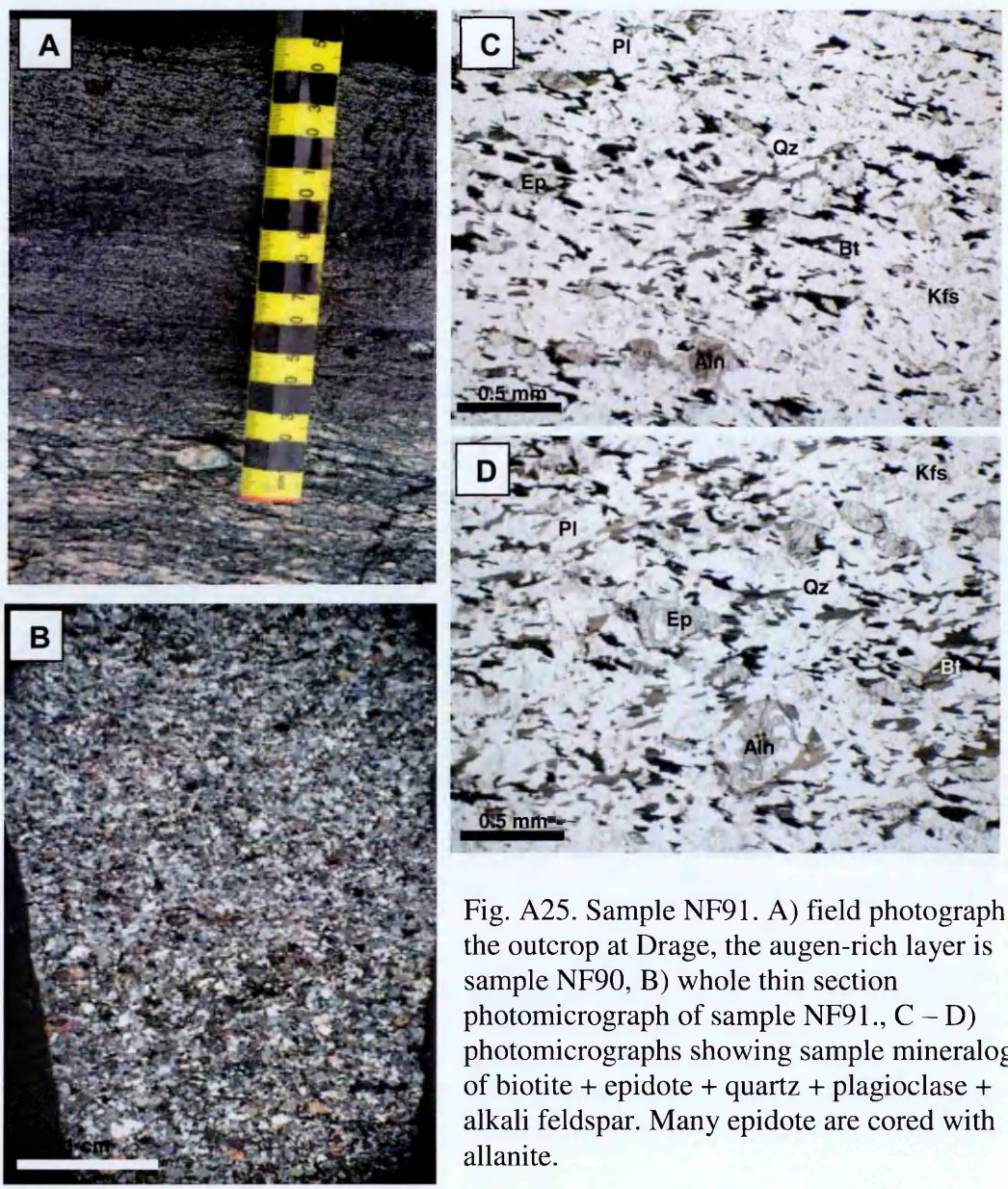

Fig. A25. Sample NF91. A) field photograph of the outcrop at Drage, the augen-rich layer is sample NF90, B) whole thin section photomicrograph of sample NF91., C – D) photomicrographs showing sample mineralogy of biotite + epidote + quartz + plagioclase + alkali feldspar. Many epidote are cored with allanite.

Flatraket Granulite

Undeformed Granulite

NF44A: represents the undeformed granulite collected from within the quarry. It contains an assemblage of quartz, biotite, and plagioclase with minor garnet, and pyroxene. This sample also contain large (3-10 cm) augen of alkali feldspar that range from near-circular to ovoid in shape. The texture of these augen has been likened to that of rapakivi granite (Krabbendam2000). The biotite form 'clots' that separate quartz-rich domains from plagioclase-rich domains. The plagioclase forms a granoblastic texture that contains numerous fine-grained acicular crystals. These acicular crystals have been recorded by Wain2001 as clinozoisite and kyanite and were interpreted to represent the onset of static eclogitisation within the Flatraket granulite. Biotite from this sample ranges in composition from 0.41-0.43 Mg# and Ti 0.34-0.41.

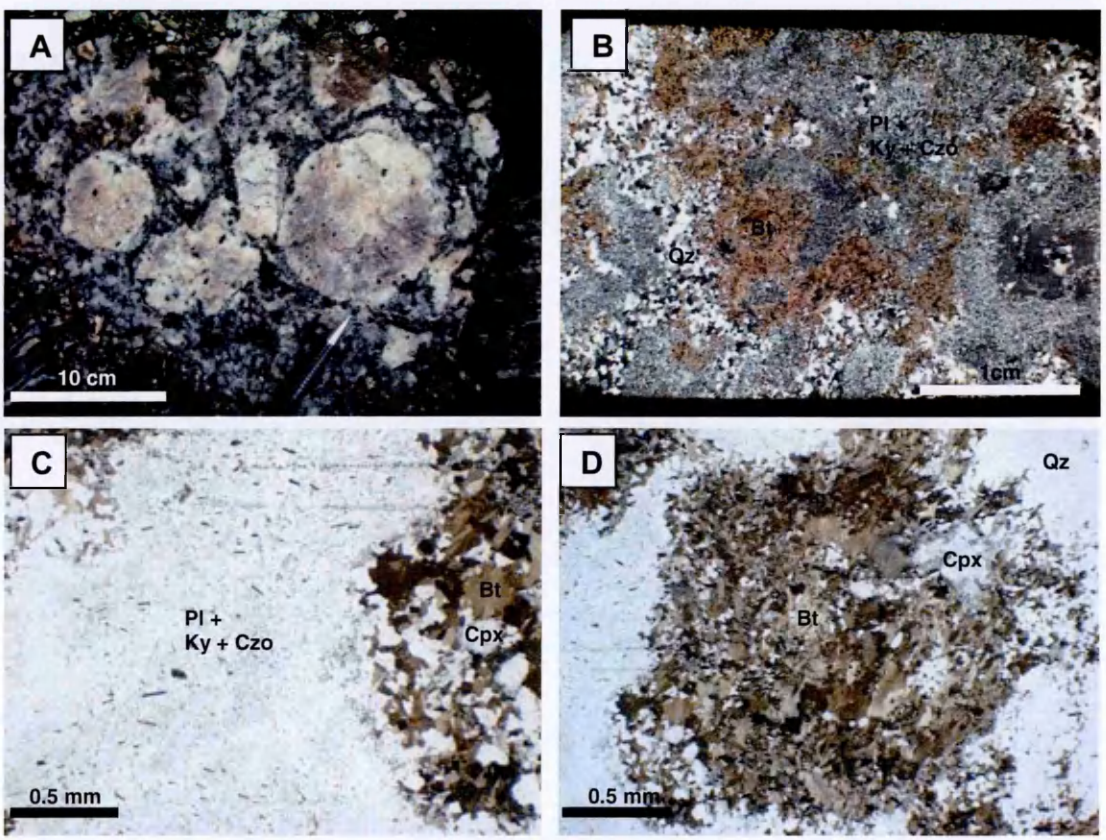

Fig. A26. Sample NF44A. A) field outcrop photograph showing the rapakivi-like texture of the granulite, B) whole thin section photomicrograph, C – D) photomicrographs showing mineralogy of biotite + quartz + plagioclase + clinopyroxene. The 'fuzzy' texture of the plagioclase is due to the presence of needles of clinozoisite + kyanite.

Sheared Granulite

NF44F: was collected from a shear zone that cross-cuts the undeformed granulite. These shear zones have been interpreted to have formed under amphibolite-facies conditions (Corfu2013). The sample contains an assemblage of quartz, plagioclase, and biotite with minor alkali feldspar, epidote, and titanite. This sample is finer grained than NF44A, with no augen preserved. NF44F has a strong mylonitic fabric defined by alternating layers of biotite-rich and quartz-rich domains. Biotite from this sample has a different chemistry from those from the undeformed sample, with a composition of Mg# 0.45-0.46 and Ti 0.30-0.35

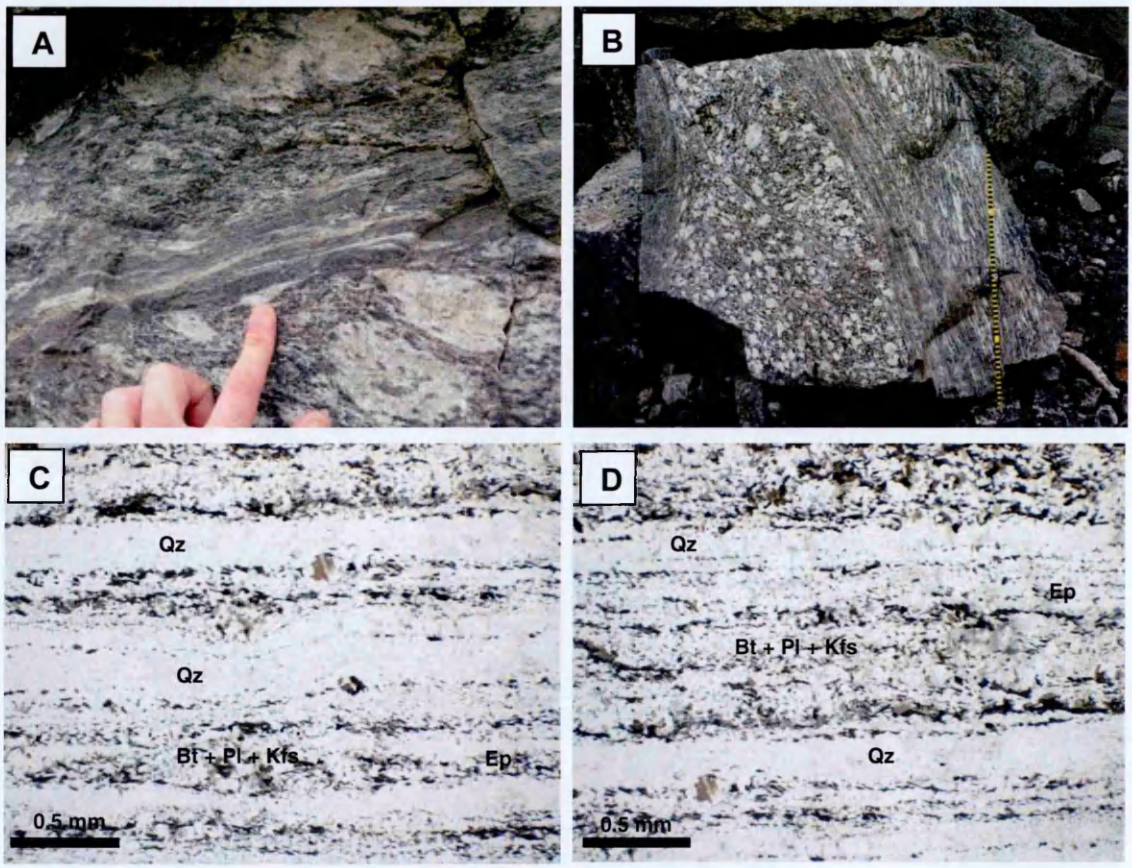

Fig. A27. Sample NF44F. A) field outcrop photograph showing the texture of the sheared granulite, B) a large (1.5 x 1.5 m) boulder showing granulite with anastomosing shear zones, C – D) photomicrographs showing the sheared granulite has an amphibolite-facie assemblage of quartz + biotite + plagioclase + alkali feldspar + epidote + titanite.

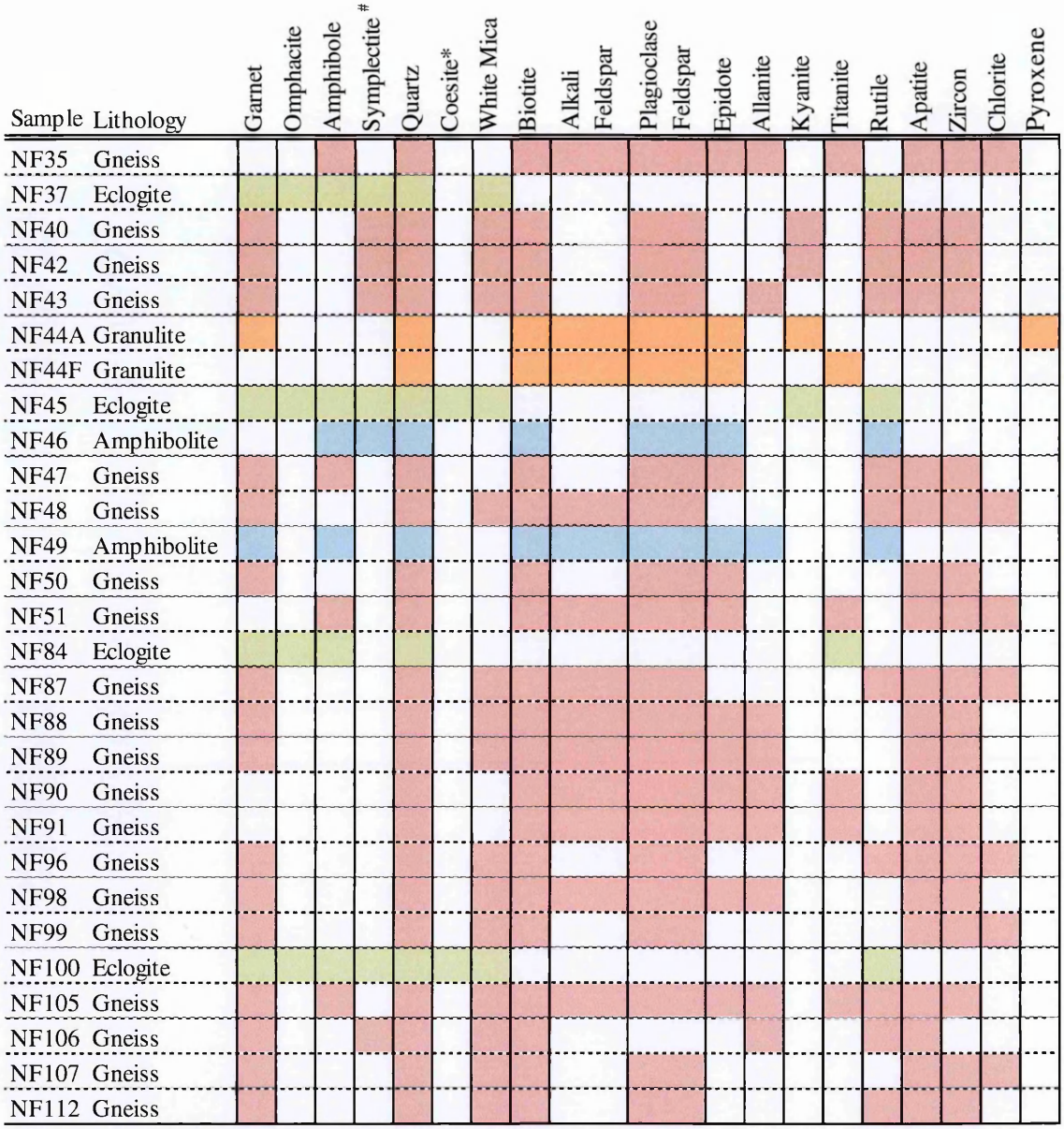

Symplectites of bitoite-plagioclase after white mica and clinopyroxene/amphibole-plagioclase symplectites after omphacite

* polycrystalline quartz inclusions in garnet and omphacite interpreted as pseudomorphs after coesite

Table A1. A tabulated sample catalogue

Appendix B:

Electron Microprobe Analysis Datasets

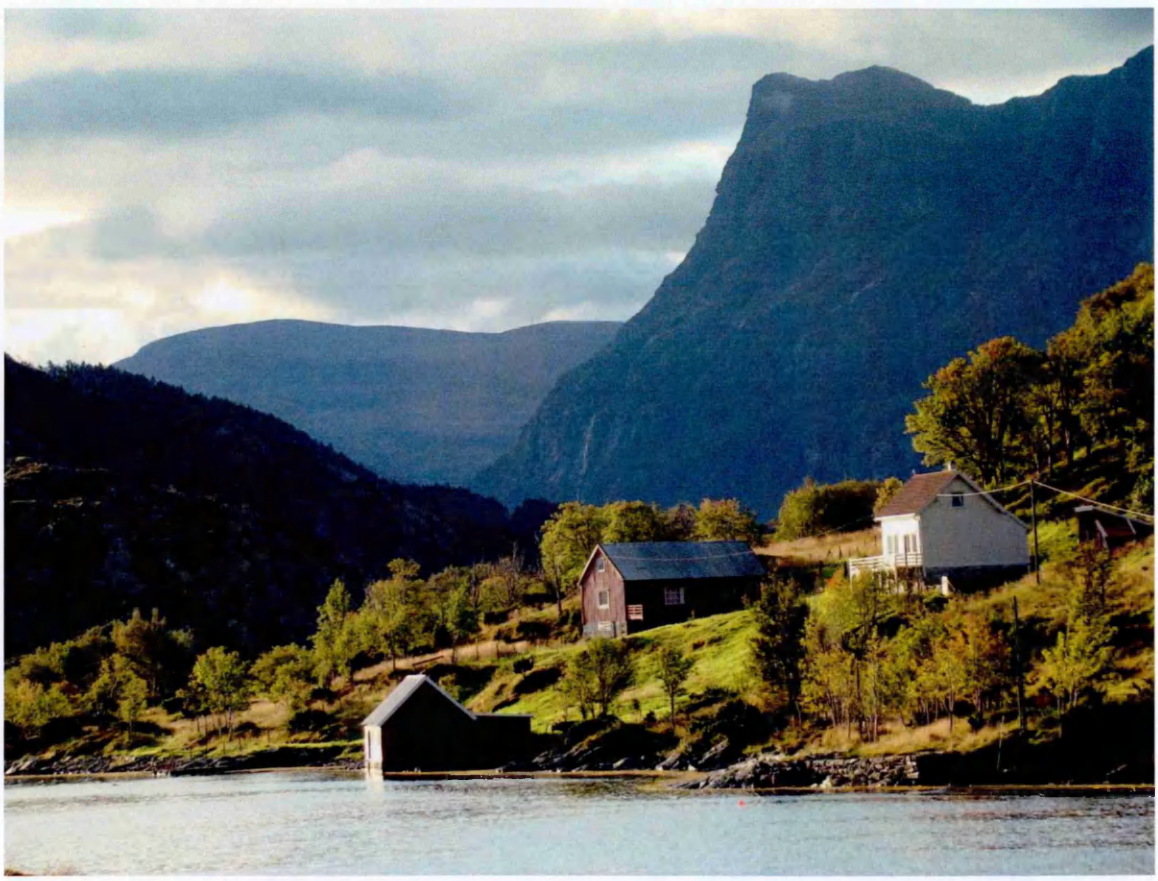

Norwegian fjordland living

Electron Microprobe Analysis
B.1: NF35 Krokkenakken Biotite-Epidote Gneiss
61°54'53.73" N
005°20'16.49" E

Mineral	Biotite		Plagioclase	Amphibole	Epidote
Position	Core	Rim	Feldspar		
F	0.21	0.17	0.06	0.09	0.11
Cl	0.01	0.01	0.00	0.02	0.01
Na_2O	0.08	0.09	8.10	1.26	0.00
K_2O	9.65	9.73	0.13	1.33	0.00
MgO	10.08	9.96	0.00	8.08	0.08
CaO	0.00	0.00	6.30	11.52	23.42
MnO	0.39	0.43	0.01	0.45	0.19
FeO	19.21	19.49	0.04	18.84	9.81
Al_2O_3	16.24	16.30	24.72	13.20	24.84
Cr_2O_3	0.03	0.00	0.00	0.00	0.01
SiO_2	36.60	36.22	60.84	41.04	38.25
TiO_2	2.27	2.60	0.00	0.78	0.14
Total	94.84	95.06	100.21	96.62	96.92
F	0.10	0.08	0.01	0.05	0.03
Cl	0.00	0.01	0.00	0.01	0.00
Na	0.02	0.03	0.70	0.38	0.00
K	1.90	1.91	0.01	0.26	0.00
Mg	2.32	2.29	0.00	1.86	0.01
Ca	0.00	0.00	0.30	1.90	2.03
Mn	0.05	0.06	0.00	0.06	0.01
Fe	2.48	2.51	0.00	2.43	0.67
Al	2.95	2.96	1.29	2.40	2.38
Cr	0.01	0.00	0.00	0.00	0.00
Si	5.64	5.58	2.70	6.34	3.10
Ti	0.26	0.30	0.00	0.09	0.01
Total	15.74	15.73	5.01	15.77	8.24

Electron Microprobe Analysis
B.2: NF37 Krokkenakken Eclogite
61°54'53.73" N
005°20'16.49" E

Mineral	White Mica		Garnet		Omphacite		Amphibole	Epidote
Position	Core	Rim	Core	Rim	Core	Rim		
F	0.04	0.00	0.00	0.00	0.01	0.02	0.09	0.01
Cl	0.00	0.00	0.00	0.00	0.01	0.00	0	0
Na_2O	0.52	0.40	0.03	0.01	5.53	5.57	3.36	0
K_2O	10.59	10.63	0.00	0.00	0.00	0.00	0.45	0
MgO	4.13	3.80	8.80	9.67	9.98	9.99	15.03	0.2
CaO	0.00	0.02	7.82	8.09	14.81	14.66	9.47	23.65
MnO	0.01	0.02	0.37	0.31	0.00	0.01	0.06	0.09
FeO	1.53	1.76	22.02	20.37	3.67	3.60	8.16	6.76
Al_2O_3	25.67	26.23	22.28	22.51	9.34	9.57	11.87	27.13
Cr_2O_3	0.07	0.18	0.05	0.03	0.05	0.05	0.04	0.1
SiO_2	51.78	49.62	38.79	39.62	54.93	54.59	48.55	38.83
TiO_2	0.28	0.42	0.06	0.00	0.05	0.06	0.32	0.15
Total	94.64	93.09	100.22	100.61	98.38	98.14	97.4	96.94
F	0.02	0.00	0.00	0.00	0.00	0.00	0.04	0
Cl	0.00	0.00	0.00	0.00	0.00	0.00	0	0
Na	0.14	0.10	0.00	0.00	0.39	0.39	0.93	0
K	1.81	1.85	0.00	0.00	0.00	0.00	0.08	0
Mg	0.83	0.78	1.00	1.09	0.54	0.54	3.19	0.03
Ca	0.00	0.00	0.64	0.65	0.57	0.57	1.44	2.01
Mn	0.00	0.00	0.02	0.02	0.00	0.00	0.01	0.01
Fe	0.17	0.20	1.40	1.28	0.11	0.11	0.97	0.45
Al	4.05	4.23	2.00	2.00	0.40	0.41	2	2.54
Cr	0.01	0.02	0.00	0.00	0.00	0.00	0.01	0.01
Si	6.94	6.79	2.96	2.98	1.99	1.98	6.92	3.08
Ti	0.03	0.04	0.00	0.00	0.00	0.00	0.03	0.01
Total	14.00	14.03	8.04	8.02	4.01	4.01	15.62	8.14

Electron Microprobe Analysis
B.3: NF40 Krokkenakken Garnet-bearing Gneiss with HP Relicts
61°54'53.73" N
005°20'16.49" E

Mineral	White Mica		Biotite		Garnet			Plagioclase	Kyanite
Position	Core	Rim	Core	Rim	Core	Mantle	Rim	Feldspar	
F	0.22	0.14	0.14	0.22	0.00	0.00	0.00	0.12	0.05
Cl	0.00	0.01	0.01	0.01	0.00	0.00	0.00	0.00	0.00
Na_2O	0.67	0.75	0.27	0.25	0.03	0.03	0.01	9.05	0.00
K_2O	9.44	9.70	8.61	8.92	0.00	0.00	0.00	0.08	0.00
MgO	2.58	2.16	12.58	12.43	8.38	6.93	6.97	0.00	0.00
CaO	0.00	0.00	0.13	0.06	4.28	7.90	5.21	4.79	0.01
MnO	0.01	0.00	0.07	0.05	1.36	0.54	0.83	0.00	0.00
FeO	2.66	2.72	15.54	15.36	24.91	23.92	26.41	0.05	0.52
Al_2O_3	28.41	29.72	17.94	17.90	22.04	21.80	21.60	23.53	61.88
Cr_2O_3	0.02	0.01	0.04	0.03	0.01	0.01	0.01	0.01	0.04
SiO_2	50.24	49.08	37.13	36.73	39.09	39.31	38.95	62.80	37.16
TiO_2	0.33	0.56	1.89	1.95	0.01	0.01	0.00	0.00	0.01
Total	94.58	94.88	94.43	93.98	100.15	100.47	100.00	100.43	99.66
F	0.09	0.06	0.07	0.10	0.00	0.00	0.00	0.02	0.01
Cl	0.00	0.00	0.00	0.01	0.00	0.00	0.00	0.00	0.00
Na	0.18	0.19	0.08	0.08	0.01	0.00	0.00	0.78	0.00
K	1.62	1.66	1.65	1.72	0.00	0.00	0.00	0.00	0.00
Mg	0.52	0.43	2.82	2.81	0.96	0.79	0.80	0.00	0.00
Ca	0.00	0.00	0.02	0.01	0.35	0.65	0.43	0.23	0.00
Mn	0.00	0.00	0.01	0.01	0.09	0.04	0.05	0.00	0.00
Fe	0.30	0.31	1.95	1.95	1.60	1.53	1.71	0.00	0.01
Al	4.50	4.71	3.18	3.20	2.00	1.97	1.97	1.23	1.98
Cr	0.00	0.00	0.01	0.01	0.00	0.00	0.00	0.00	0.00
Si	6.75	6.59	5.58	5.57	3.00	3.02	3.02	2.78	1.01
Ti	0.03	0.06	0.21	0.22	0.00	0.00	0.00	0.00	0.00
Total	14.00	14.01	15.58	15.68	8.00	8.00	8.00	5.03	3.01

Electron Microprobe Analysis
B.4: NF42 Krokkenakken Garnet-bearing Gneiss with HP Relicts
61°54'53.73" N
005°20'16.49" E

Mineral	White Mica		Biotite		Garnet			Plagioclase	Amphibole
Position	Core	Rim	Core	Rim	Core	Mantle	Rim	Feldspar	
F	0.05	0.02	0.12	0.15	0.00	0.00	0.00	0.03	0.04
Cl	0.00	0.01	0.00	0.00	0.00	0.01	0.00	0.00	0.01
Na_2O	0.39	0.41	0.15	0.10	0.01	0.03	0.01	5.61	1.13
K_2O	9.59	9.92	9.07	8.76	0.00	0.00	0.00	0.07	0.59
MgO	3.68	3.04	15.37	15.63	4.82	6.47	8.09	0.00	14.04
CaO	0.01	0.00	0.03	0.08	6.68	7.41	6.12	10.71	11.76
MnO	0.02	0.00	0.03	0.03	0.83	0.11	0.29	0.02	0.08
FeO	1.99	1.81	12.96	12.59	28.33	25.66	24.93	0.06	9.28
Al_2O_3	27.32	29.00	16.95	17.40	21.44	21.84	22.00	28.64	12.95
Cr_2O_3	0.02	0.03	0.03	0.02	0.04	0.00	0.00	0.00	0.06
SiO_2	49.68	48.86	37.85	37.65	37.49	38.26	38.57	55.28	46.65
TiO_2	0.19	0.41	2.27	2.22	0.02	0.06	0.00	0.00	0.53
Total	93.00	93.49	94.93	94.68	99.65	99.85	100.04	100.42	97.11
F	0.02	0.01	0.06	0.07	0.00	0.00	0.00	0.00	0.02
Cl	0.00	0.00	0.00	0.00	0.00	0.00	0.00	0.00	0.00
Na	0.10	0.11	0.04	0.03	0.00	0.01	0.00	0.49	0.32
K	1.67	1.72	1.71	1.65	0.00	0.00	0.00	0.00	0.11
Mg	0.75	0.62	3.39	3.44	0.57	0.75	0.93	0.00	3.01
Ca	0.00	0.00	0.01	0.01	0.57	0.62	0.51	0.52	1.81
Mn	0.01	0.00	0.01	0.01	0.05	0.01	0.02	0.00	0.01
Fe	0.23	0.20	1.61	1.56	1.88	1.67	1.61	0.00	1.12
Al	4.38	4.63	2.95	3.03	2.00	2.00	2.00	1.52	2.20
Cr	0.00	0.01	0.01	0.00	0.00	0.00	0.00	0.00	0.01
Si	6.77	6.62	5.60	5.57	2.97	2.97	2.97	2.48	6.72
Ti	0.02	0.04	0.25	0.25	0.00	0.00	0.00	0.00	0.06
Total	13.94	13.95	15.64	15.61	8.03	8.03	8.03	5.01	15.38

Electron Microprobe Analysis
B.5: NF43 Krokkenakken Garnet-bearing Gneiss with HP Relicts
61°54'53.73" N
005°20'16.49" E

Mineral	White Mica		Biotite		Garnet		Epidote
Position	Core	Rim	Core	Rim	Core	Rim	
F	0.10	0.08	0.10	0.02	0.00	0.00	0.00
Cl	0.00	0.00	0.00	0.00	0.00	0.00	0.01
Na_2O	0.20	0.17	0.13	0.09	0.02	0.00	0.01
K_2O	10.41	10.59	9.53	9.46	0.00	0.00	0.40
MgO	3.29	2.74	10.61	10.64	7.34	7.90	1.07
CaO	0.00	0.02	0.00	0.00	6.69	6.53	21.96
MnO	0.02	0.00	0.17	0.16	1.00	0.72	0.17
FeO	2.68	2.69	17.21	17.38	24.62	24.22	9.63
Al_2O_3	26.73	28.14	18.52	18.64	21.84	22.32	24.53
Cr_2O_3	0.07	0.07	0.04	0.05	0.01	0.04	0.04
SiO_2	50.25	48.80	35.81	35.74	38.22	38.49	38.45
TiO_2	0.30	0.38	2.64	2.70	0.04	0.02	0.18
Total	94.07	93.68	94.81	94.92	99.85	100.29	96.45
F	0.04	0.03	0.05	0.01	0.00	0.00	0.00
Cl	0.00	0.00	0.00	0.00	0.00	0.00	0.00
Na	0.05	0.04	0.04	0.03	0.00	0.00	0.00
K	1.80	1.84	1.85	1.83	0.00	0.00	0.04
Mg	0.67	0.56	2.40	2.40	0.85	0.90	0.13
Ca	0.00	0.01	0.00	0.00	0.56	0.54	1.91
Mn	0.00	0.00	0.02	0.02	0.07	0.05	0.01
Fe	0.30	0.31	2.19	2.21	1.60	1.56	0.65
Al	4.27	4.53	3.32	3.33	2.00	2.02	2.34
Cr	0.01	0.01	0.01	0.01	0.00	0.00	0.00
Si	6.82	6.66	5.44	5.42	2.96	2.96	3.12
Ti	0.03	0.04	0.30	0.31	0.00	0.00	0.01
Total	14.00	14.03	15.61	15.55	8.04	8.03	8.22

Electron Microprobe Analysis
B.6: NF105 Krokkenakken Biotite-Epidote Gneiss with Relict White Mica
61°54'53.73" N
005°20'16.49" E

Mineral	White Mica		Biotite		Plagioclase	Alkali	Epidote
Position	Core	Rim	Core	Rim	Feldspar	Feldspar	
F	0.07	0.09	0.25	0.08	0.02	0.02	0.00
Cl	0.01	0.00	0.02	0.01	0.00	0.01	0.02
Na_2O	0.22	0.22	0.06	0.05	9.08	0.95	0.01
K_2O	10.79	10.82	9.63	9.56	0.17	15.21	0.00
MgO	2.17	2.16	8.85	8.72	0.01	0.00	0.08
CaO	0.00	0.00	0.00	0.00	4.53	0.02	23.27
MnO	0.02	0.03	0.54	0.56	0.00	0.00	0.29
FeO	4.56	4.55	20.98	20.83	0.10	0.03	10.07
Al_2O_3	26.70	27.16	15.88	16.59	23.40	18.39	24.37
Cr_2O_3	0.00	0.03	0.00	0.00	0.00	0.00	0.00
SiO_2	48.05	47.80	34.65	34.12	62.74	63.41	37.87
TiO_2	0.87	0.86	2.94	2.86	0.02	0.00	0.11
Total	93.46	93.72	93.80	93.41	100.07	98.04	96.07
F	0.03	0.04	0.13	0.04	0.00	0.00	0.00
Cl	0.00	0.00	0.01	0.01	0.00	0.00	0.00
Na	0.06	0.06	0.02	0.02	0.78	0.09	0.00
K	1.91	1.91	1.95	1.94	0.01	0.91	0.00
Mg	0.45	0.45	2.09	2.06	0.00	0.00	0.01
Ca	0.00	0.00	0.00	0.00	0.21	0.00	2.04
Mn	0.00	0.01	0.07	0.08	0.00	0.00	0.02
Fe	0.53	0.53	2.78	2.76	0.00	0.00	0.69
Al	4.36	4.43	2.96	3.10	1.22	1.02	2.35
Cr	0.00	0.01	0.00	0.00	0.00	0.00	0.00
Si	6.66	6.62	5.49	5.41	2.78	2.98	3.10
Ti	0.09	0.09	0.35	0.34	0.00	0.00	0.01
Total	14.10	14.12	15.85	15.74	5.01	5.01	8.22

Electron Microprobe Analysis
B.7: NF106 Krokkenakken Garnet-bearing Gneiss without HP Relicts
61°54'53.73" N
005°20'16.49" E

Mineral	White Mica		Biotite		Garnet		Plagioclase
Position	Core	Rim	Core	Rim	Core	Rim	Feldspar
F	0.00	0.00	0.14	0.21	0.00	0.00	0.00
Cl	0.01	0.00	0.01	0.02	0.01	0.01	0.01
Na_2O	0.32	0.46	0.08	0.09	0.03	0.03	9.12
K_2O	10.29	10.32	8.84	9.34	0.00	0.00	0.19
MgO	2.62	1.06	11.32	11.47	3.64	4.01	0.00
CaO	0.00	0.01	0.06	0.01	9.76	11.02	4.27
MnO	0.01	0.00	0.16	0.17	0.25	0.53	0.00
FeO	2.95	2.85	18.38	17.95	27.13	24.88	0.03
Al_2O_3	28.19	32.96	16.70	16.41	20.90	21.24	23.11
Cr_2O_3	0.03	0.00	0.02	0.01	0.00	0.01	0.00
SiO_2	47.75	43.72	36.26	36.78	38.58	38.35	63.36
TiO_2	0.40	0.59	2.93	3.28	0.18	0.05	0.00
Total	92.58	91.97	94.90	95.74	100.48	100.11	100.09
F	0.00	0.00	0.07	0.10	0.00	0.00	0.00
Cl	0.00	0.00	0.01	0.01	0.00	0.00	0.00
Na	0.09	0.13	0.02	0.03	0.01	0.00	0.78
K	1.82	1.84	1.72	1.80	0.00	0.00	0.01
Mg	0.54	0.22	2.57	2.59	0.43	0.47	0.00
Ca	0.00	0.00	0.01	0.00	0.82	0.92	0.20
Mn	0.00	0.00	0.02	0.02	0.02	0.04	0.00
Fe	0.34	0.33	2.34	2.27	1.78	1.63	0.00
Al	4.59	5.42	3.00	2.93	1.93	1.96	1.20
Cr	0.01	0.00	0.00	0.00	0.00	0.00	0.00
Si	6.60	6.11	5.52	5.56	3.02	3.00	2.80
Ti	0.04	0.06	0.34	0.37	0.01	0.00	0.00
Total	14.02	14.11	15.61	15.68	8.01	8.02	5.00

Electron Microprobe Analysis
B.8: NF45 Flatraket Harbour Kyanite Eclogite
61°58'41.50" N
005°14'43.20" E

Mineral	White Mica		Garnet		Omphacite		Amphibole	Kyanite
Position	Core	Rim	Core	Rim	Core	Rim		
F	0.04	0.06	0.00	0.00	0.00	0.06	0.00	0.00
Cl	0.01	0.01	0.00	0.00	0.01	0.00	0.00	0.00
Na_2O	0.56	0.58	0.00	0.02	6.35	6.25	4.48	0.01
K_2O	10.64	10.56	0.00	0.00	0.00	0.00	0.06	0.01
MgO	3.82	4.02	13.32	11.60	9.39	9.42	10.21	0.00
CaO	0.02	0.03	6.66	7.74	14.34	14.40	9.09	0.02
MnO	0.00	0.01	0.19	0.32	0.02	0.01	0.21	0.00
FeO	1.32	1.43	17.02	17.89	2.60	2.76	12.48	0.34
Al_2O_3	28.12	27.88	22.82	22.91	11.20	11.30	21.13	62.71
Cr_2O_3	0.09	0.09	0.06	0.01	0.14	0.06	0.06	0.07
SiO_2	50.48	50.39	39.08	38.96	55.34	55.16	38.94	35.91
TiO_2	0.42	0.46	0.05	0.05	0.12	0.11	0.01	0.02
Total	95.51	95.52	99.22	99.53	99.51	99.53	96.66	99.09
F	0.02	0.03	0.00	0.00	0.00	0.01	0.00	0.00
Cl	0.00	0.00	0.00	0.00	0.00	0.00	0.00	0.00
Na	0.14	0.15	0.00	0.00	0.44	0.43	1.29	0.00
K	1.80	1.79	0.00	0.00	0.00	0.00	0.01	0.00
Mg	0.76	0.80	1.49	1.30	0.50	0.50	2.25	0.00
Ca	0.00	0.00	0.53	0.62	0.55	0.55	1.44	0.00
Mn	0.00	0.00	0.01	0.02	0.00	0.00	0.02	0.00
Fe	0.15	0.16	1.07	1.13	0.08	0.08	1.55	0.01
Al	4.40	4.37	2.02	2.03	0.47	0.48	3.69	2.02
Cr	0.01	0.01	0.00	0.00	0.00	0.00	0.01	0.00
Si	6.71	6.70	2.93	2.93	1.97	1.97	5.77	0.98
Ti	0.04	0.05	0.00	0.00	0.00	0.00	0.00	0.00
Total	14.04	14.06	8.06	8.05	4.01	4.02	16.03	3.01

Electron Microprobe Analysis
B.9: NF46 Flatraket Harbour Amphibolite
61°58'41.50" N
005°14'43.20" E

Mineral	Biotite		Plagioclase	Amphibole	Epidote
Position	Core	Rim	Feldspar		
F	0.00	0.00	0.00	0.04	0.00
Cl	0.06	0.03	0.00	0.03	0.00
Na_2O	0.37	0.25	8.43	1.94	0.00
K_2O	8.69	8.86	0.05	0.70	0.00
MgO	13.75	13.76	0.02	11.02	0.09
CaO	0.07	0.13	5.92	11.30	23.35
MnO	0.07	0.12	0.00	0.29	0.15
FeO	15.59	15.58	0.25	14.62	9.17
Al_2O_3	16.73	16.59	24.47	14.02	25.28
Cr_2O_3	0.01	0.02	0.01	0.03	0.03
SiO_2	35.06	34.89	61.15	41.90	38.25
TiO_2	2.00	1.85	0.00	0.41	0.00
Total	92.42	92.12	100.29	96.32	96.33
F	0.00	0.00	0.00	0.02	0.00
Cl	0.02	0.01	0.00	0.01	0.00
Na	0.11	0.08	0.72	0.56	0.00
K	1.72	1.75	0.00	0.14	0.00
Mg	3.17	3.18	0.00	2.48	0.01
Ca	0.01	0.02	0.28	1.83	2.03
Mn	0.01	0.02	0.00	0.03	0.01
Fe	2.02	2.02	0.01	1.85	0.62
Al	3.05	3.04	1.28	2.49	2.42
Cr	0.00	0.00	0.00	0.01	0.00
Si	5.42	5.42	2.71	6.32	3.10
Ti	0.23	0.21	0.00	0.05	0.00
Total	15.76	15.77	5.01	15.78	8.19

Electron Microprobe Analysis
B.10: NF47 Flatraket Harbour Garnet-bearing Gneiss without White Mica or HP Relicts
61°58'41.50" N
005°14'43.20" E

Mineral	Biotite		Garnet		Plagioclase	Epidote
Position	Core	Rim	Core	Rim	Feldspar	
F	0.06	0.17	0.00	0.00	0.03	0.05
Cl	0.07	0.07	0.01	0.00	0.00	0.01
Na_2O	0.15	0.19	0.01	0.00	7.94	0.00
K_2O	9.06	9.13	0.00	0.00	0.14	0.00
MgO	11.84	11.85	7.31	7.14	0.00	0.14
CaO	0.07	0.08	8.00	7.35	6.81	23.33
MnO	0.26	0.21	0.58	0.66	0.00	0.10
FeO	18.51	18.54	23.58	24.57	0.13	8.08
Al_2O_3	16.04	16.04	21.69	21.91	25.48	26.49
Cr_2O_3	0.04	0.03	0.00	0.01	0.00	0.06
SiO_2	36.71	36.73	39.40	39.22	59.74	38.62
TiO_2	2.80	2.62	0.02	0.01	0.00	0.19
Total	95.63	95.77	100.63	100.87	100.26	97.08
F	0.03	0.08	0.00	0.00	0.00	0.01
Cl	0.02	0.02	0.00	0.00	0.00	0.00
Na	0.04	0.06	0.00	0.00	0.69	0.00
K	1.75	1.77	0.00	0.00	0.01	0.00
Mg	2.67	2.68	0.83	0.81	0.00	0.02
Ca	0.01	0.01	0.65	0.60	0.32	2.00
Mn	0.03	0.03	0.04	0.04	0.00	0.01
Fe	2.34	2.35	1.51	1.57	0.00	0.54
Al	2.87	2.87	1.96	1.97	1.34	2.50
Cr	0.01	0.01	0.00	0.00	0.00	0.00
Si	5.56	5.57	3.02	3.00	2.66	3.09
Ti	0.32	0.30	0.00	0.00	0.00	0.01
Total	15.66	15.76	8.34	8.34	5.02	8.18

Electron Microprobe Analysis
B.11: NF48 Flatraket Harbour Garnet-bearing Gneiss without HP Relicts
61°58'41.50" N
005°14'43.20" E

Mineral	White Mica		Biotite		Garnet		Plagioclase
Position	Core	Rim	Core	Rim	Core	Rim	Feldspar
F	0.07	0.15	0.13	0.13	0.00	0.00	0.02
Cl	0.00	0.00	0.04	0.03	0.00	0.00	0.00
Na_2O	0.53	0.63	0.14	0.10	0.00	0.00	9.25
K_2O	9.90	9.89	9.18	9.31	0.00	0.00	0.09
MgO	1.98	1.38	10.62	10.69	7.92	7.43	0.00
CaO	0.00	0.05	0.02	0.02	5.41	5.35	4.34
MnO	0.00	0.00	0.14	0.15	0.65	0.63	0.03
FeO	2.51	2.67	18.22	18.22	25.67	26.16	0.07
Al_2O_3	29.28	31.17	17.73	17.88	21.63	21.54	23.17
Cr_2O_3	0.01	0.02	0.02	0.00	0.02	0.00	0.00
SiO_2	48.86	46.60	35.76	36.07	39.01	39.06	63.27
TiO_2	0.73	0.91	2.43	2.35	0.04	0.01	0.00
Total	93.89	93.48	94.48	94.96	100.38	100.18	100.23
F	0.03	0.07	0.07	0.07	0.00	0.00	0.00
Cl	0.00	0.00	0.01	0.01	0.00	0.00	0.00
Na	0.14	0.17	0.04	0.03	0.00	0.00	0.79
K	1.71	1.73	1.79	1.81	0.00	0.00	0.00
Mg	0.40	0.28	2.43	2.43	0.91	0.86	0.00
Ca	0.00	0.01	0.01	0.00	0.45	0.44	0.21
Mn	0.00	0.00	0.02	0.02	0.04	0.04	0.00
Fe	0.29	0.30	2.34	2.32	1.65	1.69	0.00
Al	4.68	5.03	3.20	3.21	1.96	1.96	1.21
Cr	0.00	0.00	0.00	0.00	0.00	0.00	0.00
Si	6.62	6.38	5.48	5.49	3.00	3.02	2.79
Ti	0.07	0.09	0.28	0.27	0.00	0.00	0.00
Total	13.94	14.05	15.67	15.65	8.02	8.00	5.01

Electron Microprobe Analysis
B.12: NF49 Flatraket Harbour Amphibolite
61°58'41.50" N
005°14'43.20" E

Mineral	Biotite		Garnet		Plagioclase	Amphibole	Epidote
Position	Core	Rim	Core	Rim	Feldspar		
F	0.04	0.10	0.00	0.00	0.00	0.00	0.00
Cl	0.06	0.04	0.00	0.01	0.00	0.04	0.00
Na_2O	0.12	0.14	0.00	0.03	7.60	1.36	0.00
K_2O	9.20	9.20	0.00	0.00	0.04	1.00	0.00
MgO	12.25	12.38	8.02	5.28	0.00	9.39	0.14
CaO	0.00	0.02	6.78	6.49	7.32	10.57	23.55
MnO	0.20	0.19	0.55	2.88	0.02	0.44	0.09
FeO	17.80	17.30	23.83	25.61	0.05	16.58	8.18
Al_2O_3	16.96	16.97	21.63	21.34	25.67	14.74	26.12
Cr_2O_3	0.03	0.04	0.01	0.03	0.03	0.04	0.02
SiO_2	36.67	37.09	39.36	38.33	59.39	41.74	38.38
TiO_2	2.37	2.24	0.01	0.03	0.03	0.41	0.18
Total	95.77	95.73	100.25	100.05	100.15	96.30	96.66
F	0.02	0.05	0.00	0.00	0.00	0.00	0.00
Cl	0.02	0.01	0.00	0.00	0.00	0.01	0.00
Na	0.03	0.04	0.00	0.01	0.66	0.40	0.00
K	1.77	1.76	0.00	0.00	0.00	0.20	0.00
Mg	2.75	2.77	0.92	0.62	0.00	2.12	0.02
Ca	0.00	0.01	0.56	0.55	0.35	1.72	2.03
Mn	0.03	0.02	0.04	0.19	0.00	0.06	0.01
Fe	2.24	2.17	1.53	1.68	0.00	2.10	0.55
Al	3.01	3.00	1.95	1.97	1.35	2.63	2.47
Cr	0.01	0.01	0.00	0.00	0.00	0.01	0.00
Si	5.52	5.57	3.02	3.00	2.65	6.33	3.08
Ti	0.27	0.25	0.00	0.00	0.00	0.05	0.01
Total	15.66	15.66	8.00	8.02	5.01	15.62	8.17

Electron Microprobe Analysis
B.13: NF50 Flatraket Harbour Garnet-bearing Gneiss without white mica or HP Relicts
61°58'41.50" N
005°14'43.20" E

Mineral	Biotite		Garnet		Plagioclase	Epidote
Position	Core	Rim	Core	Rim	Feldspar	
F	0.09	0.18	0.00	0.00	0.00	0.00
Cl	0.05	0.05	0.00	0.00	0.01	0.00
Na_2O	0.16	0.14	0.02	0.01	7.63	0.00
K_2O	9.04	9.05	0.00	0.00	0.07	0.00
MgO	12.71	12.46	8.17	7.14	0.00	0.15
CaO	0.03	0.02	6.84	6.57	7.22	23.48
MnO	0.18	0.23	0.54	0.84	0.00	0.17
FeO	17.10	17.01	23.77	25.36	0.10	8.01
Al_2O_3	16.13	16.51	22.02	21.90	25.78	26.66
Cr_2O_3	0.02	0.06	0.01	0.03	0.00	0.02
SiO_2	36.26	36.20	37.77	37.70	59.70	37.43
TiO_2	2.34	2.24	0.02	0.01	0.00	0.17
Total	94.18	94.17	99.16	99.57	100.51	96.13
F	0.04	0.09	0.00	0.00	0.00	0.00
Cl	0.01	0.01	0.00	0.00	0.00	0.00
Na	0.05	0.04	0.00	0.00	0.66	0.00
K	1.77	1.77	0.00	0.00	0.00	0.00
Mg	2.90	2.84	0.95	0.83	0.00	0.02
Ca	0.01	0.01	0.57	0.55	0.34	2.03
Mn	0.02	0.03	0.04	0.05	0.00	0.01
Fe	2.19	2.18	1.55	1.66	0.00	0.54
Al	2.91	2.98	2.02	2.01	1.35	2.54
Cr	0.00	0.01	0.00	0.00	0.00	0.00
Si	5.54	5.54	2.94	2.94	2.65	3.03
Ti	0.27	0.26	0.00	0.00	0.00	0.01
Total	15.71	15.76	8.06	8.05	5.01	8.19

Electron Microprobe Analysis
B.14: NF51 Flatraket Harbour Biotite-Epidote Gneiss
61°58'41.50" N
005°14'43.20" E

Mineral	Biotite		Plagioclase	Alkali	Amphibole	Epidote
Position	Core	Rim	Feldspar	Feldspar		
F	0.13	0.15	0.04	0.12	0.02	0.16
Cl	0.05	0.04	0.00	0.01	0.04	0.01
Na_2O	0.24	0.24	9.79	8.37	1.51	0.02
K_2O	9.28	9.27	0.41	3.32	1.13	0.00
MgO	11.34	11.33	0.00	0.47	9.56	0.17
CaO	0.06	0.08	3.10	0.26	11.44	22.71
MnO	0.25	0.24	0.01	0.00	0.44	0.07
FeO	19.24	18.94	0.06	0.32	16.56	7.04
Al_2O_3	15.30	15.13	22.10	23.64	13.86	27.16
Cr_2O_3	0.00	0.00	0.00	0.00	0.00	0.02
SiO_2	36.19	36.16	65.00	62.42	41.66	37.14
TiO_2	2.59	2.58	0.01	0.00	0.60	0.15
Total	94.72	94.25	100.53	98.94	96.85	94.64
F	0.06	0.07	0.01	0.02	0.01	0.04
Cl	0.01	0.01	0.00	0.00	0.01	0.00
Na	0.07	0.07	0.83	0.73	0.44	0.00
K	1.83	1.83	0.02	0.19	0.22	0.00
Mg	2.61	2.62	0.00	0.03	2.16	0.02
Ca	0.01	0.01	0.15	0.01	1.86	1.99
Mn	0.03	0.03	0.00	0.00	0.06	0.01
Fe	2.48	2.45	0.00	0.01	2.10	0.48
Al	2.78	2.77	1.14	1.25	2.48	2.62
Cr	0.00	0.00	0.00	0.00	0.00	0.00
Si	5.59	5.60	2.85	2.81	6.32	3.04
Ti	0.30	0.30	0.00	0.00	0.07	0.01
Total	15.79	15.79	5.01	5.05	15.73	8.21

Electron Microprobe Analysis
B.15: NF112 Flatraket Harbour Garnet-bearing Gneiss without white mica or HP Relicts
61°58'41.50" N
005°14'43.20" E

Mineral	White Mica#		Biotite		Garnet		Plagioclase
Position	Core	Rim	Core	Rim	Core	Rim	Feldspar
F	0.10	0.05	0.07	0.06	0.00	0.00	0.00
Cl	0.01	0.00	0.06	0.05	0.01	0.01	0.01
Na_2O	0.31	0.42	0.14	0.12	0.05	0.03	8.73
K_2O	9.88	10.29	9.34	9.39	0.00	0.00	0.19
MgO	3.15	1.93	12.54	12.44	7.21	3.74	0.00
CaO	0.02	0.01	0.03	0.04	6.95	7.01	5.27
MnO	0.04	0.02	0.21	0.20	0.66	5.14	0.00
FeO	2.37	2.48	16.27	15.83	25.01	24.69	0.05
Al_2O_3	26.15	30.89	17.31	16.74	21.21	21.16	23.84
Cr_2O_3	0.03	0.01	0.00	0.03	0.02	0.02	0.00
SiO_2	50.54	47.52	36.71	36.57	39.03	38.53	62.50
TiO_2	0.40	0.56	2.47	2.53	0.06	0.00	0.00
Total	93.01	94.17	95.15	94.00	100.22	100.32	100.60
F	0.04	0.02	0.03	0.03	0.00	0.00	0.00
Cl	0.00	0.00	0.02	0.01	0.00	0.00	0.00
Na	0.08	0.11	0.04	0.03	0.01	0.00	0.75
K	1.72	1.78	1.79	1.83	0.00	0.00	0.01
Mg	0.64	0.39	2.82	2.82	0.83	0.44	0.00
Ca	0.01	0.00	0.01	0.01	0.58	0.59	0.25
Mn	0.01	0.00	0.03	0.03	0.04	0.34	0.00
Fe	0.27	0.28	2.05	2.01	1.61	1.62	0.00
Al	4.21	4.93	3.07	3.00	1.93	1.96	1.24
Cr	0.00	0.00	0.00	0.01	0.00	0.00	0.00
Si	6.90	6.44	5.52	5.57	3.02	3.03	2.76
Ti	0.04	0.06	0.28	0.29	0.00	0.00	0.00
Total	13.92	14.01	15.65	15.64	8.02	7.99	5.00

Electron Microprobe Analysis
B.16: NF87 Drage Garnet-bearing Gneiss without white mica and HP Relicts
62°06'08.3" N
005°12'48.0" E

Mineral	White Mica#		Biotite		Garnet		Plagioclase
Position	Core	Rim	Core	Rim	Core	Rim	Feldspar
F	0.18	0.06	0.04	0.07	0.05	0.00	0.01
Cl	0.01	0.00	0.03	0.03	0.00	0.00	0.00
Na_2O	0.49	0.54	0.14	0.10	0.01	0.02	6.51
K_2O	10.19	10.20	9.13	9.46	0.00	0.00	0.11
MgO	1.81	1.45	11.86	11.81	6.09	5.98	0.01
CaO	0.00	0.00	0.09	0.07	7.36	7.49	9.38
MnO	0.02	0.00	0.15	0.15	0.68	0.83	0.00
FeO	1.84	1.67	16.23	16.18	26.18	26.17	0.10
Al_2O_3	30.09	31.60	17.79	18.26	21.01	21.00	27.54
Cr_2O_3	0.00	0.00	0.05	0.04	0.01	0.00	0.00
SiO_2	48.12	47.12	37.07	37.06	38.76	38.64	57.03
TiO_2	0.96	1.11	1.98	1.62	0.10	0.06	0.02
Total	93.70	93.76	94.57	94.85	100.26	100.19	100.71
F	0.08	0.03	0.02	0.03	0.01	0.00	0.00
Cl	0.00	0.00	0.01	0.01	0.00	0.00	0.00
Na	0.13	0.14	0.04	0.03	0.00	0.00	0.56
K	1.77	1.77	1.75	1.82	0.00	0.00	0.01
Mg	0.37	0.29	2.67	2.65	0.71	0.69	0.00
Ca	0.00	0.00	0.02	0.01	0.61	0.62	0.45
Mn	0.00	0.00	0.02	0.02	0.05	0.05	0.00
Fe	0.21	0.19	2.05	2.04	1.70	1.70	0.00
Al	4.82	5.05	3.16	3.24	1.93	1.93	1.45
Cr	0.00	0.00	0.01	0.01	0.00	0.00	0.00
Si	6.55	6.39	5.59	5.58	3.02	3.01	2.54
Ti	0.10	0.12	0.23	0.18	0.01	0.00	0.00
Total	14.01	13.97	15.54	15.60	8.03	8.02	5.02

n.b. small white mica are relict grains preserved within quartz ribbons

Electron Microprobe Analysis
B.17: NF88 Drage Garnet-bearing Gneiss without HP Relicts
62°06'08.3" N
005°12'48.0" E

Mineral	White Mica		Biotite		Garnet		Plagioclase
Position	Core	Rim	Core	Rim	Core	Rim	Feldspar
F	0.10	0.00	0.09	0.12	0.00	0.00	0.00
Cl	0.01	0.00	0.03	0.03	0.01	0.01	0.00
Na_2O	0.46	0.54	0.11	0.10	0.03	0.01	8.33
K_2O	10.33	10.45	9.44	9.39	0.00	0.00	0.13
MgO	1.64	1.03	9.36	9.37	4.11	2.71	0.01
CaO	0.01	0.01	0.01	0.05	9.93	10.73	6.19
MnO	0.02	0.01	0.16	0.20	0.79	2.60	0.00
FeO	2.22	1.99	20.20	19.81	26.16	25.62	0.01
Al_2O_3	30.65	32.55	17.84	18.35	20.89	20.29	24.25
Cr_2O_3	0.00	0.00	0.02	0.01	0.00	0.00	0.01
SiO_2	47.12	45.88	35.98	35.80	38.18	37.87	61.35
TiO_2	1.20	1.12	2.64	2.50	0.05	0.04	0.00
Total	93.76	93.58	95.87	95.74	100.13	99.90	100.29
F	0.04	0.00	0.04	0.06	0.00	0.00	0.00
Cl	0.00	0.00	0.01	0.01	0.00	0.00	0.00
Na	0.12	0.14	0.03	0.03	0.00	0.00	0.72
K	1.79	1.82	1.83	1.83	0.00	0.00	0.01
Mg	0.34	0.21	2.12	2.13	0.48	0.32	0.00
Ca	0.00	0.00	0.00	0.01	0.84	0.92	0.29
Mn	0.00	0.00	0.02	0.03	0.05	0.18	0.00
Fe	0.25	0.23	2.57	2.52	1.72	1.70	0.00
Al	4.92	5.23	3.20	3.29	1.94	1.90	1.27
Cr	0.00	0.00	0.01	0.00	0.00	0.00	0.00
Si	6.42	6.25	5.48	5.45	3.00	3.01	2.72
Ti	0.12	0.12	0.30	0.29	0.00	0.00	0.00
Total	14.02	14.00	15.63	15.64	8.03	8.04	5.01

Electron Microprobe Analysis
B.18: NF89 Drage Garnet-bearing Gneiss without HP Relicts
62°06'08.3" N
005°12'48.0" E

Mineral	White Mica		Biotite		Garnet		Plagioclase	Epidote
Position	Core	Rim	Core	Rim	Core	Rim	Feldspar	
F	0.05	0.10	0.00	0.18	0.00	0.00	0.00	0.00
Cl	0.00	0.00	0.05	0.05	0.01	0.00	0.00	0.08
Na_2O	0.35	0.37	0.13	0.10	0.00	0.03	8.11	0.16
K_2O	10.54	10.81	9.59	9.60	0.00	0.00	0.20	0.01
MgO	1.38	1.05	9.25	9.27	7.20	7.67	0.00	0.39
CaO	0.01	0.00	0.00	0.02	4.73	4.79	6.55	18.92
MnO	0.02	0.03	0.36	0.39	0.85	0.72	0.00	0.16
FeO	2.71	2.70	19.52	19.27	27.68	26.97	0.07	8.91
Al_2O_3	30.61	32.00	17.82	17.91	21.29	21.43	24.85	21.82
Cr_2O_3	0.01	0.02	0.04	0.04	0.00	0.01	0.00	0.03
SiO_2	47.09	46.16	35.83	36.05	38.60	38.42	60.75	35.33
TiO_2	1.13	0.74	3.02	2.87	0.08	0.03	0.00	0.18
Total	93.93	93.98	95.60	95.75	100.42	100.08	100.53	85.97
F	0.02	0.04	0.00	0.09	0.00	0.00	0.00	0.00
Cl	0.00	0.00	0.01	0.01	0.00	0.00	0.00	0.01
Na	0.09	0.10	0.04	0.03	0.00	0.00	0.70	0.03
K	1.83	1.89	1.86	1.87	0.00	0.00	0.01	0.00
Mg	0.28	0.21	2.10	2.11	0.83	0.89	0.00	0.05
Ca	0.00	0.00	0.00	0.01	0.39	0.40	0.31	1.83
Mn	0.01	0.01	0.04	0.05	0.06	0.05	0.00	0.01
Fe	0.31	0.31	2.49	2.46	1.80	1.75	0.00	0.68
Al	4.92	5.15	3.20	3.22	1.95	1.96	1.30	2.33
Cr	0.00	0.00	0.01	0.01	0.00	0.00	0.00	0.00
Si	6.42	6.31	5.46	5.49	3.00	2.98	2.69	3.20
Ti	0.12	0.08	0.35	0.33	0.00	0.00	0.00	0.01
Total	14.00	14.09	15.56	15.66	8.03	8.04	5.01	8.16

Electron Microprobe Analysis
B.19: NF90 Drage Biotite-Epidote Gneiss
62°06'08.3" N
005°12'48.0" E

Mineral	Biotite		Plagioclase	Alkali	Epidote
Position	Core	Rim	Feldspar	Feldspar	
F	0.15	0.17	0.00	0.00	0.12
Cl	0.05	0.04	0.00	0.01	0.00
Na_2O	0.06	0.04	7.99	1.83	0.00
K_2O	9.60	8.01	0.21	14.24	0.00
MgO	7.67	6.63	0.00	0.00	0.09
CaO	0.00	2.29	6.57	0.02	23.48
MnO	0.31	0.29	0.00	0.01	0.29
FeO	22.34	20.44	0.10	0.03	9.72
Al_2O_3	16.43	16.22	24.66	18.46	24.65
Cr_2O_3	0.00	0.01	0.01	0.00	0.02
SiO_2	36.02	38.19	60.61	64.46	38.15
TiO_2	2.78	2.37	0.01	0.03	0.17
Total	95.39	94.70	100.15	99.08	96.69
F	0.07	0.08	0.00	0.00	0.03
Cl	0.01	0.01	0.00	0.00	0.00
Na	0.02	0.01	0.69	0.16	0.00
K	1.90	1.57	0.01	0.84	0.00
Mg	1.78	1.52	0.00	0.00	0.01
Ca	0.00	0.37	0.31	0.00	2.05
Mn	0.04	0.04	0.00	0.00	0.02
Fe	2.90	2.63	0.00	0.00	0.66
Al	3.01	2.94	1.29	1.01	2.36
Cr	0.00	0.00	0.00	0.00	0.00
Si	5.60	5.87	2.70	2.99	3.10
Ti	0.32	0.28	0.00	0.00	0.01
Total	15.66	15.32	5.01	5.01	8.25

Electron Microprobe Analysis
B.20: NF91 Drage Biotite-Epidote Gneiss
62°06'08.3" N
005°12'48.0" E

Mineral	Biotite		Plagioclase	Alkali	Epidote
Position	Core	Rim	Feldspar	Feldspar	
F	0.32	0.32	0.00	0.00	0.00
Cl	0.07	0.07	0.01	0.01	0.01
Na_2O	0.07	0.06	9.17	0.55	0.00
K_2O	9.60	9.57	0.14	15.96	0.00
MgO	7.96	8.05	0.01	0.00	0.12
CaO	0.04	0.03	4.56	0.02	21.69
MnO	0.44	0.43	0.03	0.00	0.28
FeO	22.22	22.50	0.07	0.02	9.21
Al_2O_3	15.54	15.42	23.39	18.42	23.83
Cr_2O_3	0.01	0.00	0.02	0.00	0.03
SiO_2	36.12	35.89	62.78	64.08	36.31
TiO_2	2.61	2.37	0.04	0.01	0.08
Total	95.00	94.72	100.22	99.07	91.56
F	0.16	0.16	0.00	0.00	0.00
Cl	0.02	0.02	0.00	0.00	0.00
Na	0.02	0.02	0.79	0.05	0.00
K	1.93	1.93	0.01	0.95	0.00
Mg	1.86	1.89	0.00	0.00	0.02
Ca	0.01	0.01	0.22	0.00	1.99
Mn	0.06	0.06	0.00	0.00	0.02
Fe	2.92	2.97	0.00	0.00	0.66
Al	2.88	2.87	1.22	1.01	2.40
Cr	0.00	0.00	0.00	0.00	0.00
Si	5.67	5.67	2.78	2.99	3.10
Ti	0.31	0.28	0.00	0.00	0.01
Total	15.82	15.86	5.01	5.00	8.19

Electron Microprobe Analysis
B.21: NF96 Drage Garnet-bearing Gneiss without HP Relicts
62°06'08.3" N
005°12'48.0" E

Mineral	White Mica		Biotite		Garnet		Plagioclase
Position	Core	Rim	Core	Rim	Core	Rim	Feldspar
F	0.12	0.00	0.24	0.11	0.00	0.00	0.05
Cl	0.01	0.01	0.06	0.05	0.00	0.00	0.00
Na_2O	0.52	0.53	0.07	0.06	0.04	0.01	9.32
K_2O	10.53	10.51	9.59	8.57	0.00	0.00	0.10
MgO	1.78	0.85	10.41	11.00	5.01	4.78	0.00
CaO	0.01	0.01	0.00	0.02	7.97	6.92	4.12
MnO	0.04	0.00	0.22	0.22	0.62	1.91	0.00
FeO	2.84	2.50	18.95	19.07	27.11	27.42	0.06
Al_2O_3	30.00	32.69	17.85	17.81	21.46	21.96	23.10
Cr_2O_3	0.04	0.03	0.04	0.03	0.04	0.00	0.00
SiO_2	47.98	45.57	36.09	34.73	38.09	37.21	63.89
TiO_2	1.19	0.90	2.74	2.57	0.08	0.03	0.02
Total	95.06	93.61	96.25	94.24	100.43	100.25	100.66
F	0.05	0.00	0.12	0.06	0.00	0.00	0.01
Cl	0.00	0.00	0.02	0.01	0.00	0.00	0.00
Na	0.14	0.14	0.02	0.02	0.01	0.00	0.79
K	1.82	1.83	1.85	1.69	0.00	0.00	0.01
Mg	0.36	0.18	2.35	2.53	0.59	0.56	0.00
Ca	0.00	0.00	0.00	0.00	0.67	0.59	0.19
Mn	0.01	0.00	0.03	0.03	0.04	0.13	0.00
Fe	0.32	0.29	2.40	2.46	1.77	1.81	0.00
Al	4.77	5.27	3.18	3.23	1.98	2.04	1.20
Cr	0.01	0.01	0.01	0.01	0.00	0.00	0.00
Si	6.48	6.23	5.47	5.35	2.98	2.93	2.81
Ti	0.12	0.09	0.31	0.30	0.01	0.00	0.00
Total	14.06	14.03	15.75	15.68	8.03	8.05	5.01

Electron Microprobe Analysis
B.22: NF98 Drage Biotite-Epidote Gneiss with Relict White Mica and Garnet
62°06'08.3" N
005°12'48.0" E

Mineral	White Mica		Biotite		Garnet		Plagioclase	Alkali	Epidote
Position	Core	Rim	Core	Rim	Core	Rim	Feldspar	Feldspar	
F	0.04	0.10	0.06	0.21	0.00	0.00	0.05	0.00	0.00
Cl	0.01	0.00	0.02	0.02	0.01	0.00	0.01	0.00	0.00
Na_2O	0.22	0.25	0.10	0.07	0.03	0.03	7.58	0.81	0.00
K_2O	10.81	10.78	9.68	9.67	0.00	0.00	0.20	15.55	0.00
MgO	1.90	1.33	10.31	10.64	2.76	2.79	0.01	0.00	0.10
CaO	0.00	0.01	0.02	0.02	12.56	12.44	7.13	0.03	23.42
MnO	0.02	0.00	0.23	0.25	0.66	0.61	0.02	0.00	0.12
FeO	4.34	4.23	18.89	18.84	24.85	24.94	0.07	0.13	9.02
Al_2O_3	28.12	30.13	17.72	17.44	20.97	21.00	25.87	18.72	26.11
Cr_2O_3	0.02	0.00	0.02	0.05	0.00	0.02	0.00	0.00	0.00
SiO_2	47.63	46.04	35.90	36.16	38.23	38.46	59.09	64.03	37.00
TiO_2	1.23	0.94	2.29	2.27	0.01	0.05	0.00	0.00	0.19
Total	94.34	93.80	95.22	95.64	100.08	100.34	100.03	99.27	95.95
F	0.02	0.04	0.03	0.10	0.00	0.00	0.01	0.00	0.00
Cl	0.00	0.00	0.01	0.01	0.00	0.00	0.00	0.00	0.00
Na	0.06	0.07	0.03	0.02	0.01	0.01	0.66	0.07	0.00
K	1.89	1.90	1.89	1.88	0.00	0.00	0.01	0.92	0.00
Mg	0.39	0.28	2.34	2.42	0.32	0.33	0.00	0.00	0.01
Ca	0.00	0.00	0.01	0.01	1.06	1.04	0.34	0.00	2.05
Mn	0.00	0.00	0.03	0.03	0.05	0.04	0.00	0.00	0.01
Fe	0.50	0.49	2.41	2.40	1.64	1.64	0.00	0.00	0.62
Al	4.55	4.91	3.18	3.14	1.94	1.94	1.36	1.03	2.51
Cr	0.00	0.00	0.00	0.01	0.00	0.00	0.00	0.00	0.00
Si	6.53	6.36	5.48	5.51	3.01	3.02	2.64	2.98	3.02
Ti	0.13	0.10	0.26	0.26	0.00	0.00	0.00	0.00	0.01
Total	14.07	14.14	15.67	15.77	8.02	8.01	5.02	5.01	8.22

Electron Microprobe Analysis
B.23: NF99 Drage Garnet-bearing Gneiss without HP Relicts#
62°06'08.3" N
005°12'48.0" E

Mineral	White Mica		Biotite		Garnet		Plagioclase
Position	Core	Rim	Core	Rim	Core	Rim	Feldspar
F	0.11	0.00	0.12	0.08	0.00	0.00	0.10
Cl	0.00	0.01	0.04	0.08	0.00	0.01	0.01
Na_2O	0.36	0.52	0.11	0.09	0.02	0.03	8.71
K_2O	10.22	10.41	9.54	8.96	0.00	0.00	0.14
MgO	2.32	0.97	9.96	9.76	4.20	4.33	0.00
CaO	0.02	0.03	0.02	0.05	7.74	7.87	5.23
MnO	0.01	0.02	0.18	0.20	0.60	0.59	0.01
FeO	2.68	2.71	19.45	20.42	28.32	27.73	0.04
Al_2O_3	28.40	32.56	17.90	17.96	21.33	21.64	23.98
Cr_2O_3	0.01	0.00	0.00	0.03	0.03	0.00	0.00
SiO_2	49.65	45.31	35.96	35.12	37.90	38.02	62.00
TiO_2	0.86	0.42	2.34	2.51	0.01	0.04	0.02
Total	94.64	92.96	95.60	95.26	100.15	100.26	100.23
F	0.04	0.00	0.06	0.04	0.00	0.00	0.01
Cl	0.00	0.00	0.01	0.02	0.00	0.00	0.00
Na	0.09	0.14	0.03	0.03	0.00	0.00	0.75
K	1.75	1.83	1.85	1.75	0.00	0.00	0.01
Mg	0.47	0.20	2.26	2.23	0.49	0.51	0.00
Ca	0.00	0.01	0.01	0.01	0.65	0.66	0.25
Mn	0.00	0.00	0.02	0.03	0.04	0.04	0.00
Fe	0.30	0.31	2.48	2.62	1.87	1.82	0.00
Al	4.51	5.29	3.22	3.25	1.98	2.00	1.25
Cr	0.00	0.00	0.00	0.01	0.00	0.00	0.00
Si	6.69	6.24	5.48	5.40	2.99	2.98	2.75
Ti	0.09	0.04	0.27	0.29	0.00	0.00	0.00
Total	13.96	14.06	15.69	15.67	8.03	8.02	5.02

Electron Microprobe Analysis
B.24: NF100 Drage Kyanite Eclogite
62°06'08.3" N
005°12'48.0" E

Mineral	White Mica		Garnet		Omphacite		Kyanite
Position	Core	Rim	Core	Rim	Core	Rim	
F	0.02	0.00	0.00	0.00	0.00	0.06	0.00
Cl	0.01	0.01	0.00	0.00	0.00	0.00	0.01
Na_2O	0.40	0.33	0.02	0.01	4.71	4.74	0.00
K_2O	10.56	10.64	0.00	0.00	0.01	0.01	0.01
MgO	4.19	3.31	10.35	10.02	11.09	11.06	0.00
CaO	0.03	0.03	10.44	10.04	17.27	17.34	0.01
MnO	0.00	0.00	0.37	0.39	0.02	0.03	0.00
FeO	1.20	1.21	16.66	17.44	2.68	2.72	0.26
Al_2O_3	26.46	28.29	22.04	22.19	9.27	9.42	63.09
Cr_2O_3	0.07	0.09	0.05	0.02	0.06	0.04	0.11
SiO_2	50.20	47.06	40.01	39.89	54.92	54.53	36.87
TiO_2	0.44	0.67	0.05	0.02	0.11	0.19	0.01
Total	93.59	91.65	100.00	100.02	100.15	100.11	100.35
F	0.01	0.00	0.00	0.00	0.00	0.01	0.00
Cl	0.01	0.00	0.00	0.00	0.00	0.00	0.00
Na	0.10	0.09	0.00	0.00	0.33	0.33	0.00
K	1.83	1.89	0.00	0.00	0.00	0.00	0.00
Mg	0.85	0.69	1.16	1.12	0.59	0.59	0.00
Ca	0.01	0.01	0.84	0.81	0.66	0.66	0.00
Mn	0.00	0.00	0.02	0.02	0.00	0.00	0.00
Fe	0.14	0.14	1.04	1.10	0.08	0.08	0.01
Al	4.23	4.63	1.95	1.97	0.39	0.40	2.00
Cr	0.01	0.01	0.00	0.00	0.00	0.00	0.00
Si	6.80	6.54	3.00	3.00	1.96	1.95	0.99
Ti	0.04	0.07	0.00	0.00	0.00	0.00	0.00
Total	14.02	14.06	8.03	8.02	4.01	4.02	3.01

Appendix C:

Single Grain Fusion Datasets

Nordfjord in the mist

Single grain fusion analysis
C.1: NF35 Krokkenakken Biotite-Epidote Gneiss
61°54'53.73" N
005°20'16.49" E
J value 0.0115 ± 5.75E-05
MAP 215-50
Biotite

Grain	^{40}Ar V	± 1σ	^{39}Ar V	± 1σ	^{38}Ar V	± 1σ	^{37}Ar V	± 1σ	^{36}Ar V	± 1σ	$^{40}Ar^*/^{39}Ar$	± 1σ	Age Ma	± 1σ	Corr?*	Age# Ma
1	1.5890	0.0015	0.0777	0.0002	0.0009	0.0000	-0.0007	0.0002	0.0000	0.0000	20.46	0.11	381	2.47		385
2	11.6561	0.0056	0.4976	0.0003	0.0065	0.0001	0.0265	0.0002	0.0005	0.0000	23.11	0.02	425	1.93		430
3	1.7532	0.0025	0.0852	0.0002	0.0010	0.0000	-0.0005	0.0002	0.0001	0.0000	20.31	0.08	379	2.15		383
4	3.5556	0.0038	0.1727	0.0002	0.0020	0.0001	-0.0005	0.0002	0.0002	0.0000	20.29	0.05	378	1.94		382
5	2.7385	0.0025	0.1313	0.0003	0.0016	0.0000	0.0005	0.0002	0.0002	0.0000	20.37	0.07	380	2.12		384
6	10.4140	0.0720	0.5080	0.0042	0.0057	0.0001	0.0021	0.0002	0.0001	0.0000	20.43	0.22	381	4.09		385
7	2.5587	0.0020	0.1266	0.0002	0.0015	0.0000	0.0005	0.0002	0.0000	0.0000	20.11	0.06	375	1.96		379
8	5.3660	0.0049	0.2650	0.0004	0.0031	0.0001	0.0037	0.0002	0.0000	0.0000	20.19	0.05	377	1.88		381
9	5.9213	0.0049	0.2869	0.0003	0.0033	0.0000	0.0007	0.0002	0.0001	0.0000	20.51	0.04	382	1.83		386
10	4.5762	0.0033	0.2199	0.0003	0.0026	0.0000	-0.0001	0.0002	0.0001	0.0000	20.72	0.05	386	1.91		390
11	7.4688	0.0059	0.3602	0.0006	0.0043	0.0001	0.0007	0.0002	0.0001	0.0000	20.65	0.04	384	1.85		388
12	9.7451	0.0116	0.4813	0.0006	0.0055	0.0001	-0.0003	0.0002	0.0001	0.0000	20.16	0.04	376	1.82		380
Average Blank	0.0082	0.0001	0.0001	0.0000	0.0000	0.0000	0.0001	0.0000	0.0001	0.0000						

* Data corrected for ^{36}Ar where the ^{36}Ar measurement is > 2x the ^{36}Ar background (blank) measurement
# Recalculated ages using the decay constant of Min et al., (2000) and GA1550 biotite standard age of 99.8 of Renne et al., (2010)

Single grain fusion analysis
C.2: NF37 Eclogite
61°54'53.73'' N
005°20'16.49'' E
J value 0.0090 ± 1.81E-05
ARGUS
White Mica

Grain	^{40}Ar V	± 1σ	^{39}Ar V	± 1σ	^{38}Ar V	± 1σ	^{37}Ar V	± 1σ	^{36}Ar V	± 1σ	$^{40}Ar^*/^{39}Ar$	± 1σ	Age Ma	± 1σ	Corr?*	Age# Ma
1	0.5797	0.0003	0.0194	0.0000	0.0001	0.0000	-0.0002	0.0000	-0.0001	0.0000	32.12	0.27	460	3.39		464
2	5.5629	0.0023	0.1943	0.0002	0.0023	0.0000	-0.0001	0.0000	0.0002	0.0000	28.24	0.04	410	0.47		414
3	1.6032	0.0010	0.0535	0.0001	0.0006	0.0000	0.0000	0.0000	0.0001	0.0000	29.39	0.12	425	1.49		429
4	0.9320	0.0006	0.0331	0.0001	0.0003	0.0000	-0.0001	0.0000	0.0000	0.0000	28.47	0.14	413	1.82		417
5	0.8653	0.0004	0.0314	0.0001	0.0004	0.0000	-0.0001	0.0000	-0.0001	0.0000	28.08	0.17	408	2.24		412
6	1.3248	0.0008	0.0463	0.0001	0.0005	0.0000	0.0000	0.0000	0.0000	0.0000	28.84	0.12	418	1.61		422
7	0.7419	0.0003	0.0266	0.0000	0.0002	0.0000	-0.0001	0.0000	-0.0001	0.0000	29.16	0.18	422	2.26		426
8	2.4200	0.0012	0.0826	0.0001	0.0009	0.0000	-0.0001	0.0000	-0.0001	0.0000	29.48	0.07	426	0.86		430
9	2.1838	0.0010	0.0775	0.0001	0.0008	0.0000	-0.0001	0.0000	-0.0001	0.0000	28.36	0.06	412	0.82		416
10	0.5006	0.0009	0.0170	0.0001	0.0002	0.0000	0.0000	0.0000	-0.0001	0.0000	30.88	0.26	444	3.34		449
11	2.2768	0.0011	0.0801	0.0001	0.0009	0.0000	-0.0001	0.0000	0.0000	0.0000	28.50	0.06	413	0.80		418
12	1.5876	0.0008	0.0561	0.0001	0.0006	0.0000	-0.0001	0.0000	0.0000	0.0000	28.17	0.11	409	1.41		413
13	0.9020	0.0004	0.0305	0.0001	0.0003	0.0000	-0.0001	0.0000	-0.0001	0.0000	30.24	0.14	436	1.85		440
14	3.3886	0.0014	0.1170	0.0001	0.0013	0.0000	-0.0001	0.0000	-0.0001	0.0000	29.05	0.05	421	0.64		425
15	0.4831	0.0011	0.0171	0.0001	0.0001	0.0000	-0.0002	0.0000	-0.0002	0.0000	30.71	0.25	442	3.18		446
16	3.2001	0.0014	0.1114	0.0001	0.0012	0.0000	-0.0001	0.0000	-0.0001	0.0000	28.96	0.05	419	0.63		424
17	2.2415	0.0011	0.0790	0.0001	0.0008	0.0000	-0.0001	0.0000	-0.0001	0.0000	28.57	0.08	414	1.10		418
18	2.2220	0.0011	0.0776	0.0001	0.0008	0.0000	-0.0001	0.0000	-0.0001	0.0000	28.92	0.08	419	0.99		423
19	0.7823	0.0002	0.0266	0.0000	0.0002	0.0000	-0.0001	0.0000	-0.0001	0.0000	30.43	0.15	438	1.91		443
20	1.0421	0.0005	0.0355	0.0001	0.0003	0.0000	-0.0001	0.0000	0.0000	0.0000	29.50	0.14	426	1.75		431
Average Blank	0.0046	0.0000	0.0006	0.0000	0.0002	0.0000	0.0003	0.0000	0.0003	0.0000						

* Data corrected for ^{36}Ar where the ^{36}Ar measurement is > 2x the ^{36}Ar background (blank) measurement
# Recalculated ages using the decay constant of Min et al., (2000) and GA1550 biotite standard age of 99.8 of Renne et al., (2010)

Single grain fusion analysis
C.3: NF37 Eclogite
61°54'53.73'' N
005°20'16.49'' E
J value 0.0090 ± 1.83E-05
ARGUS
Amphibole

Grain	^{40}Ar V	± 1σ	^{39}Ar V	± 1σ	^{38}Ar V	± 1σ	^{37}Ar V	± 1σ	^{36}Ar V	± 1σ	$^{40}Ar^*/^{39}Ar$	± 1σ	Age Ma	± 1σ	Corr?*	Age# Ma
1	0.1515	0.0002	0.0048	0.0000	0.0000	0.0000	0.0011	0.0000	-0.0001	0.0000	38.27	0.74	536	8.96		542
2	0.1087	0.0001	0.0034	0.0000	0.0000	0.0000	0.0008	0.0000	-0.0001	0.0000	42.59	1.30	588	15.33		594
3	0.3115	0.0009	0.0103	0.0001	0.0002	0.0000	0.0020	0.0000	0.0000	0.0000	30.03	0.54	433	6.92		438
4	0.2711	0.0010	0.0088	0.0001	0.0001	0.0000	0.0027	0.0000	0.0000	0.0000	31.70	0.64	455	8.12		459
5	0.2439	0.0009	0.0073	0.0001	0.0001	0.0000	0.0015	0.0000	0.0000	0.0000	34.93	0.69	495	8.59		500
6	0.5762	0.0004	0.0196	0.0001	0.0002	0.0000	0.0037	0.0000	0.0000	0.0000	30.14	0.32	435	4.11		439
7	0.6454	0.0006	0.0035	0.0000	0.0000	0.0000	0.0014	0.0000	-0.0001	0.0000	194.06	2.62	1829	15.52		1850
8	0.1482	0.0003	0.0049	0.0000	0.0000	0.0000	0.0010	0.0000	0.0000	0.0000	33.58	1.26	478	15.82		483
9	0.2231	0.0007	0.0037	0.0000	0.0000	0.0000	0.0011	0.0000	0.0000	0.0000	61.89	1.49	802	15.55		810
10	0.5270	0.0005	0.0176	0.0000	0.0001	0.0000	0.0018	0.0000	0.0000	0.0000	30.47	0.26	439	3.32		444
11	0.2992	0.0008	0.0088	0.0001	0.0001	0.0000	0.0026	0.0000	0.0000	0.0000	34.88	0.60	495	7.38		500
12	0.6840	0.0005	0.0137	0.0001	0.0002	0.0000	0.0044	0.0000	0.0000	0.0000	51.00	0.37	684	4.12		691
13	0.8099	0.0004	0.0162	0.0000	0.0001	0.0000	0.0035	0.0000	0.0000	0.0000	51.16	0.30	686	3.32		693
Average Blank	0.0046	0.0000	0.0006	0.0000	0.0002	0.0000	0.0003	0.0000	0.0002	0.0000						

* Data corrected for ^{36}Ar where the ^{36}Ar measurement is > 2x the ^{36}Ar background (blank) measurement
# Recalculated ages using the decay constant of Min et al., (2000) and GA1550 biotite standard age of 99.8 of Renne et al., (2010)

Single grain fusion analysis
C.4: NF40 Krokkenakken Garnetiferous Gneiss with High Pressure Relicts
61°54'53.73'' N
005°20'16.49'' E
J value 0.0118 ± 5.90E-05
MAP 215-50
White Mica

Grain	^{40}Ar V	± 1σ	^{39}Ar V	± 1σ	^{38}Ar V	± 1σ	^{37}Ar V	± 1σ	^{36}Ar V	± 1σ	$^{40}Ar^*/^{39}Ar$	± 1σ	Age Ma	± 1σ	Corr?*	$Age^{\#}$ Ma
1	8.4335	0.0144	0.4097	0.0014	0.0047	0.0002	-0.0002	0.0003	0.0004	0.0000	20.33	0.08	388	2.21		392
2	12.2988	0.0349	0.5972	0.0027	0.0072	0.0003	-0.0003	0.0003	0.0001	0.0000	20.55	0.11	392	2.60		396
3	3.9475	0.0087	0.1949	0.0011	0.0025	0.0001	-0.0002	0.0003	0.0001	0.0000	20.11	0.13	384	2.84		388
4	10.8229	0.0241	0.5320	0.0011	0.0065	0.0002	0.0000	0.0003	0.0003	0.0001	20.16	0.07	385	2.09		389
5	13.1409	0.0132	0.6421	0.0018	0.0073	0.0001	0.0004	0.0003	0.0005	0.0001	20.23	0.07	386	2.08		390
6	5.8054	0.0069	0.2877	0.0019	0.0035	0.0002	0.0003	0.0003	0.0000	0.0000	20.14	0.13	385	2.89		388
7	10.1168	0.0158	0.5013	0.0021	0.0061	0.0002	-0.0006	0.0003	0.0000	0.0000	20.18	0.09	385	2.33		389
8	8.8530	0.0108	0.4244	0.0026	0.0052	0.0002	-0.0001	0.0003	0.0008	0.0000	20.34	0.13	388	2.84		392
Average Blank	0.0017	0.0002	0.0000	0.0000	0.0000	0.0000	0.0005	0.0001	0.0000	0.0000						

* Data corrected for ^{36}Ar where the ^{36}Ar measurement is > 2x the ^{36}Ar background (blank) measurement
# Recalculated ages using the decay constant of Min et al., (2000) and GA1550 biotite standard age of 99.8 of Renne et al., (2010)

Single grain fusion analysis
C.5: NF40 Krokkenakken Garnetiferous Gneiss with High Pressure Relicts
61°54'53.73" N
005°20'16.49" E
J value 0.0115 ± 5.74E-05
MAP 215-50
Biotite

Grain	^{40}Ar V	± 1σ	^{39}Ar V	± 1σ	^{38}Ar V	± 1σ	^{37}Ar V	± 1σ	^{36}Ar V	± 1σ	$^{40}Ar^*/^{39}Ar$	± 1σ	Age Ma	± 1σ	Corr?*	Age# Ma
1	8.0967	0.0130	0.3977	0.0008	0.0045	0.0001	0.0005	0.0003	0.0003	0.0000	20.17	0.05	375	1.91		379
2	2.0102	0.0068	0.0957	0.0004	0.0012	0.0000	0.0003	0.0003	0.0001	0.0000	20.86	0.12	387	2.68		391
3	1.6143	0.0065	0.0781	0.0004	0.0009	0.0000	-0.0004	0.0003	0.0001	0.0000	20.42	0.13	380	2.83		383
4	2.6957	0.0069	0.1325	0.0004	0.0015	0.0000	0.0007	0.0003	0.0000	0.0000	20.25	0.08	377	2.18		381
5	1.0224	0.0065	0.0495	0.0003	0.0006	0.0000	0.0005	0.0003	0.0000	0.0000	20.64	0.20	383	3.84		387
6	0.5902	0.0065	0.0287	0.0003	0.0003	0.0000	0.0005	0.0003	0.0000	0.0000	20.39	0.39	379	6.74		383
7	0.8690	0.0065	0.0424	0.0003	0.0004	0.0001	-0.0001	0.0003	0.0000	0.0000	20.37	0.24	379	4.34		383
8	6.9358	0.0078	0.3398	0.0004	0.0039	0.0000	0.0023	0.0003	0.0001	0.0000	20.36	0.03	379	1.80		383
9	4.2173	0.0019	0.2081	0.0002	0.0023	0.0000	0.0002	0.0004	0.0001	0.0000	20.13	0.04	375	1.81		379
10	4.7724	0.0029	0.2371	0.0005	0.0021	0.0007	0.0007	0.0004	0.0001	0.0000	20.06	0.06	374	1.93		377
11	0.5029	0.0013	0.0245	0.0001	0.0003	0.0000	0.0007	0.0004	0.0000	0.0000	20.24	0.30	377	5.28		381
12	8.2877	0.0064	0.3414	0.0004	0.0041	0.0001	0.0045	0.0004	0.0007	0.0000	23.67	0.04	433	2.03		438
Average Blank	0.0089	0.0001	0.0002	0.0000	0.0000	0.0000	0.0000	0.0000	0.0000	0.0000						

* Data corrected for ^{36}Ar where the ^{36}Ar measurement is > 2x the ^{36}Ar background (blank) measurement
# Recalculated ages using the decay constant of Min et al., (2000) and GA1550 biotite standard age of 99.8 of Renne et al., (2010)

Single grain fusion analysis
C.6: NF42 Krokkenakken Garnetiferous Gneiss with High Pressure Relicts
61°54'53.73" N
005°20'16.49" E
J value 0.0118 ± 5.91E-05
MAP 215-50
White Mica

Grain	^{40}Ar V	± 1σ	^{39}Ar V	± 1σ	^{38}Ar V	± 1σ	^{37}Ar V	± 1σ	^{36}Ar V	± 1σ	$^{40}Ar^*/^{39}Ar$	± 1σ	Age Ma	± 1σ	Corr?*	Age# Ma
1	1.1473	0.0044	0.0541	0.0007	0.0006	0.0001	0.0008	0.0001	0.0000	0.0000	20.94	0.31	399	5.58		403
2	5.2662	0.0191	0.2522	0.0019	0.0030	0.0001	0.0019	0.0001	0.0001	0.0000	20.71	0.18	395	3.52		399
3	3.5884	0.0055	0.1659	0.0008	0.0020	0.0002	0.0005	0.0004	0.0005	0.0000	20.75	0.12	396	2.75		400
4	0.8921	0.0025	0.0423	0.0005	0.0005	0.0000	-0.0001	0.0004	0.0000	0.0000	21.02	0.29	401	5.23		405
5	0.5121	0.0036	0.0237	0.0004	0.0003	0.0000	-0.0001	0.0004	0.0001	0.0000	20.78	0.48	396	8.40		401
6	2.9519	0.0070	0.1423	0.0011	0.0016	0.0001	0.0001	0.0004	0.0000	0.0000	20.65	0.17	394	3.41		398
7	0.7711	0.0033	0.0380	0.0003	0.0004	0.0000	-0.0002	0.0005	0.0000	0.0000	20.01	0.27	383	4.96		387
8	2.3795	0.0053	0.1140	0.0007	0.0013	0.0001	0.0001	0.0005	0.0000	0.0000	20.89	0.14	398	3.01		402
9	0.3546	0.0016	0.0172	0.0003	0.0002	0.0000	0.0000	0.0005	0.0000	0.0000	20.13	0.46	385	8.11		389
10	9.5714	0.0123	0.4600	0.0020	0.0052	0.0002	0.0018	0.0005	0.0003	0.0000	20.64	0.10	394	2.43		398
11	6.9941	0.0095	0.3374	0.0015	0.0041	0.0002	0.0004	0.0005	0.0001	0.0000	20.63	0.10	394	2.44		398
12	6.2020	0.0098	0.2988	0.0013	0.0038	0.0001	0.0002	0.0005	0.0000	0.0000	20.71	0.10	395	2.44		399
Average Blank	0.0014	0.0002	0.0000	0.0000	0.0000	0.0000	0.0004	0.0001	0.0000	0.0000						

* Data corrected for ^{36}Ar where the ^{36}Ar measurement is > 2x the ^{36}Ar background (blank) measurement
# Recalculated ages using the decay constant of Min et al., (2000) and GA1550 biotite standard age of 99.8 of Renne et al., (2010)

Single grain fusion analysis
C.7: NF42 Krokkenakken Garnetiferous Gneiss with High Pressure Relicts
61°54'53.73" N
005°20'16.49" E
J value 0.0114 ± 5.69E-05
MAP 215-50
Biotite

Grain	^{40}Ar V	± 1σ	^{39}Ar V	± 1σ	^{38}Ar V	± 1σ	^{37}Ar V	± 1σ	^{36}Ar V	± 1σ	$^{40}Ar^*/^{39}Ar$	± 1σ	Age Ma	± 1σ	Corr?*	Age# Ma
1	6.1706	0.0138	0.3022	0.0007	0.0035	0.0000	0.0016	0.0009	0.0002	0.0001	20.20	0.09	373	2.30		376
2	4.7322	0.0080	0.2326	0.0004	0.0026	0.0001	0.0033	0.0006	0.0001	0.0000	20.17	0.06	372	1.97		376
3	7.1846	0.0103	0.3569	0.0009	0.0039	0.0001	0.0002	0.0006	0.0001	0.0000	20.06	0.06	370	1.97		374
4	10.7376	0.0133	0.4501	0.0008	0.0058	0.0001	0.0065	0.0006	0.0013	0.0000	23.00	0.05	419	2.04		423
5	7.0855	0.0078	0.3279	0.0005	0.0037	0.0000	0.0114	0.0006	0.0002	0.0000	21.46	0.05	393	1.92		397
6	13.1282	0.0095	0.6197	0.0007	0.0074	0.0001	0.0004	0.0006	0.0019	0.0000	20.30	0.03	374	1.77		378
7	6.4720	0.0122	0.3304	0.0006	0.0039	0.0001	0.4075	0.0006	0.0004	0.0000	19.25	0.06	357	1.87		360
8	4.6351	0.0130	0.2306	0.0008	0.0027	0.0000	0.0012	0.0003	0.0001	0.0000	19.98	0.09	369	2.23		373
9	9.5707	0.0175	0.4598	0.0008	0.0043	0.0012	0.0014	0.0003	0.0007	0.0000	20.36	0.05	375	1.92		379
10	5.3844	0.0133	0.2596	0.0007	0.0028	0.0005	0.0014	0.0003	0.0004	0.0000	20.23	0.08	373	2.13		377
Average Blank	0.0078	0.0001	0.0001	0.0000	0.0000	0.0000	0.0001	0.0000	0.0001	0.0000						

* Data corrected for ^{36}Ar where the ^{36}Ar measurement is > 2x the ^{36}Ar background (blank) measurement
# Recalculated ages using the decay constant of Min et al., (2000) and GA1550 biotite standard age of 99.8 of Renne et al., (2010)

Single grain fusion analysis
C.8: NF43 Krokkenakken Garnetiferous Gneiss with High Pressure Relicts
61°54'53.73" N
005°20'16.49" E
J value 0.0073 ± 3.63E-05
MAP 215-50
White Mica

Grain	^{40}Ar V	± 1σ	^{39}Ar V	± 1σ	^{38}Ar V	± 1σ	^{37}Ar V	± 1σ	^{36}Ar V	± 1σ	$^{40}Ar^*/^{39}Ar$	± 1σ	Age Ma	± 1σ	Corr?*	Age# Ma
1	1.0341	0.0033	0.0321	0.0003	0.0004	0.0001	0.0053	0.0039	0.0001	0.0000	32.23	0.35	380	4.08		383
2	4.1283	0.0059	0.1267	0.0008	0.0016	0.0001	0.0053	0.0039	0.0001	0.0001	32.58	0.22	383	2.87		387
3	2.5470	0.0061	0.0760	0.0007	0.0010	0.0001	0.0016	0.0039	0.0001	0.0000	33.50	0.34	393	3.96		397
4	4.8218	0.0098	0.1413	0.0009	0.0018	0.0001	0.0060	0.0039	0.0003	0.0000	33.47	0.25	393	3.13	Y	397
5	2.7436	0.0070	0.0832	0.0005	0.0012	0.0001	0.0067	0.0040	0.0001	0.0000	32.98	0.22	388	2.91		392
6	1.2124	0.0029	0.0360	0.0004	0.0005	0.0001	0.0012	0.0046	0.0000	0.0001	33.68	0.34	395	4.02		399
7	3.4969	0.0091	0.1026	0.0006	0.0011	0.0001	0.0004	0.0046	0.0001	0.0000	34.09	0.23	399	3.02		403
8	4.6323	0.0090	0.1417	0.0009	0.0018	0.0001	0.0041	0.0046	0.0000	0.0000	32.69	0.22	384	2.92		388
9	1.1966	0.0032	0.0354	0.0004	0.0005	0.0001	0.0049	0.0046	0.0001	0.0001	33.82	0.44	396	4.93		400
10	1.8743	0.0023	0.0550	0.0005	0.0007	0.0000	-0.0003	0.0046	0.0003	0.0001	32.29	0.45	380	5.05	Y	384
11	1.8743	0.0023	0.0550	0.0005	0.0007	0.0000	-0.0003	0.0046	0.0003	0.0001	34.09	0.33	399	3.91		403
12	1.5712	0.0042	0.0472	0.0007	0.0007	0.0001	-0.0018	0.0046	0.0000	0.0000	33.32	0.48	391	5.34		395
13	0.9103	0.0027	0.0265	0.0004	0.0003	0.0001	-0.0033	0.0046	0.0000	0.0000	34.41	0.47	403	5.29		407
14	0.5243	0.0014	0.0156	0.0002	0.0002	0.0000	0.0094	0.0046	0.0000	0.0000	33.65	0.47	395	5.25		399
Average Blank	0.0098	0.0003	0.0002	0.0001	0.0001	0.0000	0.0006	0.0001	0.0002	0.0000						

* Data corrected for ^{36}Ar where the ^{36}Ar measurement is > 2x the ^{36}Ar background (blank) measurement

Recalculated ages using the decay constant of Min et al., (2000) and GA1550 biotite standard age of 99.8 of Renne et al., (2010)

Single grain fusion analysis
C.9: NF43 Krokkenakken Garnetiferous Gneiss with High Pressure Relicts
61°54'53.73" N
005°20'16.49" E
J value 0.0116 ± 5.79E-05
MAP 215-50
Biotite

Grain	^{40}Ar V	± 1σ	^{39}Ar V	± 1σ	^{38}Ar V	± 1σ	^{37}Ar V	± 1σ	^{36}Ar V	± 1σ	$^{40}Ar^*/^{39}Ar$	± 1σ	Age Ma	± 1σ	Corr?*	Age# Ma
1	2.3587	0.0075	0.1157	0.0004	0.0014	0.0000	0.0006	0.0002	0.0000	0.0000	20.27	0.11	381	2.51		385
2	8.3923	0.0098	0.4129	0.0008	0.0048	0.0001	0.0060	0.0002	0.0001	0.0000	20.29	0.05	381	1.90		385
3	4.2504	0.0076	0.2098	0.0005	0.0023	0.0004	0.0044	0.0002	0.0001	0.0000	20.18	0.07	379	2.07		383
4	2.7916	0.0075	0.1365	0.0005	0.0013	0.0002	0.0003	0.0002	0.0000	0.0000	20.36	0.10	382	2.37		386
5	1.1223	0.0079	0.0547	0.0004	0.0006	0.0001	0.0003	0.0002	0.0000	0.0000	20.39	0.26	382	4.68		386
6	1.5927	0.0074	0.0782	0.0004	0.0009	0.0001	0.0001	0.0002	0.0000	0.0000	20.27	0.16	381	3.26		384
7	3.7729	0.0076	0.1847	0.0005	0.0018	0.0003	0.0329	0.0002	0.0000	0.0000	20.35	0.08	382	2.17		386
8	5.2716	0.0086	0.2595	0.0005	0.0027	0.0006	0.0010	0.0002	0.0001	0.0000	20.25	0.06	380	1.97		384
9	4.2251	0.0068	0.2071	0.0007	0.0024	0.0000	0.0137	0.0005	0.0000	0.0000	20.36	0.08	382	2.18		386
10	2.6506	0.0071	0.1283	0.0004	0.0015	0.0001	0.0008	0.0005	0.0000	0.0000	20.60	0.10	386	2.37		390
11	7.8840	0.0106	0.3887	0.0004	0.0045	0.0001	0.0010	0.0005	0.0000	0.0000	20.25	0.04	380	1.82		384
12	3.0235	0.0066	0.1483	0.0004	0.0018	0.0000	0.0052	0.0005	0.0000	0.0000	20.34	0.08	382	2.22		386
Average Blank	0.0049	0.0001	0.0001	0.0000	0.0000	0.0000	0.0001	0.0000	0.0000	0.0000						

* Data corrected for ^{36}Ar where the ^{36}Ar measurement is > 2x the ^{36}Ar background (blank) measurement
# Recalculated ages using the decay constant of Min et al., (2000) and GA1550 biotite standard age of 99.8 of Renne et al., (2010)

Single grain fusion analysis
C.10: NF105 Krokkenakken Biotite-Epidote Gneiss with Relict White Mica
61°54'53.73'' N
005°20'16.49'' E
J value 0.0094 ± 4.72E-05
MAP 215-50
White Mica

Grain	^{40}Ar V	± 1σ	^{39}Ar V	± 1σ	^{38}Ar V	± 1σ	^{37}Ar V	± 1σ	^{36}Ar V	± 1σ	$^{40}Ar^*/^{39}Ar$	± 1σ	Age Ma	± 1σ	Corr?*	Age# Ma
1	2.5147	0.0048	0.0980	0.0006	0.0012	0.0001	0.0079	0.0029	0.0000	0.0000	25.65	0.16	391	2.81		395
2	0.9702	0.0036	0.0390	0.0005	0.0004	0.0001	-0.0063	0.0029	0.0000	0.0000	24.90	0.32	381	4.72		385
3	1.7756	0.0063	0.0691	0.0007	0.0008	0.0001	0.0002	0.0029	0.0001	0.0000	25.71	0.28	392	4.19		396
4	0.8910	0.0020	0.0341	0.0004	0.0003	0.0001	-0.0047	0.0029	0.0000	0.0000	26.14	0.29	398	4.28		402
5	0.7389	0.0021	0.0279	0.0004	0.0002	0.0001	0.0002	0.0029	0.0000	0.0000	26.46	0.35	402	5.14		406
6	0.6085	0.0018	0.0227	0.0003	0.0004	0.0000	-0.0047	0.0029	0.0000	0.0000	26.84	0.33	407	4.85		411
7	1.0808	0.0035	0.0425	0.0007	0.0005	0.0000	-0.0019	0.0029	0.0001	0.0000	25.43	0.40	388	5.75		392
8	0.3722	0.0021	0.0139	0.0003	0.0001	0.0001	-0.0003	0.0029	0.0000	0.0000	26.84	0.62	407	8.66		411
9	0.8970	0.0019	0.0350	0.0003	0.0005	0.0001	0.0068	0.0029	0.0000	0.0000	25.61	0.19	390	3.16		394
10	0.7612	0.0019	0.0302	0.0005	0.0004	0.0001	0.0008	0.0029	0.0000	0.0000	25.24	0.40	385	5.71		389
11	0.6677	0.0019	0.0258	0.0006	0.0003	0.0001	-0.0041	0.0029	0.0000	0.0000	25.86	0.57	394	7.94		398
12	0.8610	0.0032	0.0335	0.0003	0.0005	0.0000	0.0035	0.0029	0.0001	0.0000	25.71	0.21	392	3.43		396
13	0.7157	0.0023	0.0272	0.0005	0.0004	0.0000	0.0013	0.0029	0.0000	0.0000	26.30	0.49	400	6.90		404
14	0.2628	0.0018	0.0102	0.0003	0.0001	0.0000	-0.0003	0.0029	0.0000	0.0000	25.67	0.83	391	11.48		395
15	0.9797	0.0028	0.0375	0.0004	0.0005	0.0000	-0.0003	0.0029	0.0000	0.0000	26.13	0.29	398	4.37		402
Average Blank	0.0059	0.0003	0.0001	0.0000	0.0001	0.0000	0.0004	0.0000	0.0001	0.0000						

* Data corrected for ^{36}Ar where the ^{36}Ar measurement is > 2x the ^{36}Ar background (blank) measurement
# Recalculated ages using the decay constant of Min et al., (2000) and GA1550 biotite standard age of 99.8 of Renne et al., (2010)

Single grain fusion analysis

C.11: NF105 Krokkenakken Biotite-Epidote Gneiss with Relict White Mica

61°54'53.73" N

005°20'16.49" E

J value 0.0094 ± 4.70E-05

MAP 215-50

Biotite

Grain	^{40}Ar V	± 1σ	^{39}Ar V	± 1σ	^{38}Ar V	± 1σ	^{37}Ar V	± 1σ	^{36}Ar V	± 1σ	$^{40}Ar^*/^{39}Ar$	± 1σ	Age Ma	± 1σ	Corr?*	Age# Ma
1	0.2471	0.0016	0.0095	0.0003	0.0000	0.0000	-0.0002	0.0016	0.0000	0.0000	26.02	0.85	394	11.76		398
2	0.8198	0.0026	0.0324	0.0005	0.0005	0.0001	-0.0018	0.0016	0.0001	0.0000	25.30	0.40	385	5.72		388
3	0.9003	0.0018	0.0365	0.0004	0.0004	0.0001	0.0008	0.0016	0.0000	0.0000	24.64	0.28	375	4.20		379
4	1.1837	0.0028	0.0459	0.0008	0.0006	0.0001	0.0040	0.0016	0.0000	0.0000	25.77	0.47	391	6.64		395
5	1.0952	0.0031	0.0435	0.0004	0.0006	0.0000	-0.0018	0.0016	0.0000	0.0000	25.15	0.26	382	3.93		386
6	0.9362	0.0025	0.0382	0.0005	0.0004	0.0001	0.0014	0.0016	0.0000	0.0000	24.54	0.34	374	4.99		378
7	0.6575	0.0025	0.0254	0.0004	0.0003	0.0001	0.0057	0.0016	0.0000	0.0000	25.87	0.41	392	5.81		396
8	0.8045	0.0020	0.0326	0.0004	0.0005	0.0001	0.0062	0.0016	0.0000	0.0000	24.69	0.32	376	4.75		380
9	0.9747	0.0031	0.0380	0.0003	0.0005	0.0001	-0.0013	0.0016	0.0000	0.0000	25.65	0.23	389	3.57		393
10	1.2701	0.0016	0.0501	0.0005	0.0006	0.0001	-0.0008	0.0016	0.0000	0.0000	25.37	0.27	385	4.03		389
11	2.4466	0.0055	0.0970	0.0008	0.0011	0.0001	-0.0002	0.0016	0.0000	0.0000	25.22	0.21	383	3.39		387
12	0.5251	0.0019	0.0211	0.0003	0.0002	0.0001	0.0051	0.0016	0.0000	0.0000	24.93	0.37	379	5.40		383
13	0.6883	0.0021	0.0275	0.0004	0.0004	0.0001	-0.0036	0.0028	0.0000	0.0000	25.05	0.41	381	5.82		385
14	0.9616	0.0014	0.0393	0.0005	0.0006	0.0000	0.0008	0.0028	0.0000	0.0000	24.50	0.30	374	4.47		377
15	1.1407	0.0035	0.0455	0.0003	0.0006	0.0001	-0.0030	0.0028	0.0000	0.0000	25.07	0.18	381	3.00		385
Average Blank	0.0056	0.0002	0.0001	0.0000	0.0001	0.0000	0.0004	0.0001	0.0001	0.0000						

* Data corrected for ^{36}Ar where the ^{36}Ar measurement is > 2x the ^{36}Ar background (blank) measurement

Recalculated ages using the decay constant of Min et al., (2000) and GA1550 biotite standard age of 99.8 of Renne et al., (2010)

Single grain fusion analysis
C.12: NF106 Krokkenakken Garnetiferous Gneiss without High-Pressure Relicts
61°54'53.73" N
005°20'16.49" E
J value 0.0095 ± 4.74E-05
MAP 215-50
White Mica

Grain	^{40}Ar V	± 1σ	^{39}Ar V	± 1σ	^{38}Ar V	± 1σ	^{37}Ar V	± 1σ	^{36}Ar V	± 1σ	$^{40}Ar^*/^{39}Ar$	± 1σ	Age Ma	± 1σ	Corr?*	Age# Ma
1	0.6651	0.0014	0.0255	0.0002	0.0004	0.0001	0.0011	0.0040	0.0000	0.0000	26.12	0.25	399	3.92		403
2	1.2410	0.0019	0.0469	0.0004	0.0005	0.0001	0.0040	0.0040	0.0001	0.0000	26.43	0.23	403	3.59		408
3	1.5914	0.0028	0.0603	0.0004	0.0007	0.0001	0.0028	0.0040	0.0000	0.0000	26.16	0.24	400	3.77	Y	404
4	1.9440	0.0050	0.0743	0.0006	0.0010	0.0001	0.0064	0.0040	0.0000	0.0000	26.18	0.21	400	3.41		404
5	1.1869	0.0036	0.0452	0.0005	0.0006	0.0001	-0.0007	0.0040	0.0001	0.0000	26.25	0.32	401	4.70		405
6	1.5258	0.0051	0.0563	0.0009	0.0007	0.0001	-0.0013	0.0040	0.0000	0.0000	27.11	0.42	413	6.05		417
7	1.1833	0.0019	0.0464	0.0004	0.0005	0.0001	-0.0048	0.0040	0.0000	0.0000	25.26	0.31	387	4.56	Y	391
8	0.5267	0.0029	0.0194	0.0004	0.0003	0.0001	0.0046	0.0040	0.0000	0.0000	27.10	0.53	412	7.44		417
9	0.7128	0.0008	0.0273	0.0005	0.0003	0.0001	-0.0043	0.0040	0.0000	0.0000	26.07	0.49	398	6.90		403
10	0.6099	0.0018	0.0229	0.0005	0.0002	0.0001	-0.0025	0.0040	0.0000	0.0000	26.69	0.56	407	7.91		411
11	0.3070	0.0008	0.0121	0.0003	0.0001	0.0001	0.0040	0.0040	0.0000	0.0000	25.39	0.58	389	8.13		393
12	0.9166	0.0025	0.0342	0.0004	0.0004	0.0001	-0.0054	0.0040	0.0000	0.0000	26.79	0.29	408	4.42		413
13	0.7970	0.0025	0.0289	0.0005	0.0003	0.0001	-0.0025	0.0040	0.0000	0.0000	27.54	0.50	419	7.05		423
14	0.4451	0.0011	0.0165	0.0003	0.0002	0.0001	-0.0066	0.0040	0.0001	0.0000	27.03	0.55	412	7.74		416
15	0.7930	0.0015	0.0291	0.0003	0.0004	0.0000	-0.0001	0.0040	0.0001	0.0000	27.28	0.27	415	4.12		419
Average Blank	0.0056	0.0002	0.0002	0.0000	0.0001	0.0000	0.0005	0.0000	0.0001	0.0000						

* Data corrected for ^{36}Ar where the ^{36}Ar measurement is > 2x the ^{36}Ar background (blank) measurement
# Recalculated ages using the decay constant of Min et al., (2000) and GA1550 biotite standard age of 99.8 of Renne et al., (2010)

Single grain fusion analysis

C.13: NF106 Krokkenakken Garnetiferous Gneiss without High-Pressure Relicts

61°54'53.73" N

005°20'16.49" E

J value 0.0095 ± 4.76E-05

MAP 215-50

Biotite

Grain	^{40}Ar V	± 1σ	^{39}Ar V	± 1σ	^{38}Ar V	± 1σ	^{37}Ar V	± 1σ	^{36}Ar V	± 1σ	$^{40}Ar^*/^{39}Ar$	± 1σ	Age Ma	± 1σ	Corr?*	Age# Ma
1	0.6141	0.0015	0.0237	0.0003	0.0003	0.0001	-0.0050	0.0031	0.0000	0.0000	25.97	0.29	399	4.43		403
2	0.9879	0.0028	0.0377	0.0005	0.0006	0.0001	0.0034	0.0031	0.0000	0.0000	26.18	0.33	402	4.83		406
3	0.7043	0.0027	0.0272	0.0004	0.0002	0.0000	-0.0026	0.0031	0.0000	0.0000	25.92	0.41	398	5.92		402
4	0.5080	0.0022	0.0192	0.0003	0.0003	0.0001	-0.0044	0.0031	0.0000	0.0000	26.43	0.44	405	6.37		409
5	0.8501	0.0021	0.0328	0.0004	0.0004	0.0001	0.0022	0.0031	0.0000	0.0000	25.88	0.33	398	4.94		402
6	1.7952	0.0043	0.0686	0.0005	0.0008	0.0001	-0.0002	0.0031	0.0001	0.0000	26.19	0.21	402	3.43		406
7	1.5243	0.0028	0.0594	0.0006	0.0007	0.0000	-0.0014	0.0031	0.0000	0.0000	25.65	0.27	394	4.16		398
8	1.9064	0.0035	0.0736	0.0005	0.0008	0.0001	-0.0014	0.0031	0.0000	0.0000	25.90	0.19	398	3.12		402
9	0.9904	0.0024	0.0378	0.0004	0.0005	0.0001	-0.0008	0.0031	0.0000	0.0000	26.21	0.30	402	4.44		406
10	0.8716	0.0026	0.0327	0.0005	0.0004	0.0001	-0.0008	0.0031	0.0000	0.0000	26.69	0.40	409	5.76		413
11	1.1324	0.0053	0.0437	0.0007	0.0006	0.0001	0.0010	0.0031	0.0000	0.0000	25.90	0.46	398	6.56		402
12	1.9028	0.0028	0.0725	0.0006	0.0009	0.0001	0.0010	0.0031	0.0000	0.0000	26.24	0.22	403	3.53		407
13	0.9559	0.0025	0.0373	0.0005	0.0004	0.0000	-0.0032	0.0031	0.0000	0.0000	25.64	0.32	394	4.78		398
14	1.1410	0.0021	0.0436	0.0004	0.0005	0.0000	-0.0026	0.0031	0.0001	0.0000	26.18	0.26	402	4.01		406
15	0.7217	0.0008	0.0270	0.0004	0.0002	0.0001	-0.0014	0.0031	0.0001	0.0000	26.74	0.39	409	5.68		414
Average Blank	0.0054	0.0002	0.0001	0.0000	0.0001	0.0000	0.0004	0.0001	0.0001	0.0000						

* Data corrected for ^{36}Ar where the ^{36}Ar measurement is > 2x the ^{36}Ar background (blank) measurement

\# Recalculated ages using the decay constant of Min et al., (2000) and GA1550 biotite standard age of 99.8 of Renne et al., (2010)

Single grain fusion analysis
C.14: NF44A Undeformed Flatraket Granulite
61°54'53.73'' N
005°20'16.49'' E
J value 0.0071 ± 3.56E-05
MAP 215-50
Biotite

Grain	^{40}Ar V	± 1σ	^{39}Ar V	± 1σ	^{38}Ar V	± 1σ	^{37}Ar V	± 1σ	^{36}Ar V	± 1σ	$^{40}Ar^*/^{39}Ar$	± 1σ	Age Ma	± 1σ	Corr?*	Age# Ma
1	3.0768	0.0064	0.0924	0.0006	0.0013	0.0001	-0.0056	0.0044	0.0001	0.0000	33.31	0.24	384	3.02		388
2	1.9485	0.0029	0.0583	0.0004	0.0007	0.0001	0.0046	0.0044	0.0000	0.0000	33.41	0.22	385	2.84		389
3	1.7036	0.0037	0.0487	0.0006	0.0010	0.0001	0.0005	0.0044	0.0000	0.0000	34.95	0.42	401	4.65		405
4	2.7773	0.0032	0.0831	0.0004	0.0012	0.0001	0.0059	0.0044	0.0000	0.0000	33.42	0.18	385	2.59		389
5	5.9888	0.0075	0.1779	0.0010	0.0026	0.0001	-0.0124	0.0044	0.0001	0.0000	33.66	0.20	388	2.68		392
6	3.0776	0.0082	0.0924	0.0005	0.0013	0.0001	-0.0118	0.0044	0.0000	0.0000	33.29	0.21	384	2.82		388
7	2.3141	0.0018	0.0690	0.0010	0.0009	0.0001	0.0039	0.0044	0.0000	0.0000	33.54	0.47	386	5.17		390
8	3.1599	0.0045	0.0922	0.0008	0.0014	0.0001	0.0046	0.0044	0.0000	0.0000	34.27	0.29	394	3.48		398
9	3.4071	0.0029	0.1029	0.0006	0.0015	0.0001	0.0012	0.0044	0.0001	0.0000	33.12	0.21	382	2.75		386
10	3.8032	0.0056	0.1157	0.0006	0.0018	0.0001	-0.0070	0.0044	0.0001	0.0000	32.86	0.16	379	2.42		383
11	5.9322	0.0068	0.1743	0.0007	0.0025	0.0001	0.0028	0.0050	0.0000	0.0000	34.04	0.15	392	2.31		396
12	2.4782	0.0048	0.0743	0.0006	0.0011	0.0001	0.0055	0.0050	0.0000	0.0000	33.36	0.27	385	3.32		389
13	1.8844	0.0046	0.0559	0.0007	0.0007	0.0001	0.0021	0.0050	0.0000	0.0000	33.68	0.44	388	4.93		392
14	5.3967	0.0105	0.1639	0.0009	0.0025	0.0001	0.0062	0.0050	0.0000	0.0000	32.93	0.20	380	2.67		384
Average Blank	0.0116	0.0004	0.0003	0.0001	0.0002	0.0000	0.0007	0.0001	0.0002	0.0000						

* Data corrected for ^{36}Ar where the ^{36}Ar measurement is > 2x the ^{36}Ar background (blank) measurement
# Recalculated ages using the decay constant of Min et al., (2000) and GA1550 biotite standard age of 99.8 of Renne et al., (2010)

Single grain fusion analysis
C.15: NF44F Sheared Flatraket Granulite
61°54'53.73" N
005°20'16.49" E
J value 0.0072 ± 3.61E-05
MAP 215-50
Biotite

Grain	^{40}Ar V	± 1σ	^{39}Ar V	± 1σ	^{38}Ar V	± 1σ	^{37}Ar V	± 1σ	^{36}Ar V	± 1σ	$^{40}Ar^*/^{39}Ar$	± 1σ	Age Ma	± 1σ	Corr?*	Age# Ma
1	1.6815	0.0030	0.0514	0.0007	0.0006	0.0001	0.0023	0.0036	0.0000	0.0000	32.70	0.43	382	4.81		386
2	2.6853	0.0036	0.0796	0.0005	0.0012	0.0001	-0.0026	0.0036	0.0000	0.0000	33.73	0.23	393	2.94		397
3	2.9691	0.0045	0.0902	0.0007	0.0013	0.0001	0.0037	0.0036	0.0001	0.0000	32.91	0.24	384	3.09		388
4	2.5222	0.0050	0.0769	0.0006	0.0012	0.0001	0.0016	0.0036	0.0001	0.0000	32.81	0.28	383	3.44		387
5	4.8836	0.0110	0.1441	0.0008	0.0019	0.0001	0.0051	0.0036	0.0002	0.0000	33.89	0.19	395	2.69		399
6	2.3154	0.0043	0.0699	0.0005	0.0009	0.0001	0.0037	0.0036	0.0001	0.0000	33.12	0.23	387	2.98		391
7	1.4525	0.0055	0.0417	0.0004	0.0006	0.0001	0.0141	0.0036	0.0001	0.0000	34.81	0.33	404	3.84		409
8	1.8634	0.0072	0.0555	0.0008	0.0007	0.0001	0.0030	0.0036	0.0000	0.0000	33.57	0.48	391	5.29		395
9	1.6207	0.0024	0.0492	0.0005	0.0006	0.0001	-0.0012	0.0036	0.0000	0.0000	32.94	0.37	385	4.22		389
10	2.6039	0.0073	0.0766	0.0007	0.0011	0.0001	0.0072	0.0036	0.0001	0.0000	33.98	0.31	396	3.69		400
11	2.2967	0.0033	0.0694	0.0009	0.0008	0.0001	0.0058	0.0036	0.0001	0.0000	33.10	0.42	386	4.77		390
12	2.1101	0.0053	0.0640	0.0007	0.0008	0.0001	-0.0040	0.0036	0.0000	0.0000	32.99	0.36	385	4.19		389
13	2.9800	0.0059	0.0900	0.0011	0.0013	0.0001	0.0065	0.0041	0.0000	0.0000	33.11	0.42	387	4.75		391
14	4.1740	0.0077	0.1280	0.0008	0.0019	0.0001	0.0015	0.0041	0.0000	0.0000	32.61	0.20	381	2.76		385
15	5.4248	0.0074	0.1677	0.0007	0.0024	0.0001	0.0107	0.0041	0.0001	0.0000	32.34	0.15	379	2.31		382
Average Blank	0.0122	0.0004	0.0003	0.0001	0.0002	0.0000	0.0006	0.0001	0.0002	0.0000						

* Data corrected for ^{36}Ar where the ^{36}Ar measurement is > 2x the ^{36}Ar background (blank) measurement
# Recalculated ages using the decay constant of Min et al., (2000) and GA1550 biotite standard age of 99.8 of Renne et al., (2010)

Single grain fusion analysis
C.16: NF45 Flatraket Harbour Eclogite
61°58'41.50'' N
005°14'43.20'' E
J value 0.0090 ± 1.77E-05
ARGUS
White Mica

Grain	^{40}Ar V	± 1σ	^{39}Ar V	± 1σ	^{38}Ar V	± 1σ	^{37}Ar V	± 1σ	^{36}Ar V	± 1σ	$^{40}Ar^*/^{39}Ar$	± 1σ	Age Ma	± 1σ	Corr?*	Age# Ma
1	4.4569	0.0022	0.1363	0.0001	0.0016	0.0000	-0.0001	0.0000	0.0000	0.0000	32.57	0.05	467	0.69		471
2	3.4938	0.0015	0.1090	0.0001	0.0013	0.0000	0.0000	0.0000	0.0000	0.0000	31.98	0.05	459	0.70		464
3	7.2012	0.0030	0.1807	0.0002	0.0022	0.0000	-0.0001	0.0000	0.0004	0.0000	39.15	0.04	548	0.51		553
4	1.8062	0.0013	0.0515	0.0001	0.0006	0.0000	0.0000	0.0000	0.0000	0.0000	34.99	0.13	497	1.59		502
5	1.4086	0.0013	0.0423	0.0001	0.0005	0.0000	-0.0001	0.0000	0.0000	0.0000	33.27	0.17	475	2.11		480
6	5.7027	0.0024	0.1492	0.0001	0.0018	0.0000	-0.0001	0.0000	0.0004	0.0000	37.34	0.05	526	0.62		531
7	1.6296	0.0013	0.0417	0.0001	0.0005	0.0000	-0.0001	0.0000	0.0001	0.0000	38.15	0.15	536	1.81		541
8	2.0418	0.0013	0.0518	0.0001	0.0006	0.0000	0.0000	0.0000	0.0002	0.0000	38.04	0.10	534	1.17		540
9	2.1210	0.0013	0.0570	0.0001	0.0007	0.0000	-0.0001	0.0000	0.0000	0.0000	37.07	0.09	523	1.09		528
10	0.3287	0.0014	0.0111	0.0001	0.0001	0.0000	0.0000	0.0000	0.0001	0.0000	26.80	0.48	392	6.30		396
11	1.9818	0.0013	0.0548	0.0001	0.0006	0.0000	-0.0001	0.0000	0.0001	0.0000	35.70	0.11	506	1.41		511
12	3.5577	0.0017	0.0811	0.0001	0.0010	0.0000	-0.0001	0.0000	0.0001	0.0000	43.62	0.07	601	0.86		607
13	3.5191	0.0016	0.0927	0.0001	0.0011	0.0000	-0.0001	0.0000	0.0001	0.0000	37.45	0.07	527	0.81		533
14	1.5663	0.0013	0.0509	0.0001	0.0006	0.0000	0.0000	0.0000	0.0001	0.0000	29.94	0.12	433	1.48		438
15	2.0225	0.0013	0.0637	0.0001	0.0008	0.0000	-0.0001	0.0000	0.0000	0.0000	31.76	0.07	456	0.85		461
16	0.5489	0.0007	0.0164	0.0001	0.0001	0.0000	-0.0001	0.0000	-0.0001	0.0000	34.43	0.32	490	4.03		495
17	1.1489	0.0012	0.0364	0.0001	0.0004	0.0000	0.0000	0.0000	0.0001	0.0000	31.07	0.15	448	1.94		452
18	1.3835	0.0012	0.0352	0.0001	0.0004	0.0000	-0.0001	0.0000	0.0000	0.0000	38.93	0.17	545	2.00		551
19	1.4543	0.0013	0.0400	0.0001	0.0005	0.0000	-0.0001	0.0000	0.0001	0.0000	35.84	0.16	507	2.00		513
Average Blank	0.0046	0.0000	0.0006	0.0000	0.0002	0.0000	0.0003	0.0000	0.0003	0.0000						

* Data corrected for ^{36}Ar where the ^{36}Ar measurement is > 2x the ^{36}Ar background (blank) measurement
# Recalculated ages using the decay constant of Min et al., (2000) and GA1550 biotite standard age of 99.8 of Renne et al., (2010)

Single grain fusion analysis
C.17: NF45 Flatraket Harbour Eclogite
61°58'41.50'' N
005°14'43.20'' E
J value 0.0090 ± 1.79E-05
ARGUS
Amphibole

Grain	^{40}Ar V	± 1σ	^{39}Ar V	± 1σ	^{38}Ar V	± 1σ	^{37}Ar V	± 1σ	^{36}Ar V	± 1σ	$^{40}Ar^*/^{39}Ar$	± 1σ	Age Ma	± 1σ	Corr?*	Age# Ma
1	0.7737	0.0007	0.0085	0.0001	0.0001	0.0000	0.0028	0.0000	0.0000	0.0000	0.56	92.08	1095	6.49		1107
2	2.1234	0.0011	0.0075	0.0000	0.0004	0.0000	0.0031	0.0000	0.0001	0.0000	1.49	283.80	2298	7.34		2325
3	0.4555	0.0003	0.0092	0.0001	0.0002	0.0000	0.0022	0.0000	0.0001	0.0000	0.34	48.10	653	5.74		660
4	0.7942	0.0005	0.0130	0.0001	0.0003	0.0000	0.0028	0.0000	0.0001	0.0000	0.25	59.27	776	4.03		784
5	0.4147	0.0003	0.0078	0.0001	0.0001	0.0000	0.0017	0.0000	0.0000	0.0000	0.34	52.26	699	7.19		707
6	0.2874	0.0011	0.0063	0.0001	0.0001	0.0000	0.0013	0.0000	0.0000	0.0000	0.53	45.84	627	11.30		633
7	0.3614	0.0004	0.0080	0.0001	0.0001	0.0000	0.0017	0.0000	0.0000	0.0000	0.30	46.06	629	7.86		636
8	0.9910	0.0006	0.0176	0.0001	0.0005	0.0000	0.0042	0.0000	0.0001	0.0000	0.21	55.36	734	3.78		741
9	0.2082	0.0008	0.0040	0.0001	0.0001	0.0000	0.0008	0.0000	0.0000	0.0000	0.79	51.01	686	15.56		693
10	0.7582	0.0005	0.0161	0.0001	0.0003	0.0000	0.0031	0.0000	0.0001	0.0000	0.18	46.16	630	4.72		637
11	0.6632	0.0004	0.0120	0.0001	0.0003	0.0000	0.0028	0.0000	0.0001	0.0000	0.27	54.48	724	5.14		732
12	0.1904	0.0009	0.0042	0.0001	0.0001	0.0000	0.0029	0.0000	0.0000	0.0000	0.70	45.75	626	17.25		632
13	0.6914	0.0003	0.0152	0.0001	0.0003	0.0000	0.0041	0.0000	0.0001	0.0000	0.15	45.41	622	3.22		628
14	0.3463	0.0003	0.0077	0.0001	0.0002	0.0000	0.0018	0.0000	0.0001	0.0000	0.34	43.20	596	8.39		602
15	0.2477	0.0005	0.0042	0.0001	0.0001	0.0000	0.0019	0.0000	0.0001	0.0000	0.85	56.39	745	13.85		753
16	0.2271	0.0005	0.0054	0.0001	0.0001	0.0000	0.0013	0.0000	0.0001	0.0000	0.45	40.54	565	12.00		570
17	2.7815	0.0016	0.0971	0.0001	0.0013	0.0000	0.0032	0.0000	0.0001	0.0000	0.04	28.47	414	0.77		418
18	0.1701	0.0007	0.0059	0.0001	0.0001	0.0000	0.0025	0.0000	0.0001	0.0000	0.35	26.44	388	12.85		391
19	0.8004	0.0006	0.0128	0.0001	0.0004	0.0000	0.0031	0.0000	0.0001	0.0000	0.25	62.45	809	4.79		818
20	0.3785	0.0004	0.0047	0.0001	0.0002	0.0000	0.0010	0.0000	0.0000	0.0000	0.83	80.63	990	11.77		1001
21	0.2688	0.0007	0.0060	0.0000	0.0001	0.0000	0.0014	0.0000	0.0000	0.0000	0.37	44.72	614	9.44		620
22	0.3330	0.0005	0.0060	0.0001	0.0001	0.0000	0.0015	0.0000	0.0001	0.0000	0.51	53.58	714	10.45		722
23	0.6262	0.0005	0.0129	0.0000	0.0002	0.0000	0.0028	0.0000	0.0000	0.0000	0.17	48.84	661	4.07		668
Average Blank	0.0046	0.0000	0.0006	0.0000	0.0002	0.0000	0.0003	0.0000	0.0002	0.0000						

* Data corrected for ^{36}Ar where the ^{36}Ar measurement is > 2x the ^{36}Ar background (blank) measurement
# Recalculated ages using the decay constant of Min et al., (2000) and GA1550 biotite standard age of 99.8 of Renne et al., (2010)

Single grain fusion analysis
C.18: NF46 Flatraket Harbour Amphibolitised Eclogite
61°58'41.50" N
005°14'43.20" E
J value 0.0071 ± 3.54E-05
MAP 215-50
Biotite

Grain	^{40}Ar V	± 1σ	^{39}Ar V	± 1σ	^{38}Ar V	± 1σ	^{37}Ar V	± 1σ	^{36}Ar V	± 1σ	$^{40}Ar^*/^{39}Ar$	± 1σ	Age Ma	± 1σ	Corr?*	Age# Ma
1	2.7586	0.0086	0.0715	0.0010	0.0013	0.0001	-0.0084	0.0054	0.0015	0.0001	32.27	0.55	371	5.99	Y	375
2	4.0349	0.0073	0.1225	0.0009	0.0017	0.0001	-0.0050	0.0054	0.0000	0.0000	32.95	0.24	378	2.99		382
3	3.0155	0.0105	0.0891	0.0008	0.0010	0.0001	-0.0037	0.0054	0.0001	0.0000	33.83	0.32	387	3.71		391
4	6.6567	0.0089	0.2011	0.0009	0.0030	0.0001	-0.0090	0.0054	0.0002	0.0000	33.10	0.16	380	2.35		383
5	4.2701	0.0060	0.1269	0.0007	0.0017	0.0001	-0.0031	0.0054	0.0002	0.0000	33.08	0.20	379	2.66	Y	383
6	1.6465	0.0024	0.0490	0.0005	0.0007	0.0001	-0.0071	0.0054	0.0001	0.0000	33.62	0.38	385	4.25		389
7	2.9101	0.0045	0.0758	0.0006	0.0012	0.0001	0.0023	0.0054	0.0015	0.0001	32.56	0.48	374	5.25	Y	378
8	6.6017	0.0121	0.1955	0.0013	0.0026	0.0002	-0.0084	0.0055	0.0003	0.0000	33.26	0.24	381	2.99	Y	385
9	1.8429	0.0033	0.0525	0.0005	0.0007	0.0001	-0.0024	0.0055	0.0005	0.0000	32.21	0.41	370	4.60	Y	374
10	2.8409	0.0064	0.0858	0.0007	0.0012	0.0001	-0.0004	0.0055	0.0001	0.0000	33.10	0.29	380	3.49		384
11	5.9577	0.0057	0.1803	0.0009	0.0024	0.0001	-0.0051	0.0060	0.0002	0.0000	32.64	0.17	375	2.44	Y	379
12	2.8421	0.0034	0.0873	0.0008	0.0012	0.0001	-0.0119	0.0060	0.0002	0.0000	32.54	0.31	374	3.65		378
13	1.2603	0.0033	0.0377	0.0004	0.0006	0.0001	0.0050	0.0060	0.0001	0.0000	33.44	0.36	383	4.13		387
14	0.9713	0.0016	0.0289	0.0004	0.0003	0.0001	-0.0038	0.0060	0.0002	0.0000	31.22	0.60	360	6.53	Y	364
15	1.6874	0.0028	0.0522	0.0006	0.0007	0.0001	-0.0031	0.0060	0.0001	0.0000	32.31	0.39	371	4.38		375
Average Blank	0.0129	0.0004	0.0003	0.0001	0.0001	0.0000	0.0007	0.0001	0.0002	0.0000						

* Data corrected for ^{36}Ar where the ^{36}Ar measurement is > 2x the ^{36}Ar background (blank) measurement
\# Recalculated ages using the decay constant of Min et al., (2000) and GA1550 biotite standard age of 99.8 of Renne et al., (2010)

Single grain fusion analysis
C.19: NF46 Flatraket Harbour Amphibolitised Eclogite
61°58'41.50" N
005°14'43.20" E
J value 0.0071 ± 3.53E-05
MAP 215-50
Biotite

Grain	^{40}Ar V	± 1σ	^{39}Ar V	± 1σ	^{38}Ar V	± 1σ	^{37}Ar V	± 1σ	^{36}Ar V	± 1σ	$^{40}Ar^*/^{39}Ar$	± 1σ	Age Ma	± 1σ	Corr?*	Age# Ma
1	1.2079	0.0036	0.0327	0.0004	0.0007	0.0001	0.1931	0.0046	0.0001	0.0000	36.95	0.48	418	5.18		422
2	0.3246	0.0017	0.0084	0.0002	0.0003	0.0001	0.1015	0.0046	0.0000	0.0000	38.82	0.85	436	8.68		441
3	0.5138	0.0026	0.0138	0.0003	0.0003	0.0001	0.1529	0.0046	0.0001	0.0000	37.12	0.81	419	8.33		424
4	0.6768	0.0024	0.0202	0.0002	0.0004	0.0001	0.1100	0.0046	0.0000	0.0000	33.48	0.39	382	4.37		386
5	0.9712	0.0023	0.0229	0.0004	0.0004	0.0001	0.2117	0.0046	0.0001	0.0000	42.41	0.83	472	8.36		477
6	1.2469	0.0030	0.0316	0.0004	0.0005	0.0001	0.1903	0.0046	0.0001	0.0000	39.43	0.49	443	5.22		447
7	0.6288	0.0020	0.0162	0.0003	0.0004	0.0001	0.1291	0.0046	0.0000	0.0000	38.90	0.69	437	7.16		442
8	1.5519	0.0033	0.0428	0.0005	0.0010	0.0001	0.1520	0.0046	0.0000	0.0000	36.27	0.45	411	4.92		415
9	0.3740	0.0019	0.0108	0.0002	0.0003	0.0001	0.1228	0.0046	0.0001	0.0000	34.66	0.77	395	8.08		399
10	2.5092	0.0048	0.0647	0.0009	0.0011	0.0001	0.1862	0.0046	0.0001	0.0000	38.76	0.53	436	5.62		440
11	0.6389	0.0022	0.0174	0.0005	0.0003	0.0001	0.1020	0.0046	0.0001	0.0000	36.73	1.03	416	10.56		420
12	0.3805	0.0015	0.0106	0.0003	0.0002	0.0001	0.0563	0.0046	0.0000	0.0000	35.99	0.94	408	9.70		412
13	0.7573	0.0034	0.0181	0.0002	0.0004	0.0001	0.2068	0.0046	0.0001	0.0000	41.79	0.59	466	6.16		471
14	0.8876	0.0024	0.0232	0.0004	0.0004	0.0001	0.1270	0.0046	0.0000	0.0000	38.24	0.69	431	7.15		435
15	0.8710	0.0023	0.0242	0.0004	0.0004	0.0001	0.0773	0.0046	0.0000	0.0000	36.04	0.65	409	6.87		413
16	0.7373	0.0024	0.0167	0.0004	0.0003	0.0001	0.1285	0.0046	0.0000	0.0000	44.14	1.07	489	10.62		494
17	1.4358	0.0053	0.0319	0.0005	0.0009	0.0001	0.3048	0.0046	0.0001	0.0000	45.03	0.69	497	6.99		503
Average Blank	0.0139	0.0004	0.0003	0.0001	0.0002	0.0000	0.0007	0.0001	0.0002	0.0000						

* Data corrected for ^{36}Ar where the ^{36}Ar measurement is > 2x the ^{36}Ar background (blank) measurement
# Recalculated ages using the decay constant of Min et al., (2000) and GA1550 biotite standard age of 99.8 of Renne et al., (2010)

Single grain fusion analysis
C.20: NF47 Flatraket Harbour Garnet-Biotite Gneiss
61°58'41.50" N
005°14'43.20" E
J value 0.0116 ± 5.81E-05
MAP 215-50
Biotite

Grain	^{40}Ar V	± 1σ	^{39}Ar V	± 1σ	^{38}Ar V	± 1σ	^{37}Ar V	± 1σ	^{36}Ar V	± 1σ	$^{40}Ar^*/^{39}Ar$	± 1σ	Age Ma	± 1σ	Corr?*	Age# Ma
1	1.6005	0.0022	0.0742	0.0002	0.0011	0.0000	-0.0001	0.0004	0.0001	0.0000	21.03	0.08	394	2.27		398
2	0.9278	0.0021	0.0428	0.0001	0.0006	0.0000	0.0003	0.0004	0.0001	0.0000	21.05	0.13	394	2.86		399
3	2.6890	0.0024	0.1203	0.0002	0.0015	0.0000	0.0135	0.0004	0.0004	0.0000	21.46	0.06	401	2.05		406
4	5.7715	0.0033	0.2714	0.0004	0.0015	0.0007	0.0019	0.0004	0.0003	0.0000	20.98	0.04	393	1.89		397
5	8.8981	0.0046	0.4275	0.0003	0.0033	0.0011	0.0019	0.0004	0.0007	0.0000	20.33	0.02	382	1.77		386
6	10.6521	0.0044	0.4640	0.0005	0.0060	0.0000	0.0001	0.0004	0.0014	0.0000	22.04	0.03	411	1.91		415
7	8.1475	0.0067	0.3854	0.0005	0.0042	0.0008	0.0003	0.0004	0.0004	0.0000	20.84	0.03	391	1.85		395
8	11.3316	0.0081	0.5409	0.0004	0.0070	0.0001	0.0012	0.0004	0.0003	0.0000	20.79	0.02	390	1.80		394
9	6.8723	0.0130	0.3282	0.0005	0.0044	0.0001	0.0021	0.0005	0.0001	0.0000	20.84	0.05	391	1.97		395
10	5.1821	0.0142	0.2462	0.0006	0.0033	0.0000	0.0028	0.0005	0.0001	0.0000	20.89	0.08	392	2.20		396
11	3.8494	0.0094	0.1802	0.0005	0.0025	0.0001	0.0026	0.0005	0.0002	0.0000	20.98	0.08	393	2.22		397
12	10.0425	0.0119	0.4872	0.0007	0.0065	0.0001	0.0005	0.0005	0.0002	0.0000	20.50	0.04	385	1.87		389
Average Blank	0.0064	0.0001	0.0001	0.0000	0.0000	0.0000	0.0001	0.0000	0.0000	0.0000						

* Data corrected for ^{36}Ar where the ^{36}Ar measurement is > 2x the ^{36}Ar background (blank) measurement
# Recalculated ages using the decay constant of Min et al., (2000) and GA1550 biotite standard age of 99.8 of Renne et al., (2010)

Single grain fusion analysis

C.21: NF48 Flatraket Harbour Garnetiferous Gneiss without High-Pressure Relicts

61°58'41.50" N

005°14'43.20" E

J value 0.0118 ± 5.88E-05

MAP 215-50

White Mica

Grain	^{40}Ar V	± 1σ	^{39}Ar V	± 1σ	^{38}Ar V	± 1σ	^{37}Ar V	± 1σ	^{36}Ar V	± 1σ	$^{40}Ar^*/^{39}Ar$	± 1σ	Age Ma	± 1σ	Corr?*	Age# Ma
1	6.8819	0.0257	0.3429	0.0013	0.0042	0.0001	0.0006	0.0004	0.0002	0.0000	19.89	0.11	379	2.55		383
2	6.9139	0.0180	0.3401	0.0014	0.0038	0.0002	0.0008	0.0004	0.0002	0.0000	20.14	0.10	384	2.46		388
3	5.5331	0.0113	0.2716	0.0018	0.0033	0.0002	-0.0002	0.0004	0.0002	0.0000	20.20	0.14	385	3.02		389
4	10.6108	0.0219	0.5275	0.0019	0.0062	0.0003	0.0008	0.0004	0.0004	0.0001	19.90	0.09	380	2.28		383
5	4.3676	0.0121	0.2195	0.0014	0.0026	0.0001	0.0001	0.0004	0.0000	0.0000	19.86	0.14	379	2.98		383
6	6.2684	0.0165	0.3138	0.0012	0.0036	0.0002	0.0009	0.0004	0.0001	0.0000	19.90	0.09	379	2.34		383
7	7.1078	0.0161	0.3526	0.0014	0.0041	0.0002	0.0008	0.0004	0.0002	0.0000	19.98	0.10	381	2.40		385
8	2.4425	0.0065	0.1228	0.0007	0.0014	0.0001	0.0004	0.0004	0.0001	0.0000	19.75	0.14	377	2.88		381
9	7.8371	0.0122	0.3941	0.0018	0.0049	0.0002	0.0001	0.0004	0.0000	0.0000	19.86	0.10	379	2.39		383
10	11.6851	0.0309	0.5791	0.0027	0.0072	0.0003	0.0005	0.0004	0.0004	0.0000	19.99	0.11	381	2.54		385
11	5.5421	0.0093	0.2767	0.0006	0.0033	0.0002	0.0000	0.0004	0.0000	0.0000	20.00	0.06	381	1.99		385
12	0.8885	0.0026	0.0431	0.0007	0.0006	0.0000	0.0007	0.0004	0.0000	0.0000	20.35	0.36	387	6.45		391
13	5.3242	0.0081	0.2645	0.0012	0.0032	0.0002	0.0009	0.0004	0.0000	0.0000	20.09	0.10	383	2.43		387
Average Blank	0.0016	0.0002	0.0001	0.0000	0.0000	0.0000	0.0004	0.0001	0.0000	0.0000						

* Data corrected for ^{36}Ar where the ^{36}Ar measurement is > 2x the ^{36}Ar background (blank) measurement

\# Recalculated ages using the decay constant of Min et al., (2000) and GA1550 biotite standard age of 99.8 of Renne et al., (2010)

Single grain fusion analysis
C.22: NF48 Flatraket Harbour Garnetiferous Gneiss without High-Pressure Relicts
61°58'41.50" N
005°14'43.20" E
J value 0.0116 ± 7.25E-05
MAP 215-50
Biotite

Grain	^{40}Ar V	± 1σ	^{39}Ar V	± 1σ	^{38}Ar V	± 1σ	^{37}Ar V	± 1σ	^{36}Ar V	± 1σ	$^{40}Ar^*/^{39}Ar$	± 1σ	Age Ma	± 1σ	Corr?*	$Age^{\#}$ Ma
1	3.1828	0.0038	0.1532	0.0005	0.0019	0.0001	-0.0033	0.0016	0.0001	0.0000	20.49	0.09	386	2.63		390
2	1.4617	0.0021	0.0722	0.0004	0.0009	0.0000	-0.0001	0.0016	0.0000	0.0000	20.10	0.15	379	3.30		383
3	5.5934	0.0039	0.2737	0.0005	0.0035	0.0001	0.0026	0.0016	0.0001	0.0000	20.28	0.05	382	2.34		386
4	5.2115	0.0019	0.2564	0.0005	0.0033	0.0001	0.0004	0.0016	0.0002	0.0000	20.09	0.05	379	2.32		383
5	8.0836	0.0052	0.3954	0.0005	0.0049	0.0001	0.0020	0.0016	0.0003	0.0000	20.21	0.04	381	2.25		385
6	1.0524	0.0032	0.0518	0.0003	0.0006	0.0000	-0.0027	0.0017	0.0000	0.0000	20.12	0.24	380	4.62		383
7	3.9516	0.0110	0.1900	0.0004	0.0022	0.0001	0.0020	0.0017	0.0003	0.0000	20.39	0.08	384	2.60		388
8	4.7087	0.0034	0.2257	0.0004	0.0027	0.0000	0.0005	0.0017	0.0002	0.0000	20.61	0.05	388	2.34		392
9	2.4160	0.0030	0.1177	0.0003	0.0014	0.0000	-0.0006	0.0017	0.0001	0.0000	20.36	0.09	384	2.63		388
10	2.7798	0.0024	0.1372	0.0004	0.0018	0.0001	0.0052	0.0017	0.0001	0.0000	20.09	0.08	379	2.52		383
11	3.2322	0.0037	0.1578	0.0008	0.0019	0.0001	0.0026	0.0017	0.0001	0.0000	20.38	0.12	384	2.94		388
12	4.5409	0.0565	0.2213	0.0028	0.0028	0.0001	0.0016	0.0017	0.0001	0.0000	20.33	0.36	383	6.51	Y	387
Average Blank	0.0109	0.0001	0.0001	0.0000	0.0000	0.0000	0.0001	0.0000	0.0001	0.0000						

* Data corrected for ^{36}Ar where the ^{36}Ar measurement is > 2x the ^{36}Ar background (blank) measurement

\# Recalculated ages using the decay constant of Min et al., (2000) and GA1550 biotite standard age of 99.8 of Renne et al., (2010)

Single grain fusion analysis
C.23: NF49 Flatraket Harbour Garnet Amphibolite
61°58'41.50" N
005°14'43.20" E
J value 0.0114 ± 5.71E-05
MAP 215-50
Biotite

Grain	^{40}Ar V	± 1σ	^{39}Ar V	± 1σ	^{38}Ar V	± 1σ	^{37}Ar V	± 1σ	^{36}Ar V	± 1σ	$^{40}Ar^*/^{39}Ar$	± 1σ	Age Ma	± 1σ	Corr?*	Age# Ma
1	4.0420	0.0087	0.1755	0.0006	0.0023	0.0001	0.0000	0.0006	0.0003	0.0000	22.45	0.10	412	2.47		416
2	10.3651	0.0145	0.4496	0.0009	0.0058	0.0001	0.0009	0.0006	0.0008	0.0000	22.53	0.06	413	2.08		417
3	7.1874	0.0096	0.3011	0.0006	0.0039	0.0001	-0.0002	0.0006	0.0012	0.0000	22.72	0.06	416	2.10		420
4	5.9868	0.0089	0.2577	0.0004	0.0034	0.0001	-0.0002	0.0004	0.0010	0.0000	22.09	0.06	406	2.05		410
5	4.4197	0.0075	0.1791	0.0004	0.0025	0.0000	0.0008	0.0004	0.0012	0.0000	22.67	0.08	415	2.23		419
6	9.5146	0.0097	0.4048	0.0004	0.0054	0.0001	0.0006	0.0004	0.0018	0.0000	22.22	0.04	408	1.93		412
7	11.1317	0.0081	0.4860	0.0004	0.0064	0.0001	0.0180	0.0004	0.0006	0.0000	22.54	0.03	413	1.91		417
8	1.8247	0.0072	0.0759	0.0004	0.0011	0.0000	0.0000	0.0004	0.0004	0.0000	22.30	0.16	409	3.16		413
9	3.4945	0.0074	0.1480	0.0004	0.0020	0.0001	-0.0004	0.0004	0.0003	0.0000	22.95	0.09	420	2.37		424
10	4.4003	0.0074	0.1908	0.0005	0.0025	0.0000	0.0006	0.0004	0.0003	0.0000	22.53	0.08	413	2.25		417
11	5.7894	0.0055	0.2490	0.0004	0.0020	0.0005	0.0054	0.0003	0.0004	0.0000	22.83	0.05	418	2.02		422
12	3.6373	0.0045	0.1619	0.0003	0.0020	0.0000	0.0001	0.0003	0.0001	0.0000	22.32	0.07	409	2.14		414
Average Blank	0.0063	0.0001	0.0001	0.0000	0.0000	0.0000	0.0001	0.0000	0.0001	0.0000						

* Data corrected for ^{36}Ar where the ^{36}Ar measurement is > 2x the ^{36}Ar background (blank) measurement
# Recalculated ages using the decay constant of Min et al., (2000) and GA1550 biotite standard age of 99.8 of Renne et al., (2010)

Single grain fusion analysis
C.24: NF49 Flatraket Harbour Garnet Amphibolite
61°58'41.50" N
005°14'43.20" E
J value 0.0114 ± 5.71E-05
MAP 215-50
Amphibole

Grain	^{40}Ar V	± 1σ	^{39}Ar V	± 1σ	^{38}Ar V	± 1σ	^{37}Ar V	± 1σ	^{36}Ar V	± 1σ	$^{40}Ar^*/^{39}Ar$	± 1σ	Age Ma	± 1σ	Corr?*	Age# Ma
1	0.1810	0.0011	0.0035	0.0002	0.0002	0.0001	-0.0044	0.0037	0.0001	0.0000	52.25	2.43	569	22.81		575
2	0.7122	0.0013	0.0181	0.0004	0.0005	0.0001	0.1674	0.0062	0.0002	0.0000	39.29	0.82	444	8.40		448
3	1.5212	0.0019	0.0235	0.0004	0.0004	0.0001	0.1775	0.0062	0.0001	0.0000	64.82	1.21	683	10.97		690
4	0.5563	0.0021	0.0066	0.0002	0.0002	0.0001	0.0953	0.0069	0.0001	0.0000	84.68	2.76	849	22.31		858
5	2.4557	0.0023	0.0703	0.0008	0.0011	0.0001	0.1357	0.0069	0.0001	0.0000	34.93	0.39	400	4.41		404
6	0.6052	0.0015	0.0118	0.0003	0.0002	0.0001	0.1403	0.0069	0.0002	0.0000	51.49	1.16	562	11.14		568
7	3.0791	0.0100	0.0919	0.0009	0.0014	0.0001	0.0024	0.0069	0.0002	0.0000	33.50	0.35	385	4.05		389
Average Blank	0.0102	0.0003	0.0002	0.0001	0.0001	0.0000	0.0006	0.0001	0.0002	0.0000						

* Data corrected for ^{36}Ar where the ^{36}Ar measurement is > 2x the ^{36}Ar background (blank) measurement
# Recalculated ages using the decay constant of Min et al., (2000) and GA1550 biotite standard age of 99.8 of Renne et al., (2010)

Single grain fusion analysis
C.25: NF50 Flatraket Harbour Garnet-Biotite Gneiss
61°58'41.50" N
005°14'43.20" E
J value 0.0116 ± 5.78E-05
MAP 215-50
Biotite

Grain	^{40}Ar V	± 1σ	^{39}Ar V	± 1σ	^{38}Ar V	± 1σ	^{37}Ar V	± 1σ	^{36}Ar V	± 1σ	$^{40}Ar^*/^{39}Ar$	± 1σ	Age Ma	± 1σ	Corr?*	Age# Ma
1	1.0555	0.0014	0.0505	0.0002	0.0007	0.0000	0.0004	0.0003	0.0000	0.0000	20.70	0.11	387	2.48		391
2	2.3878	0.0027	0.1134	0.0002	0.0015	0.0000	0.0075	0.0003	0.0000	0.0000	20.95	0.07	391	2.11		395
3	3.3463	0.0021	0.1590	0.0003	0.0021	0.0000	0.0036	0.0003	0.0001	0.0000	20.93	0.04	391	1.91		395
4	1.8242	0.0019	0.0875	0.0002	0.0011	0.0000	-0.0007	0.0002	0.0000	0.0000	20.74	0.09	388	2.31		391
5	2.8501	0.0015	0.1360	0.0003	0.0018	0.0000	0.0005	0.0002	0.0001	0.0000	20.80	0.05	389	1.95		393
6	2.2260	0.0012	0.1096	0.0001	0.0013	0.0000	0.0003	0.0002	0.0000	0.0000	20.25	0.06	379	2.00		383
7	2.8266	0.0018	0.1335	0.0002	0.0018	0.0000	0.0011	0.0002	0.0001	0.0000	20.89	0.04	390	1.87		394
8	3.9750	0.0028	0.1908	0.0002	0.0026	0.0000	0.0009	0.0002	0.0001	0.0000	20.70	0.03	387	1.84		391
9	1.8588	0.0021	0.0884	0.0002	0.0008	0.0002	0.0000	0.0004	0.0000	0.0000	21.00	0.08	392	2.26		396
10	9.8314	0.0091	0.4684	0.0005	0.0058	0.0001	0.0122	0.0004	0.0010	0.0000	20.37	0.03	381	1.81		385
11	6.3321	0.0296	0.3031	0.0013	0.0037	0.0001	0.0117	0.0004	0.0001	0.0000	20.76	0.13	388	2.86		392
12	4.8457	0.0064	0.2260	0.0004	0.0024	0.0007	0.0000	0.0004	0.0001	0.0000	21.28	0.06	397	2.02		401
Average Blank	0.0057	0.0001	0.0001	0.0000	0.0000	0.0000	0.0000	0.0000	0.0000	0.0000						

* Data corrected for ^{36}Ar where the ^{36}Ar measurement is > 2x the ^{36}Ar background (blank) measurement
# Recalculated ages using the decay constant of Min et al., (2000) and GA1550 biotite standard age of 99.8 of Renne et al., (2010)

Single grain fusion analysis
C.26: NF51 Flatraket Harbour Biotite-Epidote Gneiss without Relict White Mica
61°58'41.50" N
005°14'43.20" E
J value 0.0090 ± 1.84E-05
ARGUS
Biotite

Grain	^{40}Ar V	± 1σ	^{39}Ar V	± 1σ	^{38}Ar V	± 1σ	^{37}Ar V	± 1σ	^{36}Ar V	± 1σ	$^{40}Ar^*/^{39}Ar$	± 1σ	Age Ma	± 1σ	Corr?*	$Age^{\#}$ Ma
1	0.4217	0.0013	0.0153	0.0001	0.0002	0.0000	-0.0001	0.0000	0.0000	0.0000	28.33	0.41	412	5.32		417
2	1.0932	0.0009	0.0416	0.0001	0.0004	0.0000	-0.0001	0.0000	0.0000	0.0000	26.28	0.11	385	1.44		389
3	0.4516	0.0013	0.0166	0.0001	0.0001	0.0000	-0.0001	0.0000	0.0000	0.0000	27.93	0.33	407	4.26		411
4	1.6238	0.0011	0.0599	0.0001	0.0007	0.0000	-0.0001	0.0000	0.0000	0.0000	26.86	0.08	393	1.05		397
5	0.7957	0.0006	0.0296	0.0001	0.0003	0.0000	-0.0001	0.0000	0.0000	0.0000	26.85	0.16	393	2.13		397
6	1.2325	0.0008	0.0452	0.0001	0.0005	0.0000	-0.0001	0.0000	0.0000	0.0000	27.22	0.11	398	1.39		402
7	1.3709	0.0009	0.0514	0.0001	0.0006	0.0000	-0.0001	0.0000	-0.0001	0.0000	26.90	0.10	394	1.35		398
8	1.4616	0.0012	0.0545	0.0001	0.0006	0.0000	-0.0002	0.0000	0.0000	0.0000	26.85	0.11	393	1.45		397
9	1.3583	0.0012	0.0505	0.0001	0.0006	0.0000	-0.0001	0.0000	0.0000	0.0000	27.03	0.09	395	1.20		399
10	3.6616	0.0017	0.1363	0.0001	0.0016	0.0000	-0.0002	0.0000	0.0001	0.0000	26.57	0.05	389	0.60		393
11	1.1678	0.0010	0.0443	0.0001	0.0005	0.0000	0.0000	0.0000	0.0001	0.0000	25.97	0.13	381	1.76		385
12	2.4784	0.0015	0.0923	0.0001	0.0011	0.0000	-0.0001	0.0000	0.0000	0.0000	26.65	0.05	390	0.59		394
13	1.1121	0.0009	0.0414	0.0001	0.0005	0.0000	-0.0001	0.0000	0.0000	0.0000	26.54	0.15	389	1.98		393
14	1.7136	0.0010	0.0629	0.0001	0.0007	0.0000	-0.0001	0.0000	0.0001	0.0000	26.84	0.08	393	0.99		397
15	0.8565	0.0008	0.0320	0.0001	0.0003	0.0000	-0.0001	0.0000	-0.0001	0.0000	27.28	0.15	399	1.98		403

Single grain fusion analysis
C.26: NF51 Flatraket Harbour Biotite-Epidote Gneiss without Relict White Mica
61°58'41.50" N
005°14'43.20" E
J value 0.0090 ± 1.84E-05
ARGUS
Biotite

Grain	^{40}Ar V	± 1σ	^{39}Ar V	± 1σ	^{38}Ar V	± 1σ	^{37}Ar V	± 1σ	^{36}Ar V	± 1σ	$^{40}Ar^*/^{39}Ar$	± 1σ	Age Ma	± 1σ	Corr?*	Age# Ma
16	0.7901	0.0008	0.0293	0.0001	0.0003	0.0000	-0.0001	0.0000	0.0000	0.0000	27.22	0.20	398	2.66		402
17	1.5440	0.0013	0.0579	0.0001	0.0007	0.0000	-0.0001	0.0000	0.0000	0.0000	26.58	0.11	389	1.40		393
18	0.8904	0.0007	0.0331	0.0001	0.0003	0.0000	0.0000	0.0000	-0.0001	0.0000	27.30	0.18	399	2.30		403
19	1.4677	0.0011	0.0562	0.0001	0.0006	0.0000	-0.0001	0.0000	0.0000	0.0000	26.04	0.11	382	1.43		386
20	1.2783	0.0009	0.0475	0.0001	0.0006	0.0000	0.0000	0.0000	0.0000	0.0000	26.99	0.11	395	1.43		399
21	2.1550	0.0013	0.0805	0.0001	0.0010	0.0000	0.0000	0.0000	0.0000	0.0000	26.83	0.06	393	0.76		397
22	0.8780	0.0006	0.0327	0.0001	0.0003	0.0000	-0.0001	0.0000	0.0000	0.0000	26.78	0.16	392	2.11		396
23	1.4108	0.0010	0.0522	0.0001	0.0006	0.0000	-0.0001	0.0000	0.0001	0.0000	26.68	0.09	391	1.23		395
24	1.3467	0.0010	0.0496	0.0001	0.0005	0.0000	-0.0001	0.0000	0.0000	0.0000	26.93	0.12	394	1.57		398
25	1.7217	0.0010	0.0624	0.0001	0.0007	0.0000	-0.0002	0.0000	0.0000	0.0000	27.38	0.08	400	1.09		404
Average Blank	0.0046	0.0000	0.0006	0.0000	0.0002	0.0000	0.0003	0.0000	0.0003	0.0000						

* Data corrected for ^{36}Ar where the ^{36}Ar measurement is > 2x the ^{36}Ar background (blank) measurement
# Recalculated ages using the decay constant of Min et al., (2000) and GA1550 biotite standard age of 99.8 of Renne et al., (2010)

Single grain fusion analysis
C.27: NF112 Flatraket Harbour Garnet-Biotite Gneiss
61°58'41.50" N
005°14'43.20" E
J value 0.0097 ± 4.83E-05
MAP 215-50
Biotite

Grain	^{40}Ar V	± 1σ	^{39}Ar V	± 1σ	^{38}Ar V	± 1σ	^{37}Ar V	± 1σ	^{36}Ar V	± 1σ	$^{40}Ar^*/^{39}Ar$	± 1σ	Age Ma	± 1σ	Corr?*	Age# Ma
1	1.1644	0.0029	0.0451	0.0003	0.0007	0.0001	-0.0038	0.0050	0.0000	0.0000	25.82	0.17	402	2.95		406
2	0.5297	0.0015	0.0207	0.0004	0.0003	0.0000	-0.0006	0.0050	0.0000	0.0000	25.59	0.55	399	7.96		403
3	1.3720	0.0043	0.0522	0.0005	0.0008	0.0000	-0.0069	0.0050	0.0001	0.0000	26.30	0.26	408	4.03		413
4	1.4051	0.0059	0.0552	0.0006	0.0007	0.0001	0.0002	0.0040	0.0000	0.0000	25.45	0.28	397	4.31		401
5	0.7442	0.0017	0.0286	0.0005	0.0003	0.0001	-0.0024	0.0040	0.0000	0.0000	26.01	0.42	404	6.17		409
6	2.1509	0.0058	0.0828	0.0007	0.0010	0.0001	-0.0049	0.0040	0.0001	0.0000	25.61	0.24	399	3.75	Y	403
7	1.8316	0.0026	0.0703	0.0005	0.0009	0.0001	0.0002	0.0040	0.0001	0.0000	26.05	0.19	405	3.16		409
8	1.7204	0.0030	0.0653	0.0006	0.0008	0.0001	-0.0024	0.0040	0.0000	0.0000	26.33	0.23	409	3.66		413
9	1.0096	0.0025	0.0390	0.0006	0.0004	0.0001	-0.0011	0.0040	0.0000	0.0000	25.88	0.41	403	6.03		407
10	0.6273	0.0012	0.0239	0.0004	0.0003	0.0001	-0.0043	0.0040	0.0000	0.0000	26.27	0.39	408	5.69		412
11	0.7302	0.0026	0.0287	0.0004	0.0003	0.0001	-0.0030	0.0040	0.0000	0.0000	25.44	0.37	396	5.42		400
12	0.6444	0.0019	0.0238	0.0005	0.0002	0.0000	-0.0030	0.0040	0.0000	0.0000	27.02	0.53	418	7.55		423
13	0.7743	0.0023	0.0291	0.0006	0.0003	0.0001	-0.0011	0.0040	0.0000	0.0000	26.57	0.58	412	8.32		416
14	0.8002	0.0028	0.0306	0.0003	0.0004	0.0001	-0.0043	0.0040	0.0000	0.0000	26.16	0.26	406	4.10		411
15	0.7951	0.0031	0.0308	0.0003	0.0004	0.0001	-0.0005	0.0040	0.0000	0.0000	25.83	0.30	402	4.59		406
Average Blank	0.0053	0.0003	0.0001	0.0000	0.0001	0.0000	0.0004	0.0001	0.0001	0.0000						

* Data corrected for ^{36}Ar where the ^{36}Ar measurement is > 2x the ^{36}Ar background (blank) measurement
# Recalculated ages using the decay constant of Min et al., (2000) and GA1550 biotite standard age of 99.8 of Renne et al., (2010)

Single grain fusion analysis
C.28: NF87 Drage Garnet-Biotite Gneiss
62°06'08.3'' N
005°12'48.0'' E
J value 0.0090 ± 1.80E-05
ARGUS
Biotite

Grain	^{40}Ar V	± 1σ	^{39}Ar V	± 1σ	^{38}Ar V	± 1σ	^{37}Ar V	± 1σ	^{36}Ar V	± 1σ	$^{40}Ar^*/^{39}Ar$	± 1σ	Age Ma	± 1σ	Corr?*	$Age^{\#}$ Ma
1	1.5307	0.0014	0.0584	0.0001	0.0007	0.0000	-0.0001	0.0000	0.0000	0.0000	26.26	0.09	385	1.13		389
2	2.0678	0.0014	0.0798	0.0001	0.0010	0.0000	-0.0001	0.0000	0.0000	0.0000	25.98	0.07	381	0.95		385
3	2.0930	0.0014	0.0798	0.0001	0.0010	0.0000	-0.0001	0.0000	0.0000	0.0000	26.21	0.06	384	0.82		388
4	1.6003	0.0015	0.0608	0.0001	0.0007	0.0000	0.0000	0.0000	0.0000	0.0000	26.35	0.11	386	1.42		390
5	1.3861	0.0014	0.0517	0.0001	0.0006	0.0000	-0.0001	0.0000	0.0000	0.0000	26.60	0.10	390	1.32		394
6	1.9783	0.0015	0.0759	0.0001	0.0009	0.0000	-0.0001	0.0000	0.0000	0.0000	26.05	0.06	382	0.80		386
7	1.7656	0.0015	0.0676	0.0001	0.0008	0.0000	-0.0001	0.0000	0.0000	0.0000	26.07	0.10	383	1.30		387
8	1.1556	0.0014	0.0439	0.0001	0.0006	0.0000	-0.0001	0.0000	0.0000	0.0000	26.10	0.10	383	1.30		387
9	1.2539	0.0014	0.0479	0.0001	0.0006	0.0000	0.0000	0.0000	0.0000	0.0000	26.07	0.15	383	1.93		387
10	1.7099	0.0016	0.0656	0.0001	0.0008	0.0000	0.0000	0.0000	0.0000	0.0000	25.97	0.09	381	1.20		385
11	0.5174	0.0007	0.0197	0.0001	0.0002	0.0000	0.0000	0.0000	0.0000	0.0000	25.72	0.32	378	4.26		382
12	0.6897	0.0009	0.0261	0.0001	0.0003	0.0000	0.0000	0.0000	0.0000	0.0000	26.47	0.20	388	2.61		392
13	0.7308	0.0012	0.0279	0.0001	0.0003	0.0000	0.0000	0.0000	0.0000	0.0000	26.12	0.18	383	2.41		387
14	0.9827	0.0010	0.0375	0.0001	0.0005	0.0000	-0.0001	0.0000	0.0000	0.0000	26.39	0.16	387	2.17		391
15	3.1118	0.0017	0.1198	0.0001	0.0015	0.0000	0.0000	0.0000	0.0000	0.0000	25.83	0.05	379	0.65		383

Single grain fusion analysis
C.28: NF87 Drage Garnet-Biotite Gneiss
62°06'08.3" N
005°12'48.0" E
J value 0.0090 ± 1.80E-05
ARGUS
Biotite

Grain	^{40}Ar V	± 1σ	^{39}Ar V	± 1σ	^{38}Ar V	± 1σ	^{37}Ar V	± 1σ	^{36}Ar V	± 1σ	$^{40}Ar^*/^{39}Ar$	± 1σ	Age Ma	± 1σ	Corr?*	Age# Ma
16	2.5828	0.0015	0.0981	0.0001	0.0012	0.0000	-0.0001	0.0000	0.0000	0.0000	26.32	0.05	386	0.69		390
17	3.5134	0.0018	0.1345	0.0001	0.0016	0.0000	-0.0001	0.0000	0.0000	0.0000	26.02	0.04	382	0.58		386
18	3.5596	0.0017	0.1351	0.0001	0.0016	0.0000	-0.0001	0.0000	0.0000	0.0000	26.22	0.04	385	0.58		389
19	1.8477	0.0015	0.0703	0.0001	0.0008	0.0000	-0.0001	0.0000	0.0000	0.0000	26.39	0.06	387	0.85		391
20	4.4594	0.0019	0.1702	0.0002	0.0021	0.0000	0.0000	0.0000	0.0001	0.0000	26.06	0.04	383	0.47		386
21	0.6557	0.0007	0.0249	0.0001	0.0003	0.0000	-0.0001	0.0000	0.0000	0.0000	26.05	0.25	382	3.35		386
22	1.3478	0.0013	0.0511	0.0001	0.0006	0.0000	-0.0001	0.0000	0.0000	0.0000	26.14	0.12	384	1.58		387
23	1.1202	0.0012	0.0424	0.0001	0.0005	0.0000	-0.0001	0.0000	0.0000	0.0000	26.16	0.12	384	1.61		388
24	2.7249	0.0016	0.1045	0.0001	0.0013	0.0000	-0.0001	0.0000	0.0000	0.0000	25.99	0.07	382	0.89		386
25	3.6451	0.0018	0.1384	0.0001	0.0016	0.0000	-0.0001	0.0000	0.0000	0.0000	26.32	0.04	386	0.54		390
Average Blank	0.0046	0.0000	0.0006	0.0000	0.0002	0.0000	0.0003	0.0000	0.0003	0.0000						

* Data corrected for ^{36}Ar where the ^{36}Ar measurement is > 2x the ^{36}Ar background (blank) measurement
# Recalculated ages using the decay constant of Min et al., (2000) and GA1550 biotite standard age of 99.8 of Renne et al., (2010)

Single grain fusion analysis
C.29: NF88 Drage Garnetiferous Gneiss without High-Pressure Relicts
62°06'08.3" N
005°12'48.0" E
J value 0.0091 ± 1.80E-05
ARGUS
White Mica

Grain	^{40}Ar V	± 1σ	^{39}Ar V	± 1σ	^{38}Ar V	± 1σ	^{37}Ar V	± 1σ	^{36}Ar V	± 1σ	$^{40}Ar^*/^{39}Ar$	± 1σ	Age Ma	± 1σ	Corr?*	$Age^{\#}$ Ma
1	2.1901	0.0011	0.0829	0.0001	0.0009	0.0000	-0.0001	0.0000	-0.0001	0.0000	26.70	0.06	393	0.76		397
2	2.4443	0.0015	0.0924	0.0001	0.0012	0.0000	0.0000	0.0000	0.0001	0.0000	25.99	0.06	383	0.84		387
3	1.8321	0.0015	0.0695	0.0001	0.0009	0.0000	0.0000	0.0000	0.0000	0.0000	26.12	0.08	385	1.05		389
4	3.9443	0.0017	0.1489	0.0002	0.0019	0.0000	-0.0001	0.0000	0.0001	0.0000	26.18	0.05	386	0.67		390
5	6.0300	0.0027	0.2280	0.0002	0.0027	0.0000	-0.0001	0.0000	0.0001	0.0000	26.23	0.03	386	0.45		390
6	2.6981	0.0014	0.1016	0.0001	0.0013	0.0000	-0.0001	0.0000	0.0001	0.0000	26.18	0.06	386	0.78		390
7	2.8360	0.0014	0.1070	0.0001	0.0013	0.0000	0.0000	0.0000	0.0001	0.0000	26.22	0.06	386	0.74		390
8	1.2730	0.0014	0.0481	0.0001	0.0006	0.0000	0.0000	0.0000	0.0000	0.0000	26.25	0.13	387	1.66		390
9	2.2803	0.0015	0.0863	0.0001	0.0011	0.0000	0.0000	0.0000	0.0000	0.0000	26.25	0.06	387	0.83		391
10	0.7303	0.0010	0.0271	0.0001	0.0004	0.0000	0.0001	0.0000	0.0001	0.0000	26.22	0.22	386	2.88		390
11	1.8420	0.0012	0.0695	0.0001	0.0009	0.0000	0.0000	0.0000	0.0001	0.0000	26.20	0.08	386	1.06		390
12	1.6386	0.0013	0.0621	0.0001	0.0008	0.0000	-0.0001	0.0000	0.0001	0.0000	26.05	0.09	384	1.26		388
13	3.6351	0.0015	0.1381	0.0001	0.0017	0.0000	-0.0001	0.0000	0.0000	0.0000	26.21	0.04	386	0.50		390
14	2.2654	0.0012	0.0858	0.0001	0.0011	0.0000	0.0000	0.0000	0.0000	0.0000	26.25	0.06	387	0.76		391
15	2.4886	0.0013	0.0929	0.0001	0.0011	0.0000	-0.0001	0.0000	0.0002	0.0000	26.27	0.06	387	0.86		391

Single grain fusion analysis
C.29: NF88 Drage Garnetiferous Gneiss without High-Pressure Relicts
62°06'08.3'' N
005°12'48.0'' E
J value 0.0091 ± 1.80E-05
ARGUS
White Mica

Grain	^{40}Ar V	± 1σ	^{39}Ar V	± 1σ	^{38}Ar V	± 1σ	^{37}Ar V	± 1σ	^{36}Ar V	± 1σ	$^{40}Ar^*/^{39}Ar$	± 1σ	Age Ma	± 1σ	Corr?*	Age# Ma
16	1.5490	0.0010	0.0587	0.0001	0.0007	0.0000	0.0000	0.0000	0.0000	0.0000	26.26	0.10	387	1.37		391
17	1.8209	0.0012	0.0688	0.0001	0.0008	0.0000	0.0000	0.0000	0.0000	0.0000	26.36	0.08	388	1.02		392
18	2.8250	0.0012	0.1065	0.0001	0.0012	0.0000	-0.0001	0.0000	0.0000	0.0000	26.45	0.06	389	0.78		393
19	1.1648	0.0009	0.0435	0.0001	0.0005	0.0000	-0.0001	0.0000	0.0000	0.0000	26.91	0.11	395	1.43		399
20	3.2798	0.0014	0.1244	0.0001	0.0014	0.0000	-0.0001	0.0000	-0.0001	0.0000	26.48	0.04	390	0.52		394
21	2.6966	0.0013	0.1022	0.0001	0.0011	0.0000	-0.0001	0.0000	0.0000	0.0000	26.45	0.06	389	0.81		393
22	4.0259	0.0016	0.1518	0.0001	0.0018	0.0000	-0.0001	0.0000	0.0000	0.0000	26.54	0.04	390	0.51		394
23	2.1374	0.0010	0.0800	0.0001	0.0009	0.0000	-0.0001	0.0000	-0.0001	0.0000	26.91	0.06	395	0.80		399
24	3.2607	0.0014	0.1232	0.0001	0.0013	0.0000	-0.0001	0.0000	-0.0001	0.0000	26.68	0.05	392	0.63		396
25	8.7594	0.0035	0.3308	0.0003	0.0039	0.0000	-0.0001	0.0000	0.0001	0.0000	26.34	0.03	388	0.36		392
Average Blank	0.0046	0.0000	0.0006	0.0000	0.0002	0.0000	0.0003	0.0000	0.0003	0.0000						

* Data corrected for ^{36}Ar where the ^{36}Ar measurement is > 2x the ^{36}Ar background (blank) measurement
# Recalculated ages using the decay constant of Min et al., (2000) and GA1550 biotite standard age of 99.8 of Renne et al., (2010)

Single grain fusion analysis
C.30: NF88 Drage Garnetiferous Gneiss without High-Pressure Relicts
62°06'08.3" N
005°12'48.0" E
J value 0.0092 ± 1.72E-05
ARGUS
Biotite

Grain	^{40}Ar V	± 1σ	^{39}Ar V	± 1σ	^{38}Ar V	± 1σ	^{37}Ar V	± 1σ	^{36}Ar V	± 1σ	$^{40}Ar^*/^{39}Ar$	± 1σ	Age Ma	± 1σ	Corr?*	$Age^{\#}$ Ma
1	5.2708	0.0024	0.2020	0.0002	0.0025	0.0000	0.0000	0.0000	0.0001	0.0000	25.90	0.03	384	0.46		388
2	3.3425	0.0015	0.1276	0.0001	0.0016	0.0000	0.0000	0.0000	0.0001	0.0000	25.95	0.05	385	0.65		389
3	2.5052	0.0014	0.0958	0.0001	0.0012	0.0000	0.0000	0.0000	0.0001	0.0000	25.87	0.06	384	0.86		388
4	3.0495	0.0014	0.1165	0.0001	0.0015	0.0000	0.0000	0.0000	0.0001	0.0000	25.98	0.04	385	0.58		389
5	0.9387	0.0011	0.0359	0.0001	0.0005	0.0000	0.0000	0.0000	0.0001	0.0000	25.64	0.17	381	2.34		385
6	1.7892	0.0012	0.0675	0.0001	0.0009	0.0000	0.0000	0.0000	0.0001	0.0000	25.93	0.09	385	1.16		389
7	4.9270	0.0023	0.1871	0.0002	0.0023	0.0000	-0.0001	0.0000	0.0001	0.0000	26.09	0.04	387	0.48		391
8	1.0372	0.0012	0.0395	0.0001	0.0005	0.0000	0.0000	0.0000	0.0000	0.0000	25.82	0.14	383	1.82		387
9	1.5003	0.0011	0.0571	0.0001	0.0007	0.0000	0.0000	0.0000	0.0002	0.0000	25.36	0.09	377	1.17		381
10	1.2585	0.0011	0.0481	0.0001	0.0006	0.0000	0.0000	0.0000	0.0001	0.0000	25.56	0.11	380	1.43		384
11	1.0907	0.0012	0.0418	0.0001	0.0006	0.0000	0.0001	0.0000	0.0001	0.0000	25.38	0.14	377	1.83		381
12	1.1837	0.0012	0.0453	0.0001	0.0006	0.0000	0.0000	0.0000	0.0000	0.0000	26.10	0.10	387	1.36		391
13	5.3199	0.0023	0.2030	0.0002	0.0025	0.0000	0.0000	0.0000	0.0001	0.0000	26.00	0.03	386	0.46		390
14	2.5172	0.0014	0.0956	0.0001	0.0012	0.0000	0.0000	0.0000	0.0000	0.0000	26.14	0.06	388	0.86		392
15	1.8055	0.0014	0.0691	0.0001	0.0009	0.0000	0.0000	0.0000	0.0000	0.0000	25.88	0.08	384	1.03		388

Single grain fusion analysis
C.30: NF88 Drage Garnetiferous Gneiss without High-Pressure Relicts
62°06'08.3" N
005°12'48.0" E
J value 0.0092 ± 1.72E-05
ARGUS
Biotite

Grain	^{40}Ar V	± 1σ	^{39}Ar V	± 1σ	^{38}Ar V	± 1σ	^{37}Ar V	± 1σ	^{36}Ar V	± 1σ	$^{40}Ar^*/^{39}Ar$	± 1σ	Age Ma	± 1σ	Corr?*	Age# Ma
16	3.2248	0.0014	0.1239	0.0001	0.0016	0.0000	0.0000	0.0000	0.0001	0.0000	25.77	0.04	383	0.57		387
17	1.3319	0.0013	0.0502	0.0001	0.0006	0.0000	0.0000	0.0000	0.0001	0.0000	26.05	0.09	386	1.19		390
18	1.1281	0.0013	0.0428	0.0001	0.0006	0.0000	0.0000	0.0000	0.0001	0.0000	25.74	0.11	382	1.47		386
19	0.6363	0.0009	0.0241	0.0001	0.0003	0.0000	0.0000	0.0000	0.0001	0.0000	25.43	0.21	378	2.83		382
20	2.7018	0.0014	0.1026	0.0001	0.0013	0.0000	-0.0001	0.0000	0.0001	0.0000	25.93	0.05	385	0.62		389
21	2.7837	0.0015	0.1062	0.0001	0.0014	0.0000	0.0000	0.0000	0.0000	0.0000	26.06	0.05	387	0.65		391
22	2.0942	0.0014	0.0796	0.0001	0.0010	0.0000	0.0000	0.0000	0.0001	0.0000	25.87	0.05	384	0.71		388
23	0.7113	0.0010	0.0273	0.0001	0.0004	0.0000	0.0000	0.0000	0.0001	0.0000	25.20	0.17	375	2.22		379
24	4.0055	0.0017	0.1527	0.0001	0.0019	0.0000	-0.0001	0.0000	0.0001	0.0000	26.04	0.04	386	0.55		390
25	2.8052	0.0016	0.1070	0.0001	0.0014	0.0000	-0.0001	0.0000	0.0001	0.0000	25.95	0.07	385	0.92		389
Average Blank	0.0046	0.0000	0.0006	0.0000	0.0002	0.0000	0.0003	0.0000	0.0003	0.0000						

* Data corrected for ^{36}Ar where the ^{36}Ar measurement is > 2x the ^{36}Ar background (blank) measurement
# Recalculated ages using the decay constant of Min et al., (2000) and GA1550 biotite standard age of 99.8 of Renne et al., (2010)

Single grain fusion analysis
C.31: NF89 Drage Garnetiferous Gneiss without High-Pressure Relicts
62°06'08.3" N
005°12'48.0" E
J value 0.0092 ± 1.74E-05
ARGUS
White Mica

Grain	^{40}Ar V	± 1σ	^{39}Ar V	± 1σ	^{38}Ar V	± 1σ	^{37}Ar V	± 1σ	^{36}Ar V	± 1σ	$^{40}Ar^*/^{39}Ar$	± 1σ	Age Ma	± 1σ	Corr?*	$Age^{\#}$ Ma
1	6.1305	0.0027	0.2306	0.0002	0.0027	0.0000	-0.0002	0.0000	0.0002	0.0000	26.30	0.04	392	0.47		396
2	1.3642	0.0012	0.0519	0.0001	0.0007	0.0000	0.0000	0.0000	0.0001	0.0000	25.77	0.10	385	1.31		389
3	1.1693	0.0012	0.0444	0.0001	0.0006	0.0000	0.0000	0.0000	0.0001	0.0000	25.74	0.13	384	1.73		388
4	2.4019	0.0014	0.0910	0.0001	0.0011	0.0000	0.0000	0.0000	0.0001	0.0000	26.12	0.07	389	0.98		393
5	1.9474	0.0013	0.0736	0.0001	0.0009	0.0000	0.0000	0.0000	0.0001	0.0000	26.15	0.08	390	1.10		394
6	2.4409	0.0013	0.0919	0.0001	0.0012	0.0000	0.0000	0.0000	0.0002	0.0000	26.00	0.06	388	0.77		392
7	1.4302	0.0012	0.0540	0.0001	0.0007	0.0000	0.0000	0.0000	0.0001	0.0000	25.97	0.09	387	1.26		391
8	2.8185	0.0014	0.1071	0.0001	0.0014	0.0000	0.0000	0.0000	0.0001	0.0000	26.01	0.06	388	0.76		392
9	0.5765	0.0008	0.0215	0.0001	0.0004	0.0000	0.0000	0.0000	0.0001	0.0000	25.22	0.27	377	3.64		381
10	0.7315	0.0010	0.0279	0.0001	0.0004	0.0000	0.0000	0.0000	0.0001	0.0000	25.15	0.16	376	2.19		380
11	0.8201	0.0010	0.0313	0.0001	0.0004	0.0000	0.0000	0.0000	0.0001	0.0000	25.34	0.21	379	2.86		383
12	2.3647	0.0012	0.0901	0.0001	0.0011	0.0000	0.0000	0.0000	0.0001	0.0000	25.87	0.06	386	0.83		390
13	2.1668	0.0012	0.0815	0.0001	0.0010	0.0000	0.0000	0.0000	0.0001	0.0000	26.07	0.09	389	1.14		393
14	1.5988	0.0011	0.0606	0.0001	0.0008	0.0000	0.0000	0.0000	0.0001	0.0000	25.96	0.08	387	1.13		391
15	4.3708	0.0020	0.1659	0.0002	0.0020	0.0000	0.0000	0.0000	0.0001	0.0000	26.11	0.04	389	0.51		393

Single grain fusion analysis
C.31: NF89 Drage Garnetiferous Gneiss without High-Pressure Relicts
62°06'08.3" N
005°12'48.0" E
J value 0.0092 ± 1.74E-05
ARGUS
White Mica

Grain	^{40}Ar V	± 1σ	^{39}Ar V	± 1σ	^{38}Ar V	± 1σ	^{37}Ar V	± 1σ	^{36}Ar V	± 1σ	$^{40}Ar^*/^{39}Ar$	± 1σ	Age Ma	± 1σ	Corr?*	$Age^{\#}$ Ma
16	1.6325	0.0012	0.0617	0.0001	0.0008	0.0000	0.0000	0.0000	0.0001	0.0000	26.09	0.08	389	1.06		393
17	0.5009	0.0005	0.0192	0.0001	0.0003	0.0000	0.0000	0.0000	0.0001	0.0000	25.06	0.33	375	4.43		379
18	1.7373	0.0011	0.0662	0.0001	0.0009	0.0000	0.0000	0.0000	0.0001	0.0000	25.83	0.07	385	1.00		389
19	3.1020	0.0013	0.1175	0.0001	0.0015	0.0000	0.0000	0.0000	0.0001	0.0000	26.14	0.05	390	0.70		394
20	3.0552	0.0014	0.1162	0.0001	0.0014	0.0000	-0.0001	0.0000	0.0000	0.0000	26.15	0.05	390	0.63		394
21	0.9291	0.0008	0.0344	0.0001	0.0005	0.0000	0.0000	0.0000	0.0001	0.0000	25.81	0.17	385	2.26		389
22	1.0331	0.0008	0.0388	0.0001	0.0004	0.0000	-0.0001	0.0000	0.0001	0.0000	26.03	0.10	388	1.39		392
23	1.4319	0.0009	0.0541	0.0001	0.0007	0.0000	0.0000	0.0000	0.0000	0.0000	26.40	0.11	393	1.47		397
24	3.6233	0.0016	0.1376	0.0001	0.0017	0.0000	-0.0001	0.0000	0.0001	0.0000	26.12	0.05	389	0.66		393
Average Blank	0.0046	0.0000	0.0006	0.0000	0.0002	0.0000	0.0003	0.0000	0.0003	0.0000						

* Data corrected for ^{36}Ar where the ^{36}Ar measurement is > 2x the ^{36}Ar background (blank) measurement
# Recalculated ages using the decay constant of Min et al., (2000) and GA1550 biotite standard age of 99.8 of Renne et al., (2010)

Single grain fusion analysis
C.32: NF89 Drage Garnetiferous Gneiss without High-Pressure Relicts
62°06'08.3" N
005°12'48.0" E
J value 0.0092 ± 1.84E-05
ARGUS
Biotite

Grain	^{40}Ar V	± 1σ	^{39}Ar V	± 1σ	^{38}Ar V	± 1σ	^{37}Ar V	± 1σ	^{36}Ar V	± 1σ	$^{40}Ar^*/^{39}Ar$	± 1σ	Age Ma	± 1σ	Corr?*	Age# Ma
1	2.8153	0.0013	0.1066	0.0001	0.0014	0.0000	0.0000	0.0000	0.0001	0.0000	26.12	0.05	389	0.62		393
2	1.5311	0.0010	0.0584	0.0001	0.0008	0.0000	0.0000	0.0000	0.0000	0.0000	26.02	0.09	388	1.16		392
3	3.0846	0.0015	0.1182	0.0001	0.0015	0.0000	0.0000	0.0000	0.0001	0.0000	25.81	0.04	385	0.58		389
4	1.0440	0.0010	0.0397	0.0001	0.0006	0.0000	0.0000	0.0000	0.0001	0.0000	25.28	0.12	378	1.58		382
5	1.5713	0.0012	0.0597	0.0001	0.0008	0.0000	0.0000	0.0000	0.0001	0.0000	25.65	0.12	383	1.60		387
6	3.3973	0.0015	0.1285	0.0001	0.0017	0.0000	0.0000	0.0000	0.0001	0.0000	26.09	0.05	389	0.62		393
7	3.1328	0.0015	0.1189	0.0001	0.0015	0.0000	0.0000	0.0000	0.0001	0.0000	25.96	0.04	387	0.60		391
8	3.2246	0.0015	0.1215	0.0001	0.0015	0.0000	0.0000	0.0000	0.0001	0.0000	26.15	0.05	390	0.72		394
9	1.4829	0.0010	0.0564	0.0001	0.0008	0.0000	0.0000	0.0000	0.0001	0.0000	25.79	0.11	385	1.47		389
10	1.7452	0.0011	0.0665	0.0001	0.0008	0.0000	0.0000	0.0000	0.0001	0.0000	25.96	0.08	387	1.07		391
11	0.9194	0.0008	0.0350	0.0001	0.0005	0.0000	0.0000	0.0000	0.0001	0.0000	25.53	0.13	381	1.80		385
12	1.6786	0.0011	0.0638	0.0001	0.0008	0.0000	0.0000	0.0000	0.0001	0.0000	26.00	0.08	388	1.06		392
13	1.4772	0.0011	0.0564	0.0001	0.0008	0.0000	0.0000	0.0000	0.0001	0.0000	25.75	0.10	384	1.38		388
14	1.6574	0.0012	0.0631	0.0001	0.0009	0.0000	0.0000	0.0000	0.0001	0.0000	25.79	0.08	385	1.10		389
15	0.7012	0.0007	0.0268	0.0001	0.0004	0.0000	0.0000	0.0000	0.0001	0.0000	25.22	0.24	377	3.20		381

Single grain fusion analysis
C.32: NF89 Drage Garnetiferous Gneiss without High-Pressure Relicts
62°06'08.3" N
005°12'48.0" E
J value 0.0092 ± 1.84E-05
ARGUS
Biotite

Grain	^{40}Ar V	± 1σ	^{39}Ar V	± 1σ	^{38}Ar V	± 1σ	^{37}Ar V	± 1σ	^{36}Ar V	± 1σ	$^{40}Ar^*/^{39}Ar$	± 1σ	Age Ma	± 1σ	Corr?*	Age# Ma
16	1.1004	0.0011	0.0415	0.0001	0.0006	0.0000	0.0000	0.0000	0.0001	0.0000	25.76	0.12	385	1.65		388
17	0.4105	0.0007	0.0155	0.0001	0.0003	0.0000	0.0000	0.0000	0.0001	0.0000	25.02	0.35	375	4.73		378
18	0.9991	0.0009	0.0382	0.0001	0.0006	0.0000	-0.0001	0.0000	0.0001	0.0000	25.32	0.15	379	1.98		382
19	3.0223	0.0015	0.1157	0.0001	0.0015	0.0000	0.0000	0.0000	0.0001	0.0000	25.88	0.04	386	0.60		390
20	1.0524	0.0010	0.0399	0.0001	0.0006	0.0000	0.0000	0.0000	0.0001	0.0000	25.46	0.12	380	1.62		384
21	0.9730	0.0011	0.0369	0.0001	0.0005	0.0000	0.0000	0.0000	0.0001	0.0000	25.88	0.15	386	2.04		390
22	2.2545	0.0013	0.0860	0.0001	0.0012	0.0000	0.0000	0.0000	0.0002	0.0000	25.62	0.06	383	0.82		387
23	1.0794	0.0010	0.0412	0.0001	0.0006	0.0000	0.0000	0.0000	0.0001	0.0000	25.43	0.14	380	1.89		384
24	0.4400	0.0005	0.0167	0.0001	0.0003	0.0000	0.0000	0.0000	0.0000	0.0000	25.67	0.28	383	3.76		387
25	2.3823	0.0014	0.0899	0.0001	0.0012	0.0000	0.0000	0.0000	0.0002	0.0000	25.91	0.07	386	0.87		390
Average Blank	0.0046	0.0000	0.0006	0.0000	0.0002	0.0000	0.0003	0.0000	0.0003	0.0000						

* Data corrected for ^{36}Ar where the ^{36}Ar measurement is > 2x the ^{36}Ar background (blank) measurement
# Recalculated ages using the decay constant of Min et al., (2000) and GA1550 biotite standard age of 99.8 of Renne et al., (2010)

Single grain fusion analysis
C.33: NF90 Drage Biotite-Epidote Gneiss without Relict White Mica
62°06'08.3" N
005°12'48.0" E
J value 0.0092 ± 1.93E-05
ARGUS
Biotite

Grain	^{40}Ar V	± 1σ	^{39}Ar V	± 1σ	^{38}Ar V	± 1σ	^{37}Ar V	± 1σ	^{36}Ar V	± 1σ	$^{40}Ar^*/^{39}Ar$	± 1σ	Age Ma	± 1σ	Corr?*	$Age^{\#}$ Ma
1	1.0964	0.0011	0.0414	0.0001	0.0006	0.0000	0.0000	0.0000	0.0001	0.0000	25.62	0.13	383	1.71		387
2	3.2435	0.0014	0.1203	0.0001	0.0015	0.0000	0.0000	0.0000	0.0002	0.0000	26.46	0.05	394	0.61		398
3	4.4462	0.0021	0.1661	0.0002	0.0021	0.0000	0.0000	0.0000	0.0002	0.0000	26.40	0.04	394	0.53		398
4	2.0393	0.0012	0.0765	0.0001	0.0010	0.0000	0.0000	0.0000	0.0001	0.0000	26.11	0.07	390	0.92		394
5	5.1994	0.0025	0.1952	0.0002	0.0024	0.0000	-0.0001	0.0000	0.0001	0.0000	26.36	0.04	393	0.51		397
6	1.7064	0.0012	0.0642	0.0001	0.0009	0.0000	0.0000	0.0000	0.0001	0.0000	25.91	0.08	387	1.05		391
7	1.8481	0.0011	0.0688	0.0001	0.0009	0.0000	0.0001	0.0000	0.0002	0.0000	26.11	0.07	390	0.96		394
8	2.4881	0.0013	0.0935	0.0001	0.0012	0.0000	0.0000	0.0000	0.0001	0.0000	26.20	0.05	391	0.69		395
9	3.0526	0.0013	0.1145	0.0001	0.0016	0.0000	0.0000	0.0000	0.0001	0.0000	26.29	0.04	392	0.55		396
10	1.1604	0.0010	0.0432	0.0001	0.0007	0.0000	0.0000	0.0000	0.0001	0.0000	26.02	0.10	388	1.35		392
11	3.9755	0.0018	0.1485	0.0002	0.0019	0.0000	0.0000	0.0000	0.0002	0.0000	26.38	0.05	393	0.68		397
12	1.2648	0.0011	0.0474	0.0001	0.0006	0.0000	0.0000	0.0000	0.0001	0.0000	26.06	0.10	389	1.38		393
13	1.2036	0.0010	0.0452	0.0001	0.0007	0.0000	0.0000	0.0000	0.0002	0.0000	25.60	0.13	383	1.69		387
14	3.3966	0.0015	0.1275	0.0001	0.0017	0.0000	0.0000	0.0000	0.0001	0.0000	26.32	0.04	393	0.56		397
15	2.2806	0.0013	0.0853	0.0001	0.0012	0.0000	0.0000	0.0000	0.0001	0.0000	26.21	0.07	391	0.87		395

Single grain fusion analysis
C.33: NF90 Drage Biotite-Epidote Gneiss without Relict White Mica
62°06'08.3" N
005°12'48.0" E
J value 0.0092 ± 1.93E-05
ARGUS
Biotite

Grain	^{40}Ar V	± 1σ	^{39}Ar V	± 1σ	^{38}Ar V	± 1σ	^{37}Ar V	± 1σ	^{36}Ar V	± 1σ	$^{40}Ar^*/^{39}Ar$	± 1σ	**Age** Ma	± 1σ	**Corr?***	**Age#** Ma
16	0.5523	0.0007	0.0204	0.0001	0.0004	0.0000	0.0000	0.0000	0.0001	0.0000	24.94	0.24	374	3.21		378
17	2.2650	0.0013	0.0850	0.0001	0.0011	0.0000	-0.0001	0.0000	0.0001	0.0000	26.29	0.06	392	0.78		396
18	6.1487	0.0024	0.2308	0.0002	0.0029	0.0000	-0.0001	0.0000	0.0003	0.0000	26.25	0.03	391	0.41		396
19	1.4575	0.0010	0.0544	0.0001	0.0008	0.0000	0.0000	0.0000	0.0002	0.0000	25.91	0.11	387	1.43		391
20	3.2049	0.0014	0.1192	0.0001	0.0016	0.0000	0.0000	0.0000	0.0002	0.0000	26.37	0.05	393	0.74		397
21	2.1104	0.0013	0.0784	0.0001	0.0011	0.0000	0.0000	0.0000	0.0002	0.0000	26.22	0.06	391	0.82		395
22	2.6308	0.0012	0.0986	0.0001	0.0014	0.0000	0.0000	0.0000	0.0002	0.0000	26.12	0.05	390	0.72		394
23	1.2174	0.0011	0.0458	0.0001	0.0007	0.0000	0.0000	0.0000	0.0001	0.0000	25.64	0.16	383	2.18		387
24	2.1861	0.0013	0.0812	0.0001	0.0011	0.0000	0.0000	0.0000	0.0002	0.0000	26.23	0.07	391	0.97		395
25	8.6994	0.0036	0.3255	0.0002	0.0041	0.0000	-0.0001	0.0000	0.0002	0.0000	26.48	0.03	395	0.35		399
Average Blank	0.0046	0.0000	0.0006	0.0000	0.0002	0.0000	0.0003	0.0000	0.0003	0.0000						

* Data corrected for ^{36}Ar where the ^{36}Ar measurement is > 2x the ^{36}Ar background (blank) measurement
# Recalculated ages using the decay constant of Min et al., (2000) and GA1550 biotite standard age of 99.8 of Renne et al., (2010)

Single grain fusion analysis
C.34: NF91 Drage Biotite-Epidote Gneiss without Relict White Mica
62°06'08.3'' N
005°12'48.0'' E
J value 0.0092 ± 1.91E-05
ARGUS
Biotite

Grain	**^{40}Ar** V	± 1σ	**^{39}Ar** V	± 1σ	**^{38}Ar** V	± 1σ	**^{37}Ar** V	± 1σ	**^{36}Ar** V	± 1σ	**$^{40}Ar^*/^{39}Ar$**	± 1σ	**Age** Ma	± 1σ	**Corr?***	**Age#** Ma
1	1.2850	0.0009	0.0490	0.0001	0.0007	0.0000	0.0000	0.0000	0.0001	0.0000	25.86	0.12	386	1.62		390
2	0.8452	0.0008	0.0323	0.0001	0.0005	0.0000	0.0000	0.0000	0.0002	0.0000	24.68	0.15	370	1.98		374
3	0.8357	0.0008	0.0318	0.0001	0.0005	0.0000	0.0000	0.0000	0.0001	0.0000	25.43	0.18	381	2.40		385
4	2.2116	0.0012	0.0848	0.0001	0.0011	0.0000	0.0000	0.0000	0.0001	0.0000	25.64	0.06	383	0.79		387
5	1.7757	0.0011	0.0673	0.0001	0.0009	0.0000	0.0000	0.0000	0.0001	0.0000	25.91	0.09	387	1.19		391
6	0.8234	0.0008	0.0312	0.0001	0.0005	0.0000	0.0001	0.0000	0.0001	0.0000	25.35	0.20	380	2.64		384
7	0.7253	0.0006	0.0278	0.0001	0.0005	0.0000	0.0000	0.0000	0.0001	0.0000	25.39	0.17	380	2.32		384
8	0.6757	0.0006	0.0260	0.0001	0.0004	0.0000	0.0000	0.0000	0.0001	0.0000	25.28	0.17	379	2.36		382
9	0.8757	0.0008	0.0333	0.0001	0.0005	0.0000	0.0001	0.0000	0.0001	0.0000	25.67	0.17	384	2.34		388
10	0.7687	0.0007	0.0278	0.0001	0.0005	0.0000	0.0000	0.0000	0.0003	0.0000	24.81	0.21	372	2.83		376

Single grain fusion analysis
C.34: NF91 Drage Biotite-Epidote Gneiss without Relict White Mica
62°06'08.3" N
005°12'48.0" E
J value 0.0092 ± 1.91E-05
ARGUS
Biotite

Grain	^{40}Ar V	± 1σ	^{39}Ar V	± 1σ	^{38}Ar V	± 1σ	^{37}Ar V	± 1σ	^{36}Ar V	± 1σ	$^{40}Ar^*/^{39}Ar$	± 1σ	**Age** Ma	± 1σ	**Corr?***	**Age#** Ma
11	2.0682	0.0012	0.0782	0.0001	0.0011	0.0000	0.0000	0.0000	0.0002	0.0000	25.85	0.07	386	0.93		390
12	0.9968	0.0008	0.0377	0.0001	0.0006	0.0000	0.0000	0.0000	0.0001	0.0000	25.70	0.14	384	1.87		388
13	1.3685	0.0009	0.0513	0.0001	0.0008	0.0000	0.0001	0.0000	0.0002	0.0000	25.59	0.12	383	1.62		387
14	2.0829	0.0011	0.0796	0.0001	0.0011	0.0000	0.0000	0.0000	0.0001	0.0000	25.78	0.07	385	0.90		389
15	2.4575	0.0013	0.0939	0.0001	0.0013	0.0000	0.0000	0.0000	0.0001	0.0000	25.91	0.06	387	0.87		391
16	0.5897	0.0006	0.0224	0.0001	0.0004	0.0000	0.0000	0.0000	0.0001	0.0000	25.31	0.21	379	2.80		383
17	2.6935	0.0013	0.1016	0.0001	0.0013	0.0000	0.0000	0.0000	0.0002	0.0000	25.84	0.05	386	0.70		390
18	2.0318	0.0012	0.0772	0.0001	0.0010	0.0000	0.0000	0.0000	0.0001	0.0000	25.85	0.08	386	1.02		390
19	0.7343	0.0007	0.0282	0.0001	0.0004	0.0000	0.0001	0.0000	0.0001	0.0000	25.01	0.20	375	2.73		379
20	3.7792	0.0018	0.1438	0.0001	0.0018	0.0000	0.0000	0.0000	0.0002	0.0000	25.90	0.04	387	0.54		391
Average Blank	0.0046	0.0000	0.0006	0.0000	0.0002	0.0000	0.0003	0.0000	0.0003	0.0000						

* Data corrected for ^{36}Ar where the ^{36}Ar measurement is > 2x the ^{36}Ar background (blank) measurement
# Recalculated ages using the decay constant of Min et al., (2000) and GA1550 biotite standard age of 99.8 of Renne et al., (2010)

Single grain fusion analysis
C.35: NF96 Drage Garnetiferous Gneiss without High-Pressure Relicts
61°58'41.50" N
005°14'43.20" E
J value 0.0093 ± 4.64E-05
MAP 215-50
White Mica

Grain	^{40}Ar V	± 1σ	^{39}Ar V	± 1σ	^{38}Ar V	± 1σ	^{37}Ar V	± 1σ	^{36}Ar V	± 1σ	$^{40}Ar^*/^{39}Ar$	± 1σ	Age Ma	± 1σ	Corr?*	Age# Ma
1	0.6201	0.0017	0.0240	0.0003	0.0003	0.0000	0.0037	0.0029	0.0000	0.0000	25.81	0.37	387	5.35		391
2	1.1933	0.0037	0.0457	0.0005	0.0006	0.0001	-0.0013	0.0029	0.0001	0.0000	26.13	0.31	392	4.57		396
3	1.2879	0.0036	0.0494	0.0005	0.0007	0.0001	0.0010	0.0029	0.0000	0.0000	26.08	0.26	391	3.88		395
4	0.3159	0.0018	0.0124	0.0003	0.0001	0.0001	-0.0029	0.0029	0.0000	0.0000	25.47	0.55	383	7.68		387
5	0.3584	0.0013	0.0137	0.0001	0.0001	0.0001	-0.0013	0.0029	0.0000	0.0000	26.19	0.30	392	4.38		396
6	0.8991	0.0023	0.0331	0.0003	0.0004	0.0001	-0.0017	0.0029	0.0000	0.0000	27.16	0.24	406	3.69		410
7	2.5705	0.0062	0.1004	0.0008	0.0012	0.0001	-0.0037	0.0029	0.0001	0.0000	25.61	0.22	385	3.39		389
8	1.1034	0.0044	0.0420	0.0004	0.0005	0.0001	0.0026	0.0029	0.0001	0.0000	26.28	0.26	394	3.94		398
9	0.5013	0.0015	0.0197	0.0003	0.0002	0.0000	0.0014	0.0029	0.0000	0.0000	25.48	0.34	383	4.98		387
10	0.8984	0.0027	0.0349	0.0005	0.0004	0.0001	-0.0002	0.0029	0.0000	0.0000	25.78	0.40	387	5.66		391
11	2.2222	0.0040	0.0857	0.0008	0.0011	0.0001	-0.0045	0.0029	0.0000	0.0000	25.92	0.23	389	3.60		393
12	2.4428	0.0050	0.0949	0.0005	0.0010	0.0001	-0.0037	0.0029	0.0001	0.0000	25.74	0.16	386	2.75		390
13	0.5519	0.0024	0.0207	0.0003	0.0002	0.0001	-0.0029	0.0029	0.0000	0.0000	26.61	0.40	398	5.69		402
14	0.5477	0.0015	0.0210	0.0004	0.0004	0.0000	-0.0049	0.0029	0.0000	0.0000	26.07	0.52	391	7.22		395
15	0.7452	0.0029	0.0293	0.0004	0.0004	0.0000	-0.0025	0.0029	0.0000	0.0000	25.42	0.39	382	5.55		386
Average Blank	0.0060	0.0003	0.0002	0.0000	0.0001	0.0000	0.0005	0.0001	0.0001	0.0000						

* Data corrected for ^{36}Ar where the ^{36}Ar measurement is > 2x the ^{36}Ar background (blank) measurement
\# Recalculated ages using the decay constant of Min et al., (2000) and GA1550 biotite standard age of 99.8 of Renne et al., (2010)

Single grain fusion analysis
C.36: NF96 Drage Garnetiferous Gneiss without High-Pressure Relicts
61°58'41.50" N
005°14'43.20" E
J value 0.0093 ± 4.64E-05
MAP 215-50
Biotite

Grain	^{40}Ar V	± 1σ	^{39}Ar V	± 1σ	^{38}Ar V	± 1σ	^{37}Ar V	± 1σ	^{36}Ar V	± 1σ	$^{40}Ar^*/^{39}Ar$	± 1σ	Age Ma	± 1σ	Corr?*	Age# Ma
1	1.0081	0.0025	0.0406	0.0004	0.0005	0.0001	0.0022	0.0025	0.0000	0.0000	24.81	0.23	374	3.56		378
2	0.8743	0.0021	0.0351	0.0006	0.0005	0.0001	0.0030	0.0025	0.0001	0.0000	24.92	0.42	375	6.00		379
3	0.9188	0.0028	0.0375	0.0003	0.0004	0.0001	0.0006	0.0025	0.0000	0.0000	24.52	0.24	370	3.63		374
4	2.1820	0.0050	0.0887	0.0007	0.0011	0.0001	-0.0009	0.0025	0.0001	0.0000	24.60	0.19	371	3.14		375
5	1.0506	0.0032	0.0443	0.0007	0.0005	0.0001	0.0034	0.0025	0.0000	0.0000	23.71	0.36	359	5.23		363
6	1.0664	0.0029	0.0432	0.0006	0.0004	0.0001	0.0030	0.0025	0.0000	0.0000	24.66	0.34	372	4.97		376
7	0.8200	0.0019	0.0337	0.0003	0.0005	0.0000	0.0006	0.0025	0.0000	0.0000	24.31	0.23	367	3.58		371
8	1.4229	0.0022	0.0581	0.0007	0.0009	0.0001	0.0002	0.0025	0.0001	0.0000	24.50	0.30	370	4.41		373
9	0.6907	0.0038	0.0286	0.0004	0.0004	0.0000	0.0002	0.0025	0.0000	0.0000	24.19	0.40	365	5.72		369
10	1.3500	0.0035	0.0562	0.0006	0.0008	0.0001	0.0010	0.0025	0.0000	0.0000	24.03	0.25	363	3.76		367
11	1.3986	0.0030	0.0564	0.0006	0.0007	0.0001	0.0022	0.0025	0.0000	0.0000	24.79	0.25	374	3.82		377
12	1.2667	0.0030	0.0499	0.0004	0.0006	0.0001	0.0030	0.0025	0.0000	0.0000	25.38	0.23	382	3.55		386
13	0.7051	0.0020	0.0289	0.0004	0.0004	0.0001	-0.0002	0.0025	0.0000	0.0000	24.40	0.36	368	5.15		372
14	1.1137	0.0032	0.0459	0.0003	0.0005	0.0001	-0.0014	0.0032	0.0001	0.0000	24.24	0.20	366	3.15		370
15	2.9816	0.0057	0.1224	0.0011	0.0014	0.0001	0.0007	0.0032	0.0001	0.0000	24.36	0.22	368	3.48		371
Average Blank	0.0070	0.0002	0.0001	0.0000	0.0001	0.0000	0.0004	0.0001	0.0001	0.0000						

* Data corrected for ^{36}Ar where the ^{36}Ar measurement is > 2x the ^{36}Ar background (blank) measurement
# Recalculated ages using the decay constant of Min et al., (2000) and GA1550 biotite standard age of 99.8 of Renne et al., (2010)

Single grain fusion analysis
C.37: NF98 Drage Biotite-Epidote with Relict White Mica
61°58'41.50" N
005°14'43.20" E
J value 0.0093 ± 4.64E-05
MAP 215-50
White Mica

Grain	^{40}Ar V	± 1σ	^{39}Ar V	± 1σ	^{38}Ar V	± 1σ	^{37}Ar V	± 1σ	^{36}Ar V	± 1σ	$^{40}Ar^*/^{39}Ar$	± 1σ	Age Ma	± 1σ	Corr?*	Age# Ma
1	0.9200	0.0020	0.0350	0.0004	0.0004	0.0001	-0.0051	0.0023	0.0001	0.0000	25.14	0.47	379	6.63	Y	383
2	1.3521	0.0045	0.0531	0.0007	0.0006	0.0001	-0.0004	0.0023	0.0000	0.0000	25.46	0.35	383	5.02		387
3	2.0716	0.0021	0.0785	0.0007	0.0010	0.0001	0.0001	0.0023	0.0002	0.0000	25.75	0.23	387	3.61	Y	391
4	1.0865	0.0030	0.0424	0.0008	0.0006	0.0001	0.0038	0.0023	0.0001	0.0000	25.65	0.50	386	6.99		390
5	0.9903	0.0034	0.0381	0.0003	0.0004	0.0001	-0.0018	0.0023	0.0001	0.0000	25.12	0.33	378	4.75	Y	382
6	0.8657	0.0037	0.0333	0.0002	0.0004	0.0001	-0.0055	0.0023	0.0000	0.0000	25.97	0.18	390	3.04		394
7	1.2362	0.0027	0.0477	0.0005	0.0006	0.0001	-0.0009	0.0023	0.0001	0.0000	25.91	0.27	389	3.99		393
8	2.1099	0.0054	0.0821	0.0005	0.0010	0.0001	-0.0023	0.0023	0.0000	0.0000	25.69	0.17	386	2.87		390
9	1.5375	0.0039	0.0592	0.0006	0.0007	0.0001	-0.0023	0.0023	0.0001	0.0000	25.41	0.32	382	4.71	Y	386
10	1.1511	0.0027	0.0461	0.0003	0.0006	0.0001	-0.0041	0.0023	0.0000	0.0000	24.99	0.15	377	2.63		380
11	1.7978	0.0049	0.0691	0.0006	0.0007	0.0000	0.0056	0.0023	0.0001	0.0000	26.04	0.23	391	3.61		395
12	0.7155	0.0031	0.0276	0.0005	0.0004	0.0000	-0.0041	0.0023	0.0001	0.0000	24.75	0.59	373	8.26	Y	377
13	1.1622	0.0026	0.0448	0.0005	0.0005	0.0001	-0.0032	0.0023	0.0000	0.0000	25.94	0.30	389	4.41		393
14	2.1815	0.0037	0.0849	0.0006	0.0010	0.0001	0.0001	0.0023	0.0001	0.0000	25.69	0.18	386	3.03		390
15	1.3447	0.0043	0.0532	0.0007	0.0007	0.0001	-0.0055	0.0023	0.0000	0.0000	25.26	0.32	380	4.73		384
Average Blank	0.0073	0.0002	0.0001	0.0000	0.0001	0.0000	0.0005	0.0001	0.0001	0.0000						

* Data corrected for ^{36}Ar where the ^{36}Ar measurement is > 2x the ^{36}Ar background (blank) measurement
\# Recalculated ages using the decay constant of Min et al., (2000) and GA1550 biotite standard age of 99.8 of Renne et al., (2010)

Single grain fusion analysis
C.38: NF98 Drage Biotite-Epidote with Relict White Mica
61°58'41.50" N
005°14'43.20" E
J value 0.0093 ± 4.64E-05
MAP 215-50
Biotite

Grain	^{40}Ar V	± 1σ	^{39}Ar V	± 1σ	^{38}Ar V	± 1σ	^{37}Ar V	± 1σ	^{36}Ar V	± 1σ	$^{40}Ar^*/^{39}Ar$	± 1σ	Age Ma	± 1σ	Corr?*	$Age^{\#}$ Ma
1	1.2244	0.0032	0.0471	0.0005	0.0006	0.0001	-0.0033	0.0030	0.0000	0.0000	25.98	0.26	390	3.93		394
2	0.1642	0.0010	0.0067	0.0002	0.0001	0.0000	0.0013	0.0030	0.0000	0.0000	24.34	0.59	368	8.21		371
3	1.1676	0.0022	0.0457	0.0005	0.0007	0.0001	0.0034	0.0030	0.0000	0.0000	25.52	0.27	384	4.05		388
4	0.3216	0.0018	0.0130	0.0003	0.0002	0.0000	-0.0029	0.0030	0.0000	0.0000	24.83	0.56	374	7.75		378
5	1.0289	0.0027	0.0407	0.0003	0.0005	0.0000	-0.0008	0.0030	0.0000	0.0000	25.30	0.21	381	3.34		385
6	0.8972	0.0031	0.0355	0.0003	0.0004	0.0000	-0.0008	0.0030	0.0000	0.0000	25.25	0.24	380	3.74		384
7	1.9292	0.0042	0.0750	0.0007	0.0009	0.0001	-0.0016	0.0030	0.0000	0.0000	25.72	0.23	386	3.61		390
8	0.4607	0.0023	0.0163	0.0003	0.0002	0.0001	0.0119	0.0030	0.0002	0.0000	25.24	0.69	380	9.49	Y	384
9	0.5404	0.0015	0.0214	0.0005	0.0002	0.0000	-0.0021	0.0030	0.0000	0.0000	25.25	0.57	380	7.88		384
10	0.9305	0.0023	0.0367	0.0004	0.0005	0.0001	-0.0006	0.0016	0.0000	0.0000	25.38	0.27	382	4.07		386
11	1.5019	0.0051	0.0582	0.0005	0.0007	0.0001	0.0021	0.0016	0.0000	0.0000	25.82	0.23	388	3.54		392
12	1.2734	0.0029	0.0500	0.0005	0.0004	0.0001	0.0008	0.0016	0.0001	0.0000	25.49	0.28	383	4.16		387
13	0.5840	0.0030	0.0228	0.0003	0.0003	0.0000	-0.0015	0.0016	0.0001	0.0000	25.65	0.37	386	5.24		389
14	0.7430	0.0023	0.0305	0.0005	0.0004	0.0000	0.0030	0.0016	0.0001	0.0000	24.38	0.40	368	5.74		372
15	0.4485	0.0023	0.0175	0.0002	0.0001	0.0001	-0.0001	0.0017	0.0000	0.0000	25.65	0.32	385	4.62		389
Average Blank	0.0067	0.0003	0.0001	0.0000	0.0001	0.0000	0.0004	0.0001	0.0001	0.0000						

* Data corrected for ^{36}Ar where the ^{36}Ar measurement is > 2x the ^{36}Ar background (blank) measurement
\# Recalculated ages using the decay constant of Min et al., (2000) and GA1550 biotite standard age of 99.8 of Renne et al., (2010)

Single grain fusion analysis
C.39: NF99 Drage Garnetiferous Gneiss without High-Pressure Relicts
61°58'41.50" N
005°14'43.20" E
J value 0.0093 ± 4.65E-05
MAP 215-50
White Mica

Grain	^{40}Ar V	± 1σ	^{39}Ar V	± 1σ	^{38}Ar V	± 1σ	^{37}Ar V	± 1σ	^{36}Ar V	± 1σ	$^{40}Ar^*/^{39}Ar$	± 1σ	Age Ma	± 1σ	Corr?*	Age# Ma
1	0.5517	0.0013	0.0213	0.0003	0.0003	0.0001	0.0016	0.0029	0.0000	0.0000	25.93	0.39	390	5.50		394
2	0.6935	0.0027	0.0279	0.0004	0.0005	0.0001	-0.0017	0.0029	0.0000	0.0000	24.88	0.38	375	5.49		379
3	0.5957	0.0021	0.0239	0.0003	0.0003	0.0001	0.0021	0.0029	0.0000	0.0000	24.92	0.33	376	4.77		380
4	0.9222	0.0047	0.0372	0.0004	0.0005	0.0001	0.0002	0.0029	0.0000	0.0000	24.81	0.30	374	4.48		378
5	2.6468	0.0085	0.1038	0.0007	0.0014	0.0001	0.0006	0.0029	0.0001	0.0000	25.50	0.19	384	3.06		388
6	0.2134	0.0010	0.0082	0.0002	0.0000	0.0001	0.0002	0.0029	0.0000	0.0000	26.01	0.71	390	9.72		394
7	0.6658	0.0025	0.0264	0.0002	0.0004	0.0001	-0.0055	0.0029	0.0000	0.0000	25.25	0.23	380	3.59		384
8	0.8904	0.0019	0.0349	0.0004	0.0004	0.0001	0.0063	0.0029	0.0000	0.0000	25.51	0.27	384	4.07		388
9	0.1344	0.0008	0.0050	0.0002	0.0001	0.0001	-0.0027	0.0029	0.0000	0.0000	27.06	1.05	405	14.14		409
10	0.1637	0.0009	0.0066	0.0002	0.0001	0.0001	-0.0003	0.0029	0.0000	0.0000	24.83	0.69	375	9.55		378
11	0.5351	0.0011	0.0206	0.0003	0.0003	0.0001	0.0016	0.0029	0.0000	0.0000	25.95	0.38	390	5.48		394
12	0.3316	0.0015	0.0127	0.0003	0.0002	0.0001	-0.0074	0.0029	0.0000	0.0000	26.06	0.65	391	8.95		395
13	0.6528	0.0015	0.0263	0.0001	0.0003	0.0001	0.0006	0.0029	0.0000	0.0000	24.86	0.14	375	2.50		379
14	0.1882	0.0009	0.0072	0.0002	0.0000	0.0000	-0.0058	0.0002	0.0000	0.0000	26.07	0.80	391	10.97		395
15	0.1503	0.0011	0.0059	0.0002	0.0000	0.0000	-0.0058	0.0002	-0.0001	0.0000	25.35	0.96	382	13.07		386
Average Blank	0.0066	0.0003	0.0001	0.0000	0.0001	0.0000	0.0005	0.0001	0.0001	0.0000						

* Data corrected for ^{36}Ar where the ^{36}Ar measurement is > 2x the ^{36}Ar background (blank) measurement
\# Recalculated ages using the decay constant of Min et al., (2000) and GA1550 biotite standard age of 99.8 of Renne et al., (2010)

Single grain fusion analysis
C.40: NF99 Drage Garnetiferous Gneiss without High-Pressure Relicts
61°58'41.50" N
005°14'43.20" E
J value 0.0093 ± 4.65E-05
MAP 215-50
Biotite

Grain	^{40}Ar V	± 1σ	^{39}Ar V	± 1σ	^{38}Ar V	± 1σ	^{37}Ar V	± 1σ	^{36}Ar V	± 1σ	$^{40}Ar^*/^{39}Ar$	± 1σ	Age Ma	± 1σ	Corr?*	Age# Ma
1	1.5594	0.0035	0.0602	0.0005	0.0008	0.0001	-0.0013	0.0022	0.0001	0.0000	25.46	0.25	383	3.74	Y	387
2	1.5275	0.0032	0.0606	0.0006	0.0008	0.0001	0.0018	0.0022	0.0000	0.0000	25.22	0.24	380	3.72		384
3	1.5313	0.0041	0.0599	0.0005	0.0009	0.0001	-0.0013	0.0022	0.0000	0.0000	25.58	0.22	385	3.39		389
4	2.0317	0.0060	0.0804	0.0006	0.0012	0.0001	0.0008	0.0022	0.0001	0.0000	25.28	0.20	381	3.21		385
5	1.6400	0.0028	0.0655	0.0007	0.0008	0.0001	-0.0018	0.0022	0.0000	0.0000	25.03	0.27	377	4.08		381
6	1.4437	0.0045	0.0569	0.0009	0.0008	0.0001	-0.0008	0.0022	0.0000	0.0000	25.38	0.40	382	5.64		386
7	0.6326	0.0032	0.0251	0.0005	0.0004	0.0001	-0.0024	0.0032	0.0000	0.0000	25.23	0.52	380	7.23		384
8	0.8292	0.0023	0.0328	0.0005	0.0004	0.0000	-0.0024	0.0032	0.0000	0.0000	25.26	0.40	381	5.66		384
9	0.5766	0.0016	0.0224	0.0005	0.0003	0.0001	0.0002	0.0032	0.0000	0.0000	25.69	0.60	386	8.27		390
10	0.7376	0.0030	0.0294	0.0002	0.0004	0.0001	-0.0051	0.0032	0.0000	0.0000	25.11	0.18	378	3.02		382
11	2.1630	0.0051	0.0859	0.0008	0.0013	0.0001	-0.0035	0.0032	0.0001	0.0000	24.78	0.25	374	3.79	Y	378
12	0.7581	0.0025	0.0290	0.0005	0.0003	0.0001	-0.0056	0.0032	0.0000	0.0000	26.14	0.44	392	6.17		396
13	0.3340	0.0017	0.0132	0.0003	0.0002	0.0001	-0.0019	0.0032	0.0000	0.0000	25.25	0.61	380	8.46		384
14	0.6928	0.0025	0.0275	0.0005	0.0003	0.0000	-0.0019	0.0032	0.0000	0.0000	25.20	0.50	380	7.04		384
15	0.4892	0.0022	0.0193	0.0005	0.0002	0.0000	-0.0051	0.0032	0.0000	0.0000	25.36	0.69	382	9.54		386
Average Blank	0.0059	0.0002	0.0001	0.0000	0.0001	0.0000	0.0005	0.0001	0.0001	0.0000						

* Data corrected for ^{36}Ar where the ^{36}Ar measurement is > 2x the ^{36}Ar background (blank) measurement
# Recalculated ages using the decay constant of Min et al., (2000) and GA1550 biotite standard age of 99.8 of Renne et al., (2010)

Single grain fusion analysis
C.41: NF100 Drage Eclogite
61°58'41.50" N
005°14'43.20" E
J value 0.0093 ± 4.67E-05
MAP 215-50
White Mica

Grain	^{40}Ar V	± 1σ	^{39}Ar V	± 1σ	^{38}Ar V	± 1σ	^{37}Ar V	± 1σ	^{36}Ar V	± 1σ	$^{40}Ar^*/^{39}Ar$	± 1σ	Age Ma	± 1σ	Corr?*	Age# Ma
1	1.0046	0.0023	0.0272	0.0004	0.0003	0.0001	0.0006	0.0031	0.0000	0.0000	36.87	0.57	534	7.47		540
2	0.4719	0.0018	0.0142	0.0003	0.0002	0.0000	-0.0004	0.0031	0.0000	0.0000	33.33	0.67	489	8.89		494
3	1.9615	0.0035	0.0623	0.0004	0.0008	0.0001	0.0001	0.0031	0.0001	0.0000	31.50	0.23	466	3.60		470
4	1.3084	0.0032	0.0377	0.0004	0.0004	0.0001	0.0063	0.0031	0.0000	0.0000	34.75	0.38	507	5.34		513
5	1.9401	0.0059	0.0352	0.0005	0.0005	0.0001	0.0030	0.0025	0.0000	0.0000	55.11	0.77	749	9.07		757
6	1.7854	0.0024	0.0565	0.0007	0.0008	0.0001	0.0009	0.0025	0.0000	0.0000	31.61	0.37	467	5.28		472
7	0.5859	0.0012	0.0179	0.0003	0.0003	0.0001	0.0025	0.0025	0.0000	0.0000	32.76	0.56	482	7.53		487
8	1.6661	0.0061	0.0562	0.0004	0.0008	0.0001	0.0035	0.0025	0.0000	0.0000	29.65	0.23	441	3.62		446
9	2.4494	0.0042	0.0765	0.0005	0.0010	0.0001	0.0004	0.0025	0.0000	0.0000	32.02	0.23	472	3.66		477
10	0.4098	0.0024	0.0147	0.0004	0.0001	0.0001	-0.0049	0.0026	0.0000	0.0000	27.94	0.71	418	9.73		423
11	0.4259	0.0018	0.0115	0.0002	0.0002	0.0001	0.0586	0.0026	0.0000	0.0000	37.15	0.58	538	7.60		543
12	1.0031	0.0020	0.0346	0.0005	0.0003	0.0001	0.0020	0.0026	0.0000	0.0000	28.98	0.40	432	5.70		437
13	0.8146	0.0013	0.0265	0.0002	0.0004	0.0000	0.0077	0.0026	0.0000	0.0000	30.68	0.28	455	4.23		460
14	0.6468	0.0013	0.0189	0.0003	0.0003	0.0001	0.0004	0.0026	0.0000	0.0000	34.14	0.61	500	8.05		505
Average Blank	0.0059	0.0003	0.0001	0.0000	0.0001	0.0000	0.0004	0.0000	0.0001	0.0000						

* Data corrected for ^{36}Ar where the ^{36}Ar measurement is > 2x the ^{36}Ar background (blank) measurement
# Recalculated ages using the decay constant of Min et al., (2000) and GA1550 biotite standard age of 99.8 of Renne et al., (2010)

Appendix D:

UV Laser Ablation $^{40}Ar/^{39}Ar$ Dataset

Hornelen basin

UV laser spot data

D.1: NF37 Krokkenakken Eclogite

61°54'53.73" N

005°20'16.49" E

J value 0.0096 ± 4.79E-05

Nu

Sample	**^{40}Ar** Counts	± 1σ	**^{39}Ar** Counts	± 1σ	**^{38}Ar** Counts	± 1σ	**^{37}Ar** Counts	± 1σ	**^{36}Ar** Counts	± 1σ	**$^{40}Ar^*/^{39}Ar$**	± 1σ	**Age** Ma	± 1σ	**Corr?***	**Age#** Ma
Gt	47.2	53.6	3.3	0.5	0.8	0.5	3923.2	8.2	1.5	0.8	14.5	16.7	235	505.9		238
Pheng (Gt)	120501.7	102.3	4667.8	15.0	50.7	1.2	21.9	8.2	1.2	0.8	25.8	0.1	398.7	4.3		403
Pheng (Gt) 2	120565.3	90.5	4253.5	14.0	51.3	1.6	8.0	8.2	11.6	0.8	28.4	0.1	433.4	2.3	Y	438
Bt rim to Mu2	70653.7	79.5	2724.2	13.0	35.4	1.3	264.1	8.2	2.6	0.8	25.9	0.1	400.3	5.0		404
symp next to bi	4904.2	55.7	179.9	2.8	2.8	0.5	2393.2	8.2	1.6	0.8	27.3	0.5	418.6	15.0		423
Mu3 (6)	95636.6	136.0	3465.2	12.0	42.8	3.0	1.6	4.4	4.7	1.3	27.6	0.1	423.2	4.7		428
bt rim to Mu3 (6)	36866.6	129.3	1483.6	7.4	17.6	1.0	549.8	4.4	-1.7	1.4	24.9	0.2	385.2	5.5		389
symp rim to Mu3 (6)	6256.7	125.8	240.7	3.4	4.3	0.6	1995.8	4.4	1.9	1.3	26.0	0.6	401.1	18.0		405
mu mu contact 9	99285.5	143.9	3761.0	12.0	40.5	1.5	-26.6	4.4	4.0	1.3	26.4	0.1	406.7	4.5		411
mu10	69285.2	134.8	2638.1	11.0	32.3	2.0	223.8	4.4	4.3	1.3	26.3	0.1	404.9	4.9		409
mu11	87085.3	138.6	3078.1	13.0	40.1	2.3	51.0	4.4	12.2	1.3	28.3	0.1	432.6	2.6	Y	437
mu12	84635.5	140.0	3109.9	12.0	38.9	2.3	8.2	4.4	1.8	1.3	27.2	0.1	417.9	4.9		422
mu13	81437.3	140.9	2994.0	13.0	39.4	2.9	6.8	4.4	1.7	1.3	27.2	0.1	417.7	5.1		422
mu14	78200.6	136.0	2905.4	11.0	32.1	1.2	46.3	4.4	1.9	1.3	26.9	0.1	413.8	4.8		418
mu15	81830.7	138.1	2997.3	12.0	37.6	2.4	25.2	4.4	3.7	1.3	27.3	0.1	419.1	5.0		423
Average Blank	3411.5	13.0	12.9	0.4	2.5	0.4	49.6	1.0	13.9	0.3						

Mu1 - T3 - 1	37508.4	114.3	1453.0	22.1	13.9	0.9	232.0	318.5	0.4	0.7	25.8	0.4	398.7	11.7		403
Mu1 - T3 - 2	41379.6	117.4	1608.0	22.1	20.1	2.0	178.6	318.5	0.6	0.6	25.7	0.4	397.5	10.6		402
Mu1 - T4 - 1	40542.0	87.2	1486.7	8.3	15.4	0.9	-808.8	318.5	0.4	0.7	27.3	0.2	418.7	5.8		423
Mu1 - T4 - 2	34699.7	109.8	1296.5	18.1	14.0	0.8	479.2	318.5	0.8	0.7	26.8	0.4	411.8	11.1		416
Mu1 - T4 - 3	36770.1	112.0	1342.4	16.1	19.4	1.6	1073.5	318.5	0.8	0.7	27.4	0.3	420.4	10.0		425
Mu1 - T4 - 4	35658.4	118.1	1344.1	21.1	17.8	2.1	-102.3	185.9	1.0	0.9	26.5	0.4	408.5	12.3		413
Mu1 - T4 - 5	40236.7	129.9	1539.0	22.1	15.0	0.8	-134.4	185.9	-0.2	0.9	26.1	0.4	403.2	11.2		407
Mu1 - T3 - 3	39439.3	123.9	1451.6	19.1	17.8	1.9	54.7	185.9	-0.1	0.9	27.2	0.4	417.3	10.7		422
Omp2	230.2	84.6	1.1	0.6	-0.4	0.8	808.0	185.9	0.7	0.9	203.7	134.6	1952.2	1577.0		1975
Omp1	451.7	84.6	12.9	1.2	-0.7	0.6	689.4	185.9	1.6	0.9	35.1	7.4	522.7	190.8		528
Symp1	3312.8	37.3	72.7	1.8	1.8	0.7	294.5	194.8	6.9	0.5	17.4	2.2	278.5	32.3	Y	281
Symp2	4134.6	36.8	109.1	2.6	2.2	0.7	948.3	194.8	6.1	0.5	21.5	1.5	337.3	21.4	Y	341
Gt Rim 1	29640.9	51.2	1060.8	7.4	17.4	1.8	-423.1	194.8	9.9	0.9	27.9	0.2	427.9	6.7		432
Gt Rim 2	5442.4	37.7	175.3	3.1	6.1	0.7	618.4	194.8	5.5	0.5	21.7	0.9	341	13.6	Y	344
Gt Rim 3	709.4	42.8	7.4	0.5	-1.4	0.8	781.6	194.8	1.9	0.7	95.7	8.7	1174	156.9		1187
Average Blank	1186.4	14.8	10.6	0.3	1.4	0.3	41.3	0.8	5.3	0.5						

* Data are corrected for ^{36}Ar where the ^{36}Ar measurement is > 2x the ^{36}Ar background (blank) measurement

Ages recalculated using the deacy constants of Min et al., (2000) and biotite standard age of 99.7 of Renne et al., (2010)

UV laser spot data

D.2: NF40 Krokkenakken Garnetiferous Gneiss with High Pressure Relicts

61°54'53.73" N

005°20'16.49" E

J value 0.0096 ± 4.78E-05

Nu

Sample	**^{40}Ar** Counts	± 1σ	**^{39}Ar** Counts	± 1σ	**^{38}Ar** Counts	± 1σ	**^{37}Ar** Counts	± 1σ	**^{36}Ar** Counts	± 1σ	**$^{40}Ar^*/^{39}Ar$**	± 1σ	**Age** Ma	± 1σ	**Corr?***	**Age#** Ma
Biotite Rim 1	103704.2	171.8	4129.8	24.1	56.9	2.4	6.5	8.4	4.4	0.9	25.1	0.2	389	5.5		392
Biotite Core 1	117455.8	171.8	4678.9	28.1	62.3	3.5	10.8	8.4	5.0	0.9	25.1	0.2	388	5.6		392
Biotite Rim 2	112952.5	141.3	4517.0	17.0	59.8	3.0	10.0	8.4	4.9	0.9	25.0	0.1	387	4.5		391
Biotite 2	50468.9	48.6	2016.4	10.0	22.0	1.0	24.0	4.3	0.3	1.3	25.0	0.1	387	5.0		391
Biotite 2 (i)	25456.2	33.4	1026.7	7.1	12.7	0.7	246.6	4.3	-1.0	1.3	24.8	0.2	384	6.0		388
Mu1	58968.6	54.5	2308.7	11.0	28.0	1.9	2.0	4.3	-1.6	1.3	25.5	0.1	395	4.9		399
Mu1(i)	56611.5	54.5	2203.1	9.5	23.4	0.9	2.8	4.3	1.2	1.2	25.7	0.1	397	4.8		401
Mu1(ii)	43210.7	48.6	1622.3	8.7	22.5	1.5	10.8	4.3	8.2	1.2	26.6	0.2	410	5.4		414
Mu1(iv)	56258.5	48.6	2205.6	9.7	25.0	1.1	32.5	4.3	3.1	1.2	25.5	0.1	394	4.8		398
bt 3(i)	38860.8	46.7	1573.4	8.3	18.8	0.8	79.8	4.3	3.2	1.2	24.7	0.1	383	5.1		387
bt 3 (ii)	56478.6	82.9	2276.5	9.4	25.2	1.0	9.7	7.9	2.6	1.2	24.8	0.1	384	4.6		388
mu 2 br	40736.8	75.5	1582.8	8.2	22.4	1.5	54.7	7.9	5.0	1.2	25.7	0.1	397	5.3		401
mu 2	22922.9	70.3	903.0	7.2	9.9	0.7	121.6	7.9	1.2	1.2	25.4	0.2	392	7.0		396
Mu2	34805.4	178.3	1377.3	8.9	16.0	1.6	-15.3	7.2	-0.3	1.6	25.3	0.2	391	3.4	Y	395
Average Blank	3168.8	13.0	12.7	0.4	2.6	0.3	48.7	1.0	12.8							

J value	0.0096	±	4.78E-05													
Sample	^{40}Ar Counts	± 1σ	^{39}Ar Counts	± 1σ	^{38}Ar Counts	± 1σ	^{37}Ar Counts	± 1σ	^{36}Ar Counts	± 1σ	$^{40}Ar^*/^{39}Ar$	± 1σ	Age Ma	± 1σ	Corr?*	Age# Ma
Mu1 - T1 - 1	33581.5	68.3	1320.7	8.6	15.3	0.8	72.9	23.0	1.1	0.9	25.4	0.2	393	6.0		397
Mu1 - T1 - 2	61218.8	80.4	2433.3	12.0	26.3	1.1	64.6	23.0	1.0	0.9	25.2	0.1	389	5.0		393
Mu1 - T1 - 3	74136.3	77.1	2954.6	12.0	36.7	2.3	4.7	23.0	-0.1	0.9	25.1	0.1	388	4.6		392
Mu1 - T1 - 4	64623.5	79.8	2563.6	11.0	29.6	1.0	17.1	23.0	0.8	0.9	25.2	0.1	389	4.7		393
Mu1 - T1 - 5	63421.7	77.8	2533.6	9.7	29.3	0.9	13.0	23.0	-0.2	0.9	25.0	0.1	387	4.5		391
Mu1 - T1 - 6	63621.9	82.5	2553.6	11.0	29.0	1.0	8.9	23.0	0.1	0.9	24.9	0.1	385	4.7		389
Mu1 - T1 - 7	61118.4	74.6	2463.4	12.0	28.1	1.2	17.1	23.0	0.7	0.9	24.8	0.1	384	4.9		388
Mu1 - T2 - 1	59416.3	84.0	2373.2	10.0	31.4	2.3	4.7	23.0	0.2	0.9	25.0	0.1	387	4.7		391
Mu1 - T2 - 2	56812.7	79.8	2273.0	9.8	25.7	1.1	10.9	23.0	0.5	0.9	25.0	0.1	387	4.7		390
Mu1 - T2 - 3	59818.4	77.1	2202.8	11.0	27.1	1.0	31.6	23.0	16.8	0.9	24.9	0.2	385	3.0	Y	389
Mu1 - T2 - 4	54597.6	66.0	2179.9	9.2	25.6	2.1	37.4	24.5	0.1	0.7	25.1	0.1	387	2.3	Y	391
Mu1 - T2 - 5	54910.2	77.8	2192.8	11.0	25.1	1.1	-115.0	23.0	0.4	0.9	25.0	0.1	387	5.0		391
Mu1 - T2 - 6	56712.6	77.8	2273.0	11.0	25.8	1.1	54.3	23.0	2.7	0.9	25.0	0.1	386	4.9		390
Mu1 - T2 - 7	39689.7	71.0	1571.3	8.5	22.1	1.8	200.9	23.0	2.1	0.9	25.3	0.1	390	5.3		394
Mu2 - T1 - 1	47940.4	97.8	1921.9	9.6	21.2	1.1	45.3	32.2	0.1	0.7	24.9	0.1	386	5.1		390

Sample	^{40}Ar Counts	± 1σ	^{39}Ar Counts	± 1σ	^{38}Ar Counts	± 1σ	^{37}Ar Counts	± 1σ	^{36}Ar Counts	± 1σ	$^{40}Ar^*/^{39}Ar$	± 1σ	Age Ma	± 1σ	Corr?*	Age# Ma
Mu2 - T1 - 2	56252.1	99.7	2202.5	9.8	25.1	1.1	43.2	32.2	-0.1	0.8	25.5	0.1	394	4.9		398
Mu2 - T1 - 3	52346.6	101.3	2072.2	11.1	24.4	1.1	43.2	32.2	-0.7	0.7	25.3	0.1	390	5.3		394
Mu2 - T1 - 4	58255.9	99.2	2152.4	10.1	24.7	1.1	45.3	32.2	5.5	0.8	26.3	0.2	405	3.0	Y	409
Mu2 - T1 - 5	55952.3	101.3	2122.3	10.1	24.7	1.2	36.9	32.2	2.0	0.8	26.4	0.1	405	5.2		410
Mu2 - T1 - 6	65865.6	312.6	2533.3	14.1	32.4	2.1	49.5	32.2	0.9	0.7	26.0	0.2	400	6.4		405
Mu2 - T1 - 7	47540.0	97.3	1891.8	10.0	20.0	1.0	-1.1	32.2	2.8	0.8	25.1	0.1	388	5.3		392
Mu2 - T1 - 8	21405.2	92.4	783.2	7.3	12.3	0.9	45.3	32.2	5.7	0.8	25.2	0.4	389	6.0	Y	393
Mu2 - T1 - 9	24408.6	93.1	977.6	6.9	11.6	1.0	140.1	32.2	2.2	0.8	25.0	0.2	386	6.5		390
Mu2 - T1 - 10	68568.2	98.3	2763.9	12.1	37.5	2.3	22.1	32.2	2.2	0.8	24.8	0.1	384	4.7		388
Mu2 - T2 - 1	45356.7	80.9	1621.4	8.1	19.3	1.0	-6.7	13.5	11.0	0.5	26.0	0.2	400	3.0	Y	404
Mu2 - T2 - 2	57572.6	80.9	2192.8	10.0	27.5	1.9	-41.1	13.5	0.0	0.6	26.3	0.1	404	5.0		408
Mu2 - T3 - 1	42652.0	81.5	1641.5	9.1	21.4	1.7	23.4	13.5	3.2	0.7	26.0	0.2	400	5.5		404
Mu2 - T3 - 2	52065.2	85.0	1962.2	9.1	22.1	1.1	16.9	13.5	1.2	0.6	26.5	0.1	408	5.1		412
Mu3 - T1 - 1	51163.2	80.4	2022.4	11.0	21.7	1.1	6.2	13.5	0.8	0.6	25.3	0.1	391	5.3		395
Mu3 - T1 - 2	51663.7	82.0	2062.5	10.0	22.6	1.1	-4.6	13.5	0.4	0.6	25.1	0.1	387	5.0		391

Sample	^{40}Ar Counts	± 1σ	^{39}Ar Counts	± 1σ	^{38}Ar Counts	± 1σ	^{37}Ar Counts	± 1σ	^{36}Ar Counts	± 1σ	$^{40}Ar^*/^{39}Ar$	± 1σ	Age Ma	± 1σ	Corr?*	Age# Ma
Mu3 - T1 - 3	55269.1	109.3	2142.7	17.1	24.1	1.0	1.9	13.5	3.0	0.7	25.8	0.2	398	6.9		402
Mu3 - T1 - 4	39711.0	98.6	1551.2	9.5	18.8	0.9	-1.2	43.1	3.1	1.3	25.6	0.2	395	5.9		399
Mu3 - T1 - 5	40311.5	98.6	1601.3	9.2	17.9	0.8	-3.4	43.1	-0.2	1.3	25.2	0.2	389	5.6		393
Mu3 - T1 - 6	50825.6	102.6	2042.4	9.8	25.1	2.5	3.2	43.1	-1.0	1.3	24.9	0.1	385	5.0		389
Mu3 - T1 - 7	37607.7	100.7	1511.1	8.6	19.4	1.6	42.6	43.1	-0.2	1.3	24.9	0.2	385	5.6		389
Mu3 - T1 - 8	37507.6	99.0	1511.1	8.7	17.6	0.8	323.1	43.1	0.3	1.3	24.8	0.2	384	5.6		388
Mu3 - T1 - 9	19783.6	94.9	803.4	6.2	11.5	1.3	318.7	43.1	0.5	1.3	24.6	0.2	381	7.2		385
Mu3 - T1 - 10	27093.4	95.9	1110.2	7.2	12.7	0.8	274.9	43.1	0.3	1.3	24.4	0.2	378	6.1		382
Bt1 - 1	25591.5	95.9	1030.0	6.8	13.5	0.8	123.7	43.1	0.4	1.3	24.9	0.2	384	6.3		388
Bt1 - 2	26786.3	165.2	1060.3	8.0	12.2	1.0	-22.0	19.1	0.2	0.9	25.3	0.3	390	7.7		394
Bt2 - 1	17373.5	163.5	699.4	5.5	11.1	1.4	22.7	19.1	0.0	0.9	24.8	0.3	384	9.2		388
Bt2 - 2	57527.7	169.3	2313.3	11.1	32.0	2.6	49.5	19.1	2.2	0.9	24.9	0.1	385	5.2		389
Bt3 - 1	19376.2	163.8	779.6	5.9	9.8	1.0	141.1	19.1	0.5	0.9	24.9	0.3	385	8.6		389
Bt3 - 2	33295.1	167.1	1320.9	8.5	15.8	1.0	154.5	19.1	2.9	0.9	25.2	0.2	389	6.7		393
Bt4 - 1	51519.6	169.0	2072.7	9.5	25.3	1.3	94.2	19.1	1.5	0.9	24.9	0.1	385	5.2		389
Bt4 - 2	28788.9	165.9	1160.5	8.2	14.5	1.1	239.4	19.1	2.2	0.9	24.8	0.2	384	7.2		388
Bt4 - 3	34797.1	166.6	1391.1	7.7	17.2	1.1	127.7	19.1	1.0	0.9	25.0	0.2	387	6.2		391
Average Blank	1213.8	10.5	12.4	0.4	1.2	0.3	44.8	0.9	5.0	0.4						

* Data are corrected for ^{36}Ar where the ^{36}Ar measurement is > 2x the ^{36}Ar background (blank) measurement

Ages recalculated using the deacy constants of Min et al., (2000) and biotite standard age of 99.7 of Renne et al., (2010)

UV laser spot data

D.3: NF42 Krokkenakken Garnetiferous Gneiss with High Pressure Relicts

61°54'53.73" N

005°20'16.49" E

J value 0.0095 ± 4.47E-05

Nu

Sample	**^{40}Ar** Counts	± 1σ	**^{39}Ar** Counts	± 1σ	**^{38}Ar** Counts	± 1σ	**^{37}Ar** Counts	± 1σ	**^{36}Ar** Counts	± 1σ	**$^{40}Ar^*/^{39}Ar$**	± 1σ	**Age** Ma	± 1σ	**Corr?***	**Age#** Ma
Mu1 - T1 - 1	111917.2	129.3	3693.4	13.0	46.0	1.5	1.1	8.9	27.0	1.3	28.1	0.2	429	2.8	Y	434
Mu1 - T1 - 2	122323.0	130.5	4145.2	13.0	52.9	1.6	20.1	8.9	25.5	1.3	27.7	0.1	423	2.6	Y	428
Mu1 - T1 - 3	80023.3	74.4	3088.0	11.0	40.3	1.9	-2.4	6.0	1.7	0.9	25.9	0.1	399	4.5		403
Mu1 - T1 - 4	48665.3	79.7	1872.5	9.1	23.5	0.8	-1.4	16.3	-1.4	1.1	26.0	0.1	400	5.1		404
Mu1 - T1 - 5	75305.4	91.8	2957.6	11.0	41.8	3.1	7.3	16.3	2.4	1.1	25.5	0.1	393	4.5		397
Mu1 - T2 - 1	63541.6	83.6	2390.8	12.0	34.5	2.7	257.7	16.3	5.8	1.0	26.6	0.1	408	5.3		412
Mu1 - T2 - 2	102430.6	104.1	3508.7	12.0	39.1	1.2	270.6	16.3	3.0	1.0	29.2	0.1	444	4.8		448
Mu1 - T2 - 3	73370.8	64.3	2262.7	11.0	28.6	1.4	23.5	13.3	0.9	1.4	32.4	0.2	487	6.0		492
Mu1 - T2 - 4	76173.4	73.4	2513.2	12.0	28.5	1.0	78.1	13.3	0.4	1.4	30.3	0.2	459	5.7		463
Mu1 - T2 - 5	73467.4	65.9	2683.6	12.0	30.5	1.0	-13.4	13.3	-0.3	1.4	27.4	0.1	419	5.1		423
Mu1 - T2 - 6	80578.1	81.2	2833.9	12.0	36.7	2.4	-5.1	13.3	-1.2	1.4	28.4	0.1	433	5.1		438
Mu1 - T2 - 7	62453.0	61.2	2182.5	10.0	29.2	1.1	22.3	13.3	20.1	1.4	25.9	0.2	399	3.6	Y	403
Mu1 - T2 - 8	107812.0	79.4	4267.0	17.1	51.2	1.5	-0.3	13.3	-0.7	1.4	25.3	0.1	390	4.5		394
Mu1 - T2 - 9	91389.8	82.9	3615.6	12.0	45.8	2.3	10.4	13.3	-1.1	1.4	25.3	0.1	390	4.3		394
Mu1 - T2 - 10	79072.8	70.0	3164.6	14.0	38.2	2.0	-5.1	13.3	-0.8	1.4	25.0	0.1	386	4.7		390

Sample	^{40}Ar Counts	± 1σ	^{39}Ar Counts	± 1σ	^{38}Ar Counts	± 1σ	^{37}Ar Counts	± 1σ	^{36}Ar Counts	± 1σ	$^{40}Ar^*/^{39}Ar$	± 1σ	Age Ma	± 1σ	Corr?*	Age# Ma
Mu1 - T2 - 11	80975.3	72.6	3244.8	14.0	42.7	2.9	16.3	13.3	0.4	1.4	25.0	0.1	386	4.6		390
Mu1 - T2 - 12	55140.5	65.1	2192.5	9.9	30.0	2.2	277.6	13.3	-0.4	1.4	25.2	0.1	388	4.8		392
Mu2 - T1 - 1	75573.1	71.7	2433.0	12.0	28.6	1.0	100.7	13.3	0.7	1.4	31.1	0.2	469	5.9		473
Mu2 - T1 - 2	100840.4	111.3	3565.3	14.0	42.9	1.5	15.9	13.1	0.6	1.1	28.3	0.1	431	5.0		436
Mu2 - T1 - 3	82513.2	104.7	3114.3	12.0	32.7	1.4	38.9	13.1	-1.2	1.1	26.5	0.1	407	4.7		411
Mu2 - T1 - 4	79107.6	103.1	3094.3	13.0	34.0	1.3	14.7	13.1	0.3	1.1	25.6	0.1	394	4.7		398
Mu2 - T2 - 1	15420.9	91.2	612.9	5.8	13.3	1.5	139.5	13.1	1.4	1.0	25.2	0.3	388	8.6		392
Mu2 - T2 - 2	37350.8	96.2	1460.8	8.3	19.3	1.0	380.6	13.1	2.0	1.0	25.6	0.2	394	5.7		398
Mu2 - T2 - 3	66991.5	97.5	2573.2	11.0	34.2	2.1	272.7	13.1	1.3	1.1	26.0	0.1	401	4.8		405
Mu2 - T2 - 4	101842.0	112.0	3575.3	15.0	40.9	1.5	32.9	13.1	-0.9	1.2	28.5	0.1	434	5.1		439
Mu2 - T2 - 5	122877.7	113.2	3565.3	13.0	53.6	1.8	80.1	13.1	71.6	1.2	28.5	0.2	435	2.8	Y	439
Mu2 - T2 - 6	76205.8	99.9	2723.5	11.0	36.4	1.3	86.2	13.1	5.5	1.0	28.0	0.1	427	5.0		432
Mu2 - T2 - 7	74000.8	109.5	2873.8	12.0	35.4	1.2	202.5	13.1	2.7	1.0	25.8	0.1	397	4.8		401
Mu3 - T1 - 1	71797.9	102.5	2783.6	11.0	31.4	1.2	58.3	13.1	-0.7	1.1	25.8	0.1	397	4.7		401
Mu3 - T1 - 2	81911.9	108.2	3144.4	13.0	35.6	1.4	6.2	13.1	-0.8	1.1	26.1	0.1	401	4.8		405
Mu3 - T1 - 3	67691.7	99.4	2693.4	12.0	41.0	2.7	3.8	13.1	-0.4	1.1	25.1	0.1	388	4.8		392
Mu3 - T1 - 4	93927.0	107.0	3765.7	15.0	45.6	1.2	35.3	13.1	2.5	1.0	24.9	0.1	385	4.5		389
Mu4 - T1 - 1	70084.4	68.2	2753.8	11.0	34.5	2.5	10.1	10.1	0.2	1.4	25.5	0.1	392	4.6		397
Mu4 - T1 - 2	78896.6	67.4	3074.4	12.0	35.2	1.1	5.2	10.1	-0.1	1.4	25.7	0.1	395	4.6		399
Mu4 - T1 - 3	80399.0	74.3	3094.5	14.0	39.5	2.4	-2.3	10.1	1.4	1.4	26.0	0.1	400	4.9		404
Mu4 - T1 - 4	76193.5	61.5	2904.1	11.0	33.1	1.3	16.3	10.1	1.1	1.3	26.2	0.1	403	4.6		408
Mu4 - T1 - 5	71285.9	70.8	2813.9	11.0	33.2	1.3	1.4	10.1	0.2	1.3	25.3	0.1	391	4.5		395
Mu4 - T1 - 6	71185.5	65.7	2843.9	12.0	34.0	1.4	471.0	10.1	0.9	1.3	25.0	0.1	387	4.6		391
Mu5 - T1 - 1	53662.6	59.1	2042.2	9.5	26.7	1.7	3.9	10.1	1.6	1.4	26.3	0.1	404	5.0		408
Mu5 - T1 - 2	76994.0	66.5	2994.3	13.0	34.4	1.1	31.1	10.1	0.0	1.4	25.7	0.1	396	4.8		400
Mu5 - T1 - 3	76793.4	71.7	3024.3	13.0	38.0	2.9	162.1	10.1	0.2	1.4	25.4	0.1	392	4.7		396
Average Blank	2283.5	11.4	12.3	0.4	1.8	0.4	48.2	0.9	9.4	0.4						

J value	0.0095	±	4.77E-05													
Sample	^{40}Ar Counts	± 1σ	^{39}Ar Counts	± 1σ	^{38}Ar Counts	± 1σ	^{37}Ar Counts	± 1σ	^{36}Ar Counts	± 1σ	$^{40}Ar^*/^{39}Ar$	± 1σ	Age Ma	± 1σ	Corr?*	$Age^{\#}$ Ma
Bt1 - 1	9030.3	35.1	277.1	3.5	7.0	0.9	3.4	88.3	7.3	0.4	32.6	0.4	488	6.1		493
Bt1 - 2	8300.2	35.1	335.3	3.9	4.6	0.6	168.7	88.3	0.4	0.4	24.8	0.3	382	4.6		386
Bt1 - 3	10924.2	36.9	439.0	3.9	7.2	1.0	-5.0	88.3	0.6	0.5	24.9	0.2	384	3.7		388
Bt1 - 4	6528.6	34.0	264.8	3.3	4.0	0.5	404.0	88.3	0.6	0.5	24.7	0.3	381	5.0		385
GM1	1577.9	31.3	59.4	1.9	1.0	0.5	91.9	88.3	1.0	0.5	26.6	1.0	408	13.7		412
GM2	1902.7	31.3	76.9	2.3	1.5	0.5	212.2	88.3	0.2	0.5	24.7	0.8	382	11.7		386
GM3	1969.3	44.1	77.9	2.2	1.1	0.4	-160.0	408.5	-0.1	0.7	25.3	0.9	390	12.9		394
GM4	1849.1	43.8	68.4	2.1	1.5	0.4	-265.9	408.5	0.3	0.7	27.0	1.1	414	14.6		418
Bt2 - 1	62588.9	85.3	2539.3	18.1	37.9	2.6	2102.5	408.5	5.2	0.7	24.7	0.2	381	3.0		385
Bt2 - 2	32815.6	75.9	1335.0	14.1	14.8	0.7	1551.9	408.5	3.0	0.7	24.6	0.3	380	4.1		384
Bt2 - 3	24104.3	35.2	1163.9	7.8	26.4	1.5	714.4	309.3	5.3	0.5	19.4	0.2	306	3.1		309
Bt3 - 1	14260.6	26.6	585.0	4.9	9.8	1.4	162.3	309.3	0.1	0.6	24.4	0.2	377	3.4		381
Bt3 - 2	16930.2	24.7	696.2	5.4	8.6	0.7	129.1	309.3	1.5	0.6	24.3	0.2	376	3.2		380
Bt3 - 3	12783.1	46.9	513.1	8.5	6.4	0.7	258.0	309.3	0.9	0.6	24.9	0.4	385	6.2		389
GM5	3330.2	57.4	131.3	2.3	1.6	0.5	-144.3	114.3	-0.4	0.5	25.4	0.6	391	8.9		395
GM6	1059.1	56.2	39.4	1.4	1.0	0.5	-55.3	114.3	-0.4	0.5	26.9	1.7	412	23.7		416
GM7	311.4	56.2	6.3	0.5	0.3	0.5	71.7	114.3	0.9	0.5	49.6	9.9	698	115.2		705
GM8	1554.7	56.9	61.0	1.7	0.5	0.5	32.2	114.3	0.2	0.5	25.5	1.2	393	16.4		397
GM9	780.8	56.2	25.7	1.4	-0.2	0.6	107.7	114.3	0.4	0.6	30.4	2.8	460	37.0		465
GM10	576.3	56.2	18.3	1.1	1.3	0.5	230.5	114.3	1.5	0.5	31.4	3.6	473	48.1		478
GM11	230.0	74.5	13.8	1.0	0.4	0.5	-145.1	165.6	0.3	0.6	16.7	5.6	266	82.4		269
GM12	235.6	73.4	7.3	0.6	-0.4	0.8	12.6	165.6	0.0	0.6	32.4	10.4	486	136.8		491
BS1	24945.0	90.5	1015.4	12.0	16.8	1.5	630.1	165.6	0.9	0.6	24.6	0.3	380	4.6		384
BS2	52359.1	113.4	2149.3	17.1	36.0	1.9	522.2	165.6	2.2	0.6	24.4	0.2	377	3.3		381
BS3	39858.9	96.8	1681.0	16.1	27.9	2.5	517.1	165.6	2.0	0.6	23.7	0.2	368	3.7		372
Qz	310.7	73.2	-0.3	0.5	1.4	0.6	245.8	165.6	0.4	0.6	-1000.1	-1545.4	NaN	3114.2		NaN
BS4	39456.3	75.1	1664.0	17.1	27.0	1.8	401.5	67.2	2.0	0.6	23.7	0.3	368	3.9		372
Average Blank	1090.5	15.0	7.1	0.3	11.0	0.3	1.2	0.3								

J value	0.0095	±	4.76E-05													
Sample	^{40}Ar	±	^{39}Ar	±	^{38}Ar	±	^{37}Ar	±	^{36}Ar	±	$^{40}Ar^*/^{39}Ar$	±	Age	±	Corr?*	Age#
	Counts	1σ	Counts	1σ	Counts	1σ	Counts	1σ	Counts	1σ		1σ	Ma	1σ		Ma
Bt1 - 1	46770.3	69.3	1598.4	7.8	27.0	2.1	-138.4	96.1	22.6	0.5	25.1	0.2	387	2.8	Y	391
Bt1 - 2	44885.6	70.0	1756.7	9.5	22.8	1.1	91.5	96.1	2.1	0.6	25.6	0.1	393	5.3		397
Bt1 - 3	51251.5	71.4	2052.5	10.0	32.3	2.3	-21.9	96.1	2.1	0.6	25.0	0.1	385	5.0		389
Bt1 - 4	51342.5	71.4	2067.1	9.9	31.1	1.8	17.5	96.1	2.4	0.6	24.8	0.1	383	4.9		387
Bt1 - T2 - 1	40518.8	68.6	1627.1	8.3	20.2	0.9	77.3	96.1	0.4	0.6	24.9	0.1	384	5.1		388
Bt1 - T2 - 2	42867.0	68.6	1675.5	8.7	29.0	2.2	162.4	96.1	2.9	0.6	25.6	0.1	394	5.2		398
Bt2 - 1	28246.4	121.0	1124.9	7.3	13.9	0.9	34.9	96.1	0.0	0.6	25.1	0.2	387	6.5		391
Bt2 - 2	33387.8	64.2	1330.4	8.4	19.4	2.0	-28.6	99.3	0.4	0.6	25.1	0.2	387	5.8		391
Bt2 - 3	28172.0	72.2	1122.8	6.4	13.3	0.8	-2.0	88.1	1.1	0.5	25.1	0.2	387	5.6		391
Bt2 - 4	30765.6	88.6	1241.8	15.1	19.3	1.7	25.3	88.1	-0.1	0.5	24.8	0.3	382	9.3		386
Bt3 - 1	29305.3	73.3	1155.9	7.7	16.1	1.0	4.4	88.1	3.8	0.4	25.4	0.2	390	6.1		394
Bt3 - 2	27623.9	81.5	1085.3	15.1	13.7	1.0	46.1	88.1	4.8	0.4	24.2	0.4	374	5.3	Y	377
Bt3 - 3	21255.3	69.0	851.2	6.3	10.4	0.8	-48.6	88.1	0.4	0.5	25.0	0.2	385	6.6		389
Bt4 - 1	34178.1	73.9	1353.4	7.2	22.9	1.5	-53.5	88.1	0.9	0.5	25.3	0.2	389	5.3		393
Bt4 - 2	37490.3	88.6	1499.4	15.1	20.9	1.5	155.5	88.1	0.7	0.5	25.0	0.3	386	8.0		390
Bt4 - 3	35351.5	85.0	1368.7	15.1	16.7	0.9	20.5	88.1	7.2	0.4	24.3	0.3	375	4.4	Y	379
Bt4 - 4	30863.0	61.7	1237.2	6.8	16.0	0.9	79.1	100.5	-0.1	0.8	25.0	0.2	385	5.3		389
Bt5 - 1	35792.5	57.7	1373.8	8.1	23.5	1.8	-9.7	100.5	6.9	0.8	24.6	0.2	379	7.1		383
Bt5 - 2	31761.9	61.0	1248.4	7.6	17.6	0.9	34.9	100.5	1.8	0.8	25.4	0.2	392	5.7		396
Bt5 - 3	28154.6	57.1	1092.7	6.7	15.8	0.9	34.9	100.5	3.1	0.9	25.8	0.2	396	5.8		400
Bt5 - 4	33748.9	59.0	1334.0	8.3	17.0	1.2	-386.9	100.5	1.2	0.8	25.3	0.2	390	5.7		394
Bt6 - 1	26074.6	56.4	1043.0	7.0	18.5	1.3	-374.2	100.5	0.7	0.8	25.0	0.2	386	6.0		389
Bt6 - 2	30686.7	58.4	1206.1	6.7	15.3	1.0	264.2	100.5	1.7	0.8	25.4	0.2	392	5.4		396
Bt6 - 3	29054.6	55.8	1161.4	6.6	15.5	1.1	244.5	100.5	1.3	0.8	25.0	0.2	386	5.4		390
Bt6 - 4	33779.6	60.4	1332.8	7.8	18.7	1.0	-63.4	100.5	2.3	0.9	25.3	0.2	390	5.6		394
Bt6 - 5	32665.9	58.4	1302.8	8.7	16.9	0.8	51.3	100.5	2.0	0.9	25.1	0.2	387	6.0		391
Average Blank	1128.4	10.1	10.9	0.3	1.1	0.3	44.6	0.8	4.6	0.4						

* Data are corrected for ^{36}Ar where the ^{36}Ar measurement is > 2x the ^{36}Ar background (blank) measurement

Ages recalculated using the deacy constants of Min et al., (2000) and biotite standard age of 99.7 of Renne et al., (2010)

UV laser spot data

D.4: NF43 Krokkenakken Eclogite and Garnetiferous Gneiss with High Pressure Relicts

61°54'53.73" N

005°20'16.49" E

J value 0.0095 ± 4.76E-05

Nu

Sample	**^{40}Ar**	±	**^{39}Ar**	±	**^{38}Ar**	±	**^{37}Ar**	±	**^{36}Ar**	±	**$^{40}Ar^*/^{39}Ar$**	±	**Age**	±	**Corr?***	**Age#**
Eclogite	Counts	1σ	Counts	1σ	Counts	1σ	Counts	1σ	Counts	1σ		1σ	Ma	1σ		Ma
T1 - 1	19505.5	39.1	811.0	7.0	10.2	0.9	517.2	5.9	1.2	0.9	24.1	0.2	372	6.9		376
T1 - 2	34842.0	41.7	977.0	7.0	17.7	1.0	535.0	5.9	33.9	1.0	25.4	0.4	391	5.2	Y	395
T1 - 3	34867.0	38.2	1327.0	9.3	18.1	1.7	274.9	5.9	-2.1	1.0	26.3	0.2	403	6.3		407
T1 - 4	55415.3	55.6	2059.7	10.0	22.3	2.4	-3.7	6.1	-2.2	1.0	26.9	0.1	411	2.6	Y	416
T1 - 5	47306.3	48.1	1762.5	9.1	20.2	1.0	6.3	5.9	-0.7	1.1	26.8	0.1	411	5.3		415
T1 - 6	52653.9	52.7	2017.5	8.3	27.3	2.3	3.8	5.9	-1.7	1.0	26.1	0.1	400	4.7		404
T1 - 7	41169.1	79.8	1562.3	8.4	18.0	1.0	204.2	5.9	-0.6	1.3	26.4	0.2	404	5.5		408
T1 - 8	19333.8	76.3	758.5	5.6	9.2	0.8	1304.7	5.9	2.0	1.2	25.5	0.2	392	6.9		396
T1 - 9	12183.4	72.6	417.6	4.3	4.9	0.7	492.9	5.9	1.7	1.2	29.2	0.4	442	10.2		447
T1 - 10a	5968.6	70.4	223.4	3.4	3.9	0.7	1138.3	5.9	1.7	1.2	26.7	0.5	409	14.6		413
T1 - 11	3242.8	69.9	129.9	2.4	2.8	0.6	987.9	5.9	-0.4	1.3	25.0	0.7	385	20.1		388
T2 - 1	41255.4	81.4	1557.2	7.9	17.8	1.2	125.8	5.9	1.9	1.2	26.5	0.1	406	5.4		410
T2 - 2	33849.9	81.4	1278.2	8.7	13.4	0.9	106.2	5.9	-0.9	1.3	26.5	0.2	406	6.4		410
T2 - 3	57502.6	83.7	2150.8	10.0	29.5	2.4	88.4	5.9	2.4	1.2	26.7	0.1	409	5.1		413
T2 - 4	41425.8	264.0	1482.2	8.2	17.4	1.1	67.9	7.5	0.3	1.4	28.0	0.2	426	7.5		430

Sample	^{40}Ar	±	^{39}Ar	±	^{38}Ar	±	^{37}Ar	±	^{36}Ar	±	$^{40}Ar^*/^{39}Ar$	±	Age	±	Corr?*	Age#
Eclogite	Counts	1σ	Counts	1σ	Counts	1σ	Counts	1σ	Counts	1σ		1σ	Ma	1σ		Ma
T2 - 5	49168.1	264.5	1859.5	9.0	24.6	1.9	81.6	7.5	-0.9	1.4	26.4	0.2	405	6.4		409
T2 - 6	55190.8	263.8	2120.0	9.7	24.4	1.1	-1.1	7.5	1.2	1.4	26.0	0.2	399	6.0		404
T2 - 7	62322.8	265.8	2217.3	11.0	25.7	1.1	11.2	7.5	1.9	1.4	28.1	0.2	428	6.3		432
T2 - 8	58376.0	266.2	2173.6	9.9	24.1	1.1	7.8	7.5	2.5	1.4	26.9	0.2	411	6.0		415
T2 - 9	125170.9	272.5	2501.7	9.9	62.6	1.9	14.2	7.5	194.6	2.4	27.1	0.3	413	4.8	Y	418
T2 - 10	67126.6	268.2	2458.3	11.0	26.6	1.1	5.1	7.5	2.2	1.4	27.3	0.2	417	5.8		421
T2 - 11	64615.2	267.1	2370.6	10.0	27.3	1.2	4.2	7.5	4.7	1.4	27.3	0.2	416	5.8		420
T2 - 12	52236.5	240.5	1986.2	9.9	21.8	1.2	5.0	3.2	1.0	1.5	26.3	0.2	403	6.1		407
T2 - 13	57212.6	240.7	2180.0	9.4	23.8	1.3	119.2	3.2	-1.1	1.6	26.2	0.2	402	5.7		406
T2 - 14	22645.3	237.4	919.6	6.5	11.3	1.1	839.7	3.2	0.3	1.5	24.6	0.3	380	9.3		384
T2 - 15	17967.2	254.1	693.9	6.4	9.0	1.1	617.6	3.2	1.8	1.5	25.9	0.4	398	12.6		402
T2 - 16	19024.3	237.3	780.8	6.1	8.3	1.1	699.2	3.2	-1.9	1.6	24.4	0.4	376	10.6		380
T2 - 17	25544.2	237.4	1038.3	7.2	12.0	1.2	302.8	3.2	-2.4	1.6	24.6	0.3	380	8.7		384
T2 - 18	32074.4	237.7	1243.9	7.2	14.0	1.2	129.1	3.2	0.5	1.5	25.8	0.2	396	7.6		400
T2 - 19	15474.3	236.9	620.0	5.1	8.0	1.6	538.8	3.2	0.4	1.5	25.0	0.4	385	12.5		389
T2 - 20	13350.0	109.3	528.6	5.8	4.6	1.2	677.4	8.4	1.8	1.1	25.3	0.4	389	10.2		393
T2 - 21	14620.1	110.3	594.9	4.6	8.1	1.0	694.7	8.4	1.7	1.1	24.6	0.3	379	8.2		383
T2 - 22	33235.1	113.2	1307.9	7.3	15.7	1.1	352.0	8.4	2.0	1.1	25.4	0.2	391	5.8		395
Bt 1	20061.4	111.3	808.2	6.2	13.9	1.7	197.6	8.4	1.4	1.1	24.8	0.2	383	7.4		387
Bt 2	49964.1	118.7	1958.3	9.9	22.9	1.1	92.5	8.4	-0.5	1.2	25.5	0.1	392	5.3		396
Bt 3	39012.1	113.6	1523.5	9.3	22.3	2.1	151.1	8.4	2.6	1.1	25.6	0.2	394	6.0		398
Average Blank	3093.4	12.8	12.5	0.4	2.4	0.4	48.6	0.9	12.4	0.4						

J Value	0.0095	±	4.75E-05													
Sample	**^{40}Ar**	**±**	**^{39}Ar**	**±**	**^{38}Ar**	**±**	**^{37}Ar**	**±**	**^{36}Ar**	**±**	**$^{40}Ar^*/^{39}Ar$**	**±**	**Age**	**±**	**Corr?***	**Age#**
Eclogite-Gneiss Contact	Counts	1σ	Counts	1σ	Counts	1σ	Counts	1σ	Counts	1σ		1σ	Ma	1σ		Ma
Mu1 - T1 - 1	5123.5	52.5	231.3	3.2	3.6	0.6	671.6	24.5	0.3	0.6	22.2	0.4	345	11.3		348
Mu1 - T1 - 2	28826.6	59.3	1125.9	7.6	13.8	0.9	393.7	24.5	0.9	0.6	25.6	0.2	393	6.1		397
Mu1 - T1 - 3	74885.7	81.7	2849.5	11.0	30.0	1.2	9.6	24.5	1.8	0.7	26.3	0.1	402	4.6		407
Mu1 - T1 - 4	83573.8	74.7	2781.3	11.0	35.9	1.3	0.7	24.5	29.7	0.6	26.9	0.1	411	2.5	Y	415
Mu1 - T1 - 5	80656.9	80.1	3021.9	12.0	38.5	2.9	-65.7	24.5	3.6	0.7	26.7	0.1	408	4.7		412
Mu1 - T1 - 6	73719.1	274.9	2686.5	13.0	37.0	2.0	-26.9	24.5	10.9	0.5	26.2	0.2	402	3.0	Y	406
Mu1 - T1 - 7	67756.2	101.0	2582.3	20.1	27.5	1.1	7.9	24.5	-0.3	0.6	26.2	0.2	402	6.7		406
Mu1 - T1 - 8	9510.5	54.0	371.2	3.9	4.0	0.7	26.0	24.5	0.9	0.6	25.6	0.3	393	9.2		397
Mu1 - T1 - 9	62587.8	76.2	2464.0	11.0	25.4	1.1	124.1	24.5	0.1	0.6	25.4	0.1	390	4.8		394
Mu1 - T1 - 10	65079.1	79.3	2579.1	9.7	28.4	1.3	39.0	24.5	1.3	0.6	25.2	0.1	388	4.5		392
Mu1 - T1 - 11	62169.1	73.2	2470.2	11.0	26.4	1.1	153.0	24.5	0.5	0.6	25.2	0.1	387	4.7		391
Mu1 - T2 - 1	6999.2	66.1	288.8	3.9	3.8	0.7	478.0	34.8	0.2	0.7	24.2	0.4	374	11.7		378
Mu1 - T2 - 2	23634.5	72.4	932.2	6.1	11.5	0.9	501.6	34.8	0.3	0.7	25.4	0.2	390	6.2		394
Mu1 - T2 - 3	72720.4	90.9	2728.3	12.0	28.2	1.1	17.2	34.8	1.9	0.7	26.7	0.1	408	5.0		412
Mu1 - T2 - 4	71910.7	90.2	2690.1	12.0	35.6	2.1	4.3	34.8	0.4	0.7	26.7	0.1	409	5.0		413
Mu1 - T2 - 5	63966.9	81.2	2415.5	10.0	26.0	1.1	25.7	34.8	3.2	0.7	26.5	0.1	405	4.8		409
Mu1 - T2 - 6	60064.0	84.3	2246.7	11.0	24.3	1.0	34.4	34.8	3.9	0.8	26.7	0.1	409	5.2		413
Mu1 - T2 - 7	63085.9	83.7	2416.5	11.0	24.7	1.1	22.2	34.8	0.2	0.7	26.1	0.1	400	5.0		404
Mu1 - T2 - 8	58020.5	87.5	2250.3	11.0	27.2	2.2	35.1	34.8	1.0	0.7	25.8	0.1	396	5.1		400
Mu1 - T2 - 9	61657.7	83.0	2364.4	9.4	23.4	1.1	49.2	34.8	0.4	0.6	26.1	0.1	400	4.7		404

Sample Eclogite-Gneiss Contact	^{40}Ar Counts	± 1σ	^{39}Ar Counts	± 1σ	^{38}Ar Counts	± 1σ	^{37}Ar Counts	± 1σ	^{36}Ar Counts	± 1σ	$^{40}Ar^*/^{39}Ar$	± 1σ	Age Ma	± 1σ	Corr?*	Age# Ma
Mu1 - T2 - 10	56604.2	72.2	2240.3	11.0	31.3	2.2	-37.2	32.1	1.2	0.9	25.3	0.1	388	5.0		392
Mu1 - T2 - 11	49695.7	76.4	1968.0	9.0	21.2	1.1	60.6	32.1	0.6	0.9	25.3	0.1	388	4.9		392
Mu1 - T2 - 12	66106.9	74.3	2622.2	9.6	28.8	1.1	88.9	32.1	1.2	0.9	25.2	0.1	388	4.4		392
Mu1 - T3 - 1	12512.0	57.7	538.0	5.4	6.6	0.9	563.5	32.1	-0.8	0.8	23.3	0.3	360	8.0		364
Mu1 - T3 - 2	5218.0	55.3	209.3	3.1	2.9	0.7	337.5	32.1	0.4	0.8	24.9	0.5	384	13.2		388
Mu1 - T3 - 3	35631.1	64.6	1336.2	8.9	15.2	0.9	298.7	32.1	2.5	0.9	26.7	0.2	408	6.2		412
Mu1 - T3 - 4	59009.1	77.1	2282.2	11.0	29.4	2.2	11.0	32.1	-0.3	0.9	25.9	0.1	397	5.0		401
Mu1 - T3 - 5	67978.5	79.3	2686.3	11.0	31.1	1.0	30.0	32.1	4.1	0.8	25.3	0.1	389	4.6		393
Mu1 - T3 - 6	57133.6	76.4	2213.8	9.6	25.6	1.0	51.7	32.1	1.6	0.9	25.8	0.1	396	4.8		400
Mu1 - T3 - 7	40331.9	79.3	1537.6	8.1	17.4	1.0	-28.8	63.1	-1.2	0.6	26.2	0.2	402	5.4		406
Mu1 - T3 - 8	47519.8	86.3	1852.8	8.6	20.1	0.9	6.7	63.1	-1.0	0.6	25.7	0.1	394	5.0		398
Mu1 - T3 - 9	44297.7	95.7	1669.4	18.1	18.0	0.9	-0.7	63.1	-0.1	0.6	26.5	0.3	406	8.8		410
Mu1 - T3 - 10	51184.4	85.7	1940.8	9.5	27.3	2.3	72.0	63.1	2.4	0.7	26.4	0.1	404	5.2		408
Mu1 - T4 - 1	8297.4	70.1	330.3	4.3	4.2	0.6	392.2	63.1	1.1	0.6	25.1	0.4	386	11.4		390
Mu1 - T4 - 2	7207.5	69.6	216.0	3.1	1.1	0.8	299.2	63.1	0.8	0.6	33.4	0.6	497	15.5		502
Mu1 - T4 - 3	15775.0	72.8	625.9	5.1	7.0	0.8	326.0	63.1	0.4	0.6	25.2	0.2	388	7.4		392
Mu1 - T4 - 4	31068.0	77.2	1197.5	7.1	12.1	0.9	297.8	63.1	0.1	0.6	25.9	0.2	398	5.8		402
Mu1 - T4 - 5	44886.9	53.9	1787.0	9.6	19.6	0.8	74.4	3.6	1.2	0.6	25.1	0.1	386	5.2		390
Mu1 - T4 - 6	46641.3	57.5	1842.7	9.7	24.7	2.0	108.8	15.9	0.1	0.7	25.3	0.1	389	5.2		393
Mu1 - T4 - 7	46341.5	61.8	1762.5	10.0	20.3	1.0	49.3	15.9	1.3	0.7	26.3	0.2	403	5.6		407
Mu1 - T4 - 8	45640.8	60.3	1702.4	7.7	18.5	0.9	15.3	15.9	2.8	0.7	26.8	0.1	410	5.1		414

Sample Eclogite-Gneiss Contact	^{40}Ar Counts	± 1σ	^{39}Ar Counts	± 1σ	^{38}Ar Counts	± 1σ	^{37}Ar Counts	± 1σ	^{36}Ar Counts	± 1σ	$^{40}Ar^*/^{39}Ar$	± 1σ	Age Ma	± 1σ	Corr?*	Age# Ma
Mu1 - T4 - 9	48945.2	63.2	1842.7	7.7	19.7	1.0	40.8	15.9	0.6	0.7	26.6	0.1	406	4.8		410
Mu1 - T4 - 10	39511.1	53.7	1431.7	7.4	17.0	1.1	-1.8	34.0	0.7	0.9	27.6	0.2	420	5.5		425
Mu1 - T4 - 11	49924.7	58.6	1902.8	11.0	22.0	1.1	-4.7	34.0	-0.3	0.9	26.2	0.2	402	5.6		406
Mu1 - T4 - 12	53331.0	61.9	1842.7	8.4	23.2	1.7	15.5	34.0	0.7	0.9	28.9	0.1	439	5.4		443
Mu1 - T4 - 13	47021.5	57.7	1702.3	9.3	22.5	1.9	12.6	34.0	0.3	0.9	27.6	0.2	421	5.6		425
Mu1 - T4 - 14	51226.4	56.9	1963.0	9.1	24.8	2.0	35.7	34.0	-0.1	0.9	26.1	0.1	400	5.0		404
Mu1 - T4 - 15	41413.4	80.4	1531.9	11.0	16.3	1.0	21.3	34.0	-0.7	0.9	27.0	0.2	413	6.6		417
Mu1 - T4 - 16	51326.9	58.6	1922.9	11.0	20.5	1.2	12.6	34.0	-0.4	0.9	26.7	0.2	408	5.6		412
Mu1 - T4 - 17	35271.8	73.9	1341.7	8.7	17.8	1.8	-52.2	25.6	-0.1	0.6	26.3	0.2	403	6.1		407
Mu1 - T4 - 18	52295.0	81.3	1993.3	8.7	21.0	1.1	-24.1	25.6	0.6	0.6	26.2	0.1	402	4.9		406
Mu1 - T4 - 19	53696.8	82.5	2063.5	10.0	21.2	1.3	-158.5	25.6	0.3	0.6	26.0	0.1	399	5.1		403
Mu1 - T4 - 20	45885.8	86.3	1802.9	9.0	23.0	2.0	76.0	25.6	-0.1	0.6	25.5	0.1	391	5.2		395
Mu1 - T4 - 21	24556.8	76.3	966.8	7.2	11.2	0.8	413.6	25.6	1.7	0.6	25.4	0.2	390	6.7		394

Sample Eclogite-Gneiss Contact	**^{40}Ar** Counts	± 1σ	**^{39}Ar** Counts	± 1σ	**^{38}Ar** Counts	± 1σ	**^{37}Ar** Counts	± 1σ	**^{36}Ar** Counts	± 1σ	**$^{40}Ar^*/^{39}Ar$**	± 1σ	**Age** Ma	± 1σ	**Corr?***	**Age#** Ma
Mu1 - T4 - 22	8906.0	69.2	296.1	3.7	5.0	0.7	157.3	25.6	3.1	0.6	30.1	0.4	454	12.4		459
Qt1 - 1	53.5	66.3	1.1	0.6	0.8	0.6	-33.4	25.6	0.0	0.6	51.1	70.4	714	812.6		722
Qt1-2	163.8	66.1	-10.3	0.9	54.6	2.6	-1393.9	25.6	0.4	0.6	-15.8	-6.5	-295	131.8		NaN
Qt1 - 3	146.9	35.4	7.5	0.6	0.5	0.5	228.7	44.2	0.3	0.6	19.6	5.0	309	72.3		312
Qt1 - 4	9041.7	40.7	34.1	1.7	2.0	0.6	362.6	44.2	2.5	0.6	265.6	13.0	2273	63.7		2300
Qt2 - 1	3010.8	37.4	119.7	2.5	2.6	0.6	129.9	44.2	-0.8	0.6	25.2	0.6	387	8.8		391
Qt2 - 2	77257.4	68.3	1.3	0.6	3.2	0.6	-7.2	44.2	4.4	0.7	61161.7	27713.8	11488	816.1		11647
Qt2 - 3	21262.6	44.9	1.0	0.6	2.2	0.6	69.3	44.2	4.7	0.5	22093.1	12991.4	9656	1055.9		9789
Qt2 - 4	447.4	35.2	1.8	0.6	2.1	0.6	-39.1	44.2	1.1	0.7	253.6	89.4	2214	449.4		2240
Qt2 - 5	7719.7	40.7	0.2	0.6	3.0	0.6	-20.0	44.2	13.7	0.5	48127.4	166029.4	11056	6210.1		11209
Qt2 - 6	6177.1	35.4	0.7	0.6	3.4	0.6	43.8	44.2	4.3	0.5	9335.8	7985.2	8114	1525.9		8224
Qt2 - 7	297.2	36.0	2.0	0.6	3.5	0.6	78.9	44.2	0.6	0.6	151.2	48.6	1608	342.3		1626
Gt1 - 1	46.7	35.7	1.0	0.6	0.1	0.6	853.6	44.2	-1.1	0.6	48.6	47.6	685	558.9		692
Gt1 - 2	287.2	35.5	0.3	0.5	0.4	0.5	974.8	44.2	1.3	0.6	1101.7	2291.6	4402	3425.7		4459
Gt1 - 3	-3.3	35.5	0.7	0.5	-0.3	0.7	965.2	44.2	0.0	0.6	-5.1	-53.8	-89	969.6		NaN
Average Blank	1179.8	9.7	11.9	0.4	1.1	0.3	44.3	0.9	455.7	0.4						

J Value	0.0095	±	4.75E-05													
Sample	**^{40}Ar**	**±**	**^{39}Ar**	**±**	**^{38}Ar**	**±**	**^{37}Ar**	**±**	**^{36}Ar**	**±**	**$^{40}Ar^*/^{39}Ar$**	**±**	**Age**	**±**	**Corr?***	**Age#**
Gneiss	Counts	1σ	Counts	1σ	Counts	1σ	Counts	1σ	Counts	1σ		1σ	Ma	1σ		Ma
Mu1 - T1 - 1	8849.9	58.5	348.8	4.5	6.3	1.1	-128.3	201.5	-0.4	1.1	25.4	0.4	390	10.8		394
Mu1 - T1 - 2	37587.6	109.1	1399.4	20.1	15.9	1.1	91.8	201.5	0.5	1.1	26.9	0.4	410	11.3		414
Mu1 - T1 - 3	41036.9	100.5	1529.7	21.1	14.9	0.8	48.4	201.5	-0.8	1.1	26.8	0.4	410	10.9		414
Mu1 - T1 - 4	40473.0	71.2	1484.1	9.4	19.4	1.8	168.5	201.5	0.3	1.1	27.3	0.2	416	6.1		420
Mu1 - T1 - 5	35735.7	98.0	1363.8	17.1	14.7	0.9	215.1	201.5	0.9	1.1	26.2	0.3	401	9.9		405
Mu1 - T2 - 1	31010.6	102.2	1253.9	17.1	15.5	2.0	271.8	201.5	0.8	1.1	24.7	0.4	381	10.2		385
Mu1 - T2 - 2	34407.8	71.2	1303.5	8.1	17.7	1.7	448.5	201.5	0.9	1.1	26.4	0.2	404	6.0		408
Mu1 - T3 - 1	37297.3	70.7	1445.6	9.3	14.7	1.0	140.1	209.8	-1.0	0.8	25.8	0.2	395	6.0		400
Mu1 - T3 - 2	49535.1	75.4	1861.4	9.8	21.5	0.9	7.9	209.8	0.9	0.8	26.6	0.2	407	5.4		411
Mu1 - T4 - 1	40799.6	74.7	1598.4	9.3	15.6	0.9	38.5	209.8	0.1	0.8	25.5	0.2	392	5.6		396
Mu1 - T4 - 2	36614.2	108.3	1418.5	18.1	14.6	0.8	120.2	209.8	0.1	0.8	25.8	0.3	396	9.9		400
Mu2 - T1 - 1	37681.3	68.1	1474.3	8.1	19.4	1.8	181.6	209.8	0.4	0.8	25.6	0.2	392	5.4		396
Mu2 - T1 - 2	46910.5	68.7	1837.0	10.0	19.8	1.1	14.7	209.8	0.1	0.8	25.5	0.1	392	5.3		396
Mu2 - T1 - 3	36490.1	72.7	1405.1	9.3	15.7	1.1	50.2	209.8	0.1	0.8	26.0	0.2	398	6.1		402
Mu2 - T1 - 4	27185.5	75.5	1035.4	6.6	10.3	0.9	-233.0	382.6	-0.6	0.7	26.3	0.2	402	6.2		406

Sample Gneiss	^{40}Ar Counts	± 1σ	^{39}Ar Counts	± 1σ	^{38}Ar Counts	± 1σ	^{37}Ar Counts	± 1σ	^{36}Ar Counts	± 1σ	$^{40}Ar^*/^{39}Ar$	± 1σ	Age Ma	± 1σ	Corr?*	Age# Ma
Mu2 - T1 - 5	29709.0	82.8	1109.1	6.8	14.8	1.7	-229.5	382.6	3.1	0.6	26.8	0.2	409	6.2		413
Mu2 - T1 - 6	38636.3	110.4	1468.3	16.1	14.7	1.0	367.1	382.6	0.4	0.7	26.3	0.3	403	8.9		407
Mu2 - T1 - 7	35690.9	78.7	1430.1	8.1	18.9	2.0	-50.5	382.6	0.7	0.7	25.0	0.2	384	5.5		388
Mu2 - T2 - 1	40400.8	77.0	1512.0	8.2	18.1	1.9	266.5	382.6	2.7	0.8	26.7	0.2	408	5.6		412
Mu2 - T2 - 2	11708.4	70.2	472.6	4.4	6.1	0.8	502.4	382.6	0.6	0.7	24.8	0.3	381	8.4		385
Mu2 - T3 - 1	38200.6	77.6	1440.8	8.8	17.9	1.8	179.8	382.6	0.0	0.7	26.5	0.2	405	5.9		409
Mu2 - T3 - 2	16613.6	75.2	683.5	14.1	7.1	0.7	-364.3	394.4	-0.7	0.8	24.3	0.5	375	14.6		379
Mu2 - T4 - 1	37512.3	93.7	1456.3	22.1	17.7	1.6	-304.1	394.4	0.2	0.8	25.8	0.4	395	11.5		399
Mu2 - T4 - 2	34782.0	100.4	1355.0	19.1	15.5	1.6	46.1	394.4	-0.3	0.7	25.7	0.4	394	10.8		398
Mu2 - T5 - 1	33377.3	101.3	1245.7	18.1	11.5	0.8	201.8	394.4	0.4	0.8	26.8	0.4	409	11.4		413
Mu2 - T5 - 2	29952.6	101.3	1138.1	16.1	11.2	0.8	-113.1	394.4	0.0	0.8	26.3	0.4	403	11.1		407
Mu2 - T6 - 1	37182.6	101.3	1420.8	19.1	12.6	0.9	24.9	394.4	0.5	0.8	26.2	0.4	401	10.5		405
Mu2 - T6 - 2	36973.0	103.0	1406.6	19.1	16.0	1.5	-17.6	394.4	1.4	0.8	26.3	0.4	402	10.6		406
Mu2 - T7 - 1	38530.6	97.0	1578.4	22.1	15.5	0.8	-176.8	394.4	0.6	0.8	24.4	0.4	376	10.2		380
Mu2 - T7 - 2	33921.6	101.3	1368.3	21.1	17.7	2.3	60.3	394.4	0.3	0.8	24.8	0.4	382	11.3		385

Sample Gneiss	^{40}Ar Counts	± 1σ	^{39}Ar Counts	± 1σ	^{38}Ar Counts	± 1σ	^{37}Ar Counts	± 1σ	^{36}Ar Counts	± 1σ	$^{40}Ar^*/^{39}Ar$	± 1σ	Age Ma	± 1σ	Corr?*	Age# Ma
Mu2 - T8 - 1	13934.4	78.8	557.9	12.0	4.1	1.2	453.0	394.4	0.2	0.8	25.0	0.6	384	15.8		388
Mu2 - T8 - 2	15776.6	84.1	645.9	16.1	8.6	1.1	402.2	394.4	1.1	0.8	24.4	0.6	376	17.6		380
Bt1 - T1 - 1	12449.7	62.3	507.6	5.4	5.3	0.6	-31.8	129.4	-0.6	0.7	24.5	0.3	378	8.7		382
Bt1 - T1 - 2	17807.5	84.1	749.8	15.1	9.6	1.0	-122.0	129.4	0.0	0.7	23.8	0.5	367	14.1		371
Bt1 - T1 - 3	39467.0	123.4	1528.1	19.1	16.4	1.0	101.8	129.4	-0.1	0.7	25.8	0.3	396	9.8		400
Bt1 - T1 - 4	30352.6	95.1	1205.0	18.1	13.8	2.0	62.1	129.4	0.5	0.8	25.2	0.4	387	11.2		391
Bt1 - T1 - 5	28266.1	93.5	1136.5	19.1	14.9	2.2	-12.9	129.4	0.8	0.7	24.9	0.4	383	12.3		387
Bt1 - T1 - 6	21961.2	65.8	876.1	6.9	9.8	0.8	54.8	129.4	0.8	0.8	25.1	0.2	385	6.8		389
Bt1 - T1 - 7	43210.6	123.4	1744.9	20.1	24.1	1.9	224.4	129.4	0.2	0.7	24.8	0.3	381	8.8		385
Bt1 - T2 - 1	17220.5	48.3	687.7	6.4	7.0	0.8	-203.8	162.9	0.0	0.7	25.0	0.2	385	7.6		389
Bt1 - T2 - 2	29362.8	88.3	1207.5	20.1	11.1	0.7	-248.8	162.9	-0.5	0.7	24.3	0.4	375	11.9		379

Sample Gneiss	^{40}Ar Counts	± 1σ	^{39}Ar Counts	± 1σ	^{38}Ar Counts	± 1σ	^{37}Ar Counts	± 1σ	^{36}Ar Counts	± 1σ	$^{40}Ar^*/^{39}Ar$	± 1σ	Age Ma	± 1σ	Corr?*	Age# Ma
Bt1 - T2 - 3	24687.8	54.6	977.9	6.2	9.7	0.7	120.1	162.9	0.2	0.7	25.3	0.2	388	5.9		392
Bt1 - T2 - 4	29077.7	81.1	1183.6	16.1	14.9	1.2	20.7	162.9	0.8	0.7	24.6	0.3	378	10.1		382
Bt1 - T2 - 5	34306.7	57.6	1341.5	8.2	15.1	0.8	248.9	162.9	0.1	0.7	25.6	0.2	392	5.7		396
Bt1 - T2 - 6	42193.4	98.4	1680.5	20.1	17.1	0.8	204.7	162.9	-0.4	0.7	25.1	0.3	386	9.1		390
Bt1 - T2 - 7	31894.5	80.2	1286.9	19.1	19.4	1.9	204.7	162.9	0.7	0.7	24.8	0.4	381	10.9		385
Bt1 - T3 - 1	43727.9	66.8	1747.7	9.3	24.7	1.9	101.0	135.0	-0.3	0.7	25.0	0.1	385	5.2		389
Bt1 - T3 - 2	41332.4	68.8	1633.4	9.7	18.8	0.9	142.3	135.0	0.4	0.7	25.3	0.2	389	5.6		393
Bt1 - T3 - 3	34926.8	67.4	1414.8	7.9	15.6	0.8	82.2	135.0	1.3	0.6	24.7	0.2	380	5.3		384
Bt1 - T3 - 4	30871.2	63.6	1248.3	8.2	14.4	0.7	157.3	135.0	-0.4	0.6	24.7	0.2	381	5.9		385
Bt1 - T3 - 5	21786.3	59.0	874.9	7.1	9.7	0.6	-97.9	135.0	-0.1	0.6	24.9	0.2	383	6.9		387
Bt1 - T3 - 6	23180.5	60.6	939.6	6.3	10.7	0.8	575.6	135.0	1.0	0.6	24.7	0.2	380	6.0		384
Bt1 - T3 - 7	29453.5	63.6	1188.6	7.1	13.1	0.9	74.7	135.0	1.2	0.6	24.8	0.2	381	5.6		385
Average Blank	1194.3	14.3	10.9	0.3	1.4	0.3	43.0	0.9	5.4	0.5						

* Data are corrected for ^{36}Ar where the ^{36}Ar measurement is > 2x the ^{36}Ar background (blank) measurement

Ages recalculated using the deacy constants of Min et al., (2000) and biotite standard age of 99.7 of Renne et al., (2010)

UV laser spot data

D.5: NF48 Flatraket Harbour Garnetiferous Gneiss without High Pressure Relicts

61°54'53.73" N

005°20'16.49" E

J value 0.0095 ± 4.74E-05

Nu

Sample	**^{40}Ar** Counts	± 1σ	**^{39}Ar** Counts	± 1σ	**^{38}Ar** Counts	± 1σ	**^{37}Ar** Counts	± 1σ	**^{36}Ar** Counts	± 1σ	**$^{40}Ar^*/^{39}Ar$**	± 1σ	**Age** Ma	± 1σ	**Corr?***	**Age#** Ma
biotite 1 rim	92695.5	116.2	3741.1	13.0	145.8	3.7	-3.7	5.4	1.7	1.3	24.8	0.1	381	4.3		385
biotite 1 core	94447.5	117.4	3804.4	13.0	134.2	4.8	1.4	5.4	2.2	1.3	24.8	0.1	382	4.3		386
bt 1 rim (2)	74522.0	108.1	3012.0	11.0	117.0	3.9	6.2	5.4	1.7	1.3	24.7	0.1	381	4.4		384
bt f1	7952.5	94.8	326.1	3.8	11.7	0.9	5.6	5.4	-2.4	1.4	24.4	0.4	376	11.9		379
bt f2	10568.5	97.5	423.8	5.0	14.9	0.9	1.4	5.4	1.2	1.3	24.9	0.4	383	10.9		387
bt f3	30098.3	101.6	1236.8	8.2	47.9	3.2	7.0	5.4	1.8	1.2	24.3	0.2	375	6.1		379
bt f4	25475.0	100.5	1017.1	7.7	34.8	1.3	138.8	5.4	-0.9	1.4	25.1	0.2	385	6.9		389
bt f5	47475.6	104.4	1919.8	8.8	22.3	1.1	3.2	5.4	1.5	1.3	24.7	0.1	380	4.9		384
bt5 rim	41401.3	61.9	1683.2	8.9	63.2	2.6	-8.3	10.9	-0.5	1.4	24.6	0.1	378	5.1		382
bt5 core 1	44705.0	293.6	1762.1	15.0	61.9	1.5	-17.0	10.9	-0.1	1.4	25.4	0.3	389	8.3		393
bt5 core 2	47979.1	732.5	1632.3	20.1	59.6	3.9	-0.3	10.9	0.2	1.5	29.4	0.6	444	15.9		448
bt 5 rim	37761.3	60.4	1554.9	8.5	57.1	3.2	3.7	10.9	2.1	1.2	24.3	0.1	374	5.1		378
bt 6	59685.6	74.3	2444.8	10.0	83.5	2.7	-21.8	10.9	-1.8	1.3	24.4	0.1	376	4.5		380
bt qtz boundary	44973.8	60.4	1855.5	10.0	72.9	2.9	15.2	10.9	0.2	1.4	24.2	0.1	374	5.1		377
bt qtz core	31816.5	75.2	1150.8	13.0	48.3	3.7	-0.4	10.9	15.2	1.3	27.7	0.3	420	4.7	Y	425
bt 7	52792.9	69.5	2152.4	10.0	79.8	3.3	1.5	10.9	2.0	1.2	24.5	0.1	378	4.7		381
Biotite 8	30826.8	189.2	1244.3	6.9	45.3	2.6	-2.4	5.3	-1.2	1.7	24.8	0.2	381	6.7		385
Biotite 9	17971.4	188.3	714.1	5.3	29.0	2.3	1.7	5.3	0.4	1.6	25.2	0.3	386	9.6		390
Average Blank	3273.3	13.1	12.7	0.4	2.5	0.4	49.6	1.0	13.1	0.4						

J Value	0.0095	±	4.76E-05													
Sample	^{40}Ar Counts	± 1σ	^{39}Ar Counts	± 1σ	^{38}Ar Counts	± 1σ	^{37}Ar Counts	± 1σ	^{36}Ar Counts	± 1σ	$^{40}Ar^*/^{39}Ar$	± 1σ	Age Ma	± 1σ	Corr?*	Age# Ma
Mu1 - T1 - 1	45120.9	85.9	1809.0	10.0	20.3	1.0	-99.4	83.1	-0.7	0.9	24.9	0.2	384	5.3		388
Mu1 - T1 - 2	67618.1	114.6	2698.8	21.7	36.4	2.2	60.7	83.1	1.4	0.9	25.1	0.2	386	6.7		390
Mu1 - T1 - 3	41211.4	83.1	1638.2	8.0	26.9	1.8	-73.4	83.1	-1.1	0.9	25.2	0.1	387	5.1		391
Mu1 - T1 - 4	50188.8	92.8	2035.2	8.4	22.7	1.0	-44.6	83.1	-0.5	0.9	24.7	0.1	380	4.6		384
Mu1 - T1 - 5	53449.4	89.5	2140.0	9.7	22.3	1.2	82.3	83.1	0.1	0.9	25.0	0.1	385	4.8		388
Mu1 - T1 - 6	57034.0	111.4	2285.8	20.7	28.2	2.4	-40.3	83.1	-0.1	0.9	25.0	0.2	384	7.3		388
Mu1 - T1 - 7	50507.1	85.3	2025.6	9.3	26.5	2.7	-79.2	83.1	-0.4	0.9	24.9	0.1	384	4.8		388
Mu1 - T1 - 8	40891.1	81.5	1611.7	9.0	25.5	2.0	17.5	83.1	4.0	0.8	25.4	0.2	390	5.4		394
Mu1 - T2 - 1	43688.0	101.9	1766.2	17.6	31.6	1.4	-35.7	57.6	-0.1	0.9	24.7	0.3	381	7.8		385
Mu1 - T2 - 2	35136.4	84.9	1408.9	14.5	15.6	0.9	450.9	57.6	-0.5	0.9	24.9	0.3	384	8.1		388
Mu1 - T2 - 3	36849.2	82.5	1478.9	15.5	14.9	0.8	-203.8	47.3	-0.1	0.8	24.9	0.3	384	8.2		388
Mu1 - T2 - 4	38932.8	85.6	1553.9	15.5	16.8	0.8	-107.8	47.3	0.3	0.8	25.1	0.3	386	7.9		390
Mu1 - T2 - 5	38733.4	205.8	1582.7	20.7	14.9	0.8	-17.8	47.3	2.0	0.7	24.5	0.4	378	10.2		381
Mu1 - T3 - 1	34895.4	84.8	1395.9	15.5	16.4	1.6	34.6	47.3	1.8	0.7	25.0	0.3	385	8.6		389
Mu1 - T3 - 2	36382.1	74.0	1461.9	8.1	20.3	2.0	-35.0	46.6	-0.2	0.8	24.9	0.2	383	5.4		387
Mu1 - T3 - 3	29911.4	83.3	1124.4	12.4	12.0	0.8	-85.3	47.3	7.2	0.7	24.7	0.3	381	5.0		385
Mu1 - T4 - 1	33442.0	86.5	1356.0	17.6	19.6	3.0	-101.8	47.3	1.1	0.8	24.7	0.3	380	9.7		384
Mu1 - T4 - 2	34261.5	77.9	1368.9	14.5	16.6	1.5	-52.3	47.3	-0.2	0.8	25.0	0.3	385	8.3		389
Mu1 - T4 - 3	32554.0	67.4	1306.8	7.3	18.0	2.1	50.3	46.6	1.2	0.8	24.9	0.2	384	5.4		388
Average Blank	1115.9	12.5	11.1	0.3	1.1	0.3	45.5	0.9	4.9	0.4						

* Data are corrected for ^{36}Ar where the ^{36}Ar measurement is > 2x the ^{36}Ar background (blank) measurement

Ages recalculated using the deacy constants of Min et al., (2000) and biotite standard age of 99.7 of Renne et al., (2010)

UV laser spot data

D.6: NF50 Flatraket Harbour Garnet-Biotite Gneiss

61°58'41.50" N

005°14'43.20" E

J value 0.0095 ± 4.77E-05

Nu

Sample	**^{40}Ar**	**±**	**^{39}Ar**	**±**	**^{38}Ar**	**±**	**^{37}Ar**	**±**	**^{36}Ar**	**±**	**$^{40}Ar^*/^{39}Ar$**	**±**	**Age**	**±**	**Corr?***	**Age#**
	Counts	1σ	Counts	1σ	Counts	1σ	Counts	1σ	Counts	1σ		1σ	Ma	1σ		Ma
GtBt1 - T1 - 1	27259.0	82.1	1070.9	7.0	56.0	1.5	650.2	64.5	-0.1	0.9	25.5	0.2	392	6.2		396
GtBt1 - T1 - 2	37673.3	84.3	1471.9	6.9	87.5	4.1	272.9	64.5	2.8	0.9	25.6	0.1	394	5.1		398
GtBt1 - T1 - 3	19448.4	79.9	764.1	5.2	44.6	2.4	354.2	64.5	-0.5	0.9	25.5	0.2	392	6.6		396
GtBt1 - T2 - 1	3887.3	76.5	153.6	2.8	7.7	0.8	676.2	64.5	-0.2	0.9	25.3	0.7	390	19.2		394
GtBt1 - T2 - 2	7532.2	76.9	302.9	3.7	15.9	1.0	494.1	64.5	0.2	0.9	24.9	0.4	384	11.6		388
GtBt1 - T2 - 3	8934.1	77.8	354.1	3.7	20.1	1.0	627.4	64.5	0.0	1.0	25.2	0.3	389	10.2		393
GtBt1 - T3	36872.0	84.7	1461.8	7.5	82.3	3.4	201.4	64.5	0.3	0.9	25.2	0.1	389	5.3		393
GtBt2 - T1 - 1	10636.5	78.3	415.2	4.1	23.1	1.0	448.5	64.5	0.5	1.0	25.6	0.3	395	9.5		399
GtBt2 - T1 - 2	16844.9	79.2	659.8	5.4	36.8	1.2	211.2	64.5	0.2	1.0	25.5	0.2	393	7.6		397
GtBt2 - T1 - 3	15642.6	90.6	618.1	4.9	37.0	2.1	287.7	42.3	-0.5	0.9	25.3	0.3	390	7.8		394
GtBt3	9734.7	88.6	379.5	4.5	25.0	2.4	311.4	42.3	-0.2	0.9	25.7	0.4	395	11.2		399
Gt1	1.4	86.3	1.4	0.6	-0.4	0.7	730.9	42.3	0.1	0.9	1.0	61.7	17	2104.6		17
Gt2	-28.6	86.3	1.3	0.6	2.0	0.6	906.8	42.3	-0.6	0.9	-22.1	-67.2	-427	2930.9		NaN
Gt3	-28.6	86.3	0.7	0.5	-0.3	0.6	673.4	42.3	0.1	0.9	-41.1	-127.9	-899	7246.3		NaN
Bt1	20749.6	90.6	815.6	6.0	43.5	1.2	277.6	42.3	-0.3	0.9	25.4	0.2	392	7.0		396
Bt2	11236.6	88.8	450.6	4.5	23.7	1.0	247.1	42.3	0.2	0.9	24.9	0.3	385	9.5		389

Sample	^{40}Ar Counts	± 1σ	^{39}Ar Counts	± 1σ	^{38}Ar Counts	± 1σ	^{37}Ar Counts	± 1σ	^{36}Ar Counts	± 1σ	$^{40}Ar^*/^{39}Ar$	± 1σ	Age Ma	± 1σ	Corr?*	Age# Ma
Bt3	34468.1	94.7	1372.0	8.7	85.2	3.6	3.6	42.3	0.2	1.0	25.1	0.2	388	6.0		392
Bt4 - 1	13139.5	88.8	488.7	4.5	30.1	2.3	111.8	42.3	5.3	0.9	23.7	0.6	367	8.6	Y	371
Bt4 - 2	18246.6	90.6	668.2	5.6	35.6	1.2	179.5	42.3	0.3	0.9	27.3	0.3	418	8.2		422
Bt5 - 1	32065.0	93.8	1261.7	6.8	76.1	3.7	47.5	42.3	1.4	0.9	25.4	0.2	392	5.6		396
Bt5 - 2	29461.3	93.4	1171.5	7.5	70.9	3.2	84.8	42.3	0.3	1.0	25.2	0.2	388	6.1		392
Bt6 - 1	27258.5	95.1	1071.2	6.3	61.1	3.4	101.7	42.3	2.6	0.9	25.5	0.2	392	6.0		396
Bt6 - 2	23653.5	91.6	940.9	6.6	58.1	2.7	115.2	42.3	0.5	0.9	25.1	0.2	388	6.6		392
Bt7 - 1	32664.7	78.8	1274.4	8.0	78.0	4.3	-40.2	31.2	0.6	0.6	25.6	0.2	395	6.0		399
Bt7 - 2	33633.4	73.9	1332.2	7.5	79.9	3.5	15.6	34.5	1.5	0.6	25.3	0.2	389	5.5		393
Bt8	49855.7	83.7	1933.7	9.5	114.0	4.2	-20.3	34.5	5.4	0.7	25.8	0.1	397	5.1		401
Qt1	87.9	67.9	2.0	0.5	0.9	0.5	-13.2	34.5	0.7	0.6	44.3	35.9	637	867.5		643
Qt2	97.9	67.8	1.0	0.5	0.2	0.5	1.2	34.5	-1.0	0.6	99.9	86.9	1208	1531.4		1221
Qt3	4434.1	68.9	145.2	2.8	7.8	0.7	184.3	34.5	0.7	0.6	30.6	0.8	462	20.7		466
Average Blank	1099.8	9.4	11.6	0.3	1.0	0.3	45.1	0.9	4.7	0.4						

J Value	0.0096	±	4.79E-05													
Sample	^{40}Ar Counts	± 1σ	^{39}Ar Counts	± 1σ	^{38}Ar Counts	± 1σ	^{37}Ar Counts	± 1σ	^{36}Ar Counts	± 1σ	$^{40}Ar^*/^{39}Ar$	± 1σ	Age Ma	± 1σ	Corr?*	Age# Ma
Bt1a - 1	32759.2	57.5	1299.8	8.3	82.9	4.1	45.5	149.8	1.4	0.9	25.2	0.2	390	5.8		394
Bt1a - 2	23997.7	49.8	955.6	7.0	57.3	3.2	59.5	149.8	-0.1	0.9	25.1	0.2	389	6.4		393
Bt2	36513.7	53.8	1464.1	8.3	92.0	4.2	-144.7	149.8	0.9	0.9	24.9	0.2	386	5.4		390
Bt3	28445.1	93.3	1129.0	7.9	71.5	3.1	-100.0	149.8	0.8	0.9	25.2	0.2	390	6.5		394
Bt4	33140.4	55.3	1305.4	6.5	80.3	3.9	-11.9	149.8	0.9	0.9	25.4	0.1	393	5.1		397
Bt5	31579.4	53.1	1258.6	7.6	76.4	3.1	9.1	149.8	1.3	0.9	25.1	0.2	388	5.6		392
Bt6-1	26308.3	46.4	1055.5	7.0	62.3	2.4	316.7	154.2	0.0	0.9	24.9	0.2	386	5.9		390
Bt6 - 2	28688.0	53.1	1135.9	6.9	74.0	2.9	-48.9	149.8	0.5	0.9	25.3	0.2	391	5.7		395
Bt6 - 3	19005.9	47.9	779.8	5.7	49.4	2.7	6.3	149.8	0.6	0.9	24.4	0.2	378	6.3		382
Bt7	21983.4	49.8	869.4	5.7	48.2	1.2	49.7	149.8	0.5	0.9	25.3	0.2	391	6.0		395
Average Blank	1176.0	11.1	11.2	0.4	1.3	0.3	46.1	1.0	5.1	0.4						

* Data are corrected for ^{36}Ar where the ^{36}Ar measurement is > 2x the ^{36}Ar background (blank) measurement

Ages recalculated using the deacy constants of Min et al., (2000) and biotite standard age of 99.7 of Renne et al., (2010)

UV laser spot data

D.7: NF51 Flatraket Harbour Biotite-Epidote Gneiss

61°58'41.50" N

005°14'43.20" E

J value 0.0096 ± 4.80E-05

Nu

Sample	**^{40}Ar** Counts	± 1σ	**^{39}Ar** Counts	± 1σ	**^{38}Ar** Counts	± 1σ	**^{37}Ar** Counts	± 1σ	**^{36}Ar** Counts	± 1σ	**$^{40}Ar^*/^{39}Ar$**	± 1σ	**Age** Ma	± 1σ	**Corr?***	**Age#** Ma
Bt1 - 1	31515.6	55.1	1260.4	8.3	45.6	2.8	60.3	21.5	1.0	1.1	25.0	0.2	388	5.9		392
Bt1 - 2	49940.5	62.3	2002.0	9.4	78.1	3.4	37.1	21.5	7.0	1.0	25.0	0.1	388	4.9		392
Bt1 - 3	53144.7	62.3	2152.3	11.0	69.5	1.6	26.2	21.5	1.4	1.1	24.7	0.1	384	5.0		388
Bt1 - 4	45133.8	64.6	1831.6	8.3	55.1	1.6	33.0	21.5	4.2	1.0	24.6	0.1	383	4.8		387
Bt2 - 1	26409.3	53.2	989.8	6.2	30.7	0.9	188.5	21.5	0.8	1.0	26.7	0.2	412	6.1		416
Bt2 - 2	35020.7	57.9	1360.6	7.4	47.9	3.4	112.1	21.5	-0.1	1.1	25.7	0.2	399	5.4		403
Bt2 - 3	51942.9	59.4	2122.3	11.0	60.2	2.8	5.7	21.5	2.8	1.0	24.5	0.1	381	5.0		385
Bt3 - 1	28575.4	52.9	1160.5	8.1	37.3	1.2	-1.0	15.9	-0.1	1.1	24.6	0.2	383	6.1		387
Bt3 - 2	30679.1	54.9	1150.5	7.9	35.5	1.3	93.6	15.9	1.0	1.1	26.7	0.2	412	6.4		416
Bt4 - 1	26773.1	51.1	1080.3	7.0	31.0	0.9	287.0	15.9	0.5	1.1	24.8	0.2	385	5.8		389
Bt4 - 2	29878.5	54.3	1060.3	7.6	34.1	1.3	214.7	15.9	1.8	1.1	28.2	0.2	432	6.9		436
Bt4 - 3	37787.7	57.7	1551.4	8.9	38.7	1.4	17.1	15.9	0.4	1.1	24.4	0.2	379	5.3		383
Bt5 - 2	34583.7	58.4	1381.0	8.8	39.9	1.1	61.6	15.9	-0.4	1.1	25.0	0.2	389	5.8		393
Bt5 - 2	16660.2	49.3	585.3	5.6	18.1	1.0	19.9	15.9	8.8	1.0	28.5	0.3	436	8.7		441
Bt5 - 3	45999.0	59.1	1852.1	8.4	49.9	1.8	38.0	15.9	0.3	1.1	24.8	0.1	386	4.8		390
Bt6 - 1	24670.3	57.0	981.1	7.1	35.6	2.5	54.7	15.9	0.4	1.1	25.2	0.2	390	6.4		394

Sample	^{40}Ar Counts	± 1σ	^{39}Ar Counts	± 1σ	^{38}Ar Counts	± 1σ	^{37}Ar Counts	± 1σ	^{36}Ar Counts	± 1σ	$^{40}Ar^*/^{39}Ar$	± 1σ	Age Ma	± 1σ	Corr?*	Age# Ma
Bt6 - 2	23553.4	124.0	974.2	7.6	29.6	1.2	129.5	17.3	0.6	1.2	24.2	0.2	377	7.2		381
Bt6 - 3	21751.4	122.4	855.9	6.7	30.9	1.9	160.7	17.3	2.0	1.2	25.4	0.3	394	7.7		398
Bt6 - 4	22051.7	122.9	874.9	7.8	30.2	2.1	174.9	17.3	1.5	1.2	25.2	0.3	391	8.2		395
Bt7 - 1	38563.9	49.7	1550.1	8.4	48.8	2.8	47.0	17.7	0.4	1.3	24.9	0.1	387	2.6		391
Bt7 - 2	33267.5	124.6	1249.8	8.6	48.1	2.8	155.0	17.3	0.3	1.2	26.6	0.2	411	6.8		415
Bt7 - 3	21551.1	122.9	851.9	6.9	28.8	1.3	218.9	17.3	-0.3	1.2	25.3	0.3	393	7.8		397
Bt8 - 1	30162.7	123.5	1199.7	9.6	37.9	1.4	98.3	17.3	0.6	1.2	25.1	0.2	390	7.2		394
Bt8 - 2	30864.8	124.3	1089.4	9.1	38.6	1.2	135.2	17.3	1.4	1.3	28.3	0.3	434	8.2		438
Ep1 - 1	1463.7	23.7	2.6	0.6	1.5	0.6	2408.9	25.2	1.7	0.6	561.5	131.2	3348	355.8		3390
Ep1 - 2	211.6	23.4	1.7	0.6	-0.3	0.7	2229.4	25.2	1.0	0.6	124.1	48.3	1417	381.7		1433
Ep1 - 3	2675.7	26.8	3.7	0.7	4.0	0.6	2731.9	25.2	1.2	0.6	721.3	129.7	3736	283.6		3783
Ep1 - 4	5479.2	28.1	160.1	2.9	6.7	0.7	2049.9	25.2	0.7	0.7	34.2	0.6	513	8.6		518
Ep2 - 1	1994.1	25.1	59.6	1.9	2.1	0.6	2983.1	25.2	2.0	0.6	33.5	1.1	503	15.1		508
Ep2 - 2	10616.1	33.0	366.6	3.9	5.5	0.7	2552.4	25.2	4.0	0.7	29.0	0.3	443	4.8		448
Ep2 - 3	1954.5	25.1	3.8	0.6	2.1	0.6	2588.3	25.2	1.7	0.6	513.0	85.1	3211	248.8		3251
Ep2 - 4	27283.5	46.2	1111.4	7.4	35.3	1.2	924.4	19.1	1.0	0.5	24.5	0.2	382	2.9		386
Ep2 - 5	12965.6	42.5	369.5	4.1	17.0	1.2	2425.3	19.1	4.1	0.3	35.1	0.4	524	5.8		529
Average Blank	1939.7	11.1	12.5	0.4	1.6	0.3	46.4	0.9	7.8	0.4						

* Data are corrected for ^{36}Ar where the ^{36}Ar measurement is > 2x the ^{36}Ar background (blank) measurement

Ages recalculated using the deacy constants of Min et al., (2000) and biotite standard age of 99.7 of Renne et al., (2010)

UV laser spot data

D.8: NF90 Drage Biotite-Epidote Gneiss

62°06'08.3" N

005°12'48.0" E

J value 0.0072 ± 3.59E-05

Nu

Sample	**^{40}Ar** Counts	± 1σ	**^{39}Ar** Counts	± 1σ	**^{38}Ar** Counts	± 1σ	**^{37}Ar** Counts	± 1σ	**^{36}Ar** Counts	± 1σ	**$^{40}Ar^*/^{39}Ar$**	± 1σ	**Age** Ma	± 1σ	**Corr?***	**Age#** Ma
Ks1 - T1 - 1	4827.9	41.4	156.4	2.9	1.5	0.5	77.9	3.4	0.3	0.7	31	0.6	361	6.9		364
Ks1 - T1 - 2	10182.8	44.3	367.9	3.6	3.2	0.6	27.8	3.4	0.8	0.7	28	0.3	327	3.6		330
Ks1 - T1 - 3	11939.4	61.6	420.2	10.0	8.3	1.3	20.7	3.4	0.5	0.7	28	0.7	334	7.6		338
Ks1 - T1 - 4	3487.6	38.0	90.8	2.0	0.9	0.6	46.7	3.4	1.0	0.7	38	1.0	439	9.9		444
Ks1 - T1 - 5	2675.2	40.6	58.8	1.9	-0.3	0.8	75.5	3.4	3.3	0.6	45	1.7	509	16.3		514
Ks1 - T1 - 6	4418.6	40.6	54.2	1.9	-0.1	0.8	51.1	3.4	0.2	0.7	82	3.0	830	24.9		839
Qz - 1	1913.4	40.2	12.2	1.2	-0.8	0.8	66.2	3.4	0.5	0.8	157	15.4	1358	93.9		1373
Qz - 2	4459.2	41.0	0.5	0.5	0.6	0.5	7.9	3.4	-0.1	0.7	8455	8515.4	7435	1787.6		7535
Ks1 - T3 - 1	7493.9	43.4	297.8	4.1	3.8	0.6	29.3	10.6	1.2	0.8	25	0.4	299	4.4		302
Ks1 - T3 - 2	13124.2	43.9	488.2	5.3	5.2	0.7	28.1	10.6	0.5	0.8	27	0.3	318	3.6		321
Ks1 - T3 - 3	13286.7	50.3	461.9	5.1	5.4	0.6	25.3	10.6	0.6	0.8	29	0.3	338	3.9		342
Ks1 - T3 - 4	17133.7	50.3	571.6	4.8	8.9	1.6	29.2	10.6	0.4	0.8	30	0.3	351	3.3		355
Ks1 - T3 - 5	16447.9	47.8	527.2	5.2	5.9	0.7	29.0	10.6	9.5	0.7	31	0.3	364	3.8		368
Ks1 - T3 - 6	19038.3	51.0	653.1	5.6	9.9	1.6	18.8	10.6	0.6	0.8	29	0.3	342	3.2		346
Ks1 - T3 - 7	10169.6	44.9	349.5	4.1	3.7	0.6	35.5	10.6	0.8	0.8	29	0.4	342	4.2		345
Ks1 - T3 - 8	17983.1	49.1	428.5	4.9	7.6	0.8	44.4	10.6	17.6	0.7	42	0.5	475	5.3		480

Sample	^{40}Ar Counts	± 1σ	^{39}Ar Counts	± 1σ	^{38}Ar Counts	± 1σ	^{37}Ar Counts	± 1σ	^{36}Ar Counts	± 1σ	$^{40}Ar^*/^{39}Ar$	± 1σ	Age Ma	± 1σ	Corr?*	Age# Ma
Ks1 - T4 - 1	14696.6	79.0	263.1	3.9	7.0	0.7	27.3	5.3	26.1	1.0	56	0.9	608	8.6		614
Ks1 - T4 - 2	2046.0	76.2	28.2	1.6	0.8	0.6	112.2	5.3	4.4	1.0	72	5.0	755	42.5		763
Ks1 - T4 - 3	3718.2	77.0	158.2	3.0	0.8	0.8	102.6	5.3	-0.7	1.1	24	0.7	281	7.4		284
Ks1 - T4 - 4	6984.8	77.5	307.4	4.4	2.8	0.7	49.0	5.3	0.1	1.1	23	0.4	272	4.8		275
Ks1 - T4 - 5	12427.8	91.2	482.4	9.3	6.1	0.7	67.3	5.3	6.3	1.0	26	0.5	306	6.0		309
Ks1 - T4 - 6	11360.8	79.3	478.4	4.8	5.7	0.7	50.6	5.3	4.4	1.0	24	0.3	284	3.5		287
Ks1 - T4 - 7	6671.1	77.8	239.7	3.3	3.4	0.7	96.8	5.3	1.5	1.1	28	0.5	328	5.6		332
Ks1 - T4 - 8	8339.8	78.4	319.1	4.1	3.5	0.7	55.9	5.3	1.7	1.1	26	0.4	310	4.8		313
Ks1 - T4 - 9	10484.5	61.0	458.0	11.0	3.7	0.7	29.6	4.3	-0.3	1.1	23	0.6	274	6.4		277
Ks1 - T4 - 10	7808.7	45.7	338.3	3.7	3.7	0.7	35.2	4.3	1.4	1.1	23	0.3	276	3.4		279
Ks1 - T4 - 11	6350.9	47.1	254.9	3.0	3.1	0.7	57.3	4.3	0.7	1.1	25	0.3	297	4.1		300
Ks1 - T4 - 12	11880.5	67.1	443.9	11.0	7.6	1.0	25.3	4.3	1.1	1.1	27	0.7	317	7.5		320
Ks1 - T4 - 13	3326.8	44.1	36.3	1.4	0.9	0.7	42.3	4.3	2.1	1.1	92	3.8	911	29.9		921
Qz - 3	543.1	49.2	8.6	1.0	0.3	0.7	65.0	4.3	0.3	1.1	63	9.1	673	81.0		680
Average Blank	1387.2	19.0	10.9	0.3	1.4	0.3	40.8	0.8	6.2	0.5						

* Data are corrected for ^{36}Ar where the ^{36}Ar measurement is > 2x the ^{36}Ar background (blank) measurement

Ages recalculated using the deacy constants of Min et al., (2000) and biotite standard age of 99.7 of Renne et al., (2010)

UV laser spot data

D.9: NF91 Drage Biotite-Epidote Gneiss

62°06'08.3" N

005°12'48.0" E

J value 0.0072 ± 3.60E-05

Nu

Sample	^{40}Ar Counts	± 1σ	^{39}Ar Counts	± 1σ	^{38}Ar Counts	± 1σ	^{37}Ar Counts	± 1σ	^{36}Ar Counts	± 1σ	$^{40}Ar^*/^{39}Ar$	± 1σ	Age Ma	± 1σ	Corr?*	$Age^{\#}$ Ma
Qz - 1	1135.0	25.2	5.1	0.4	-1.1	0.7	21.8	6.2	0.6	0.7	220.7	17.9	1715	89.9		1735
Qz - 2	3011.3	26.8	4.7	0.4	0.3	0.4	27.5	6.2	0.9	0.7	639.7	58.9	3109	136.5		3147
Bt2 - T1 - 1	20825.9	41.5	687.8	6.4	7.3	0.6	-0.5	6.2	0.0	0.7	30.3	0.3	356	3.5		359
Bt2 - T1 - 2	31546.4	87.0	1016.5	17.0	12.8	1.6	9.2	6.2	0.1	0.7	31.0	0.5	364	5.8		367
Bt3 - T1 - 1	27149.3	82.4	883.5	7.0	10.1	0.9	6.0	8.1	-0.3	0.9	30.7	0.3	360	3.2		364
Bt3 - T1 - 2	34524.4	111.2	1069.3	15.0	12.0	1.1	-1.3	8.1	0.1	0.9	32.3	0.5	377	5.2		381
Bt3 - T1 - 3	26624.2	79.9	852.8	7.2	9.8	0.8	0.9	8.1	0.9	0.9	31.2	0.3	366	3.4		369
Bt4 - T1 - 1	27714.9	81.9	734.2	6.3	10.5	1.4	19.2	8.1	0.7	0.9	37.8	0.3	433	4.0		438
Bt4 - T1 - 2	33482.5	83.5	1095.0	7.2	12.1	0.9	-0.8	8.1	1.0	0.9	30.6	0.2	359	2.8		362
Bt5 - T1 - 1	21846.0	78.5	725.7	6.0	7.5	0.9	1.0	8.1	0.4	0.9	30.1	0.3	354	3.3		357
Bt5 - T1 - 2	24438.7	80.4	873.6	6.3	10.0	0.9	8.6	8.1	-0.1	0.9	28.0	0.2	331	2.8		334
Bt6 - T1 - 1	24980.9	80.4	817.0	6.4	9.7	0.9	6.4	8.1	0.1	0.9	30.6	0.3	359	3.2		362
Bt6 - T1 - 2	19309.1	84.9	639.8	14.0	6.9	0.6	-0.1	14.6	-0.1	1.0	30.2	0.7	354	7.4		358
Bt7 - T1 - 1	29372.3	97.2	913.7	14.0	9.0	0.6	18.5	14.6	0.1	1.0	32.1	0.5	375	5.6		379
Bt7 - T1 - 2	19188.1	78.7	504.1	12.0	5.4	0.6	14.9	14.6	0.3	1.0	38.1	0.9	437	9.6		441

Sample	^{40}Ar Counts	± 1σ	^{39}Ar Counts	± 1σ	^{38}Ar Counts	± 1σ	^{37}Ar Counts	± 1σ	^{36}Ar Counts	± 1σ	$^{40}Ar^*/^{39}Ar$	± 1σ	Age Ma	± 1σ	Corr?*	Age# Ma
Bt8	23774.3	81.8	770.4	14.0	10.1	1.4	2.4	14.6	0.1	1.0	30.9	0.6	362	6.3		365
Bt9 - T1 - 1	24985.8	93.0	821.5	15.0	7.9	0.7	11.6	14.6	-0.3	1.0	30.4	0.6	357	6.3		361
Bt9 - T1 - 2	26820.7	93.8	870.3	15.0	11.8	1.3	3.0	14.6	-0.3	1.0	30.8	0.5	361	6.0		365
Bt10 - T1 - 1	27939.9	92.2	906.8	14.0	7.8	0.7	0.6	14.6	-0.4	1.0	30.8	0.5	361	5.4		365
Bt10 - T1 - 2	18509.2	86.5	624.9	15.0	7.8	1.3	36.5	14.6	-0.1	1.0	29.6	0.7	348	7.9		352
Bt11 - T1 - 1	12184.1	47.4	391.9	7.6	4.2	0.6	62.0	6.6	1.1	0.5	31.1	0.6	364	6.7		368
Bt11 - T1 - 2	23157.1	55.7	743.3	11.0	10.1	1.3	8.0	6.6	0.8	0.5	31.2	0.5	365	5.2		369
Bt11 - T1 - 3	26508.3	56.7	835.4	10.0	10.2	1.1	-1.8	6.6	0.7	0.5	31.7	0.4	371	4.4		375
Bt11 - T1 - 4	24779.6	58.6	799.9	10.0	8.4	0.7	8.0	6.6	1.7	0.3	31.0	0.4	363	4.5		367
Bt12 - T1 - 1	25035.4	47.5	824.7	5.7	9.7	0.8	-0.7	4.7	0.8	0.7	30.4	0.2	356	2.8		360
Bt12 - T1 - 2	16458.0	42.5	691.1	5.6	6.7	0.7	12.0	4.7	2.7	0.6	23.8	0.2	285	2.6		288
Bt12 - T1 - 3	21988.0	59.8	716.3	13.0	7.1	0.7	96.0	4.7	1.5	0.7	30.7	0.6	360	6.2		364
Bt12 - T1 - 4	30377.4	73.0	990.0	14.0	12.4	1.1	-4.9	4.7	0.7	0.7	30.7	0.4	360	5.0		364
Average Blank	1284.9	16.4	10.7	0.3	1.2	0.4	41.8	0.9	5.8	0.5						

* Data are corrected for ^{36}Ar where the ^{36}Ar measurement is > 2x the ^{36}Ar background (blank) measurement

Ages recalculated using the deacy constants of Min et al., (2000) and biotite standard age of 99.7 of Renne et al., (2010)

UV laser spot data

D.10: NF44A Undeformed Flatraket Granulite

62°06'08.3" N

005°12'48.0" E

J value 0.0071 ± 3.57E-05

Nu

Sample	**^{40}Ar**	**±**	**^{39}Ar**	**±**	**^{38}Ar**	**±**	**^{37}Ar**	**±**	**^{36}Ar**	**±**	**$^{40}Ar^*/^{39}Ar$**	**±**	**Age**	**±**	**Corr?***	**Age#**
	Counts	1σ	Counts	1σ	Counts	1σ	Counts	1σ	Counts	1σ		1σ	Ma	1σ		Ma
C5 Mica1-1	21359.8	380.0	629.4	9.3	8.9	0.7	7.5	56.2	-2.9	0.9	33.9	0.8	392	8.3		396
C5 Mica1-2	15551.4	379.6	463.0	9.1	5.9	0.7	7.5	56.2	0.0	0.7	33.6	1.1	388	11.1		392
C5 Mica1-3	22561.4	380.1	678.5	9.4	8.8	0.8	-0.7	56.2	-0.2	0.7	33.3	0.7	385	7.8		389
C5 Mica1-4	24564.3	380.4	743.6	10.0	9.3	0.7	136.1	56.2	-0.3	0.7	33.0	0.7	382	7.3		386
C5 Mica1-5	28269.8	380.6	825.8	10.2	10.5	0.7	-19.8	56.2	2.7	0.7	34.2	0.6	395	6.7		399
C5 mica2-1	41399.9	94.6	1197.2	8.0	15.9	0.7	12.4	8.4	1.9	1.2	34.6	0.2	398	3.1		402
C5 mica2-2	22472.4	89.3	661.1	6.8	8.7	0.6	5.4	8.4	0.9	1.2	34.0	0.4	392	4.3		396
C5 mica2-3	24475.4	90.1	704.2	6.4	12.2	1.2	-18.3	8.4	1.3	1.2	34.8	0.3	400	4.0		404
C5 mica2-4	23774.4	89.0	689.1	6.2	9.1	0.6	4.0	8.4	-2.1	1.4	34.5	0.3	398	3.9		402
C5 fsp1-2	7953.1	83.3	44.5	3.4	1.1	0.5	172.7	8.4	3.4	1.2	178.7	13.8	1485	78.6		1502
C5 fsp1-3	113418.2	109.7	1618.2	9.1	17.1	0.8	62.6	8.4	3.7	1.2	70.1	0.4	733	4.6		741
C5 fsp1-4	42400.0	99.8	1387.7	8.2	14.6	0.7	2.6	8.4	1.6	1.2	30.6	0.2	356	2.6		360
Average Blank	5353.2	16.7	62.7	1.2	5.4	0.3	78.8	1.0	19.2	0.4						

* Data are corrected for ^{36}Ar where the ^{36}Ar measurement is > 2x the ^{36}Ar background (blank) measurement

Ages recalculated using the deacy constants of Min et al., (2000) and biotite standard age of 99.7 of Renne et al., (2010)

Appendix E:

Whole Rock XRF Dataset

The beach at Rifvika

Methodology:

Major elements were determined using sample-glass discs prepared by fusing a 5:1 ratio mix of lithium metaborate/tetraborate flux (Spectroflux 105) and powdered samples prepared by jaw crushing and tema mill. Aliquots of ~3 g of sample powder were dried overnight in porcelain crucibles in an over at ~ 100 °C. 3.5900g of flux and 0.7000g of sample powder were weighted into platinum crucibles and stirred with a glass rod to ensure homogeneity, before being fired in a furnace at 1100 °C for ~ 20 minutes. Sample mixtures were stirred every 5 minutes to remove gas bubbles and promote homogeneity.

The melt was poured into a pre-heated brass mould and formed using a sprung press. Discs were left to cool prior to analysis. 1.2g of sample powder from the dried aliquots was weighed to four decimal places into pre-ignited alumina crucibles. Samples were ignited in the furnace at 1000 °C for one hour, cooled for 15 minutes and reweighed to four decimal places. The difference in weight before and after ignition was used to assess the mass loss on ignition for each sample.

Trace elements were determined from pressed sample powder pellets formed by thoroughly mixing approximately 9.5 g of sample powder with 0.9 ml of Polyvinylpyrollidone(PVP)-methyl cellulose binder using the 'bag technique' (Watson 1996). The mixture was emptied into a hardened steel mould and formed into a pellet using a hydraulic press. The sample pellets were dried overnight in the oven at ~ 100 °C prior to analysis.

E.1: XRF Major Element Analysis

Sample	NF-11-035	NF-11-037	NF-11-040	NF-11-042	NF-11-045	NF-11-046	NF-11-047	NF-11-048	NF-11-049	NF-11-050	NF-11-051	NF-11-084	NF-11-087	NF-11-088	NF-11-089	NF-11-090	NF-11-091
Lithology	Gneiss	Eclogite	Gneiss	Gneiss	Eclogite	Amphibolite	Gneiss	Gneiss	Amphibolite	Gneiss	Gneiss	Eclogite	Gneiss	Gneiss	Gneiss	Gneiss	Gneiss
SiO_2	64.90	51.51	71.79	60.02	49.48	49.09	55.01	62.49	56.43	64.86	60.13	47.21	64.77	65.25	61.34	64.95	66.79
TiO_2	0.76	1.10	0.62	1.12	0.73	0.31	1.29	0.90	0.97	0.76	0.92	0.94	0.83	0.82	0.94	0.85	0.68
Al_2O_3	15.54	14.64	12.59	16.86	16.68	15.73	17.91	15.91	16.34	15.34	16.75	14.33	15.21	15.30	16.26	15.31	15.43
Fe_2O_3	5.98	11.55	4.58	8.60	9.11	9.24	10.24	8.09	8.98	6.08	6.55	14.08	6.34	6.16	8.08	5.49	4.34
MnO	0.12	0.19	0.07	0.10	0.13	0.14	0.22	0.15	0.15	0.09	0.10	0.23	0.10	0.10	0.18	0.08	0.08
MgO	2.18	8.56	2.17	4.90	10.45	8.62	4.63	3.73	5.56	3.48	3.04	10.16	3.31	2.33	3.23	2.10	1.47
CaO	3.14	10.81	1.42	3.77	10.54	10.10	4.04	2.45	5.59	2.98	4.41	10.08	2.94	2.24	2.02	3.19	3.01
Na_2O	3.61	2.36	1.66	2.19	3.24	3.37	2.76	2.91	2.75	3.17	3.80	2.04	2.21	2.13	2.53	3.06	3.46
K_2O	2.54	0.08	2.19	2.32	0.37	0.73	3.31	2.83	1.81	2.41	2.64	0.02	2.54	3.21	3.86	3.31	3.87
P_2O_5	0.19	0.09	0.09	0.16	0.07	0.11	0.13	0.14	0.08	0.14	0.31	0.36	0.18	0.17	0.16	0.32	0.20
LOI	0.50	0.09	0.86	0.99	0.27	1.63	0.53	0.51	1.02	0.60	0.76	0.40	0.95	1.07	0.84	0.80	0.72
Total	99.44	101.00	98.04	101.01	101.06	99.08	100.07	100.12	99.68	99.92	99.40	99.85	99.40	98.79	99.44	99.46	100.06

E2: XRF Trace Element Analysis

Sample	NF-11-035	NF-11-037	NF-11-040	NF-11-042	NF-11-045	NF-11-046	NF-11-047	NF-11-048	NF-11-049	NF-11-050	NF-11-051	NF-11-084	NF-11-087	NF-11-088	NF-11-089	NF-11-090	NF-11-091
Lithology	Gneiss	Eclogite	Gneiss	Gneiss	Eclogite	Amphibolite	Gneiss	Gneiss	Amphibolite	Gneiss	Gneiss	Eclogite	Gneiss	Gneiss	Gneiss	Gneiss	Gneiss
Rb	94.50	1.20	59.70	91.10	11.00	18.00	113.40	98.50	53.20	80.30	61.30	0.00	99.10	115.90	140.40	91.70	111.50
Sr	219.00	68.60	47.10	119.70	88.60	357.00	96.70	104.60	122.70	183.20	372.20	119.90	173.10	156.20	127.30	402.20	420.40
Y	31.60	26.10	19.60	31.20	16.40	22.20	34.90	27.00	28.60	21.00	28.10	22.00	27.10	35.30	21.70	29.00	24.40
Zr	209.50	61.30	203.70	172.10	39.90	29.00	180.60	192.70	150.80	186.90	218.10	59.80	177.40	209.40	168.90	237.10	291.90
Nb	13.60	5.10	10.80	13.50	4.90	4.00	23.50	18.00	14.60	14.00	13.30	8.30	16.70	18.50	19.30	13.80	14.40
Ba	882.20	18.00	525.60	401.70	124.60	254.70	772.80	721.00	364.80	733.60	772.40	9.60	588.00	769.20	686.70	1261.10	980.40
Pb	12.70	2.70	7.20	13.00	8.10	10.60	9.40	14.20	16.70	11.30	6.80	12.40	10.80	14.30	11.90	15.60	21.80
Th	12.50	3.20	7.60	11.20	0.00	0.50	3.40	7.00	5.60	5.20	4.00	1.80	6.40	16.10	12.30	9.40	13.00
U	2.90	0.30	1.60	3.30	1.30	0.00	1.00	2.10	1.40	0.80	2.80	0.20	2.20	1.70	1.70	1.70	2.50
Sc	13.40	45.20	7.40	20.70	30.40	34.40	28.30	21.60	29.60	16.20	11.90	36.00	16.20	15.50	21.10	12.80	10.50
V	104.40	317.50	74.20	202.30	232.30	253.60	206.60	146.70	171.30	126.60	115.70	228.30	133.30	102.90	146.50	90.20	71.50
Cr	43.90	234.50	61.00	183.80	584.00	408.00	183.10	136.90	212.60	101.00	50.90	513.30	100.70	65.70	115.30	42.80	16.10
Co	14.60	40.90	5.40	21.10	42.20	23.80	25.30	12.90	21.80	16.10	15.70	47.50	7.90	11.70	20.20	7.10	8.30
Ni	19.50	84.70	27.70	71.10	267.60	120.50	41.00	40.80	71.00	40.80	32.80	214.20	22.50	23.30	48.30	18.80	13.50
Cu	14.90	119.80	67.10	21.60	18.70	7.60	42.30	15.40	34.50	50.20	27.20	111.00	15.80	13.40	13.70	39.10	11.60
Zn	64.20	102.30	54.80	90.30	72.70	109.20	105.10	104.00	113.50	73.90	91.10	131.70	83.50	78.30	91.40	61.60	63.10
Ga	17.70	16.20	13.60	23.40	16.40	18.70	20.90	19.90	17.60	18.40	20.50	19.60	18.30	18.60	20.50	17.50	17.80
Mo	0.40	0.00	0.00	1.00	0.10	0.00	0.60	0.00	0.00	0.30	9.10	0.20	2.10	0.20	0.00	0.60	1.10
As	0.00	2.30	0.00	0.00	-3.50	0.10	0.00	0.00	0.00	0.40	0.60	0.20	0.50	2.20	2.50	0.00	0.00
S	33.10	21.60	87.80	82.20	25.60	78.90	109.60	37.80	118.40	95.40	67.50	55.50	166.30	21.30	30.20	45.10	32.00

Appendix F:

DiffArg_inverse Model Results

Kjenndalsbreen glacier

F.1: White Mica Linear Models

T (°C)	Grain Radius (mm)	Cooling Rate (°CMa^{-1})	Age Diff (Ma)
450	0.25	5	2.246
		10	0.802
		25	0.204
		50	0.070
		70	0.041
	0.5	5	1.138
		10	0.396
		25	0.090
		50	0.025
		70	0.012
	1	5	0.520
		10	0.153
		25	0.022
		50	0.004
		70	0.001

T (°C)	Grain Radius (mm)	Cooling Rate (°CMa^{-1})	Age Diff (Ma)
500	0.25	5	9.267
		10	3.580
		25	0.964
		50	0.350
		70	0.211
	0.5	5	5.329
		10	1.942
		25	0.503
		50	0.180
		70	0.108
	1	5	2.798
		10	1.001
		25	0.255
		50	0.089
		70	0.052

T (°C)	Grain Radius (mm)	Cooling Rate (°CMa^{-1})	Age Diff (Ma)
600	0.25	5	29.248
		10	13.500
		25	4.784
		50	2.151
		70	1.456
	0.5	5	24.683
		10	11.147
		25	3.804
		50	1.645
		70	1.088
	1	5	19.829
		10	8.643
		25	2.759
		50	1.109
		70	0.703

T (°C)	Grain Radius (mm)	Cooling Rate (°CMa^{-1})	Age Diff (Ma)
700	0.25	5	49.248
		10	23.500
		25	8.740
		50	4.151
		70	2.879
	0.5	5	44.683
		10	21.147
		25	7.804
		50	3.645
		70	2.512
	1	5	39.828
		10	18.642
		25	6.758
		50	3.105
		70	2.120

F.2: White Mica 1/T Models

T (°C)	Grain Radius (mm)	Cooling Rate (°CMa^{-1})	Age Diff (Ma)
450	0.25	5	0.626
		10	0.220
		25	0.053
		50	0.014
		70	0.009
	0.5	5	0.302
		10	0.097
		25	0.053
		50	0.014
		70	0.009
	1	5	0.107
		10	0.024
		25	0.002
		50	0.000
		70	0.000

T (°C)	Grain Radius (mm)	Cooling Rate (°CMa^{-1})	Age Diff (Ma)
500	0.25	5	2.636
		10	0.967
		25	0.251
		50	0.090
		70	0.054
	0.5	5	1.397
		10	0.500
		25	0.127
		50	0.045
		70	0.026
	1	5	0.711
		10	0.251
		25	0.061
		50	0.019
		70	0.010

T (°C)	Grain Radius (mm)	Cooling Rate (°CMa^{-1})	Age Diff (Ma)
600	0.25	5	10.301
		10	4.611
		25	1.560
		50	0.672
		70	0.445
	0.5	5	8.145
		10	3.535
		25	1.130
		50	0.458
		70	0.126
	1	5	5.995
		10	2.461
		25	0.710
		50	0.265
		70	0.163

T (°C)	Grain Radius (mm)	Cooling Rate (°CMa^{-1})	Age Diff (Ma)
700	0.25	5	18.073
		10	8.455
		25	3.045
		50	1.409
		70	0.924
	0.5	5	15.660
		10	7.234
		25	2.572
		50	1.170
		70	0.794
	1	5	13.260
		10	6.019
		25	2.097
		50	0.930
		70	0.623

F.3: Biotite Linear Models

T (°C)	Grain Radius (mm)	Cooling Rate (°CMa^{-1})	Age Diff (Ma)
450	0.25	5	26.214
		10	12.111
		25	4.298
		50	1.934
		70	1.298
	0.5	5	22.165
		10	10.020
		25	3.425
		50	1.484
		70	0.974
	1	5	17.846
		10	7.793
		25	2.501
		50	1.014
		70	0.639

T (°C)	Grain Radius (mm)	Cooling Rate (°CMa^{-1})	Age Diff (Ma)
500	0.25	5	36.213
		10	17.110
		25	6.296
		50	2.933
		70	2.005
	0.5	5	32.160
		10	15.015
		25	5.421
		50	2.480
		70	1.678
	1	5	27.828
		10	12.775
		25	4.483
		50	1.995
		70	1.328

T (°C)	Grain Radius (mm)	Cooling Rate (°CMa^{-1})	Age Diff (Ma)
600	0.25	5	56.213
		10	27.110
		25	10.296
		50	4.933
		70	3.459
	0.5	5	52.160
		10	25.015
		25	9.420
		50	4.479
		70	3.129
	1	5	47.826
		10	22.772
		25	8.481
		50	3.993
		70	2.774

T (°C)	Grain Radius (mm)	Cooling Rate (°CMa^{-1})	Age Diff (Ma)
700	0.25	5	76.082
		10	37.043
		25	14.296
		50	6.918
		70	4.875
	0.5	5	72.159
		10	35.015
		25	13.420
		50	6.479
		70	4.546
	1	5	67.826
		10	32.772
		25	12.481
		50	5.993
		70	4.192

F.4: Biotite 1/T Models

T (°C)	Grain Radius (mm)	Cooling Rate (°CMa^{-1})	Age Diff (Ma)
450	0.25	5	11.313
		10	5.079
		25	1.727
		50	0.748
		70	0.492
	0.5	5	9.004
		10	3.926
		25	1.268
		50	0.521
		70	0.332
	1	5	6.706
		10	2.785
		25	0.822
		50	0.310
		70	0.189
500	0.25	5	15.990
		10	7.377
		25	2.624
		50	1.188
		70	0.800
	0.5	5	13.517
		10	6.141
		25	2.130
		50	0.942
		70	0.625
	1	5	11.046
		10	4.906
		25	1.637
		50	0.696
		70	0.452

T (°C)	Grain Radius (mm)	Cooling Rate (°CMa^{-1})	Age Diff (Ma)
600	0.25	5	25.134
		10	11.918
		25	4.238
		50	2.073
		70	1.437
	0.5	5	22.574
		10	10.589
		25	3.866
		50	1.793
		70	1.237
	1	5	19.781
		10	9.192
		25	3.308
		50	1.514
		70	1.037
700	0.25	5	34.522
		10	16.550
		25	6.248
		50	2.960
		70	2.060
	0.5	5	31.295
		10	14.948
		25	5.650
		50	2.649
		70	1.838
	1	5	28.214
		10	13.275
		25	4.980
		50	2.337
		70	1.616